# *Catalytic Enantioselective 6π Photocyclization of Acrylanilides*

**and**

# *Enantiomerisation Processes of Indolyl-Naphthyl Atropisomers*




**Pearse Solon**

Wadham College

*A dissertation presented in partial fulfilment of requirements for the award of the degree*

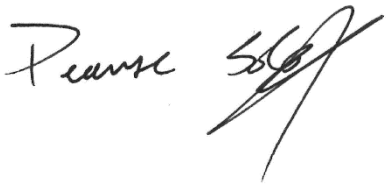
**Doctor of Philosophy**

*of the*

**University of Oxford**

# Declaration

*This dissertation describes work carried out in the Chemistry Research Laboratory at the University of Oxford between February 2019 and March 2023. The dissertation is a product of my own work and includes no results obtained through collaboration, unless explicitly stated otherwise in the text.*



*Pearse Solon*

# Acknowledgements

I would firstly like to thank Prof. Martin D. Smith for accepting me for a summer studentship in 2015. Little did I know at the time that it would be the start of a years long ordeal spanning two degrees, a pandemic, and what felt like a million stumbling blocks. Your support over the years has been indispensable and has allowed me to grow as a scientist and to become confident in my abilities as one.

Starting from the beginning, I would especially like to thank Kat, my summer project supervisor. Though I'm sure the experience was harrowing from your point of view, your help and guidance in those early days encouraged me to pursue organic chemistry. To Ben, my part II supervisor, for patiently helping me through my first venture into atropisomerism and kinetic resolution, and also to Alison for all of her support in chemistry, crosswords, and teatime. Thanks also to Jack and Liz, for suffering through with me.

In the lab, I'd like to thank Zac both for resurfacing from nowhere, and for graciously sharing his hood and supervising me when I returned for rotation. Thanks to Maddie for all of her help in F4 and for being an all-round good egg and teatime proponent, and thanks to Ben D for providing light relief, grounding, and dramatics. There are too many people from the lab to thank individually, but thanks to Ricky, Owen, Mihai, Jiyuan, Yao, Morgan, Mengxue, Qing, Ben, and all the part IIs we've had, in addition to all the recent recruits.

Outside the lab, I'd like to thank Charlie, Dani, Kate, and again Zac for peacefully cohabitating, and for all the great times we had in Howard Street. It's sad that it's time for us to go our separate ways, but I'm excited to see where everyone ends up. Also, a big thanks to Oli for his continuous support and for putting up with the endless DPhil while working through his own.

Finally, I’d also like to thank my family for their continued support.

# List of Abbreviations

| | |
|---|---|
| * | Chiral or excited state |
| +/- | Racemic |
| ∝ | Proportional to |
| Å | Angstrom |
| -$d_n$ | n deutero |
| $\Delta G^{\ddagger}_{T(K)}$ | Free energy barrier at a given temperature T (in Kelvin) |
| °C | Degrees Celsius |
| $\lambda_{10\%}$ | Wavelength at which 10% of maximum emission/absorption occurs |
| Φ | Quantum yield |
| $t^{rac}_{\frac{1}{2}}$ | Half-life of racemization |
| (ox) | Oxidant or oxidation |
| (red) | Reduction |
| [X] | Concentration of X |
| A | Acceptor |
| ABS | Absorbance or absorbance units |
| Ac | Acetyl |
| Anti | On the opposite side/face |
| Ar | Aryl |
| $BAr^F_4$ | Tetrakis[3,5-bis(trifluoromethyl)phenyl]borate |
| BINAM | 2,2′-Bis(diphenylphosphinoamino)-1,1′-binaphthyl |
| BINAP | 2,2′-Bis(diphenylphosphino)-1,1′-binaphthyl |
| BINOL | 1,1′-Bi-2-naphthol |
| Bn | Benzyl |
| Boc | *tert*-Butyloxycarbonyl |
| BOX | Bisoxazoline |
| Bu | Butyl |
| Cat. | Catalyst |
| Cbz | Benzyloxycarbonyl |
| CFL | Compact Fluorescent Lamp |
| CPA | Chiral Phosphoric Acid |
| Cy | Cyclohexyl |
| Cyoct | Cyclooctyl |
| D | Diffusion coefficient or donor |

| | |
|---|---|
| δ | Chemical shift |
| Da | Dalton |
| DCE | 1,2-Dichloroethane |
| Δ | Change or heat |
| Dexter | Dexter electron transfer |
| dFppy | 2-(2,4-Difluorophenyl)pyridine |
| DIBAL-H | Diisobutylaluminium hydride |
| DIPA | Di*iso*propyl amine |
| DIPEA | *N,N*-Diisopropyl ethylamine |
| DMAP | Dimethylaminopyridine |
| DME | 1,2-dimethoxyethane |
| DMF | *N,N*-Dimethylformamide |
| DMSO | Dimethyl Sulfoxide |
| DOSY | Diffusion Ordered NMR Spectroscopy |
| dr | diastereomeric ratio |
| dtbpy | 4,4'-Di-*tert*-butyl-2,2'-bipyridine |
| $E_{1/2}$ | Half-cell potential |
| $E_T$ | Triplet Energy |
| ee | Enantiomeric excess |
| ent | Enantiomer |
| $E_NT$ | Energy Transfer |
| eq. | Equivalent(s) |
| er | Enantiomeric ratio |
| ESI | Electrospray ionisation |
| Et | Ethyl |
| FDA | Food and Drug Administration (US) |
| Fluo | Fluorescence |
| FMO | Frontier molecular orbital |
| FRET | Forster Resonance Energy Transfer |
| FTIR | Fourier-Transform Infrared Spectroscopy |
| G12C | A kRAS oncogenic driver mutation |
| HFIP | Hexfluoro *iso*propanol |
| HOMO | Highest occupied molecular orbital |
| HPLC | High Performance Liquid Chromatography |
| HRMS | High Resolution Mass Spectrometry |
| HSOMO | Highest singly occupied molecular orbital |

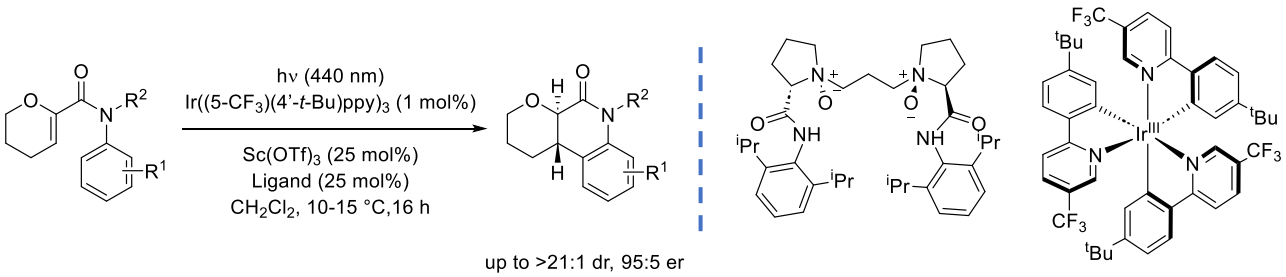
| | |
|---|---|
| HTS | High Throughput Screening |
| hv | Radiation or light |
| *i* | *iso* |
| $I_{10\%}$ | 10% intensity |
| IC | Internal conversion |
| $IC_{50}$ | Half-maximal inhibitory concentration |
| IPA | 2-propanol/isopropyl alcohol/isopropanol |
| ISC | Inter-system crossing |
| *k* | Rate constant |
| K | Kelvin |
| kcal | Kilocalorie |
| $K_{eq}$ | Equilibrium constant |
| KRas | Kirsten Rat Sarcoma Viral Oncogene Homologue |
| L | Ligand |
| LA | Lewis Acid |
| λ | Wavelength |
| LC | Liquid chromatography |
| LC/MS | Liquid chromatography coupled mass spectrometry |
| LED | Light emitting diode |
| LiHMDS | Lithium bis(trimethylsilyl)amide |
| Lit. | Literature |
| ln | Natural logarithm |
| LSOMO | Lowest singly occupied molecular orbital |
| LUMO | Lowest unoccupied molecular orbital |
| m | metre |
| M | Molar |
| *m*- | *meta* |
| *m*-CPBA | *meta*-chloroperbenzoic acid |
| Me | Methyl |
| MeCN | Acetonitrile |
| µ | Micro |
| mol | Mole |
| mol% | Mole percent |
| molal | Mole per kilogram solvent |
| mr | Molar ratio of heterocoupled to combined homocoupled products |
| MS | Mass spectrometry |

| | |
|---|---|
| MW | Molecular Weight/Molecular Mass |
| *n* | Normal |
| n | Nano |
| NMR | Nuclear Magnetic Resonance |
| nOe | Nuclear Overhauser Effect |
| *o*- | *ortho* |
| ODE | Ordinary differential equation |
| OLED | Organic light emitting diode |
| *p*- | *para* |
| PC | Photocatalyst |
| pERK | Protein kinase R (PKR)-like endoplasmic reticulum kinase |
| Ph | Phenyl |
| PhMe | Toluene |
| PHOLED | Phosphorescent organic light-emitting diode |
| Phos | Phosphorescence |
| PMB | *Para*methoxybenzyl |
| ppm | Parts per million |
| ppy | 2-Phenylpyridine |
| Pr | Propyl |
| PyBOX | Pyridinebisoxazoline |
| R | Alkyl group |
| r.t. | Room temperature |
| $R^2$ | Correlation coefficient |
| rac. | Racemic mixture/racemate |
| rr | Regioisomeric ratio |
| s gauge | Small inner diameter gauge |
| s/m/d/h | second(s)/minute(s)/day(s)/hour(s) |
| $S_n$ | Singlet State |
| SET | Single electron transfer |
| SIDA | Self-induced diastereomeric anisochronism |
| $^1$ | Singlet |
| SM | Starting material |
| syn | One the same side/face |
| *t* | Time |
| $T_n$ | Triplet state |
| TAS | Transient absorption spectroscopy |

| | |
|---|---|
| *t*-Bu/*t*Bu | *tert*-Butyl |
| TET | Triplet energy transfer |
| Tf | Trifluoromethanesulfonyl |
| TFA | Trifluoroacetic acid |
| THF | Tetrahydrofuran |
| TLC | Thin-layer chromatography |
| TMEDA | *N,N,N',N'*-Tetramethylethylenediamine |
| TMS | Trimethylsilyl |
| Tol | Toluyl |
| $^3$ | Triplet |
| Ts | Tosyl |
| TS | Transition state |
| UV | Ultraviolet |
| UV-VIS | Ultraviolet-Visible |
| V | Volts |
| W | Watts |
| w/w | Percent by weight |
| XantPhos | 4,5-Bis(diphenylphosphino)-9,9-dimethylxanthene |

# Abstract

This thesis is composed of two parts. The first part describes the development of a dual catalytic enantioselective 6π photocyclization (Scheme A1).




Scheme A1 The dual catalytic enantioselective 6π photocyclization of acrylanilides

We go on to describe the work carried out to validate the predicted reaction pathway and determine whether the photocatalytic portion of the cycle operates by photoredox catalysis or energy transfer catalysis (Figure A1).

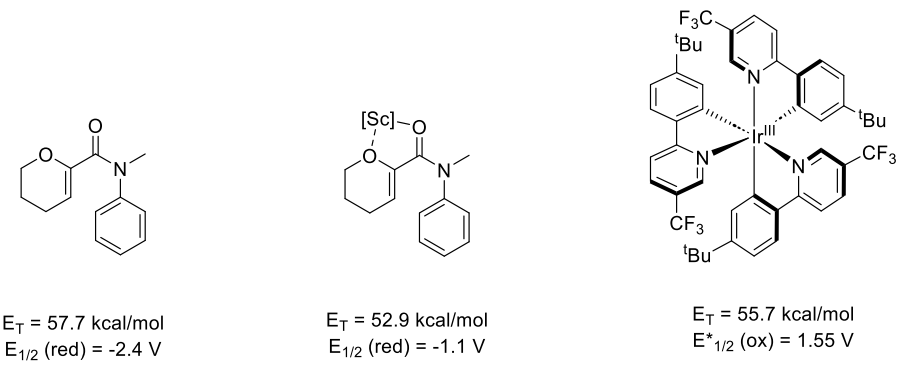



Figure A1 Measurement and calculation of properties indicates that either form of photocatalysis may be in operation

The second part describes the observation of non-first order racemisation of an indolyl-naphthyl atropisomer and the work carried out to reproducibly observe the effect and gather data across a number of concentrations (Figure A2).

This work is now part of a publication.[1]

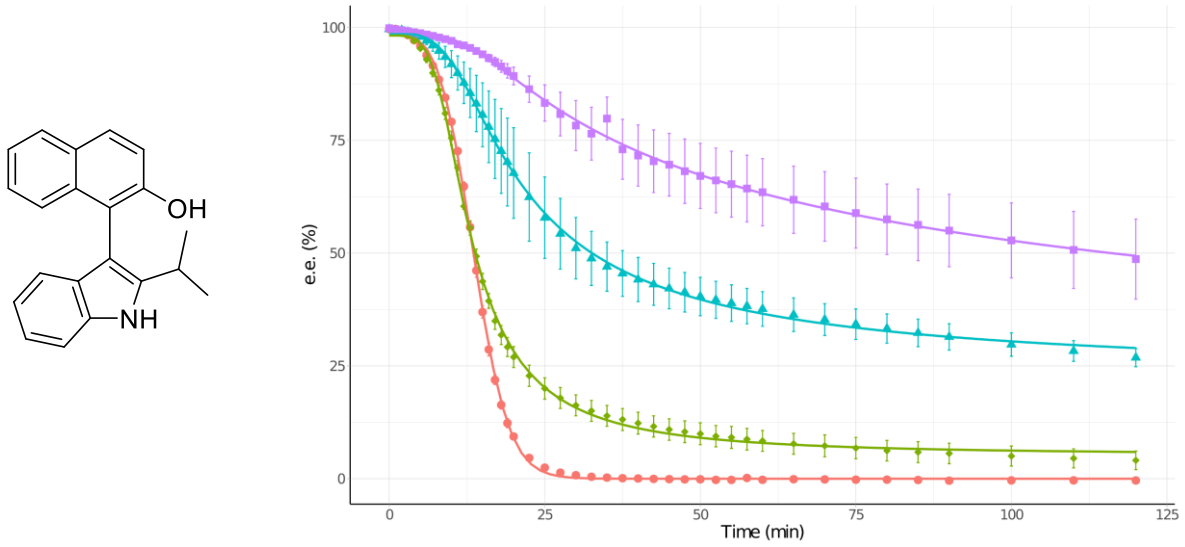



Figure A2 Erosion data recorded in toluene across a number of concentrations

We then describe the combination of experimental probes and modelling carried out in the hopes of determining the underlying cause of the observed behaviour (Figure A3).

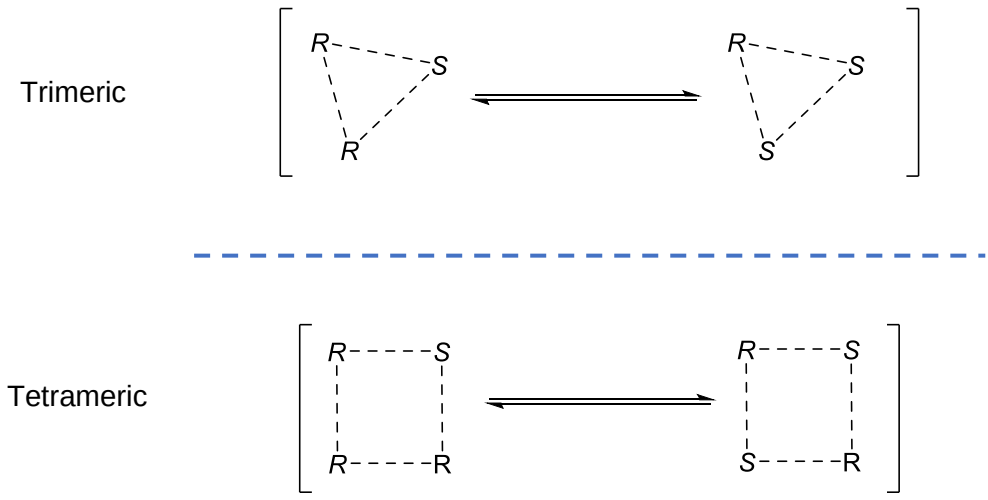



Figure A3 Rapid erosion of enantiomeric excess may be due to the presence of trimers and/or tetramers in solution

# Contents

Part I: Catalytic Enantioselective 6π Photocyclization of Acrylanilides ..... 1
I.1 Introduction ..... 2
I.1.1 Organic Photochemistry – the $T_1$ State ..... 2
I.1.1.1 Direct excitation ..... 3
I.1.1.2 Sensitized Photochemistry ..... 4
I.1.2 Asymmetric Photocyclization ..... 6
I.1.2.1 Lewis Acid Catalysis ..... 7
I.1.3 Asymmetric 6π Photocyclization of Acrylanilides ..... 11
I.1.4 Iridium Photosensitizers ..... 13
I.1.5 Previous work in the Smith Group ..... 15
I.1.6 This Project ..... 16
I.3 Results and Discussion ..... 19
I.3.1 Reaction Optimisation ..... 19
I.3.1.1 The Photocatalyst ..... 19
I.3.1.2 Lewis Acid Sources, Additives, and Preformation ..... 23
I.3.2 Reaction Scope ..... 26
I.3.2.1 *N*-Alkylation ..... 26
I.3.2.1 *o*-Substitution ..... 28
I.3.2.2 *p*-Substitution ..... 29
I.3.2.3 *m*-Substitution ..... 30
I.3.2.4 Alteration of the etheric ring ..... 31
I.3.2.1 Absolute Configuration ..... 34
I.3.3 Mechanistic Studies ..... 36
I.3.3.1 Possible Pathways ..... 36
I.3.3.2 Validation of the 1,5-H shift ..... 39
I.3.3.3 Diastereoselectivity and Meta substitution ..... 42
I.3.3.1 Additional Mechanistic Insights ..... 45
I.3.3.1 Energy Transfer vs Photoredox ..... 47
I.3.3.2 Selectivity ..... 50
I.4 Conclusion and Future Work ..... 53

Part II: Enantiomerisation Processes of Indolyl-Naphthyl Atropisomers ..... 55
II.1 Introduction ..... 56
II.1.1 Atropisomerism ..... 56
II.1.2 The Barrier to Rotation ..... 57
II.1.3 Alternative Enantiomerisation Pathways ..... 62
II.1.4 Autocatalysis ..... 64
II.1.5 Dimerization ..... 67
II.1.6 This Work ..... 70
II.2 Results and Discussion ..... 73
II.2.1 Initial synthesis ..... 73
II.2.2 Data Gathering and Methodology ..... 75
II.2.2.1 Methodology Development ..... 75
II.2.2.2 Collected Data ..... 77
II.2.2.3 Meaningful Fits ..... 79
II.2.3 Evidence for Hydrogen Bonding ..... 80
II.2.3.1 Erosion Studies of Modified Substrates ..... 81
II.2.3.2 NMR Studies ..... 86
II.2.3.3 Hydrogen Bonding Solvents ..... 91
II.2.3.4 Spiking ..... 93
II.2.4 Possible Models ..... 95
II.2.4.1 The Boundary Case ..... 96
II.2.4.2 Spiking Studies ..... 104
II.2.4.3 Lower Concentrations ..... 106
II.3 Conclusion and Future Work ..... 111
References ..... 113
Experimental Data ..... S-i

# Part I:

# Catalytic Enantioselective 6π

# Photocyclization of Acrylanilides

# I.1 Introduction

Light is an abundant fuel on which all forms of life rely. It is therefore unsurprising that the study of light, whether it be its generation, or the harnessing of its energy, is a key area of many scientific disciplines.[2] These studies have led to many discoveries and inventions ranging from LEDs to generate light, the conversion of light to storable energy by photovoltaics, and the use of light energy to drive chemical transformations.

## I.1.1 Organic Photochemistry – the $T_1$ State

Broadly speaking, the transformation of organic molecules using visible light falls into two categories: those involving the photomediated transfer of electrons, and those involving access to a substrate's excited states using light energy.[3]

The first of these fields, referred to as photoredox catalysis, is a field which has received much attention in recent times, with a huge number of useful and unique reactions being developed, but which will not be discussed in detail.[4, 5]

The latter, with which we are concerned, falls into two broad categories based on the way in which access to the triplet state* is gained. In the first, more traditional approach, known as direct excitation, the triplet state is generated by direct irradiation of a substrate.[6] The second, more recent approach, is photosensitization or energy transfer catalysis. In this approach a photosensitizer is used to access the triplet state of the substrate of interest.[3]

* Though reactions can also take place from excited singlet states, we will focus on reactivity from the triplet state.

### I.1.1.1 Direct excitation

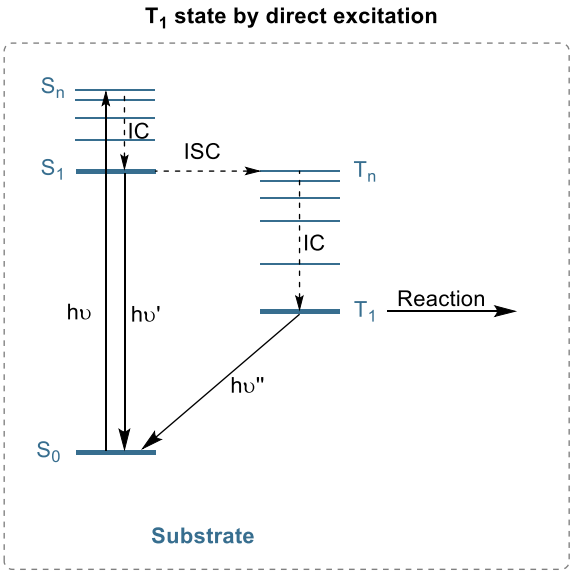
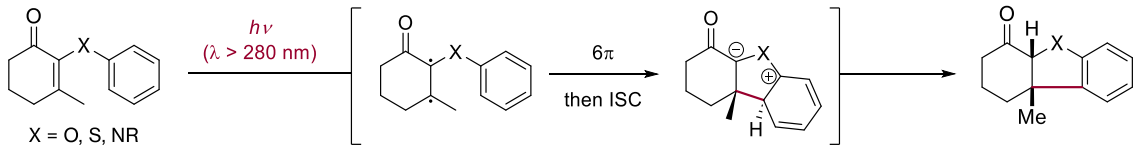



Figure 1 Access to the $T_1$ state by direct excitation/irradiation. A substrate in the ground state, $S_0$, is excited by light (hv) to an appropriate excited singlet state, $S_n$, from where it quickly relaxes by internal conversion (IC) to the first excited singlet state, $S_1$. From $S_1$, the substrate may return to the ground state by fluorescence (hv'), or undergo intersystem crossing (ISC) to access the triplet state, from where it may react or return to the ground state by phosphorescence (hv'').

As mentioned, early work in synthetic photochemistry focussed primarily on the direct excitation of organic molecules. In this regime (Figure 1), a substrate is directly irradiated with light (hv) in order to electronically excite the substrate to an excited singlet state, $S_n$. From this excited state internal conversion (IC) allows relaxation to $S_1$, the lowest lying excited singlet state. A molecule in the $S_1$ state can then either relax back to the ground state ($S_0$) by fluorescence (hv'); or undergo inter-system crossing (ISC) to generate the $T_1$ state (either directly or by internal conversion from a $T_n$ state). From $T_1$ a substrate can either phosphoresce (hv'') back to the $S_0$ state or go on to react.[6]

Of note in this regime are the large energy gaps between $S_0$ and $S_n$ states in most organic molecules. Because of this, promotion between these states necessitates the use of high energy UV light.[6] Coupled with this is the low rate of intersystem crossing to $T_n$ states from $S_n$ states in organic molecules due to small spin-orbit coupling constants, which leads to inefficient reactions.[7]




1 2

Scheme 1 Schultz' 6π cyclization is achieved by direct excitation. Generation of a triplet species leads to cyclisation, followed by intersystem crossing and a 1,5-H shift to form **2**.

A representative example of this reaction type is the 6π photocyclization of **1** to form **2** reported by Schultz (Scheme 1).[8] Though highly selective and high yielding for a number of substrates, most substitution of the aryl ring is incompatible with the conditions used and leads to unpredictable decomposition.

### I.1.1.2 Sensitized Photochemistry

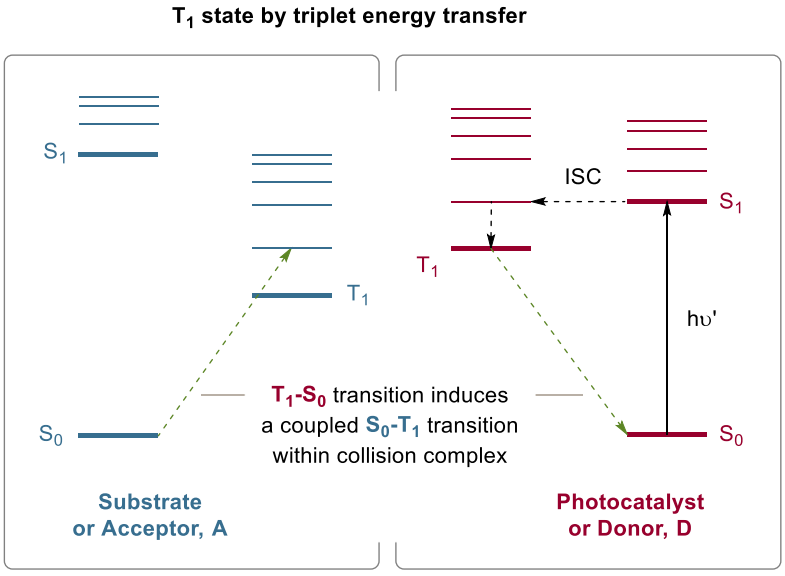



Figure 2 Access to the $T_1$ state by sensitization relies on the generation of a donor triplet state ($T_1$, right) as previously described. This donor triplet state can relax to its ground state ($S_0$, right) by exciting an acceptor directly to its triplet state ($T_1$, left) from its ground state ($S_0$, left).

In contrast to direct excitation, sensitized photochemistry (Figure 2) makes use of a donor (D) which readily and repeatedly undergoes direct excitation and inter-system crosses to a long-lived triplet state.[3] This long-lived triplet state ($T_1$) can then relax back to its ground state, $S_0$, either directly by phosphorescence, or by acting as a donor and coupling its transition with

a simultaneous excitation of an acceptor directly to a triplet state. This may occur by either dipole interaction (FRET) or formal electron exchange (Dexter energy transfer).[9, 10] For our purposes, Dexter is the more common mechanism of the two (Figure 3).[11]

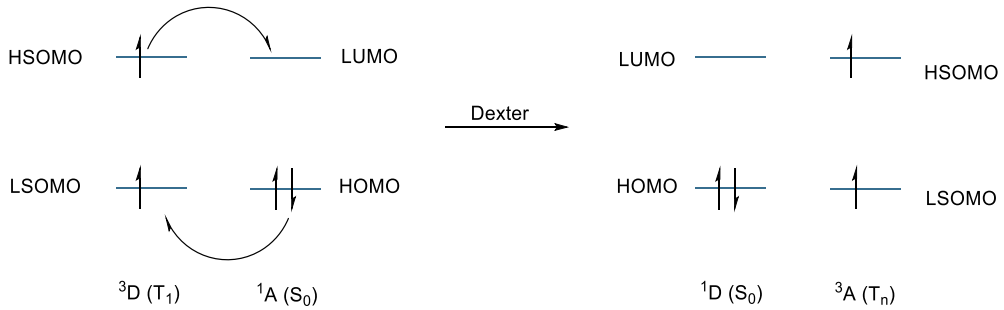
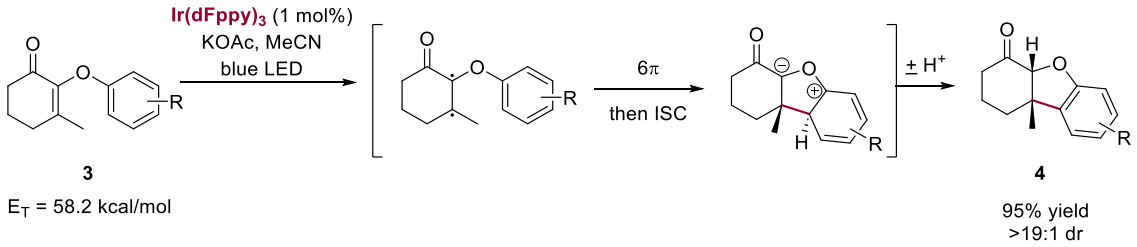



Figure 3 Dexter energy transfer proceeds by formal electron exchange to simultaneously promote the acceptor to a triplet state ($^3$A ($T_n$), right) and relax the donor to a ground state singlet ($^1$D ($S_0$), right).

This regime, wherein a coupled excitation and relaxation gives rise to a substrate $T_n$ state, obviates the need to access the substrate $T_1$ state *via* an excited singlet state ($S_n$). This side-steps issues associated with inefficient inter-system crossing in small organic molecules and ensures that high energy singlet states, which can cause undesired reactivity, are never generated. In addition to this, a sensitized approach allows for flexibility in the sensitizer used, facilitating tailoring for desirable properties, such as excitation with benign visible light rather than harmful UV.[3]




Scheme 2 Analogous to Schultz' cyclization, Smith *et al*'s cyclization proceeds from the triplet state. In this case, however, the triplet state is accessed directly by sensitization.

A representative example of this form of catalysis is the 6π cyclization of **3** reported by Smith *et al* (Scheme 2). This is the same cyclisation reported by Schultz, but using a sensitization strategy.[12] In place of high energy UV light, blue light was used in combination with an iridium

based photocatalyst. This both widens the method's tolerance to substitution and improves the safety of the methodology.

### I.1.2 Asymmetric Photocyclization

Though energy transfer (and indeed photoredox) mediated reactions exhibit exquisite specificity and tolerance, control of absolute stereochemistry remains an enduring challenge.[13-17]

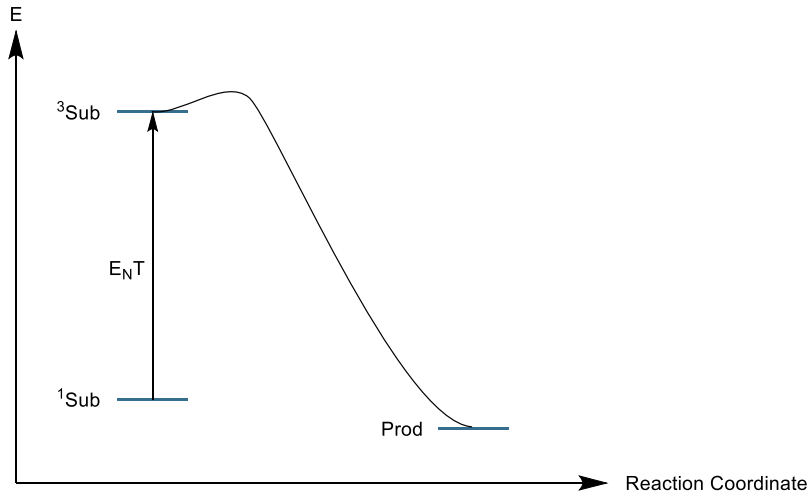



Figure 4 Illustrative reaction coordinate for a photochemical reaction. Small activation barriers to reaction from the triplet state make control difficult.

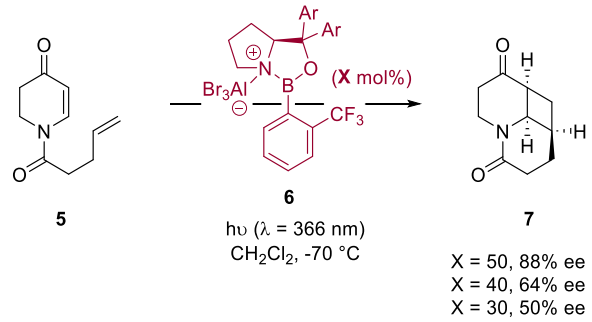
Much of the difficulty faced in controlling the stereochemical outcomes of photochemical reactions arises from the highly reactive nature of the intermediates generated. In an illustrative reaction coordinate (Figure 4) a ground state substrate is excited to its lowest lying triplet state ($T_1$). This high energy species then reacts rapidly *via* low barrier pathways, giving little chance to influence stereochemical outcomes.

In traditional, ground state asymmetric catalysis, stereoinduction arises from reaction of a substrate only within a chiral environment.[18] This is achieved either by use of a chiral reagent or catalyst. In the case of photochemical reactions, the $T_1$ state is generated either by direct excitation or by energy transfer, both of which are ordinarily achiral phenomena. It can

therefore be difficult to ensure that access to this state is possible only when in the presence of/bound to a source of chirality.

### I.1.2.1 Lewis Acid Catalysis

One notable method by which asymmetric photocyclizations can be achieved is with Lewis acid catalysis.[19-21]




Scheme 3 Bach's asymmetric [2 + 2] photocyclization makes use of a chiral Lewis acid (**6**) to form **7** stereoselectively

In one early report, Bach and co-workers achieve high enantioselectivity in the intramolecular [2 + 2] cyclization of **5** by making use of chiral Lewis acid **6** under direct irradiation with UV light (Scheme 3).

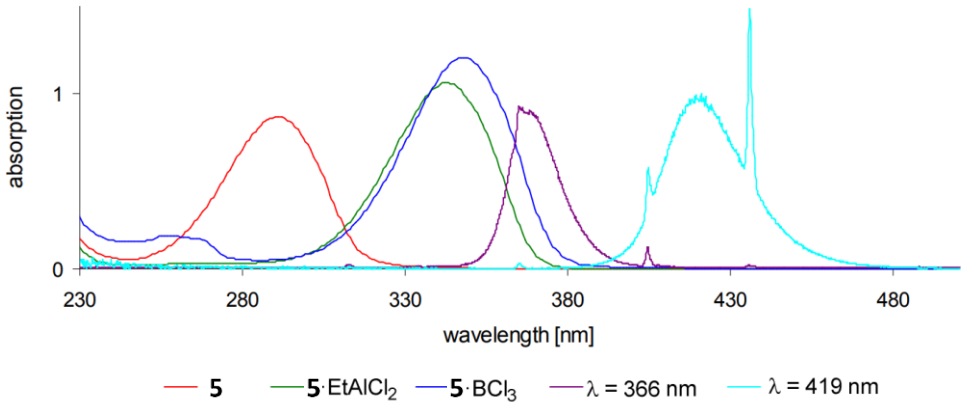
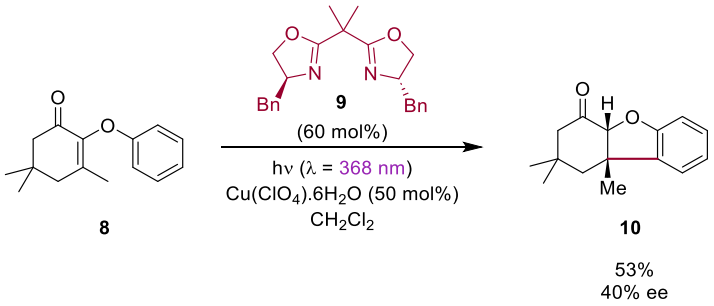



Figure 5 UV-VIS spectra of **5** with various Lewis acids reveal a shift in the absorbance profile of **5** when complexed to a Lewis acid.

Key to understanding the selectivity of the cyclization is the shift in absorbance that **5** exhibits on coordination to a Lewis acid (Figure 5). It can be seen that **5** alone exhibits an

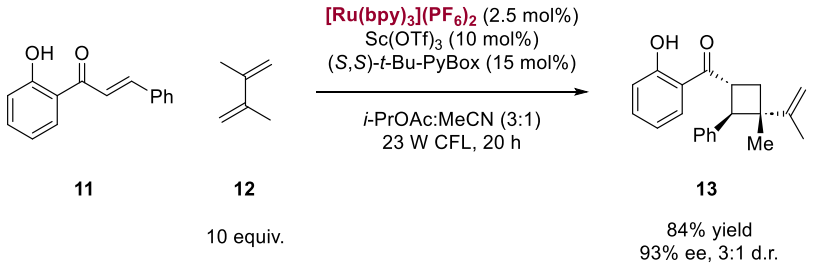
absorbance maximum at ~290 nm, but when a Lewis acid is added, this absorbance maximum shifts to longer wavelengths (343 nm for addition of $EtAlCl_2$, 348 nm for addition of $BCl_3$). This bathochromic shift is significant as, if a chiral Lewis acid can cause the same shift to occur, irradiation with an appropriate wavelength of light ($\lambda$ = 366 nm) would only excite the substrate when bound, facilitating stereoselective reaction from the $T_1$ state.




Scheme 4 Bach's Lewis acid catalysed asymmetric 6π photocyclization makes use of a similar shift in absorption on complexation, but utilises a metallic Lewis acid in combination with a chiral ligand to furnish **10** in moderate ee.

Another variation of this approach also developed by Bach is the use of a metallic Lewis acid with chiral ligand **9** (Scheme 4).[22] Again, this method makes use of the occurrence of a bathochromic shift on binding of the Lewis acid to substrate **8**, but the combination of a Lewis acidic metal with a chiral ligand allows the use of a range of chiral ligands. This is a particularly attractive approach because it can exploit chiral ligands developed for ground state Lewis acid catalysis since the 1990's.[23]

Though high selectivity is possible using Bach's methods, the use of direct excitation by UV light still presents many problems with compatibility and safety.




Scheme 5 Yoon's Lewis acid catalysed [2 + 2] cycloaddition again takes advantage of a chiral Lewis acid complex, but combines it with sensitization to achieve high stereoselectivity in an intermolecular [2 +2] cycloaddition.

An answer to the use of direct excitation is presented by Yoon *et al* in their combination of asymmetric Lewis acid catalysis with energy transfer catalysis (Scheme 5).[24] Using this approach, the intermolecular [2 + 2] reaction of **11** and **12** to form **13** can be made enantioselective by the use of a metallic Lewis acid/chiral ligand combination.

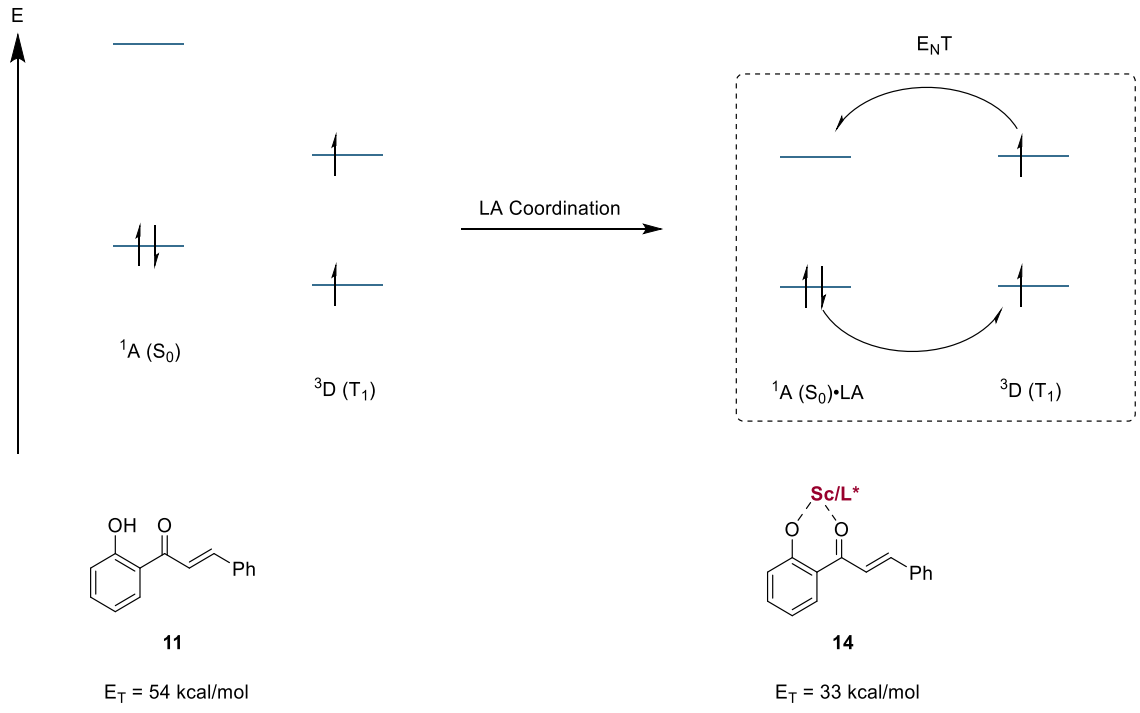
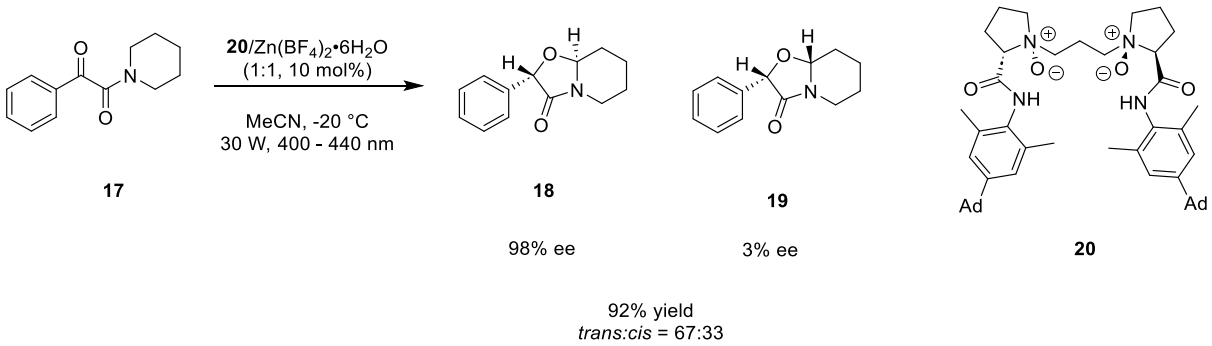



Figure 6 $E_NT$ enabled by Lewis acid coordination. A Lewis acid can coordinate to **11**, producing complex **14**, whose frontier molecular orbitals are suitably aligned (energetically and spatially) to allow energy transfer from a donor($^3D$ ($T_1$)). to occur.

Much like the bathochromic shift approach, this approach makes use of changes in electronics on coordination of a Lewis acid. In this regime, however, coordination of a Lewis acid induces a change in the electronics of the frontier molecular orbitals (FMOs) of a

substrate, allowing them to interact with the FMOs of an excited photosensitizer when they previously could not (Figure 6).[25, 26] This overlap allows energy transfer to occur, and as interaction is only made possible by coordination of the chiral Lewis acid, the substrate $T_1$ state is only generated when bound.

In addition to BOX and PyBOX ligands, which in combination with copper(II) salts have long been used as ligands for asymmetric Lewis acid catalysis, recent work by Feng *et al* has shown amino acid derived *N,N'*-dioxide ligands to be effective alternatives.[23, 27]

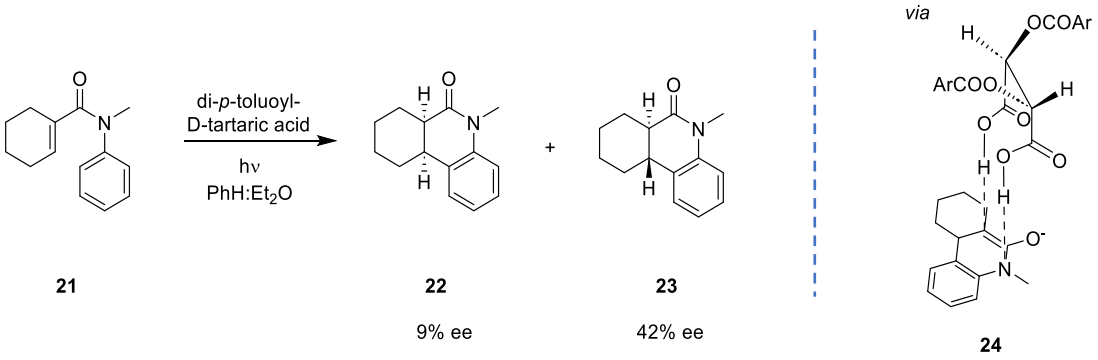



Scheme 6 Feng's enantioselective Norrish Type II cyclization makes use of chiral ligand **20** and Zinc to facilitate asymmetric photocyclization of **17** to form **18** and **19**.

In Feng's system an α-oxamide forms oxazolidinones **18** and **19** in the presence of a substoichiometric amount of chiral zinc•**20** complex (Scheme 6).[28] Though **19** is essentially racemic, **18** is formed in high enantiomeric excess. This reaction operates using principles similar to those used by Bach and Yoon above. Zinc•**20** coordinates to **17** allowing it to more efficiently directly absorb light and intersystem cross to its $T_1$ state. From there the reaction proceeds with the Lewis acid still bound and influencing the stereochemical outcome.

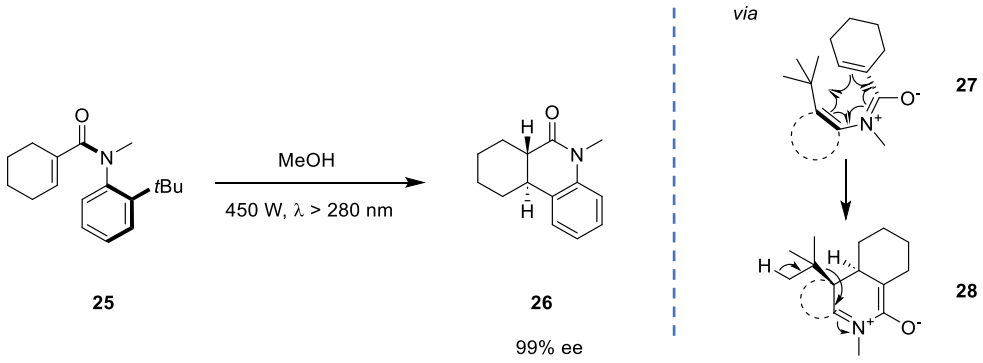
### I.1.3 Asymmetric 6π Photocyclization of Acrylanilides

In addition to the Schultz type enone chromophore, acrylanilides have also found common usage as amenable starting materials for 6π photocyclizations due to their favourable conformational profile.[29, 30] A number of attempts have been made to make this photocyclization enantioselective.



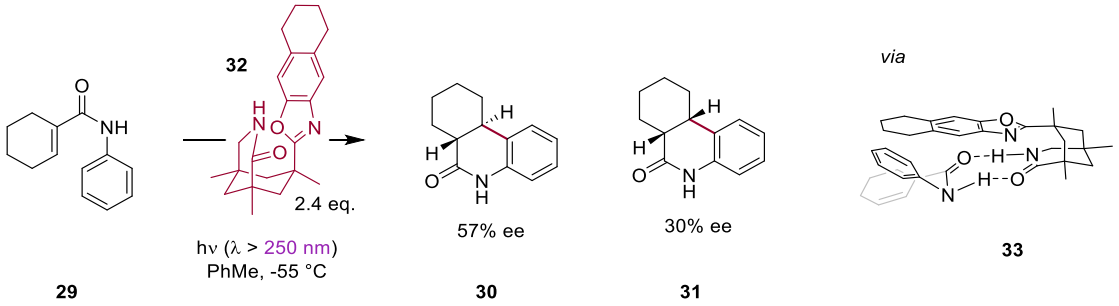

Scheme 7 An early example of an enantioselective 6π acrylanilide photocyclization by Ninomiya. Rationalisation of the stereochemical outcome is provided by the formation of intermediate chiral enolate complex **24**.

One of the earliest examples of an asymmetric 6π photocyclization of an acrylanilide is that reported by Ninomiya in 1984 (Scheme 7).[31] In their report, direct irradiation of a solution of **21** in the presence of di-*p*-toluoyl-D-tartaric acid leads to formation of enantioenriched **22** and **23**. Rationalisation of this comes from the postulation that the diacid can interact with reversibly formed excited state intermediate **24**, thereby controlling the absolute stereochemistry.




Scheme 8 Enantiospecific 6π cyclization *via* axial to point chirality transfer reported by Sivaguru. Selectivity arises from the preference for compound **25** to exclusively form helix **27** due to bulk about its chiral axis.

Another enantioselective 6π photocyclization, reported by Sivaguru and co-workers, makes use of enantiopure, axially chiral acrylanilide **25** (Scheme 8).[32, 33] In this reaction the axial chirality of **25** means that, in the reactive conformation, it sits as a helix and upon excitation to the triplet state (**27**), cyclization can only occur onto one face of the aryl ring. Subsequent loss of isobutene from **28** furnishes an enolate which is reprotonated with high diastereoselectivity to furnish **26** in nearly 100% ee.




Scheme 9 Bach's enantioselective 6π acrylanilide photocyclization exploits a chiral host photosensitizer (**33**). Promotion of **29** to the triplet state only when bound to **33** constrains its conformation, thereby forming **30** and **31** stereoselectively.

A different approach to this cyclization was developed by Bach wherein acrylanilide **29** could be cyclised to form **30** and **31** in moderate enantiomeric excess (Scheme 9).[34] In this reaction stereoselectivity is established using chiral lactam-based host **32**, which hydrogen bonds to acrylanilide **29**, restricting its conformation. Direct irradiation of the guest-host complex then promotes **33** to the $T_1$ state still in this constrained geometry, from which it cyclises stereoselectively.

### I.1.4 Iridium Photosensitizers

Ligated iridium complexes have many exceptional photophysical properties which have led to their widespread study and adoption across many fields ranging from materials science to biology.[35] With the development of photoredox catalysis and sensitized energy transfer, iridium complexes have found even more use as catalysts of choice.[36]

One major use of iridium complexes is in the field of organic light emitting diodes (OLEDs).[37] Research by materials scientists in this area has been ongoing since their development began in 1987 due to their much-increased efficiency when compared to traditional lighting.[38]

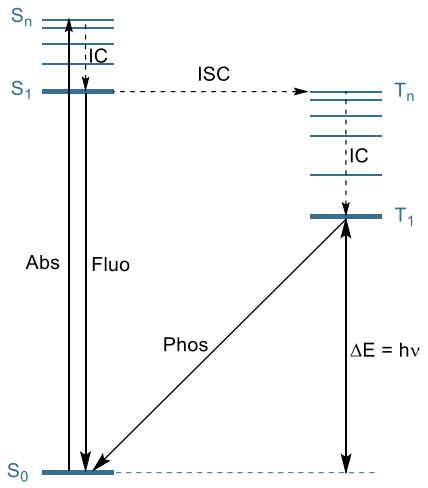



Figure 7 The wavelength of phosphorescence of iridium complexes is dependent on the $S_0$ - $T_1$ energy gap.

The way in which a specific class of iridium based OLEDS known as PHOLEDs produce light is by phosphorescence.[39] This involves the promotion of a complex to its lowest triplet state ($T_1$) by direct excitation to a singlet state, followed by internal conversion, intersystem crossing, and relaxation *via* internal conversion (Figure 7). Modern PHOLEDS undergo this process incredibly efficiently, with some reaching 100% internal quantum efficiency.[40-43] From this state the OLED produces light of the desired wavelength by phosphorescence (emitting a

photon to return to the ground state, $S_0$). In order to produce OLEDs which emit varied wavelengths of light, a vast number of cyclometallated iridium complexes have been developed and their characteristics studied.

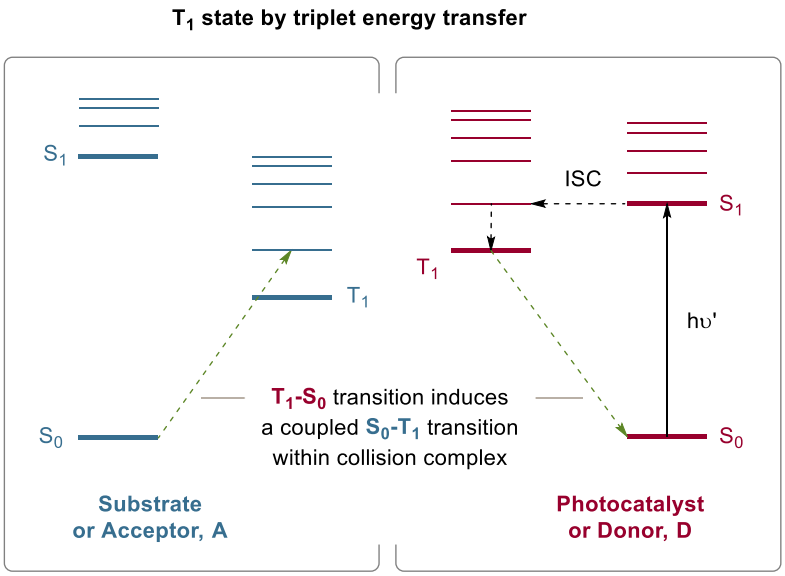


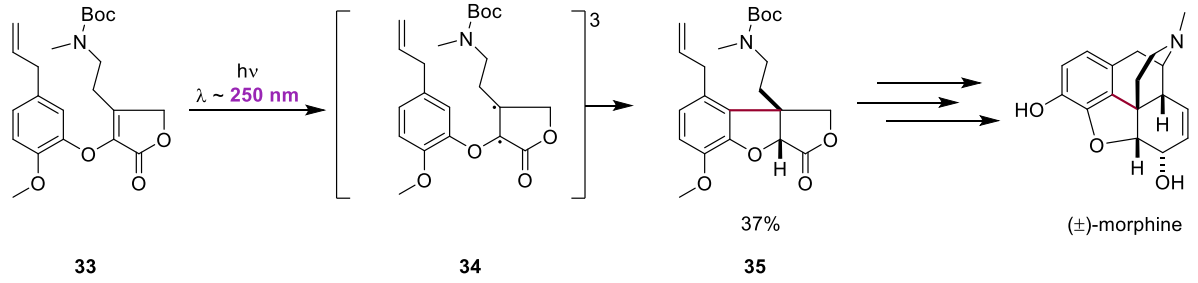

Figure 8 Instead of phosphorescing, complexes (D) may undergo energy transfer to a suitable acceptor (A). This is dependent on favourable interaction between the HSOMO and LSOMO of the triplet state complex and the HOMO and LUMO of the ground state acceptor.

Analogous to the phosphorescence of PHOLEDs is the process of energy transfer. In this regime, instead of phosphorescing to return to the ground state, the iridium complex transfers its energy to an acceptor *via* a non-radiative process (Figure 8). As this process requires good frontier molecular orbital interaction, it is very sensitive to the electronics of the two systems.

Because of the wide range of PHOLEDs already synthesised and characterised, and the ease with which modern computational chemistry can compute triplet energies for organic substrates, iridium-based photosensitizers present an attractive and convenient choice for use in energy transfer catalysis.[36, 44, 45]

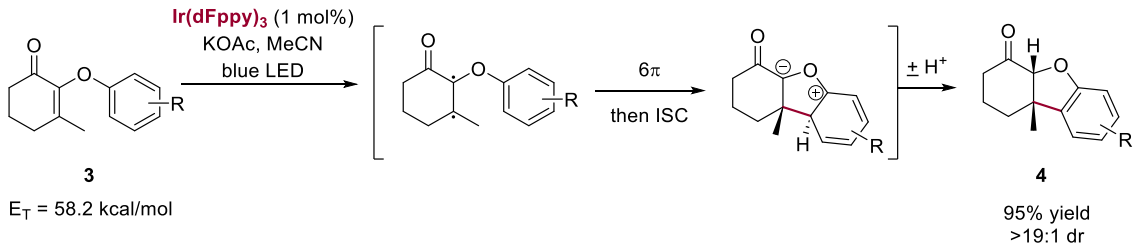
### I.1.5 Previous work in the Smith Group

The Smith group's work in photochemistry has primarily focussed on the use of 6π photocyclizations to enable the synthesis of complex multicyclic frameworks.




Scheme 10 Smith *et al*'s total synthesis of morphine included a key 6π photocyclization of **33** to form **35** *via* triplet diradical **34**.

The first photocatalytic 6π photocyclization developed in the group was in the total synthesis of morphine reported in 2016 (Scheme 10).[46] This strategy enabled complexity to be rapidly built around a tricyclic core and is a key feature of the synthesis. The use of a direct excitation strategy in the cyclization, however, leads to a poor yield due to large amounts of decomposition upon irradiation.




Scheme 11 Smith's methodology was subsequently extended to make use of visible light and a photosensitizer to facilitate the same reaction.

A refinement of this methodology was subsequently developed wherein the 6π photocyclization can be carried out using energy transfer catalysis (Scheme 11).[12] This development removes the need to use hazardous high energy UV light and allows a wide range of substrates to undergo cyclization due to the mild nature of the reaction conditions employed.

### I.1.6 This Project

This project was initiated by Dr Benjamin Jones and initial exploratory studies were carried out in collaboration with Dr Mihai V. Popescu and Dr Ji Yuan Du [†].[1] The aim of the study was to determine whether a highly enantioselective 6π photocyclization could be carried out under energy transfer conditions using chiral Lewis acid catalysis. As discussed, this had been reported for photochemical [2 + 2] cycloadditions, but there were no reports of highly selective 6π variations.

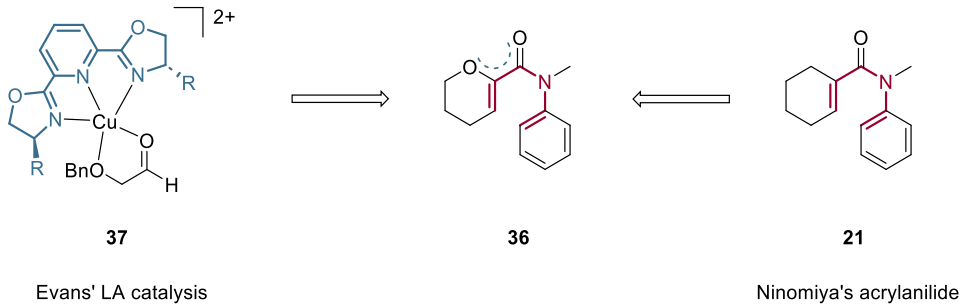
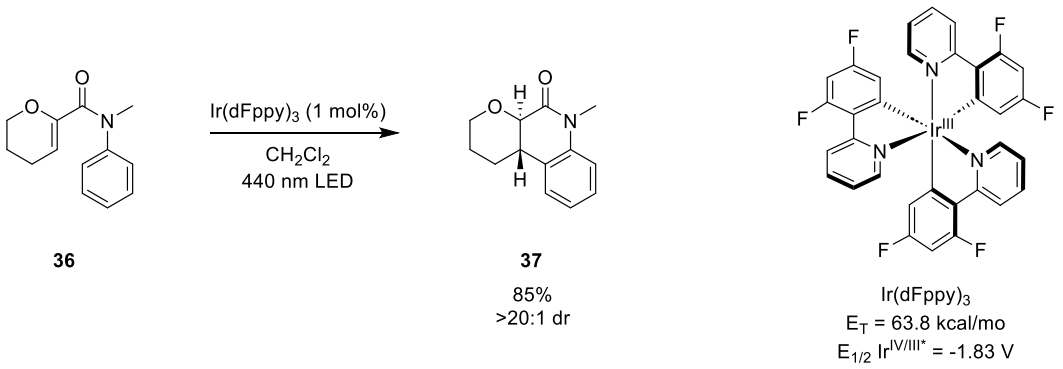



Figure 9 The model substrate devised by Dr Ben Jones is a combination of Ninomiya's acrylanilide core and a Lewis acid binding motif previously exploited by Evans.

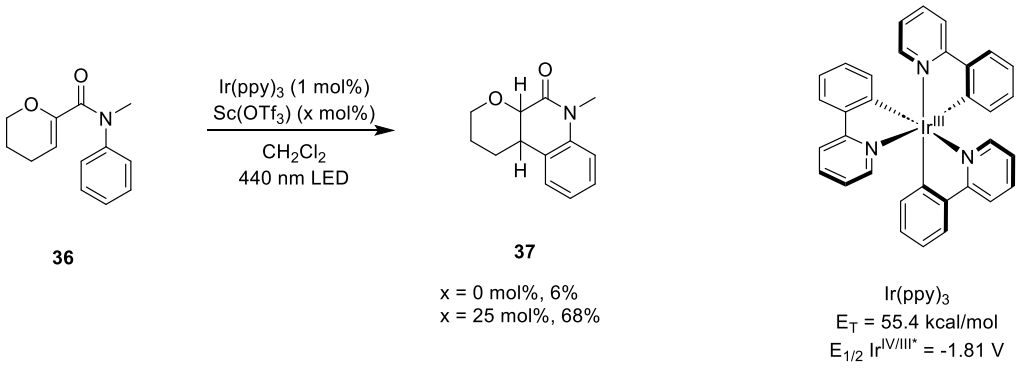
Design of the model substrate (**36**) was influenced by a combination of previously reported 6π photocyclizations and classical Lewis acid catalysis (Figure 9). Acrylanilide **21**, reported by Ninomiya, was chosen as the framework for the substrate due to acrylanilides' favourable conformational preferences.[30] A slight modification of this framework allowed the incorporation of an α-ketoether binding motif previously used by Evans in highly enantioselective aldol reactions.[47]

[†] To ensure clarity in relative contributions, all compounds/data generated by Drs Jones and Popescu will be denoted BJXX and MVPXX, respectively.



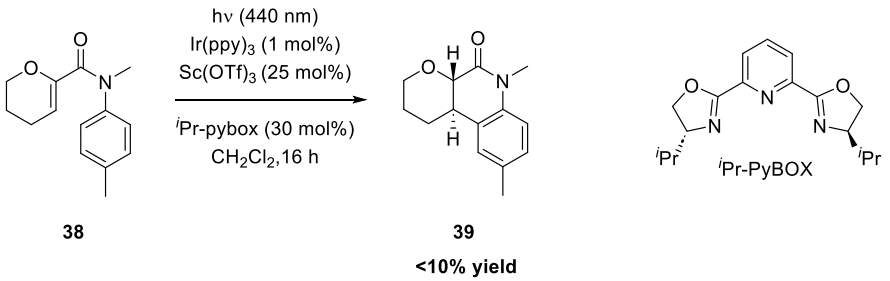

Scheme 12 Photocyclization of **36** using $Ir(dFppy)_3$ furnished **37** as a single diastereomer in high yield. Dr was determined using quantitate NMR analysis of the crude reaction mixture.

Initial development of the reaction showed that cyclization of **36** to the corresponding dihydroquinolone, **37**, proceeded rapidly under energy transfer conditions using $Ir(dFppy)_3$ in the absence of a Lewis acid (Scheme 12).




Scheme 13 The use of $Sc^{3+}$ as a Lewis acid additive in combination with $Ir(ppy)_3$, facilitated selective "switching on" of reactivity. Yield refers to NMR yield using 1 eq. dibromomethane as an internal standard.

Further screening identified that $Ir(ppy)_3$, a catalyst with both a lower triplet energy and less reducing power could provide **37** in just 6% yield when used alone, but that the addition of 25 mol% of scandium(III) triflate increased the yield of **37** to 68% (Scheme 13). This indicated that reactivity of **36** could be effectively modulated by the presence or absence of Lewis acid.

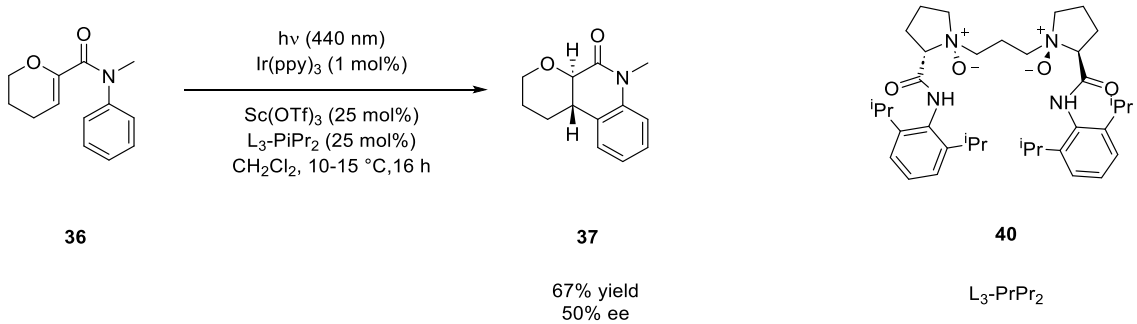



**38** **39**

**<10% yield**

Scheme 14 Tests using PyBOX ligands were unsuccessful, leading primarily to recovery of **38**. Yield refers to NMR yield using 1 eq. dibromomethane as an internal standard.

Having observed this promising chromophore activation effect, the next step was to attempt the cyclization with the addition of a chiral ligand. Unfortunately, attempts to use PyBOX and BOX ligands resulted in much lower yields of **39** (Scheme 14). This was reasoned to be due to the highly reducing nature of the excited state photocatalysts being used.




**36** **37** **40**

67% yield
50% ee

$L_3$-Pr$Pr_2$

Scheme 15 Lead conditions using Feng ligand **40** were found to furnish **37** in moderate yield and ee. Yield refers to isolated yield; ee was determined by normal phase HPLC using a chiral stationary phase.

A review of enantioselective Lewis acid catalysed reactions led to the testing of commercial Feng ligand **40**. Pleasingly, this was found to restore reactivity and furnish **37** in 50% ee (Scheme 15).

It was at this point in the evolution of the project that the author joined Drs Jones, Popescu, and Du in working on this project.

This work is now part of a publication.[1]

# I.2 Results and Discussion

## I.2.1 Aim

The aim of this project was to optimise the enantioselective 6π photocyclization described and to elucidate the catalytic manifold by which the reaction occurs.

## I.2.2 Reaction Optimisation

In the reaction we are considering there are two catalysts, a Lewis acid/chiral ligand catalyst and a photocatalyst. The absolute stereochemistry of the products is determined by the chiral Lewis acid complex. In combination with the photocatalyst, the Lewis acid plays a second role enabling reactivity only in its presence. As we had already found a suitable Lewis acid/ligand combination (scandium triflate and **40**), optimisation of the photocatalyst was the next step.

### I.2.2.1 The Photocatalyst

Though the photocatalyst in our system is racemic, as our aim is for energy transfer to occur exclusively to the bound substrate (**42**), tuning of the photocatalyst's photophysical properties to facilitate this process was vital (Figure 10).

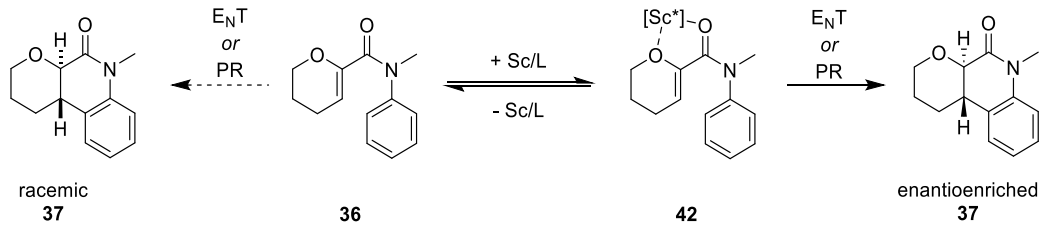
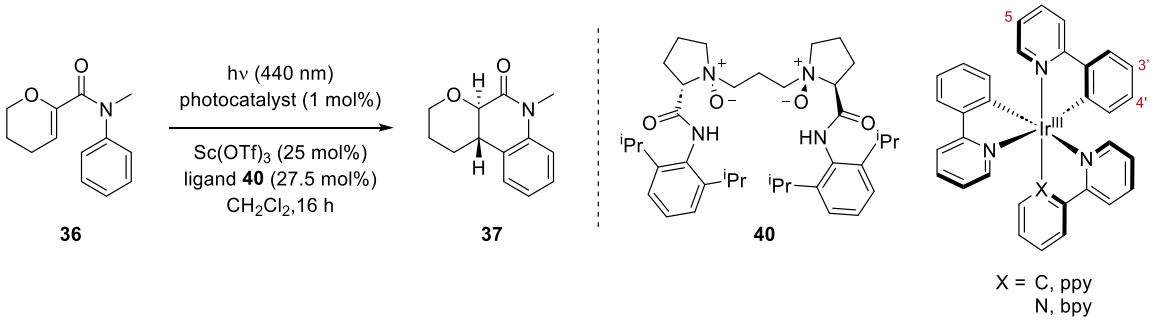



Figure 10 Selective energy transfer to **42** in the presence of **36** was hypothesised to give enantioenriched **37**.

A screen of commercially available and previously reported catalysts was carried out to determine whether any reactivity or selectivity trends could be identified in the Lewis acid catalysed photocyclization of **36** (Figure 10).[1]

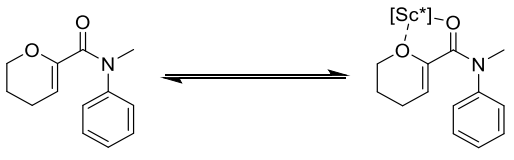
Table 1 Known photocatalyst screen.




| Entry | Photocatalyst | $E_T$ ($I_{10\%}$) (kcal·mol$^{-1}$) | $E_{½}^{red}$ $Ir^{IV/*III}$ (V) | Lewis acid /ligand | Yield (%) | er | dr |
|---|---|---|---|---|---|---|---|
| **1** | Ir(4',6'-Fppy)$_3$ | 63.8 | -1.83 | Sc(OTf)$_3$/**40** | 95 | 53:47 | >20:1 |
| **2** | Ir(4'-Fppy)$_3$ | 62.3 | -1.74 | Sc(OTf)$_3$/**40** | 67 | 54:46 | 1:1 |
| **3** | Ir(ppy)$_3$ | 59.4 | -1.81 | Sc(OTf)$_3$/**40** | 67 | 75:25 | >20:1 |
| **4** | Ir((3'-OMe)ppy)$_3$ | 55.3 | -1.89 | Sc(OTf)$_3$/**40** | 26 | 79:21 | >20:1 |
| **5** | Ir(ppy)$_2$(dtbbpy)(PF$_6$) | 56.4 | -1.19 | Sc(OTf)$_3$/**40** | <5 | 68:32 | - |
| **6** | Ir(Fppy)$_2$(dtbbpy)(PF$_6$) | 61.0 | -1.19 | Sc(OTf)$_3$/**40** | 20 | 62:38 | >20:1 |
| **7** | Ir(dFppy)$_2$(dtbbpy)(PF$_6$) | 63.3 | -1.15 | Sc(OTf)$_3$/**40** | 70 | 58:42 | 14:1 |
| **8** | Ir(dF(CF$_3$)ppy)$_2$(dtbbpy)(PF$_6$) | 63.3 | -1.01 | Sc(OTf)$_3$/**40** | 97 | 52:48 | 18:1 |

$E_T$ ($I_{10\%}$) is the triplet energy at 10% max emission. $E_{½}^{red}$ $Ir^{IV/*III}$ is the excited state reduction potential of the listed photocatalyst as calculated according to Experimental p.S-44. Yield refers to NMR yield using 1 eq. dibromomethane as an internal standard. Enantiomeric ratio was determined by normal phase HPLC analysis using a chiral stationary phase. Diastereomeric ratio was determined by quantitate NMR analysis of the crude reaction mixture.

It was found that cationic photocatalysts (Table 1, entries 5 – 8) performed less well than neutral homoleptic complexes (Table 1, entries 1-4), while, among the neutral homoleptic complexes, enantioselectivity appears to increase with deceasing photocatalyst triplet energy and with increasing strength as an excited state reductant. Though not displayed here, a number of ruthenium based photocatalysts and organic photocatalysts were also tested, but none yielded **37** (see Experimental p.S-1).



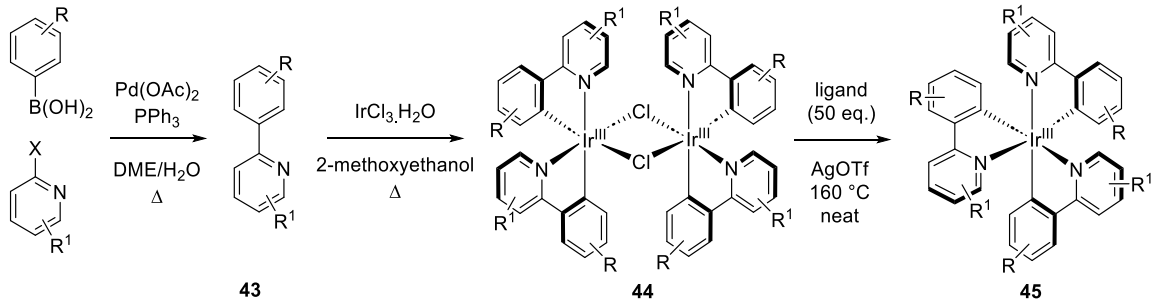

**36**
$E_T$ = 57.7 kcal mol$^{-1}$
$E_{1/2}$ (red) = -2.4 V

**42**
$E_T$ = 52.9 kcal mol$^{-1}$
$E_{1/2}$ (red) = -1.3 V

Figure 11 A change in reduction potential is observed upon complexation of **36** to form **42**. The predicted triplet energy of **42** is also lower than that of **36**.

To aid the design of new photocatalysts, the influence of Sc/**40** binding to **36** was probed. Triplet energy calculations (carried out by Dr Mihai V. Popescu) indicated a reduction in triplet energy on coordination. In addition to this, a shift in reduction potential was observed upon coordination to scandium (Figure 11).

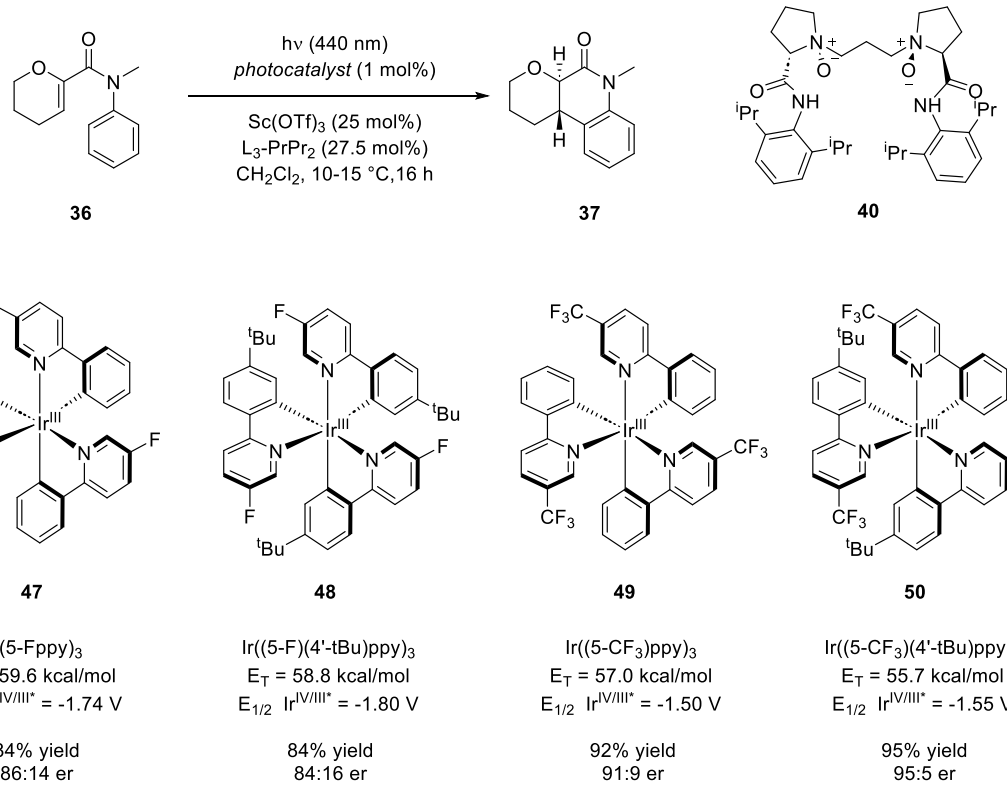
These results suggest that selective energy *or* electron transfer are viable strategies for enantioinduction. Thus, we approached further optimisation empirically, synthesising a range of photocatalysts based on the homoleptic iridium/phenylpyridine framework which earlier provided modest selectivity.




Scheme 16 General scheme for the synthesis of homoleptic iridium photocatalysts. Suzuki coupling of an aryl boronic acid with a pyridyl bromide furnishes phenylpyridines **43**, which when heated with iridium chloride in 2-methoxyethanol produces dimers **44**. Heating dimers **44** in the presence of silver triflate and an appropriate ligand furnishes catalysts **45.**

The desired iridium photosensitizers (**45**) were accessed *via* the corresponding dimers (**44**) which were prepared from **43** according to literature methods.[36] Formation of the sensitizers themselves was promoted by heating the dimers in the presence of silver triflate and a vast excess of the corresponding phenylpyridine ligand (Scheme 16).

A number of novel photocatalysts with varied substitution (**47** – **50**) were synthesised in this way. It was envisioned that the groups incorporated would alter the electronics of the system, lowering or raising the frontier molecular orbital energies and thereby altering their photophysical properties and excited-state reactivity.




Scheme 17 Cyclization with novel photocatalysts **47** – **50** led to higher yields and enantioselectivities.

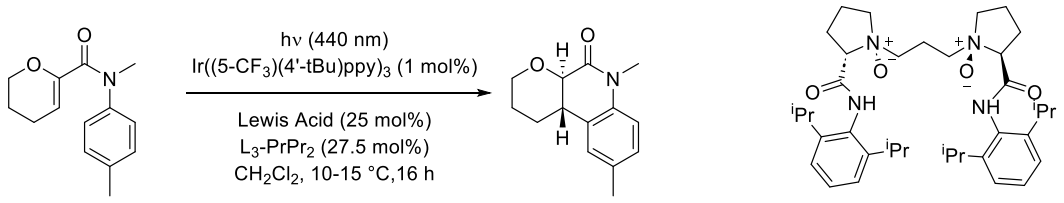
$E_T$ is the triplet energy at 10% max emission. $E_{½}$ $Ir^{IV/*III}$ is the excited state reduction potential of the listed photocatalyst as calculated according to Experimental p.S-44. Yield refers to NMR yield using 1 eq. dibromomethane as an internal standard. Enantiomeric ratio was determined by normal phase HPLC analysis using a chiral stationary phase.

Pleasingly, cyclization with the synthesised photocatalysts (**47** – **50**) led to increased yield and enantioselectivity (Scheme 17). The addition of an electron withdrawing group (-F, -$CF_3$) at the pyridine 4 position and an electron donating group (*t*-Bu) at the phenyl 4' position furnished much improved results. Photocatalyst **50** provided optimal results, producing **37** in 95% isolated yield and 95:5 er.

### I.2.2.2 Lewis Acid Sources, Additives, and Preformation

It was recognised that the Lewis acid source may affect reactivity for several reasons, including solubility, degree of coordination, and coordinating ability.[27] For this reason we sought to explore the use of different scandium sources to test if the reaction could be improved further. In the same vein, additives were screened to determine if an increase in reactivity or selectivity could be achieved.

Table 2 Lewis acid source and additive screen.




38 39 40

| Entry | Scandium source | Additive | Yield (%) | er | dr |
|---|---|---|---|---|---|
| **1** | $ScCl_3.6H_2O$ | - | - | - | - |
| **2** | $ScCl_3.THF_3$ | - | 6 | 51:49 | ND |
| **3** | $Sc(NTf_2)_3$ | - | - | - | - |
| **4** | $Sc(OTf)_3$ | $LiClO_4$ (1 eq.) | 68 | 71:29 | 17:1 |
| **5** | $Sc(OTf)_3$ | LiOTf (1 eq.) | 27 | 81:19 | >20:1 |
| **6** | $Sc(OTf)_3$ | LiI (1.0 eq.) | - | - | - |
| **7** | $Sc(OTf)_3$ | $KClO_4$ (1.0 eq.) | 10 | 57:43 | 14:1 |
| **8** | $Sc(OTf)_3$ | 4Å MS | 30 | 93:7 | >20:1 |
| **9** | $Sc(OTf)_3$ | $H_2O$ (5.0 eq.) | 78 | 94:6 | >20:1 |

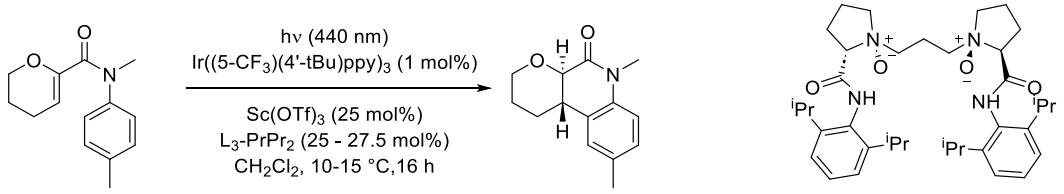
Yield refers to NMR yield using 1 eq. dibromomethane as an internal standard. Enantiomeric ratio was determined by normal phase HPLC analysis using a chiral stationary phase. Diastereomeric ratio was determined by quantitate NMR analysis of the crude reaction mixture.

Unfortunately, the use of scandium sources other than scandium triflate gave little or no conversion (Table 2, entries 1 -3) and the inclusion of additives decreased the yield of the product, with most also negatively impacting the enantiomeric excess (Table 2, entries 4 – 9).

We reasoned that perhaps one of the reasons for sub-optimal selectivity may be the low solubility of Lewis acids in dichloromethane and the presence of small amounts of unligated (i.e. without chiral ligand) scandium, which could promote a racemic background reaction.

We sought to investigate a number of preforming methodologies to ensure the maximum amount of scandium/**40** complex was in solution while minimising the amount of unligated scandium that was present.

Table 3 Preformation screen.




**38** **39** **40**

| Entry | $CH_2Cl_2$ source | Preformation method | Lewis acid solution | Sc:L | Yield (%) | er | dr |
|---|---|---|---|---|---|---|---|
| **1** | SPS | Sonication | Unfiltered | 1:1.1 | 83 | 94.5:5.5 | >20:1 |
| **2** | SPS | Heat (60 °C) | Unfiltered | 1:1.1 | 74 | 94.5:5.5 | >20:1 |
| **3** | SPS | Sonication | Filtered | 1:1.1 | 85 | 93:7 | >20:1 |
| **4** | Winchester | Heat (60 °C) | Filtered | 1:1.1 | 90 | 94:6 | >20:1 |
| **5** | Winchester | Sonication + Heat | Filtered | 1:1.1 | 87 | 95:5 | >20:1 |
| **6** | Winchester | Sonication + Heat | Filtered, then $H_2O$ (5 eq.) | 1:1.1 | 94 | 93:7 | >20:1 |
| **7** | Winchester | Sonication + Heat | Filtered | 1:1 | 95 | 95:5 | >20:1 |
| **8** | SPS | Sonication + Heat | Filtered | 1:1 | 95 | 95:5 | >20:1 |

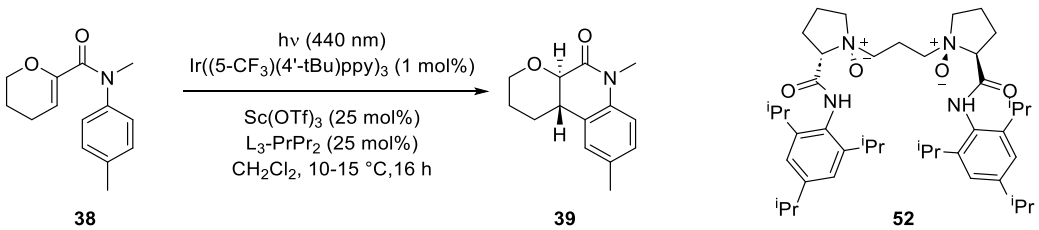
SPS indicates dichloromethane dried by passage through an activated alumina column. Filtered indicates that preformed Lewis acid solution was passed through a 0.2 µm PTFE syringe filter prior to reaction. See Experimental p.S-6 for a representative procedure. Yield refers to NMR yield using 1 eq. dibromomethane as an internal standard. Enantiomeric ratio was determined by normal phase HPLC analysis using a chiral stationary phase. Diastereomeric ratio was determined by quantitate NMR analysis of the crude reaction mixture.

The results of this investigation showed that the use of commercial solvents, which contain a small amount of water, resulted in increased yield (Table 3, entries 1-3 vs entries 4-8); however, deliberate spiking of the reaction medium with excess water (5.0 eq.) negatively impacted enantioselectivity (entry 6). Preforming the scandium-ligand catalyst in dichloromethane solution by sonication in a warm water bath prior to its addition to **38** and **40** provided an increase in yield and a marginal improvement in enantioselectivity (Table 3,

entries 5). Finally, using equimolar amounts of scandium and ligand furnished optimal results (95% yield, 95:5 er, >20:1 dr; Table 3, entry 7).

As a final check, a number of alternative reaction conditions were tested to ensure that all opportunities for improvement were explored.

Table 4 Alternative reaction condition screen.




38 39 52

| Entry | Deviation | Yield (%) | er | dr |
|---|---|---|---|---|
| **0** | None | 95 | 95:5 | >20:1 |
| **1** | Preform with 0.3 eq. $K[BAr^F]_4$ | 55 | 92:8 | >20:1 |
| **2** | Preform with **52** | 47 | 91:9 | >20:1 |
| **3** | 0 °C | 69 | 95:5 | >20:1 |
| **4** | 10 °C | 97 | 94:6 | >20:1 |
| **5** | 427 nm lamp | 92 | 94:6 | >20:1 |
| **6** | Preform and evaporate to solid | 28 | 50:50 | 10:1 |
| **7** | Unsparged dichloromethane | 80 | 94:6 | >20:1 |
| **8** | 20 mol% Sc/L | 37 | 92:8 | >20:1 |
| **9** | 15 mol% Sc/L | 31 | 92:8 | >20:1 |
| **10** | 10 mol% Sc/L | 26 | 92:8 | >20:1 |
| **11** | 5 mol% Sc/L | 12 | 78:22 | >20:1 |

Yield refers to NMR yield using 1 eq. dibromomethane as an internal standard. Enantiomeric ratio was determined by normal phase HPLC analysis using a chiral stationary phase. Diastereomeric ratio was determined by quantitate NMR analysis of the crude reaction mixture.

Addition of $KB(Ar_F)_4$ during the catalyst preformation step, envisaged to increase the Lewis acidity of the resulting complex by reducing anion coordination, led to no improvement in enantioselectivity and a decrease in yield (Table 4, entry 1). The use of related Feng ligand **52**, containing an additional *iso*-propyl group at the aryl *para*- position, also resulted in a decrease in both yield and enantioselectivity (Table 4, entry 2). Decreasing the temperature of the reaction impacted yield negatively (Table 4, entries 3,4), with the use of a shorter wavelength light source (427 nm) giving the same result (Table 4, entry 5). Preformation of scandium/ligand complex followed by its evaporation to dryness and subsequent addition to

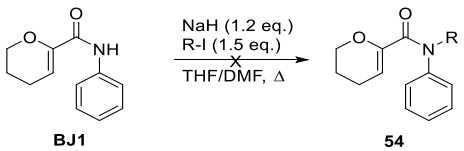
the reaction mixture as a solid resulted in both a highly unselective and low yielding reaction (Table 1, entry 6). Omitting degassing of the reaction solvent resulted only in a decrease in yield (Table 4, entry 7). Finally, lowering the loading of scandium/ligand complex dramatically decreased yield (Table 4, entries 8-11), but enantioselectivity suffered significantly only at the lowest loading tested (Table 4, entry 11).

While many alterations to the reaction conditions were well tolerated, none improved upon the conditions identified previously. Thus, it was decided to use these conditions to test the substrate scope of the developed reaction.

### I.2.3 Reaction Scope

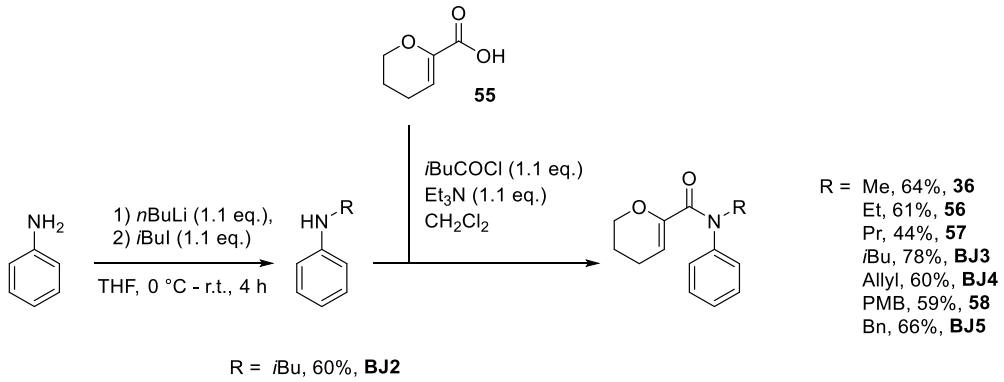
#### I.2.3.1 *N*-Alkylation

With the reaction optimised and the core of the substrate established, our attention turned initially to the tolerance of the reaction to *N*-substitution.




Scheme 18 Attempted alkylation of **BJ1** using sodium hydride and alkyl iodides was unsuccessful.

Though early attempts to cyclise the free *N*-H substrate (**BJ1**) failed, it was thought that it could provide direct access to the desired *N* alkyl structures (**54**) (Scheme 18). Despite the use of forcing conditions, this alkylation was uncooperative.




Scheme 19 The final route to *N*-alkylated substrates was by initial alkylation to afford secondary anilines, which were then coupled with **55** to afford the desired acrylanilides.

Thankfully, many *N*-alkylated anilines were found to be commercially available and could be subjected directly to amide coupling with **55** (Scheme 19). In the case of *N-iso*butyl aniline, which was not commercially available, access was by direct alkylation of aniline.

Having synthesised the desired *N*-alkylated substrates in acceptable yields, they were subjected to cyclization under the previously optimised conditions.

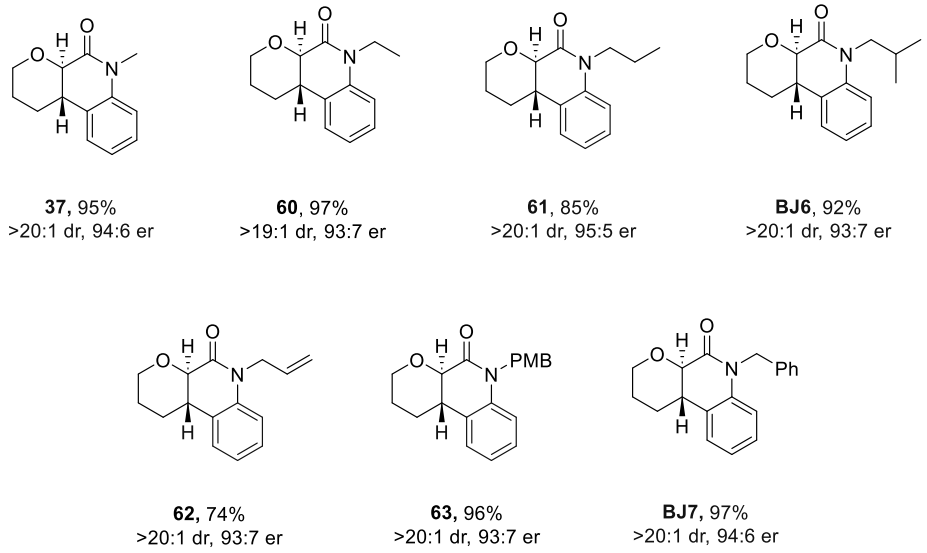


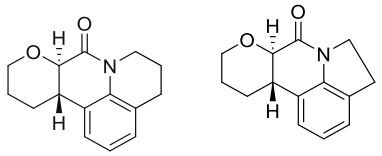

Figure 12 Photocyclization of *N*-alkylated substrates was generally successful, with a wide range of alkyl groups tolerated. Quoted yields are isolated; diastereomeric ratio was determined by NMR analysis of the crude reaction mixture; enantiomeric ratios were determined by normal phase HPLC using a chiral stationary phase.

In general *N*-alkylation was well tolerated even for branched alkyl groups and easily cleaved groups such as *p*-methoxybenzyl (**63**) and benzyl (**BJ7**) groups (Figure 12). Yields ranged from good to excellent and just one diastereomer was observed in all cases. Enantioselectivities were similarly excellent, the lowest being 93:7 er.

Attempts to carry out the reaction with branched *N*-alkyl groups (2-propyl, etc) were unsuccessful and led exclusively to recovery of starting material. This can be rationalised as arising from unfavourable strain disfavouring the reactive conformation (a similar effect is seen with *o*-substitution, over).

### I.2.3.1 *o*-Substitution

Access to substrates with *ortho*-substituted phenyl groups could be achieved *via* the same route as before. Cyclization was unfortunately unsuccessful in all cases where the *ortho* group was not tethered to the amide *N*.

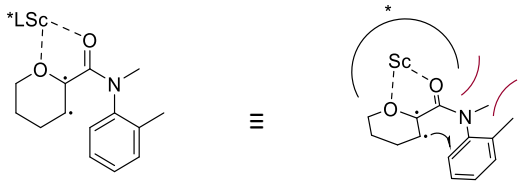


**BJ8**, 52%
>20:1 dr, 82:18 er

**64**, 65%
>20:1 dr, 78:22 er

Figure 13 Successfully cyclised *ortho*-substituted examples tethered the ortho alkyl group to the amide *N*-.

Two key examples of this are terahydroquinoline and indoline derived compounds **BJ8** and **64**. Conversion and yield for both of these examples are substantially lower than those recorded for other substitution patterns, and though diastereoselectivity is still high, enantioselectivity is also unfortunately lower (Figure 13).




**65**

Figure 14 Allylic strain in *ortho*-substituted substrates was hypothesised to prevent the cyclisation from proceeding.

Though disappointing, these observations can be rationalised in light of transition state strain induced by *ortho* substitution (**65**, Figure 14).

### I.2.3.2 *p*-Substitution

*Para*-substituted substrates were again accessed by direct amide coupling of the corresponding *N*-methyl anilines with carboxylic acid **55**. Where the desired *N*-methyl anilines were not commercially available they were synthesised by methylation of the corresponding $NH_2$ anilines.

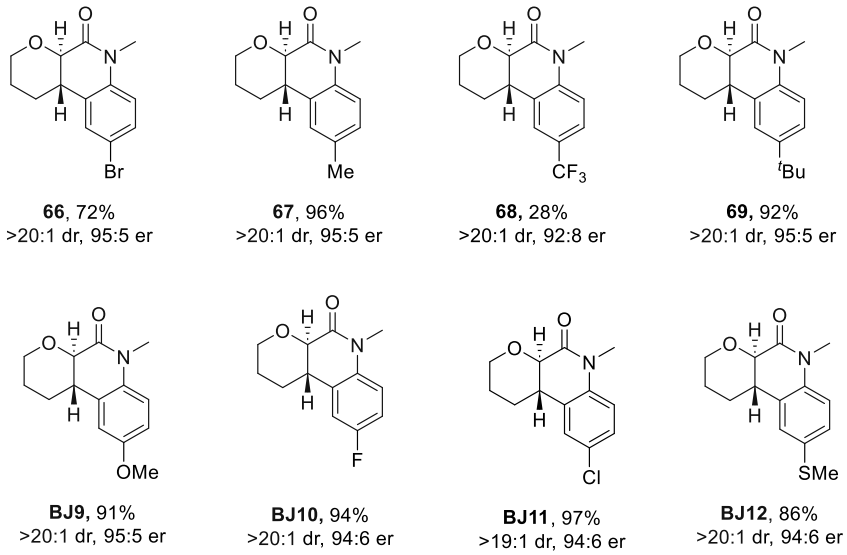



Figure 15 Successful *para*-substituted examples included a wide range of electron withdrawing and donating groups spanning a range of steric demands. Quoted yields are isolated; diastereomeric ratio was determined by NMR analysis of the crude reaction mixture; enantiomeric ratios were determined by normal phase HPLC using a chiral stationary phase.

Cyclization of *para*-substituted substrates proved to be exceedingly successful (Figure 15). Halogens, electron donating groups and even bulky alkyl groups were well tolerated and

furnished cyclised products in excellent yields and with uniformly high enantioselectivities. A notable exception is the *para*-trifluoromethyl example (**68**) where yields were low, but unreacted starting material is recovered, indicating that extended reaction times could lead to an increase in yield.

### I.2.3.3 *m*-Substitution

Once again *meta*-substituted substrates were synthesised by direct amide coupling of the appropriate *N*-methylated, *meta* substituted anilines with **55**.

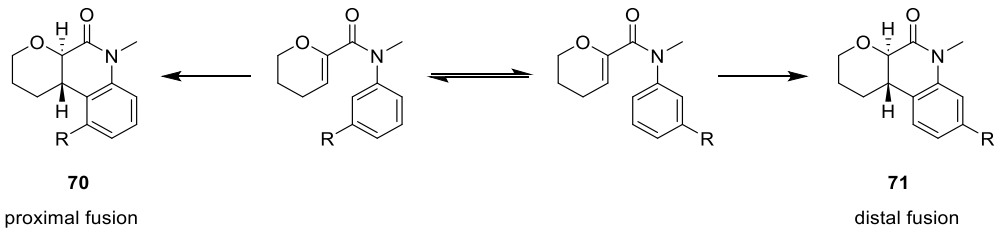



Figure 16 In the case of *meta*-substituted substrates, cyclization may be either proximal or distal to the substituent.

In the case of the cyclization of *meta*-substituted substrates, an added complication comes from the generation of distinct regioisomers arising from cyclization to the aryl *ortho* position either proximal (**70**) or distal (**71**) to the substituent (Figure 16).

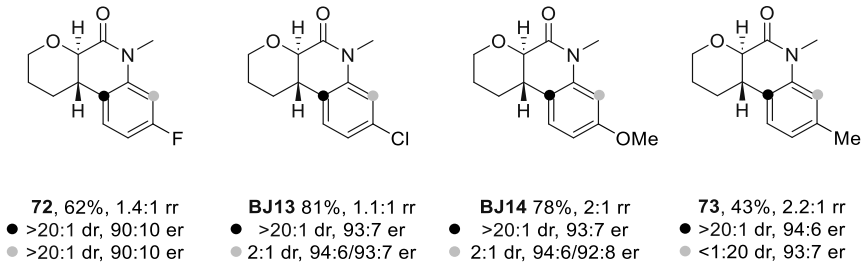
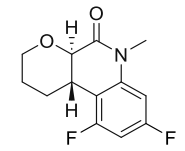



Figure 17 Successful *meta*-substituted examples are fewer and have a complex distribution of product isomers. Quoted yields are isolated; diastereomeric ratio was determined by NMR analysis of the crude reaction mixture; enantiomeric ratios were determined by normal phase HPLC using a chiral stationary phase.

Regioisomer selectivity in *meta* substituted examples is in general low, the highest being 2.2:1 rr (**73**), and appears to trend with the steric bulk of the *meta*- substituent. This is

unsurprising given the strain that can be anticipated in creating a fused ring proximal to a large substituent. Diastereoselectivity of the distally fused regioisomers is uniformly excellent, though that of the proximally fused regioisomers is notably variable (this is discussed in detail in Section I.2.4.3). Enantioselectivities are all good to excellent, indicating that the stereodetermining step remains robust.

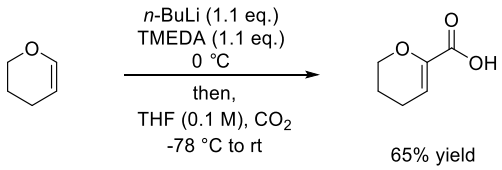


**BJ15,** 57%
4:1 dr, 88:12 er (major)
84:16 (minor)

Figure 18 A single di-*meta*-substituted example was found, though diastereoselectivity was disappointingly low. Quoted yields are isolated; diastereomeric ratio was determined by NMR analysis of the crude reaction mixture; enantiomeric ratios were determined by normal phase HPLC using a chiral stationary phase.

Attempts to eschew regioisomer formation by using a di-*meta* substituted substrate (**BJ15**) proved to be detrimental. *Meta* difluorination saw a significant drop in diastereoselectivity and a small decrease in enantioselectivity. Decreased yields in both mono- and di-*meta* substitution may be attributed to both steric (transition state strain) and electronic (radical accepting ability) effects.

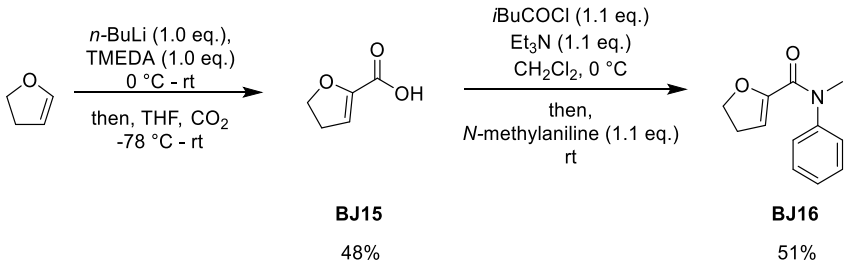
### I.2.3.4 Alteration of the etheric ring




65% yield
**55**

Scheme 20 Synthesis of **55** was achieved by lithiation with *n*-BuLi/TMEDA and trapping of $CO_2$.

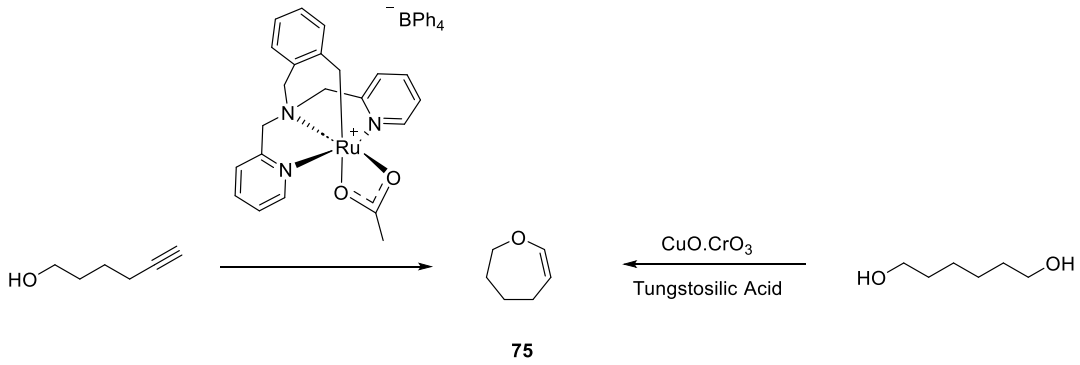
Hitherto the 3,4-dihydropyran moiety has remained unchanged. This is partly due to the ease of access to the carboxylic acid (**55**) by lithiation and trapping with $CO_2$ (Scheme 20).




Scheme 21 Preparation of the 5-membered analogue proceeded by first lithiating 3,4-dihydropyran and trapping $CO_2$ with the resulting anion. Amide coupling of the resulting acid with *N*-methylaniline yielded the desired amide, **BJ16**.

Access to the five membered analogue is similarly straightforward due to the commercial availability of 2,3-dihydrofuran (Scheme 21).

Accessing the 8-membered ring, however, proved to be challenging due to the commercial unavailability of 2,3,4,5-tetrahydrooxepine (**75**). Initial attempts centered around its synthesis from either 1,6-hexanediol or 5-hexyn-1-ol by literature methods (Scheme 22).[48, 49]




Scheme 22 Routes explored to synthesise **75** included by dehydration of the corresponding diol, and ruthenium mediated annulation of the appropriate alkynol.

Unfortunately, neither route furnished **75** in synthetically useful amounts (perhaps due to its volatility) or in high enough purity for further use (Scheme 22).

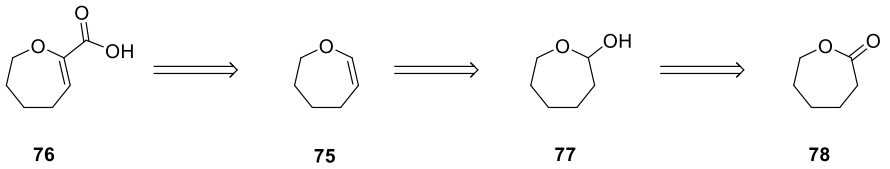
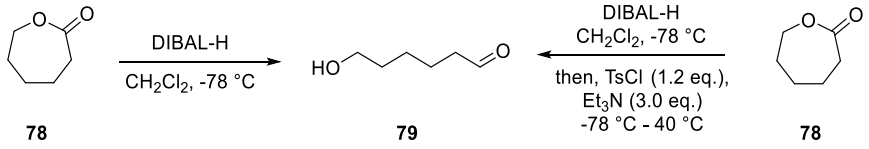



Figure 19 Proposed route to **76** *via* lactol **77**.

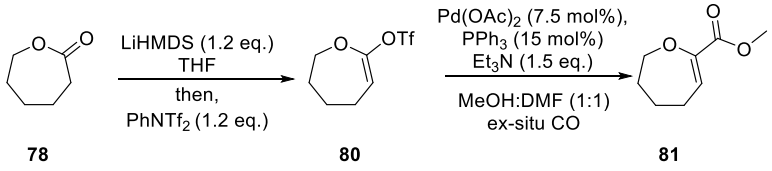
Given the unsuccessful nature of these routes, synthesis from the corresponding lactone (**78**) was explored. Reduction was expected to give lactol **77** which could then be converted to **75** by elimination (Figure 19).




Scheme 23 Attempts to synthesise lactol **77** from lactone **78** were unsuccessful, leading to aldehyde **79**.

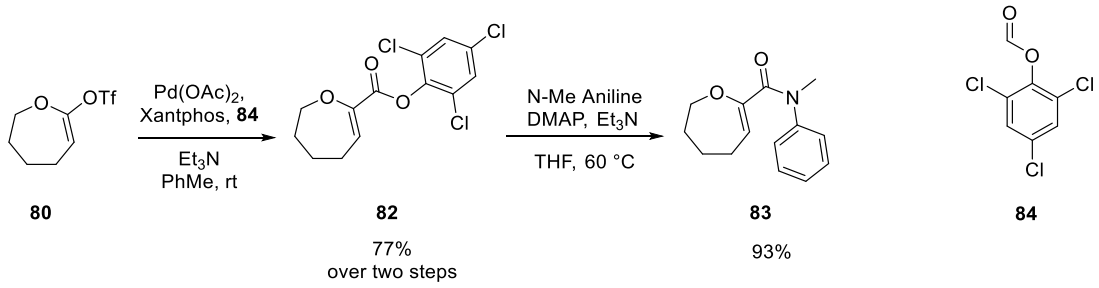
In reality, reduction of lactone **78** with DIBAL-H even at low temperatures resulted in formation of only the corresponding aldehyde, **79** (Scheme 23). Attempts to trap the lactol *in situ* using tosyl chloride also resulted only in isolation of aldehyde **79** (Scheme 23).

With these methods having proven unfruitful, a final route utilising the same lactone (**78**), but proceeding *via* carbonylation of the corresponding enol triflate was devised.[50]




Scheme 24 Carbonylation of **80** with ex-situ generated CO was unsuccessful.

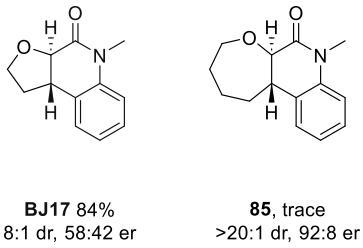
Although triflate **80** was observed to form by NMR, carrying out the carbonylation using ex-situ generated CO did not lead to recovery of **81** (Scheme 24).[51, 52]




Scheme 25 Successful synthesis of **83** was achieved by carbonylation using CO surrogate **84**.

Finally, the use of previously reported CO surrogate 2,4,6-trichlorophenylformate (**84**) in combination with triflate **80** formed ester **82** in moderate yield (Scheme 25).[53] Ester **82** could then be used directly to give the desired amide (**83**) in excellent yield by treatment with *N*-methylaniline and DMAP (Scheme 25).

With both **BJ16** and **83** in hand, their cyclization was investigated.




**BJ17** 84%
8:1 dr, 58:42 er

**85**, trace
>20:1 dr, 92:8 er

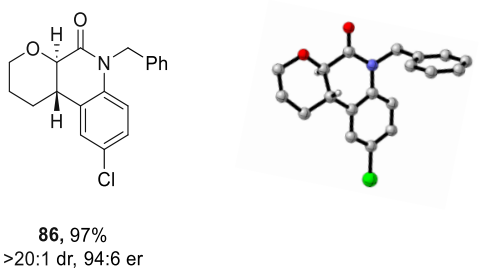
Figure 20 Cyclization of other etheric rings led to either low selectivity or reactivity. Quoted yields are isolated; diastereomeric ratio was determined by NMR analysis of the crude reaction mixture; enantiomeric ratios were determined by normal phase HPLC using a chiral stationary phase.

Interestingly, the five-membered analogue, **BJ16**, yielded **BJ17** in high yield but in very poor diastereo- and enantioselectivity, and the seven-membered analogue, **83**, yielded **85** in only trace amounts, but with very high diastereo- and enantioselectivity.

### I.2.3.5 Absolute Configuration

Though the relative configuration of the point chiral centers formed in the reaction was known to be trans based on NMR data, determination of the absolute configuration was still

necessary. To do this, a substrate with a high chance of providing an appropriate Flack parameter was devised with the help of Dr. Owen Smith.




**86**, 97%
>20:1 dr, 94:6 er

Figure 21 **86** was devised to maximise the chances of producing a crystalline product with a sufficiently heavy atom and high enantiomeric ratio to determine absolute configuration by single crystal x-ray crystallography.

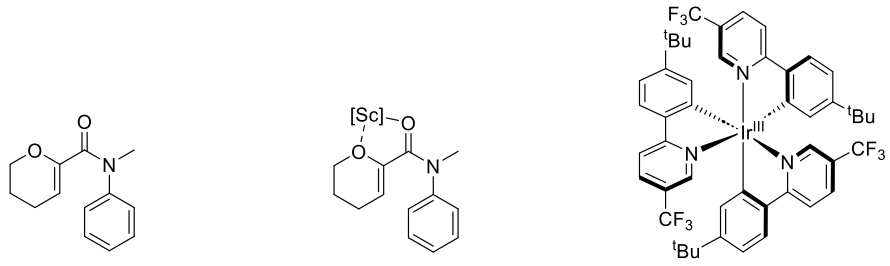
Cyclization of the substrate proceeded in high yield, and diastereo- and enantioselectivity. Crystallisation of the product and measurement of the crystals performed by Dr Smith confirmed the configuration to be that illustrated and to be in agreement with computation carried out by Dr Mihai V. Popescu.

### I.2.4 Mechanistic Studies

Much of the mechanistic insight into the reaction was gained only with the help and guidance of computational work carried out by Dr Mihai V. Popescu.

#### I.2.4.1 Possible Pathways

Heretofore we have not especially considered the mechanism underlying the photocyclization. Two obvious possibilities for the active catalytic mode exist: photoredox catalysis and energy transfer catalysis.




**36**
$E_T$ = 57.7 kcal/mol
$E_{1/2}$ (red) = -2.4 V

**42**
$E_T$ = 52.9 kcal/mol
$E_{1/2}$ (red) = -1.1 V

**50**
$E_T$ = 55.7 kcal/mol
$E^*_{1/2}$ (ox) = 1.55 V

Figure 22 Calculated and measured redox and photophysical data for **36**, **42**, and **50.**

Surveyance of optimisation data and correlation of yields and enantioselectivities with triplet energies and excited state redox properties of photocatalysts led us to the conclusion that either or both of these catalytic manifolds could be active (Figure 22). Indeed, measurement of the redox properties of substrate **36** in the absence and presence (**42**) of scandium indicated that single electron reduction by an excited state photocatalyst is feasible and calculation of substrate triplet energies under the same conditions indicated that triplet energy transfer is also feasible.

### I.2.4.1a The Pathways

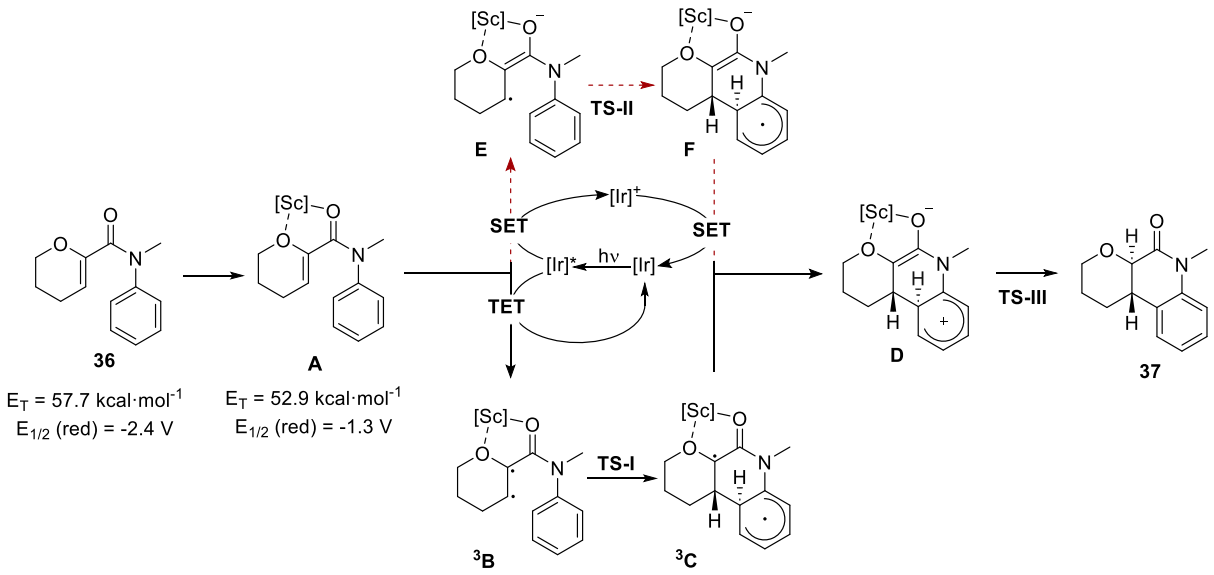



Figure 23 Proposed reaction pathways under both photoredox and energy transfer regimes.

To begin to determine which or whether both forms of photocatalysis are active, two pathways were proposed based on past work within the group and reported mechanistic observations (Figure 23).[12] For both pathways, binding of ligated scandium to the substrate to form **A** is predicted to be the first step and to facilitate reactivity.

In the photoredox pathway (upper Figure 23), the excited state iridium photocatalyst undergoes single electron transfer to **A** to produce radical anion **E**. The radical in **E**, localised β to the oxygen/amide, can then undergo addition to the aryl ring, producing **F**. A second electron transfer from **F** to a ground state $Ir^{IV}$ species closes the catalytic cycle and furnishes intermediate **D**, which is common to both pathways.

In the energy transfer pathway (lower Figure 23), the excited state iridium photocatalyst undergoes energy transfer to **A**, giving rise to triplet intermediate $^3$**B**. From here, $^3$**B** can either unproductively relax back to the ground state, **A**, or the radical localised β to the

oxygen/amide can again undergo addition to the aryl ring, thereby producing **$^3$C**. Intersystem crossing of **$^3$C** gives rise to intermediate **D**[‡].

From convergence of the pathways, a suprafacial 1,5-H shift is calculated as the lowest energy pathway to rearomatisation. After dissociation from scandium, we arrive at **37**.

### I.2.4.1b Pathway Energies

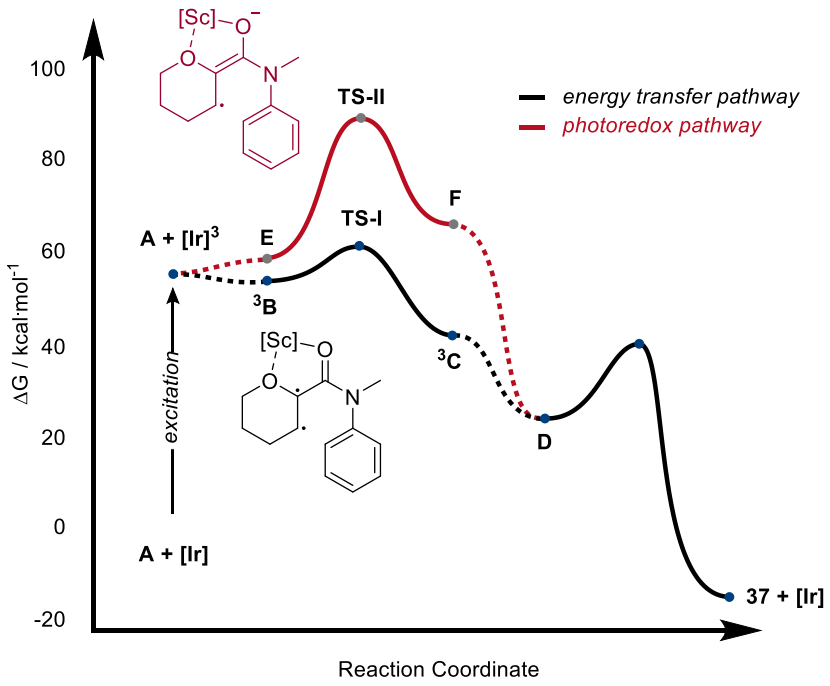



Figure 24 Reaction coordinates for photoredox (red) and energy transfer (black) pathways. Computational studies performed using the M06-2X-D3/Def2-TZVPP(SMD =$CH_2Cl_2$)//M06-2X-D3/6-31+G(d,p);def2TZVP[Sc](CPCM = $CH_2Cl_2$) level of theory.

From calculation of the energy barriers associated with the described pathways, reaction coordinates for each can be produced and compared (Figure 24). From these coordinates we can see that, in agreement with experimental measurements, both energy transfer and single electron transfer from a photosensitizer are possible and that both **$^3$C** and radical anion **E** can be formed.

[‡] It should be noted that intermediate D, though here represented as a zwitterion, could also be represented as a triplet diradical. The zwitterion representation is shown as calculations indicate that this is the most faithful representation of the species.

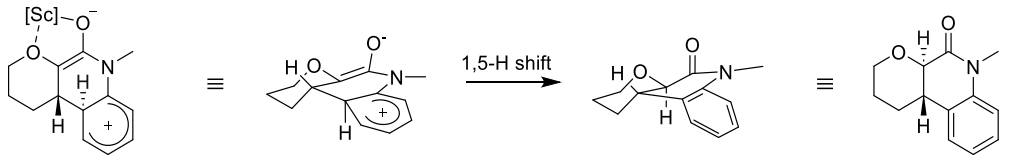
The key difference in these pathways comes when comparing the addition of the β radical to the π system. In the case of cyclization from $^3$**B**, the barrier is calculated to be quite low (~6.6 kcal mol$^{-1}$); however, in the case of cyclization from radical anion **E**, the barrier is calculated to be prohibitively high at ~29 kcal mol$^{-1}$. To compound this, cyclization from $^3$**C** is calculated to be exergonic by approximately 12 kcal mol$^{-1}$, while cyclization from **E** is calculated to be endergonic by approximately 9 kcal mol$^{-1}$. Subsequent steps to form **D** are similarly barrierless for both pathways.

The results of these calculations and the procession of the reaction at room temperature indicates that although both $^3$**C** and **E** are likely produced under our conditions, the energy transfer pathway is presumed to be the only productive pathway.

Though these calculations seem conclusive as to the mechanism of the reaction, experimental validation is necessary to definitively confirm that the predicted pathway is active.

### I.2.4.2 Validation of the 1,5-H shift

Though unhelpful in discriminating between photoredox and energy transfer mediated pathways, experimental validation of the 1,5-H shift is important as this step potentially explains the high diastereoselectivity that we observe in the reaction.




**D** **37**

Figure 25 Conformational representation of the 1,5-H shift.

To probe this step, substrate **BJ18**, bearing a perdeutero aryl ring was synthesised. If our active pathway does proceed *via* a 1,5-H shift, then subjection of this substrate to the reaction should induce a 1,5-D shift. If it does, this should be reflected in high retention of deuterium and its migration to the indicated position.

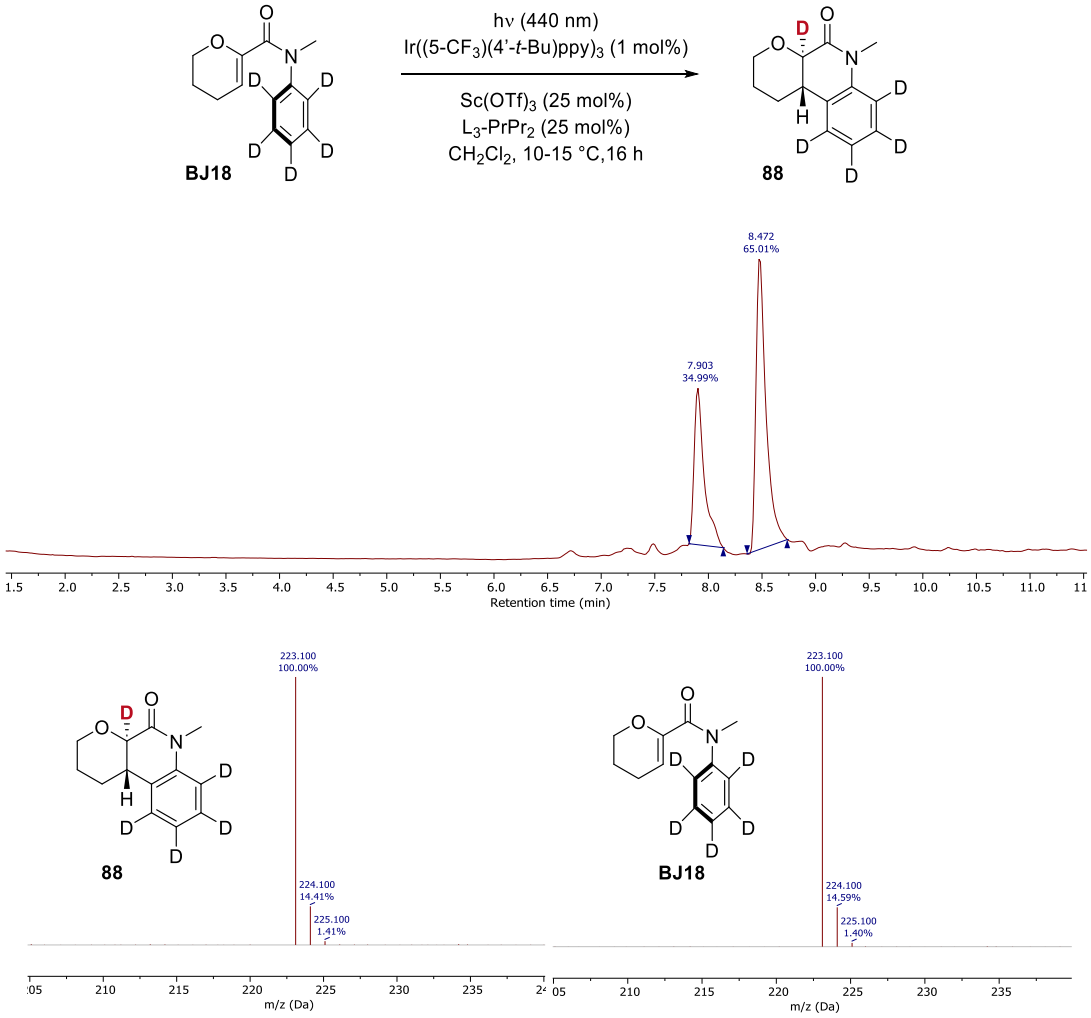



Figure 26 LC/MS analysis of deuterium retention in **BJ18**. Top: UV chromatogram; bottom: mass spectra for each peak.

Analysis of the crude reaction mixture by LC/MS at approximately 60% conversion shows two distinct peaks, the identities of which can be confirmed with authentic samples. As can be seen from the extracted mass chromatograms, complete retention of deuterium is observed (Figure 26). Confirmation of the migration of deuterium to the expected position was confirmed by NMR analysis (Figure 27).

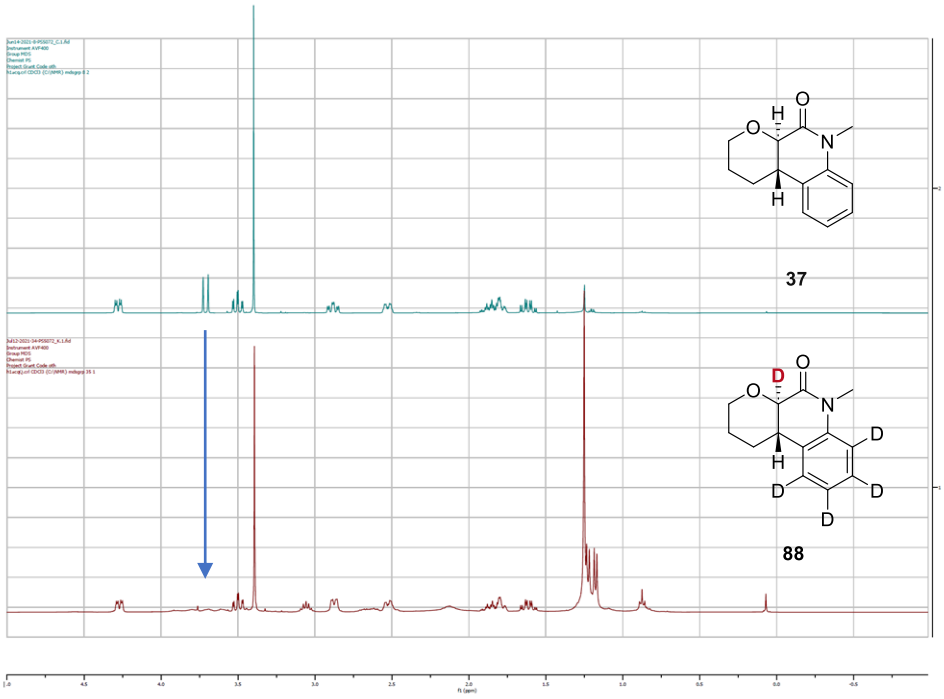



Figure 27 NMR confirmation of the position of the migrated deuterium. The peak of interest (~3.75 ppm) is not present in **88**, indicating full migration of deuterium to the position indicated.

Though this labelling experiment is in line with the prediction of a 1,5-H shift, the results do not distinguish whether the process by which the rearrangement occurs is intramolecular or intermolecular.

In order to tell the difference between these two possibilities, a crossover experiment was devised. In this experiment equimolar amounts of **BJ18** and **57**[§] are mixed and subjected to the reaction. If the process is intramolecular and no intermolecular process is active, then full retention of deuterium should be observed in **88** and full retention of hydrogen should be observed in **57**.

[§] **BJ18** and **57** were chosen to maximise chromatographic discrimination between substrates and to minimally affect substrate reactivity.

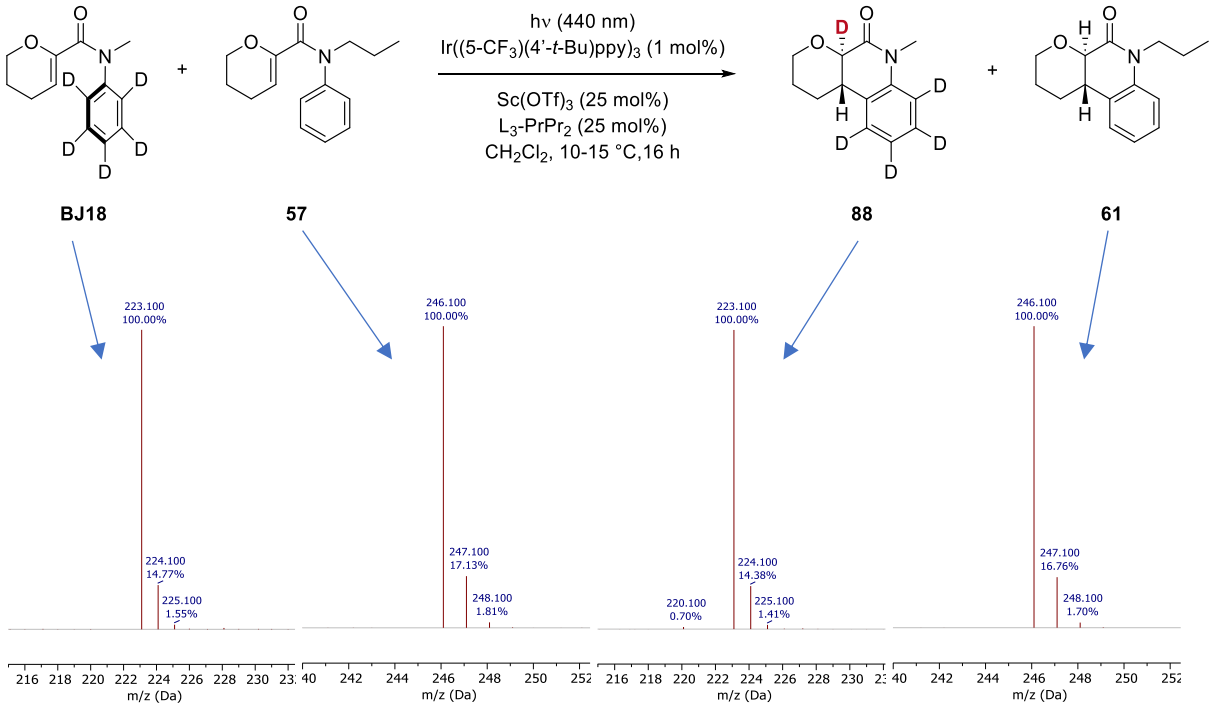



Figure 28 Crossover experiment and LC/MS analysis. Mass spectra for each eluted peak are shown, indicating intramolecular retention of deuterium.

Again, LC/MS analysis of the crude reaction mixture was carried out and the chromatogram peaks identified by correlation with samples of confirmed structure. The results indicate that no crossover occurs between the substrates (i.e. there is full retention of deuterium/hydrogen on cyclization) and serves as experimental validation of the predicted suprafacial 1,5-H shift (Figure 28).

### I.2.4.3 Diastereoselectivity and Meta substitution

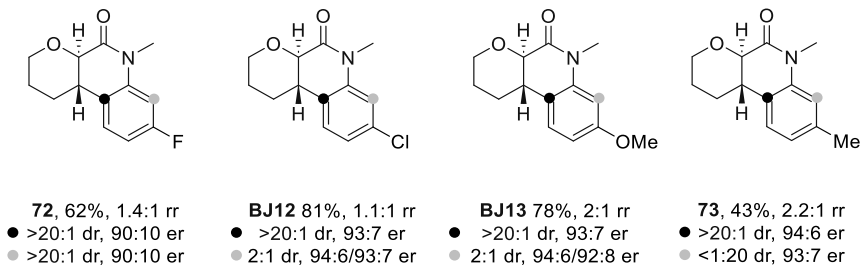



Figure 29 Meta substituted scope examples. Quoted yields are isolated; diastereomeric ratio was determined by NMR analysis of the crude reaction mixture; enantiomeric ratios were determined by normal phase HPLC using a chiral stationary phase.

As previously discussed, diastereoselectivity is almost universally perfect except for in the case of *meta* substituted substrates (Figure 29). Given the prediction that the diastereodetermining step is the aforementioned 1,5-H shift; that we have experimentally validated the occurrence of this shift; and given such shifts are stereospecific in nature, we reasoned that another mechanism must be at play in these examples.

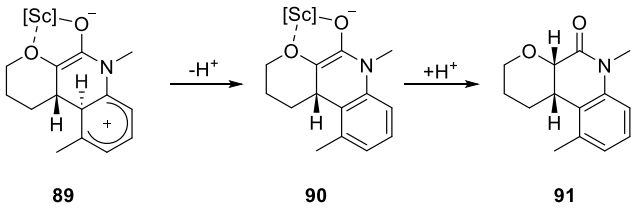



Figure 30 The proposed deprotonation/protonation mechanism by which zwitterion **89** can be converted to **91.**

We postulated that in proximally fused species such as **89**, the steric bulk of proximal ring fusion causes distortion, and an alternative mechanism for the conversion of zwitterion **89** to **91** is active (Figure 30). In this pathway, rearomatisation of **89** is achieved by deprotonation to form **90**, which is then converted to **91** by enolate protonation. In this way the diastereomer formed is determined entirely by the facial selectivity of the final protonation and not by the stereochemistry of the Lewis acid/ligand controlled radical addition as in the 1,5-H shift.

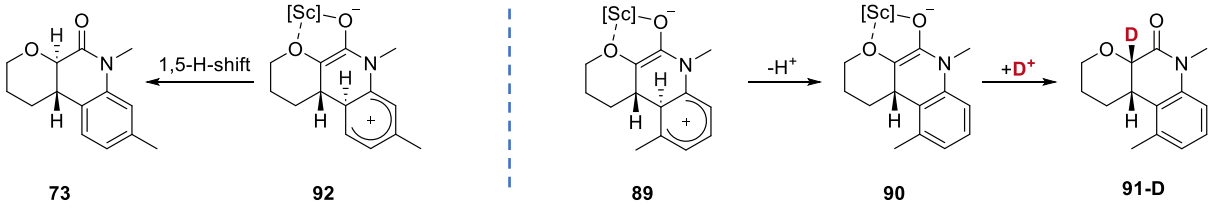



Figure 31 Anticipated divergent outcomes of exogenous deuterium incorporation.

Based on this postulation, we reasoned that in the presence of a deuteron source any products formed by the deprotonation-protonation pathway would be liable to be partially deuterated α to the amide and that this would not occur in any products formed *via* the 1,5-

H shift (Figure 31). Substrate **93** (Figure 32) was an ideal probe due to the complete inversion of diastereoselectivity between regioisomers as this may indicate that each regiosisomer is formed by just one mechanism (1,5-H shift, or deprotonation-protonation).

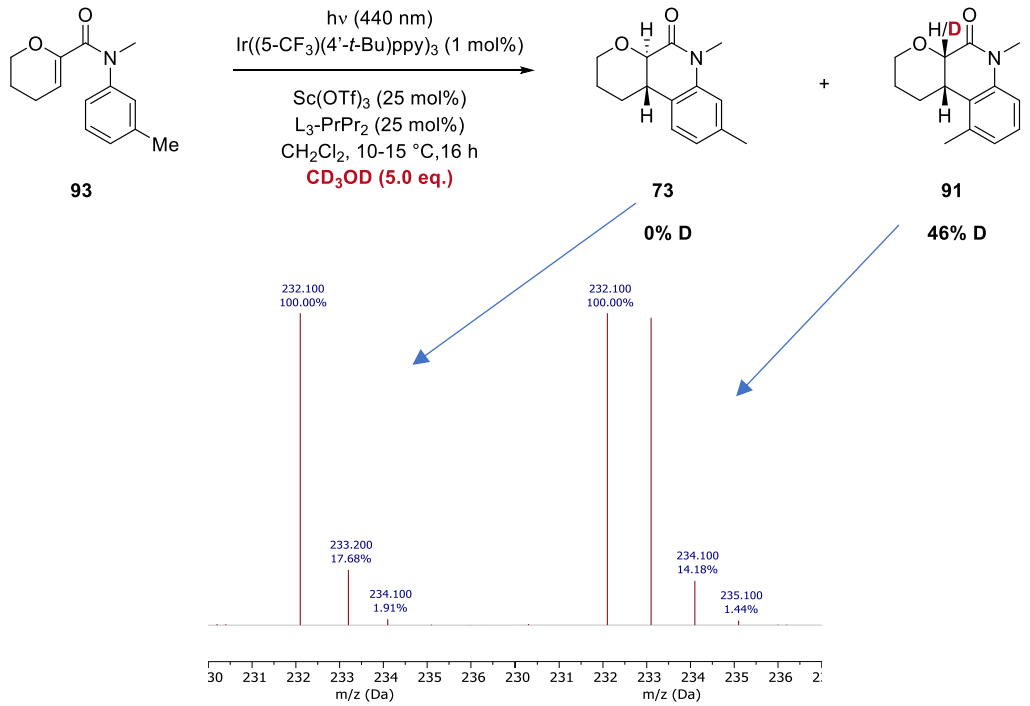



Figure 32 Experimental validation of a deprotonation/protonation mechanism. Mass spectra for the eluted peaks are shown, indicating incorporation of deuterium only in the *cis*-fused product, **91**.

To test the hypothesis, **93** was subjected to cyclization in the presence of methanol-$d_4$ and the reaction mixture was analysed by LC/MS (Figure 32). As predicted, the distally fused regioisomer showed no incorporation of exogeneous deuterium, which is consistent with formation *via* 1,5-H shift. As also predicted, the proximally fused regiosiomer was recovered with significant deuterium incorporation (46%). As the only source of deuterium in the reaction mixture was the added methanol-$d_4$, this incorporation can only have arisen from a protonation event like that proposed. In addition, the level of deuteration measured is in line with that reported for similar systems in protic environments.[54]

### I.2.4.4 Additional Mechanistic Insights

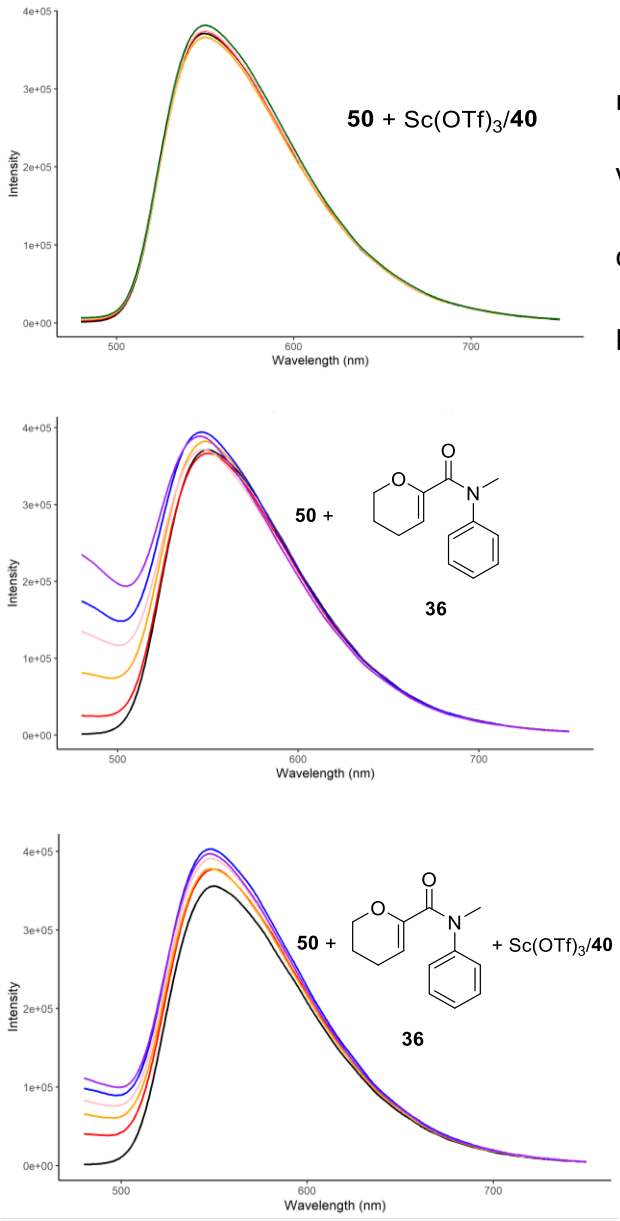



Figure 33 Stern-Volmer quenching studies showed no quenching of excited photocatalyst. Top to bottom: preformed scandium/ligand (**40**) added to photocatalyst solution; **36** added to photocatalyst solution; scandium/ligand (**40**) + **36** added to photocatalyst solution. None show significant quenching of the excited state photocatalyst, **50**.

Though uninformative in terms of catalytic manifold, both quantum yield and Stern-Volmer quenching studies are routinely carried out to characterise photochemical processes. Measurement of the quantum yield of the process showed that it was unlikely to proceed *via* a chain process and indeed that the process was remarkably inefficient in terms of photonic efficiency ($\Phi = 0.003$).

Stern-Volmer quenching proved to be equally as uninformative, with no quenching of the excited photocatalyst recorded in the presence of substrate **36**, scandium complex, or a combination of the two (experimental p173). This is likely due to the vanishingly small quantum yield of the process which was not enough to provide measurable quenching even in vast excess (~40,000-fold excess relative to photocatalyst).[**]

[**] In the case of quenching studies involving **36**, the substrate was found to itself be emissive. Quenching would therefore only be apparent in parts of the spectrum where **36** is not emissive (>650 nm).

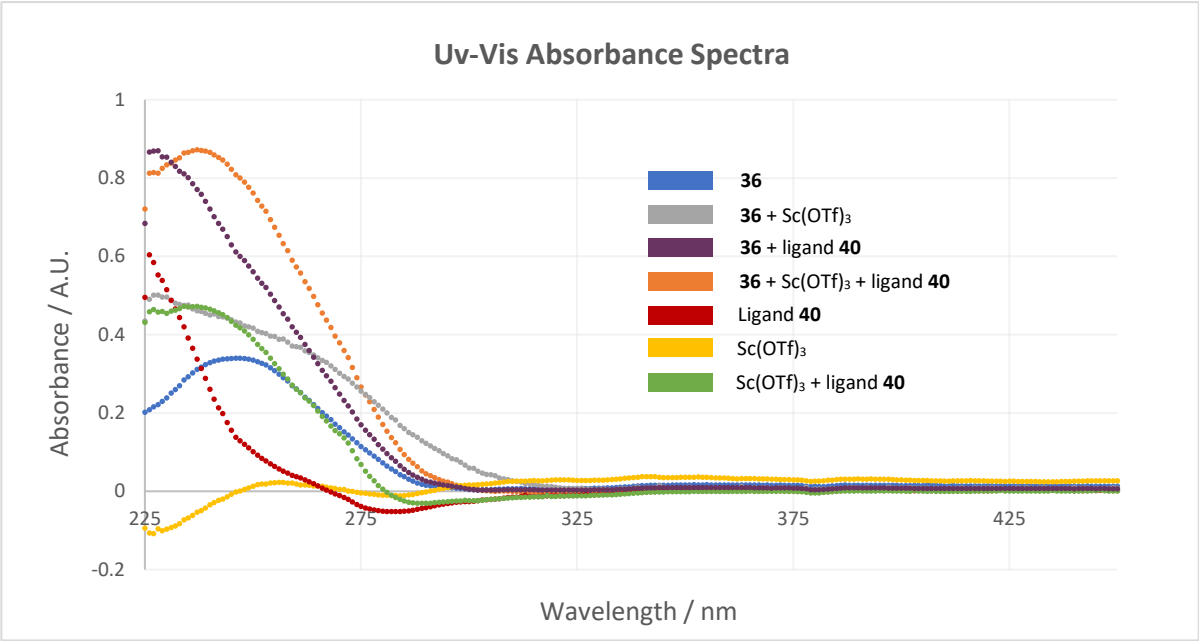



Figure 34 UV-Vis absorbance spectra of reaction components. substrate (**36**), blue; substrate (**36**) + scandium(III) triflate, grey; substrate (**36**) + ligand (**40**), purple; substrate (**36**) + scandium(III) triflate + ligand (**40**), orange; ligand (**40**), red; scandium(III) triflate, yellow; scandium(III) triflate + ligand (**40**), green.

In addition to quantum yield and Stern-Volmer quenching, the UV-VIS absorbance spectrum of **36** in the presence of combinations of Lewis acid and ligand **40** were recorded (Figure 34).

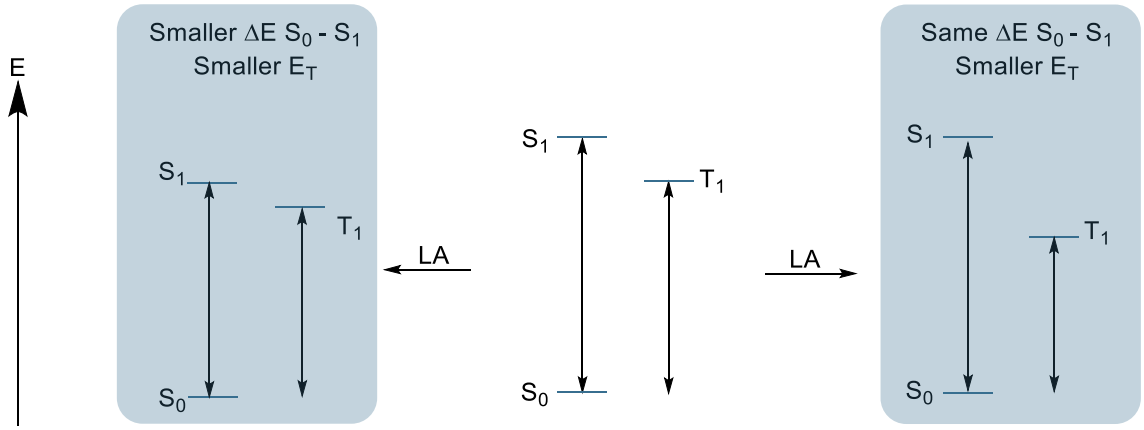



Figure 35 Coordination can induce a change in triplet energy without inducing a bathochromic shift.

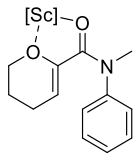
The purpose of the measurements was to determine whether **36** exhibited a bathochriomic shift on binding to the Lewis acid. No such shift was observed, but as absorbance can only inform us about excitation ($\Delta E\ S_0 - S_n$), this does not mean that the triplet energy ($\Delta E\ S_0 - T_1$) is unchanged by binding (Figure 35).

### I.2.4.5 Energy Transfer vs Photoredox

The discussed mechanistic probes have given an understanding of the mechanism of the common 1,5 H shift and the origins of the diastereoselectivity of the reaction. However, the central question of the whether the reaction proceeds *via* photoredox or energy transfer catalysis has not yet been addressed.

Though transient absorption spectroscopy (TAS) can be invaluable in validating mechanistic predictions for photoredox mediated reactions, its use is resource intensive and unfortunately was outside of our means. In addition to this, the low quantum yield of our reaction makes the likelihood of observing electron transfer low, and the absence of this observation could not be used to rigorously exclude a photoredox pathway.[55]

#### I.2.4.5a Weakly Reducing Photocatalyst Study




**42**

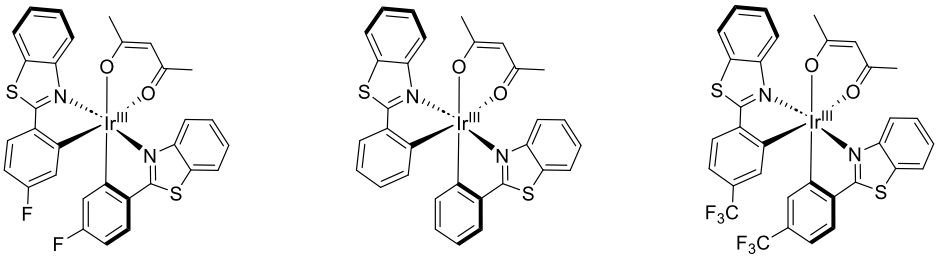
$E_T$ = 52.9 kcal·mol$^{-1}$
$E_{1/2}$ (red) = -1.3 V

| Photoredox | Energy Transfer |
|---|---|
| $E_{red}$ $PC^{X+1/X*}$ < -1.3 V | $E_{red}$ $PC^{X+1/X*}$ > -1.3 V |
| $E_T$ < 52.9 kcal mol$^{-1}$ | $E_T$ > 52.9 kcal mol$^{-1}$ |

Figure 36 Probing catalytic manifold can be achieved by carefully selecting catalysts based on photophysical properties.

Given these restrictions, we instead turned to an approach developed by other groups, most notably the Yoon and Macmillan groups.[24, 56] In this approach, the reaction is run with a number of photocatalysts which are carefully selected for their photophysical properties. The catalysts should have either the requisite triplet energy *or* redox properties to enable the reaction the occur, but not both. By eliminating the possibility of one manifold based on

catalyst properties, it can reasonably be assumed that, if the reaction proceeds, it does so *via* the other manifold. Repeating this with a number of catalysts and correlating yield and enantioselectivity strengthens the argument.



**94**
$E_{1/2}$ $Ir^{IV/III*}$ = -1.12 V
$E_T$ = 56.3 kcal $mol^{-1}$

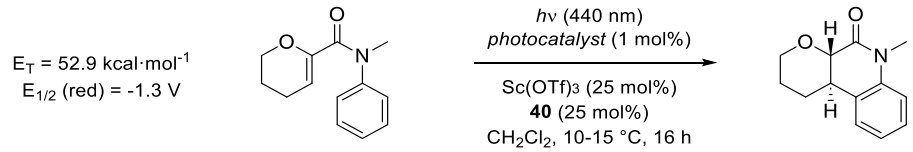
**95**
$E_{1/2}$ $Ir^{IV/III*}$ = -1.27 V
$E_T$ = 54.8 kcal $mol^{-1}$

**96**
$E_{1/2}$ $Ir^{IV/III*}$ = -0.8 V
$E_T$ = 53.6 kcal $mol^{-1}$

Figure 37 The series of iridium complexes reported by Chen which were chosen for the study. None have the reduction potential necessary for the cyclisation to occur.

With this in mind, we searched the literature for a set of photocatalysts with suitable photophysical properties. A series of iridium complexes reported by Chen and co-worker was chosen (Figure 37).[57]

Table 5 Weakly reducing photocatalyst study. [††]




**36** **37**

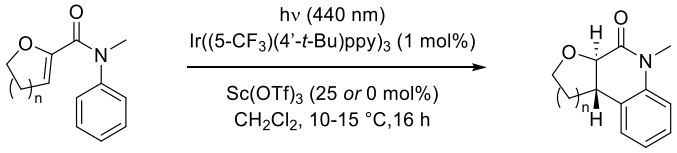
| Entry | Photocatalyst | $E_T$ ($I_{10\%}$) (kcal·$mol^{-1}$) | $E_{1/2}$ $Ir^{IV/III*}$ (V) | Yield (%) | er | dr |
|---|---|---|---|---|---|---|
| **1** | **94** | 56.3 | -1.12 | 33 | 76:24 | >20:1 |
| **2** | **95** | 54.8 | -1.27 | 15 | 79:21 | >20:1 |
| **3** | **96** | 53.6 | -0.8 | 8 | 88:12 | >20:1 |

$E_T$ ($I_{10\%}$) is the triplet energy at 10% max emission. $E_{½}^{red}$ $Ir^{IV/*III}$ is the excited state reduction potential of the listed photocatalyst as calculated according to Experimental p.S-44. Yield refers to NMR yield using 1/3 eq. trimethoxybenzene as an internal standard. Enantiomeric ratio was determined by normal phase HPLC analysis using a chiral stationary phase. Diastereomeric ratio was determined by quantitate NMR analysis of the crude reaction mixture.

[††] It is acknowledged that strongly reducing photocatalysts with very low triplet energy were not tested and that an electron transfer mechanism cannot be rigorously excluded.

As can be seen from the results of the cyclization, while none of the photocatalysts have the requisite redox properties to enter the photoredox pathway, they do have appropriate triplet energies and the reaction does proceed in their presence (Table 5). Additionally, the yield of **37** increases with increasing triplet energy and its enantiomeric excess drops with increasing triplet energy. Both of these are hallmarks of energy transfer mediated reactions.[24, 56]

### I.2.4.5b Consequences for Reactivity




Scheme 26 Cyclization of other etheric rings indicated that triplet energy varies significantly with ring size.

| Entry | n | Lewis Acid? | Yield (%) |
|---|---|---|---|
| **1** | 1 | No | 84* |
| **2** | 1 | Yes | 84* |
| **3** | 2 | No | trace |
| **4** | 2 | Yes | 95* |
| **5** | 3 | Yes | trace |

*Indicates isolated yield. Trace yields were confirmed by NMR analysis of the crude reaction mixture.

With the knowledge that the reaction is most likely energy transfer mediated, we can explain clearly the very different reactivity of dihydrofuran and 2,3,4,5-tetrahydrooxepine derived substrates. Though the redox properties of these substrates are very similar to the diydropyran substrate, calculations suggest that their triplet energies are quite different. Indeed, cyclization of the five membered substrate proceeds in good yield even in the absence of Lewis acid, while the seven membered ring struggles even in its presence (Scheme 26).

### I.2.4.6 Selectivity

Based on computational and experimental studies the selectivity found in this reaction arises from several different sources

#### I.2.4.6a Enantioselectivity

Calculations (again, carried out by Dr Mihai V. Popescu) indicate that the enantioselectivity observed is due to distortion of the active octahedral scandium complex. Four binding points are provided by the Feng ligand, locking the chirality of the complex as a whole, and the final two points are the oxygen atoms that form the binding motif of the substrate.

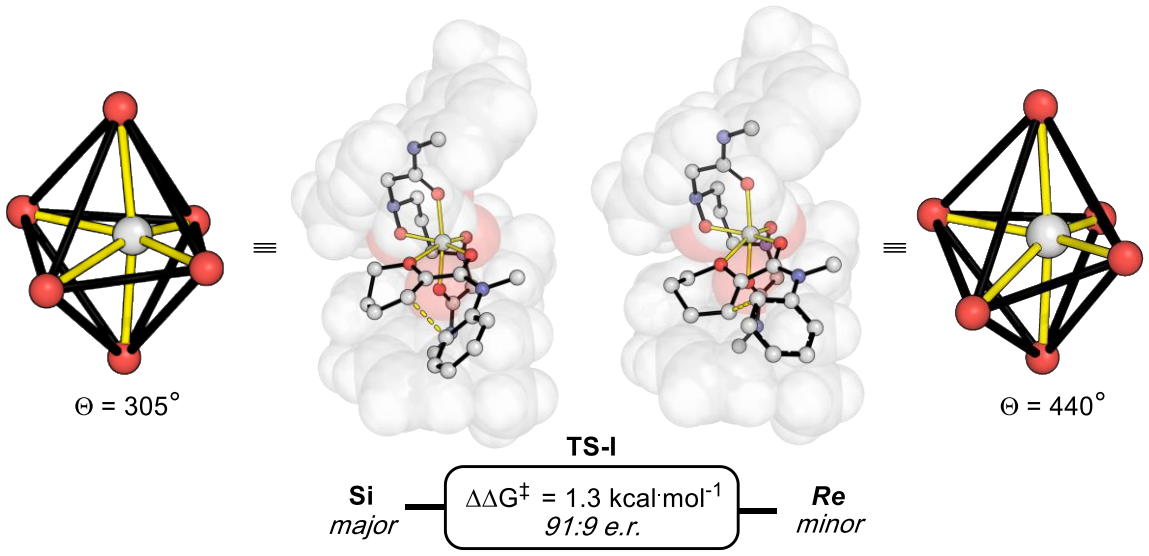



Figure 38 Octahedral distortion provides a rationale for enantioselectivity. Computational studies performed using the M06-2X-D3/Def2-TZVPP(SMD = $CH_2Cl_2$)//M06-2X-D3/6-31+G(d,p);def2TZVP[Sc](CPCM = $CH_2Cl_2$) level of theory.

The distortion of this octahedral complex as the reaction proceeds through cyclization (**TS-I**, the enantiodetermining step) can be quantified by a distortion angle, Θ (Figure 38). Calculations of the difference in energy between these diastereomeric transitions states predict a theoretical er of 91:9, which is close to our experimental value.

### I.2.4.6b Suppression of Background Reactivity

Though a racemic component of the reaction mixture, the photocatalyst developed plays a key role in ensuring high selectivity in the reaction. The reduction in triplet energy on complexation to scandium is moderate (~4.8 kcal $mol^{-1}$), especially when compared to the broad emission of iridium photosensitizers and the large changes in redox potential on complexation ($E_{½}^{red}$= 1.1 V).

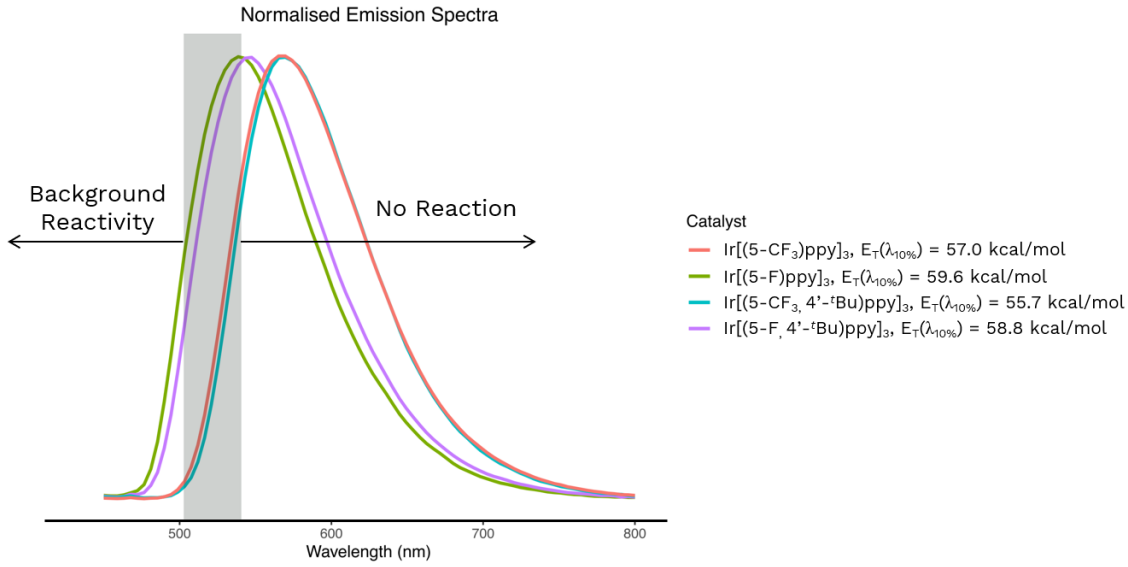



Figure 39 Illustration of the narrow window within which selective energy transfer can occur.

| Entry | Photocatalyst | $E_T$ ($I_{10\%}$) kcal $mol^{-1}$ | Yield (%) | er |
|---|---|---|---|---|
| **1** | Ir[(5-$CF_3$)ppy]$_3$ | 57.0 | 92 | 91:9 |
| **2** | Ir[(5-F)ppy]$_3$ | 59.6 | 84 | 86:14 |
| **3** | Ir[(5-$CF_3$, 4'-$^t$Bu)ppy]$_3$ | 55.7 | 95 | 95:5 |
| **4** | Ir[(5-F, 4'-$^t$Bu)ppy]$_3$ | 58.8 | 84 | 84:16 |

$E_T$ ($I_{10\%}$) is the triplet energy at 10% max emission. Yield refers to NMR yield using 1/3 eq. trimethoxybenzene as an internal standard. Enantiomeric ratio was determined by normal phase HPLC analysis using a chiral stationary phase.

The narrow window within which the success of this reaction lies becomes apparent when illustrated in comparison to the broad emission of the novel photosensitizers developed for

this system (Figure 39)[‡‡]. Emission at wavelengths shorter than approximately 500 nm leads to energy transfer giving rise to uncontrolled background reactivity, while emission at wavelengths longer than approximately 530 nm means that the catalyst does not have sufficient energy to undergo energy transfer to the substrate. Additionally, though we use triplet energies as surrogates to predict potential reactivity, in reality many other factors are at play (orbital overlap, triplet lifetime, etc.).

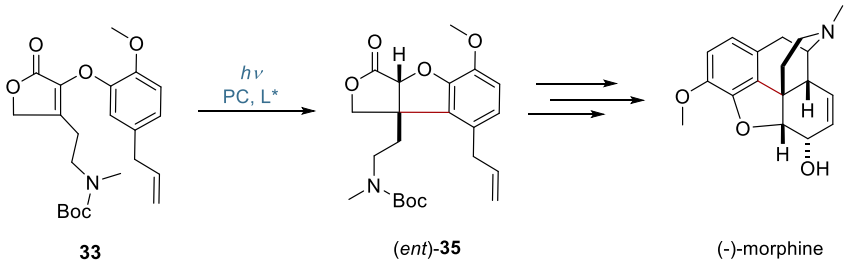
#### I.2.4.6c Diastereoselectivity

As previously discussed, the diastereoselectivity of the reaction can easily be rationalised as a consequence of the stereospecific nature of the suprafacial 1,5-H shift. In this way high enantioselectivity is translated to high diastereoselectivity. Even in the complicated case of *meta* substituents, diastereomeric ratios can be rationalised based on a 1,5-H shift where favourable and a deprotonation-protonation mechanism where the 1,5-H shift is disfavoured due to steric interactions.

[‡‡] It is worth noting that all triplet energy values quoted are calculated using the short wavelength at which emission intensity is 10% of its maximum. We have found that these values are more reflective of the capability of the catalyst, especially in selective reactions where a narrow transfer window is desired.

## I.3 Conclusion and Future Work

In conclusion, our work has led to the development of a highly enantioselective 6π cyclization enabled by dual Lewis acid-energy transfer catalysis. The small reduction in triplet energy caused by Lewis acid coordination in combination with careful photosensitizer development allows for precise control of the reaction and provides a new avenue for future enantioselective 6π cyclizations, for example, in a proposed enantioselective synthesis of morphine (Scheme 27).




Scheme 27 Potential application of the developed enantioselective cyclization to the synthesis of (-)-morphine.

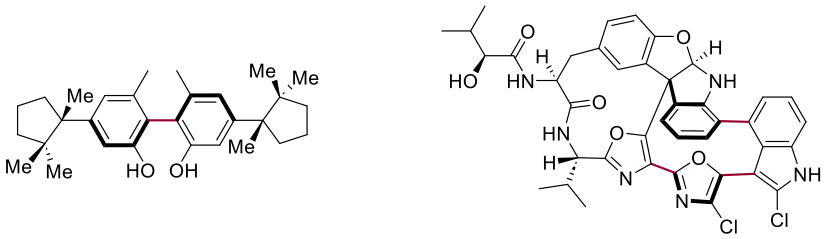
# Part II:

# Enantiomerisation Processes of Indolyl-Naphthyl Atropisomers

# II.1 Introduction

## II.1.1 Atropisomerism

Atropisomers are axially chiral molecules whose chirality arises from hindered rotation about a single bond.[58, 59] For practical reasons, to be considered atropisomeric a molecule must have a half-life to interconversion of greater than 1000 s at room temperature (i.e. it must take more than 1000 s for half of the molecules in a sample to enantiomerise[§§]).[61]




**100**

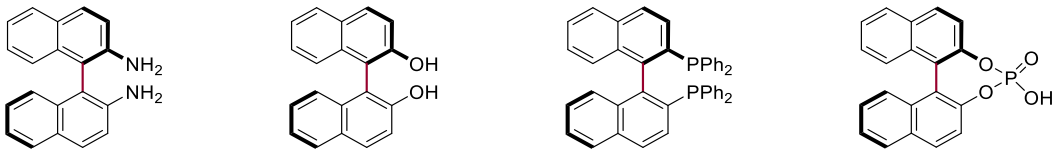
Mastigophorene A

**101**

Diazonamide A

Figure 40 Examples of atropisomers include natural products and ligands such as mastigophorene A (**100**) and diazonamide A (**101**). Chiral axes are shown in red.

Perhaps the most widely recognised form of atropisomer, biaryl atropisomeric fragments can be found in a wide range of compounds including natural products such as mastigophorene A and diazonamide A (Figure 40).[62-65]




**102**

(R)-BINAM

**103**

(R)-BINOL

**104**

(R)-BINAP

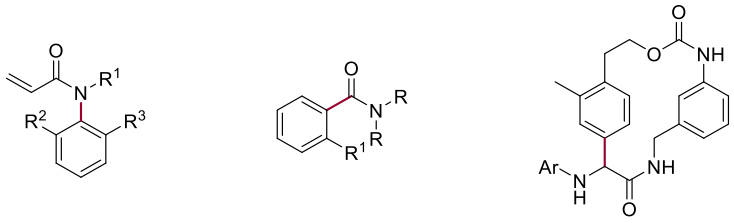
**105**

(R)-CPA

Figure 41 Some atropisomeric chiral ligand classes include BINAM (**102**), BINOL (**103**), BINAP (**104**), and CPAs (**105**). Chiral axes are shown in red.

[§§] Enantiomerisation refers to the inversion of stereochemistry of a single molecule. Racemisation is the bulk property of becoming racemic.[60]

In addition to this, many widely used chiral ligands and organocatalysts such as BINAM (**102**), BINOL (**103**), BINAP (**104**), and chiral phosphoric acids (CPAs, **105**) are based around an atropisomeric binaphthyl core (Figure 41).[66-70]



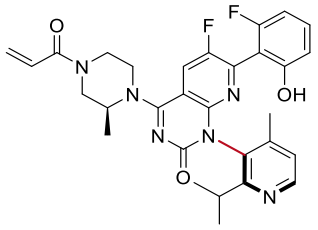

**106** **107** **108**

Figure 42 Examples of non-biaryl atropisomers include hindered amides (**106**, **107**) and constrained rings (**108**). Chiral axes are shown in red.

Though much literature focuses on biaryl atropisomers a wide variety of other atropisomeric scaffolds have been reported including hindered amides (**106**, **107**) and constrained rings (**108**) (Figure 42).[70-74]

### II.1.2 The Barrier to Rotation

The barrier to rotation, while interesting in a purely academic sense, is especially important in the context of atropisomeric fragments in drug discovery.[75-77] This is particularly pertinent given the recent rise in drug candidates exhibiting atropisomerism.[78, 79] This trend is typified by Amgen's sotorasib, the first FDA approved KRas G12C inhibitor, notable for its remarkable ability to drug the protein's shallow, hinge-like binding pocket.[80, 81]




(*M*)-**AMG-510 "sotorasib"**
*KRas G12C covalent inhibitor*
*$IC_{50}$ = 0.027 μM*
*pERK $IC_{50}$ = 0.016 μM*
*Nature*, 2019, **575**, 217

Figure 43 Sotorasib, the first approved KRas G12C inhibitor is atropisomeric. Chiral axis shown in red.

As with all drugs, the stability of all stereogenic elements needs to be well characterised under physiological conditions due to the risk of lower activity or deleterious effects arising from conversion to other species/enantiomers in vivo.[82-84]

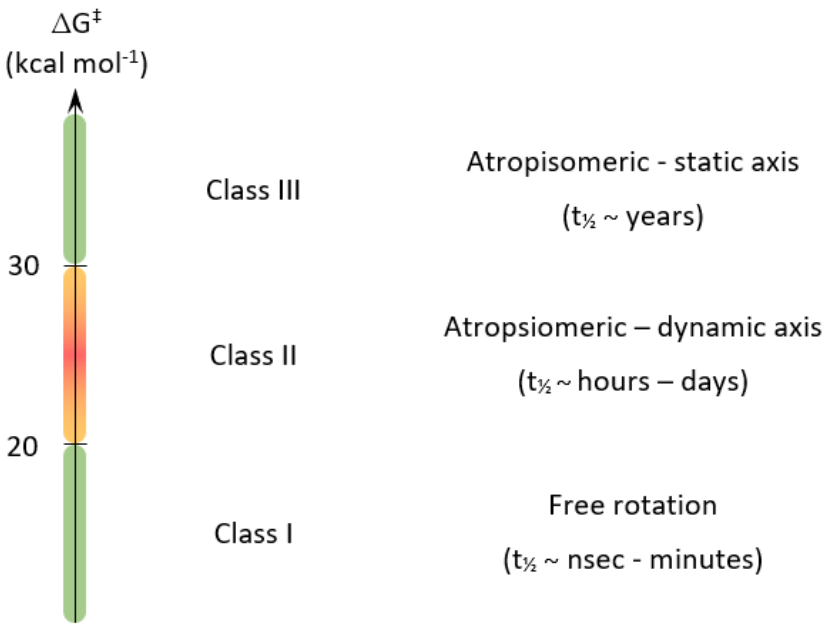



Figure 44 Atropisomeric classes applied to drug design divide atropisomers according to the rate at which rotation occurs.

To aid with development, drug discovery classifies atropsiomers based on their barrier to inversion under physiological conditions.[76] Class I atropisomers have barriers to inversion smaller than 20 kcal mol$^{-1}$, corresponding to a half-life in the range of nanoseconds to seconds at 37 °C. These compounds are considered achiral because of rapid interconversion and are therefore developed as such.

Class II atropisomers have a larger barrier to inversion (20 kcal mol$^{-1}$ to 30 kcal mol$^{-1}$) and interconvert on intermediate timescales (hours to days) at 37 °C. This class of atropisomer is the most problematic as, while compounds can be developed and characterised as a single enantiomer, their interconversion in vivo can cause harmful effects. This class of axis is generally avoided or designed out of a candidate.[85-87]

The third and final class of atropisomer, Class III, have barriers to inversion greater than 30 kcal $mol^{-1}$. As the barrier is so large, this class of atropisomer is essentially static under physiological conditions and timescales. Because of this, this class of atropisomer is usually developed as a single enantiomer and treated in much the same way as molecules containing point chiral centres are.

#### II.1.2.1a Enantiomerisation

As mentioned, characterisation of the barrier to inversion is key to understanding the stereochemical lability of an atropisomer. To arrive at representative measurements for inversion barriers, a good understanding of the process must be established.

In general, the barrier we speak about is the thermal (ground state) barrier that an atropisomer must traverse to invert its stereochemistry.[88-90]

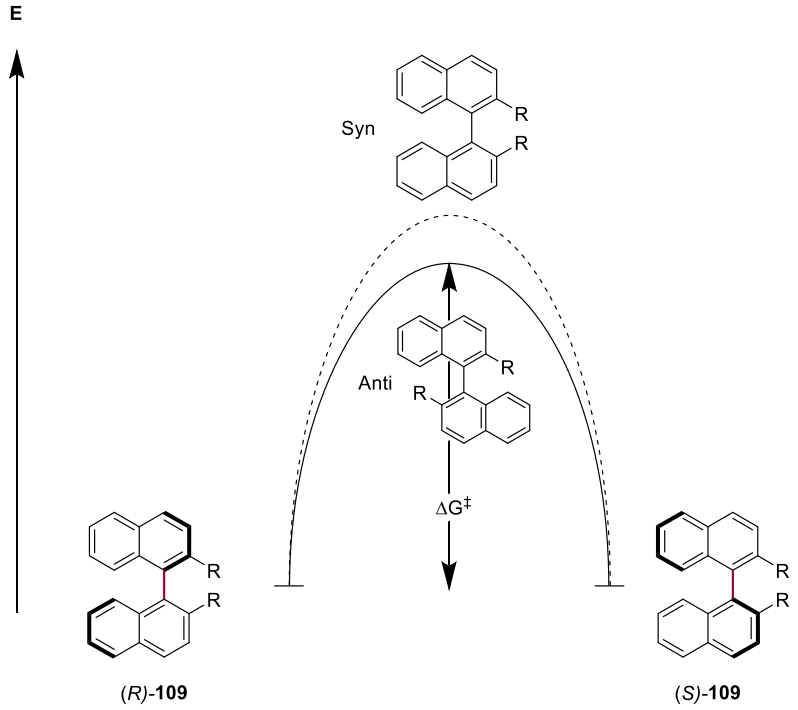



Figure 45 Biaryl enantiomerisation proceeds *via* the *anti* or *syn* conformation. The *anti* pathway is generally the lower energy of the two.

This process has been well studied for axially chiral binaphthyls wherein interconversion is by direct rotation about the axis.[90-92] For steric reasons the lower energy pathway for this interconversion is generally *via* the *anti*- transition state.[92]

Though most research investigating enantiomerisation pathways has focussed on biaryl frameworks, enantiomerisation of non-biaryl atropsiomers has been observed to follow the same kinetic regime.[73, 91, 93-96]

#### II.1.2.1b First Order Kinetics

Once the pathway by which an atropisomer interconverts is understood, describing the kinetics of this process is trivial.[97, 98]

If we assume enantiomerisation proceeds as above we can see that an equilibrium between enantiomers is established. By symmetry, the rate of the forward and backwards reactions must be the same ($k_{ent}$).

$$\mathrm{R} \underset{k_{ent}}{\overset{k_{ent}}{\rightleftharpoons}} \mathrm{S}$$

In this regime, a first order differential can easily be written to describe the system:

$$\frac{d[R]}{dt} = -k_{ent} \cdot [R] + k_{ent} \cdot [S]$$

After integration and rearrangement and substitution (Experimental p S-88), this yields:

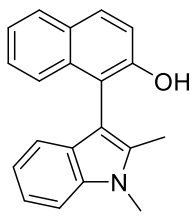
$$ln\left(\frac{e.e._0}{e.e._t}\right) = 2k_{ent} \cdot t$$

The utility of this equation is that, in this first order regime, simple measurements of ee over time can be used to determine the rate of enantiomerisation, ($k_{ent}$), which can then be used to calculate the enantiomerisation energy barrier.

#### II.1.2.1c Measuring the barrier

Practically, there are several approaches which can be used to measure the rate of thermal enantiomerisation including dynamic NMR (DNMR), dynamic HLPC, polarimetry, and circular dichroism.[89, 91, 97, 99, 100] All of these methods make use of either the observation of erosion of enantiomeric excess over time (erosion studies), or the observation of dynamic behaviour on a stationary phase or in solution (DHPLC, DNMR).

Perhaps the most common method used for the measurement of an enantiomerisation barrier is by erosion study. This involves the incubation of an enantioenriched solution of the compound of interest and the monitoring of its enantiomeric excess over time.[97]




**111**

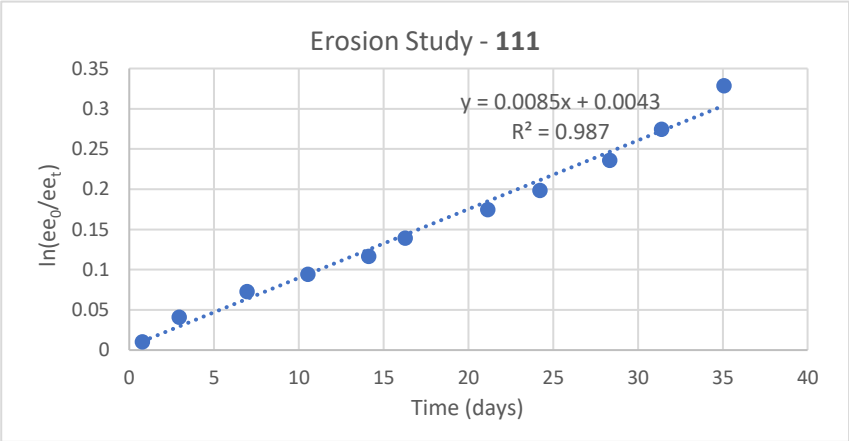



Figure 46 Measurement of the inversion barrier of **111** yields a straight line with slope $k_{rac}$.

For an erosion study of **111**, aliquots were taken from an enantioenriched solution incubated at 22 °C. HPLC analysis of the aliquots allowed tracking of the enantiomeric excess of the solution over the course of the study. Manipulation of the data yielded the straight-

line plot shown, the slope of which corresponds to the rate of racemisation ($k_{rac}$). By using this value in the Eyring equation, a barrier to inversion of 27 kcal mol$^{-1}$ was obtained.

### II.1.3 Alternative Enantiomerisation Pathways

Though quoted barriers are usually measured using solutions of pure enantiomer at neutral pH under heating/cooling, it is important to note that alternative enantiomerisation pathways with accompanying barriers have been reported. Many of these alternative pathways have been investigated as possible ways to enable resolution of chiral materials.[101, 102]

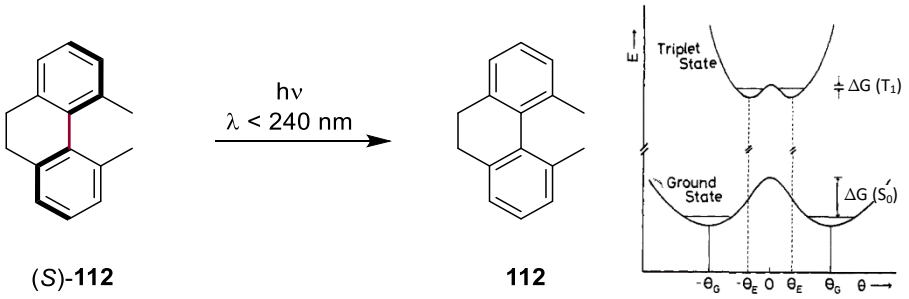



Figure 47 Mislow's reported biaryl photoracemisation. Diagram reproduced from *J. Phys. Chem.*, 1977, **81**, 969.[103]

One area which has recently received renewed interest is photoracemisation.[103-106] Pioneering work by Mislow in 1963 showed that biaryl **112** could be photoracemised by irradiation with high energy UV light (λ < 240 nm).[107] Upon irradiation **112** is excited to its triplet state in which the barrier to enantiomerisation is greatly reduced (Figure 47).[108]

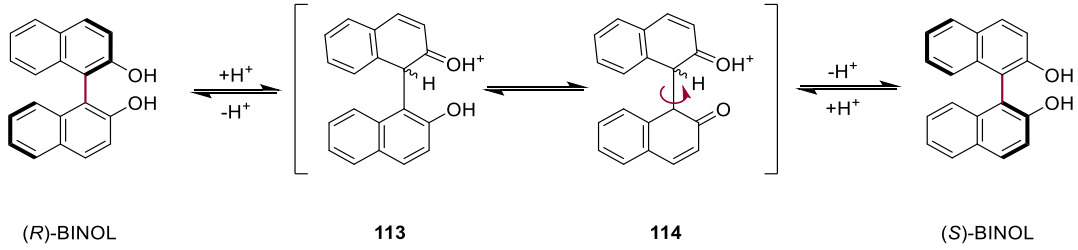
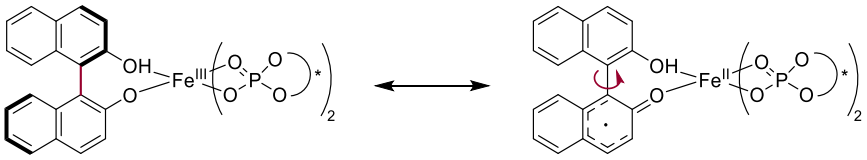



Figure 48 Acid mediated racemisation of BINOL proceeds *via* enone **114**.

Another reported method of altering the inversion barrier, this time of BINOL is by protonation or deprotonation.[109] Under acidic conditions BINOL will protonate first at the *C*-1

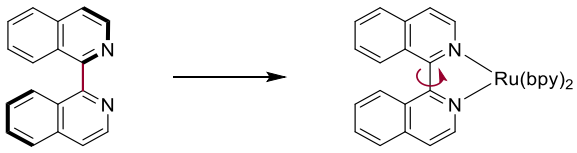
position. While this protonation does reduce the barrier marginally, computational studies have shown that tautomer **114** has a much lower barrier to inversion (23.3 kcal $mol^{-1}$) which is in line with experimentally observed barriers in acidic media.[110-112]




**115** **116**

Figure 49 Single electron oxidation of BINOL significantly reduces the rotational barrier.

Yet another way to access species with lower inversion barriers is by single electron transfer (SET). Work by Pappo on the enantioselective synthesis of BINOL has shown that radical cation intermediate **116** undergoes rapid rotation about the biaryl carbon-carbon bond.[113] Use of a chiral phosphoric acid bound to the oxidant, iron, means that this oxidised intermediate can be made to favour one conformer over the other, and when reduction occurs, the large barrier is restored, furnishing the biaryl enantioselectively.




**117** **118**

Figure 50 Rapid rotation of the biaryl axis *via* the *syn* transition state is observed on coordination to ruthenium.

One final way that inversion barriers of atropisomers may be modulated is by coordination to a metal. A report from Ashby in 1994 showed that 1,1'-bisisoquinoline (**117**) underwent rapid rotation about the biaryl axis when coordinated to ruthenium (**118**).[114] While the barrier to rotation of 1,1'-bisisoquinoline is not prohibitively high when uncoordinated, the rotation *via* the more sterically demanding *syn* transition state when coordinated is notable.[115]

While this is not an exhaustive list and new examples of barrier modulations are disclosed regularly, it is clear that the barrier to rotation in the sense of an isolated molecule is not the only barrier that must be considered when dealing with atropisomerism.

### II.1.4 Autocatalysis

Autocatalysis occurs when the product of a reaction is itself a catalyst for the reaction. The process of autocatalysis underlies all forms of life and has understandably been widely studied.[116, 117]

In purely practical terms an autocatalytic reaction will be observed to speed up as more product is formed and catalyses its own production.

$$\mathrm{A} \xrightarrow{k_1} \mathrm{B} \qquad \text{(ac 1)}$$

$$\mathrm{A} + \mathrm{B} \xrightarrow{k_2} 2\,\mathrm{B} \qquad \text{(ac 2)}$$

Perhaps one of the simplest autocatalytic regimes is presented in equations ac 1 and ac 2. In this regime, A reacts at rate $k_1[A]$ to produce B. Once B is present a second reaction can take place at rate $k_2[A][B]$ wherein A can react with B to produce two equivalents of B. While the rate constants are not directly comparable because of molecularity, it's clear that if the second reaction takes place faster than the first, B is acting as a catalyst in its own production.

$$\frac{d[B]}{dt} = -k_1 \cdot [A] + k_2 \cdot [A] \cdot [B] \qquad \text{(ode 1)}$$

An ordinary differential equation (ODE) can easily be written for equations ac 1 and 2 (ode 1), and through substitution and integration is readily soluble. For the purposes of considering the characteristics of autocatalysis, a visual representation of the regime is helpful.[117]

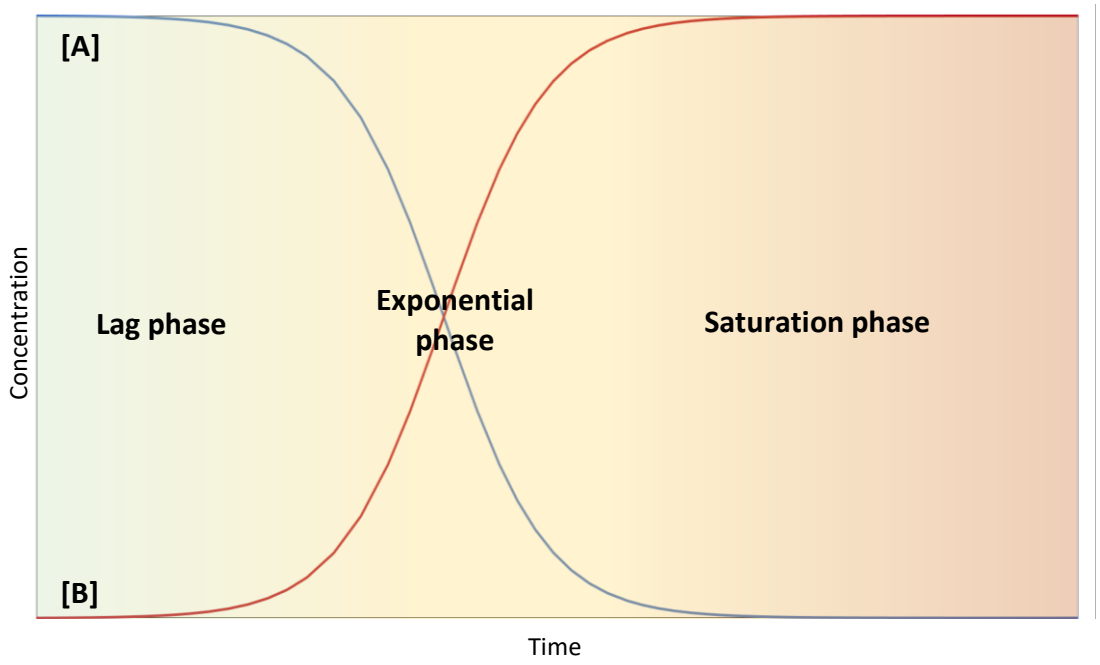


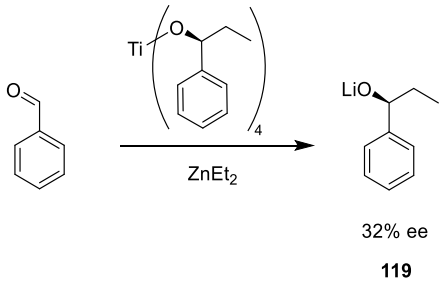

Figure 51 Sigmoidal growth/decay is characteristic of autocatalysis and can be divided into lag, exponential, and saturation phases.

From examination of the plotted concentrations, we obtain the characteristic sigmoidal growth/decay curve. We can also begin to distinguish three distinct phases which arise from the kinetics underlying the regime (Figure 51). Firstly, a lag phase is observed wherein B is only generated directly from A by a first order process. Once B has formed, catalysis starts to occur. In this phase growth is exponential as more and more B is produced and catalyses its own production. Thirdly and finally, the concentration of B increases to a point where the system is saturated in catalyst and the rate can no longer increase.

#### II.1.4.1a Asymmetric Autocatalysis

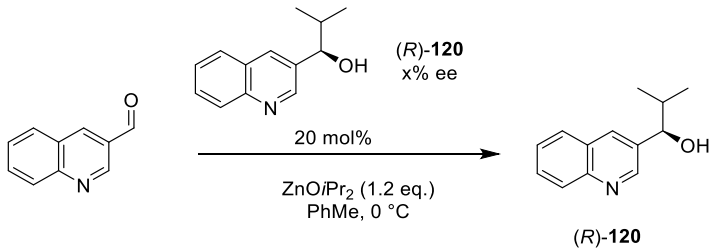
Asymmetric autocatalysis is an extension of autocatalysis where, in addition to the product of a reaction catalysing its own formation, the product is chiral and catalyses the formation

of the same enantiomer.[118-121] Just as autocatalysis underlies the origins of life, asymmetric autocatalysis underlies the origin of homochirality.[122, 123]




Scheme 28 Wynberg's autoinductive alkylation of benzaldehyde produces **119**, the reaction's chiral ligand.

Though not strictly autocatalysis, perhaps the earliest example of synthetic asymmetric autoinduction*** was reported by Wynberg and Alberts in 1989 (Scheme 28).[124] In the work alkylation of benzaldehyde is carried out using a chiral metal alkoxide. The chiral ligand (**119**) and the product of the reaction (**119**), however, are one in the same, and the chiral ligand effectively promotes its own production.




| Catalyst ee (%) | Product ee (%) |
|---|---|
| - | 8.9 |
| 8.9 | 43.3 |
| 43.3 | 67.0 |
| 67.0 | 81.6 |
| 81.6 | 85.5 |
| 85.5 | 86.2 |
| 86.2 | 88.1 |

Scheme 29 Autocatalytic amplification of enantiomeric excess reported by Soai.

The first example of true asymmetric autocatalysis is that reported by Soai in 1990, which was subsequently further refined to the reaction widely known as the Soai reaction.[125] In this reaction quinoline-3-carbaldehyde is alkylated with di*iso*propyl zinc using substoichiometric amounts (10 mol%) of (*R*)-**120** with low enantiomeric excess (Scheme 29). Running the

*** Autoinduction refers to instances where the product does not itself catalyse the reaction, but does influence the outcome of the reaction

reaction a single time leads to recovery of (*R*)-**120** with an increased enantiomeric excess of 8.9%, but by repeatedly running the reaction using the obtained product as the starting catalyst, the enantiomeric excess of the recovered product can be amplified to 88.1% over 7 rounds[†††].

### II.1.5 Dimerization

Chiral recognition is, in its purest sense, the ability of a chiral entity to discriminate between enantiomers of another.[127, 128] This is possible because interactions between enantiomers are diastereomeric.

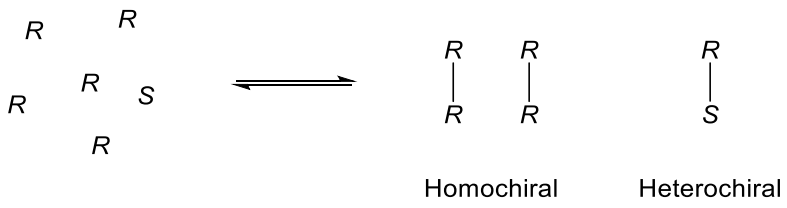



Figure 52 Binary association of chiral monomers can form hetero- and homo-dimers.

One way in which chiral recognition is commonly encountered is in the formation of dimers.[129-132] When a monomer is chiral, it is easy to see that two different dimers can form, one in which both monomers in the dimer are of the same handedness, and one in which they are of opposite handedness. These are referred to homo- and heterochiral dimers, respectively, and they are diastereomers of each other.

[†††] Much research has been carried out into the mechanism of the Soai reaction, but is outside of our scope[121, 126]

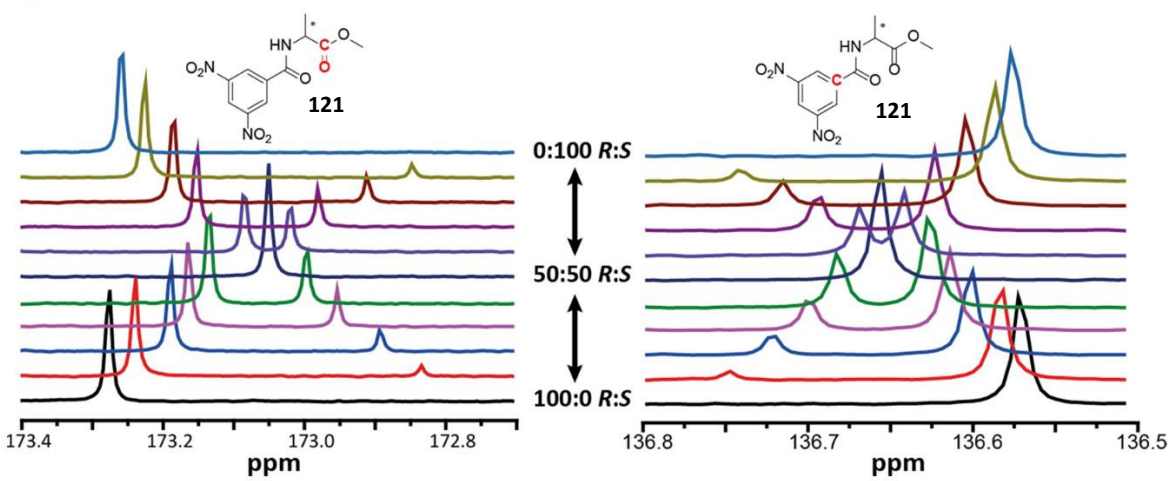



Figure 53 The SIDA effect observed for *N*-3,5-dinitrobenzoylalanine methyl ester as reported by Trapp. Reproduced from *Chem.Eur.J.* **2017**, 23, 5414[133]

One way in which the effect of such association become clear is in the case of self-induced diastereomeric anisochronism, SIDA.[133-136] This occurs when the formation of hetero- and homodimers (or higher order aggregates) in solution leads to distinct sets of NMR peaks. In a report from Trapp, the SIDA effect is astonishingly pronounced in the carbon NMR spectra of *N*-3,5-dinitrobenzoylalanine methyl ester (**121**) at varying enantiomeric excess (Figure 53). It can be seen that when enantiopure and racemic only one set of peaks are apparent, indicating exclusively heterochiral and homochiral dimers, respectively. At intermediate concentrations, however, two sets of well-defined peaks ($\Delta\delta > 1$ ppm for the carbonyl peak) are present, one for the homochiral dimer and one for the heterochiral dimer.[‡‡‡]

Far from being a niche observation, chiral recognition can be seen in a wide variety of chiral molecules which can participate in intermolecular interactions. The most relevant example to this work is that of BINOL.

[‡‡‡] Peaks in the spectra of scalemic mixtures have intermediate shifts due to exchange on the NMR timescale.

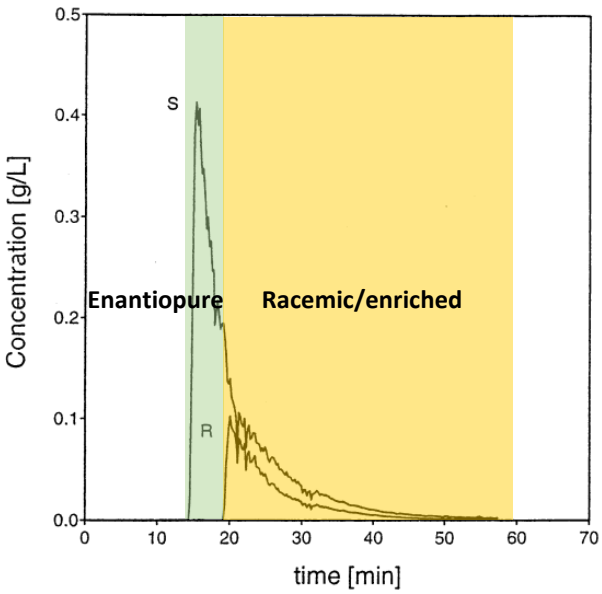


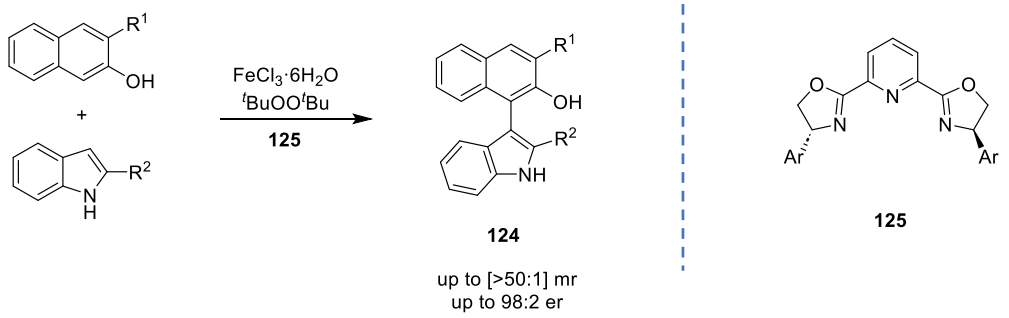

Figure 54 Disproportionation of enantioenriched (*R/S;* 80/20) BINOL can occur on achiral separation media. Reproduced from *J. Phys. Chem. A,* **2002,** 106, 10461.[137]

In the case of BINOL intermolecular hydrogen bonding between hydroxyl moieties gives rise to homo- and hetero-dimers. Interestingly, although the SIDA effect is absent or undetectable (i.e. just one set of peaks is seen in all NMR spectra), self-association is apparent in non-linear effects observed in polarimetric measurements and, most strikingly, in the ability for enantioenriched BINOL to "disproportionate" into enantiopure and racemic/enriched fractions on achiral separation media (Figure 54).[137-141]

It is clear from the wide range of effects which arise from self-association that the phenomenon is powerful and can greatly alter fundamental properties of chiral molecules.

## II.1.6 This Work

One longstanding focus of the Smith Group is the development of atropselective syntheses. In this vein, Dr Richard Surgenor developed an iron catalysed dehydrogenative cross coupling for the atropselective synthesis of indolyl-naphthyl atropisomers (**124**, Scheme 30).[142]




Scheme 30 Iron catalysed dehydrogenative atropselective cross coupling developed by Dr Richard Surgenor.

Routine characterisation of atropisomers within the group includes the determination of their barrier to inversion by erosion study. As per literature, the biaryl atropisomers produced are expected to enantiomerise according to a first-order rate law.

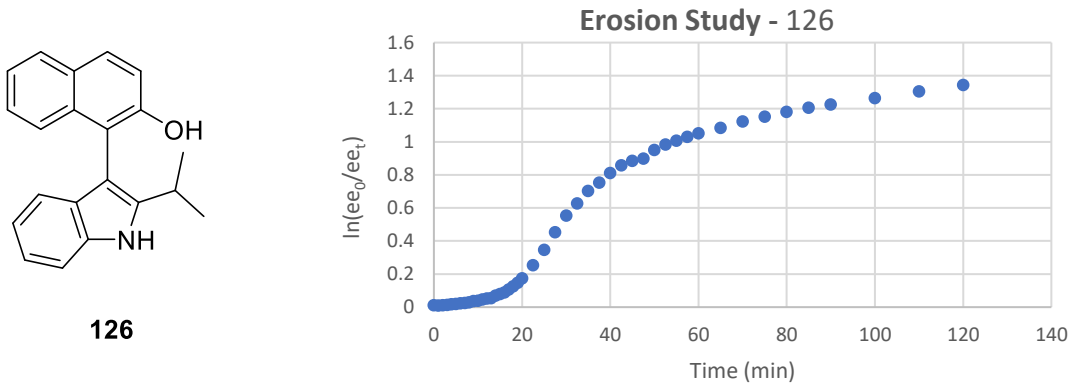



Figure 55 Erosion of enriched **126** at 80 °C in toluene proceeds in a non-first order manner. Erosion was monitored by chiral normal phase HPLC analysis of aliquots taken at predefined timepoints.

While analysing data collected from the erosion of compound **126**, it was found that **126** eroded at much lower temperatures than expected based on computation and experience

with similar scaffolds, and that a first order plot of the data did not yield a straight line (Figure 55). Rather the plotted data deviated strongly from the expected behaviour, with erosion of enantioenriched **126** appearing to erode slowly at first and then much faster.

This is of particular note given the importance of barriers in the use of atropisomers in any application. Attempts to locate similar effects in literature; however, were unsuccessful and so this work was initiated to determine the origin of the observed phenomenon.

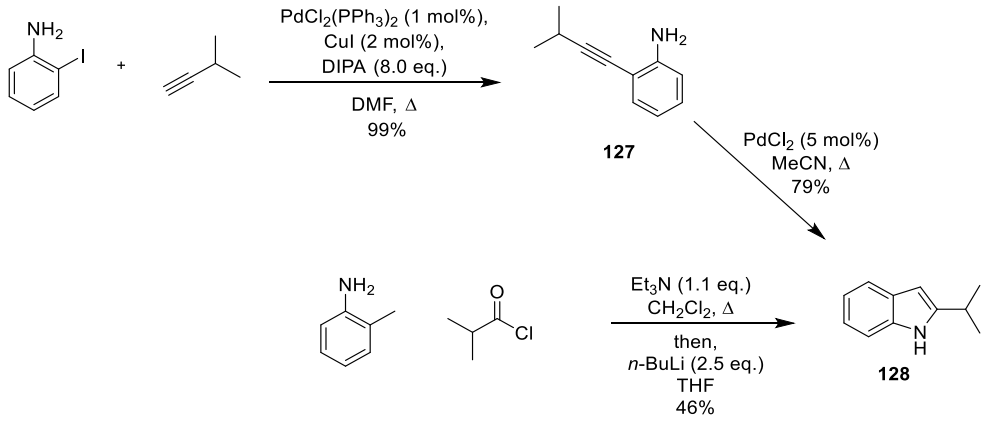
# II.2 Results and Discussion

## II.2.1 Aim

The aim of this project was to describe the underlying mechanism by which non-first order enantiomerisation of **126** occurs.

## II.2.2 Initial synthesis

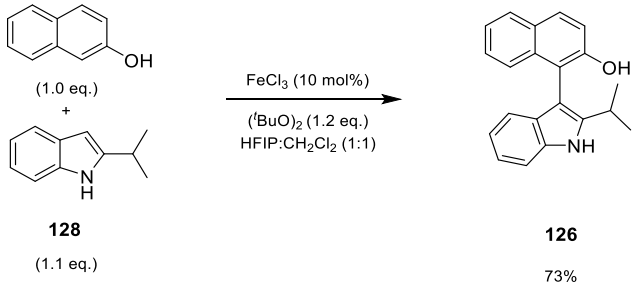
The initial focus of the project was to develop a method to acquire reproducible kinetic data. Access to enantiopure material was therefore a priority.




Scheme 31 Synthesis of 2-isopropyl indole, **128** is achieved by LaRock indole synthesis (top route) or by coupling of *o*-toluidine with *iso*butyryl chloride and subsequent *n*-BuLi mediated annulation.

Synthesis of 2-*iso*propyl indole could be achieved by two routes (Scheme 31). The first is by a Larock indole synthesis wherein intermediate **127** is formed by Sonogashira coupling of 2-iodoaniline and 3-methylbut-1-yne.[143] This is followed by a palladium mediated annulation to yield **128**. [142] The second route proceeds by amide coupling of 2-methyl aniline and *iso*butyryl chloride followed by treatment with *n*-butyl lithium to form **128**. Though the first route has a higher overall yield (78% vs 46%), the high cost of reagents and starting materials used in the

Larock synthesis and the speed with which **128** can be formed *via* the second route makes it an appealing alternative.




Scheme 32 Access to **126** *via* iron mediated cross-coupling.

Access to the desired racemic atropisomer, **126**, is then *via* a dehydrogenative iron mediated cross-coupling developed within the group by Dr Richard Surgenor (Scheme 32).[142]

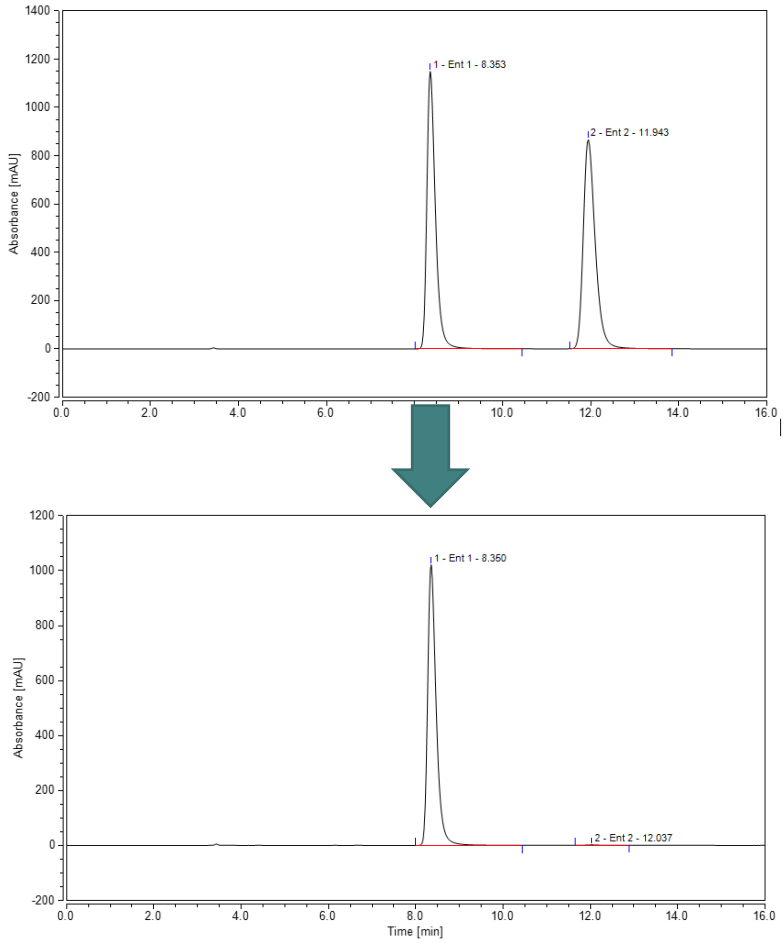



Figure 56 Resolution of **126** is by semi-preparative normal phase HPLC.

Access to enantiopure **126**, while trivial in theory and with access to appropriate resources, proved challenging in reality. Nonetheless, sufficient amounts of **126** (~100 mg) could be resolved to provide material (>99.5% enantiomeric excess) for further investigation.

## II.2.3 Data Gathering and Methodology

### II.2.3.1 Methodology Development

With sufficient enantiopure material in hand, the first hurdle was to develop a methodology which could generate data reproducibly.

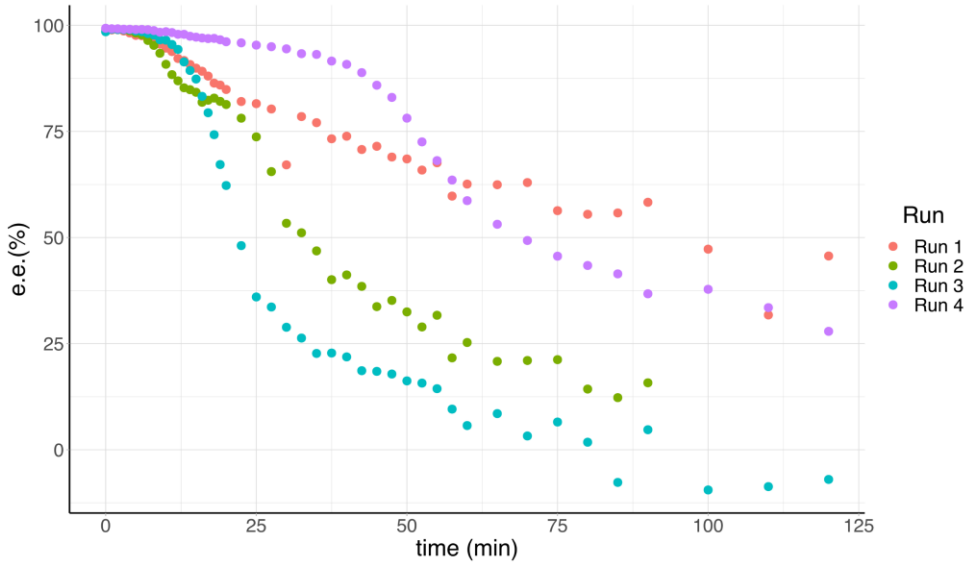



Figure 57 Initial attempts to study the enantiomerisation were irreproducible. Concentration: 0.2 M; temperature: 80 °C; solvent: toluene.

Initial attempts to led to wildly irreproducible data (Figure 57). Though a great many precautions were taken to ensure control, a number of issues were identified. Firstly, the temperature of the oil bath in which the samples were submersed for the kinetics runs was observed to fluctuate by approximately 1 °C despite a large thermal mass and adequate pre-equilibration. Secondly, the enantiomeric excess of a stock solution of **126** prepared to be used for all runs of a single concentration was observed to erode slowly over time, even when

stored at -18 °C. Thirdly, and finally, the solvent used for the erosion study (toluene) was observed to evaporate over the course of the study, with some runs drying out before conclusion.

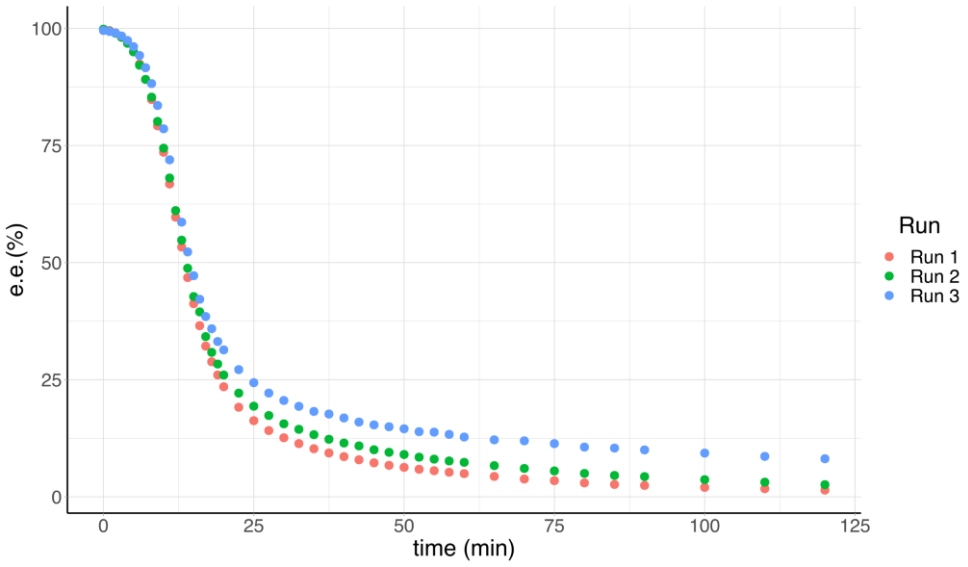



Figure 58 Reproducibility was gained using methodology changes. Concentration: 0.1 molal; temperature: 80 °C; solvent: toluene.

To combat these issues, a number of changes to the collection methodology were necessary. Firstly, to combat temperature fluctuations all apparatus (vial, vial holder, vial cap, stirrer bar) was preheated in the position it would be throughout the run. Secondly, solutions would be made up at the desired molality immediately before measurement. The use of molality in place of molarity allowed set masses to be pre-weighed into vials and stored at -18 °C until needed. Solvent could then be added immediately before commencement of the study. Additionally, once solvent was added to the solid sample the solution was vortexed for a fixed time at a fixed rpm to ensure homogeneity. Thirdly, and finally, aliquots were taken with a microlitre syringe through a 26s-gauge (~0.5 mm) hole pierced in a polypropylene cap which stayed in place throughout the study. The combination of all of these precautions allowed reproducible data to be recorded (Figure 58).

### II.2.3.2 Collected Data

With the new methodology in place data could be gathered reproducibly at a number of concentrations to facilitate analysis.[§§§]

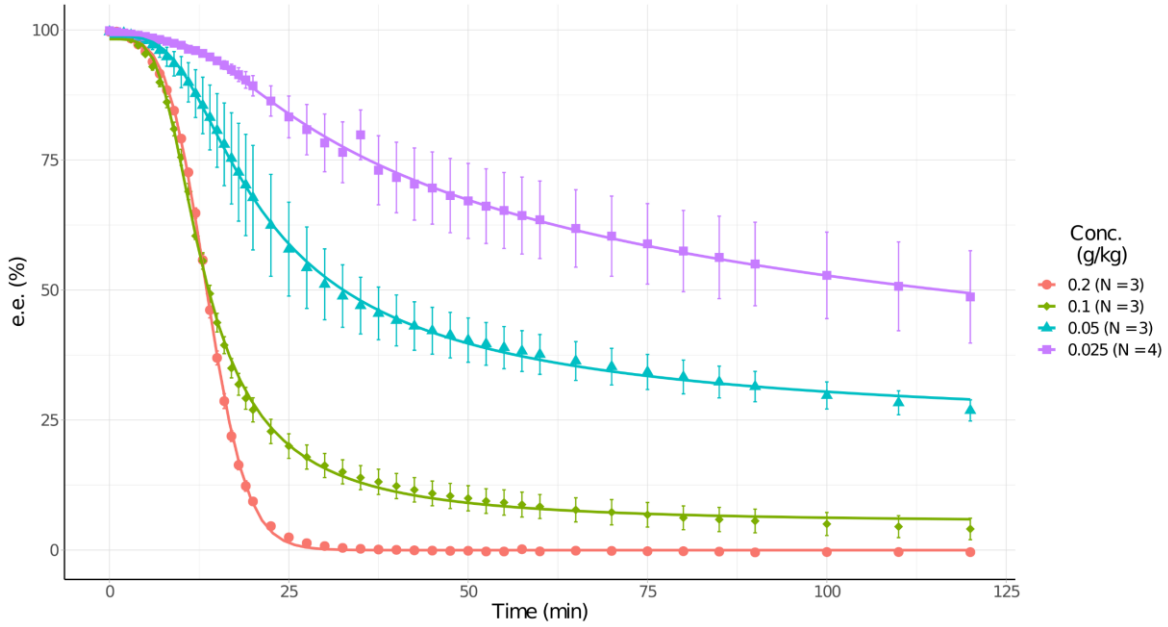



Figure 59 Data gathered across four concentrations in trip-/quadruplicate. Temperature:80 °C; solvent: toluene.

A strong concentration dependence is apparent in the data, but other than confirming deviation from the expected first order enantiomerisation process, the data in this form are difficult to interpret. As such, we sought a well-defined function which could fit the data[****].

$$y = h + \frac{h + i}{\left(1 + \left(\frac{x}{j}\right)^{k}\right)^{l}}$$

A five-parameter logistic curve above was found to fit well at all concentrations and was chosen for our initial analysis.

[§§§] For treatment of the data, please see Experimental p222

[****] Though we acknowledge that such a fit has no inherent "meaning", at this stage we merely sought a function which reproduce the sigmoidal shape observed.

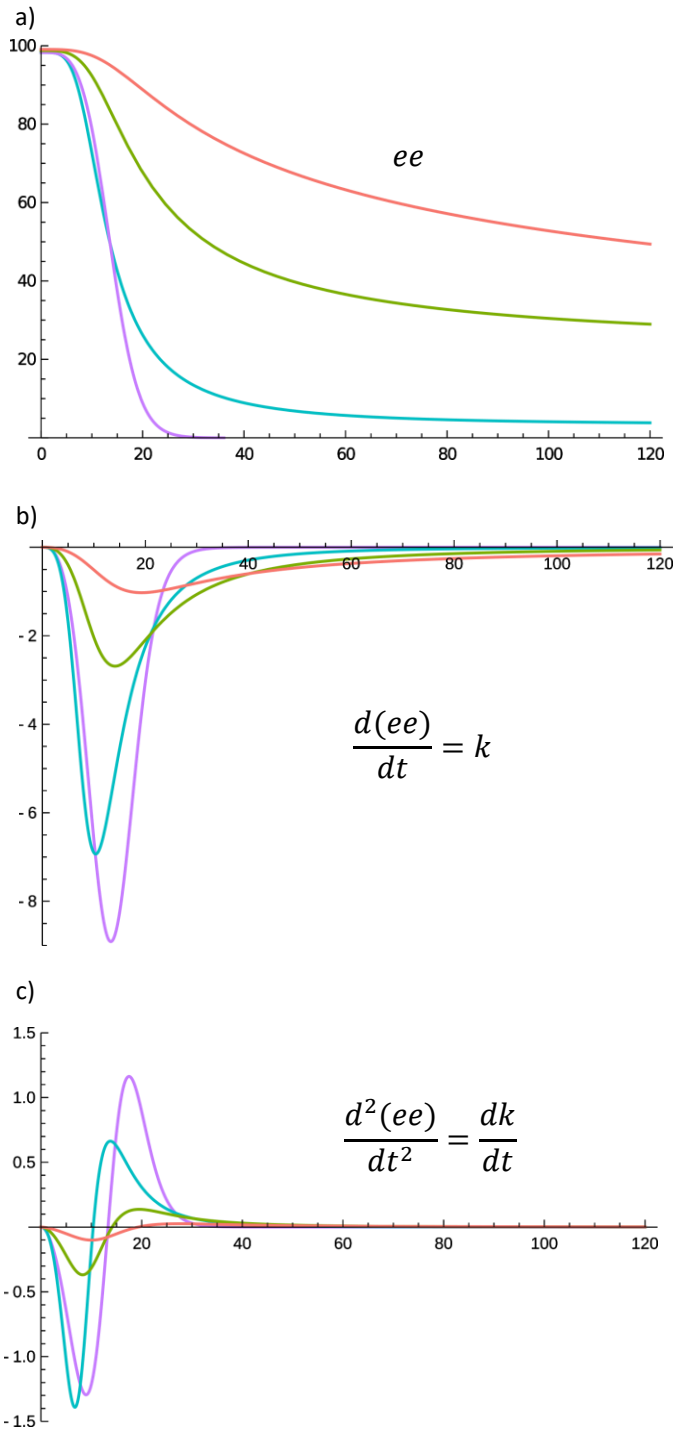



Figure 60 The fit (a) and its first (b), and second (c) derivatives.

While the closeness of the fit to the recorded data is clear, it is the derivatives of the curves which we were most interested in.

The first derivative, $\frac{d(ee)}{dt}$, is the rate at which the enantiomeric excess of the solution changes. As can be seen from the plot of this function, the peak rate of enantiomerisation increases as concentration increases. Additionally, the local minima, the points at which the rate of racemisation is highest, are relatively consistent, though the earliest peak seems to be for the 0.1 molal solution, which is unexpected.

Finally, the rate of change of the rate, $\frac{d^2(e.e.)}{dt^2}$, allows us to interpret acceleration and deceleration of racemisation. Here we see the turning points of the original fit as maxima and minima. While the minima, indicating the first turning point, or the transition to rapid racemisation are tightly clustered, the maxima, which represent the transition back to a curve of low slope, are distributed over a larger period of time, with the earliest peak again being for the 0.1 molal solution.

Though we acknowledge that these fits are merely the product of meaningless parameterisation, the trends that they make clear (i.e. the earliest maxima/turning points are not for the most concentrated solution) are nonetheless insightful.

### II.2.3.3 Meaningful Fits

As the pathway of the enantiomerisation is unknown, derivation of a rate law from first principles is not possible. Because of this, fitting our data in a meaningful way is almost impossible. Having said this, one common fit was appealing due to the similarity of its shape to our observed racemisation profile.

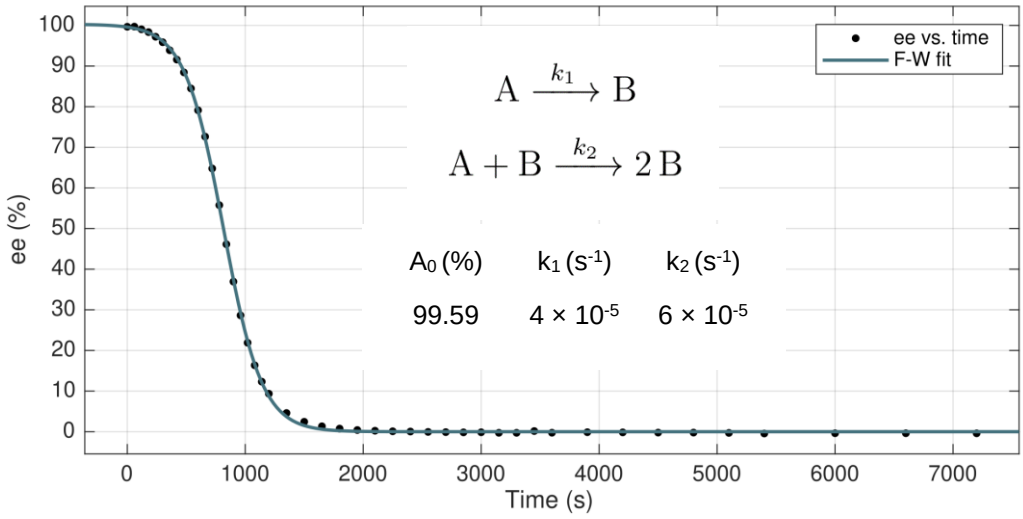



Figure 61 0.2 molal data fitted using the Finke-Watzky two-step mechanism. Data were collected at 80 °C in toluene.

The Finke-Watzky mechanism is an autocatalytic mechanism which consists of just two steps.[144] An initial first order reaction proceeds to form species B with rate constant $k_1$. B can then catalyse its own formation by a second order reaction with A which has rate constant $k_2$. This simple model fits the data recorded for the most concentrated solution (0.2 molal) with striking closeness ($R^2$ = 0.9999). Under our circumstances the meaning of $A_0$ and $k_1$ can seemingly be interpreted as the starting enantiomeric excess and the rate of first order

enantiomerisation. The meaning of $k_2$, however, is unclear but agrees with the supposition that some other process is causing rapid erosion of enantiomeric excess.

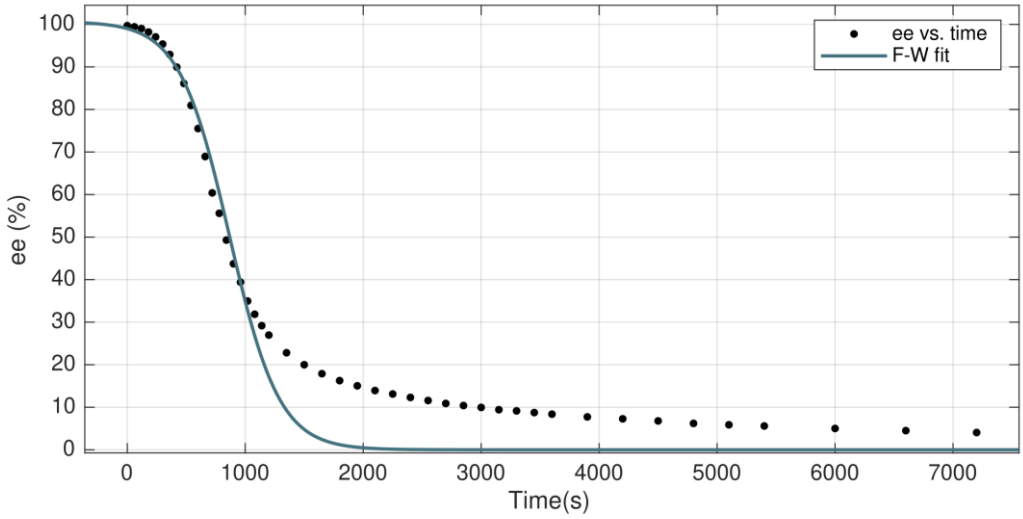



Figure 62 Fitting for concentrations other than 0.2 molal was unsuccessful. 0.1 molal fitting shown. Data were collected at 80 °C in toluene.

While the fit for the 0.2 molal kinetics runs is undeniable, attempts to fit further concentrations using this model failed to reproduce the observed tailing. Coupling this with the observation that the earliest turning points and maxima/minima were recorded not for the most concentrated (0.2 molal) solution, but for the second most concentrated (0.1 molal) solution may indicate that a complex mechanism or a change in rate limiting step may be at play.

### II.2.4 Evidence for Hydrogen Bonding

While characterisation of the racemisation profile is important to understanding our observations, we also sought chemical explanations for their origin.

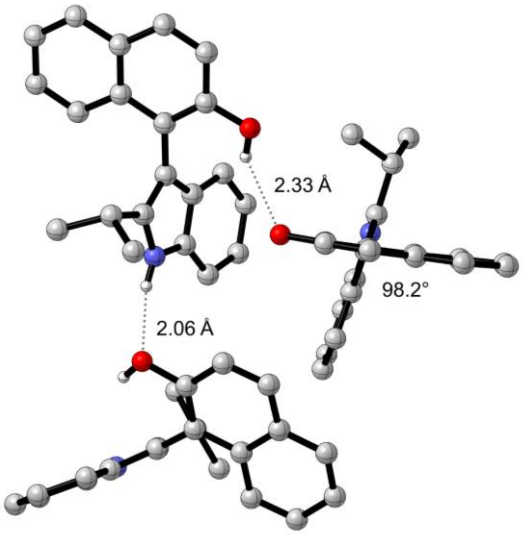



Figure 63 The single crystal X-ray structure of enantiopure **126** indicated the presence of two hydrogen bonds.

Crystallisation of enantiopure **126** at low temperature allowed for the measurement of its absolute stereochemistry and for the observation of its solid-state behaviour. The results of this measurement show a dimeric unit cell with a hydrogen bond between the indole *N*-H (donor) and the naphthol *O*- (acceptor) (Figure 63)[††††]. In addition to this, there appears to be an interaction between naphthol hydroxyl moieties. Though perhaps not close enough (2.33 Å) to deem a hydrogen bond, this interaction may still be of interest.

Though these observations are only indicative of the solid state, the presence of a hydrogen bond provides an avenue for investigation to continue.

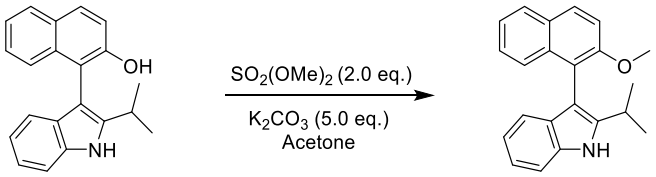
### II.2.4.1 Erosion Studies of Modified Substrates

As a probe of the importance of hydrogen bonding in the effects observed, we sought to modulate the hydrogen bonding ability of both the *N*-H and *O*-H moieties and investigate the enantiomerisation barriers of the resulting compounds.

[††††]In addition to the unit cell a third molecule has been added in Figure 63 for clarity

### II.2.4.1a The *O*-Methyl Analogue

The naphthol moiety of **126** was expected to be both the strongest hydrogen bond donor and acceptor. While modulation of an acceptor's ability can be complex, we hypothesised that the naphthol's donating ability could be easily curtailed by *O*-methylation.




**126** **129**

90%

Scheme 33 Synthesis of the *O*-methyl analogue, **129** was by methylation with dimethylsulphate and potassium carbonate in acetone.

The O-methylated analogue, **129**, was easily prepared by treatment of **126** with dimethysulfate. Access to enantiopure material was by semi-preparative normal phase chiral HPLC.

Initial attempts to observe the racemisation of **129** in toluene at 80 °C (the same temperature at which the other studies were carried out) led to no measurable erosion of enantiomeric excess over a period of four hours.

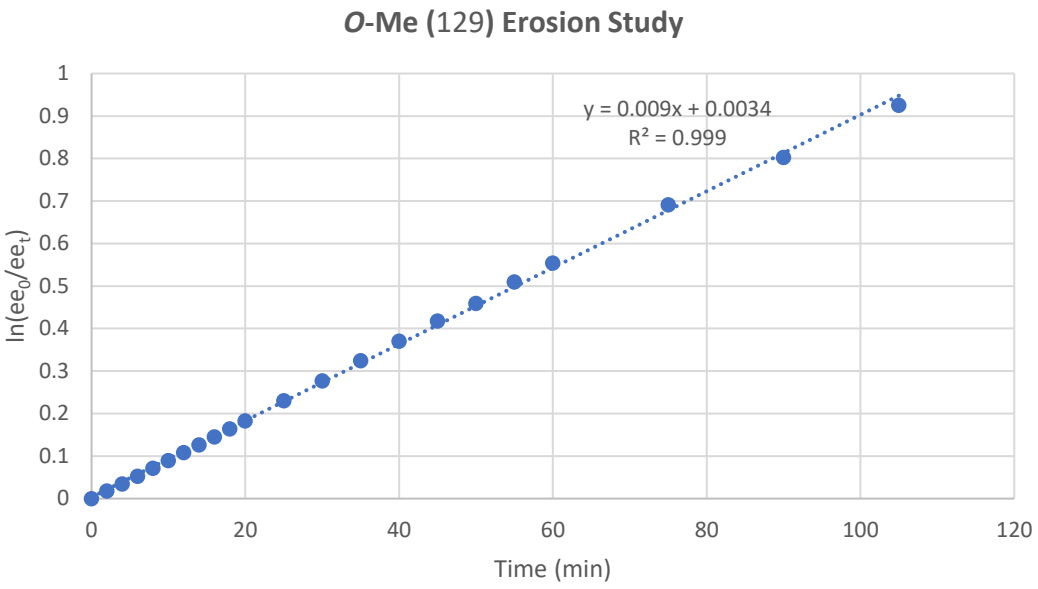


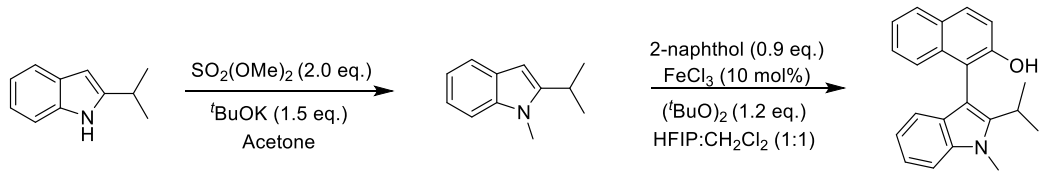

Figure 64 Racemisation Study of **129** in 1,2,4-trimethylbenzene at 155 °C. Concentration: 0.025 molal.

Erosion could only be observed on a practical timescale (1-4 hours) when the study solvent was changed to 1,2,4-trimethylbenzene and the temperature was raised to 155 °C. Under these conditions the sample could be eroded to approximately 40% ee in 105 minutes. Plotting the data according to a first order rate law yields a straight line ($R^2 = 0.999$), indicating a return to first order erosion and a barrier to enantiomerisation of 33.5 kcal $mol^{-1}$ (Figure 64). This corresponds to a half-life to racemisation of approximately 274 days at 80 °C, or 6,000 years at room temperature.

This return to first order erosion on modification of the naphthol moiety indicates that hydrogen bonding may well be the origin of the observed effects. Though modification was intended to stifle hydrogen bond donating ability, we recognise that methylation also impacts accepting ability and the steric bulk of the naphthol.

### II.2.4.1b The *N*-Methyl Analogue

In addition to modification of the naphthol moiety, we also sought to determine the effect of indole modification.




**128** **130** 71% **131** 43%

Scheme 34 Synthesis of the *N*-methyl analogue, **131** is by direct coupling of **131** with 2-naphthol.

Synthesis of the *N*-methyl analogue, while slightly more involved, was also easily achieved by first methylating indole **128** to yield **130**, which could then be directly coupled with 2-naphthol as before (Scheme 34). Access to enantiopure material was again by semi-preparative normal phase chiral HPLC.

Again, initial attempts to erode an enantiopure sample of **131** in toluene at 80 °C led to no measurable decrease in enantiomeric excess, and so further studies were conducted in 1,2,4-trimethylbenzene at 155 °C.

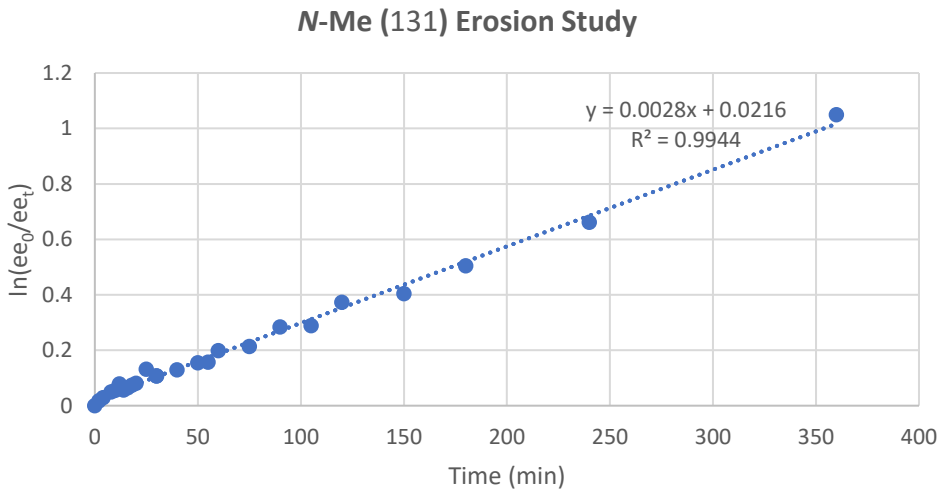



Figure 65 Erosion study of **131** in 1,2,4-trimethylbenzene at 155 °C. Concentration: 0.025 molal.

Erosion once again proceeded according to a first order kinetic regime under these conditions (Figure 65). Plotting the appropriate values yields a barrier of 34.5 kcal $mol^{-1}$ which corresponds to a half-life to racemisation of approximately 1,146 days at 80 °C and 32,000 years at 25 °C.

While the barriers measured for both modified substrates are not the exact same, they are in line with calculated barriers and expectations based on atropisomers with similar bulk around the steric axis. Most notable is that both show no measurable enantiomerisation at 80 °C, while **126** racemises under the same conditions on the timescale of minutes to hours. This provides strong evidence for the participation of both *O*-H and *N*-H moieties in the observed non-first order enantiomerisation.

### II.2.4.2 NMR Studies

To determine whether the hydrogen bonding observed in the solid state was also present in the solution state we turned to NMR.[‡‡‡‡]

#### II.2.4.2a Dilution Study

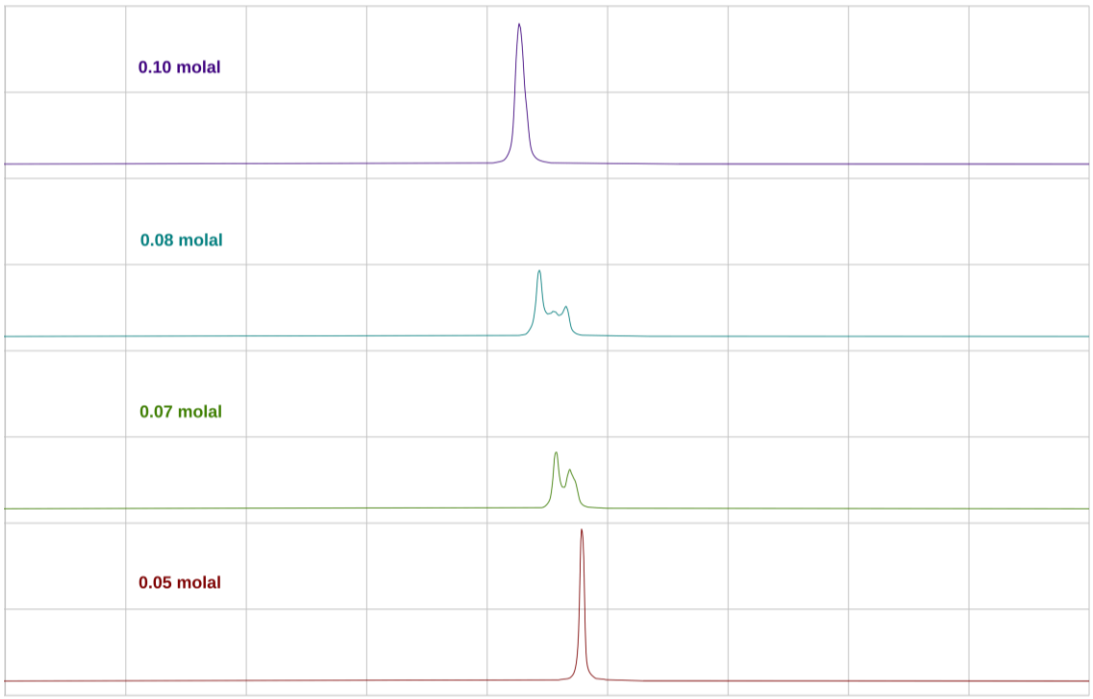



Figure 66 NMR dilution study of **126**. The *O*-H shift resonance is shown. Solvent: toluene-$d_8$; temperature: 25 °C. Concentrations are volumetric equivalents of molalities in protio toluene.

An initial dilution study carried out in toluene-$d_8$ showed that both the *O*- and *N*-H shifts varied with concentration, indicating that hydrogen bonding is present in toluene solution (Figure 66).

[‡‡‡‡] At this stage it is worth noting that SIDA was not apparent in the NMR spectra of **126**. In all cases the same set of well resolved peaks were recorded.

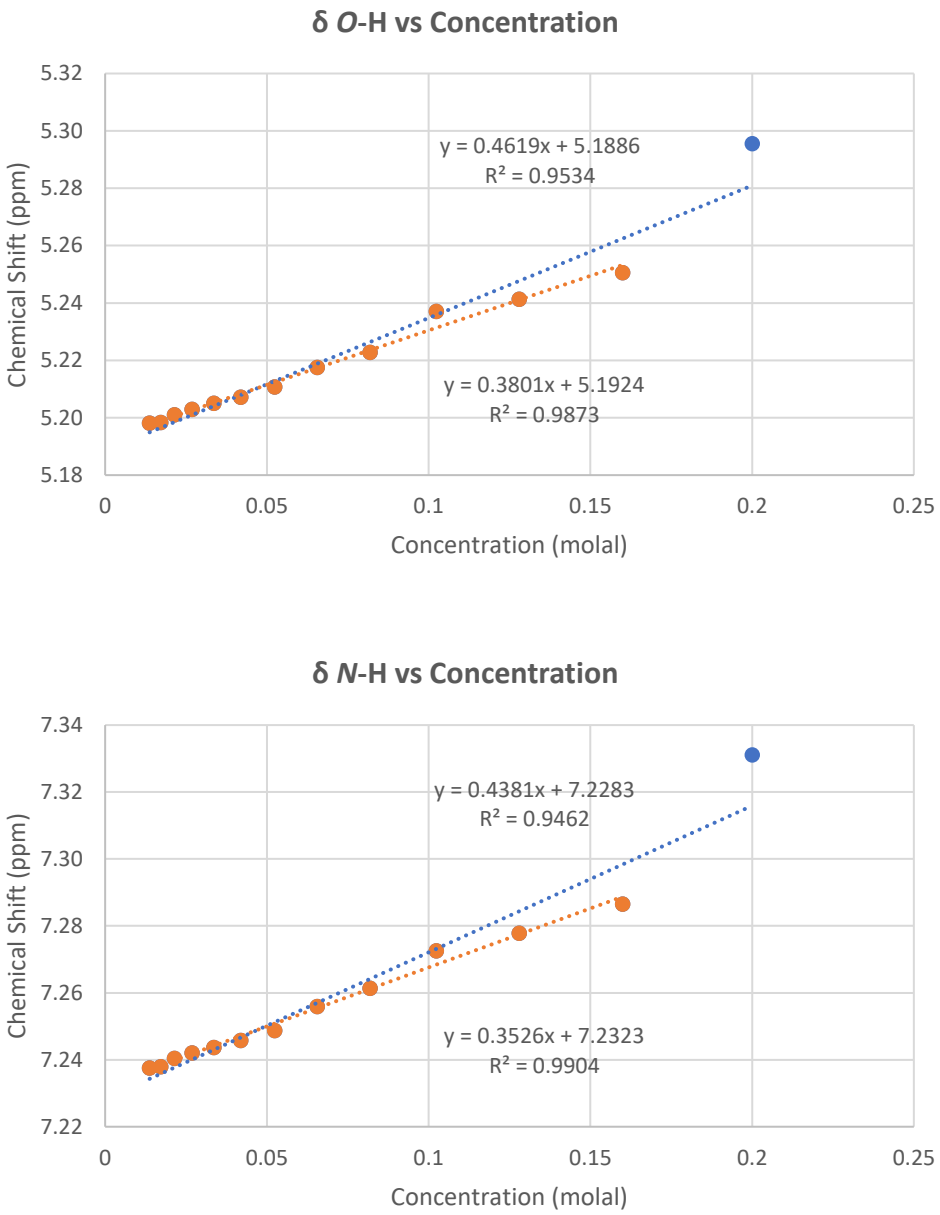



Figure 67 NMR dilution study for **126**. Top - *O*-H shift and bottom - *N*-H shift. Solvent: toluene-d8; temperature: 25 °C. Concentrations are volumetric equivalents of molalities in protio toluene.

Plots of chemical shift (δ) vs concentration (molal) for both *O*-H and *N*-H, while somewhat fatuous, show a linear relationship between chemical shift (δ) and concentration. Interestingly, for both O-H and N-H, the data recorded for the most concentrated sample (0.2 molal, blue) appears to be an outlier when compared to other datapoints (orange).

### II.2.4.2b DOSY

A common phenomenon observed in BINOLs is the formation of hydrogen bonded dimers in solution. Encouraged by the indication of hydrogen bonding in solution, we sought to determine whether well-defined dimers were also present in our system.

Detection of dimers in solution is possible through the use of diffusion ordered NMR spectroscopy (DOSY). By using this technique, a diffusion coefficient for each peak in the spectrum can be measured. As diffusion can be related to a species' mass and shape, the mass of the species can be approximated.[145] A calculated mass much more than the monomeric mass indicates the presence of dimers in solution.

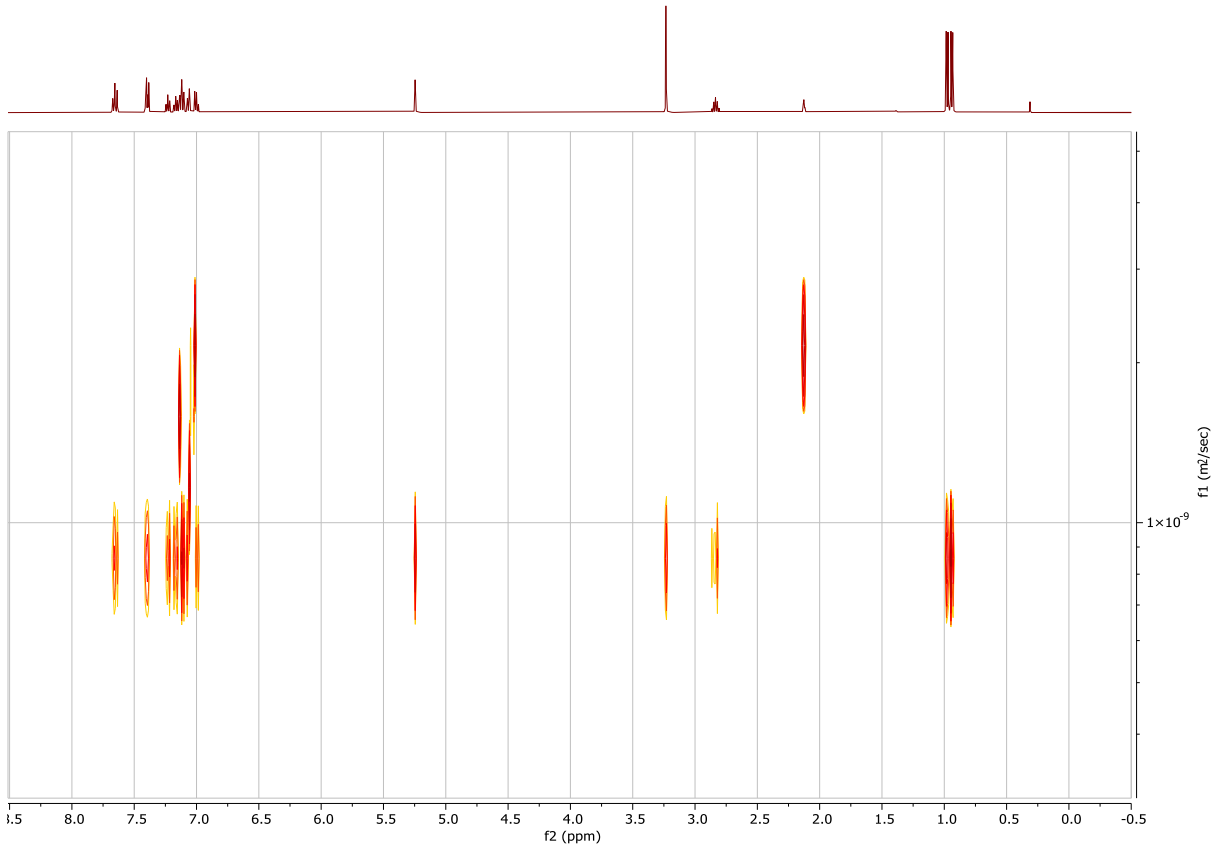



Figure 68 **131** (*N*-Me) DOSY results. Solvent: toluene-$d_8$; temperature: 25 °C; molality: 0.05 molal. Concentrations are volumetric equivalents of molalities in protio toluene. See Experimental p S-122 for more details.

Our initial measurements focussed on validation of the method for our system using *N*-methyl derivative **131** as racemisation of this substrate was observed to proceed *via* first order enantiomerisation. A diffusion coefficient of approximately $1 \times 10^{-9}\, m^2\, s^{-1}$ was measured for **131**. This value can be converted to an approximate mass using calibrations developed by Stalke, resulting in a mass of approximately 289 Daltons.[145] Though lower than the actual molar mass of 301, this value is well within the calculated error (± 9%), indicating that **131** likely exists as a monomer in solution.

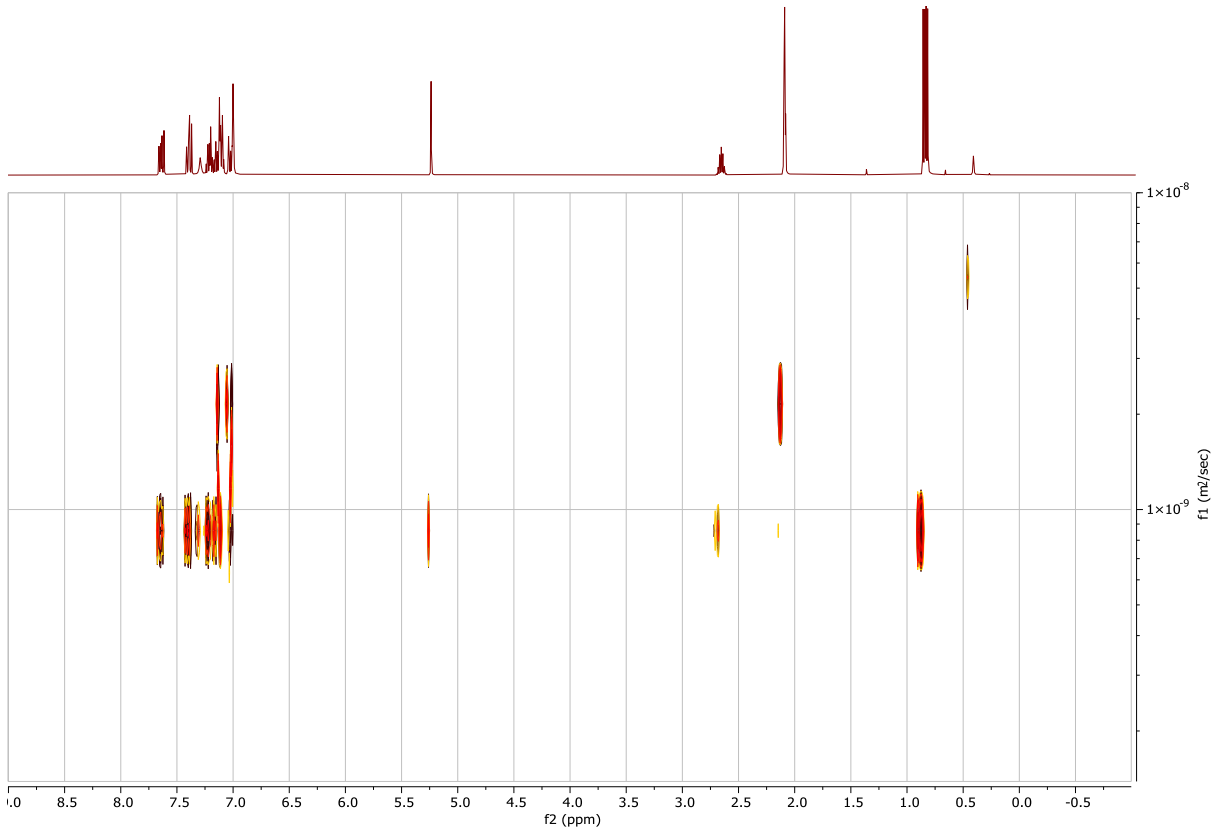



Figure 69 Overlay of enantiopure and racemic DOSY spectra of **126**. Solvent: toluene-$d_8$; temperature: 25 °C; molality: 0.05 molal. Concentrations are volumetric equivalents of molalities in protio toluene. See Experimental p S-122 for more details.

Measurement of both racemic and enantiopure **126** samples in the same manner resulted in smaller diffusion coefficients ($9.0 \times 10^{-10}\, m^2\, s^{-1}$ for racemic **126** and $8.5 \times 10^{-10}\, m^2\, s^{-1}$ for enantiopure **126**). Using the internal calibration method developed by Stalke, these values correspond to masses of 386 and 412 daltons, respectively. Both values

are significantly greater than the molar mass, 301 daltons, and indicate the presence of dimers (or higher order aggregates) in solution.

$$\mathrm{R} + \mathrm{R} \underset{k_1}{\overset{k_1}{\rightleftharpoons}} \mathrm{RR}$$

$$\mathrm{S} + \mathrm{S} \underset{k_1}{\overset{k_1}{\rightleftharpoons}} \mathrm{SS}$$

$$\mathrm{R} + \mathrm{S} \underset{k_2}{\overset{k_2}{\rightleftharpoons}} \mathrm{RS}$$

Figure 70 Dimer formation

Because of symmetry, the homochiral RR and SS dimers must form and dissociate at the same rates, but the heterochiral RS dimer, their diastereomer, needs not.

Based on the average masses measured using DOSY, it is possible to approximate the proportions of monomer and dimer present in solution as 63% and 37%, respectively.[§§§§]

$$\mathrm{R} + \mathrm{R} \rightleftharpoons \mathrm{RR}$$

$$k_{eq,homo} = \frac{[RR]}{[R] \cdot [R]}$$

In the case of the enantiopure sample, the equilibrium constant is easily calculated based on the mole fractions of monomer and dimer to yield a value of 0.93. As we start our erosion studies with enantiopure **126** in toluene solution, this equilibrium value can be used to help understand our starting concentrations of dimer and monomer.

[§§§§] As the measured masses are only marginally higher than the monomeric mass, the chances of higher order oligomers forming is vanishingly small.

Using the mass calculated from the racemic sample to determine equilibrium constants is remarkably more complex. In our case, it suffices to conclude that that the reduction in average mass indicates that formation of the heterodimer in solution is less favourable than formation of the homodimer.

### II.2.4.3 Hydrogen Bonding Solvents

While we had established that the non-linear enantiomerisation pathway could be stopped by methylation of either *N*-H or *O*-H moieties, these modifications do not just affect the hydrogen bonding ability of the moieties. We therefore sought to explore more subtle ways to disrupt hydrogen bonding in solution.

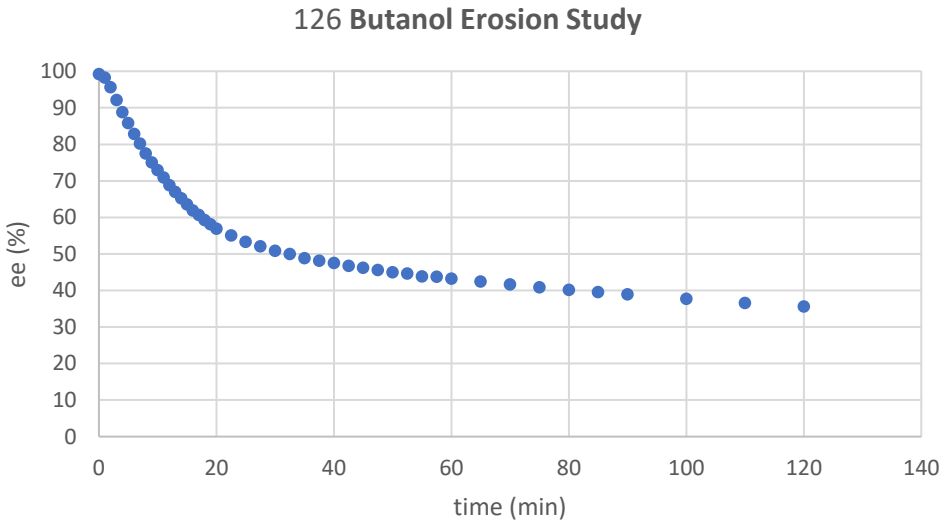



Figure 71 Erosion study of **126** in butanol (0.2 molal) at 80 °C.

Carrying the erosion study out in butanol, a protic moderately hydrogen bonding solvent produced a similar racemisation profile to that recorded in toluene, though complete racemisation was not observed on the study timescale. This could indicate a change in mechanism or possibly a dependence of the observed effect on equilibria between hydrogen bond donors and acceptors.

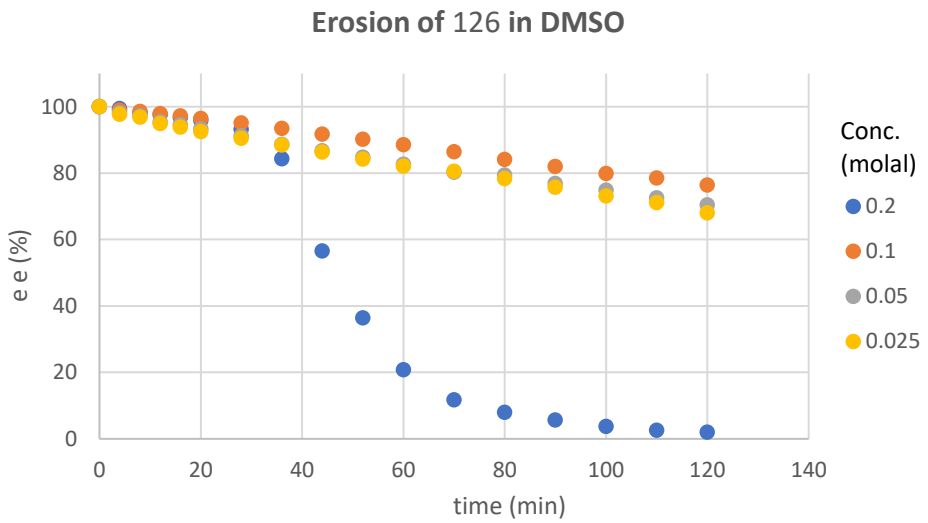



Figure 72 Racemisation study of **126** in DMSO at 155 °C.

To investigate the effect of a strongly hydrogen bonding solvent, an erosion study was carried out in DMSO. Interestingly, at low concentrations (0.1, 0.05, 0.025 molal) racemisation proceeds slowly, but at high concentration (0.2 molal) the enantiomeric excess erodes slowly at first, then rapidly, as with earlier studies carried out in toluene (Figure 72).

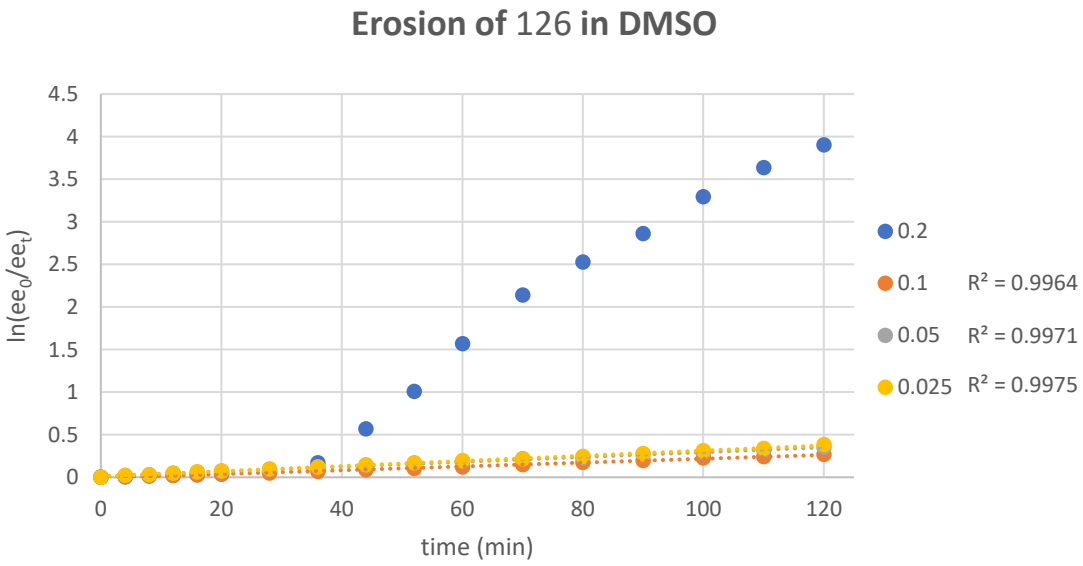



Figure 73 First order plot for racemisation of **126** in DMSO at 155 °C.

Plotting the data according to a first order rate law indicates that at low concentrations enantiomerisation occurs by the expected first order pathway with a barrier of approximately

34.5 kcal mol$^{-1}$ (Figure 73). This barrier is in line with that measured for the *O*- and *N*-methyl derivatives (33.5 and 34.5 kcal mol$^{-1}$, respectively). For the highest concentration; however, enantiomerisation appears to proceed *via* the unknown non-first order pathway that we are investigating.

Though far from a perfect probe of the effects of hydrogen bonding, the results of these studies show that a very strongly hydrogen bonding solvent can suppress non-first order enantiomerisation. More importantly though, a sufficiently high concentration of **126** can restore non-first order behaviour despite a greater than 50-fold excess of DMSO.

#### II.2.4.4 Spiking

With the observation that strongly hydrogen bonding solvents can disrupt the non-first order pathway, we sought to investigate whether inclusion of 2-naphthol or indole could also disrupt the pathway.

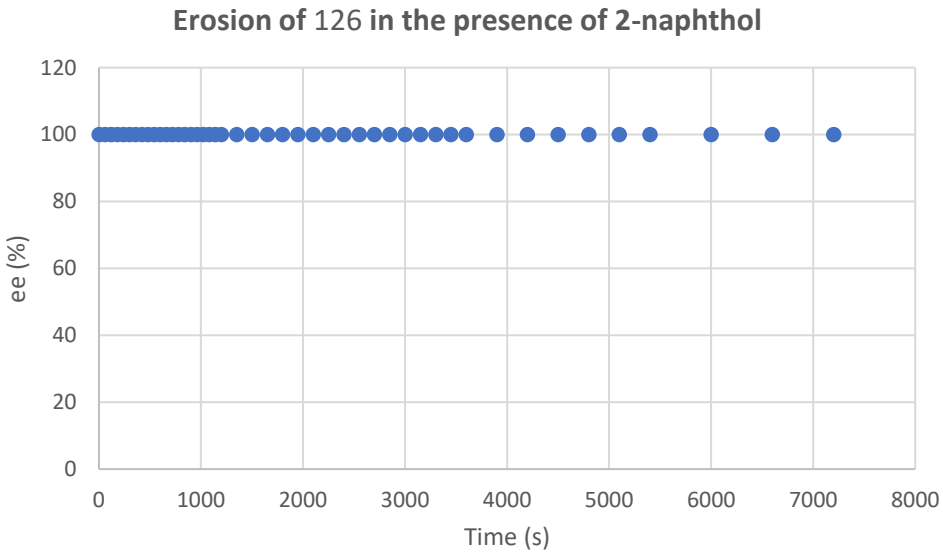



Figure 74 Erosion of **126** (0.025 molal) in the presence of 2-naphthol (0.175 molal) at 80 °C in toluene.

Indeed, inclusion of a large excess of naphthol (7 eq.) was sufficient to completely halt the alternate enantiomerisation pathway. As with the DMSO study, this may indicate that just the

presence of sufficiently strong intermolecular hydrogen bonds is sufficient to disrupt the non-first order pathway.

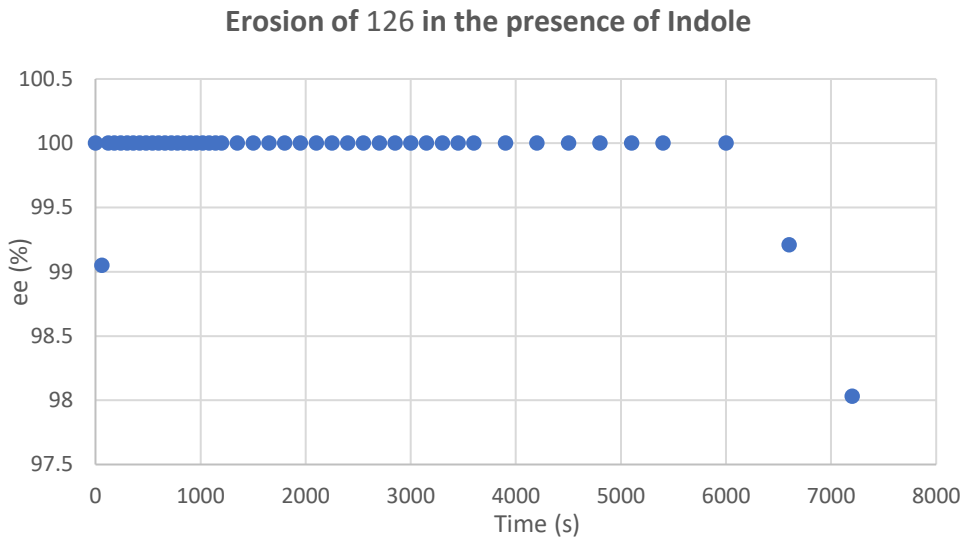



Figure 75 Erosion of **126** (0.025 molal) in the presence of indole (0.175 molal) at 80 °C in toluene.

When the same excess of indole was added in a separate study, erosion was again significantly slowed, but increased toward the end of the study (Figure 75). Although not entirely clear, this could be indicative of less effective inhibition of the alternative pathway in comparison to 2-naphthol rather than inability to inhibit or enable the pathway.

### II.2.5 Possible Models

While the experimental observations made are invaluable in unravelling the pathway by which enantiomerisation occurs, none of the observations point to a definitive explanation for our observations on a molecular level (other than the invocation of hydrogen bonds). We therefore had to consider possible explanations for the observed enantiomerisation based on experience of known phenomena and barrier modulations.

It is important to note that the pathways presented are just a selection of those considered. Other pathways were dismissed for their inability to explain different aspects of our observations (strong concentration dependence, the lag and saturation phases, symmetry, etc) and are omitted only for brevity.

At this stage it may be useful to summarise the observations thus far:

| **Experiment** | **Observation** |
|---|---|
| Erosion | Sigmoidal curve shape could indicate autocatalysis |
| Crystal Structure | Presence of hydrogen bonds |
| Methylation | Modification of either *N*-H or *O*-H moieties restores first order behaviour |
| DOSY | Dimer formation more favourable at high enantiomeric excess |
| H-bonding solvents | Enantiomerisation pathway is a function of both concentration and strength of hydrogen bond acceptors/donors |

### II.2.5.1 The Boundary Case

Though confident that the reaction exhibits autocatalytic or autoinductive characteristics, the remarkable fit of the Finke-Watzky model merits further investigation.

$$\mathrm{A} \xrightarrow{k_1} \mathrm{B}$$

$$\mathrm{A} + \mathrm{B} \xrightarrow{k_2} 2\,\mathrm{B}$$

The first step in the two-step model is a first order reaction. Though at first it seems that this step should represent classical monomeric first order enantiomerisation, the rate constant for this step is several orders of magnitude greater than we would expect based on the rates measured for both the *N*-Me analogue (**131**) and **126** in DMSO (fitted $k_1$ = 4 x $10^{-5}$ $s^{-1}$, expected $k_1$ based on other measurements = 7 x $10^{-9}$ $s^{-1}$).

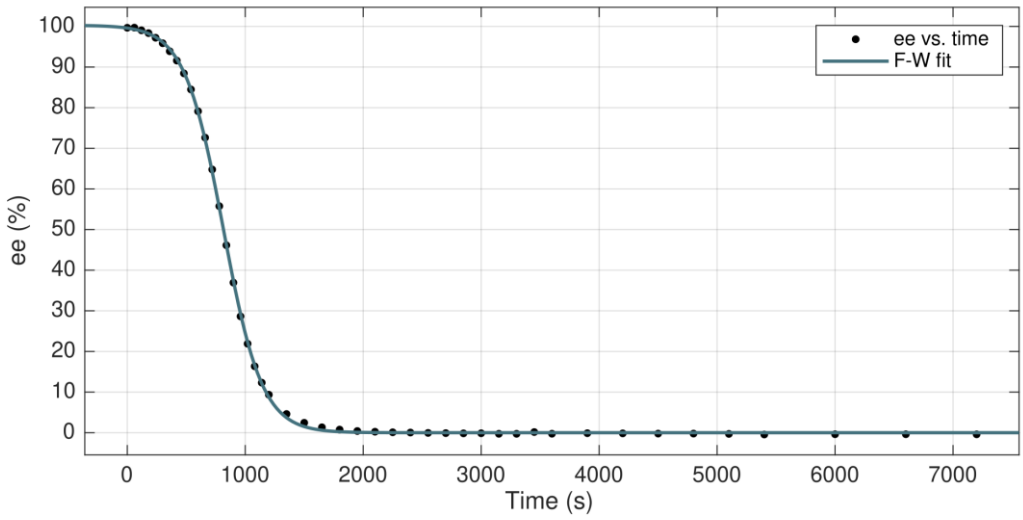



Figure 76 the Finke-Watzky fit for 0.2 molal. Data recorded at 80 °C in toluene.

Because of the large difference in rate constant, it is highly unlikely that the first order inversion process we are observing is the monomeric barrier. Rather, this first order inversion may be indicative of a different process: diastereomerisation.

#### II.2.5.1a Diastereomerisation

To try to explain how this simple model can emulate our observed racemisation profiles, we need to look at the system of elementary steps which may be active. We will first focus on the observed first order step.

$$\mathrm{R} \underset{k_1}{\overset{k_1}{\rightleftharpoons}} \mathrm{S} \qquad (\text{eq. } 7)$$

$$\mathrm{R} + \mathrm{R} \underset{k_{2'}}{\overset{k_2}{\rightleftharpoons}} \mathrm{RR} \qquad (\text{eq. } 8)$$

$$\mathrm{S} + \mathrm{S} \underset{k_{2'}}{\overset{k_2}{\rightleftharpoons}} \mathrm{SS} \qquad (\text{eq. } 9)$$

$$\mathrm{R} + \mathrm{S} \underset{k_{3'}}{\overset{k_3}{\rightleftharpoons}} \mathrm{RS} \qquad (\text{eq. } 10)$$

$$\mathrm{RR} \underset{k_{4'}}{\overset{k_4}{\rightleftharpoons}} \mathrm{RS} \underset{k_4}{\overset{k_{4'}}{\rightleftharpoons}} \mathrm{SS} \qquad (\text{eq. } 11)$$

From our measured monomeric enantiomerisation barrier, we can reasonably approximate $k_1$ as 0 at 80 °C (calculated $t_{½}$ ≈ 3.5 years). In the limit of high concentration, it seems that we can also reasonably make use of an equilibrium approximation wherein consumption of the homodimer is slow compared to the equilibrium, making its concentration approximately constant (at least for early t).

$$\mathrm{RR} \xrightarrow{k_1} \mathrm{RS} \xleftarrow{k_1} \mathrm{SS} \qquad (\text{eq } 13)$$

The combination of these assumptions leaves us with eq 13 as the observed first order process. Though the process will be reversible, we obtain a net rate from our fit.

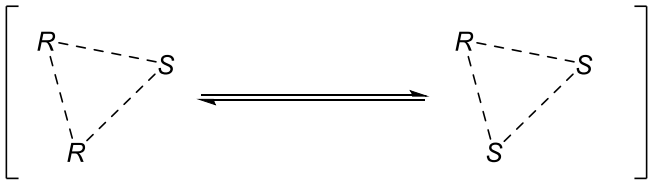
#### II.2.5.1b The Autocatalytic Step

While our assumption that diastereomerisation is the first order process we are observing seems robust, we still have very little information about the autocatalytic step. With the

assumption that we are observing autocatalysis (or autoinduction) two main possibilities for the origin of the effect present themselves: a trimeric (dimer + monomer) interaction or a tetrameric (dimer + dimer) interaction.

### Trimeric

The first possibility for the catalytic step is a barrier lowering interaction between a dimer and a monomer.




**132** **133**

Figure 77 Trimeric barrier modulation may be by reversible interconversion of **132** and **133**.

For a lag period to be present, we can rule out the activity of a homotrimer, and are left with a trimer composed of two molecules of one enantiomer and one of the other. In the same way that diastereomerisation can occur, we can envision the two possible trimers interconverting. While the forward and backward rates for this interconversion will necessarily be equal and opposite, the interconversion will lead to racemisation in the same way that the monomeric enantiomerisation does.

The creation of this interaction in solution could be from two distinct combinations: a heterodimer and a monomer of any handedness, or a homo dimer and a monomer of the opposite handedness. In addition to this, if the pathway does proceed *via* **132/133**, then we expect that the breaking up of the interaction could produce either a homodimer and a monomer of the other handedness, or a heterodimer and a monomer of either handedness.

$$\mathrm{RS} + \mathrm{R} \underset{k_{5'}}{\overset{k_5}{\rightleftharpoons}} \mathrm{RS} + \mathrm{S} \qquad \text{(eq. 14)}$$

$$\mathrm{RS} + \mathrm{R} \underset{k_{6'}}{\overset{k_6}{\rightleftharpoons}} \mathrm{SS} + \mathrm{R} \qquad \text{(eq. 15)}$$

$$\mathrm{RR} + \mathrm{S} \underset{k_{7'}}{\overset{k_7}{\rightleftharpoons}} \mathrm{RS} + \mathrm{S} \qquad \text{(eq. 16)}$$

$$\mathrm{RR} + \mathrm{S} \underset{k_{8'}}{\overset{k_8}{\rightleftharpoons}} \mathrm{SS} + \mathrm{R} \qquad \text{(eq. 17)}$$

Formulating these steps as equations leads us to recognise symmetry in these elementary steps, thereby allowing for some simplification. By symmetry, the forward reaction of eq. 15 is the same as the backward reaction of equation 16, meaning that $k_6$ = $k_{7'}$. Similarly, the backward reaction of eq. 15 is the same as the forward reaction of eq. 16, meaning that $k_{6'}$ = $k_7$.

$$\mathrm{R} + \mathrm{R} \underset{k_{2'}}{\overset{k_2}{\rightleftharpoons}} \mathrm{RR} \qquad \text{(eq. 8)}$$

$$\mathrm{S} + \mathrm{S} \underset{k_{2'}}{\overset{k_2}{\rightleftharpoons}} \mathrm{SS} \qquad \text{(eq. 9)}$$

$$\mathrm{R} + \mathrm{S} \underset{k_{3'}}{\overset{k_3}{\rightleftharpoons}} \mathrm{RS} \qquad \text{(eq. 10)}$$

$$\mathrm{RR} \underset{k_{4'}}{\overset{k_4}{\rightleftharpoons}} \mathrm{RS} \underset{k_4}{\overset{k_{4'}}{\rightleftharpoons}} \mathrm{SS} \qquad \text{(eq. 11)}$$

$$\mathrm{RS} + \mathrm{R} \underset{k_{5'}}{\overset{k_5}{\rightleftharpoons}} \mathrm{RS} + \mathrm{S} \qquad \text{(eq. 14)}$$

$$\mathrm{RS} + \mathrm{R} \underset{k_{6'}}{\overset{k_6}{\rightleftharpoons}} \mathrm{SS} + \mathrm{R} \qquad \text{(eq. 15)}$$

$$\mathrm{RR} + \mathrm{S} \underset{k_6}{\overset{k_{6'}}{\rightleftharpoons}} \mathrm{RS} + \mathrm{S} \qquad \text{(eq. 16)}$$

$$\mathrm{RR} + \mathrm{S} \underset{k_{8'}}{\overset{k_8}{\rightleftharpoons}} \mathrm{SS} + \mathrm{R} \qquad \text{(eq. 17)}$$

Making these substitutions, leaves us with equations 8-11 and 14-17 to describe our system.

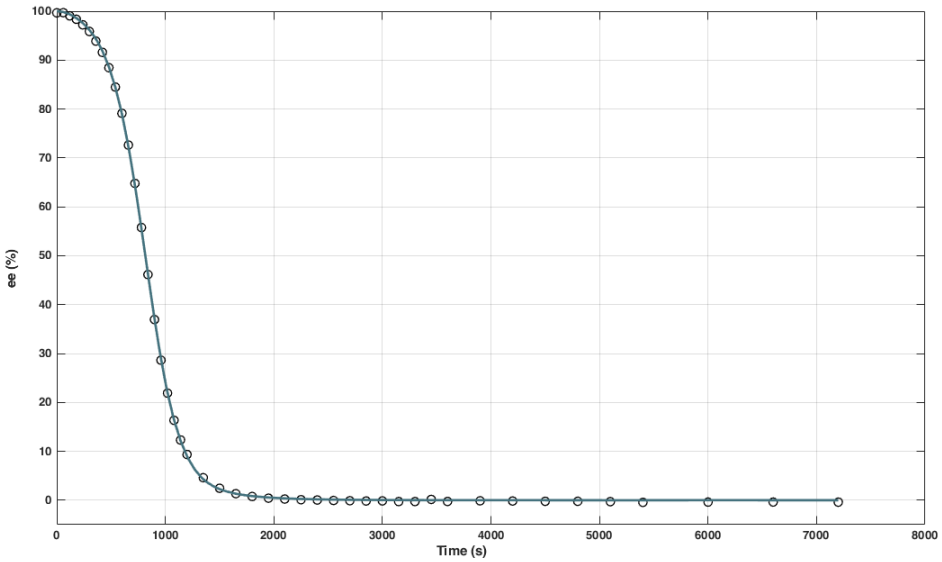



Figure 78 Fitting of the trimeric model closely matches experimental data.

Simulation and fitting of this model to our data provides a close fit. It is worth noting, however, that given that we are using many parameters to fit to just one observable, fitting at this stage simply indicates that the proposed regime could be consistent with the observed phenomenon. It is also worth noting, that though we have considered a trimer wherein all intermolecular interactions are equal, pathways where this does not occur were also modelled, but are not discussed.

## Tetrameric

In addition to a trimeric interaction leading to barrier modulation, a tetrameric interaction between two dimers is possible.

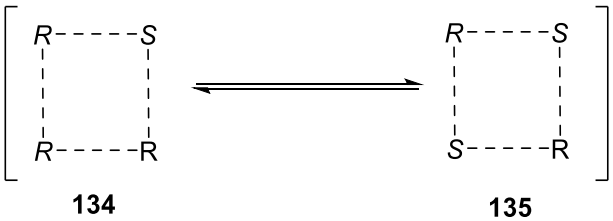



Figure 79 Possible tetrameric interaction may explain the observed effects by reversible interconversion of **134** and **135**.

Again, as we observe an induction period, we can disregard the possibility of a tetrameric interaction occurring between to homodimers. We are then left with the possibility of an

interaction between a homodimer and a heterodimer (**134**) which could lead to the formation of a tetramer composed of two heterodimers (**135**) (Figure 79). Analogous to the dimeric diastereomerisation, the forward and reverse reactions need not have the same rate constant because **134** and **135** are diastereomers of each other.

This possibility is particularly appealing as the preference for **134** to diastereomerise to **135** seems chemically intuitive, the interaction leads to a local decrease in enantioenrichment, and dissociation of **135** to form two heterodimers renders the regime autocatalytic.

$$\mathrm{RR} + \mathrm{RS} \underset{k_{-2}}{\overset{k_2}{\rightleftharpoons}} 2\,\mathrm{RS} \underset{k_2}{\overset{k_{-2}}{\rightleftharpoons}} \mathrm{SS} + \mathrm{RS} \qquad (\mathrm{eq}\ 15)$$

Equation 15 describes this autocatalytic step wherein heterodimer (RS), produced by first order diastereomerisation, is the autocatalyst.

$$\mathrm{R} + \mathrm{R} \underset{k_{2'}}{\overset{k_2}{\rightleftharpoons}} \mathrm{RR} \qquad (\mathrm{eq.}\ 8)$$

$$\mathrm{S} + \mathrm{S} \underset{k_{2'}}{\overset{k_2}{\rightleftharpoons}} \mathrm{SS} \qquad (\mathrm{eq.}\ 9)$$

$$\mathrm{R} + \mathrm{S} \underset{k_{3'}}{\overset{k_3}{\rightleftharpoons}} \mathrm{RS} \qquad (\mathrm{eq.}\ 10)$$

$$\mathrm{RR} \underset{k_{4'}}{\overset{k_4}{\rightleftharpoons}} \mathrm{RS} \underset{k_4}{\overset{k_{4'}}{\rightleftharpoons}} \mathrm{SS} \qquad (\mathrm{eq.}\ 11)$$

$$\mathrm{RR} + \mathrm{RS} \underset{k_{6'}}{\overset{k_6}{\rightleftharpoons}} 2\,\mathrm{RS} \underset{k_6}{\overset{k_{6'}}{\rightleftharpoons}} \mathrm{SS} + \mathrm{RS} \qquad (\mathrm{eq.}\ 16)$$

By describing the system using equations 8-11 and 16, we again attempted to fit the system to our recorded data.

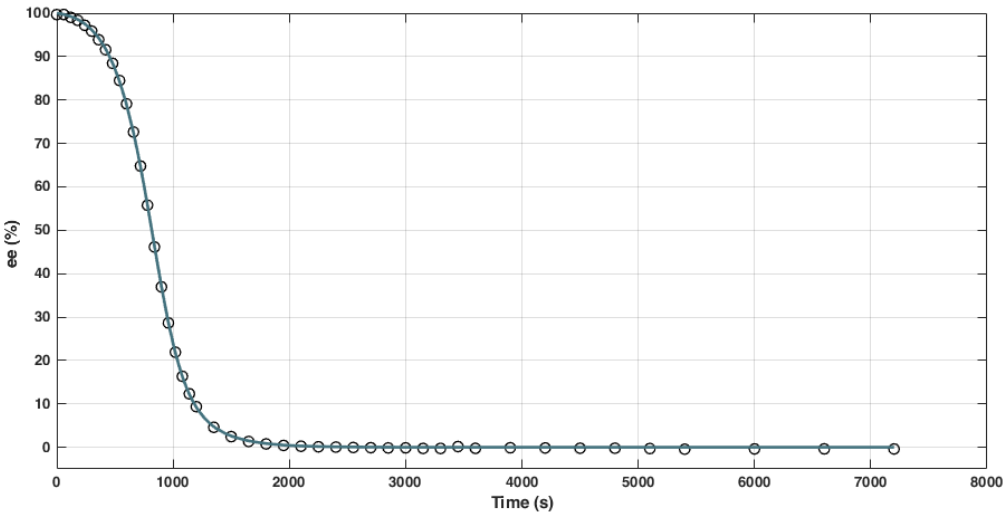



Figure 80 Fitting using equations 8-11 and 16 closely mimics experimental data.

Given the similarity to the previous model, its perhaps unsurprising that this model can also faithfully reproduce the observed racemisation profile.

#### II.2.5.1c Comparison

At this stage it is helpful to examine the similarities and differences between the profiles that the models simulate.

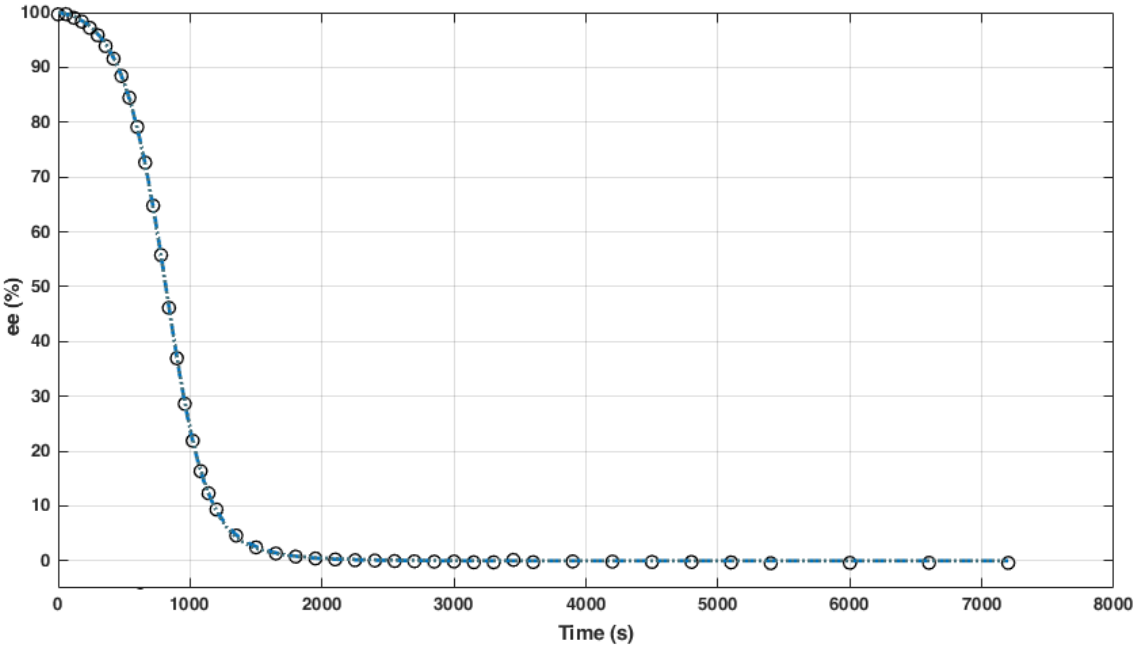



Figure 81 Overlay of both simulations showing similarly convincing fits. Trimeric: …, Tetrameric: ---.

Overlaying simulations of the models shows that both can produce a lineshape which faithfully recreates that observed (Figure 81). In particular, the exponential phase of the curves seems to describe the observed behaviour well.

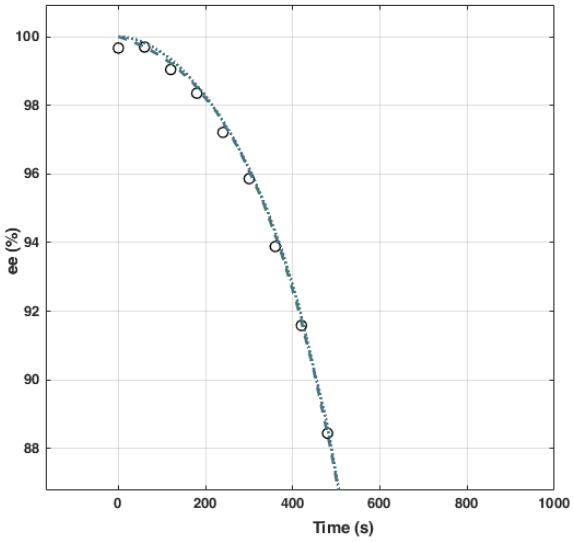



Figure 82 Fits at early t match closely and avoid over-fitting to a low $t_0$ timepoint. Trimeric: …, Tetrameric: ---

More closely examining the curves at early t shows that both are almost direct overlays. Both predict a smooth decrease in ee with a short lag period. This is a promising sign that we have not fallen victim to over parameterisation as in our raw data the first data point is actually lower than the second.

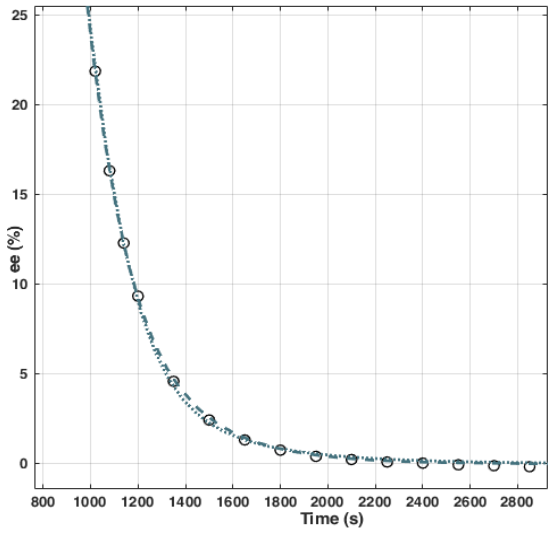



Figure 83 Fits approaching racemic bulk solution differ slightly. Trimeric: …, Tetrameric: ---

The other interesting portion of the curve is the transition to the saturation phase. Here both of the curves again overlay incredibly closely. While there is a slight difference between the curves, this could simply be a consequence of convergence parameters.

### II.2.5.2 Spiking Studies

As we were comfortable with the idea that the system might be autocatalytic, we sought a characteristic test. One way to test autocatalytic systems is by spiking with the active catalyst.[146] This ordinarily causes the exponential regime to be initiated on addition, which is observed as a shift in the recorded reaction profile. Though our system is far from average, we sought to determine whether this could provide any additional insights.

In an initial study a solid sample was prepared at 70% enantiomeric excess by addition of enantiopure material of the opposite enantiomer. The erosion study was then run as normal. The total concentration of the solution was 0.2 molal, the highest concentration previously recorded and the concentration at which our models were investigated.

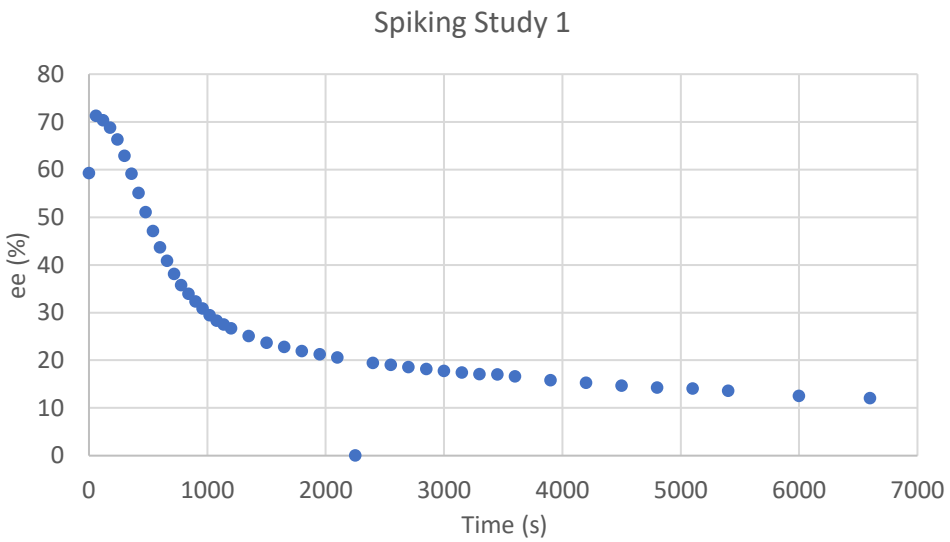



Figure 84 Spiking study with enantiopure material of the opposite enantiomer. Starting ee: 70%; concentration: 0.2 molal; temperature: 80°C; solvent: toluene.

Interestingly, spiking in this manner did not cause a shift of the recorded profile (Figure 84). Instead, the recorded profile had the same overall shape, but with much gentler slope and more gradual transitions between phases. Additionally, the bulk sample did not erode to racemic over the course of the study. In our initial studies at this concentration the bulk solution was racemic after approximately 30 minutes.

Reasoning that some of these observations may be due to spiking the solid with the opposite enantiomer instead of the racemate (which we anticipated to be the active catalyst), we decided to repeat the study, this time spiking to the same starting enantiomeric excess with racemic material.

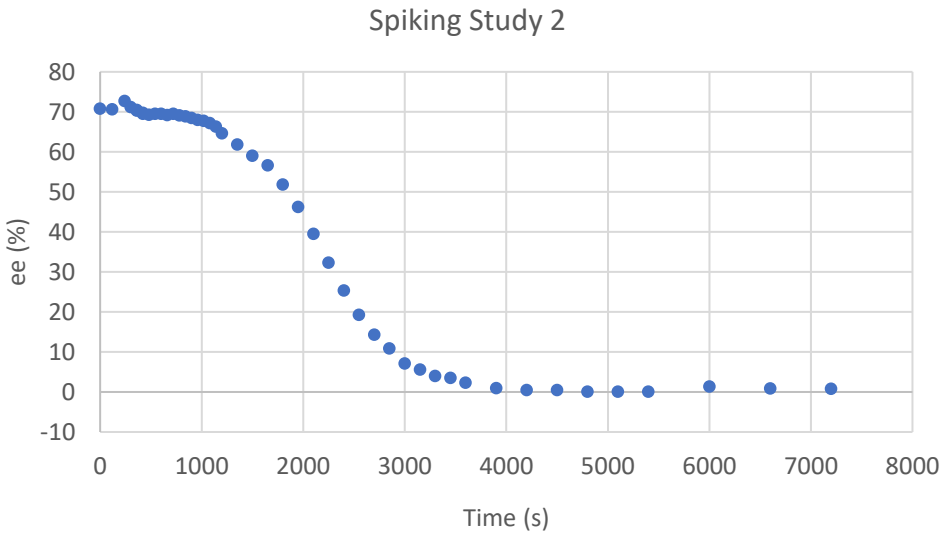



Figure 85 Spiking study carried out with racemic material. Starting ee: 70%; concentration: 0.2 molal; temperature: 80°C; solvent: toluene.

Again, the study did not produce the shift anticipated, but produced yet another curve (Figure 85). Interestingly, the addition of racemic material causes a dilation of the induction phase instead of a contraction. The rate at which the exponential part of the curve accelerates is also lessened, though the solution does now racemise entirely on the timescale of the study.

Though these spiking studies were intended to make clear whether we had correctly identified the active catalyst species, they were not able to. While this is somewhat disappointing, the data generated by these spiking studies may be the key to fully understanding the underlying mechanism of the observed effect.

#### II.2.5.3 Lower Concentrations

Though useful in gaining understanding, one of the main issues with our approach hitherto has been its focus on the most concentrated case and our use of enantiomeric excess.

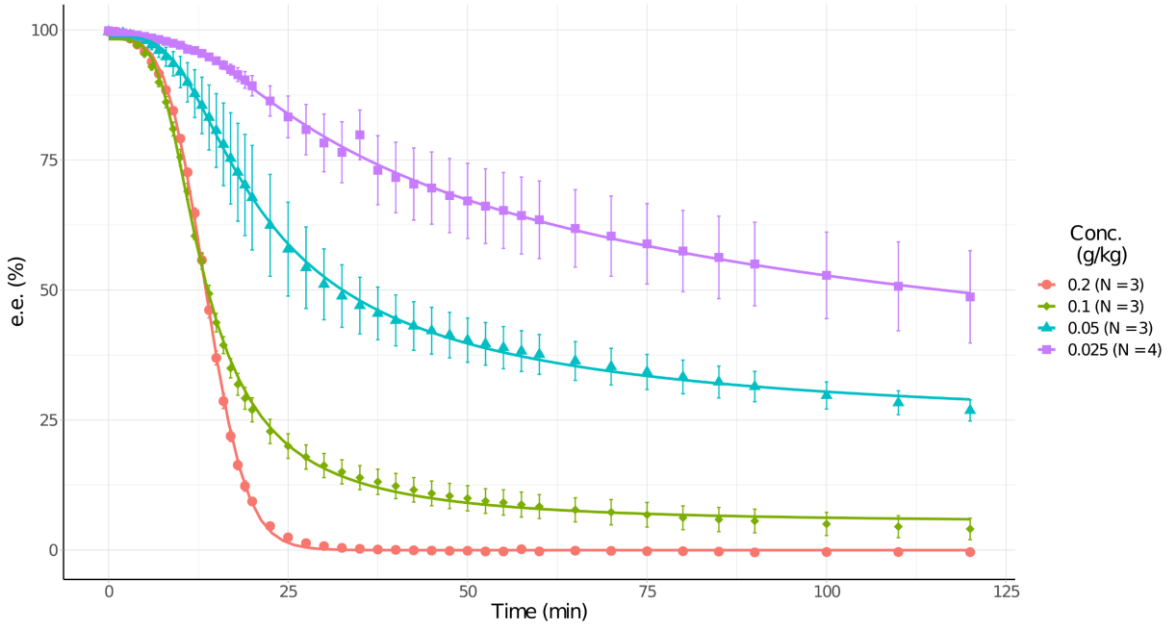



Figure 86 The collected data.

The consequences of our treatment are that we have ignored the most striking aspect of the effect – its concentration dependence. By using enantiomeric excess, we disregard the absolute concentration and so have no way of describing this dependence.

#### II.2.5.3a Qualitatively

$$\mathrm{R} + \mathrm{R} \underset{k_{2'}}{\overset{k_2}{\rightleftharpoons}} \mathrm{RR} \qquad (\text{eq. } 8)$$

$$\mathrm{S} + \mathrm{S} \underset{k_{2'}}{\overset{k_2}{\rightleftharpoons}} \mathrm{SS} \qquad (\text{eq. } 9)$$

$$\mathrm{R} + \mathrm{S} \underset{k_{3'}}{\overset{k_3}{\rightleftharpoons}} \mathrm{RS} \qquad (\text{eq. } 10)$$

The models which we described were all based on the same three dimer equilibria (eqns 8-10). Though the equilibrium constant (and indeed the forward and backward rate constants) will remain constant across all concentrations (at fixed temperature), the relative concentrations of monomers and the ability for these equilibria to remain dynamic will change.

$$Homodimer \quad formation \propto concentration^2$$
$$Diastereomerisation \propto concentration$$

For our hypothesised first order diastereomerisation the forward rate will fall in line with concentration. The same is true for homodimer dissociation, but the rate at which homodimer formation falls is with the square of concentration. After our start time diastereomerisation occurs, which puts the dimer system out of equilibrium. As we reduce concentration, the rate at which the equilibrium can try re-establish itself becomes slow relative to the rate of diastereomerisation.

$$Catalysis \propto concentration^2$$

When diastereomerisation does occur to give the heterodimer (our proposed catalyst), lower concentrations mean that the rate of the catalytic step is lower, as this also scales with the square of concentration.

$$Heterodimer \;\; dissociation \propto concentration$$

Additionally, as we begin to form heterodimer, lowering the concentration will speed up the apparent rate at which the heterodimer equilibrium is established. We know that the heterodimer is less favourable relative to its constituent monomers than the homodimer, so it is unsurprising that catalysis tails off.

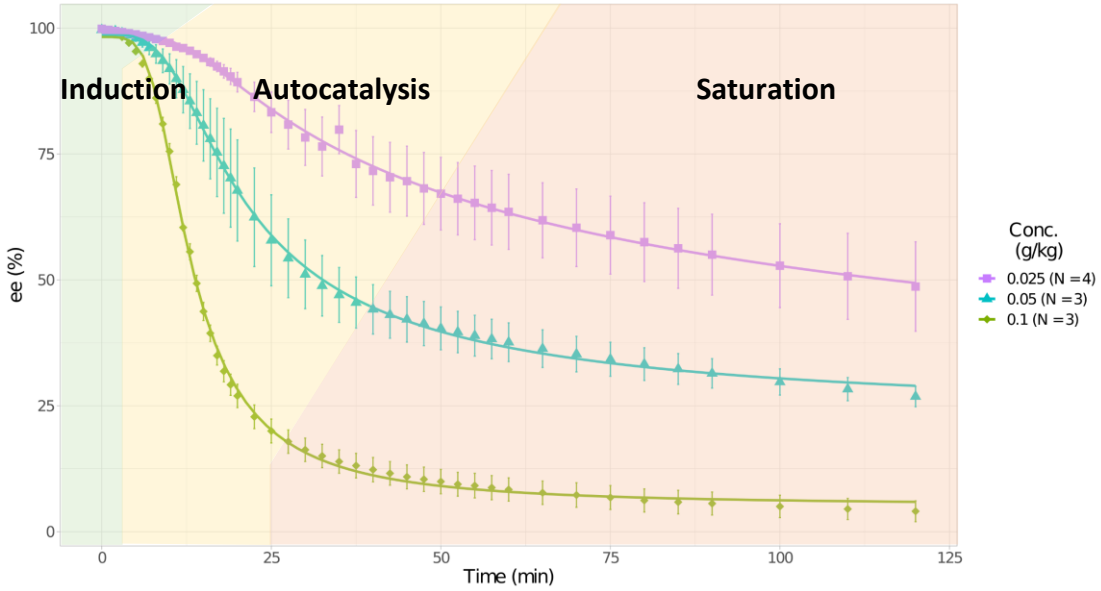



Figure 87 A qualitative illustration of the induction, autocatalysis, and saturation phases observed.

Though this is very much a qualitative understanding of our system, the addition of complex equilibria to an autocatalytic system has made its solubility elusive. With this understanding we can still identify the distinct phases present in the racemisation profiles, but through the lens of the autocatalytic pathway becoming less and less active with reducing concentration (Figure 87).

#### II.2.5.3b Quantitatively

Though we have a reasonable qualitative understanding of the kinetics of the system, our aim was to be able to extract quantitative data which can be corroborated using other techniques (e.g. equilibrium constants from DOSY). Fitting just one concentration is not sufficient because of the number of unknown rate constants in our models and the inability for our methods to track concentrations of dimers over time.

In collaboration with Prof. Martin Galpin, we have initiated work to carry out fitting across all concentrations.

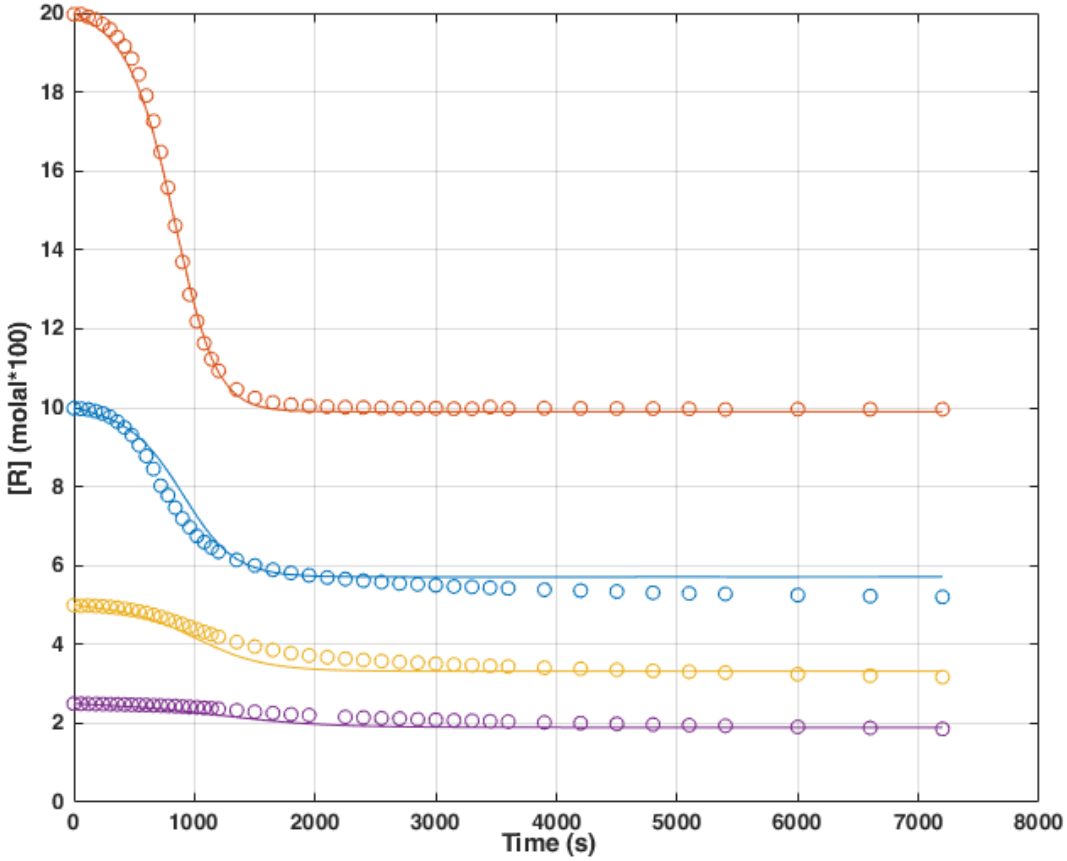



Figure 88 An early simultaneous fit of the trimeric model across all four concentrations recorded.

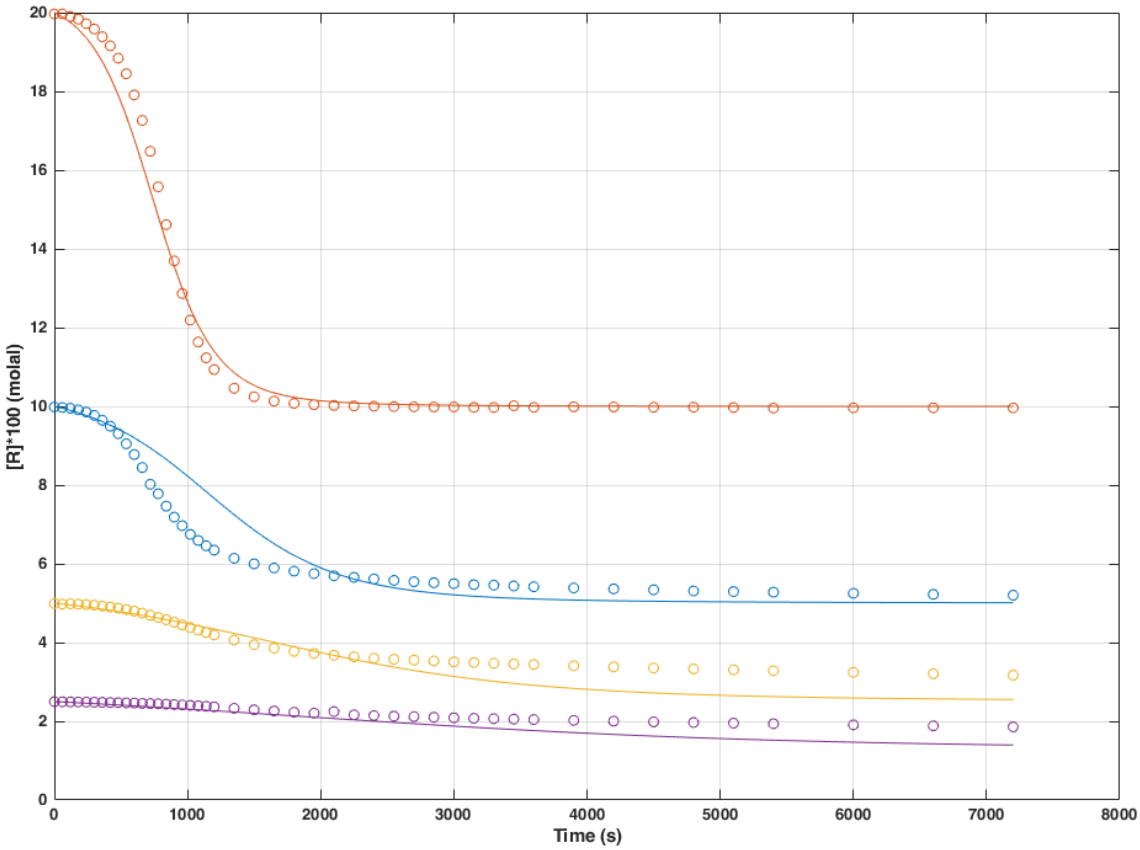



Figure 89 An early simultaneous fit of the tetrameric model across four concentrations recorded.

Though early attempts have been hindered by practical capabilities, the work is still ongoing, with the fits produced thus far showing promise (Figure 88, Figure 89)

## II.3 Conclusion and Future Work

Though the aim to fully elucidate the non-first order enantiomerisation pathway has not been achieved, we have shown the effect to be reproducible, demonstrated a number of ways in which it can be perturbed, and observed the preferential formation of homodimers in solution. In addition to this, we have proposed a number of plausible models, and begun the process of describing the models mathematically and investigating their ability to fit the recorded data with a view to validating the models based on rationalisation of the outputted rate constants.

A key limiting factor in the investigation of the observed effects was the inherent opacity of the process from the point of view of the data collected. The underlying phenomenon is enantiomerisation or diasteromerisation, both of which are local events on the scale of a molecule or oligomer. Our observation method, however, was not molecular and relied on measuring the enantiomeric excess of the solution – a bulk property.

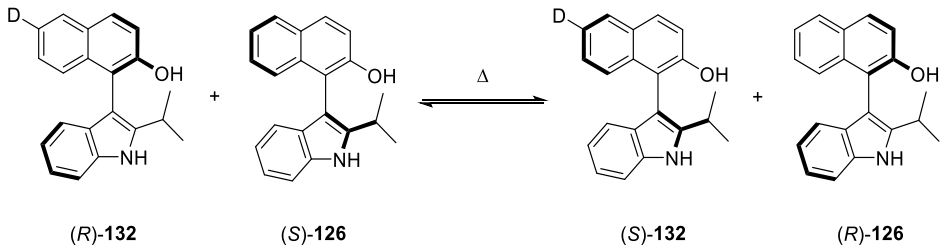



Figure 90 Observation of the enantiomerisation of **132** and **126** by SFC/MS could allow for tracking of enantiomerisation in pseudo-racemic solution. This could allow observation of the solution's "resting state".

One key experiment which may provide some insight into the enantiomerisation's underlying kinetics is by tracking the enantiomerisation of a "pseudo-racemic" solution of equal amounts of (*R*)-**132** and (*S*)-**126** by SFC/MS. Separation on a chiral stationary phase

followed by mass spectrographic analysis of each eluted peak would allow observation of the interconversion of each isotopomer in “racemic” solution.

Further future work on the project may focus more specifically on the kinetics of dimerization and dissociation events in solution. Though detection would likely not be able to discern between enantiomeric dimers, determination of the rates of association/dissociation in enantiopure and racemic solutions would aide in validating fitted models. As an extension of this, if observation of dimer concentrations over the course of an erosion study were possible, the data could facilitate rapid elucidation of the underlying kinetics.

# References


1. B. A. Jones, P. Solon, M. V. Popescu, J. Y. Du, R. Paton and M. D. Smith, *J. Am. Chem. Soc.*, 2023, **145**, 171-178.
2. P. Klán and J. Wirz, *Photochemistry of Organic Compounds*, Wiley, Chichester, U.K., 2009.
3. F. Strieth-Kalthoff, M. J. James, M. Teders, L. Pitzer and F. Glorius, *Chem. Soc. Rev.*, 2018, **47**, 7190-7202.
4. C. K. Prier, D. A. Rankic and D. W. MacMillan, *Chem. Rev.*, 2013, **113**, 5322-5363.
5. N. A. Romero and D. A. Nicewicz, *Chem. Rev.*, 2016, **116**, 10075-10166.
6. Y. Sumida and H. Ohmiya, *Chem. Soc. Rev.*, 2021, **50**, 6320-6332.
7. C. M. Marian, *Wiley Interdisciplinary Reviews-Computational Molecular Science*, 2012, **2**, 187-203.
8. M. Karplus, C. W. Kern, W. N. Lipscomb, O. J. Savers, W. E. Palke, K. S. Pitzer, R. M. Pitzer and A. G. Schultz, *Prog. Phys. Org. Chem*, 1983, **16**, 527-527.
9. D. L. Dexter, *J. Chem. Phys.*, 1953, **21**, 836-850.
10. T. Förster, *Annalen der Physik*, 2006, **437**, 55-75.
11. F. Strieth-Kalthoff and F. Glorius, *Chem*, 2020, **6**, 1888-1903.
12. N. Munster, N. A. Parker, L. van Dijk, R. S. Paton and M. D. Smith, *Angew. Chem. Int. Ed. Engl.*, 2017, **56**, 9468-9472.
13. B. C. Hong, *Org Biomol Chem*, 2020, **18**, 4298-4298.
14. Y. Inoue, *Chem. Rev.*, 1992, **92**, 741-770.
15. Y. Inoue and V. Ramamurthy, Marcel Dekker, New York, 2004, pp. 261-314.
16. C. Prentice, J. Morrisson, A. D. Smith and E. Zysman-Colman, *Beilstein J. Org. Chem.*, 2020, **16**, 2363-2441.
17. H. Rau, *Chem. Rev.*, 1983, **83**, 535-547.
18. M. Christmann and S. Bräse, *Asymmetric Synthesis II*, Wiley-VCH, Weinheim, 2012.
19. Q. Sha, Y. Deng and M. P. Doyle, Springer Verlag, 2018, vol. 62, pp. 1-25.
20. C. Wang, L. A. Chen, H. Huo, X. Shen, K. Harms, L. Gong and E. Meggers, *Chem. Sci.*, 2015, **6**, 1094-1100.
21. L. Zhang and E. Meggers, *Acc. Chem. Res.*, 2017, **50**, 320-330.
22. V. Edtmüller, A. Pöthig and T. Bach, *Tetrahedron*, 2017, **73**, 5038-5047.
23. J. S. Johnson and D. A. Evans, *Acc. Chem. Res.*, 2000, **33**, 325-335.
24. T. R. Blum, Z. D. Miller, D. M. Bates, I. A. Guzei and T. P. Yoon, *Science*, 2016, **354**, 1391-1395.
25. M. J. Genzink, J. B. Kidd, W. B. Swords and T. P. Yoon, *Chem. Rev.*, 2022, **122**, 1654-1716.
26. J. Grosskopf, T. Kratz, T. Rigotti and T. Bach, *Chem. Rev.*, 2022, **122**, 1626-1653.
27. M. Y. Wang and W. Li, *Chin. J. Chem .* 2021, **39**, 969-984.
28. T. Zhan, L. Yang, Q. Chen, R. Weng, X. Liu and X. Feng, *CCS Chem.*, **0**, 1-10.
29. Y. Ogata, K. Takagi and I. Ishino, *J. Org. Chem.*, 2002, **36**, 3975-3979.
30. G. J. Pros and A. J. Bloomfield, *J. Phys. Chem. A*, 2019, **123**, 7609-7618.
31. I. Ninomiya, T. Naito and Y. Tada, *Heterocycles*, 1984, **22**, 237-237.
32. A. J. Ayitou and J. Sivaguru, *J. Am. Chem. Soc.*, 2009, **131**, 5036-5037.
33. A. J. Ayitou and J. Sivaguru, *Chem. Commun.*, 2011, **47**, 2568-2570.

34. T. Bach, B. Grosch, T. Strassner and E. Herdtweck, *J. Org. Chem.*, 2003, **68**, 1107-1116.
35. E. Longhi and L. De Cola, John Wiley & Sons, Ltd, 2017, pp. 205-274.
36. A. Singh, K. Teegardin, M. Kelly, K. S. Prasad, S. Krishnan and J. D. Weaver, *J. Organomet. Chem.*, 2015, **776**, 51-59.
37. L. F. Gildea and J. A. G. Williams, Woodhead Publishing, 2013, pp. 77-113.
38. C. W. Tang and S. A. Vanslyke, *Appl. Phys. Lett.*, 1987, **51**, 913-915.
39. H. T. Mao, G. F. Li, G. G. Shan, X. L. Wang and Z. M. Su, *Coord. Chem. Rev.*, 2020, **413**, 213283-213283.
40. C. Adachi, M. A. Baldo, M. E. Thompson and S. R. Forrest, *J. Appl. Phys.*, 2001, **90**, 5048-5051.
41. M. A. Baldo, D. F. O'Brien, Y. You, A. Shoustikov, S. Sibley, M. E. Thompson and S. R. Forrest, *Nature*, 1998, **395**, 151-154.
42. M. A. Baldo, S. Lamansky, P. E. Burrows, M. E. Thompson and S. R. Forrest, *Appl. Phys. Lett.*, 1999, **75**, 4-6.
43. T. Tsutsui, M.-J. Yang, M. Yahiro, K. Nakamura, T. Watanabe, T. Tsuji, Y. Fukuda, T. Wakimoto and S. Miyaguchi, *Japanese Journal of Applied Physics*, 1999, **38**, L1502.
44. S. Okada, K. Okinaka, H. Iwawaki, M. Furugori, M. Hashimoto, T. Mukaide, J. Kamatani, S. Igawa, A. Tsuboyama, T. Takiguchi and K. Ueno, *Dalton Trans.*, 2005, 1583-1590.
45. D. Tordera, J. J. Serrano-Perez, A. Pertegas, E. Orti, H. J. Bolink, E. Baranoff, M. K. Nazeeruddin and J. Frey, *Chem. Mater.*, 2013, **25**, 3391-3397.
46. S. Chu, N. Munster, T. Balan and M. D. Smith, *Angew. Chem. Int. Ed. Engl.*, 2016, **55**, 14306-14309.
47. D. A. Evans and J. M. Janey, *Org. Lett.*, 2001, **3**, 2125-2128.
48. P. N. Liu, F. H. Su, T. B. Wen, H. H. Sung, I. D. Williams and G. Jia, *Chem. - Eur. J.*, 2010, **16**, 7889-7897.
49. F. T. Oakes, F. A. Yang and J. F. Sebastian, *J. Org. Chem.*, 1982, **47**, 3094-3097.
50. S. Song, S. F. Zhu, L. Y. Pu and Q. L. Zhou, *Angew. Chem. Int. Ed. Engl.*, 2013, **52**, 6072-6075.
51. S. V. F. Hansen, Z. E. Wilson, T. Ulven and S. V. Ley, *React. Chem. Eng.*, 2016, **1**, 280-287.
52. C. Veryser, S. Van Mileghem, B. Egle, P. Gilles and W. M. De Borggraeve, *React. Chem. Eng.*, 2016, **1**, 142-146.
53. T. Ueda, H. Konishi and K. Manabe, *Org. Lett.*, 2012, **14**, 5370-5373.
54. M. J. Oddy, D. A. Kusza and W. F. Petersen, *Org. Lett.*, 2021, **23**, 8963-8967.
55. L. Tian, N. A. Till, B. Kudisch, D. W. C. MacMillan and G. D. Scholes, *J. Am. Chem. Soc.*, 2020, **142**, 4555-4559.
56. E. R. Welin, C. Le, D. M. Arias-Rotondo, J. K. McCusker and D. W. C. MacMillan, *Science*, 2017, **355**, 380-385.
57. I. R. Laskar and T. M. Chen, *Chem. Mater.*, 2004, **16**, 111-117.
58. G. H. Christie and J. Kenner, *J. Chem. Soc., Trans.*, 1922, **121**, 614-620.
59. R. Kuhn, *Stereochemie*, Leipzig, 1933.
60. M. Reist, B. Testa, P. A. Carrupt, M. Jung and V. Schurig, *Chirality*, 1995, **7**, 396-400.
61. M. Ōki, in *Topics in Stereochemistry*, John Wiley & Sons, Ltd, 2007, pp. 1-81.
62. O. Baudoin and F. Guéritte, *Stud. Nat. Prod. Chem.*, 2003, **29**, 355-417.
63. G. Bringmann, J. Mutanyatta-Comar, M. Knauer and B. M. Abegaz, *Nat. Prod. Rep.*, 2008, **25**, 696-718.

64. G. Bringmann, T. Gulder, T. A. Gulder and M. Breuning, *Chem. Rev.*, 2011, **111**, 563-639.
65. M. C. Kozlowski, B. J. Morgan and E. C. Linton, *Chem. Soc. Rev.*, 2009, **38**, 3193-3207.
66. B. Tan, *Axially Chiral Compounds*, Wiley, 2021.
67. J. Brussee and A. C. A. Jansen, *Tetrahedron Lett.*, 1983, **24**, 3261-3262.
68. M. Klussmann, L. Ratjen, S. Hoffmann, V. Wakchaure, R. Goddard and B. List, *Synlett*, 2010, **2010**, 2189-2192.
69. Y. N. Ma, S. X. Li and S. D. Yang, *Acc. Chem. Res.*, 2017, **50**, 1480-1492.
70. P. Rodriguez-Salamanca, R. Fernandez, V. Hornillos and J. M. Lassaletta, *Chem. - Eur. J.*, 2022, **28**, e202104442.
71. S. Brandes, B. Niess, M. Bella, A. Prieto, J. Overgaard and K. A. Jorgensen, *Chem. - Eur. J.*, 2006, **12**, 6039-6052.
72. O. Kitagawa, *Acc. Chem. Res.*, 2021, **54**, 719-730.
73. E. Kumarasamy, R. Raghunathan, M. P. Sibi and J. Sivaguru, *Chem. Rev.*, 2015, **115**, 11239-11300.
74. G. J. Mei, W. L. Koay, C. Y. Guan and Y. X. Lu, *Chem*, 2022, **8**, 1855-1893.
75. J. Clayden, W. J. Moran, P. J. Edwards and S. R. LaPlante, *Angew. Chem. Int. Ed. Engl.*, 2009, **48**, 6398-6401.
76. S. R. LaPlante, P. J. Edwards, L. D. Fader, A. Jakalian and O. Hucke, *ChemMedChem*, 2011, **6**, 505-513.
77. S. R. Laplante, D. F. L, K. R. Fandrick, D. R. Fandrick, O. Hucke, R. Kemper, S. P. Miller and P. J. Edwards, *J. Med. Chem.*, 2011, **54**, 7005-7022.
78. M. Basilaia, M. H. Chen, J. Secka and J. L. Gustafson, *Acc. Chem. Res.*, 2022, **55**, 2904-2919.
79. S. Perreault, J. Chandrasekhar and L. Patel, *Acc. Chem. Res.*, 2022, **55**, 2581-2593.
80. FDA Approves First Targeted Therapy for Lung Cancer Mutation Previously Considered Resistant to Drug Therapy | FDA, https://www.fda.gov/news-events/press-announcements/fda-approves-first-targeted-therapy-lung-cancer-mutation-previously-considered-resistant-drug).
81. F. McCormick, *Biochem. J*, 2019, **476**, 365-374.
82. M. Eichelbaum and A. S. Gross, in *Advances in Drug Research Volume 28*, Elsevier Science & Technology, United Kingdom, 1996, vol. 28, pp. 1-64.
83. S. Fabro, R. L. Smith and R. T. Williams, *Nature*, 1967, **215**, 296.
84. R. R. Shah and S. K. Branch, Springer, Berlin, Heidelberg, 2003, pp. 379-399.
85. P. Eveleigh, E. C. Hulme, C. Schudt and N. J. M. Birdsall, *Mol. Pharmacol.*, 1989, **35**, 477-483.
86. R. J. Fiuary, M. Spangler, R. Osterman, L. Schulman and J. H. Schwerdt, *Chirality*, 1996, 8364-8371.
87. Y. S. Zhou, L. K. Tay, D. Hughes and S. Donahue, *J. Clin. Pharmacol.*, 2004, **44**, 680-688.
88. G. Bott, L. D. Field and S. Sternhell, *J. Am. Chem. Soc.*, 1980, **102**, 5618-5626.
89. F. Leroux, John Wiley & Sons, Ltd, 2004, vol. 5, pp. 644-649.
90. L. Meca, D. Reha and Z. Havlas, *J. Org. Chem.*, 2003, **68**, 5677-5680.
91. A. Ahmed, R. A. Bragg, J. Clayden, L. W. Lai, C. McCarthy, J. H. Pink, N. Westlund and S. A. Yasin, *Tetrahedron*, 1998, **54**, 13277-13294.
92. A. S. Cooke and M. M. Harris, *J. Chem. Soc.*, 1963, **0**, 2365-2373.
93. A. N. Bootsma and C. E. Anderson, *Tetrahedron Lett.*, 2016, **57**, 4834-4837.

94. S. Kayama, H. Tabata, Y. Takahashi, N. Tani, S. Wakamatsu, T. Oshitari, H. Natsugari and H. Takahashi, *Tetrahedron*, 2015, **71**, 7046-7053.
95. M. Lorentzen, I. Kalvet, F. Sauriol, T. Rantanen, K. B. Jorgensen and V. Snieckus, *J. Org. Chem.*, 2017, **82**, 7300-7308.
96. L. F. Tietze, H. J. Schuster, J. M. von Hof, S. M. Hampel, J. F. Colunga and M. John, *Chem. - Eur. J.*, 2010, **16**, 12678-12682.
97. M. Rickhaus, L. Jundt and M. Mayor, *Chimia*, 2016, **70**, 192-202.
98. M. Soustelle, *An Introduction to Chemical Kinetics*, Wiley Blackwell, 2011.
99. G. Cannazza, M. M. Carrozzo, D. Braghiroli and C. Parenti, *J. Chromatogr. B*, 2008, **875**, 192-199.
100. F. P. Gasparro and N. H. Kolodny, *J. Chem. Educ.*, 1977, **54**, 258-261.
101. A. Holzl-Hobmeier, A. Bauer, A. V. Silva, S. M. Huber, C. Bannwarth and T. Bach, *Nature*, 2018, **564**, 240-243.
102. G. Hu, D. Holmes, B. F. Gendhar and W. D. Wulff, *J. Am. Chem. Soc.*, 2009, **131**, 14355-14364.
103. M. Irie, K. Yoshida and K. Hayashi, *J. Phys. Chem.*, 1977, **81**, 969-972.
104. G. Belletti, C. Tortora, I. D. Mellema, P. Tinnemans, H. Meekes, F. Rutjes, S. B. Tsogoeva and E. Vlieg, *Chem. - Eur. J.*, 2020, **26**, 839-844.
105. Q. Wang, A. Pietropaolo, M. Fortino, Z. Song, M. Bando, N. Naga and T. Nakano, *Chirality*, 2022, **34**, 317-324.
106. Z. Zhang, Y. Wang and T. Nakano, *Molecules*, 2016, **21**, 1541-1541.
107. K. Mislow and A. J. Gordon, *J. Am. Chem. Soc.*, 1963, **85**, 3521-&.
108. J. S. J. Tan and R. S. Paton, *Chem. Sci.*, 2019, **10**, 2285-2289.
109. M. R. Boyd, Y. F. Hallock, J. H. Cardellina, 2nd, K. P. Manfredi, J. W. Blunt, J. B. McMahon, R. W. Buckheit, Jr., G. Bringmann, M. Schaffer, G. M. Cragg and et al., *J. Med. Chem.*, 1994, **37**, 1740-1745.
110. A. M. Genaev, G. E. Salnikov, A. V. Shernyukov, Z. Zhu and K. Y. Koltunov, *Org. Lett.*, 2017, **19**, 532-535.
111. A. M. Genaev, G. E. Salnikov, A. V. Shernyukov, Z. W. Zhu and K. Y. Koltunov, *Mendeleev Commun.*, 2018, **28**, 27-28.
112. F. Octa-Smolin, F. van der Vight, R. Yadav, J. Bhangu, K. Soloviova, C. Wolper, C. G. Daniliuc, C. A. Strassert, H. Somnitz, G. Jansen and J. Niemeyer, *J. Org. Chem.*, 2018, **83**, 14568-14587.
113. S. Narute, R. Parnes, F. D. Toste and D. Pappo, *J. Am. Chem. Soc.*, 2016, **138**, 16553-16560.
114. M. T. Ashby, G. N. Govindan and A. K. Grafton, *J. Am. Chem. Soc.*, 1994, **116**, 4801-4809.
115. E. C. Constable, R. M. Hartshorn and C. E. Housecroft, *Molecules*, 2021, **26**, 1584-1584.
116. A. J. Bissette and S. P. Fletcher, *Angew. Chem. Int. Ed. Engl.*, 2013, **52**, 12800-12826.
117. A. I. Hanopolskyi, V. A. Smaliak, A. I. Novichkov and S. N. Semenov, *ChemSystemsChem*, 2021, **3**, e2000026-e2000026.
118. D. G. Blackmond, *Proceedings of the National Academy of Sciences of the United States of America*, 2004, **101**, 5732-5736.
119. B. L. Feringa and R. A. van Delden, *Angew. Chem. Int. Ed.*, 1999, **38**, 3418-3438.
120. K. Soai, A. Matsumoto and T. Kawasaki, Academic Press, 2017, pp. 1-30.
121. K. Soai, T. Kawasaki and A. Matsumoto, *Asymmetric autocatalysis : the Soai reaction*, Cambridge, 1st edn., 2022.

122. H. Wynberg, *Chimia*, 1989, **43**, 150-152.
123. H. Wynberg, *J. Macromol. Sci. - A Chem.*, 1989, **26**, 1033-1041.
124. A. H. Alberts and H. Wynberg, *J. Am. Chem. Soc.*, 1989, **111**, 7265-7266.
125. K. Soai, S. Niwa and H. Hori, *J. Chem. Soc., Chem. Commun.*, 1990, 982-983.
126. S. V. Athavale, A. Simon, K. N. Houk and S. E. Denmark, *Nat. Chem.*, 2020, **12**, 412-423.
127. N. A. Seifert, C. Perez, J. L. Neill, B. H. Pate, M. Vallejo-Lopez, A. Lesarri, E. J. Cocinero and F. Castano, *Phys. Chem. Chem. Phys.*, 2015, **17**, 18282-18287.
128. H. Wynberg and B. Feringa, *Tetrahedron*, 1976, **32**, 2831-2834.
129. I. Alkorta, O. Picazo and J. Elguero, *Tetrahedron: Asymmetry*, 2004, **15**, 1391-1399.
130. I. Alkorta and J. Elguero, *J. Am. Chem. Soc.*, 2002, **124**, 1488-1493.
131. I. Alkorta and J. Elguero, *J. Chem. Phys.*, 2002, **117**, 6463-6468.
132. E. Fogassy, F. Faigl and M. Acs, *Tetrahedron*, 1985, **41**, 2841-2845.
133. G. Storch, M. Haas and O. Trapp, *Chem. - Eur. J.*, 2017, **23**, 5414-5418.
134. V. Daskova, D. Padin and B. L. Feringa, *J. Am. Chem. Soc.*, 2022, **144**, 23603-23613.
135. D. Parker, *Chem. Rev.*, 1991, **91**, 1441-1457.
136. T. Williams, R. G. Pitcher, P. Bommer, J. Gutzwiller and M. Uskoković, *J. Am. Chem. Soc.*, 1969, **91**, 1871-1872.
137. R. Baciocchi, G. Zeroni, M. Valentini, M. Mazzotti and M. Morbidelli, *J. Phys. Chem. A*, 2002, **106**, 10461-10469.
138. R. Charles and E. Gilav, *J. Chromatogr.*, 1984, **298**, 516-520.
139. K. C. Cundy and P. A. Crooks, *J. Chromatogr. A*, 1983, **281**, 17-33.
140. J. Martens and R. Bhushan, *J. Liq. Chromatogr.*, 1992, **15**, 1-27.
141. W. L. Tsai, K. Hermann, E. Hug, B. Rohde and A. S. Dreiding, *Helv. Chim. Acta*, 1985, **68**, 2238-2243.
142. R. R. Surgenor, X. Liu, M. J. H. Keenlyside, W. Myers and M. D. Smith, *Nat. Chem.*, 2023, **15**, 357-365.
143. R. C. Larock and E. K. Yum, *J. Am. Chem. Soc.*, 1991, **113**, 6689-6690.
144. M. A. Watzky and R. G. Finke, *J. Am. Chem. Soc.*, 1997, **119**, 10382-10400.
145. R. Neufeld and D. Stalke, *Chem. Sci.*, 2015, **6**, 3354-3364.
146. C. Wang, H. Zhang, L. A. Wells, T. Liu, T. Meng, Q. Liu, P. J. Walsh, M. C. Kozlowski and T. Jia, *Nat. Commun.*, 2021, **12**, 932.

# Experimental Data

# Contents


Contents ..... S-1

General Information ..... S-3

Part I: Catalytic Enantioselective 6π Photocyclization of Acrylanilides ..... S-6

I.1 Reaction Optimization ..... S-7

I.1.1 Extended Optimization Table ..... S-7

I.1.2 Summary of Enantioselective Reaction Optimization ..... S-9

I.1.3 Chiral Ligands Employed in this Study ..... S-10

I.1.4 Photocatalysts Employed in this Study ..... S-11

I.2 Experimental Procedures ..... S-12

I.2.1 General Procedures ..... S-12

I.2.2 Photocatalysts and Phenylpyridines ..... S-14

I.2.3 Precursors ..... S-21

I.2.4 Substrates ..... S-23

I.2.6 Photocyclization Products ..... S-30

I.3 Characterisation of Novel Photocatalysts ..... S-42

I.3.1 Absorbance and Emission Spectra of Novel Photocatalysts ..... S-42

I.3.2 Square-Wave Voltammograms of Novel Photocatalysts ..... S-46

I.3.3 Estimation of Excited State Redox Potentials for Novel Photocatalysts ..... S-50

I.3.4 Summary of Photocatalyst Properties ..... S-50

I.4 Mechanistic Experiments and Photophysics ..... S-51

I.4.1 Labelling and Crossover Experiments ..... S-51

I.4.2 Chemical Actinometry and Quantum Yield Measurement ..... S-57

I.4.3 Weakly Reducing Photocatalyst Study ..... S-58

I.4.4 Electrochemical Measurements ..... S-59

I.4.5 Stern-Volmer Quenching ..... S-60

I.4.6 UV-Vis Absorbance Spectra ..... S-64

I.5 X-ray Crystallography ..... S-65

I.6 HPLC Traces for Chiral Compounds ..... S-67

Part II: Enantiomerisation Processes of Indolyl-Naphthyl Atropisomers ..... S-86

II.1 General Procedures for Kinetic Data Collection ..... S-87

II.2 Experimental Data for Compounds ..... S-89

II.3 Rate Laws and Kinetic Formulae ..... S-94

II.3.1 Rate Laws ..... S-94

II.3.2 Formulae ..... S-96
II.4 HPLC Data ..... S-97
II.5 Collated Erosion Data ..... S-101
II.5.1 Data for 111 at 22 °C ..... S-101
II.5.2 Data for 126 recorded at 80 °C in toluene ..... S-103
II.5.3 Data for methylated analogues ..... S-118
II.5.4 NMR Studies ..... S-122
II.5.6 Alternative erosion conditions ..... S-144
II.6 X-Ray Crystallography ..... S-159
II.7 MATLAB SimBiology ..... S-170
II.7.1 Simulations ..... S-170
II.7.3 Concentration Based Fits ..... S-196
References ..... S-217

# General Information

**Naming and Numbering**

Systematic compound names in accordance with regulations set forth by the International Union for Pure and Applied Chemistry (IUPAC) have been generated from the appropriate structures using the PerkinElmer Informatics software ChemDraw® (version 21).

**Reaction Conditions**

Reactions requiring moisture-sensitive reagents performed in flame-dried glassware, under an atmosphere of argon (balloon pressure). Room temperature refers to 20–25 °C. Temperatures of 0 °C were obtained using an ice/water bath. Temperatures of −78 °C were obtained using a dry ice/acetone bath. Temperatures of 0 °C to −40 °C were obtained using a polar bear plus. 10-15 °C refers to reactions carried out in a tempering beaker filled with water. Reflux and heating conditions were obtained using a Drysyn® heating block or an oil bath equipped with a thermometer where the reported temperature refers to the temperature of the Drysyn® block or oil bath. Syringe filters, where used, were 0.2 µm PTFE membrane filters obtained from Fisher Scientific (cat no. 15141499).

**Solvents and Reagents**

Anhydrous dichloromethane and tetrahydrofuran were obtained using an MBraun SPS-5. All other solvents were used without further purification. Degassed solvents were prepared by sparging with argon for 10 minutes. Reagents were used directly as supplied by major chemical suppliers.

**Chromatography**

Thin layer chromatography was carried out on Merck Kieselgel 60, $F_{254}$ 0.25 mm precoated aluminium plates and visualisation was achieved by UV light ($\lambda_{max}$ = 254 nm) and/or by staining with potassium permanganate solution or phosphomolybdic acid solution. Column chromatography was performed using VWR silica gel 60 (40-63 m particle size) or Aldrich silca gel 60 (40-63 nm particle size) using a pressurised nitrogen line.

**NMR Spectroscopy**

NMR spectra were recorded on a Bruker Avance spectrometers at room temperature (unless otherwise stated) in the deuterated solvent stated and are referenced to the residual non-deuterated solvent peak. Chemical shifts are quoted in ppm with signal splittings recorded as singlet (s), doublet (d), triplet (t), quartet (q), hept. (heptet), and multiplet (m). The abbreviation br. denotes broad. Coupling constants, *J*, are measured to the nearest 0.1 Hz and are presented as observed. All $^{19}F$ NMR spectra are proton decoupled.

Assignments were carried out with the aid of homo and heteronuclear 2D NMR experiments (COSY, HSQC, HMBC, etc.), and where necessary, with the aid of the Paton group's CASCADE NMR prediction tool.[1]

NMR yields were determined using trimethoxy benzene as an internal standard (0.33 eq.) and setting the $T_1$ relaxation delay to 60 sec.

**Infrared**

Infrared spectra were recorded on a Bruker Tensor 27 FTIR spectrometer equipped with a diamond ATR module. Absorption maxima ($\nu_{max}$) are reported in wavenumbers ($cm^{-1}$).

**Mass Spectrometry**

Accurate masses (HRMS) were recorded on Bruker MicroTOF and Micromass GCT spectrometers under conditions of electrospray ionisation (ESI).

**Photochemistry Setup**

The photochemical irradiation setup used consisted of a water jacketed beaker in which sealed reaction vials were suspended and 2 Kessil PR-160L LED lamps centered at 440 nm which shone through the walls of the beaker. A picture of the setup is provided on page 129 (Figure S3).

**Polarimetry**

Optical Rotations were determined using a Schmidt + Haensch Unipol 2020 polarimeter with a path length of 1 dm (using the sodium D line, 589 nm). Concentrations are reported in g/100 mL. Temperatures are reported in °C.

**Chiral HPLC**

Chiral HPLC was performed on a Dionex Ultimate 3000 system comprising of a Dionex LPG-3400SD pump, WPS-3000SL autosampler, TCC-3000SD column compartment fitted with the appropriate Daicel Chiralpak column (dimensions: 0.46 cm ø × 25 cm) and corresponding guard column (0.4 cm ø × 1 cm), and a DAD-3000 diode array detector. Wavelengths (λ) are reported in nm, retention times ($\tau_R$) are reported in minutes and solvent flow rates are reported in mL $min^{-1}$.

**LC/MS**

LC/MS was carried out on an Agilent 1260 Infinity II system comprising of a 1260 Infinity II Quaternary Pump VL (G7111A), a 1260 Infinity II Vialsampler (G7129A) with integrated column compartment (G7130A), a Agilent 1260 Infinity II Diode Array Detector WR (G7115A), and a 6100 Series Single Quadrupole LC/MS (G7115A) using API-ES positive ionisation. Separations were carried out by gradient elution (1 minute dwell at 5% MeCN/$H_2O$, followed by a gradient to 95% MeCN/$H_2O$ over 7 minutes) using a Poroshell 120 EC-C18 USP L1 Solvent Saver 3.0 x 100mm column at a flow rate of 0.4 mL $min^{-1}$. 0.1% formic acid was added to all solvents.

**Melting Points**

Melting points were determined using a Reichert melting point apparatus and are uncorrected.

**Synthesis of Catalysts and Ligands**

The chiral ligands and photocatalysts that were not commercially available were prepared following reported literature methods.[2-4]

**Voltammetry Studies**

Voltammetry measurements were made using an EmStat3 with a glassy carbon electrode as the working electrode, a platinum wire as counter electrode and a leak free Ag/AgCl (sat. KCl) reference electrode. Voltammograms were referenced to the $Fc/Fc^+$ couple as an internal reference. Square wave voltammograms were acquired with a 5 mV step potential, 50 mV modulation amplitude and 5 Hz frequency. The supporting electrolyte, (tetra-n-butylammonium hexafluorophosphate, $Bu_4NPF_6$, $TBAPF_6$) was prepared as a 0.1 M solution in either MeCN or $CH_2Cl_2$. Samples were measured at 0.01 M concentration.

**Fluorescence spectroscopy**

Emission spectra were recorded on an Edinburgh Instruments FS5 spectrometer. Emission spectra were recorded as 5 μM solutions in degassed MeCN by irradiating at 390 nm and recording between 400 and 800 nm.

**Data analysis**

Processing of raw data was carried out using R Studio or Microsoft Excel. Treatment of the data is outlined in the relevant part of Section II.5.

**Modelling**

All models were created using MATLAB SimBiology v. 6.4 (R2022b). Fitting to and simulation of these models was also carried out in SimBiology v. 6.4, with all parameters outlined in Section II.7.

# Part I:

# Catalytic Enantioselective 6π

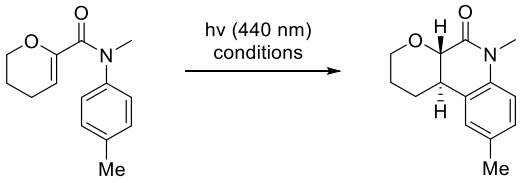
# Photocyclization of Acrylanilides

# I.1 Reaction Optimization

For completeness, the optimisation table included in the literature publication is included below.[5] Entries are from BAJ and PS.

## I.1.1 Extended Optimization Table

Table S1 Extended Optimisation Table




| Entry | Photocatalyst | Lewis acid (mol %) | Ligand (mol %) | Solvent/conc. (M) | Temp. (°C) | Conversion (%)[a] | Yield (%)[a] | er[c] | dr[d] |
|---|---|---|---|---|---|---|---|---|---|
| **1** | $Ir(ppy)_3$ | $Sc(OTf)_3$ (25) | **L1** (30) | $CH_2Cl_2$ (0.02) | 10-15[b] | 11 | 10 | - | 1:1 |
| **2** | $Ir(ppy)_3$ | $Sc(OTf)_3$ (25) | **L2** (30) | $CH_2Cl_2$ (0.02) | 10-15[b] | 9 | 10 | 50:50 | - |
| **3** | $Ir(ppy)_3$ | $Sc(OTf)_3$ (25) | **L3** (30) | $CH_2Cl_2$ (0.02) | 10-15[b] | <10 | 5 | 70:30 | - |
| **4** | $Ir(ppy)_3$ | $Sc(OTf)_3$ (25) | **3** (30) | $CH_2Cl_2$ (0.02) | 10-15[b] | 100 | 96 | 75:25 | >20:1 |
| **5** | $Ir(ppy)_3$ | $Sc(OTf)_3$ (25) | **3** (30) | DCE (0.02) | 10-15[b] | 59 | 40 | 67:33 | >20:1 |
| **6** | $Ir(ppy)_3$ | $Sc(OTf)_3$ (25) | **3** (30) | PhMe (0.02) | 10-15[b] | 37 | 17 | 64:35 | >20:1 |
| **7** | $Ir(ppy)_3$ | $Sc(OTf)_3$ (25) | **3** (30) | CPME (0.02) | 10-15[b] | 55 | 64 | - | 3:1 |
| **8** | $Ir(ppy)_3$ | $Sc(OTf)_3$ (25) | **3** (30) | EtOAc (0.02) | 10-15[b] | 79 | <10 | - | - |
| **9** | $Ir(ppy)_3$ | $Sc(OTf)_3$ (25) | **L4** (30) | $CH_2Cl_2$ (0.02) | 10-15[b] | n.d. | n.d. | 51:49 | n.d. |
| **10** | $Ir(ppy)_3$ | $Sc(OTf)_3$ (25) | **L5** (30) | $CH_2Cl_2$ (0.02) | 10-15[b] | n.d. | n.d. | 51:49 | n.d. |
| **11** | $Ir(ppy)_3$ | $Sc(OTf)_3$ (25) | **L6** (30) | $CH_2Cl_2$ (0.02) | 10-15[b] | n.d. | n.d. | 70:30 | n.d. |
| **12** | $Ir(ppy)_2(dtbbpy)PF_6$ | $Sc(OTf)_3$ (25) | **L7** (30) | $CH_2Cl_2$ (0.02) | 10-15[b] | <5 | <5 | 55:45 | - |
| **13** | $Ir(Fppy)_2(dtbbpy)PF_6$ | $Sc(OTf)_3$ (25) | **L6** (30) | $CH_2Cl_2$ (0.02) | 10-15[b] | 17 | 12 | 56:44 | >20:1 |
| **14** | $Ir(dFppy)_2(dtbbpy)PF_6$ | $Sc(OTf)_3$ (25) | **L6** (30) | $CH_2Cl_2$ (0.02) | 10-15[b] | 100 | 80 | 51:49 | 3:1 |
| **15** | $Ir(ppy)_3$ | $Cu(OTf)_2$ (25) | **3** (30) | $CH_2Cl_2$ (0.02) | 10-15[b] | 65 | <5 | 63:37 | - |
| **16** | $Ir(ppy)_3$ | $Mg(OTf)_2$ (25) | **3** (30) | $CH_2Cl_2$ (0.02) | 10-15[b] | 84 | 40 | 50:50 | - |
| **17** | $Ir(ppy)_3$ | $La(OTf)_3$ (25) | **3** (30) | $CH_2Cl_2$ (0.02) | 10-15[b] | 84 | 50 | 50:50 | 4:1 |
| **18** | $Ir(ppy)_3$ | $Sc(OTf)_3$ (10) | **3** (12) | $CH_2Cl_2$ (0.02) | 10-15[b] | 100 | 80 | 50:50 | 7:1 |
| **19** | $Ir(ppy)_3$ | $Sc(OTf)_3$ (25) | **3** (30) | $CH_2Cl_2$ (0.02) | 10-15[b] | 79 | 73 | 75:25 | 10:1 |
| **20** | $Ir(ppy)_3$ | $Sc(OTf)_3$ (50) | **3** (60) | $CH_2Cl_2$ (0.02) | 10-15[b] | - | - | 64:36 | - |
| **21** | $Ir(ppy)_3$ | $Sc(OTf)_3$ (25) | **3** (30) | $CH_2Cl_2$ (0.02) | -30 | 82 | 48 | 42:58 | 3:1 |
| **22** | $Ir(ppy)_3$ | $Sc(OTf)_3$ (25) | **3** (30) | $CH_2Cl_2$ (0.01) | 10-15[b] | 79 | 71 | 75:25 | >20:1 |
| **23** | $Ir(ppy)_3$ | $Sc(OTf)_3$ (25) | **3** (30) | $CH_2Cl_2$ (0.05) | 10-15[b] | 90 | 62 | 54:46 | 5:1 |
| **24** | $Ir(ppy)_3$ | none | none | $CH_2Cl_2$ (0.02) | 10-15[b] | 83 | 6 | - | >20:1 |
| **25** | none | $Sc(OTf)_3$ (25) | none | $CH_2Cl_2$ (0.02) | 10-15[b] | 100 | <5 | - | - |
| **26** | $Ir(dFppy)_3$ | $Sc(OTf)_3$ (25) | **3** (30) | $CH_2Cl_2$ (0.02) | 10-15[b] | 100 | 95 | 53:47 | >20:1 |

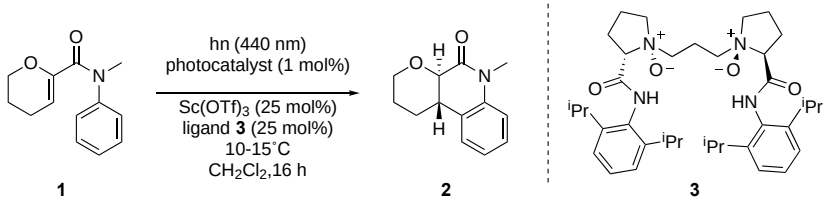
| | | | | | | | | | |
|---|---|---|---|---|---|---|---|---|---|
| **27** | $Ir(ppy)_3$ | $Sc(OTf)_3$ (25) | **L7** (30) | $CH_2Cl_2$ (0.02) | 10-15[b] | 79 | 70 | 54:46 | 5:1 |
| **28** | $Ir(ppy)_3$ | $Sc(OTf)_3$ (25) | **L8** (30) | $CH_2Cl_2$ (0.02) | 10-15[b] | 89 | 70 | 50:50 | 4:1 |
| **29** | $Ir((3'\text{-}OMe)ppy))_3$ | $Sc(OTf)_3$ (25) | **3** (30) | $CH_2Cl_2$ (0.02) | 10-15[b] | 48 | 13 | 86:14 | >20:1 |
| **30** | $Ir(dF(CF_3)ppy)_2(bpy)(PF_6)$ | $Sc(OTf)_3$ (25) | **3** (30) | $CH_2Cl_2$ (0.02) | 10-15[b] | 100 | 61 | 51:49 | 5:1 |
| **31** | $Ir(Fppy)_3$ | $Sc(OTf)_3$ (25) | **3** (30) | $CH_2Cl_2$ (0.02) | 10-15[b] | 100 | 67 | 54:46 | 1:.1 |
| **32** | $Ir((3'\text{-}OMe)ppy))_3$ | $Sc(OTf)_3$ (25) | **3** (30) | MeCN (0.02) | 10-15[b] | 30 | <5 | 70:30 | - |
| **33** | $Ir((3'\text{-}OMe)ppy))_3$ | $Sc(OTf)_3$ (25) | **L9** (30) | $CH_2Cl_2$ (0.02) | 10-15[b] | 47 | 32 | 84:16 | 5:1 |
| **34** | $Ir((3'\text{-}OMe)ppy))_3$ | $Gd(OTf)_3$ (25) | **L9** (30) | $CH_2Cl_2$ (0.02) | 10-15[b] | <5 | <5 | - | - |
| **35** | $Ir((3'\text{-}OMe)ppy))_3$ | $Y(OTf)_3$ (25) | **L9** (30) | $CH_2Cl_2$ (0.02) | 10-15[b] | <5 | <5 | - | - |
| **36** | $Ir((3'\text{-}OMe)ppy))_3$ | $Yb(OTf)_3$ (25) | **L9** (30) | $CH_2Cl_2$ (0.02) | 10-15[b] | <5 | <5 | - | - |
| **37** | $Ir((3'\text{-}OMe)ppy))_3$ | $Eu(OTf)_3$ | **L9** (30) | $CH_2Cl_2$ (0.02) | 10-15[b] | <5 | <5 | - | - |
| **38** | $Ir((3'\text{-}OMe)ppy))_3$ | $Zn(OTf)_3$ | **L9** (30) | $CH_2Cl_2$ (0.02) | 10-15[b] | <5 | <5 | - | - |
| **39** | $Ir((5\text{-}F)ppy)_3$ (**C1**) | $Sc(OTf)_3$ (25) | **L9** (30) | $CH_2Cl_2$ (0.02) | 10-15[b] | 100 | 98 | 84:16 | >20:1 |
| **40** | $Ir((5\text{-}F)ppy)_3$ (**C1**) | $Sc(OTf)_3$ (25) | **L9** (30) | $CH_2Cl_2$ (0.02) | 0 | 100 | 91 | 86:14 | >20:1 |
| **41** | $Ir((5\text{-}F)ppy)_3$ (**C1**) | $Sc(OTf)_3$ (25) | **L9** (30) | $CH_2Cl_2$ (0.02) | −30 | 100 | 92 | 88:12 | >20:1 |
| **42** | $Ir((5\text{-}F)ppy)_3$ (**C1**) | $Sc(OTf)_3$ (25) | **L9** (30) | $CH_2Cl_2$ (0.02) | −50 | <5 | <5 | - | - |
| **43** | $Ir((5\text{-}F)ppy)_3$ (**C1**) | $Sc(OTf)_3$ (25) | **L9** (30) | $CH_2Cl_2$ (0.02) | −30 | 100 | 82 | 88:12 | >20:1 |
| **44** | $Ir((5\text{-}F)ppy)_3$ (**C1**) | $Sc(OTf)_3$ (25) | **3** (30) | $CH_2Cl_2$ (0.02) | −30 | 15 | 12 | 72:28 | - |
| **45** | $Ir((5\text{-}F)ppy)_3$ (**C1**) | $Sc(OTf)_3$ (25) | **L10** (30) | $CH_2Cl_2$ (0.02) | −30 | 29 | <5 | 80:20 | - |
| **46** | $Ir((5\text{-}F)ppy)_3$ (**C1**) | $Sc(OTf)_3$ (25) | **L10** (30) | $CH_2Cl_2$ (0.02) | −20 | 88 | 80 | 88:12 | >20:1 |
| **47** | $Ir((5\text{-}F)ppy)_3$ (**C1**) | $Sc(OTf)_3$ (25) | **3** (30) | $CH_2Cl_2$ (0.02) | −20 | 72 | 56 | 88:12 | >20:1 |
| **48** | $Ir((5\text{-}F)ppy)_3$ (**C1**) | $Sc(OTf)_3$ (25) | **L10** (30) | $CH_2Cl_2$ (0.02) | −20 | <5 | <5 | 87:13 | - |
| **49** | $Ir((5\text{-}F, 4'\text{-}^tBu)ppy)_3$ (**C2**) | $Sc(OTf)_3$ (25) | **L10** (30) | $CH_2Cl_2$ (0.02) | −30 | <5 | <5 | 80:20 | - |
| **50** | $Ir((5\text{-}F, 4'\text{-}^tBu)ppy)_3$ (**C2**) | $Sc(OTf)_3$ (25) | **L10** (30) | $CH_2Cl_2$ (0.02) | 10-15[b] | 100 | 65 | 89:11 | >20:1 |
| **51** | $Ir((5\text{-}F)ppy)_3$ (**C1**) | $Sc(OTf)_3$ (25) | **L10** (27.5) | $CH_2Cl_2$ (0.02) | −30 | 100 | 90 | 89:11 | >20:1 |
| **52** | $Ir((5\text{-}F)ppy)_3$ (**C1**) | $Sc(OTf)_3$ (20) | **L10** (22) | $CH_2Cl_2$ (0.02) | −30 | 85 | 70 | 89:11 | >20:1 |
| **53** | $Ir((5\text{-}F)ppy)_3$ (**C1**) | $Sc(OTf)_3$ (15) | **L10**(16.5) | $CH_2Cl_2$ (0.02) | −30 | 74 | 57 | 89:11 | >20:1 |
| **54** | $Ir((5\text{-}F)ppy)_3$ (**C1**) | $Sc(OTf)_3$ (10) | **L10** (12) | $CH_2Cl_2$ (0.02) | −30 | 69 | 46 | 86:14 | >20:1 |
| **55** | $Ir((5\text{-}F)ppy)_3$ (**C1**) | $Sc(OTf)_3$ (25) | **3** (30) | $CH_2Cl_2$ (0.02) | 10-15[b] | 88 | 59 | 86:14 | >20:1 |
| **56** | $Ir((5\text{-}F)ppy)_3$ (**C1**) | $Sc(OTf)_3$ (25) | **L10** (30) | $CH_2Cl_2$ (0.02) | 10-15[b] | 90 | 90 | 84:16 | >20:1 |
| **57** | $Ir((5\text{-}F)ppy)_3$ (**C1**) | $Sc(OTf)_3$ (10) | **L10** (12) | $CH_2Cl_2$ (0.05) | 10-15[b] | 88 | 77 | 84:16 | >20:1 |
| **58** | $Ir((5\text{-}F, 4'\text{-}^tBu)ppy)_3$ (**C2**) | $Sc(OTf)_3$ (15) | **3** (16) | $CH_2Cl_2$ (0.02) | 10-15[b] | 85 | 65 | 88:12 | >20:1 |
| **59** | $Ir((5\text{-}F, 4'\text{-}^tBu)ppy)_3$ (**C2**) | $Sc(OTf)_3$ (15) | **3** (18) | $CH_2Cl_2$ (0.02) | −10 | 77 | 61 | 90:10 | >20:1 |
| **60** | $Ir((5\text{-}F, 4'\text{-}^tBu)ppy)_3$ (**C2**) | $Sc(OTf)_3$ (25) | **3** (27) | $CH_2Cl_2$ (0.02) | −10 | 88 | 74 | 89:11 | >20:1 |
| **61** | $Ir((5\text{-}F, 4'\text{-}^tBu)ppy)_3$ (**C2**) | $Sc(OTf)_3$ (25) | **L10** (27) | $CH_2Cl_2$ (0.02) | −10 | 87 | 84 | 89:11 | >20:1 |
| **62** | $Ir((5\text{-}CF_3)ppy)_3$ (**C3**) | $Sc(OTf)_3$ (25) | **L10** (27) | $CH_2Cl_2$ (0.02) | 10-15[b] | 55 | 45 | 89:11 | >20:1 |
| **63** | $Ir((5\text{-}CF_3, 4'\text{-}^tBu)ppy)_3$ (**4**) | $Sc(OTf)_3$ (25) | **3** (27) | $CH_2Cl_2$ (0.02) | 10-15[b] | 100 | 95 | 94:6 | >20:1 |
| **64** | $Ir((5\text{-}CF_3, 4'\text{-}^tBu)ppy)_3$ (**4**) | $Sc(OTf)_3$ (25) | **3** (25) | $CH_2Cl_2$ (0.02) | 10-15[b] | 100 | 95 | 95:5 | >20:1 |
| **65** | $Ru(deeb)_3(PF6)_2$ | $Sc(OTf)_3$ (25) | **3** (25) | $CH_2Cl_2$ (0.02) | 10-15[b] | 0 | 0 | - | - |
| **66** | $Ir(phbt)_2acac$ | $Sc(OTf)_3$ (25) | **3** (25) | $CH_2Cl_2$ (0.02) | 10-15[b] | 31 | 15 | 79:21 | >20:1 |

| | | | | | | | | | |
|---|---|---|---|---|---|---|---|---|---|
| **67** | Ir((4-F)phbt)$_2$acac | Sc(OTf)$_3$ (25) | **3** (25) | $CH_2Cl_2$ (0.02) | 10-15[b] | 54 | 33 | 76:24 | >20:1 |
| **68** | Ir((4-CF3)phbt)$_2$acac | Sc(OTf)$_3$ (25) | **3** (25) | $CH_2Cl_2$ (0.02) | 10-15[b] | 22 | 8 | 88:12 | >20:1 |
| **69** | BODIPY 1 | Sc(OTf)$_3$ (25) | **3** (25) | $CH_2Cl_2$ (0.02) | 10-15[b] | 0 | 0 | - | - |
| **70** | BODIPY 2 | Sc(OTf)$_3$ (25) | **3** (25) | $CH_2Cl_2$ (0.02) | 10-15[b] | 0 | 0 | - | - |
| **71** | BODIPY 3 | Sc(OTf)$_3$ (25) | **3** (25) | $CH_2Cl_2$ (0.02) | 10-15[b] | 0 | 0 | - | - |

Reaction optimization. a) Determined by quantitative $^1$H NMR spectroscopy using $CH_2Br_2$ as an internal standard. b) 10-15 °C refers to the internal temperature of a water-cooled water filled jacketed beaker in which the reaction vial was immersed. c) Determined by $^1$H NMR analysis of the crude reaction mixture. d) Determined by chiral stationary phase HPLC.

## I.1.2 Summary of Enantioselective Reaction Optimization

Table S2 Summary Optimisation Table




| Entry | Photocatalyst | $E_T$ (kcal mol$^{-1}$) | $E_{1/2}^{red}$ $Ir^{IV/*III}$ (V) | Lewis acid /ligand | Yield (%)[a] | er[b] | dr[c] |
|---|---|---|---|---|---|---|---|
| **1** | Ir(dFppy)$_3$ | 63.8 | -1.83 | none | 85 | 50:50 | >20:1 |
| **2** | Ir(dFppy)$_3$ | 63.8 | -1.83 | Sc(OTf)$_3$/**3** | 95 | 53:47 | >20:1 |
| **3** | Ir(ppy)$_2$(dtbbpy)($PF_6$) | 56.4 | -1.19 | Sc(OTf)$_3$/**3** | <5 | 68:32 | - |
| **4** | Ir(Fppy)$_2$(dtbbpy)($PF_6$) | 61.0 | -1.19 | Sc(OTf)$_3$/**3** | 20 | 62:38 | >20:1 |
| **5** | Ir(dFppy)$_2$(dtbbpy)($PF_6$) | 63.3 | -1.15 | Sc(OTf)$_3$/**3** | 70 | 58:42 | 14:1 |
| **6** | Ir(dF($CF_3$)ppy)$_2$(dtbbpy)($PF_6$) | 63.3 | -1.01 | Sc(OTf)$_3$/**3** | 97 | 52:48 | 18:1 |
| **7** | Ir(ppy)$_3$ | 59.4 | -1.81 | Sc(OTf)$_3$/**3** | 67 | 75:25 | >20:1 |
| **8** | Ir((3'-OMe)ppy)$_3$ | 55.3 | -1.89 | Sc(OTf)$_3$/**3** | 26 | 79:21 | >20:1 |
| **9** | Ir((5-F)ppy)$_3$ | 59.2 | -1.74 | Sc(OTf)$_3$/**3** | 84 | 86:14 | >20:1 |
| **10** | Ir((5-F)(4'-*t*-Bu)ppy)$_3$ | 59.0 | -1.80 | Sc(OTf)$_3$/**3** | 84 | 84:16 | >20:1 |
| **11** | Ir((5-$CF_3$)ppy)$_3$ | 56.0 | -1.50 | Sc(OTf)$_3$/**3** | 92 | 91:9 | >20:1 |
| **12** | Ir((5-$CF_3$)(4'-*t*-Bu)ppy)$_3$ | 55.7 | -1.55 | Sc(OTf)$_3$/**3** | 95 | 95:5 | >20:1 |
| **13** | Ir((5-$CF_3$)(4'-*t*-Bu)ppy)$_3$ | 55.7 | -1.55 | none | - | - | - |

**Table S1:** Summary of reaction optimization. a) Determined by quantitative $^1$H NMR spectroscopy using 1,3,5-trimethoxybenzene as an internal standard. b) Determined by chiral stationary phase HPLC. c) Determined by $^1$H NMR analysis of the crude reaction mixture. 10-15 °C refers to the internal temperature of a water-cooled water filled jacketed beaker in which the reaction vial was immersed

## I.1.3 Chiral Ligands Employed in this Study

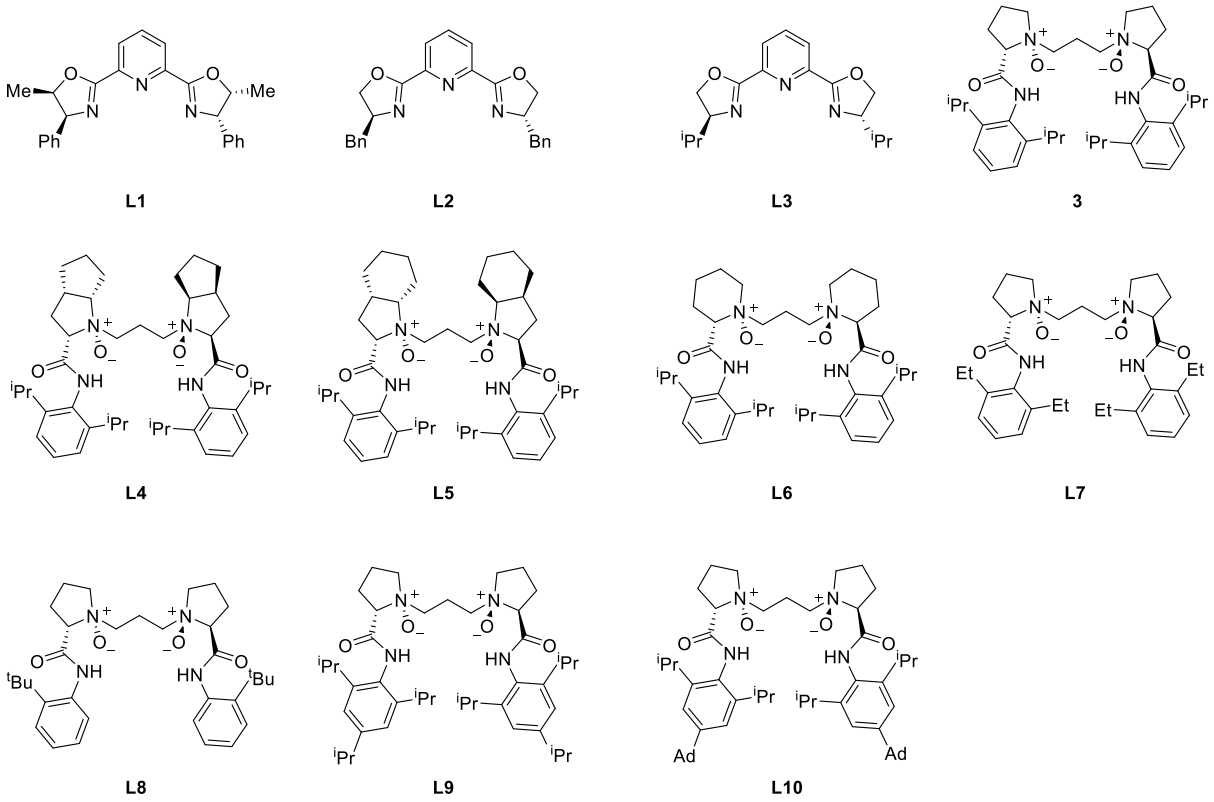



Figure S1 Chiral ligands employed in the study

## I.1.4 Photocatalysts Employed in this Study

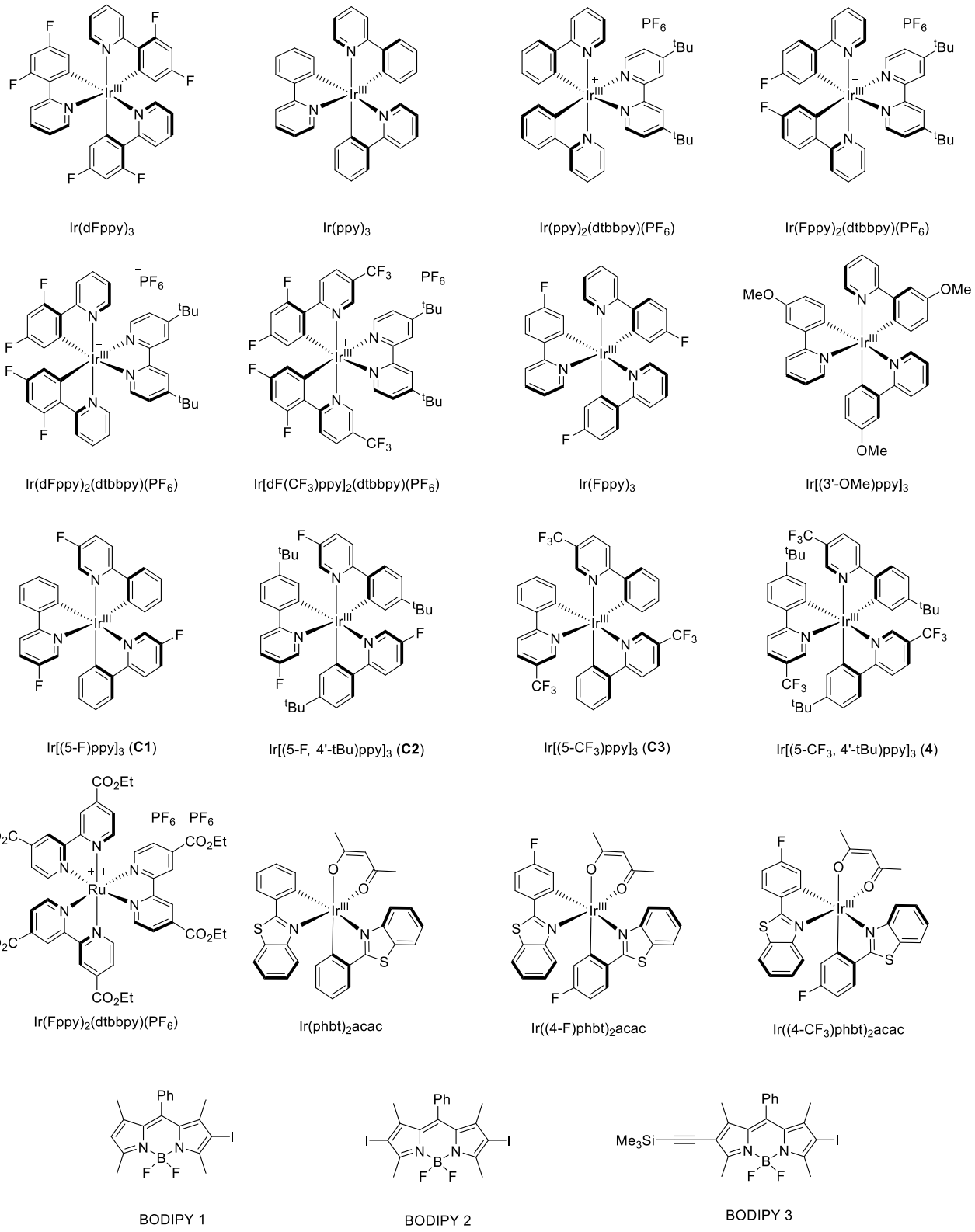



Figure S2 Photosensitizers employed in this study

# I.2 Experimental Procedures

## I.2.1 General Procedures

**General Procedure A: Preparation of alkylated anilines**

To *the appropriate aniline* in anhydrous THF (0.2 M) at 0 °C was added $^{n}$BuLi (2.6 M, 1.1 equiv.) dropwise. After a further 30 min, the appropriate alkyl halide (1.0 equiv.) was added and the reaction left to stir at room temperature for 16 hours. Upon completion, the reaction mixture was quenched by slow addition of $H_2O$, diluted with $CH_2Cl_2$, washed with sat.aq. $NaHCO_3$ (3 x), dried over $MgSO_4$, filtered, and concentrated *in vacuo*. The crude product was purified by flash column chromatography afford the corresponding *N*-alkylanilines.

**General Procedure B: Preparation of photocyclization substrates by amide coupling**

*The appropriate carboxylic acid* (1.00 equiv.) was dissolved in $CH_2Cl_2$ (0.5 M) and cooled to 0 °C and $Et_3N$ (1.10 equiv.) followed by isobutyl chloroformate (1.00 equiv.) were added. After 30 minutes at 0 °C, *the appropriate* N-*alkyl aniline* (1.10 equiv.) was added and the reaction was warmed to room temperature and stirring was continued for 16 hours. Water was added and the phases were separated, the aqueous phase was extracted twice with $CH_2Cl_2$ and the combined organic layers were dried over anhydrous $Na_2SO_4$, filtered and concentrated to give crude product, which was purified by flash column chromatography to afford the corresponding acrylanilides.

**General Procedure C: Enantioselective photocyclization**

$Sc(OTf)_3$ (51.7 mg, 0.105 mmol) and **3** (65.1 mg, 0.105 mmol) were added to a 25 mL vial equipped with a stirrer bar The vial was capped then evacuated and backfilled with argon three times. $CH_2Cl_2$ (21 mL) which had been sparged with argon for 15 minutes was added by syringe and the vial was heated to 60 °C with sonication for 30 minutes then cooled to room temperature to give a stock solution of the Lewis acid complex.

Ir((5-$CF_3$, 4'-*t*-Bu)ppy)$_3$ (**4**) (1.0 mg, 1 µmol, 1 mol%) and *the appropriate starting material* (0.100 mmol) were added to a 10 mL vial equipped with a stirrer bar The vial was capped with a 20 mm aluminium crimp cap with silicone/PTFE septum then evacuated and backfilled with argon three times. The Lewis acid complex solution was drawn into a 24 mL syringe and, under a protective layer of argon, the syringe was equipped with a syringe filter. 5 mL of the Lewis acid complex solution (0.025 equiv.) was dispensed into each reaction vial. The reaction vials were placed in a water jacketed beaker and stirred for 30 min in the dark before being irradiated with a Kessil lamp centred at 440 nm for 16 h. The reaction was transferred to a separating funnel using an additional 5 mL $CH_2Cl_2$ and washed with 1 M aqueous sodium hydroxide solution (10 mL). The aqueous phase was extracted twice with $CH_2Cl_2$ (10 mL) and the combined organic layers were dried over anhydrous $Na_2SO_4$, filtered and concentrated to give the crude product. The diastereomeric ratio was determined by quantitative $^1$H NMR analysis of the crude reaction mixture. The crude product was purified by column chromatography (EtOAc-pentane) to give the pure cyclization product.

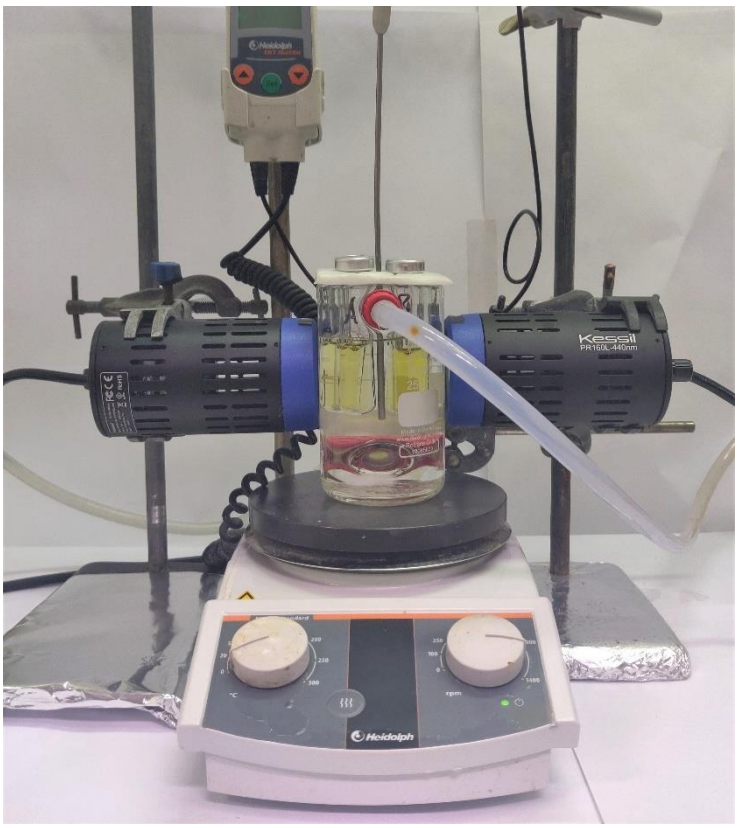



Figure S3 Experimental setup for General Procedure C showing 250 mL water jacketed beaker with reaction vials suspended in stirred water. Temperature is continuously monitored by an external probe (10 – 15 °C) . Kessil PR160L-440 nm lamps are positioned touching the edge of the jacketed vessel.

**General Procedure D1: Racemic photocyclization**

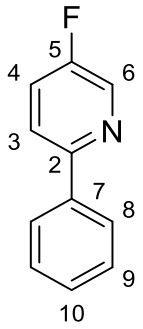
$Ir(dFppy)_3$ (0.8 mg, 1 µmol, 1 mol%) and *the appropriate starting material* (0.100 mmol) were added to a 10 mL microwave vial. The vial was capped then evacuated and backfilled with argon three times. THF (2 mL) which had been sparged with argon for 15 minutes was added by syringe and the reaction was placed in a water jacketed beaker filled with water and irradiated with a kessil lamp centred at 440 nm for 16 h. After this time, the reaction mixture was concentrated to dryness to give the crude product. $^1$H NMR analysis of the crude reaction mixture facilitated identification of the minor diastereomer peaks for determination of the dr for the enantioselective reactions. A small sample of the crude product was purified by preparative TLC to give the racemic reference material for chiral HPLC analysis.

**General Procedure D2: Racemic photocyclization for *meta*-substituted substrates**

$Ir((5\text{-}CF_3, 4'\text{-}t\text{-}Bu)ppy)_3$ (**4**) (1.0 mg, 1 µmol, 1 mol%), $Sc(OTf)_3$ (12.3 mg, 0.025 mmol, 0.25 equiv.), and *the appropriate starting material* were added to a 10 mL vial equipped with a stirrer bAr The vial was sealed and evacuated and backfilled with argon three times before $CH_2Cl_2$ (5.0 mL) sparged with argon for 15 min was added. The reaction was then irradiated with a Kessil lamp centred at 440 nm in a water jacketed beaker filled with water for 16 h. After this time, the reaction mixture was concentrated to dryness to afford the crude product. $^1$H NMR analysis of the crude reaction mixture facilitated identification of the minor diastereomer and regioisomer peaks for determination of the diastereoisomeric ration (d.r.) and regioisomeric ratio (r.r.) for the enantioselective reactions. A small sample of the crude product was purified by preparative TLC to give the racemic reference material for chiral HPLC analysis.

## I.2.2 Photocatalysts and Phenylpyridines

**5-Fluoro-2-phenylpyridine (PP1)**




This compound was synthesized by a modification of a literature procedure.[3]

2-Bromo-5-fluoropyridine (440 mg, 2.50 mmol, 1.00 equiv.), phenylboronic acid (266 mg, 3.00 mmol, 1.20 equiv.), $Pd(OAc)_2$ (14.0 mg, 0.0625 mmol, 0.0250 equiv.), $PPh_3$ (65.5 mg, 0.0250 mmol, 0.100 equiv.) and $K_2CO_3$ (931 mg, 6.75 mmol, 2.70 equiv.) were dissolved in dimethoxyethane (2.5 ml) and water (3.3 mL). The resulting mixture was sparged with argon for 15 minutes then heated under reflux for 16 hours. Upon cooling to room temperature, the reaction mixture was transferred to a separating funnel, diluted with water and extracted three times with EtOAc. The combined organic layers were washed with brine, dried over anhydrous sodium sulfate, filtered and concentrated to give the crude product which was purified by flash column chromatography (1:19, $CH_2Cl_2$: pentane) to give 5-fluoro-2-phenylpyridine (**PP1**) (303 mg, 70%) as a white solid.

**m.p.** = 38-40 °C ($CH_2Cl_2$/pentane).

**IR** (film) $\nu_{max}/cm^{-1}$: 2980, 1465, 1445, 1376, 1221, 1185, 1123, 1010, 833, 773, 727, 686.

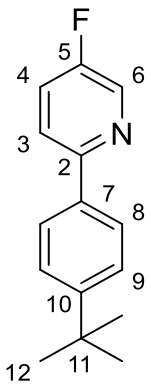
**$^1$H NMR** (400 MHz, $CDCl_3$) $\delta$ = 8.55 (d, *J* = 2.9 Hz, 1H, H-6), 7.98–7.88 (m, 2H, H-8), 7.72 (ddd, *J* = 8.8, 4.3, 0.6 Hz, 1H, H-3), 7.55–7.39 (m, 4H, H-4,9,10).

**$^{19}$F {$^1$H} NMR** (377 MHz, $CDCl_3$) $\delta$ = −129.9.

**$^{13}$C NMR** (101 MHz, $CDCl_3$) $\delta$ = 159.0 (quat., d, *J* = 256.1 Hz, C-5), 153.9 (d, *J* = 3.7 Hz, Ar CH, C-2), 138.6 (quat., C-7), 137.9 (d, *J* = 23.6 Hz, Ar CH, C-6), 129.0 (Ar CH, C-10), 128.9 (2 x Ar CH, C-9), 126.9 (2 x Ar CH, C-8), 123.6 (d, *J* = 18.4 Hz, Ar CH, C-4), 121.4 (d, *J* = 4.3 Hz, Ar CH, C-3).

**HRMS** ($ESI^+$) $C_{11}H_8FN$ $[M+H]^+$ requires 174.0714; found 174.0714, Δ 0.2 ppm.

**2-(4-(*Tert*-butyl)phenyl)-5-fluoropyridine (PP2)**




This compound was synthesized by a modification of a literature procedure.[3]

2-Bromo-5-fluoropyridine (880 mg, 5.00 mmol, 1.00 equiv.), 4-tert-butylphenylboronic acid (1.07 g, 6.00 mmol, 1.20 equiv.), $Pd(OAc)_2$ (28.0 mg, 0.125 mmol, 0.0250 equiv.), $PPh_3$ (131 mg, 0.0500 mmol, 0.100 equiv.) and $K_2CO_3$ (1.86 g, 13.5 mmol, 2.70 equiv.) were dissolved in dimethoxyethane (5 ml) and water (6.6 mL). The resulting mixture was sparged with argon for 15 minutes then heated under reflux for 16 hours. Upon cooling to room temperature, the reaction mixture was transferred to a separating funnel, diluted with water and extracted three times with EtOAc. The combined organic layers were washed with brine, dried over anhydrous sodium sulfate, filtered and concentrated to give the crude product which was purified by flash column chromatography (3:97, EtOAc: pentane) to give 2-(4-(*tert*-butyl)phenyl)-5-fluoropyridine (**PP2**) (949 mg, 83%) as a white solid.

**m.p.** = 64-66 °C (EtOAc-pentane).

**IR** (film) $\nu_{max}/cm^{-1}$: 2963, 1470, 1260, 1224, 823, 729.

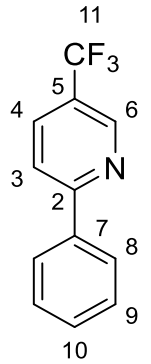
**$^1$H NMR** (400 MHz, $CDCl_3$) $\delta$ = 8.53 (d, *J* = 2.9 Hz, 1H, H-6), 7.90–7.84 (m, 2H, H-8), 7.70 (ddd, *J* = 8.8, 4.3, 0.6 Hz, 1H, H-3), 7.52–7.48 (m, 2H, H-9), 7.45 (ddd, *J* = 8.7, 8.1, 2.9 Hz, 1H, H-4), 1.36 (s, 9H, H-12).

**$^{19}$F {$^1$H} NMR** (377 MHz, $CDCl_3$) $\delta$ = 130.3.

**$^{13}$C NMR** (101 MHz, $CDCl_3$) $\delta$ = 158.8 (quat., d, *J* = 255.6 Hz, C-5), 153.9 (quat., C-2), 153.9 (quat., C-10), 137.8 (d, *J* = 23.6 Hz, Ar CH, C-6), 135.7 (quat., C-7), 126.6 (2 x Ar CH, C-8), 125.9 (2 x Ar CH, C-9), 123.6 (d, *J* = 18.4 Hz, Ar CH, C-4), 121.2 (d, *J* = 4.1 Hz, Ar CH, C-3), 34.8 (quat., C-11), 31.4 (3 x $CH_3$, C-12).

**HRMS** ($ESI^+$) $C_{16}H_{16}F_3N$ $[M+H]^+$ requires 230.1340; found 230.1340, Δ 0.3 ppm.

**2-Phenyl-5-(trifluoromethyl)pyridine (PP3)**




This compound was synthesized by a modification of a literature procedure. [3]

2-Bromo-5-trifluoromethylpyridine (2.26 g, 10.0 mmol, 1.00 equiv.), phenylboronic acid (1.46 g, 12.0 mmol, 1.20 equiv.), $Pd(OAc)_2$ (56.0 mg, 0.250 mmol, 0.0250 equiv.), $PPh_3$ (262 mg, 0.100 mmol, 0.100 equiv.) and

$K_2CO_3$ (3.73 g, 13.5 mmol, 2.70 equiv.) were dissolved in dimethoxyethane (10 ml) and water (13.5 mL). The resulting mixture was sparged with argon for 15 minutes then heated under reflux for 16 hours. Upon cooling to room temperature, the reaction mixture was transferred to a separating funnel, diluted with water and extracted three times with EtOAc. The combined organic layers were washed with brine, dried over anhydrous sodium sulfate, filtered and concentrated to give the crude product which was purified by flash column chromatography (1:19, EtOAc: pentane) then recrystallization from hexane to give 2-phenyl-5-(trifluoromethyl)pyridine (**PP3**) (949 mg, 36%) as a white needles.

**m.p.** = 60-62 °C (hexane).

**IR** (film) $\nu_{max}/cm^{-1}$: 2980, 1598, 1388, 1330, 1293, 1241, 1085, 974, 955, 940, 739, 692, 652, 641.

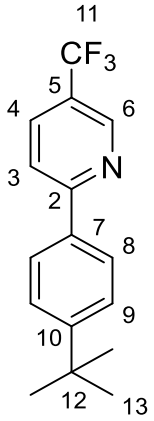
**$^1$H NMR** (400 MHz, $CDCl_3$) $\delta$ = 8.99–8.89 (m, 1H, H-6), 8.07–8.01 (m, 2H, H-8), 7.98 (dd, *J* = 8.3, 0.7 Hz, 1H, H-4), 7.84 (d, *J* = 8.4 Hz, 1H, H-3), 7.55–7.45 (m, 3H, H-9,10).

**$^{19}$F {$^1$H} NMR** (377 MHz, $CDCl_3$) $\delta$ = −62.2.

**$^{13}$C NMR** (101 MHz, $CDCl_3$) $\delta$ = 160.7 (quat., C-2), 146.6 (q, *J* = 4.1 Hz, Ar CH, C-6), 138.0 (quat., C-7), 133.9 (quat., q, *J* = 3.5 Hz, C-4), 130.1 (Ar CH, C-10), 129.0 (2 x Ar CH, C-9), 127.3 (2 x Ar CH, C-8), 124.8 (quat., q, *J* = 33.1 Hz, C-5), 123.8 (q, *J* = 272.2 Hz, C-11), 120.0 (Ar CH, C-3).

**HRMS** ($ESI^+$) $C_{12}H_8F_3N$ $[M+H]^+$ requires 224.0682; found 224.0682, Δ 0.1 ppm.

**2-(4-(*tert*-Butyl)phenyl)-5-(trifluoromethyl)pyridine (PP4)**




This compound was synthesized by a modification of a literature procedure. [3]

2-Chloro-5-trifluoromethylpyridine (908 mg, 5.0 mmol, 1.00 equiv.), (4-(*tert*-butyl)phenyl)boronic acid (1.07 g, 6.0 mmol, 1.20 equiv.), Pd(OAc)2 (28.0 mg, 0.125 mmol, 0.0250 equiv.), $PPh_3$ (131 mg, 0.050 mmol, 0.100 equiv.) and $K_2CO_3$ (1.87 g, 6.75 mmol, 2.70 equiv.) were dissolved in dimethoxyethane (5 ml) and water (6.75 mL). The resulting mixture was sparged with argon for 15 minutes then heated under reflux for 16 hours. Upon cooling to room temperature, the reaction mixture was transferred to a separating funnel, diluted with water and extracted three times with EtOAc. The combined organic layers were washed with brine, dried over anhydrous sodium sulfate, filtered and concentrated to give the crude product which was purified by flash column chromatography (1:19, EtOAc: pentane) to give 2-(4-(*tert*-butyl)phenyl)-5-(trifluoromethyl)pyridine (**PP4**) (1.23 g, 88%) as a white crystalline solid.

**m.p.** = 64-66 °C (EtOAc-pentane).

**IR** (film) $\nu_{max}/cm^{-1}$: 2917, 2849, 1601, 1326, 1163, 1122, 1084, 1012, 831.

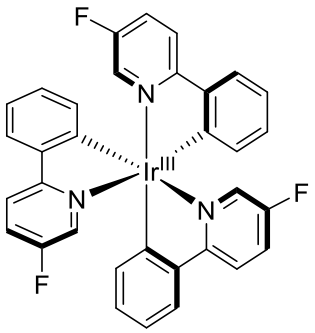
**$^1$H NMR** (400 MHz, $CDCl_3$) $\delta$ = 8.97 – 8.91 (m, 1H, H-6), 8.00 – 7.92 (m, 3H, H-4,8), 7.83 (dd, J = 8.4, 0.8 Hz, 1H, H-3), 7.58 – 7.50 (m, 2H, H-9), 1.46 – 1.29 (m, 9H, H-13).

**$^{13}$C NMR** (101 MHz, $CDCl_3$) $\delta$ = 160.7 (quat., C-2), 153.5 (quat., C-10), 146.5 (q, *J* = 4.1 Hz, Ar CH, C-6), 135.2 (quat., C-7), 133.8 (q, *J* = 3.5 Hz, Ar CH, C-4), 127.0 (2 x Ar CH, C-8), 126.0 (2 x Ar CH, C-9), 124.5 (quat., q, *J* = 32.9 Hz, C-5), 123.9 (q, *J* = 272.1 Hz, C-11), 119.6 (Ar CH, C-3), 34.8 (quat., C-12), 31.2 (3 x $CH_3$, C-13).

**$^{19}$F {$^1$H} NMR** (377 MHz, $CDCl_3$) $\delta$ = -62.2.

**HRMS** (ESI$^+$) $C_{16}H_{16}F_3N$ $[M+H]^+$ requires 280.1308; found 280.1309, Δ 0.6 ppm.

**Ir((5-F)ppy)$_3$ (47)**




$IrCl_3$ (450 mg, 1.50 mmol, 1.00 equiv.) and 5-fluoro-2-phenylpyridine (**PP1**) (585 mg, 3.39 mmol, 2.26 equiv.) in methoxyethanol-water (20/10 mL) were heated under reflux for 16 hours then cooled to room temperature. The resulting precipitate was collected by vacuum filtration and washed with water to give the chloride dimer (670 mg, 61%) as a yellow solid.

The chloride dimer (22.8 mg, 0.0200 mmol, 1.00 equiv.), AgOTf (15.4 mg, 0.0600 mmol, 3.00 equiv.) and 5-fluoro-2-phenylpyridine (173 mg, 1.00 mmol, 50.0 equiv.) were added to a 10 mL reaction vial. The vial was sealed and evacuated and backfilled with argon three times. The reaction was heated to 160 °C for 16 h then cooled to room temperature. The reaction mixture was diluted with $CH_2Cl_2$ and purified directly by flash column chromatography (7:3, $CH_2Cl_2$: pentane) to give Ir(5-Fppy)$_3$ (**47**) (25.7 mg, 91%) as a yellow solid.

**m.p.** > 250 °C ($CH_2Cl_2$/pentane).

**IR** (film) $\nu_{max}$/cm$^{-1}$: 3041, 1477, 1442, 1431, 1260, 1230, 831, 774, 736, 722.

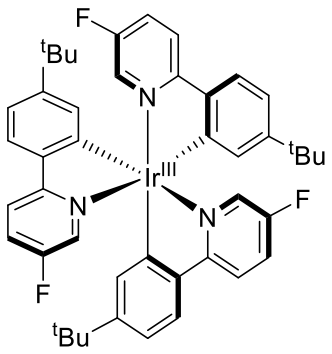
**$^1$H NMR** (500 MHz, $CDCl_3$) $\delta$ = 7.89 (dd, *J* = 8.9, 4.7 Hz, 3H), 7.59 (dd, *J* = 7.7, 1.4 Hz, 3H), 7.45 – 7.37 (m, 6H), 6.93 (ddd, *J* = 7.7, 7.5, 1.4 Hz, 3H), 6.85 (ddd, *J* = 7.3, 7.3, 1.4 Hz, 3H), 6.77 (dd, *J* = 7.6, 1.3 Hz, 3H).

**$^{13}$C NMR** (126 MHz, $CDCl_3$) $\delta$ = 163.3 (d, *J* = 3.3 Hz), 158.6 (d, *J* = 251.2 Hz), 158.6, 142.5, 137.0, 135.1 (d, *J* = 28.8 Hz), 129.9, 124.1 (obs. d), 124.0, 120.4, 119.8 (d, *J* = 5.7 Hz).

**$^{19}$F {$^1$H} NMR** (471 MHz, $CDCl_3$) $\delta$ = −128.5.

**HRMS** (ESI$^+$) $C_{33}H_{21}F_3IrN_3$ $[M+H]^+$ requires 710.1391; found 710.1384, Δ 0.7 ppm.

**Ir((5-F, 4'-*t*-Bu)ppy)$_3$ (48)**




$IrCl_3$ (450 mg, 1.50 mmol, 1.00 equiv.) and 2-(4-(*tert*-butyl)phenyl)-5-fluoropyridine (**PP2**) (585 mg, 3.39 mmol, 2.26 equiv.) in methoxyethanol-water (20/10 mL) were heated under reflux for 16 hours then cooled to room temperature. The resulting precipitate was collected by vacuum filtration and washed with water to give the chloride dimer (125 mg, 73%) as a yellow solid.

The chloride dimer (68.4 mg, 0.0500 mmol, 1.00 equiv.), AgOTf (38.6 mg, 0.0600 mmol, 3.00 equiv.) and 2-(4-(tert-butyl)phenyl)-5-fluoropyridine (572 mg, 1.00 mmol, 50.0 equiv.) were added to a 10 mL reaction vial. The vial was sealed and evacuated and backfilled with argon three times. The reaction was heated to 160 °C for 16 h then cooled to room temperature. The reaction mixture was diluted with $CH_2Cl_2$ and purified directly by flash column chromatography (7:3, $CH_2Cl_2$: pentane) to give Ir((5-F)(4'-*t*-Bu)ppy)$_3$ (**48**) (74.5 mg, 85%) as a yellow solid.

**IR** (film) $\nu_{max}/cm^{-1}$: 2961, 1584, 1473, 1259, 1234, 843, 806, 629.

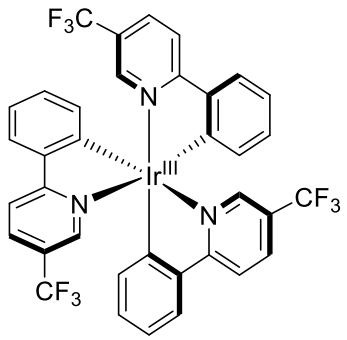
**$^1$H NMR** (500 MHz, $CDCl_3$) $\delta$ = 7.80 (dd, *J* = 9.2, 5.0 Hz, 3H), 7.48 (d, *J* = 8.2 Hz, 3H), 7.44 (app. t, *J* = 2.5 Hz, 3H), 7.35 (ddd, *J* = 9.0, 7.6, 2.8 Hz, 3H), 6.95 (dd, *J* = 8.2, 2.1 Hz, 3H), 6.82 (d, *J* = 2.1 Hz, 3H), 1.08 (s, 27H).

**$^{13}$C NMR** (126 MHz, $CDCl_3$) $\delta$ = 163.6 (d, *J* = 3.4 Hz), 158.5 (d, *J* = 250.2 Hz), 158.5, 152.2, 140.0, 135.0 (d, *J* = 28.6 Hz), 134.3, 123.8 (d, *J* = 19.1 Hz), 123.2, 119.2 (d, *J* = 5.6 Hz), 117.4, 34.5, 31.4.

**$^{19}$F {$^1$H} NMR** (471 MHz, $CDCl_3$) $\delta$ = −129.6.

**HRMS** ($ESI^+$) $C_{45}H_{44}N_3F_3Ir$ $[M+H]^+$ requires 877.3192; found 877.3190, Δ 0.1 ppm.

**Ir((5-$CF_3$)ppy)$_3$ (49)**




$IrCl_3$ (75 mg, 0.250 mmol, 1.00 equiv.) and 2-phenyl-5-(trifluoromethyl)pyridine (**PP3**) (125 mg, 0.562 mmol, 2.26 equiv.) in methoxyethanol-water (3/2 mL) were heated under reflux for 16 hours then cooled to room temperature. The resulting precipitate was collected by vacuum filtration and washed with water to give the chloride dimer (125 mg, 68%) as a yellow solid.

The chloride dimer dimer (67.2 mg, 0.0500 mmol, 1.00 equiv.), AgOTf (38.6 mg, 0.0600 mmol, 3.00 equiv.) and 2-phenyl-5-(trifluoromethyl)pyridine (557 mg, 1.00 mmol, 50.0 equiv.) were added to a 10 mL reaction vial. The vial was sealed and evacuated and backfilled with argon three times. The reaction was heated to 160 °C for 16 h then cooled to room temperature. The reaction mixture was diluted with $CH_2Cl_2$ and purified directly by flash column chromatography (7:3, $CH_2Cl_2$: pentane) to give Ir((5-$CF_3$)ppy)$_3$ (**49**) (74.5 mg, 84%) as an orange solid.

**IR** (film) $\nu_{max}/cm^{-1}$: 2359, 1612, 1582, 1328, 1309, 1265, 1232, 1175, 1135, 1084, 1054, 1034.

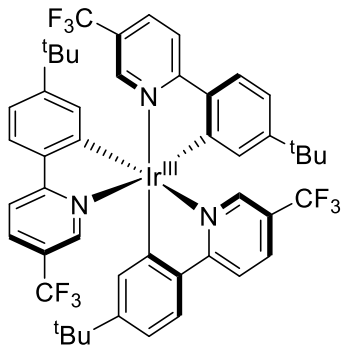
**$^1$H NMR** (500 MHz, $CDCl_3$) $\delta$ = 8.01 (d, *J* = 8.6 Hz, 3H), 7.84 (dd, *J* = 8.6, 2.1 Hz, 3H), 7.73 (dd, *J* = 7.8, 1.5 Hz, 3H), 7.67 (s, 3H), 6.99 (ddd, *J* = 7.8, 7.5, 1.4 Hz, 3H), 6.92 (ddd, *J* = 7.4, 7.2, 1.4 Hz, 3H), 6.82 (dd, *J* = 7.6, 1.3 Hz, 3H).

**$^{13}$C NMR** (126 MHz, $CDCl_3$) $\delta$ = 170.2, 144.0 (q, *J* = 4.7 Hz), 142.0, 137.3, 133.9 (d, *J* = 3.2 Hz), 131.6, 125.8, 125.1 (d, *J* = 33.8 Hz), 122.9 (d, *J* = 272.0 Hz), 121.0, 119.0.

**$^{19}$F {$^1$H} NMR** (471 MHz, $CDCl_3$) $\delta$ = −62.7.

**HRMS** ($ESI^+$) $C_{36}H_{21}F_9IrN_3$ $[M+H]^+$ requires 860.1295; found 860.1288, Δ 0.3 ppm.

**Ir((5-$CF_3$, 4'-*t*-Bu)ppy)$_3$ (50)**




$IrCl_3$ (45 mg, 0.150 mmol, 1.00 equiv.) and 2-(4-(*tert*-butyl)phenyl)-5-(trifluoromethyl)pyridine (**PP4**) (95 mg, 0.340 mmol, 2.26 equiv.) in methoxyethanol-water (2/1 mL) were heated under reflux for 16 hours then cooled to room temperature. The resulting precipitate was collected by vacuum filtration and washed with water to give the chloride dimer (129 mg, 55%) as a yellow solid.

The chloride dimer (78.0 mg, 0.050 mmol, 1.00 equiv.), AgOTf (39.0 mg, 0.150 mmol, 3.00 equiv.) and 2-(4-(*tert*-butyl)phenyl)-5-(trifluoromethyl)pyridine (390 mg, 2.50 mmol, 50.0 equiv.) were added to a 10 mL reaction vial. The vial was sealed and evacuated and backfilled with argon three times. The reaction was heated to 160 °C for 16 h then cooled to room temperature. The reaction mixture was diluted with $CH_2Cl_2$ and purified directly by flash column chromatography (1:1, $CH_2Cl_2$: pentane, followed by 1:19, EtOAc: pentane) to give Ir((5-$CF_3$)(4'-*t*-Bu)ppy)$_3$ (**50**) (50.4 mg, 98%) as an orange solid.

**IR** (film) $\nu_{max}/cm^{-1}$: 2963, 1693, 1611, 1586, 1328, 1310, 1128, 1087, 812, 773, 762, 736.

**$^1$H NMR** (500 MHz, $CDCl_3$) $\delta$ = 7.91 (d, *J* = 8.6 Hz, 3H), 7.75 (dd, *J* = 8.6, 2.1 Hz, 3H), 7.72 (s, 3H), 7.63 (d, *J* = 8.3 Hz, 3H), 7.02 (dd, *J* = 8.3, 2.1 Hz, 3H), 6.90 (d, *J* = 2.1 Hz, 3H), 1.11 (s, 27H).

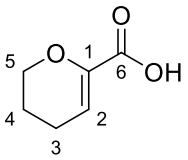
**$^{13}$C NMR** (126 MHz, $CDCl_3$) $\delta$ = 170.4, 161.3, 154.2, 143.9 (d, *J* = 4.7 Hz), 139.5, 134.6, 133.5 (q, *J* = 3.3 Hz), 125.1, 124.7 (q, *J* = 33.9 Hz), 123.1 (q, *J* = 271.9 Hz), 118.6, 118.2, 34.7, 31.3.

**$^{19}$F {$^1$H} NMR** (471 MHz, $CDCl_3$) $\delta$ = −62.8.

**HRMS** ($ESI^+$) $C_{48}H_{44}N_3F_9Ir$ $[M+H]^+$ requires 1027.3097; found 1027.3099, Δ 0.3 ppm.

## I.2.3 Precursors

**3,4-Dihydro-2H-pyran-6-carboxylic acid (55)**




This compound was synthesized by a modification of a literature procedure.[6-tetrahydrooxepin: Synthesis and Carbon-13 Nuclear Magnetic Resonance Spectrum, 7]

*n*-BuLi (2.5 M in hexane, 20 mL, 50.0 mmol, 1.00 equiv.) was cooled to 0 °C and dihydropyran (1.00 equiv.) was added. TMEDA (7.48 mL, 5.80 g, 50.0 mmol, 1.00 equiv.) was added and the reaction was warmed to room temperature and stirred for 2 hours. THF (50 mL) was added and the reaction was cooled to −78 °C. Powdered dry ice (~10 g) was added and the reaction was allowed to warm to room temperature and stirred for 3 hours. $Et_2O$ was added and the resulting solution was extracted three times with water. The combined aqueous layers were acidified with 37% hydrochloric acid and extracted three times with EtOAc. The combined EtOAc extracts were washed with water, and concentrated to give 3,4-dihydro-2*H*-pyran-6-carboxylic acid (**P1**) (4.14 g, 65%) as a waxy solid.

**m.p.** = 40-43 °C (EtOAc).

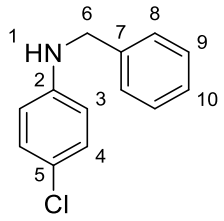
**IR** (film) $\nu_{max}/cm^{-1}$: broad signal 3467-3039, 2937, 2882, 1703, 1644, 1263, 1218, 1188, 1120, 1080, 1068, 1046, 919, 760, 702.

**$^1$H NMR** (400 MHz, $CDCl_3$) $\delta$ = 10.36 (br. s, 1H, *O*-H), 6.22 (t, *J* = 4.2 Hz, 1H, H-2), 4.19–4.02 (m, 2H, H-5), 2.31–2.15 (m, 2H, H-3), 1.93–1.79 (m, 2H, H-4).

**$^{13}$C NMR** (101 MHz, $CDCl_3$) $\delta$ = 167.6 (quat., C-6), 143.5 (quat., C-1), 113.9 (CH, C-2), 66.9 ($CH_2$, C-5), 21.4 ($CH_2$, C-4), 20.8 ($CH_2$, C-3).

**HRMS** ($ESI^+$) $C_6H_8O_3$ $[M+Na]^+$ requires 151.0366; found 151.0366, Δ 0.4 ppm.

***N*-Benzyl-4-chloroaniline (S2)**




Prepared following **General Procedure A** using 4-chloroaniline (638 mg, 5.00 mmol, 1.00 equiv.), *n*-BuLi (2.5 M in hexane, 2.00 mL, 5.00 mmol, 1.00 equiv.) and benzyl bromide (654 µL, 5.0 mmol, 1.00 equiv.). Flash column chromatography (1:49, $Et_2O$: pentane) afforded *N*-benzyl-4-chloroaniline (**S2**) (842 mg, 77%) as a white solid.

**m.p.** = 40-42 °C (EtOAc).

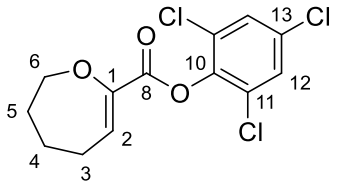
**IR** (film) $\nu_{max}/cm^{-1}$: 3422, 1602, 1509, 1494, 1482, 1449, 1325, 1295, 1274, 1172, 1124, 1089, 1070, 807, 731, 692.

**$^1$H NMR (400 MHz, $CDCl_3$)** $\delta$ = 7.27 (m, 4H, H-8,9), 7.25 – 7.15 (m, 1H, H-10), 7.08 – 6.99 (m, 2H, H-4), 6.52 – 6.44 (m, 2H, H-3), 4.23 (s, 2H, H-6).

**$^{13}$C NMR (101 MHz, $CDCl_3$)** $\delta$ = 146.5 (quat., C-2), 138.8 (quat., C-7), 129.1 (2 x Ar CH, C-9), 128.7 (2 x Ar CH, C-4), 127.5 (2 x Ar CH, C-8), 127.4 (Ar CH, C-10), 122.3 (quat., C-5), 114.1 (2 x Ar CH, C-3), 48.5 ($CH_2$, C-6).

HRMS ($ESI^+$) $C_{13}H_{13}NCl$ $[M+H]^+$ requires 218.0731; found 218.0732, Δ 0.4 ppm.

**2,4,6-Trichlorophenyl 4,5,6,7-tetrahydrooxepine-2-carboxylate (82)**




This compound was synthesized by a modification of a literature procedure.[8, 9]

To a solution of ε-caprolactone (1.1 ml, 10 mmol, 1.0 equiv.) in anhydrous THF (20 mL) was added LiHMDS (1.0 M, 12 mL, 12 mmol, 1.2 equiv.) dropwise over 10 minutes at room temperature. The mixture was then cooled to -78 °C before phenyltriflimide (4.3 g, 12 mmol, 1.2 equiv.) in anhydrous THF (10 mL) was added. Stirring was continued for 2 h before the solution was allowed to warm to 0 °C, quenched with 10% aq. NaOH (25 mL), extracted with $Et_2O$ (3 x 25 mL), dried over $MgSO_4$, filtered, and concentrated to afford an oil.

To a round bottom flask was added 2,4,6-trichlorophenyl formate (4.5 g, 20 mmol, 2.0 equiv.), $Pd(OAc)_2$ (67 mg, 0.3 mmol, 3 mol%), and Xantphos (347 mg, 0.6 mmol, 6 mol%). the flask was then evacuated and backfilled with argon three times before the crude triflate was added as a solution in sparged toluene (20 mL). The mixture was stirred for 5 minutes before $Et_3N$ (2.8 mL, 20 mmol, 2.0 equiv.) was added dropwise over 10 min and the reaction was allowed to stir for 16 h. The crude reaction mixture was directly purified by flash column chromatography (1:3, EtOAc: pentane) to yield 2,4,6-trichlorophenyl 4,5,6,7-tetrahydrooxepine-2-carboxylate (**82**) (2.5 g, 77% yield) as a white solid.

**m.p.** = 65-69 °C (EtOAc-pentane).

**IR** (film) $\nu_{max}/cm^{-1}$: 3088, 1745, 1644, 1568, 1450, 1390, 1367, 1322, 1261, 1234, 1211, 1142, 1119, 1073, 1054, 979, 928, 892, 861, 843, 818, 803, 759, 745, 690.

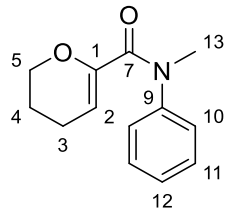
**$^1$H NMR** (400 MHz, $CDCl_3$) $\delta$ = 7.37 (s, 2H, H-12), 6.74 (t, $J$ = 6.2 Hz, 1H, H-2), 4.15 – 4.06 (m, 2H, H-6), 2.45 – 2.36 (m, 2H, H-3), 2.02 – 1.92 (m, 2H, H-5), 1.79 – 1.68 (m, 2H, H-4).

**$^{13}$C NMR** (101 MHz, $CDCl_3$) $\delta$ = 160.5 (quat., C-8), 147.8 (quat., C-10), 143.1 (quat., C-1), 131.9 (quat., C-13), 129.7 (2 x quat., C-11), 128.6 (2 x Ar CH, C-12), 126.1 (CH, C-2), 73.6 ($CH_2$, C-6), 31.4 ($CH_2$, C-5), 26.8 ($CH_2$, C-3), 24.5 ($CH_2$, C-4).

**HRMS** ($ESI^+$): $C_{13}H_{11}O_3Cl_3Na$ $[M+Na]^+$ requires 342.9666; found 342.9667, Δ 0.2 ppm.

## I.2.4 Substrates

***N*-Methyl-*N*-phenyl-3,4-dihydro-2*H*-pyran-6-carboxamide (36)**




Prepared following **General Procedure B** using *N*-methylaniline (238 mg, 2.20 mmol, 1.10 equiv.) and 3,4-dihydro-2H-pyran-6-carboxylic acid (**P1**) (256, mg, 2.00 mmol, 1.00 equiv.). Flash column chromatography (1:4, EtOAc:pentane) afforded *N*-methyl-*N*-phenyl-3,4-dihydro-2*H*-pyran-6-carboxamide (**36**) (279 mg, 64%) as a white solid.

**m.p.** = 56-58 °C (EtOAc-pentane).

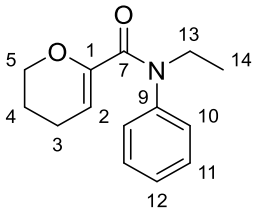
**IR** (film) $\nu_{max}$/cm$^{-1}$: 2978, 2938, 1643, 1596, 1498, 1379, 1370, 1055, 920, 775, 740, 703.

**$^1$H NMR** (400 MHz, $CDCl_3$) $\delta$ = 7.41–7.32 (m, 2H, H-10), 7.32–7.22 (m, 1H, H-12), 7.25–7.15 (m, 2H, H-11), 5.42 (t, *J* = 4.0 Hz, 1H, H-2), 3.55–3.48 (m, 2H, H-5), 3.35 (s, 3H, H-13), 2.02 (td, *J* = 6.4, 4.0 Hz, 2H, H-3), 1.72–1.61 (m, 2H, H-4).

**$^{13}$C NMR** (101 MHz, $CDCl_3$) $\delta$ = 166.1 (quat., C-7), 148.6 (quat., C-1), 145.2 (quat., C-9), 129.0 (2 x Ar CH, C-10), 126.6 (Ar CH, C-12), 125.7 (2 x Ar CH, C-11), 107.1 (CH, C-2), 65.8 ($CH_2$, C-5), 38.1 ($CH_3$, C-13), 21.7 ($CH_2$, C-4), 20.2 ($CH_2$, C-3).

**HRMS** (ESI$^+$) $C_{13}H_{15}NO_2$ $[M+Na]^+$ requires 240.0995; found 240.0997, Δ 1.0 ppm.

***N*-Ethyl-*N*-phenyl-3,4-dihydro-2*H*-pyran-6-carboxamide (56)**




Prepared following **General Procedure B** using *N*-ethylaniline (244 mg, 2.20 mmol, 1.10 equiv.) and 3,4-dihydro-2H-pyran-6-carboxylic acid (**P1**) (256 mg, 2.00 mmol, 1.00 equiv.). Flash column chromatography (3:7, EtOAc: pentane) afforded *N*-ethyl-*N*-phenyl-3,4-dihydro-2H-pyran-6-carboxamide (**56**) (284 mg, 61%) as a white solid.

**m.p.** = 84-86 °C (EtOAc-pentane).

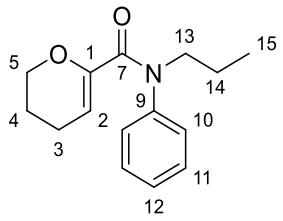
**IR** (film) $\nu_{max}$/cm$^{-1}$: 2977, 2958, 2931, 2874, 1629, 1493, 1402, 1305, 1282, 768, 747, 700.

**$^1$H NMR** (400 MHz, $CDCl_3$) $\delta$ = 7.37–7.30 (m, 2H, H-10), 7.25–7.20 (m, 1H, H-12), 7.17–7.10 (m, 2H, H-11), 5.36 (t, *J* = 4.0 Hz, 1H, H-2), 3.80 (q, *J* = 7.1 Hz, 2H, H-13), 3.51–3.37 (m, 2H, H-5), 1.99–1.94 (m, 2H, H-3), 1.65–1.58 (m, 2H, H-4), 1.13 (t, *J* = 7.1 Hz, 3H, H-14).

**$^{13}$C NMR** (101 MHz, $CDCl_3$) $\delta$ = 165.6 (quat., C-7), 148.8 (quat., C-1), 143.4 (quat., C-9), 128.9 (2 x Ar CH, C-10), 126.8 (Ar CH, C-12), 126.7 (2 x Ar CH, C-11), 106.9 (CH, C-2), 65.7 ($CH_2$, C-5), 45.1 ($CH_2$, C-13), 21.7 ($CH_2$, C-4), 20.2 ($CH_2$, C-3), 13.0 ($CH_3$, C-14).

**HRMS** (ESI$^+$) $C_{14}H_{18}NO_2$ $[M+H]^+$ requires 232.1332; found 232.1333, Δ 0.4ppm.

***N*-Phenyl-*N*-propyl-3,4-dihydro-2*H*-pyran-6-carboxamide (57)**




Prepared following **General Procedure B** using *N*-propylaniline (297 mg, 2.2 mmol, 1.1 equiv.) and 3,4-dihydro-2H-pyran-6-carboxylic acid (**P1**) (256 mg, 2.00 mmol, 1.00 equiv.). Flash column chromatography (1:4, EtOAc: pentane) afforded *N*-phenyl-*N*-propyl-3,4-dihydro-2*H*-pyran-6-carboxamide (**57**) (220 mg, 44%) as a white solid.

**m.p.** = 46-48 °C (EtOAc-pentane).

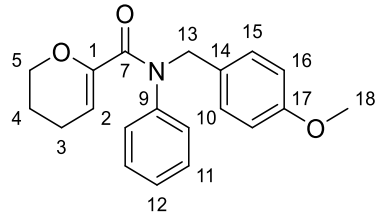
**IR** (film) $\nu_{max}$/cm$^{-1}$: 1654, 1632, 1598, 1496, 1457, 1446, 1400, 1305, 1287, 1277, 1224, 1160, 1116, 1079, 1055, 919, 782, 767, 752, 702.

**$^1$H NMR** (400 MHz, $CDCl_3$) $\delta$ = 7.37 – 7.30 (m, 2H, H-10), 7.25 – 7.19 (m, 1H, H-12), 7.18 – 7.11 (m, 2H, H-11), 5.35 (t, *J* = 4.0 Hz, 1H, H-2), 3.86 – 3.61 (m, 2H, H-13), 3.59 – 3.19 (m, 2H, H-5), 1.97 (td, *J* = 6.4, 4.0 Hz, 2H, H-3), 1.74 – 1.49 (m, 4H, H-4,14), 0.88 (t, *J* = 7.4 Hz, 3H, H-15).

**$^{13}$C NMR** (101 MHz, $CDCl_3$) $\delta$ = 165.7 (quat., C-7), 148.7 (quat., C-1), 143.5 (quat., C-9), 128.7 (2 x Ar $CH_2$, C-10), 126.6 (2 x Ar CH, C-11), 126.5 (Ar CH, C-12), 106.6 (CH, C-2), 65.6 ($CH_2$, C-5), 51.6 ($CH_2$, C-13), 21.6 ($CH_2$, C-4), 20.8 ($CH_2$, C-14), 20.0 ($CH_2$, C-3), 11.3 ($CH_3$, C-15).

**HRMS** (ESI$^+$) $C_{15}H_{20}NO_2$ $[M+H]^+$ requires 246.1489; found 246.1488, Δ -0.3 ppm.

***N*-(4-Methoxybenzyl)-*N*-phenyl-3,4-dihydro-2*H*-pyran-6-carboxamide (58)**




Prepared following **General Procedure B** using 4-methoxy-*N*-methylaniline (439 mg, 2.2 mmol, 1.1 equiv.) and 3,4-dihydro-2H-pyran-6-carboxylic acid (**P1**) (256 mg, 2.0 mmol, 1.0 equiv.). Flash column chromatography (3:17, EtOAc: pentane) afforded *N*-(4-methoxybenzyl)-*N*-phenyl-3,4-dihydro-2*H*-pyran-6-carboxamide (**58**) (381 mg, 59%) as a white solid.

**m.p.** = 74-76 °C (EtOAc-pentane).

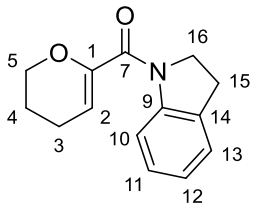
**IR** (film) $\nu_{max}$/cm$^{-1}$: 1624, 1596, 1586, 1512, 1495, 1430, 1399, 1320, 1304, 1294, 1276, 1244, 1230, 1186, 1135, 1070, 1059, 1026, 923, 820, 802, 756, 739, 694, 623.

**$^1$H NMR** (400 MHz, $CDCl_3$) $\delta$ = 7.28 – 7.09 (m, 5H, H-10,12,15), 7.03 – 6.95 (m, 2H, H-11), 6.80 – 6.72 (m, 2H, H-16), 5.39 (t, *J* = 4.0 Hz, 1H, H-2), 4.87 (s, 2H, H-13), 3.75 (s, 3H, H-18), 3.47 – 3.40 (m, 2H, H-5), 1.96 (td, *J* = 6.4, 4.0 Hz, 2H, H-3), 1.66 – 1.56 (m, 2H, H-4).

**$^{13}$C NMR** (101 MHz, $CDCl_3$) $\delta$ = 165.8 (quat., C-7), 158.8 (quat. Ar, C-17), 148.6 (quat., C-1), 143.4 (quat Ar, C-9), 129.9 (2 x Ar CH, C-15), 129.5 (quat., Ar, C-14), 128.6 (2 x Ar CH, C-11), 126.7 (2 x Ar CH, C-10), 126.6 (Ar CH, C-12), 113.7 (2 x Ar CH, C-16), 107.1 (CH, C-2), 65.6 ($CH_2$, C-5), 55.2 ($CH_3$, C-18), 52.9 ($CH_2$, C-13), 21.5 ($CH_2$, C-4), 20.1 ($CH_2$, C-3).

**HRMS** (ESI$^+$) $C_{20}H_{22}NO_3$ $[M+H]^+$ requires 324.1594; found 324.1591, Δ -1.1 ppm.

**(3,4-dihydro-2*H*-pyran-6-yl)(indolin-1-yl)methanone (S64)**




Prepared following **General Procedure B** using indoline (247 µL, 2.2 mmol, 1.1 equiv.) and 3,4-dihydro-2H-pyran-6-carboxylic acid (**55**) (256 mg, 2.0 mmol, 1.0 equiv.). Flash column chromatography (1:4, EtOAc: pentane) afforded (3,4-dihydro-2*H*-pyran-6-yl)(indolin-1-yl)methanone (**S64**) (127 mg, 28%) as an off-white solid.

**m.p.** = 76-78 °C (EtOAc-pentane).

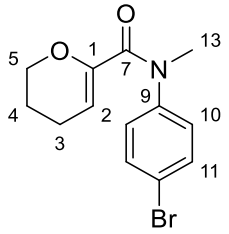
**IR** (film) $\nu_{max}$/cm$^{-1}$: 1654, 1627, 1596, 1480, 1462, 1446, 1431, 1401, 1338, 1318, 1297, 1286, 1258, 1233, 1072, 1055, 1043, 921, 874, 763, 741, 725.

**$^1$H NMR** (400 MHz, $CDCl_3$) $\delta$ = 7.97 (s, 1H, H-10), 7.23 – 7.15 (m, 2H, H-11,12), 7.01 (td, *J* = 7.5, 1.1 Hz, 1H, H-13), 5.62 (t, *J* = 4.0 Hz, 1H, H-2), 4.19 (t, *J* = 8.3 Hz, 2H, H-16), 4.14 – 4.07 (m, 2H, H-5), 3.11 (t, *J* = 8.3 Hz, 2H, H-15), 2.21 (td, *J* = 6.4, 4.0 Hz, 2H, H-3), 1.97 – 1.87 (m, 2H, H-4)

**$^{13}$C NMR** (101 MHz, $CDCl_3$) $\delta$ = 163.6 (quat., C-7), 149.4 (quat., C-1), 142.9 (quat. Ar, C-9), 132.2 (quat Ar, C-14), 127.2 (Ar CH, C-11), 124.6 (Ar CH, C-13), 123.9 (Ar CH, C-12), 117.4 (Ar CH, C-10), 106.3 (CH, C-2), 66.3 ($CH_2$, C-5), 49.4 ($CH_2$, C-16), 28.4 ($CH_2$, C-12), 21.8 ($CH_2$, C-3), 20.2 ($CH_2$, C-4)

**HRMS** (ESI$^+$) $C_{14}H_{15}NO_2Na$ [M+Na]$^+$ requires 252.0995; found 252.0997, Δ -0.8 ppm.

***N*-(4-Bromophenyl)-*N*-methyl-3,4-dihydro-2*H*-pyran-6-carboxamide (S66)**




Prepared following **General Procedure B** using 4-bromo-*N*-methylaniline (280 mg, 1.5 mmol, 1.0 equiv.) and 3,4-dihydro-2H-pyran-6-carboxylic acid (**55**) (211 mg, 1.65 mmol, 1.1 equiv.). Flash column chromatography (1:4, EtOAc: pentane) *N*-(4-bromophenyl)-*N*-methyl-3,4-dihydro-2*H*-pyran-6-carboxamide (**S66**) (262 mg, 59%) as a yellow solid.

**m.p.** = 67-70 °C (EtOAc-pentane).

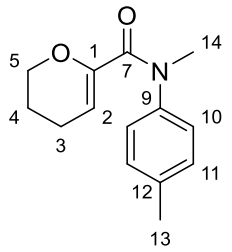
**IR** (film) $\nu_{max}$/cm$^{-1}$: 1655, 1639, 1586, 1488, 1464, 1446, 1425, 1405, 1377, 1365, 1342, 1308, 1294, 1283, 1228, 1163, 1105, 1070, 1055, 1010, 920, 838, 821, 799, 749, 714.

**$^1$H NMR** (400 MHz, $CDCl_3$) $\delta$ = 7.51 – 7.38 (m, 2H, H-10), 7.10 – 6.97 (m, 2H, H-11), 5.45 (t, *J* = 4.0 Hz, 1H, H-2), 3.61 – 3.50 (m, 2H, H-5), 3.29 (s, 3H, H-13), 2.01 (td, *J* = 6.4, 4.0 Hz, 2H, H-3), 1.72 – 1.60 (m, 2H, H-4).

**$^{13}$C NMR** (101 MHz, $CDCl_3$) $\delta$ = 165.7 (quat., C-7), 148.2 (quat., C-1), 144.1 (quat., C-9), 132.0 (Ar CH, C-10), 127.2 (Ar CH, C-11), 119.8 (quat. Ar, C-12), 107.5 ($CH_2$, C-2), 65.7 ($CH_2$, C-5), 37.9 ($CH_3$, C-13), 21.5 ($CH_2$, C-4), 20.1 ($CH_2$, C-3).

**HRMS** (ESI$^+$) $C_{13}H_{15}NO_2Br$ [M+H]$^+$ requires 296.0281; found 296.0282, Δ 0.3 ppm.

***N*-Methyl-*N*-(p-tolyl)-3,4-dihydro-2*H*-pyran-6-carboxamide (38)**




Prepared following **General Procedure B** using *N,*4-dimethylaniline (532 mg, 4.40 mmol, 1.10 equiv.) and 3,4-dihydro-2*H*-pyran-6-carboxylic acid (**55**) (512 mg, 4.00 mmol, 1.00 equiv.). Flash column chromatography (1:4, EtOAc: pentane) afforded *N*-methyl-*N*-(p-tolyl)-3,4-dihydro-2H-pyran-6-carboxamide (**38**) (693 mg, 75%) as a white solid.

**m.p.** = 46-48 °C (EtOAc-pentane).

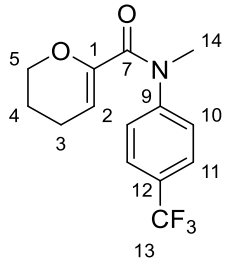
**IR** (film) $\nu_{max}/cm^{-1}$: 2977, 2931, 1633, 1511, 1366, 1053, 917, 826, 748.

**$^{1}$H NMR** (400 MHz, $CDCl_3$) $\delta$ = 7.16–7.10 (m, 2H, H-10), 7.08–7.01 (m, 2H, H-11), 5.34 (t, *J* = 4.0 Hz, 1H, H-2), 3.57–3.50 (m, 2H, H-5), 3.29 (s, 3H, H-14), 2.34 (s, 3H, H-13), 2.02–1.93 (m, 2H, H-3), 1.68–1.59 (m, 2H, H-4).

**$^{13}$C NMR** (101 MHz, $CDCl_3$) $\delta$ = 166.1 (quat., C-7), 148.5 (quat., C-1), 142.4 (quat. Ar, C-9), 136.2 (quat. Ar, C-12), 129.4 (2 x Ar CH, C-11), 125.4 (2 x Ar, C-10), 106.6 (CH, C-2), 65.7 ($CH_2$, C-5), 38.0 ($CH_3$, C-14), 21.6 ($CH_2$, C-4), 21.0 ($CH_3$, C-13), 20.0 ($CH_2$, C-3).

**HRMS** ($ESI^+$) $C_{14}H_{17}NO_2$ $[M+H]^+$ requires 232.1332; found 232.1332, Δ 0.2 ppm.

***N*-Methyl-*N*-(4-(trifluoromethyl)phenyl)-3,4-dihydro-2*H*-pyran-6-carboxamide (S68)**




Prepared following **General Procedure B** using *N*-methyl-4-(trifluoromethyl)aniline (289 mg, 1.65 mmol, 1.1 equiv.) and 3,4-dihydro-2H-pyran-6-carboxylic acid (**55**) (192 mg, 1.5 mmol, 1.0 equiv.). Flash column chromatography (1:4, EtOAc: pentane) afforded *N*-methyl-*N*-(4-(trifluoromethyl)phenyl)-3,4-dihydro-2*H*-pyran-6-carboxamide (**S68**) (280 mg, 75%) as a yellow oil.

**IR** (film) $\nu_{max}/cm^{-1}$: 1743, 1649, 1612, 1519, 1371, 1325, 1230, 1165, 1122, 1068, 1017, 920, 849, 752.

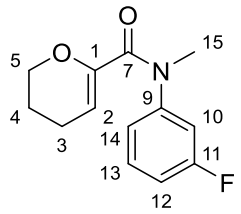
**$^{1}$H NMR** (400 MHz, $CDCl_3$) $\delta$ = 7.57 – 7.49 (m, 2H, H-10), 7.22 (d, *J* = 8.3 Hz, 2H, H-11), 5.45 (t, *J* = 4.0 Hz, 1H, H-2), 3.47 – 3.40 (m, 2H, H-5), 3.27 (s, 3H, H-14), 1.96 (td, *J* = 6.4, 4.0 Hz, 2H, H-3), 1.64 – 1.54 (m, 2H, H-4).

**$^{19}$F NMR** (377 MHz, $CDCl_3$) δ = -62.4.

**$^{13}$C NMR** (101 MHz, $CDCl_3$) $\delta$ = 165.7 (quat., C-7), 148.2 (quat., C-5), 148.0 (quat., C-9), 128.3 (quat. Ar, q, *J* = 32.7 Hz, C-12), 126.0 (2 x Ar CH, q, *J* = 3.7 Hz, C-11), 125.5 (2 x quat. Ar, C-10), 123.9 (quat., q, *J* = 271.8 Hz, C-13), 108.1 (CH, C-2), 65.7 ($CH_2$, C-5), 37.8 ($CH_3$, C-14), 21.5 ($CH_2$, C-4), 20.1 ($CH_2$, C-3).

**HRMS** ($ESI^+$) $C_{14}H_{14}F_3NO_3Na$ $[M+Na]^+$ requires 308.0869; found 308.0880, Δ 3.6 ppm.

***N*-(3-Fluorophenyl)-*N*-methyl-3,4-dihydro-2*H*-pyran-6-carboxamide (1S72)**




Prepared following **General Procedure B** using 3-fluoro-*N*-methylaniline (631 µL, 5.5 mmol, 1.1 equiv.) and 3,4-dihydro-2H-pyran-6-carboxylic acid (**55**) (640 mg, 5.0 mmol, 1.0 equiv.). Flash column chromatography (1:4, EtOAc: pentane) afforded *N*-(3-fluorophenyl)-*N*-methyl-3,4-dihydro-2*H*-pyran-6-carboxamide (**S72**) (674 mg, 57%) as a yellow oil.

**IR** (film) $\nu_{max}$/cm$^{-1}$: 1645, 1608, 1592, 1488, 1464, 1369, 1344, 1312, 1287, 1265, 1231, 1201, 1151, 1098, 1070, 1057, 1023, 967, 920, 857, 829, 786, 765, 749, 697.

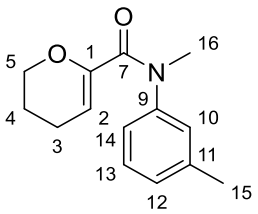
**$^1$H NMR** (400 MHz, $CDCl_3$) $\delta$ = 7.24 – 7.18 (m, 1H, H-14), 6.92 – 6.74 (m, 3H, H-10,12,13), 5.39 (t, *J* = 4.0 Hz, 1H, H-2), 3.54 – 3.37 (m, 2H, H-5), 3.23 (s, 3H, H-15), 1.94 (td, *J* = 6.4, 4.0 Hz, 2H, H-3), 1.67 – 1.47 (m, 2H, H-4).

**$^{19}$F NMR** (377 MHz, $CDCl_3$) $\delta$ = -108.5 – -115.3 (m)

**$^{13}$C NMR** (101 MHz, $CDCl_3$) $\delta$ = 164.9 (Ar CH, d, *J* = 182.0 Hz, C-11), 161.5 (quat., C-7), 148.2 (quat., C-1), 146.5 (Ar quat., d, *J* = 9.6 Hz, C-9), 129.8 (Ar CH, d, *J* = 8.9 Hz, C-13), 121.2 (Ar CH, d, *J* = 3.1 Hz, C-14), 113.3 (Ar CH, d, *J* = 20.8 Hz, C-12), 112.8 (Ar CH, d, *J* = 22.5 Hz, C-10), 107.5 (CH, C-2), 65.7 ($CH_2$, C-5), 37.9 ($CH_3$, C-15), 21.5 ($CH_2$, C-4), 20.1 ($CH_2$, C-3).

**HRMS** (ESI$^+$) $C_{13}H_{15}NO_2F$ $[M+H]^+$ requires 236.1081; found 236.1081, Δ -0.2 ppm.

***N*-Methyl-*N*-(*m*-tolyl)-3,4-dihydro-2*H*-pyran-6-carboxamide (S73)**




Prepared following **General Procedure B** using *N*,3-dimethylaniline (666 mg, 5.5 mmol, 1.1 equiv.) and 3,4-dihydro-2H-pyran-6-carboxylic acid (**55**) (640 mg, 5.0 mmol, 1.0 equiv.). Flash column chromatography (1:4, EtOAc: pentane) afforded *N*-methyl-*N*-(*m*-tolyl)-3,4-dihydro-2*H*-pyran-6-carboxamide (**S73**) (546 mg, 47%) as a yellow oil.

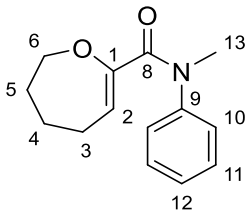
**IR** (film) $\nu_{max}$/cm$^{-1}$: 1643, 1605, 1588, 1492, 1464, 1447, 1370, 1344, 1305, 1287, 1231, 1191, 1160, 1105, 1083, 1060, 1028, 920, 789, 748, 702, 679.

**$^1$H NMR** (400 MHz, $CDCl_3$) $\delta$ = 7.21 (t, *J* = 7.7 Hz, 1H, H-10), 7.06 – 6.93 (m, 3H, H-12,13,14), 5.38 (t, *J* = 3.9 Hz, 1H, H-2), 3.58 – 3.47 (m, 2H, H-5), 3.31 (s, 3H, H-16), 2.35 (s, 3H, H-15), 2.00 (td, *J* = 6.4, 4.0 Hz, 2H, H-3), 1.73 – 1.52 (m, 2H, H-4).

**$^{13}$C NMR** (101 MHz, $CDCl_3$) $\delta$ = 166.0 (quat., C-7), 148.5 (quat., C-1), 144.9 (Ar quat., C-9), 138.7 (Ar Quat., C-11), 128.6 (Ar CH, C-13), 127.1 (Ar CH, C-12), 126.1 (Ar CH, C-10), 122.5 (Ar CH, C-14), 106.8 (CH, C-2), 65.7 ($CH_2$, C-5), 37.9 ($CH_3$, C-16), 21.6 ($CH_2$, C-4), 21.3 ($CH_3$, C-15), 20.1 ($CH_2$, C-3).

**HRMS** (ESI$^+$) $C_{14}H_{18}NO_2$ $[M+H]^+$ requires 232.1332; found 232.1332, Δ -0.1 ppm.

***N*-Methyl-*N*-phenyl-4,5,6,7-tetrahydrooxepine-2-carboxamide (83)**




To a solution of 2,4,6-trichlorophenyl 4,5,6,7-tetrahydrooxepine-2-carboxylate (**82**) (375 mg, 1.2 mmol, 1.0 equiv.) in THF (3 mL) was added $Et_3N$ (280 µl, 2.4 mmol, 2.0 equiv.), DMAP (13 mg, 0.1 mmol, 0.1 equiv.), and *N*-methylaniline (650 µl, 6.0 mmol, 5.0 equiv.). The reaction was then warmed to 60 °C and allowed to stir for 72 h. Upon complete consumption of starting material, the mixture was allowed to cool and directly purified by flash column chromatography (1:4, EtOAc: pentane) to afford *N*-methyl-*N*-phenyl-4,5,6,7-tetrahydrooxepine-2-carboxamide (**83**) as a viscous yellow oil (257 mg, 93%).

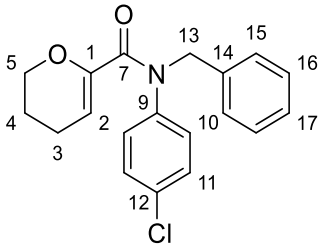
**IR** (film) $\nu_{max}/cm^{-1}$: 1624, 1596, 1586, 1512, 1495, 1430, 1399, 1320, 1304, 1294, 1276, 1244, 1230, 1186, 1135, 1070, 1059, 1026, 923, 820, 802, 756, 739, 694, 623.

**$^1$H NMR** (600 MHz, $CDCl_3$) $\delta$ = 7.40 – 7.33 (m, 2H, H-11), 7.27 – 7.21 (m, 1H, H-12), 7.20 – 7.14 (m, 2H, H-10), 5.77 (t, *J* = 5.8 Hz, 1H, H-2), 3.29 (s, 3H, H-13), 3.05 (t, *J* = 5.3 Hz, 2H, H-6), 2.17 – 2.11 (m, 2H, H-3), 1.59 (m, 2H, H-5), 1.54 – 1.47 (m, 2H, H-4).

**$^{13}$C NMR** (151 MHz, $CDCl_3$) $\delta$ = 167.2 (quat., C-8), 153.1 (quat., C-1), 145.3 (quat., C-9), 129.1 (2 x Ar CH, C-11), 126.7 (Ar CH, C-12), 126.1 (2 x Ar CH, C-10), 116.9 (CH, C-2), 72.1 ($CH_2$, C-6), 38.6 ($CH_3$, C-13), 30.7 ($CH_2$, C-5), 26.4 ($CH_2$, C-3), 25.1 ($CH_2$, C-4).

**HRMS** (ESI$^+$): $C_{14}H_{18}NO_2$ $[M+H]^+$ requires 232.1332; found 232.1332, Δ 0.0 ppm.

***N*-Benzyl-*N*-(4-chlorophenyl)-3,4-dihydro-2*H*-pyran-6-carboxamide (S86)**




Prepared following **General Procedure B** using *N*-benzyl-4-chloroaniline (**S2**) (479 mg, 2.2 mmol, 1.1 equiv.) and 3,4-dihydro-2H-pyran-6-carboxylic acid (**P1**) (256 mg, 2.0 mmol, 1.0 equiv.). Flash column chromatography (3:17, EtOAc: pentane) afforded *N*-benzyl-*N*-(4-chlorophenyl)-3,4-dihydro-2*H*-pyran-6-carboxamide (**S86**) (381 mg, 59%) as a white solid.

**m.p.** = 66-69 °C (EtOAc-pentane).

**IR** (film) $\nu_{max}/cm^{-1}$: 1651, 1627, 1493, 1434, 1412, 1394, 1319, 1303, 1282, 1229, 1139, 1090, 1077, 1048, 1030, 1016, 920, 858, 817, 744, 722, 696, 643.

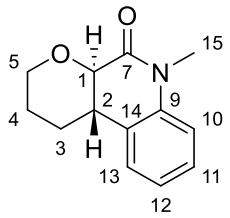
**$^1$H NMR** (400 MHz, $CDCl_3$) $\delta$ = 7.39 – 7.22 (m, 7H, H-10,11,16,17), 7.11 – 6.99 (m, 2H, H-15), 5.57 (t, *J* = 4.0 Hz, 1H, H-2), 5.00 (s, 2H, H-13), 3.58 (t, *J* = 5.1 Hz, 2H, H-5), 2.09 (td, *J* = 6.4, 4.0 Hz, 2H, H-3), 1.73 (dd, *J* = 6.4, 4.6 Hz, 2H, H-4).

**$^{13}$C NMR** (101 MHz, $CDCl_3$) $\delta$ = 165.7 (quat., C-7), 148.2 (quat., C-1), 142.0 (quat., C-9), 137.0 (quat., C-14), 132.2 (quat., C-12), 128.8 (2 x Ar CH, C-16), 128.5 (2 x Ar CH, C-11), 128.4 (Ar CH, C-17), 127.8 (2 x Ar CH, C-15), 127.4 (2 x Ar CH, C-10), 107.8 (CH, C-2), 65.7 ($CH_2$, C-5), 53.5 ($CH_2$, C-13), 21.5 ($CH_2$, C-4), 20.1 ($CH_2$, C-3).

**HRMS** ($ESI^+$) $C_{19}H_{19}NO_2Cl$ $[M+H]^+$ requires 328.1099; found 328.1097, Δ -0.5 ppm.

## I.2.6 Photocyclization Products

**(4a*R*,10b*S*)-6-Methyl-2,3,6,10b-tetrahydro-1*H*-pyrano[2,3-*c*]quinolin-5(4a*H*)-one (37)**




Prepared from *N*-methyl-*N*-phenyl-3,4-dihydro-2*H*-pyran-6-carboxamide (**36**) (21.7 mg, 0.100 mmol) following **General Procedure C**. Purification by flash column chromatography (3:2, EtOAc: pentane) afforded (4a*R*,10b*S*)-6-methyl-2,3,6,10b-tetrahydro-1*H*-pyrano[2,3-c]quinolin-5(4a*H*)-one (**37**) (21.6 mg, 95%, >20:1 dr, 94:6 er) as an off-white solid.

- or –

Prepared from *N*-methyl-*N*-phenyl-3,4-dihydro-2*H*-pyran-6-carboxamide (**36**) (435 mg, 2.0 mmol) following **General Procedure C,** but with 20 mL of preformed catalyst solution (5 mol%) and 4.0 mg (0.025 mol%) **4** in a 30 mL vial. Purification by flash column chromatography (3:2, EtOAc: pentane) afforded (4a*R*,10b*S*)-6-methyl-2,3,6,10b-tetrahydro-1*H*-pyrano[2,3-c]quinolin-5(4a*H*)-one (**37**) (288 mg, 66% (86% brsm), >20:1 dr, 80:20 er) as an off-white solid.

**m.p.** = 78-80 °C

**IR** (film) $\nu_{max}$/cm$^{-1}$: 2935, 2920, 2849, 1688, 1602, 1459, 1380, 1253, 1110.

**$^1$H NMR** (400 MHz, $CDCl_3$) $\delta$ = 7.33 – 7.28 (m, 1H, H-11), 7.22 (d, *J* = 7.7 Hz, 1H, H-13), 7.10 (ddd, *J* = 7.5, 7.5, 1.2 Hz, 1H, H-12), 7.00 (d, *J* = 1.2 Hz, 1H, H-10), 4.32 – 4.22 (m, 1H, H-5), 3.71 (d, *J* = 13.1 Hz, 1H, H-1), 3.50 (ddd, *J* = 11.9, 11.8, 2.7 Hz, 1H, H-5'), 3.40 (s, 3H, H-15), 2.97 – 2.75 (m, 1H, H-2), 2.61 – 2.47 (m, 1H, H-3), 1.95 – 1.73 (m, 2H, H-4), 1.70 – 1.54 (m, 1H, H-3').

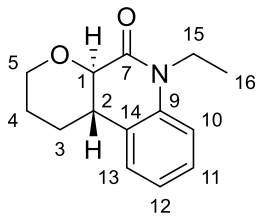
**$^{13}$C NMR** (101 MHz, $CDCl_3$) $\delta$ = 168.3 (quat., C-7), 139.3 (quat., C-9), 128.0 (Ar CH, C-11), 127.2 (quat. Ar, C-14), 124.6 (Ar CH, C-13), 123.4 (Ar CH, C-12), 114.8 (Ar CH, C-10), 76.0 (CH, C-1), 68.3 ($CH_2$, C-5), 36.5 (CH, C-2), 30.1 ($CH_3$, C-15), 26.2 ($CH_2$, C-3), 24.8 ($CH_2$, C-4).

**HRMS** (ESI$^+$): $C_{13}H_{15}NO_2$ $[M+H]^+$ requires 218.1176; found 218.1177, Δ 0.8 ppm.

**Chiral HPLC:** (Chiralpak OD-H, 30% $^i$PrOH, 70% hexane, 1.0 mL min$^{-1}$, λ = 210 nm) $\tau_R$ (major) = 11.1 min, $\tau_R$ (minor) = 16.5 min; er 95:5.

**$[\alpha]_D^{25}$** = +159.1 (*c* = 0.50, $CHCl_3$).

**(4a*R*,10b*S*)-6-Ethyl-2,3,6,10b-tetrahydro-1*H*-pyrano[2,3-c]quinolin-5(4a*H*)-one (60)**



Prepared from *N*-ethyl-*N*-phenyl-3,4-dihydro-2*H*-pyran-6-carboxamide (**56**) (23.1 mg, 0.100 mmol) following **General Procedure C**. Purification by flash column chromatography (1:1, EtOAc: pentane) afforded (4a*R*,10b*S*)-6-ethyl-2,3,6,10b-tetrahydro-1*H*-pyrano[2,3-c]quinolin-5(4a*H*)-one (**60**) (22.2 mg, 97%, >20:1 dr, 93:7 er) as an off-white solid.

**m.p.** = 80-82 °C

**IR** (film) $\nu_{max}$/cm$^{-1}$: 2970, 2935, 2850, 1687, 1458, 1389, 1242, 1113.

**$^1$H NMR** (400 MHz, $CDCl_3$) $\delta$ = 7.32–7.27 (m, 1H, H-11), 7.22 (ddd, *J* = 7.7, 1.5, 1.5 Hz, 1H, H-13), 7.09 (ddd, *J* = 7.6, 7.5, 1.1 Hz, 1H, H-12), 7.04 (dd, *J* = 8.2, 1.1 Hz, 1H, H-10), 4.27 (ddd, *J* = 11.5, 4.5, 1.7 Hz, 1H, H-5), 4.16–4.03 (m, 1H, H-15), 4.02–3.85 (m, 1H, H-15'), 3.71 (d, *J* = 13.2 Hz, 1H, H-1), 3.50 (ddd, *J* = 11.8, 11.8, 2.7 Hz, 1H, H-5'), 2.92–2.79 (m, 1H, H-2), 2.58–2.41 (m, 1H, H-3), 1.95–1.70 (m, 2H, H-4), 1.68–1.48 (m, 1H, H-3'), 1.25 (t, *J* = 7.1 Hz, 3H, H-16).

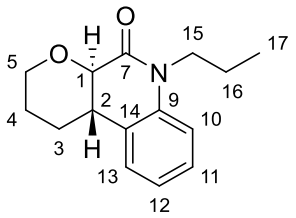
**$^{13}$C NMR** (101 MHz, $CDCl_3$) $\delta$ = 167.9 (quat., C-7), 138.3 (quat. Ar, C-9), 128.1 (Ar CH, C-11), 127.7 (quat. Ar, C-14), 125.0 (Ar CH, C-13), 123.4 (Ar CH, C-12), 114.9 (Ar CH, C-10), 76.06 (CH, C-1), 68.4 ($CH_2$, C-5), 38.0, ($CH_2$, C-15) 36.7 (Ch, C-2), 26.4 ($CH_2$, C-3), 24.9 ($CH_2$, C-4), 12.9 ($CH_3$, C-16).

**HRMS** (ESI$^+$): $C_{14}H_{17}NO_2$ $[M+Na]^+$ requires 254.1152; found 254.1153, Δ 0.6 ppm.

**Chiral HPLC:** (Chiralpak OD-H, 30% $^i$PrOH, 70% hexane, 1.0 mL min$^{-1}$, λ = 260 nm) $\tau_R$ (major) = 8.6 min, $\tau_R$ (minor) = 12.4 min; er 93:7.

**$[\alpha]_D^{25}$** = +154.7(*c* = 0.50, $CHCl_3$).

**(4a*R*,10b*S*)-6-Propyl-2,3,6,10b-tetrahydro-1*H*-pyrano[2,3-*c*]quinolin-5(4a*H*)-one (61)**



Prepared from *N*-phenyl-*N*-propyl-3,4-dihydro-2*H*-pyran-6-carboxamide (**57**) (24.5 mg, 0.100 mmol) following **General Procedure C**. Purification by flash column chromatography (2:3, EtOAc: pentane) afforded (4a*R*,10b*S*)-6-propyl-2,3,6,10b-tetrahydro-1*H*-pyrano[2,3-c]quinolin-5(4a*H*)-one (**61**) (20.9 mg, 85%, >20:1 dr, 95:5 er) as an off-white solid.

**m.p.** = 69-73 °C

**IR** (film) $\nu_{max}$/cm$^{-1}$: 1691, 1602, 1496, 1458, 1389, 1305, 1252, 1230, 1215, 1145, 1115, 1090, 963, 755, 668.

**$^1$H NMR** (400 MHz, $CDCl_3$) $\delta$ = 7.29 (ddd, *J* = 8.4, 7.3, 1.3 Hz, 1H, H-11), 7.22 (ddd, *J* = 7.6, 1.5, 1.5 Hz, 1H, H-13), 7.09 (ddd, *J* = 7.5, 7.5, 1.1 Hz, 1H, H-12), 7.01 (dd, *J* = 8.3, 1.1 Hz, 1H, H-10), 4.32 – 4.23 (m, 1H, H-5), 4.05

– 3.84 (m, 2H, H-15), 3.72 (d, *J* = 13.2 Hz, 1H, H-1), 3.50 (ddd, *J* = 11.8, 11.8, 2.6 Hz, 1H, H-5'), 2.92 – 2.80 (m, 1H, H-2), 2.53 (m, 1H, H-3), 1.97 – 1.49 (m, 5H, H-3', 4, 16), 0.94 (t, *J* = 7.4 Hz, 3H, H-17).

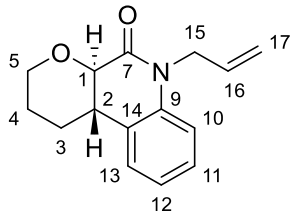
**$^{13}$C NMR** (101 MHz, $CDCl_3$) $\delta$ = 168.1 (quat., C-7), 138.2 (quat. Ar, C-9), 127.9 (Ar CH, C-11), 127.6 (quat. Ar, C-14), 124.8 (Ar CH, C-13), 123.3 (Ar CH, C-12), 115.1 (Ar CH, C-10), 75.9 (CH, C-1), 68.2 (CH, C-5), 44.0 ($CH_2$, C-15), 36.5 (CH, C-2), 26.3 ($CH_2$, C-3), 24.8 ($CH_2$, C-4), 20.4 ($CH_2$, C-16), 11.1 ($CH_3$, C-17).

**HRMS** ($ESI^+$): $C_{15}H_{20}NO_2$ $[M+H]^+$ requires 246.1489; found 246.1488, Δ 0.4 ppm.

**Chiral HPLC:** (Chiralpak OD-H, 30% $^i$PrOH, 70% hexane, 1.0 mL min$^{-1}$, λ = 210 nm) $\tau_R$ (major) = 7.1 min, $\tau_R$ (minor) = 12.0 min; er 95:5.

**$[\alpha]_D^{25}$** = +161.5 (*c* = 0.10, $CHCl_3$).

**(4a*R*,10b*S*)-6-Allyl-2,3,6,10b-tetrahydro-1*H*-pyrano[2,3-*c*]quinolin-5(4a*H*)-one (62)**




Prepared from *N*-allyl-*N*-phenyl-3,4-dihydro-2*H*-pyran-6-carboxamide (**BJ4**) (24.3 mg, 0.100 mmol) following **General Procedure C**. Purification by flash column chromatography (1:1, EtOAc: pentane) afforded (4a*R*,10b*S*)-6-allyl-2,3,6,10b-tetrahydro-1*H*-pyrano[2,3-c]quinolin-5(4a*H*)-one (**62**) (17.5 mg, 72%, >20:1 dr, 91:9 er) as an off-white solid.

**m.p.** = 80-82 °C (EtOAc-pentane).

**IR** (film) $\nu_{max}$/cm$^{-1}$: 2980, 1691, 1386, 1211.

**$^1$H NMR** (400 MHz, $CDCl_3$) $\delta$ = 7.29 – 7.18 (m, 2H, H-11,13), 7.09 (ddd, *J* = 7.5, 7.5, 1.2 Hz, 1H, H-12), 7.01 (dd, *J* = 8.1, 1.1 Hz, 1H, H-10), 5.87 (ddt, *J* = 17.2, 10.1, 4.9 Hz, 1H, H-16), 5.22 – 5.10 (m, 2H, H-17), 4.87 – 4.77 (m, 1H, H-15), 4.38 – 4.31 (m, 1H, H-15'), 4.31 – 4.24 (m, 1H, H-5), 3.78 (d, *J* = 13.2 Hz, 1H, H-1), 3.51 (td, *J* = 11.8, 2.7 Hz, 1H, H-5'), 3.10 – 2.78 (m, 1H, H-2), 2.63 – 2.42 (m, 1H, H-3), 1.94 – 1.73 (m, 2H, H-4), 1.70 – 1.52 (m, 1H, H-3').

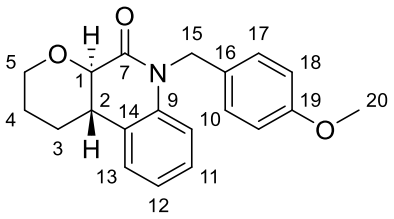
**$^{13}$C NMR** (101 MHz, $CDCl_3$) $\delta$ = 168.1 (quat., C-8), 138.6 (quat., C-9), 132.6 (CH, C-16), 128.0 (Ar CH, C-11), 127.4 (quat., C-14), 124.8 (Ar CH, C-13), 123.6 (Ar CH, C-12), 116.7 ($CH_2$, C-17), 115.6 (Ar CH, C-10), 76.0 (CH, C-1), 68.4 ($CH_2$, C-5), 45.6 ($CH_2$, C-15), 36.7 (CH, C-2), 26.4 ($CH_2$, C-3), 24.9 ($CH_2$, C-4).

**HRMS** ($ESI^+$) $C_{15}H_{17}O_2N$ $[M+H]^+$ requires 244.1332; found 244.1333, Δ 0.2 ppm.

**Chiral HPLC:** (Chiralpak OD-H, 30% $^i$PrOH, 70% hexane, 1.0 mL min$^{-1}$, λ = 210 nm) $\tau_R$ (major) = 9.1 min, $\tau_R$ (minor) = 12.0 min; er 93:7.

**$[\alpha]_D^{25}$** = +138.4 (*c* = 1.00, $CHCl_3$).

**(4a*R*,10b*S*)-6-(4-Methoxybenzyl)-2,3,6,10b-tetrahydro-1*H*-pyrano[2,3-*c*]quinolin-5(4a*H*)-one (63)**



Prepared from *N*-(4-methoxybenzyl)-*N*-phenyl-3,4-dihydro-2*H*-pyran-6-carboxamide (**58**) (32.3 mg, 0.100 mmol) following **General Procedure C**. Purification by flash column chromatography (3:7, EtOAc: pentane) afforded (4a*R*,10b*S*)-6-(4-methoxybenzyl)-2,3,6,10b-tetrahydro-1H-pyrano[2,3-*c*]quinolin-5(4a*H*)-one (**63**) (31.1 mg, 96%, >20:1 dr, 93:7 er) as an off-white solid.

**m.p.** = 138-140 °C

**IR** (film) $\nu_{max}$/cm$^{-1}$: 1688, 1603, 1513, 1496, 1460, 1391, 1304, 1249, 1212, 1178, 1114, 1034, 754.

**$^1$H NMR** (400 MHz, $CDCl_3$) $\delta$ = 7.23 – 7.12 (m, 4H, H-11,13,17), 7.05 (td, *J* = 7.5, 1.2 Hz, 1H, H-12), 6.96 (dd, *J* = 8.2, 1.2 Hz, 1H, H-10), 6.85 – 6.76 (m, 2H, H-18), 5.30 (d, *J* = 15.8 Hz, 1H, H-15), 4.98 (d, *J* = 15.8 Hz, 1H, H-15'), 4.31 (dd, *J* = 11.6, 4.4 Hz, 1H, H-5), 3.87 (d, *J* = 13.2 Hz, 1H, H-1), 3.75 (s, 3H, H-20), 3.54 (td, *J* = 11.8, 2.6 Hz, 1H, H-5'), 2.99 – 2.87 (m, 1H, H-2), 2.54 (dd, *J* = 12.8, 3.8 Hz, 1H, H-3), 1.98 – 1.81 (m, 2H, H-4), 1.63 (tdd, *J* = 12.8, 11.4, 4.2 Hz, 1H, H-3').

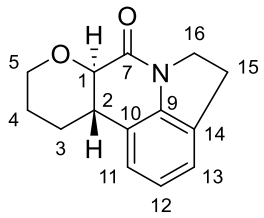
**$^{13}$C NMR** (101 MHz, $CDCl_3$) $\delta$ = 168.7 (quat., C-7), 158.8 (quat., C-19), 138.4 (quat., C-9), 128.9 (quat., C-16), 128.1 (2 x Ar CH, C-17), 127.9 (Ar CH, C-13), 127.4 (quat., C-14), 124.7 (Ar CH, C-11), 123.5 (Ar CH, C-12), 115.8 (Ar CH, C-10), 114.1 (2 x Ar CH, C-18), 76.0 (CH, C-1), 68.3 ($CH_2$, C-5), 55.2 ($CH_3$, C-20), 45.9 ($CH_2$, C-15), 36.5 (CH, C-2), 26.3 ($CH_2$, C-3), 24.8 ($CH_2$, C-4).

**HRMS** (ESI$^+$): $C_{20}H_{22}NO_3$ $[M+H]^+$ requires 324.1594; found 324.1594, Δ -0.2 ppm.

**Chiral HPLC:** (Chiralpak OD-H, 30% $^i$PrOH, 70% hexane, 1.0 mL min$^{-1}$, λ = 210 nm) $\tau_R$ (major) = 13.0 min, $\tau_R$ (minor) = 15.8 min; er 93:7.

**$[\alpha]_D^{25}$** = +98.9 (*c* = 0.10, $CHCl_3$).

**(7a*R*,11a*S*)-4,5,9,10,11,11a-hexahydropyrano[2,3-*c*]pyrrolo[3,2,1-*ij*]quinolin-7(7a*H*)-one (64)**



Prepared from (3,4-dihydro-2*H*-pyran-6-yl)(indolin-1-yl)methanone (**S64**) (22.9 mg, 0.100 mmol) following **General Procedure C**. Purification by flash column chromatography (3:7, EtOAc: pentane) afforded (7a*R*,11a*S*)-4,5,9,10,11,11a-hexahydropyrano[2,3-*c*]pyrrolo[3,2,1-*ij*]quinolin-7(7a*H*)-one (**64**) (15.0 mg, 65%, >20:1 dr, 78:22 er) as an off-white solid.

**m.p.** = 146-149 °C

**IR** (film) $\nu_{max}$/cm$^{-1}$: 2919, 2850, 1686, 1595, 1481, 1468, 1441, 1402, 1348, 1321, 1265, 1223, 1129, 1111, 1070, 1043, 956, 770, 662, 651, 621.

**$^1$H NMR** (400 MHz, $CDCl_3$) $\delta$ = 7.11 (ddd, *J* = 7.2, 1.2, 1.2 Hz, 1H, H-13), 7.03 (dd, *J* = 7.4, 7.4 Hz, 1H, H-12), 7.02 – 6.94 (m, 1H, H-11), 4.30 (ddd, *J* = 11.6, 4.7, 1.7 Hz, 1H, H-5), 4.20 (ddd, *J* = 12.1, 10.4, 4.6 Hz, 1H, H-16), 4.00

(dddd, *J* = 11.8, 10.5, 8.1, 1.0 Hz, 1H, H-16'), 3.82 (d, *J* = 12.7 Hz, 1H, H-1), 3.53 (ddd, *J* = 11.8, 11.8, 2.9 Hz, 1H, H-5'), 3.32 – 3.09 (m, 2H, H-15), 2.98 (ddd, *J* = 12.8, 12.4, 3.9 Hz, 1H, H-2), 2.57 (ddd, *J* = 12.9, 5.5, 2.9 Hz, 1H, H-3), 1.94 – 1.72 (m, 2H, H-4), 1.62 (ddd, *J* = 12.9, 11.6, 4.2 Hz, 1H, H-3')

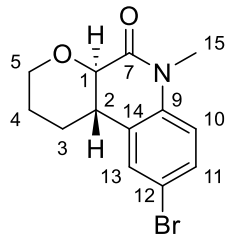
**$^{13}$C NMR** (101 MHz, $CDCl_3$) $\delta$ = 165.8 (quat., C-7), 139.9 (quat., C-9), 128.7 (quat., C-14), 123.9 (Ar CH, C-13), 123.7 (Ar CH, C-11), 122.4 (Ar CH, C-12), 122.0 (quat., C-10), 78.5 (CH, C-1), 69.2 ($CH_2$, C-5), 45.3 ($CH_2$, C-16), 38.1 (CH, C-2), 28.1 ($CH_2$, C-15), 26.1 ($CH_2$, C-3), 25.0 ($CH_2$, C-4).

**HRMS** ($ESI^+$): $C_4H_{16}NO_2$ $[M+H]^+$ requires 230.1176; found 230.1176, Δ 0.1 ppm.

**Chiral HPLC:** (Chiralpak IB N-3, 30% $^i$PrOH, 70% hexane, 1.0 mL min$^{-1}$, λ = 210 nm) $\tau_R$ (major) = 15.0 min, $\tau_R$ (minor) = 17.9 min; er 78:22

**$[\alpha]_D^{25}$** = +64.5 (*c* = 0.10, $CHCl_3$).

**(4a*R*,10b*S*)-9-Bromo-6-methyl-2,3,6,10b-tetrahydro-1*H*-pyrano[2,3-*c*]quinolin-5(4a*H*)-one (66)**




Prepared from *N*-(4-bromophenyl)-*N*-methyl-3,4-dihydro-2*H*-pyran-6-carboxamide (**S66**) (29.6 mg, 0.100 mmol) following **General Procedure C**. Purification by flash column chromatography (3:2, EtOAc: pentane) afforded (4a*R*,10b*S*)-9-bromo-6-methyl-2,3,6,10b-tetrahydro-1*H*-pyrano[2,3-*c*]quinolin-5(4a*H*)-one (**66**) (21.2 mg, 72%, >20:1 dr, 95:5 er) as an off-white solid.

**m.p.** = 130-134 °C

**IR** (film) $\nu_{max}$/cm$^{-1}$: 1691, 1489, 1469, 1415, 1374, 1252, 1218, 1112, 1082, 801, 770.

**$^1$H NMR** (400 MHz, $CDCl_3$) $\delta$ = 7.41 (ddd, *J* = 8.6, 2.3, 0.8 Hz, 1H, H-11), 7.30 (dd, *J* = 2.3, 1.2 Hz, 1H, H-13), 6.86 (d, *J* = 8.6 Hz, 1H, H-10), 4.32 – 4.24 (m, 1H, H-5), 3.68 (d, *J* = 13.1 Hz, 1H, H-1), 3.50 (ddd, *J* = 11.5, 11.5, 3.1 Hz, 1H, H-5'), 3.36 (s, 3H, H-15), 2.86 (ddd, *J* = 12.3, 12.3, 4.2 Hz, 1H, H-2), 2.48 (dd, *J* = 12.9, 3.8 Hz, 1H, H-3), 1.93 – 1.75 (m, 2H, H-4), 1.67 – 1.52 (m, 1H, H-3').

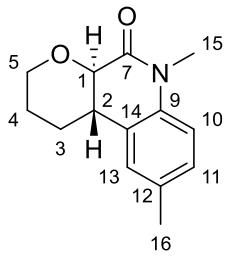
**$^{13}$C NMR** (101 MHz, $CDCl_3$) $\delta$ = 168.3 (quat., C-7), 138.5 (quat., C-9), 130.8 (Ar CH, C-11), 129.3 (2 x quat., C-12,14), 127.8 (Ar CH, C-13), 116.5 (Ar CH, C-10), 75.6 (CH, C-1), 68.3 ($CH_2$, C-5), 36.4 (CH, C-2), 30.2 ($CH_3$, C-15), 26.1 ($CH_2$, C-3), 24.7 ($CH_2$, C-4).

**HRMS** ($ESI^+$): $C_{13}H_{15}NO_2Br$ $[M+H]^+$ requires 296.0281; found 296.0282, Δ 0.3 ppm.

**Chiral HPLC:** (Chiralpak OD-H, 30% $^i$PrOH, 70% hexane, 1.0 mL min$^{-1}$, λ = 254 nm) $\tau_R$ (major) = 15.9 min, $\tau_R$ (minor) = 22.2 min; er 93:7.

**$[\alpha]_D^{25}$** = +118.8 (*c* = 0.10, $CHCl_3$).

**(4a*R*,10b*S*)-6,9-Dimethyl-2,3,6,10b-tetrahydro-1*H*-pyrano[2,3-c]quinolin-5(4a*H*)-one (39)**



Prepared from *N*-methyl-*N*-(p-tolyl)-3,4-dihydro-2H-pyran-6-carboxamide (**38**) (23.2 mg, 0.100 mmol) following **General Procedure C**. Purification by flash chromatography (7:3, EtOAc: pentane) afforded (4a*R*,10b*S*)-6,9-Dimethyl-2,3,6,10b-tetrahydro-1*H*-pyrano[2,3-c]quinolin-5(4a*H*)-one (**39**) (22.2 mg, 96%, >20:1 dr, 95:5 er) as a white solid.

**m.p.** = 112-114 °C (EtOAc-pentane).

**IR** (film) $\nu_{max}$/cm$^{-1}$: 2980, 2970, 1682, 1503, 1385, 1375, 1258, 1158, 1138, 1104, 1088, 1063, 959, 819.

**$^1$H NMR** (400 MHz, $CDCl_3$) $\delta$ = 7.10 (d, *J* = 8.3 Hz, 1H, H-11), 7.01 (s, 1H, H-13), 6.88 (d, *J* = 8.2 Hz, 1H, H-10), 4.31–4.22 (m, 1H, H-5), 3.68 (d, *J* = 13.1 Hz, 1H, H-1), 3.49 (ddd, *J* = 11.7, 11.7, 2.7 Hz, 1H, H-5'), 3.37 (s, 3H, H-15), 2.85 (ddd, *J* = 12.3, 12.3, 4.2 Hz, 1H, H-2), 2.55–2.47 (m, 1H, H-3), 2.34 (s, 3H, H-16), 1.93–1.71 (m, 2H, H-4), 1.60 (tdd, *J* = 12.8, 11.5, 4.3 Hz, 1H, H-3').

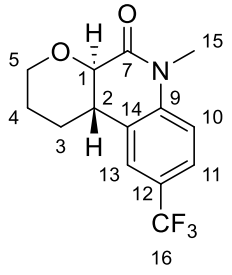
**$^{13}$C NMR** (101 MHz, $CDCl_3$) $\delta$ = 168.3 (quat., C-7), 137.0 (quat., C-9), 133.1 (quat., C-12), 128.4 (Ar CH, C-11), 127.1 (Ar CH, C-13), 125.4 (quat., C-14), 114.9 (Ar CH, C-10), 76.3 (AH, C-1), 68.4 ($CH_2$, C-5), 36.6 (CH, C2), 30.2 ($CH_3$, C-15), 26.4 ($CH_2$, C-3), 25.0 ($CH_2$, C-4), 21.0 ($CH_3$, C-16).

**HRMS** (ESI$^+$) $C_{14}H_{17}NO_2$ $[M+H]^+$ requires 232.1332; found 232.1335, Δ 1.5 ppm.

**Chiral HPLC:** (Chiralpak OD-H, 40% $^i$PrOH, 60% hexane, 1.0 mL min$^{-1}$, λ = 260 nm) $\tau_R$ (major) = 8.0 min, $\tau_R$ (minor) = 11.2 min; er 95:5.

**$[\alpha]_D^{25}$** = +155.6 (*c* = 0.50 $CHCl_3$).

**(4a*R*,10b*S*)-6-Methyl-9-(trifluoromethyl)-2,3,6,10b-tetrahydro-1*H*-pyrano[2,3-*c*]quinolin-5(4a*H*)-one (68)**



Prepared from *N*-methyl-*N*-(4-(trifluoromethyl)phenyl)-3,4-dihydro-2*H*-pyran-6-carboxamide (**S68**) (28.5 mg, 0.100 mmol) following **General Procedure C**. Purification by flash column chromatography (3:7, EtOAc: pentane) afforded (4a*R*,10b*S*)-6-methyl-9-(trifluoromethyl)-2,3,6,10b-tetrahydro-1*H*-pyrano[2,3-*c*]quinolin-5(4a*H*)-one (**68**) (28.9 mg, 28%, >20:1 dr, 92:8 er) as an off-white solid.

**m.p.** = 149-152 °C

**IR** (film) $\nu_{max}$/cm$^{-1}$: 1700, 1619, 1508, 1378, 1335, 1307, 1289, 1276, 1253, 1218, 1168, 1149, 1112, 1097, 1082, 991, 963, 827, 804, 769, 668.

**$^{1}$H NMR** (400 MHz, $CDCl_3$) $\delta$ = 7.60 – 7.55 (m, 1H, H-11), 7.44 (s, 1H, H-13), 7.08 (d, *J* = 8.5 Hz, 1H, H-10), 4.32 (ddd, J = 11.6, 4.5, 1.7 Hz, 1H, H-5), 3.73 (d, *J* = 13.2 Hz, 1H, H-1), 3.52 (td, *J* = 11.8, 2.8 Hz, 1H, H-5'), 3.43 (s, 3H, H-15), 2.92 (ddd, *J* = 12.3, 12.3, 4.2 Hz, 1H, H-2), 2.60 – 2.52 (m, 1H, H-3), 1.94 – 1.82 (m, 2H, H-4), 1.73 – 1.60 (m, 1H, H-3').

**$^{19}$F {$^{1}$H} NMR** (565 MHz, $CDCl_3$) δ -62.0.

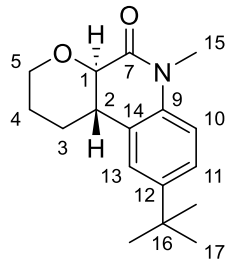
**$^{13}$C {$^{1}$H, $^{19}$F} NMR** (126 MHz, $CDCl_3$) $\delta$ = 168.2 (quat., C-7), 142.1 (quat., C-9), 127.8 (quat., C-14), 125.5 (quat., C-12), 125.4 (Ar CH, C-11), 124.1 (quat., C-16), 121.9 (Ar CH, C-13), 114.8 (Ar CH, C-10), 75.5 (CH, C-1), 68.3 ($CH_2$, C-1), 36.4 (CH, C-2), 30.2 ($CH_3$, C-15), 26.0 ($CH_2$, C-3), 24.6 ($CH_2$, C-4).

**HRMS** ($ESI^+$): $C_{14}H_{15}NO_2F_3$ $[M+H]^+$ requires 286.1049; found 286.1049, Δ -0.1 ppm.

**Chiral HPLC:** (Chiralpak OD-H, 30% $^{i}$PrOH, 70% hexane, 1.0 mL min$^{-1}$, λ = 210 nm) $\tau_R$ (major) = 14.1 min, $\tau_R$ (minor) = 19.4 min; er 92:8.

**$[\alpha]_D^{25}$** = +120.0 (*c* = 0.10, $CHCl_3$).

**(4a*R*,10b*S*)-9-(*Tert*-butyl)-6-methyl-2,3,6,10b-tetrahydro-1*H*-pyrano[2,3-c]quinolin-5(4a*H*)-one (69)**




Prepared from *N*-(4-(*tert*-butyl)phenyl)-*N*-methyl-3,4-dihydro-2*H*-pyran-6-carboxamide (**S69**) (27.3 mg, 0.100 mmol) following **General Procedure C**. Purification by flash column chromatography (1:1, EtOAc: pentane) afforded (4a*R*,10b*S*)-9-(tert-butyl)-6-methyl-2,3,6,10b-tetrahydro-1*H*-pyrano[2,3-c]quinolin-5(4a*H*)-one (**69**) (25.1 mg, 92%, >20:1 dr, 95:5 er) as a colourless oil.

**IR** (film) $\nu_{max}$/cm$^{-1}$: 2956, 2905, 2858, 1691, 1507, 1377, 1109, 1086.

**$^{1}$H NMR** (400 MHz, $CDCl_3$) $\delta$ = 7.34–7.28 (m, 1H, H-11), 7.24–7.19 (m, 1H, H-13), 6.93 (d, *J* = 8.4 Hz, 1H, H-10), 4.34–4.20 (m, 1H, H-5), 3.72 (d, *J* = 13.1 Hz, 1H, H-1), 3.51 (ddd, *J* = 11.8, 11.8, 2.7 Hz, 1H, H-5'), 3.38 (s, 3H, H-15), 2.93–2.79 (m, 1H, H-2), 2.61–2.51 (m, 1H, H-3), 1.96–1.75 (m, 2H, H-4), 1.71–1.52 (m, 1H, H-3'), 1.32 (s, 9H, H-17).

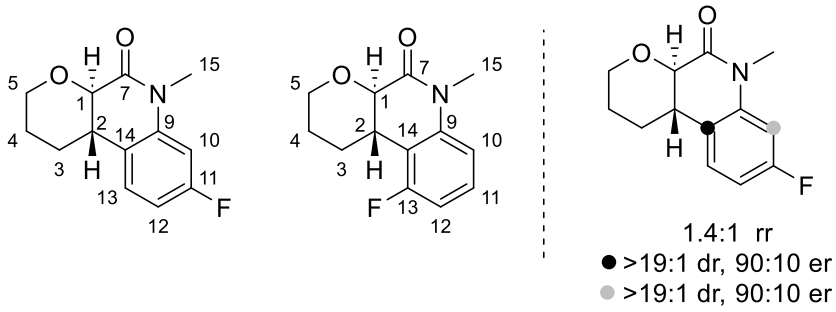
**$^{13}$C NMR** (101 MHz, $CDCl_3$) $\delta$ = 168.3 (quat., C-7), 146.3 (quat., C-12), 136.8 (quat., C-9), 126.6 (quat., C-14), 124.6 (Ar CH, C-11), 121.5 (Ar CH, C-13), 114.5 (Ar CH, C-10), 76.2 (CH, C-1), 68.3 ($CH_2$, C-5), 36.7 (CH, C-2), 34.5 (quat., C-16), 31.4 (3 x $CH_3$, C-17), 30.0 ($CH_3$, C-15), 26.2 ($CH_2$, C-3), 24.9 ($CH_2$, C-4).

**HRMS** ($ESI^+$): $C_{17}H_{24}NO_2$ $[M+H]^+$ requires 274.1802; found 274.1801, Δ 0.0 ppm.

**Chiral HPLC:** (Chiralpak OD-H, 30% $^{i}$PrOH, 70% hexane, 1.0 mL min$^{-1}$, λ = 270 nm) $\tau_R$ (major) = 9.8 min, $\tau_R$ (minor) = 13.3 min; er 95:5.

**$[\alpha]_D^{25}$** = +134.7 (*c* = 0.50, $CHCl_3$)

**(4a*R*,10b*S*)-8-Fluoro-6-methyl-2,3,6,10b-tetrahydro-1*H*-pyrano[2,3-*c*]quinolin-5(4a*H*)-one (72), and (4a*R*,10b*S*)-10-Fluoro-6-methyl-2,3,6,10b-tetrahydro-1*H*-pyrano[2,3-*c*]quinolin-5(4a*H*)-one (72b)**




Prepared from *N*-(3-fluorophenyl)-*N*-methyl-3,4-dihydro-2H-pyran-6-carboxamide (**S72**) (23.5 mg, 0.100 mmol) following **General Procedure C**. Purification by flash column chromatography (3:7→1:1, EtOAc: pentane) afforded an inseparable mixture of (4a*R*,10b*S*)-8-fluoro-6-methyl-2,3,6,10b-tetrahydro-1*H*-pyrano[2,3-*c*]quinolin-5(4a*H*)-one (**72**) (>20:1 dr, 90:10 er) and (4a*R*,10b*S*)-10-fluoro-6-methyl-2,3,6,10b-tetrahydro-1*H*-pyrano[2,3-*c*]quinolin-5(4a*H*)-one (**72b**) (>20:1 dr, 90:10 er) (1.4:1 rr) as an off-white solid. The yield refers to the combined masses of the two products (8.3 mg, 35%). The diastereomeric ratio and regioisomeric ratio was determined by quantitative $^1$H NMR analysis of the crude reaction mixture.

**(4a*R*,10b*S*)-8-Fluoro-6-methyl-2,3,6,10b-tetrahydro-1*H*-pyrano[2,3-*c*]quinolin-5(4a*H*)-one (72), and (4a*R*,10b*S*)-10-Fluoro-6-methyl-2,3,6,10b-tetrahydro-1*H*-pyrano[2,3-*c*]quinolin-5(4a*H*)-one (72b**)

**m.p.** = 96-104 °C

**IR** (film) $\nu_{max}$/cm$^{-1}$: 1697, 1613, 1509, 1470, 1437, 1378, 1346, 1312, 1253, 1237, 1218, 1142, 1110, 1086, 1061, 1003, 965, 850, 770, 667.

**(4a*R*,10b*S*)-8-Fluoro-6-methyl-2,3,6,10b-tetrahydro-1*H*-pyrano[2,3-*c*]quinolin-5(4a*H*)-one (72)**

**$^1$H NMR** (600 MHz, $CDCl_3$) δ = 7.15 (ddd, *J* = 8.1, 6.2, 1.3 Hz, 1H, H-13), 6.82 – 6.75 (m, 1H, H-12), 6.72 (dd, *J* = 10.4, 2.5 Hz, 1H, H-10), 4.32 – 4.22 (m, 1H, H-5), 3.69 (d, *J* = 13.1 Hz, 1H, H-1), 3.50 (td, *J* = 12.0, 2.6 Hz, 1H, H-5'), 3.37 (s, 3H, H-15), 2.83 (tdd, *J* = 13.1, 4.0, 1.9 Hz, 1H, H-2), 2.53 – 2.47 (m, 1H, H-3), 1.91 – 1.75 (m, 2H, H-4), 1.65 – 1.55 (m, 1H, H-3').

**$^{19}$F {$^1$H} NMR** (376 MHz, $CDCl_3$) δ = -113.14.

**$^{13}$C NMR** (151 MHz, $CDCl_3$) δ = 168.3 (quat., C-7), 162.5 (quat., d, *J* = 244.7 Hz, C-11), 140.7 (quat., d, *J* = 10.1 Hz, C-9), 125.8 (Ar CH, d, *J* = 9.5 Hz, C-13), 122.7 (quat., d, *J* = 3.2 Hz, C-14), 111.8 (Ar CH, d, *J* = 25.0 Hz, C-12), 109.5 (d, *J* = 21.1 Hz, C-10), 76.0 (CH, C-1), 68.3 ($CH_2$, C-5), 36.1 (CH ,C-2), 30.1 ($CH_3$, C-15), 26.4 ($CH_2$, C-3), 24.7 ($CH_2$, C-4).

**Chiral HPLC:** (Chiralpak IB N-3, 25% $^i$PrOH, 75% hexane, 1.0 mL min$^{-1}$, λ = 210 nm) $\tau_R$ (major) = 17.0 min, $\tau_R$ (minor) = 22.3 min; er 90:10.

**(4a*R*,10b*S*)-10-Fluoro-6-methyl-2,3,6,10b-tetrahydro-1*H*-pyrano[2,3-*c*]quinolin-5(4a*H*)-one (72b)**

**$^1$H NMR** (600 MHz, $CDCl_3$) δ = 7.26 – 7.20 (m, 1H, H-11), 6.82 – 6.75 (m, 2H, H-10,12), 4.32 – 4.22 (m, 1H, H-5), 3.81 (d, *J* = 12.8 Hz, 1H, H-1), 3.58 – 3.53 (m, 1H, H-5'), 3.38 (s, 3H, H-15), 3.04 (td, *J* = 12.2, 4.1 Hz, 1H, H-2), 2.94 – 2.88 (m, 1H, H-3), 1.91 – 1.81 (m, 2H, H-4), 1.73 (ddt, *J* = 11.5, 3.8, 1.9 Hz, 1H, H-3').

**$^{19}$F {$^1$H} NMR** (376 MHz, $CDCl_3$) δ = -113.60.

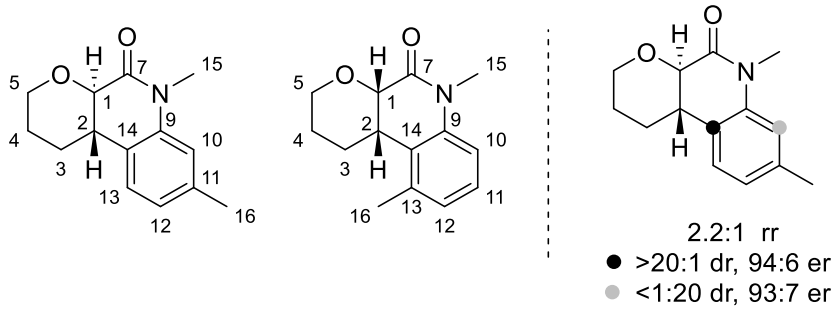
**$^{13}$C NMR** (151 MHz, $CDCl_3$) δ = 168.0 (quat., C-7), 161.5 (quat., d, *J* = 247.4 Hz, C-13), 141.2 (d, *J* = 8.2 Hz, C-9), 128.8 (Ar CH, d, *J* = 10.8 Hz, C-11), 114.1 (quat., d, *J* = 15.3 Hz, C-9), 111.1 (Ar CH, d, *J* = 2.8 Hz, C-10), 102.9 (Ar CH, d, *J* = 26.6 Hz, C-12), 75.6 (CH, C-1), 68.5 ($CH_2$, C-5), 36.5 (CH, C-2), 30.9 ($CH_3$, C-15), 27.4 ($CH_2$, C-3), 25.1 ($CH_2$, C-4).

**Chiral HPLC:** (Chiralpak IB N-3, 25% $^{i}$PrOH, 75% hexane, 1.0 mL min$^{-1}$, λ = 210 nm) $\tau_R$ (major) = 15.3 min, $\tau_R$ (minor) = 18.8 min; er 90:10.

**HRMS** (ESI$^+$): $C_{13}H_{15}NO_2F$ $[M+H]^+$ requires 236.1081; found 236.1081, Δ -0.2 ppm.

**$[\alpha]_D^{25}$** = +149.4 (*c* = 0.10, $CHCl_3$).

**(4a*R*,10b*S*)-6,8-Dimethyl-2,3,6,10b-tetrahydro-1*H*-pyrano[2,3-*c*]quinolin-5(4a*H*)-one (73), and (4a*R*,10b*S*)-6,10-dimethyl-2,3,6,10b-tetrahydro-1*H*-pyrano[2,3-*c*]quinolin-5(4a*H*) (91)**




Prepared from *N*-methyl-*N*-(*m*-tolyl)-3,4-dihydro-2*H*-pyran-6-carboxamide (**S73**) (23.1 mg, 0.100 mmol) following **General Procedure C**. Purification by flash column chromatography (3:7→3:2, EtOAc: pentane) afforded (4a*R*,10b*S*)-6,8-dimethyl-2,3,6,10b-tetrahydro-1*H*-pyrano[2,3-*c*]quinolin-5(4a*H*)-one (**73**) (6.7 mg, >20:1 dr, 94:6 er) and (4a*R*,10b*S*)-6,10-dimethyl-2,3,6,10b-tetrahydro-1*H*-pyrano[2,3-*c*]quinolin-5(4a*H*) (**91**) (3.0 mg, >20:1 dr, 93:7 er) as off-white solids. The yield refers to the combined masses of the three products (9.7 mg, 42%). The diastereomeric ratio and regiosomeric ratio was determined by quantitative $^1$H NMR analysis of the crude reaction mixture.

**(4a*R*,10b*S*)-6,8-Dimethyl-2,3,6,10b-tetrahydro-1*H*-pyrano[2,3-*c*]quinolin-5(4a*H*)-one (73)**

**m.p.** = 125-129 °C

**IR** (film) $\nu_{max}$/cm$^{-1}$: 1691, 1615, 1469, 1423, 1376 1344, 1315, 1254, 1111, 1091, 963, 769.

**$^1$H NMR** (600 MHz, $CDCl_3$) δ = 7.09 (dd, J = 7.7, 1.2 Hz, 1H, H-12), 6.92 (dd, J = 7.7, 1.6 Hz, 1H, H-13), 6.81 (d, J = 1.6 Hz, 1H, H-10), 4.27 (dd, J = 11.5, 4.5 Hz, 1H, H-5), 3.68 (d, J = 13.1 Hz, 1H, H-1), 3.50 (td, J = 11.9, 2.4 Hz, 1H, H-5'), 3.39 (s, 3H, H-15), 2.87 – 2.80 (m, 1H, H-2), 2.51 (dd, J = 12.6, 3.9 Hz, 1H, H-3), 2.37 (s, 3H, H-16), 1.85 (ddd, J = 17.0, 8.5, 4.2 Hz, 1H, H-4), 1.77 (dq, J = 13.7, 2.2 Hz, 1H, H-4), 1.58 (tdd, J = 12.9, 11.4, 4.1 Hz, 1H, H-3').

**$^{13}$C NMR** (151 MHz, $CDCl_3$) δ = 168.5 (quat., C-7), 139.1 (quat., C-9), 137.9 (quat., C-11), 124.4 (Ar CH, C-12), 124.2 (quat., C-14), 124.0 (Ar C, C-13, 115.7 (Ar CH, C-10), 76.3 (CH, C-1), 68.3 ($CH_2$, C-5), 36.2 (CH, C-2), 30.1 ($CH_3$, C-15), 26.3 ($CH_2$, C-3), 24.9 ($CH_2$, C-4), 21.4 ($CH_3$, C-16).

**HRMS** (ESI$^+$): $C_{14}H_{17}NO_2$ $[M+H]^+$ requires 232.1332; found 232.1333, Δ 0.5 ppm.

**Chiral HPLC:** (Chiralpak IG-3, 20% $^{i}$PrOH, 80% hexane, 1.0 mL min$^{-1}$, λ = 210 nm) $\tau_R$ (major) = 21.4 min, $\tau_R$ (minor) = 18.6 min; er 94:6.

**$[\alpha]_D^{25}$** = +145.3 (*c* = 0.10, $CHCl_3$).

**(4a*R*,10b*S*)-6,8-Dimethyl-2,3,6,10b-tetrahydro-1*H*-pyrano[2,3-*c*]quinolin-5(4a*H*)-one (91)**

**m.p.** = 118-120 °C

**IR** (film) $\nu_{max}$/cm$^{-1}$: 1699, 1684, 1653, 1559, 1541, 1507, 1473, 1457, 772, 668.

**$^1$H NMR** (600 MHz, $CDCl_3$) δ = 7.17 (t, J = 7.9 Hz, 1H, H-11), 6.92 (d, J = 7.6 Hz, 1H, H-12), 6.83 (d, J = 8.2 Hz, 1H, H-10), 4.56 (d, J = 6.3 Hz, 1H, H-1), 3.94 – 3.84 (m, 2H, H-5), 3.39 (s, 3H, H-15), 3.28 (ddd, J = 12.8, 6.4, 3.9 Hz, 1H, H-2), 2.35 (s, 3H, H-16), 1.90 – 1.81 (m, 2H, H-3,4), 1.70 – 1.64 (m, 1H, H-3'), 1.49 (td, J = 13.3, 3.5 Hz, 1H, H-4').

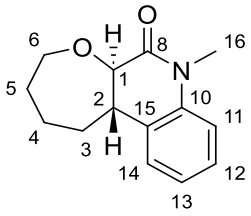
**$^{13}$C NMR** (151 MHz, $CDCl_3$) δ = 168.0 (quat., C-7), 138.7 (quat., C-9), 136.0 (quat., C-13), 127.6 (Ar CH, C-11), 126.0 (quat., C-14), 125.6 (Ar CH, C-12), 113.1 (Ar CH, C-10), 72.8 (CH, C-1), 63.2 ($CH_2$, C-5), 35.4 (CH, C-2), 30.0 ($CH_3$, C-15), 26.0 ($CH_2$, C-3), 24.4 ($CH_2$, C-4), 18.7 ($CH_3$, C-16).

**HRMS** (ESI$^+$): $C_{14}H_{17}NO_2$ $[M+H]^+$ requires 232.1332; found 232.1333, Δ 0.3 ppm.

**Chiral HPLC:** (Chiralpak IB N-3, 15% $^i$PrOH, 85% hexane, 1.0 mL min$^{-1}$, λ = 222 nm) $\tau_R$ (major) = 19.0 min, $\tau_R$ (minor) = 23.3 min; er 93:7.

**$[\alpha]_D^{25}$** = +14.3 (*c* = 0.10, $CHCl_3$).

**(5a*R*,11b*S*)-7-Methyl-1,2,3,4,7,11b-hexahydrooxepino[2,3-*c*]quinolin-6(5a*H*)-one (85)**




Prepared from *N*-methyl-*N*-phenyl-4,5,6,7-tetrahydrooxepine-2-carboxamide (**83**) (23. mg, 0.100 mmol) following **General Procedure C** using $Ir(Fppy)_3$ (1 mg, 0.001 mmol, 1 mol%). Purification by flash chromatography (3:7, EtOAc: pentane) afforded (5a*R*,11b*S*)-7-methyl-1,2,3,4,7,11b-hexahydrooxepino[2,3-*c*]quinolin-6(5a*H*)-one (**85**) (5.5 mg, 24%, >20:1 dr) as a yellow oil.

**IR** (film) $\nu_{max}$/cm$^{-1}$: 2927, 2857, 1685, 1602, 1559, 1541, 1497, 1458, 1419, 1352, 1263, 1127, 1051, 913, 740, 682, 669, 657, 618.

**$^1$H NMR** (600 MHz, $CDCl_3$) *δ* = 7.30 (m, *J* = 10.2, 2H, H-12,14), 7.10 (ddd, *J* = 7.6, 7.6, 1.2 Hz, 1H, H-13), 7.02 – 6.95 (m, 1H, H-11), 4.08 (ddd, *J* = 12.4, 6.2, 4.7 Hz, 1H, H-6), 3.84 (d, *J* = 13.7 Hz, 1H, H-1), 3.80 – 3.73 (m, 1H, H-6'), 3.39 (s, 3H, H-16), 3.08 (ddd, *J* = 13.4, 9.4, 3.7 Hz, 1H, H-2), 2.49 – 2.42 (m, 1H, H-3), 2.03 – 1.91 (m, 2H, H-4,5), 1.85 – 1.77 (m, 1H, H-3'), 1.76 – 1.64 (m, 2H, H-4',5').

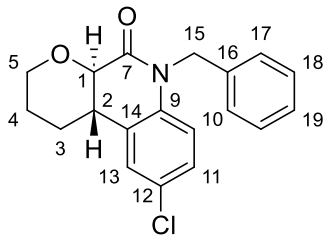
**$^{13}$C NMR** (151 MHz, $CDCl_3$) *δ* = 170.3 (quat., C-8), 139.6 (quat., C-10), 128.7 (quat., C-15), 127.7 (ArCH, C-14), 124.3 (Ar CH, C-12), 123.4 (Ar CH, C-13), 115.0 (Ar CH, C-11), 80.0 (CH, C-1), 69.2 ($CH_2$, C-6), 41.8 (CH, C-2), 30.3 ($CH_3$, C-16), 30.2($CH_2$, C-5), 27.7 ($CH_2$, C-3), 24.3 ($CH_2$, C-4).

**HRMS** (ESI$^+$): $C_{14}H_{18}NO_2$ $[M+H]^+$ requires 232.1332; found 232.1333, Δ 0.2 ppm.

**Chiral HPLC:** (Chiralpak IG-3, 25% $^i$PrOH, 75% hexane, 1.0 mL min$^{-1}$, λ = 210 nm) $\tau_R$ (major) = 17.7 min, $\tau_R$ (minor) = 16.5 min; er 87:13.

**$[\alpha]_D^{25}$** = +12.2 (*c* = 0.10, $CHCl_3$).

**(4a*R*,10b*S*)-6-Benzyl-9-chloro-2,3,6,10b-tetrahydro-1*H*-pyrano[2,3-c]quinolin-5(4a*H*)-one (86)**



Prepared from *N*-benzyl-*N*-(4-chlorophenyl)-3,4-dihydro-2*H*-pyran-6-carboxamide (**S86**) (32.9 mg, 0.100 mmol) following **General Procedure C**. Purification by flash column chromatography (3:7, EtOAc: pentane) afforded (4a*R*,10b*S*)-6-benzyl-9-chloro-2,3,6,10b-tetrahydro-1*H*-pyrano[2,3-c]quinolin-5(4a*H*)-one (**86**) (28.9 mg, 88%, >20:1 dr, 94:6 er) as an off-white solid.

**m.p.** = 158-160 °C

**IR** (film) $\nu_{max}$/cm$^{-1}$: 1694, 1489, 1455, 1422, 1376, 1303, 1253, 1212, 1182, 1122, 977, 963, 813, 771, 703, 677, 667, 633.

**$^1$H NMR** (400 MHz, $CDCl_3$) $\delta$ = 7.41 – 7.32 (m, 2H, H-18), 7.36 – 7.24 (m, 3H, H-17,19), 7.24 (dd, *J* = 2.4, 1.3 Hz, 1H, H-10), 7.19 (ddd, *J* = 8.7, 2.4, 1.0 Hz, 1H, H-11), 6.92 (d, *J* = 8.7 Hz, 1H, H-13), 5.42 (d, *J* = 16.2 Hz, 1H, H-15), 5.11 (d, *J* = 16.2 Hz, 1H, H-15'), 4.44 – 4.35 (m, 1H, H-5), 3.96 (d, *J* = 13.2 Hz, 1H, H-1), 3.63 (ddd, *J* = 11.7, 11.7, 2.8 Hz, 1H, H-5'), 3.02 (ddddd, *J* = 12.7, 11.4, 4.4, 1.1, 1.1 Hz, 1H, H-2), 2.59 (dd, *J* = 12.6, 3.8 Hz, 1H, H-3), 2.06 – 1.85 (m, 2H, H-4), 1.71 (ddd, *J* = 12.7, 11.4, 4.3 Hz, 1H, H-3').

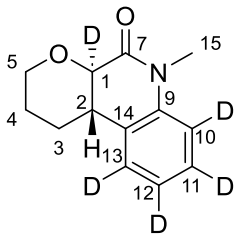
**$^{13}$C NMR** (101 MHz, $CDCl_3$) $\delta$ = 168.3 (quat., C-7), 136.9 (quat., C-16), 136.3 (quat., C-9), 129.3 (quat., C-12), 129.0 (quat., C-14), 128.8 (2 x Ar CH, C-18), 127.8 (Ar CH, C-11), 127.4 (Ar CH, C-19), 126.6 (2 x Ar CH, C-17), 125.1 (Ar CH, C-10), 117.0 (Ar CH, C-13), 75.6 CH, C-1), 68.3 ($CH_2$, C-5), 46.5 ($CH_2$, C-15), 36.5 (CH, C-2), 26.2 ($CH_2$, C-3), 24.6 ($CH_2$, C-4).

**HRMS** (ESI$^+$): $C_{19}H_{19}NO_2Cl$ $[M+H]^+$ requires 328.1099; found 328.1097, Δ -0.6 ppm.

**Chiral HPLC:** (Chiralpak IF-3, 50% $^i$PrOH, 50% hexane, 1.0 mL min$^{-1}$, λ = 210 nm) $\tau_R$ (major) = 14.7 min, $\tau_R$ (minor) = 18.6 min; er 94:6.

**$[\alpha]_D^{25}$** = +104.2 (*c* = 0.10, $CHCl_3$).

**(4a*R*,10b*S*)-6-Methyl-2,3,6,10b-tetrahydro-1*H*-pyrano[2,3-*c*]quinolin-5(4a*H*)-one-4a,7,8,9,10-$d_5$ (88)**



Prepared from *N*-Methyl-*N*-(phenyl-$d_5$)-3,4-dihydro-2*H*-pyran-6-carboxamide (**BJ18**) (22.2 mg, 0.100 mmol) following **General Procedure C**. Purification by flash column chromatography (2:3, EtOAc: pentane) afforded (4a*R*,10b*S*)-6-methyl-2,3,6,10b-tetrahydro-1*H*-pyrano[2,3-*c*]quinolin-5(4a*H*)-one-4a,7,8,9,10-$d_5$ (**88**) (22.0 mg, 99%) as an off-white solid.

**m.p.** = 76-80 °C (EtOAc-pentane).

**IR** (film) $\nu_{max}$/cm$^{-1}$: 1693, 1579, 1473, 1433, 1390, 1337, 1280, 1218, 1098, 1074, 1028, 770, 668.

**$^{1}$H NMR** (600 MHz, $CDCl_3$) $\delta$ = 4.28 (ddd, *J* = 11.5, 4.3, 2.1 Hz, 1H, H-5), 3.51 (ddd, *J* = 11.8, 11.8, 2.7 Hz, 1H, H-5'), 3.40 (s, 3H, H-15), 2.89 (dd, *J* = 11.5, 4.1 Hz, 1H, H-2), 2.53 (dd, *J* = 12.6, 3.8 Hz, 1H, H-3), 1.95 – 1.73 (m, 2H, H-4), 1.69 – 1.59 (m, 1H, H-3').

**$^{13}$C NMR** (151 MHz, $CDCl_3$) $\delta$ = 168.4 (quat., C-7), 139.2 (quat., C-9), 127.9 – 127.2 (m, Ar CD, C-11), 127.1 (quat., C-14), 124.7 – 123.9 (m, Ar CD, C-13), 123.2 – 122.5 (m, Ar CD, C-12), 115.0 – 114.1 (m, Ar CD, C-10), 75.9 – 75.3 (m, CD, C-1), 68.3 ($CH_2$, C-5), 36.4 (CH, C-2), 30.1 ($CH_3$, C-15), 26.2 ($CH_2$, C-3), 24.8 ($CH_2$, C-4).

**HRMS** ($ESI^+$) $C_{13}H_{11}D_5NO_2$ $[M+H]^+$ requires 223.1489; found 223.1491, Δ 0.6 ppm.

**Chiral HPLC:** (Chiralpak IB N-3, 30% $^{i}$PrOH, 70% hexane, 1.0 mL min$^{-1}$, $\lambda$ = 210 nm) $\tau_R$ (major) = 11.1 min, $\tau_R$ (minor) = 16.6 min; er 94:6.

**$[\alpha]_D^{25}$** = +120.0 (*c* = 1.00, $CHCl_3$).

# I.3 Characterisation of Novel Photocatalysts

## I.3.1 Absorbance and Emission Spectra of Novel Photocatalysts

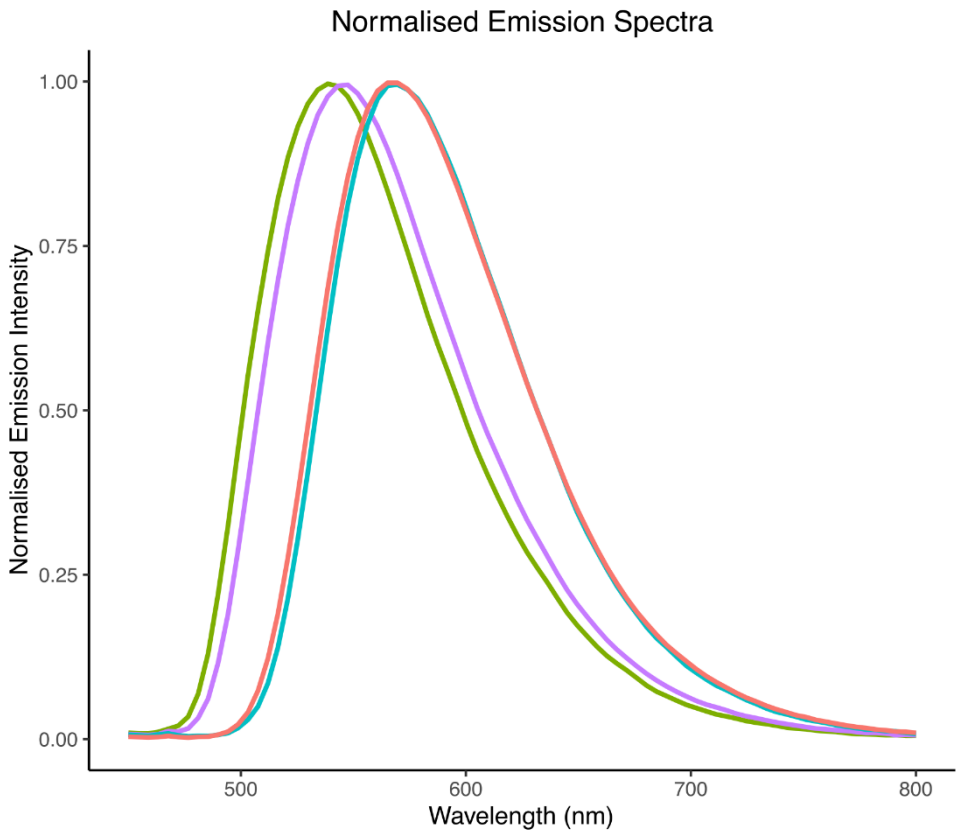



Figure S4 Emission spectra of Ir((5-F)ppy)$_3$ (**47**) (green), Ir((5-F)(4′-t-Bu)ppy)$_3$ (**48**) (purple), Ir((5-$CF_3$)ppy)$_3$ (**49**) (red) and Ir((5-$CF_3$)(4′-t-Bu)ppy)$_3$ (**50**) (blue).

Table S3 Emission values and corresponding triplet energies of photocatalysts **47** - **50**

| Photocatalyst | $\lambda_{max}$ (nm) | $E_{T\,(\lambda max)}$ (kcal/mol) | $\lambda_{10\%}$ (nm) | $E_{T(\lambda 10\%)}$ (kcal/mol) |
|---|---|---|---|---|
| Ir((5-F)ppy)$_3$ (**47**) | 541 | 52.8 | 480 | 59.6 |
| Ir((5-F,4′-*t*-Bu)ppy)$_3$ (**48**) | 547 | 52.3 | 486 | 58.8 |
| Ir((5-$CF_3$)ppy)$_3$ (**49**) | 565 | 50.6 | 502 | 57.0 |
| Ir((5-$CF_3$, 4′- *t*-Bu)ppy)$_3$ (**50**) | 567 | 50.4 | 513 | 55.7 |

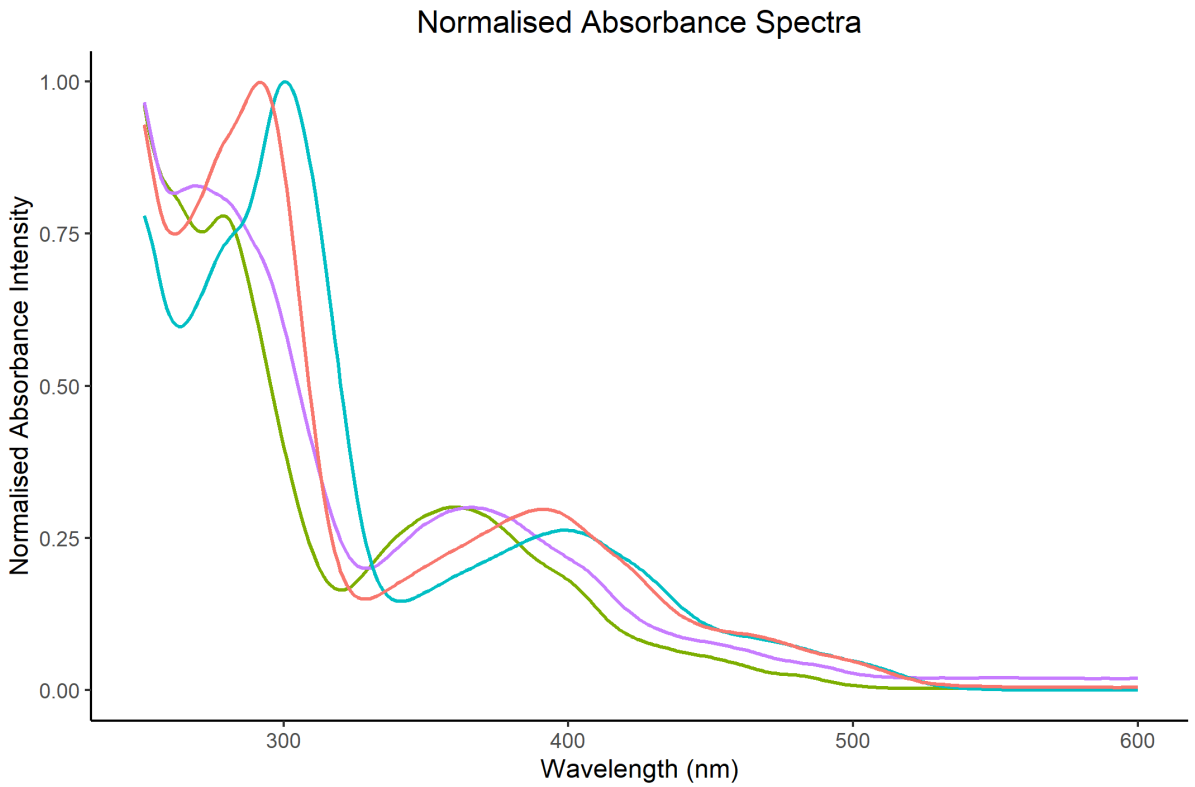



Figure S5 Absorbance spectra of Ir((5-F)ppy)$_3$ (**47**) (green), Ir((5-F)(4'-t-Bu)ppy)$_3$ (**48**) (purple), Ir((5-$CF_3$)ppy)$_3$ (**49**) (red) and Ir((5-$CF_3$)(4'-t-Bu)ppy)$_3$ (**50**) (blue).

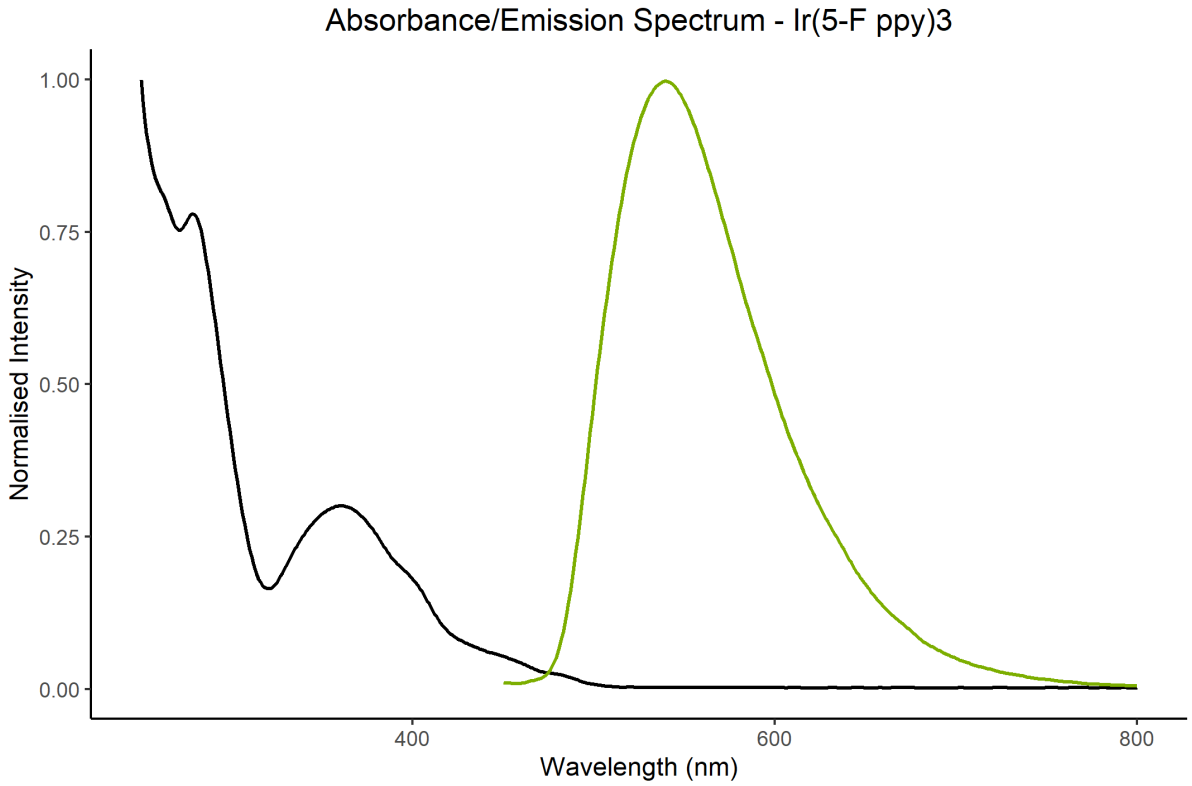



Figure S6 Absorbance (black) and emission (green) spectra of Ir((5-F)ppy)$_3$ (**47**)

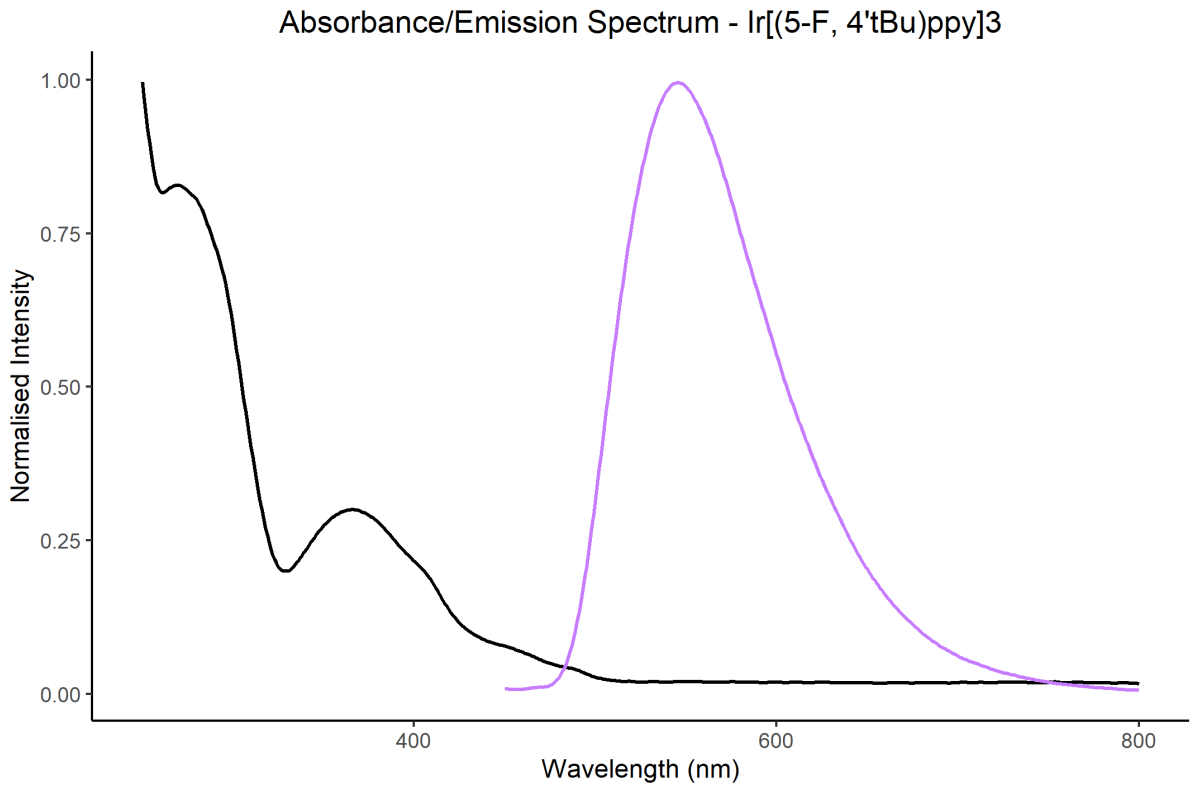



Figure S7 Absorbance (black) and emission (lilac) spectra of Ir((5-F)(4'-t-Bu)ppy)$_3$ (**48**)

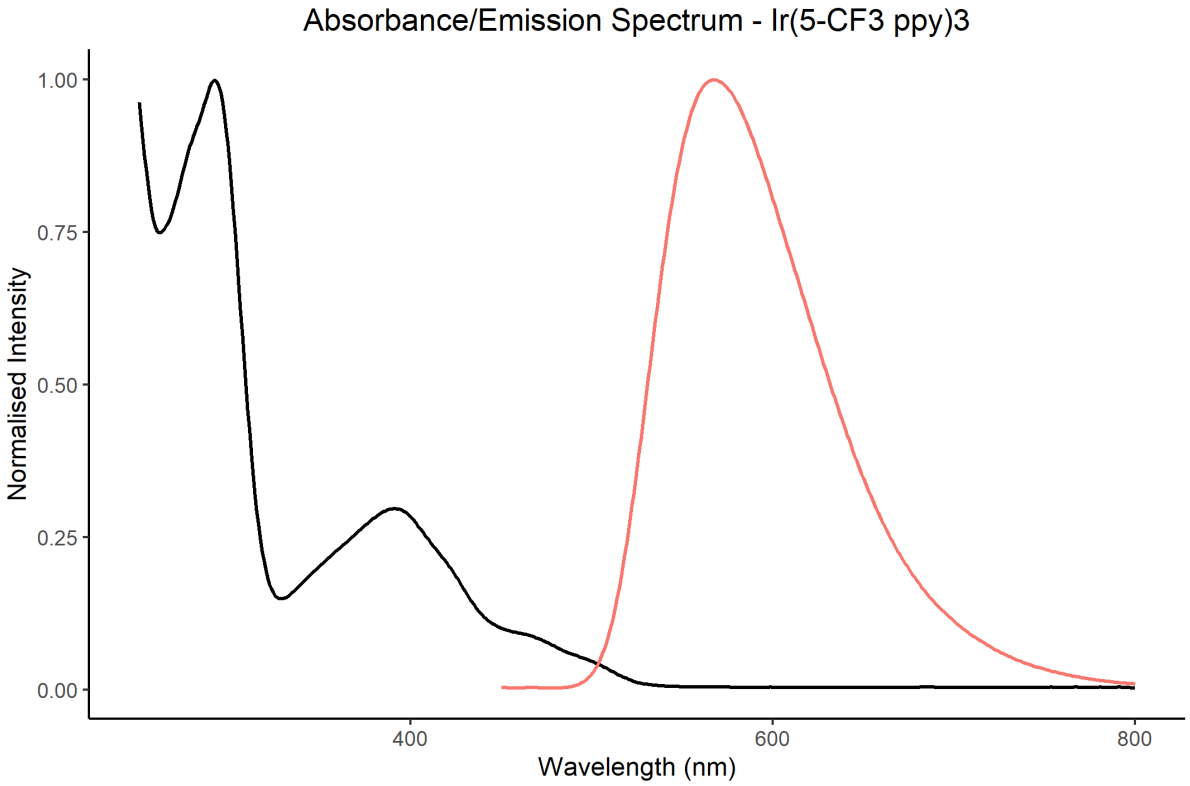



Figure S 8 Absorbance (black) and emission (orange) spectra of Ir((5-$CF_3$)ppy)$_3$ (**49**)

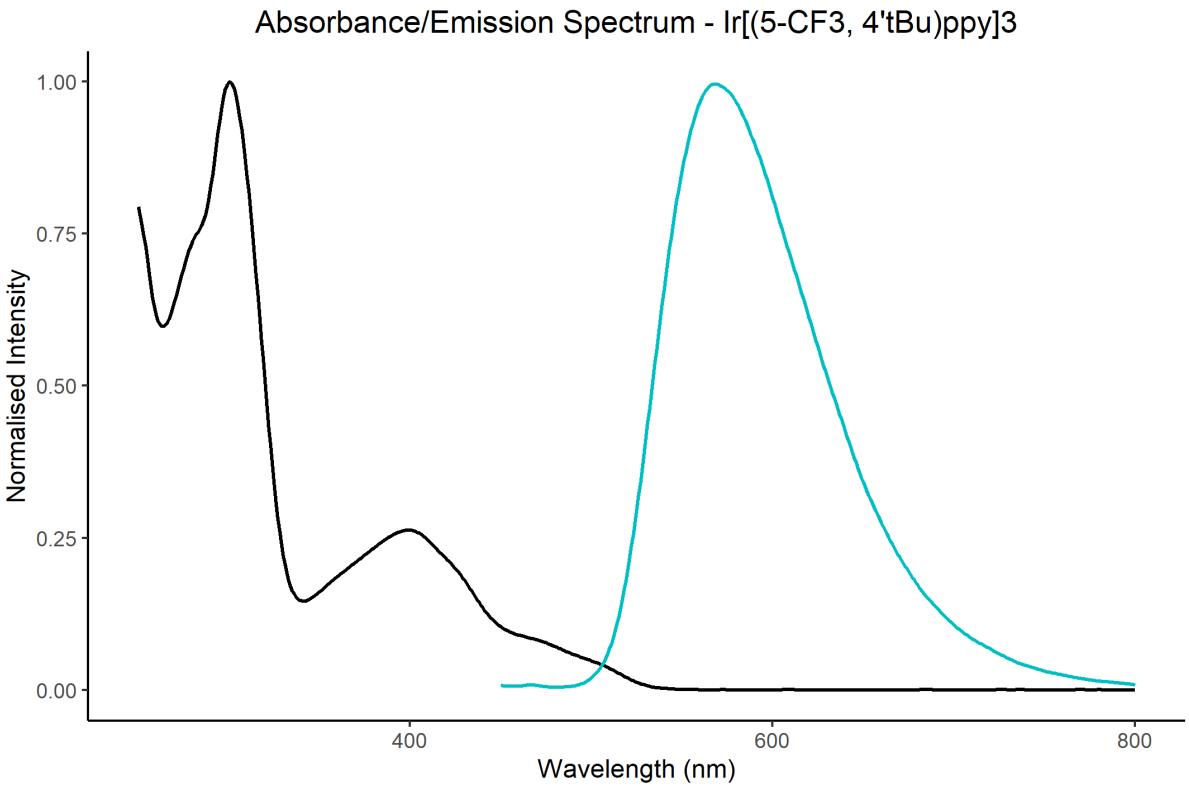



Figure S9 Absorbance (black) and emission (blue) spectra of Ir((5-$CF_3$)(4'-t-Bu)ppy)$_3$ (**50**)

### I.3.2 Square-Wave Voltammograms of Novel Photocatalysts

Voltammograms were recorded by MVP and are included for completeness

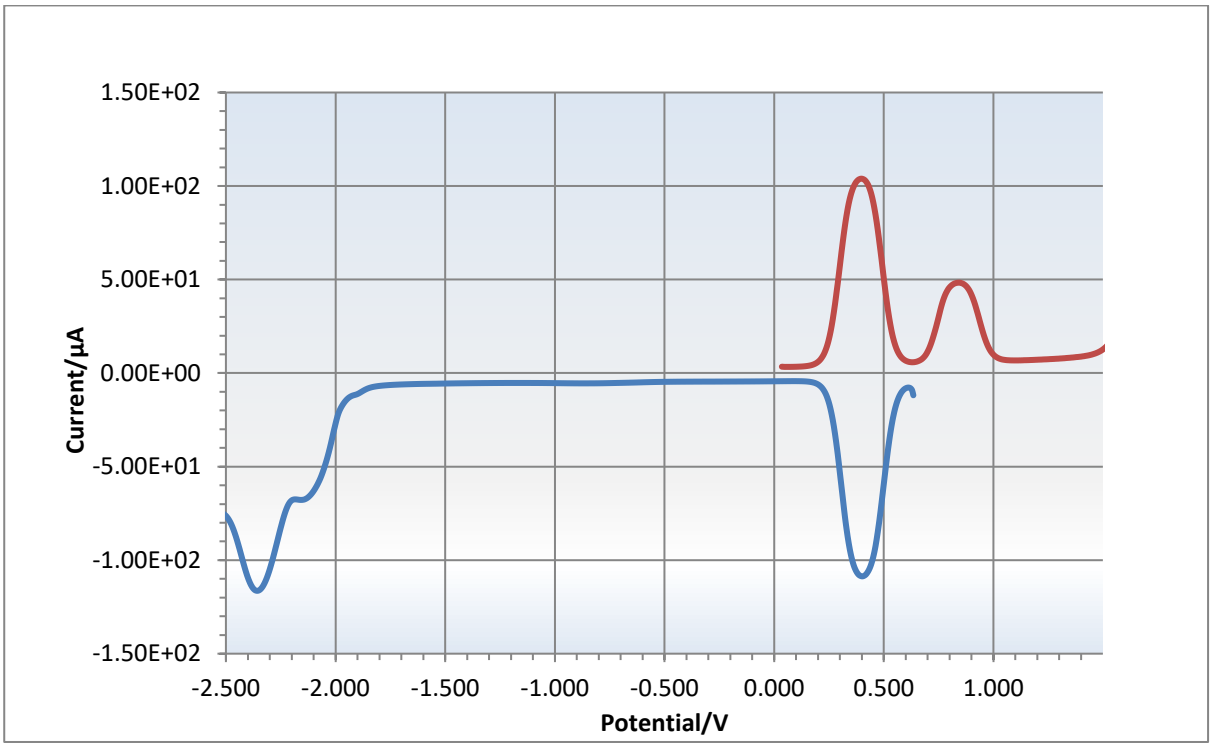



Figure S10 Square-wave voltammogram of Ir((5-F)ppy)$_3$ (**47**) in MeCN

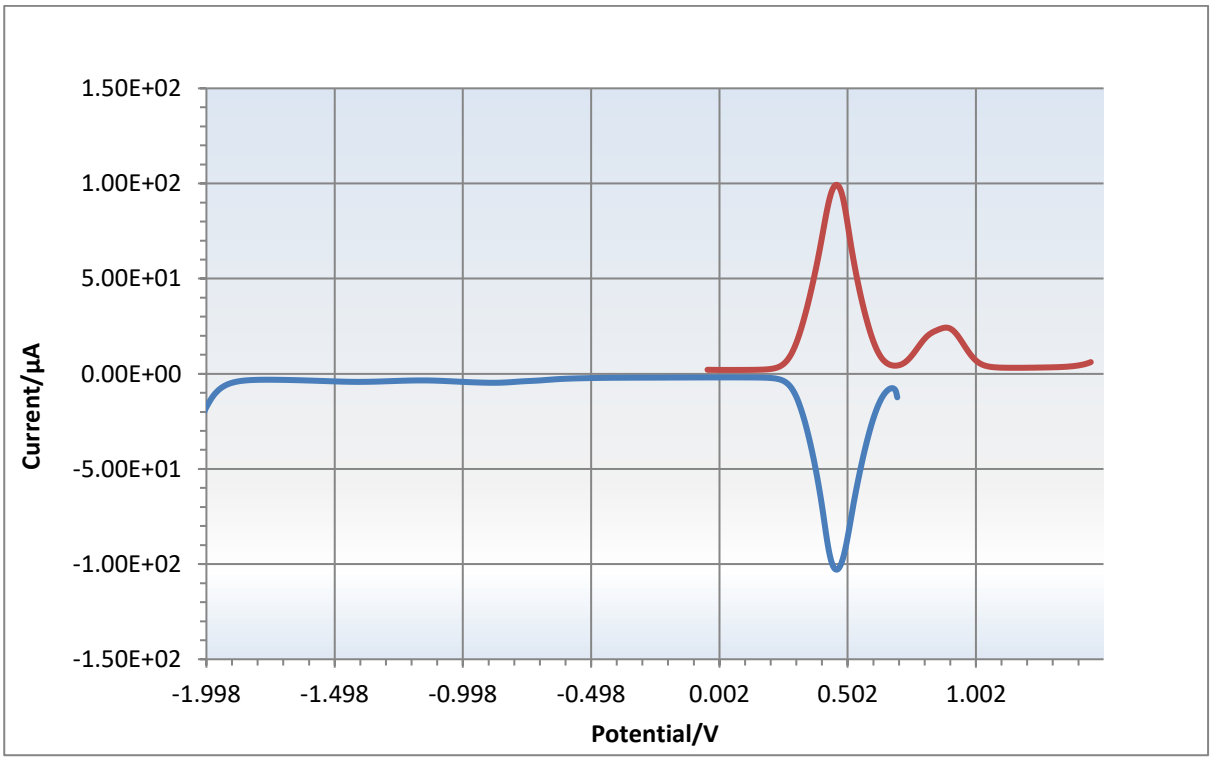



Figure S11 Square-wave voltammogram of Ir((5-F)ppy)$_3$ (**47**) in $CH_2Cl_2$

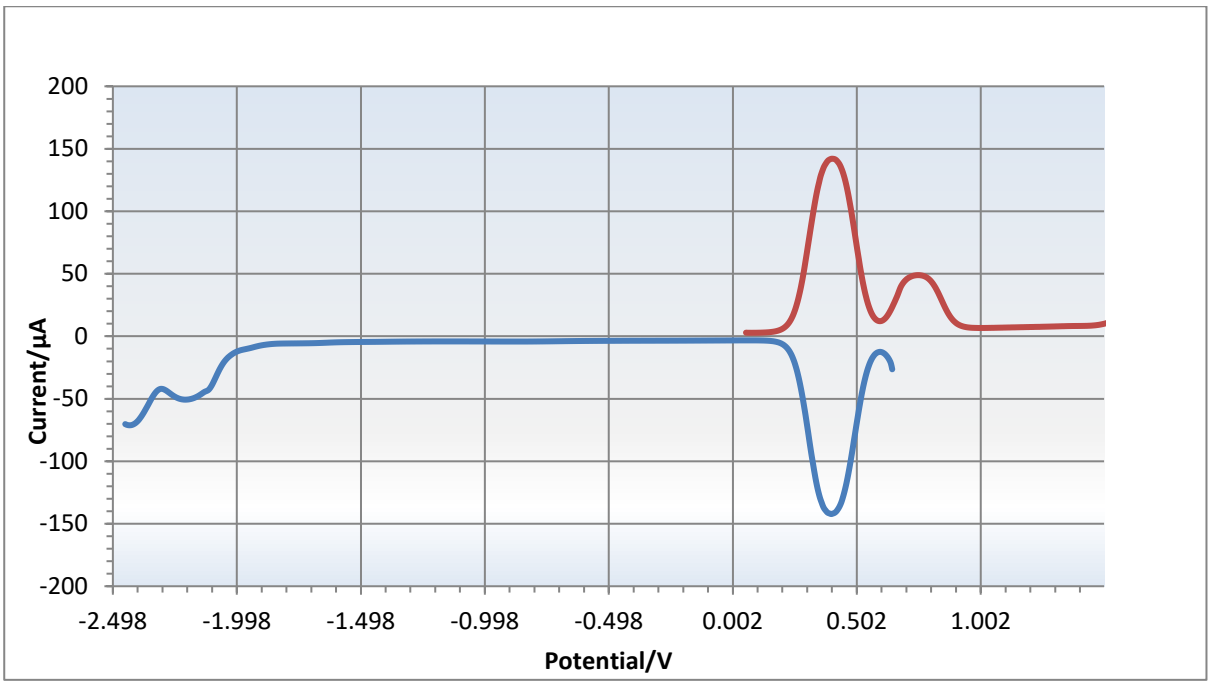



Figure S12 **:** Square-wave voltammogram of Ir((5-F)(4'-t-Bu)ppy)$_3$ (**48**) in MeCN

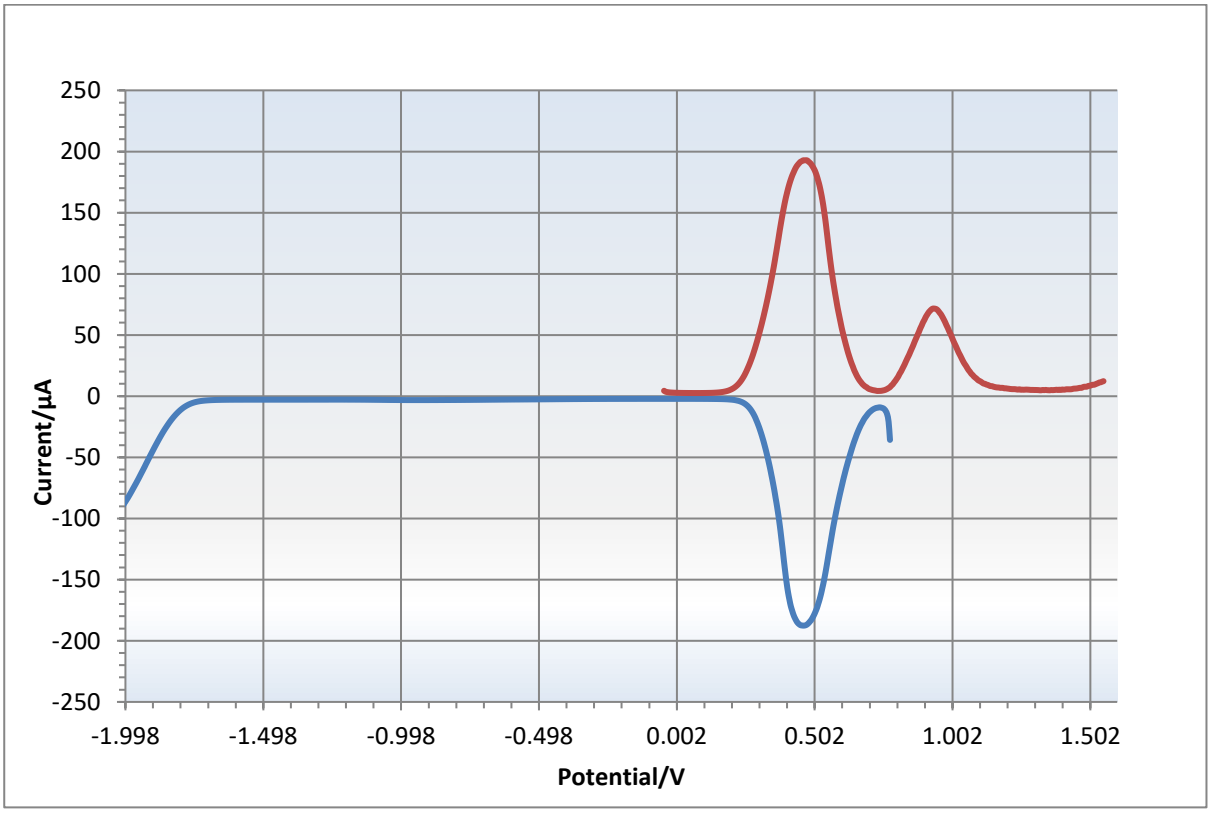



Figure S13 Square-wave voltammogram of Ir((5-F)(4'-t-Bu)ppy)$_3$ (**48**) in $CH_2Cl_2$

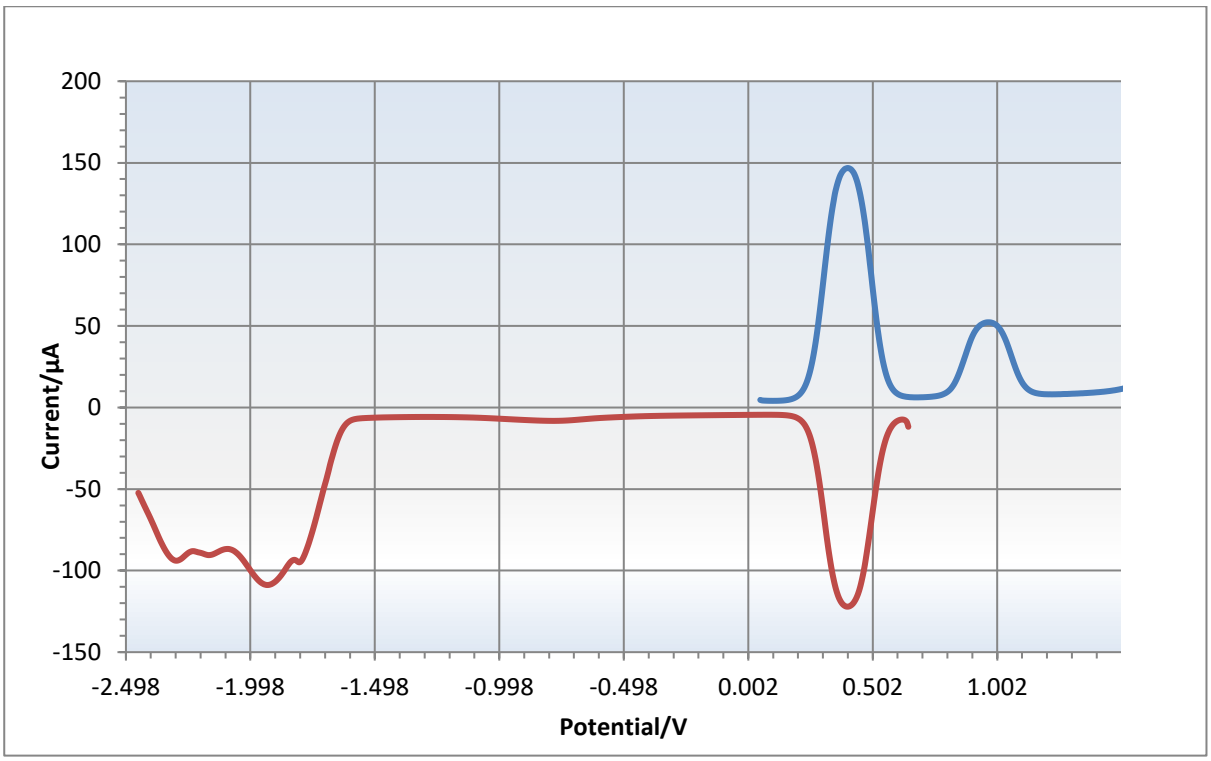



Figure S14 Square-wave voltammogram of Ir((5-$CF_3$)ppy)$_3$ (**49**) in MeCN

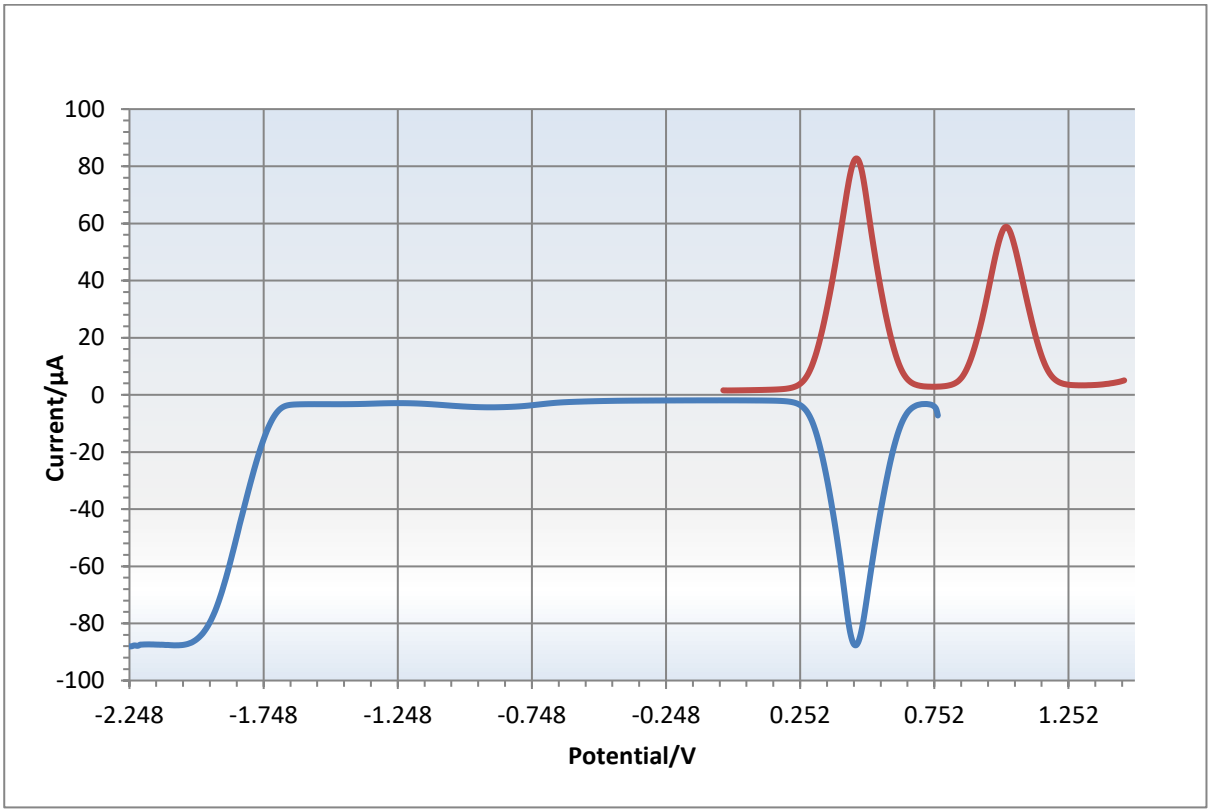



Figure S 15 Square-wave voltammogram of Ir((5-$CF_3$)ppy)$_3$ (**49**) in $CH_2Cl_2$

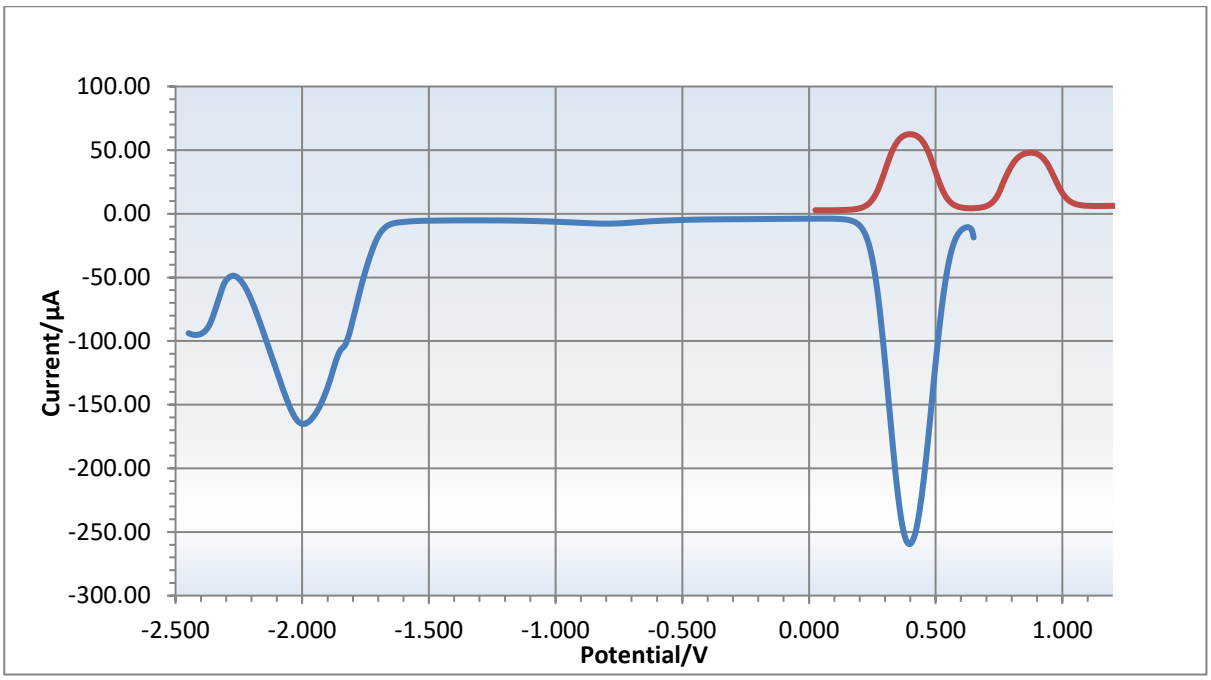



Figure S16 Square-wave voltammogram of Ir((5-$CF_3$)(4′-t-Bu)ppy)$_3$ (**50**) in MeCN

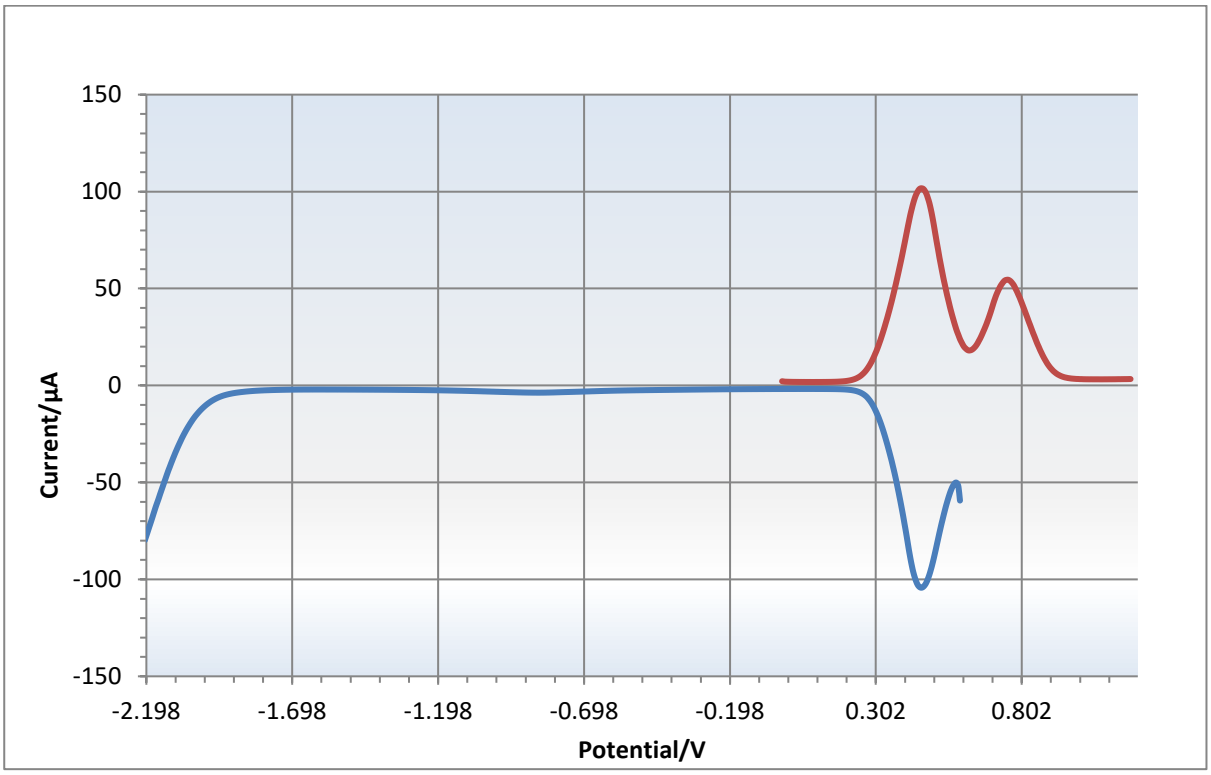



Figure S17 Square-wave voltammogram of Ir((5-$CF_3$)(4′-t-Bu)ppy)$_3$ (**50**) in $CH_2Cl_2$

### I.3.3 Estimation of Excited State Redox Potentials for Novel Photocatalysts

To be able to compare the properties of different photocatalysts, all excited state redox properties were calculated from ground state redox potentials in acetonitrile and λ (10%) values which were either recorded or available in the literature.[10-13]

The excited state redox properties were calculated using the Rehm-Weller equations:[14]

$$E_{1/2}^{red}\ Ir(IV)/*(III) = E_{1/2}^{red}\ Ir(IV)/(III) - E^{0\text{-}0}$$

$$E_{1/2}^{red}\ Ir*(III)/(II) = E_{1/2}^{red}\ Ir(III)/(II) + E^{0\text{-}0}$$

Where $E^{0\text{-}0}$ is the energy gap between the zero-level vibrational levels of the ground and excited state; estimated as the high-energy onset of phosphorescence where the emission intensity is 10% of the observed maximum.

### I.3.4 Summary of Photocatalyst Properties

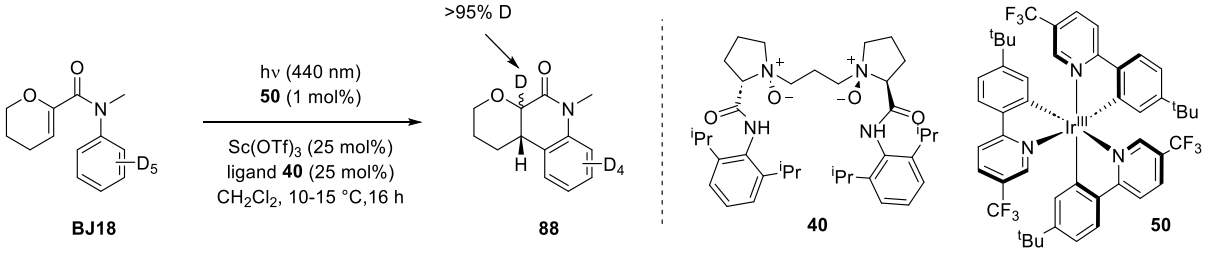
Table S4 Summary of photocatalyst properties

| Photocatalyst | $E_{1/2}^{red}$ vs. SCE in $CH_2Cl_2$ (V) | | $E_{1/2}^{red}$ vs. SCE in MeCN (V) | | | | Emission in MeCN (nm) | | $E_T$ (kcal/mol) | |
|---|---|---|---|---|---|---|---|---|---|---|
| | $Ir^{IV/III}$ | $Ir^{IV/*III}$ | $Ir^{IV/III}$ | $Ir^{IV/*III}$ | $Ir^{III/II}$ | $Ir^{*III/II}$ | λ (10%)* | λ (max) | λ (10%) | λ (max) |
| $Ir(ppy)_3$ [1] | - 0.69 | - 1.88 | - 0.77 | -1.81 | -2.23 | + 0.35 | 481 | 516 | 59.4 | 55.4 |
| $Ir((4'\text{-}^tBu)ppy)_3$ [2] | - 0.60 | - 1.97 | - 0.66 | -1.90 | -2.33 | + 0.23 | 485 | 525 | 59.0 | 54.5 |
| $Ir(Fppy)_3$ [1] | N/A | N/A | - 0.96 | -1.74 | -2.18 | + 0.52 | 459 | 488 | 62.3 | 58.6 |
| $Ir(dFppy)_3$ [1] | N/A | N/A | - 0.94 | -1.83 | -1.87 | + 0.90 | 448 | 476 | 63.8 | 60.0 |
| $Ir(dF(CF_3)ppy)_2(dtbbpy)(PF_6)$ [1] | N/A | N/A | - 1.73 | -1.01 | -1.40 | + 1.34 | 452 | 473 | 63.3 | 60.0 |
| $Ir(dFppy)_2(dtbbpy)(PF_6)$ [1] | N/A | N/A | - 1.59 | -1.15 | -1.47 | + 1.27 | 452 | 516 | 63.3 | 55.4 |
| $Ir(Fppy)_2(dtbbpy)(PF_6)$ [1] | N/A | N/A | - 1.45 | -1.19 | -1.50 | + 1.14 | 469 | 540 | 61.0 | 52.9 |
| $Ir(ppy)_2(dtbbpy)(PF_6)$ [6,7] | N/A | N/A | - 1.33 | -1.32 | -1.34 | + 0.83 | 500 | 570 | 56.4 | 48.3 |
| $Ir((3'\text{-}OMe)ppy)_3$ [2] | - 0.70 | - 1.95 | - 0.76 | -1.89 | -2.34 | + 0.26 | 517 | 557 | 55.3 | 51.3 |
| $Ir((5\text{-}F)ppy)_3$ **47** | - 0.88 | - 1.70 | - 0.84 | -1.74 | -2.17 | + 0.41 | 480 | 541 | 59.6 | 52.8 |
| $Ir((5\text{-}F)(4'\text{-}^tBu)ppy)_3$ **48** | - 0.75 | - 1.80 | - 0.75 | -1.80 | -2.22 | + 0.33 | 486 | 547 | 58.8 | 52.3 |
| $Ir((5\text{-}CF_3)ppy)_3$ **49** | - 1.02 | - 1.45 | - 0.97 | -1.50 | -1.80 | + 0.67 | 502 | 565 | 57.0 | 50.6 |
| $Ir((5\text{-}CF_3)(4'\text{-}^tBu)ppy)_3$ **50** | - 0.93 | - 1.49 | - 0.87 | -1.55 | -1.83 | +0.59 | 513 | 567 | 55.7 | 50.4 |

* Where literature values are cited, these values were obtained by graphical extraction from published emission spectra.

# I.4 Mechanistic Experiments and Photophysics

## I.4.1 Labelling and Crossover Experiments




Scheme S1 Deuterium labelling experiment to probe the proposed 1,5-H shift

The photocyclization of pentadeuterated substrate (**BJ18**) was performed according to **General Procedure C**. The crude reaction mixture was analysed by $^{1}$H NMR and LC/MS to determine the degree of deuterium transfer from the aniline *ortho*-positions to the α-carbonyl position. Results indicate >95% incorporation of deuterium at the C17 position, consistent with a intramolecular 1,5-H-shift.

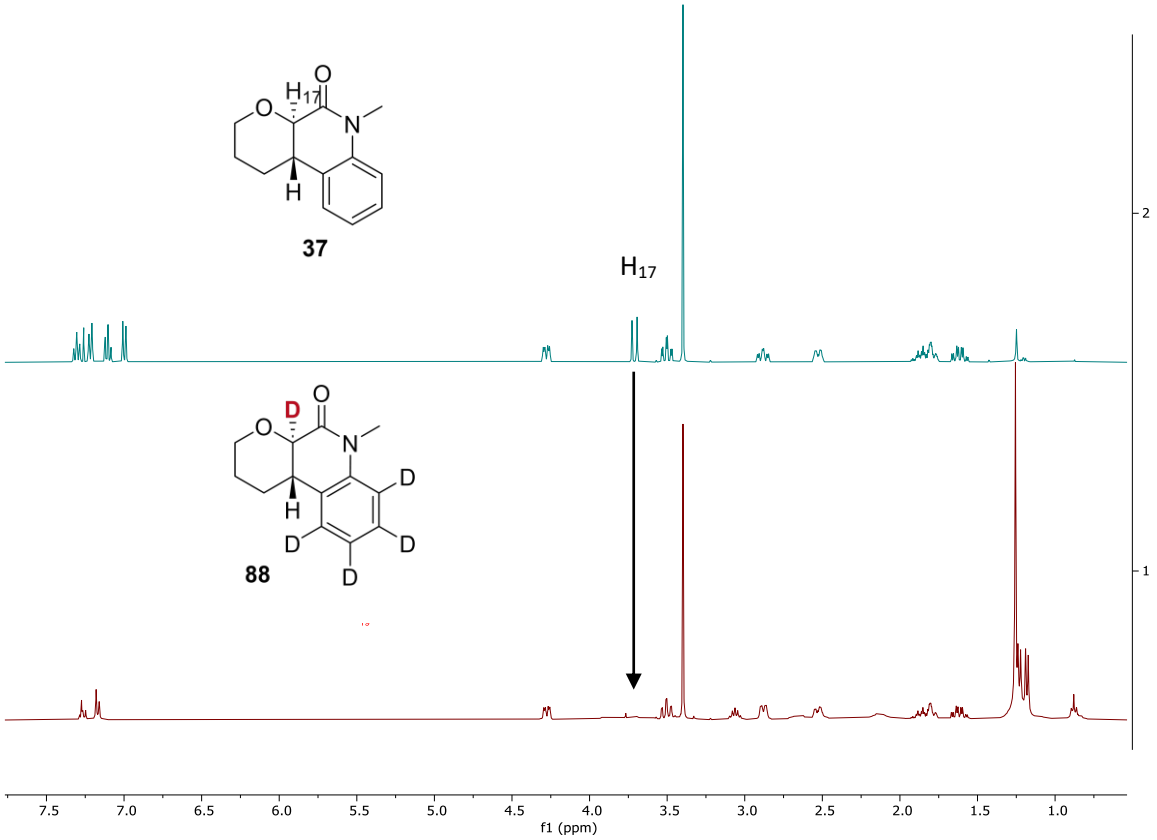



Figure S18 Top, purified $^{1}$H NMR spectrum of (4aR,10bS)-6-methyl-2,3,6,10b-tetrahydro-1H-pyrano[2,3-c]quinolin-5(4aH)-one (**37**) for comparison. Bottom, Crude $^{1}$H NMR spectrum of the product of the cyclization (**88**) using the corresponding -$d_5$ substrate (**BJ18**).

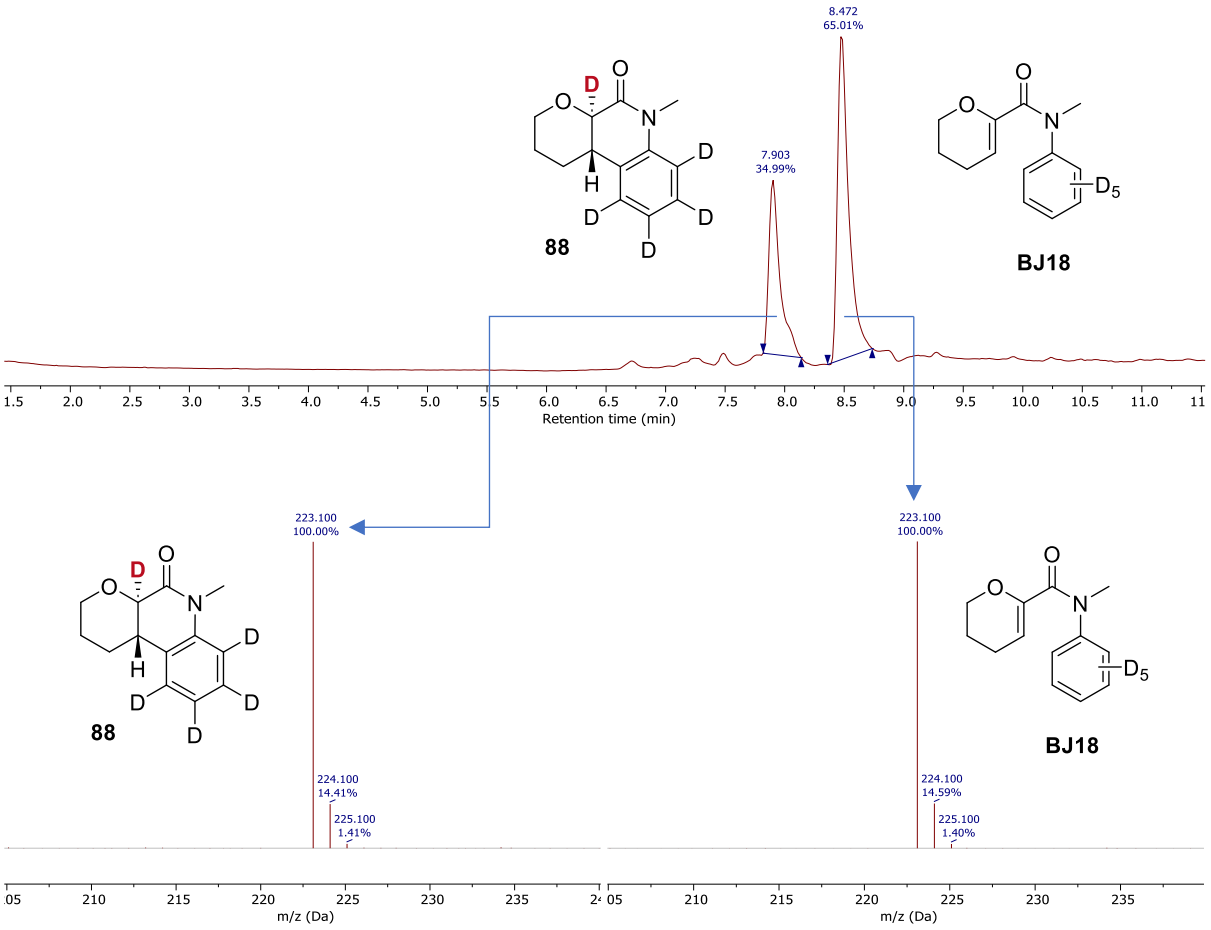


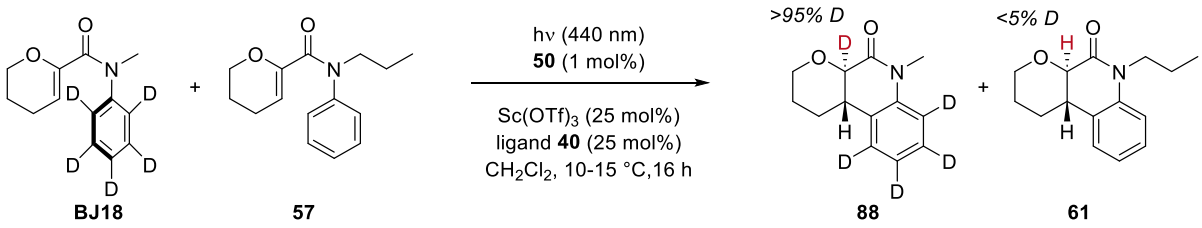

Figure S19 LC/MS (ESI) trace of crude reaction mixture of $d_5$-substrate at ≈ 60% conversion showing deuterated SM **BJ18** and deuterated product **88**. Top: total ion chromatograph. Bottom: API-ES MS analysis of each component shows no evidence of deuterium loss in **88** or **BJ18**

## Crossover Experiments

Crossover experiments were carried out to investigate the possibility of intermolecular hydrogen transfer. LC/MS analysis of the crude reaction mixtures was performed to separate the reaction components and determine their isotopic distribution. The identities of each (LC/MS) chromatogram peak were confirmed by separation of reaction components by flash column chromatography followed by re-analysis under the same separation conditions used to determine their retention times. Purified and separated products were also analysed by quantitative $^1$H NMR (d1 = 60 s) to determine the extent of crossover.

In all cases, no exchange of deuterium between substrates and products was observed, ruling out the possibility of intermolecular proton transfer.

**Crossover Experiment 1: crossover of *N*-methyl pentadeuterated substrate (BJ18) and *N*-propyl substrate (57).**




Scheme S2 Crossover experiment between **BJ18** and **57**

This experiment was carried out with **BJ18** (0.5 mmol), and **57** (0.5 mmol) according to **General Procedure C** and the crude reaction mixture analysed before reaction completion.

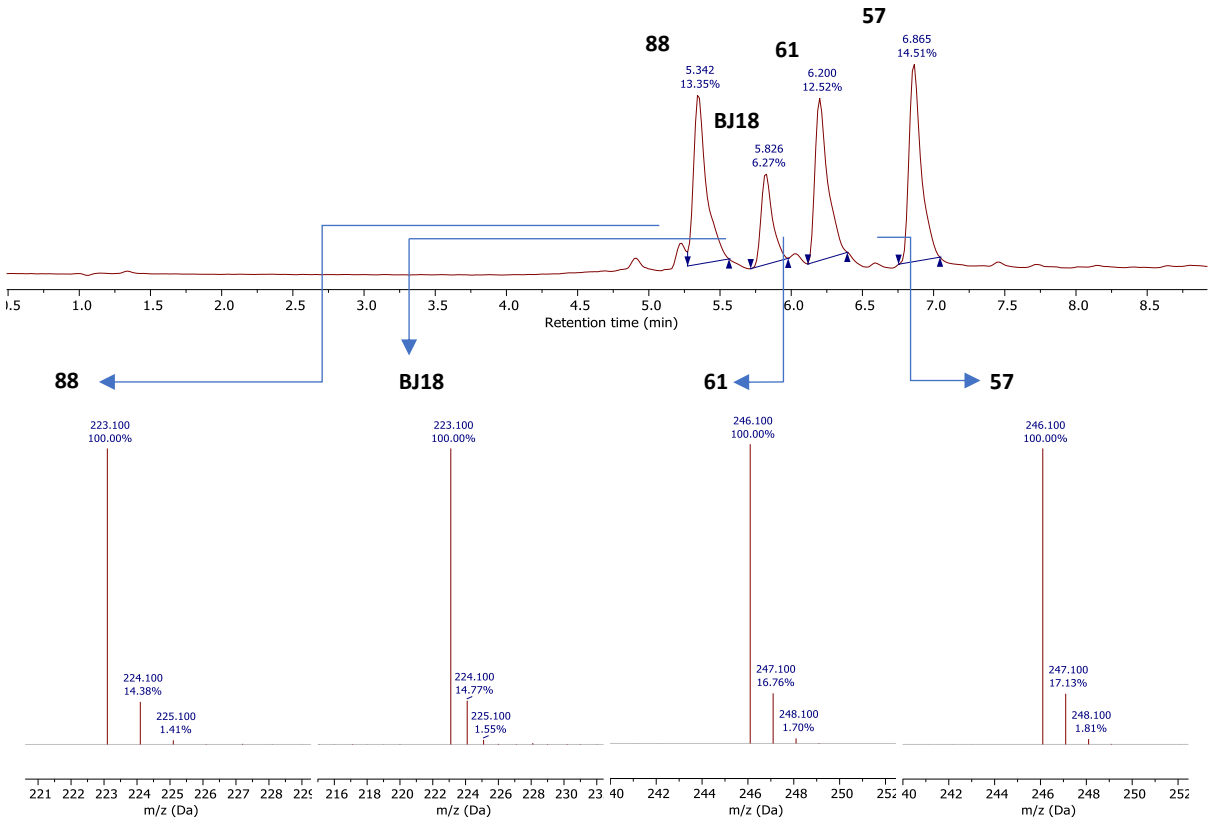
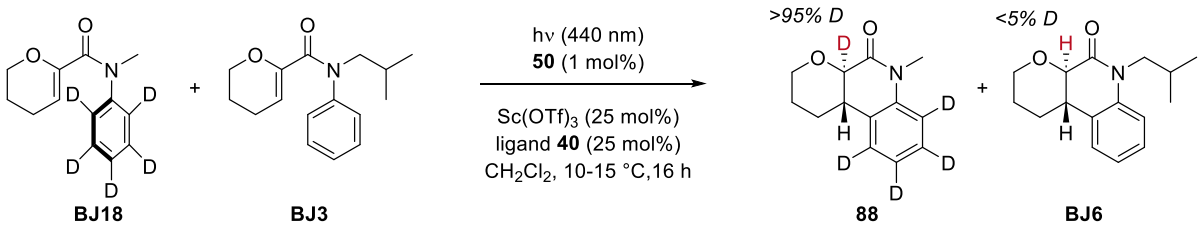



Figure S20 LC/MS analysis of crude crossover reaction mixture of $d_5$-substrate (**BJ18**), and non-deuterated substrate (**57**) at ≈60% conversion to products **88** and **61**. Top: total ion chromatograph. Bottom: API-ES MS analysis of each component.

No evidence for crossover was observed.

**Crossover Experiment 2: crossover of *N*-methyl pentadeuterated substrate (BJ18) and *N*-isobutyl substrate (88).**




Scheme S3 Crossover experiment between **BJ18** and **BJ3**

This experiment was carried out with **BJ18** (0.5 mmol), and **BJ3** (0.5 mmol) according to **General Procedure C** and the crude reaction mixture analysed before reaction completion.

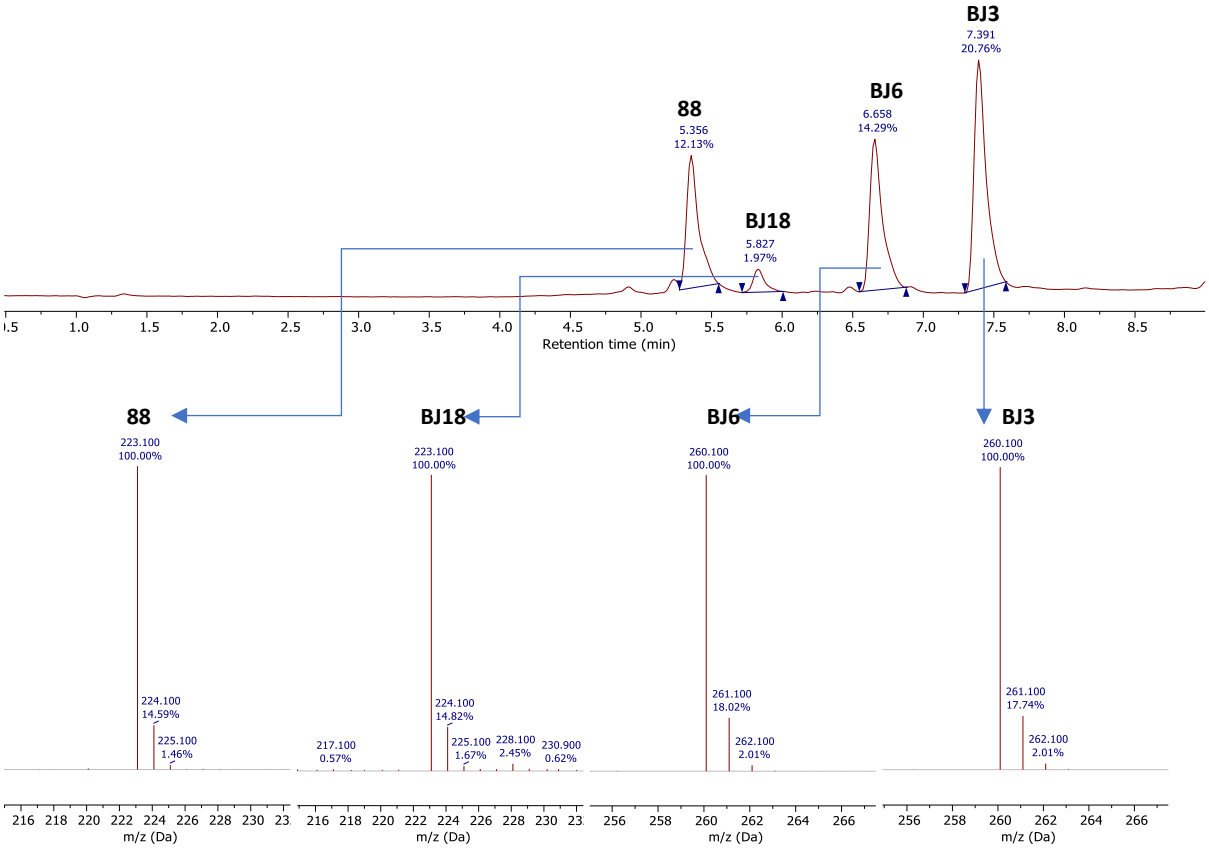
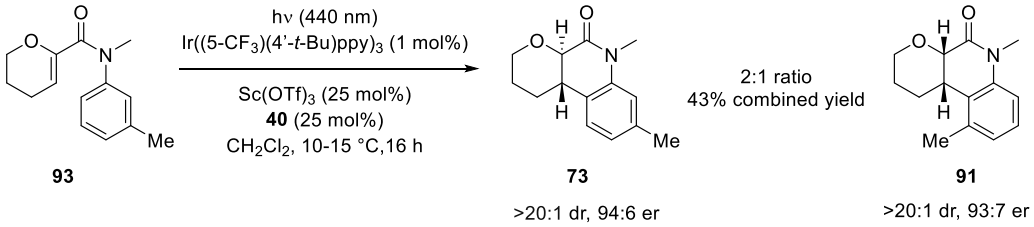



Figure S21 LC/MS analysis of crude crossover reaction mixture of $d_5$-substrate (**BJ18**), and non-deuterated substrate (**BJ3**) at ≈90% conversion to products **88** and **BJ6**. Top: total ion chromatograph. Bottom: API-ES MS analysis of each component. No evidence for crossover was observed.

**Probing the diastereoselectivity for *meta*-substituted substrates:**
**Exogenous deuterium incorporation study**




Scheme S4 Cyclization of *meta*-substituted substrate leads to an otherwise unobserved *cis*- product

Cyclization of *meta*-substituted substrates occurs to give a mixture of 2 regioisomers. For the regioisomer where the substituent is proximal to the THP ring, the product is formed as a diastereoisomeric mixture containing the (otherwise unobserved) *cis*-isomer (Scheme S4).

It was proposed that the formation of the major (*cis*-fused) diastereomer of the minor regioisomer **91** (fusion at the aniline 2-position) was due to a reaction pathway whereby intermediate **89** could rearomatize to form **90**, followed by *intermolecular* protonation to form the *cis*-fused product, **91** (Figure S22).

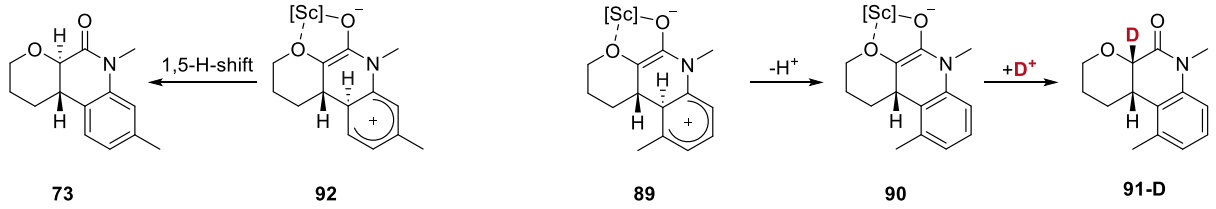
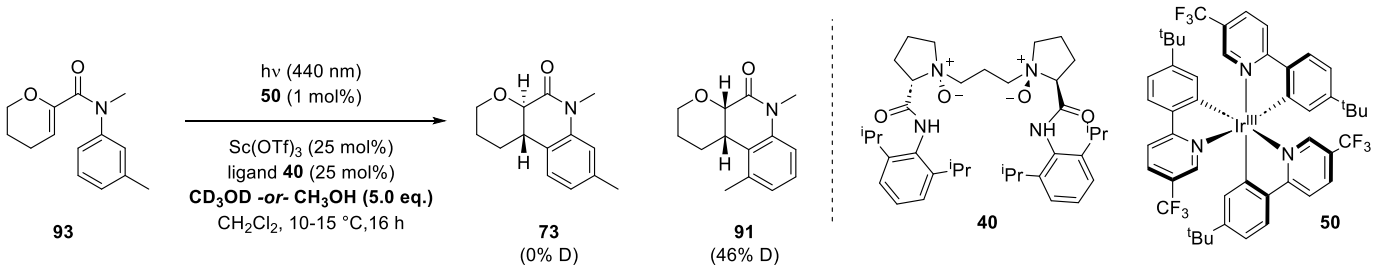



Figure S22 Left: the calculated mechanism for formation of the major diastereomer (trans-fused) of the major regioisomer (cyclization to the aniline 6-position). Right: proposed mechanism for the formation of the major diastereomer (cis-fused) of the minor regioisomer (cyclization to the aniline 2-position).

This contrasts with the *intramolecular* 1,5-H-shift predicted to be operating normally (**92** → **73**). If this deprotonation/protonation mechanism is in operation, protonation should be possible from an external H/D source whilst in the case of a 1,5-H-shift, this is unlikely.




Scheme S5 Inclusion of exogeneous D and H sources to probe the potential for a protonation/deprotonation mechanism in the formation of cis-fused diastereomers.

To probe the mechanism of formation for the *cis*-diastereomer, photocyclization of *meta*-methyl substrate **93** was performed with 5 equiv. MeOH-$d_4$ present in the reaction (Scheme S5).

To determine a baseline/control for the reaction in the presence of methanol-$d_4$, the reaction of **93** was duplicated, but with the addition of 5 equiv. methanol. A control reaction of substrate **1** as an exemplar *trans*-selective cyclization in the presence of 5 equiv. MeOH-$d_4$ was also carried out.

The reaction components were separated by preparative TLC and analysed by LC/MS to determine the degree of deuterium incorporation (as determined by comparative abundance of M+1 peak by LC/MS analysis).

No deuterium incorporation was observed in the C6-linked *trans*-diastereomer **73**. However, 46% incorporation of D was observed in the C2-linked *cis*-diastereomer **91** (an M+1 peak intensity of 98.5% corresponds to 46%[II] deuterium incorporation; see Table S5). This finding is consistent with the proposal that the *cis*-diastereomer may not form via a 1,5-H shift, but instead by an alternative intermolecular deprotonation-reprotonation mechanism

Table S5 Tabulation of relative abundance of M+1 peak in LC/MS

| **Substrate** | | **93** | **93** | **36** |
|---|---|---|---|---|
| **Additive (5.0 equiv.)** | | $CH_3OH$ | $CD_3OD$ | $CD_3OD$ |
| **Natural M+1 Abundance $[M+1+H]^+$ (%)** | | 15.1 | | 14.1 |
| **M+1 Abundance (%)** | *Cis*-fused (C2-linked) | 15.0 | 98.5 | - |
| | *Trans*-fused (C6-linked) | 15.5 | 17.7 | 14.5 |

These measurements indicate that within experimental error, deuterium incorporation only occurs in the *cis*-fused product. This observation is in line with observations made on similar systems.[15]

[II] Isotopic enrichment was calculated by subtracting the baseline M+1+H abundance from the measured M+1+H and expressing this as a percentage of the combined M+H and true M+1+H abundances. $\frac{98.5-15.0}{100+(98.5-15.0)} = 45.5\%$

## I.4.2 Chemical Actinometry and Quantum Yield Measurement

### Chemical Actinometry

To determine the quantum yield of the optimised reaction, a 430 nm LED (Thorlabs M430L5) was calibrated by ferric oxalate actinometry as follows:[10, 16, 17]

3 mL of a freshly prepared solution of ferric oxalate (0.006 M) in aqueous $H_2SO_4$ (0.05 M) was placed in a quartz cuvette and irradiated for 8 seconds under stirring. This was carried out in triplicate, and an identical control sample was kept in the dark. A sample of each of the irradiated and control samples (0.30 mL) were transferred to vials containing 1.35 mL of a 0.1% phenanthroline solution (13.56 g $CH_3COONa$ and 0.10 g phenanthroline in 100 mL 0.5 M $H_2SO_4$) and 1.35 mL $H_2O$. Samples were kept in the dark for 1 h before their absorbance was measured at 510 nm. The LED irradiation time was chosen to ensure that conversion did not exceed 5% and that absorbance did not exceed 0.5 – 1 ABS.

$$no.moles\ Fe^{2+} = \frac{v_1 v_3 \Delta A(510\ nm)}{10^3 v_2 l \varepsilon(510\ nm)}$$

Equation S1

The number of moles of $Fe^{2+}$ produced from irradiation could be calculated from these measurements according to **Equation S1** where $v_1$ (mL) is the irradiated volume, $v_2$ (mL) is the aliquot of the irradiated solution transferred, $v_3$ (mL) is the final volume of complexation solution, l (cm) is the path length, ΔA is the difference in absorption (at 510 nm) between the irradiated solution and the solution stored in the dark, and ε(510 nm) is the molar absorption coefficient of $Fe(phen)_3^{2+}$ at 510 nm (11,100 $M^{-1}$ $cm^{-1}$).

$$f\ (E\ s^{-1}) = \frac{no.moles\ Fe^{2+}}{\Phi_R t(1 - 10^{-A})}$$

Equation S2

$$f\ (mW) = 1000\ \times f(E\ s^{-1}) N_A h \frac{c}{\lambda}$$

Equation S3

Using the value calculated, the photon flux can then be calculated (first in E $s^{-1}$ and subsequently in mW) according to the above equations, where $\Phi_R$ is the quantum yield of formation of $Fe^{2+}$ in the ferric oxalate actinometer (well known for a range of wavelengths),[12] *t* is the irradiation time (s), A is the absorption of the 0.006 M ferric oxalate solution at the irradiation wavelength, $N_A$ is Avogadro's number, *h* is planck's length (m), *c* is the speed of light (m $s^{-1}$), and λ is the irradiation wavelength (nm).

### Quantum Yield Measurement

Using this methodology, our LED was determined to have an irradiation power of 73 mW using our setup. With the power known, the quantum yield was determined by preparing the reaction solution according to **General Procedure C** using substrate **36.** 3 mL of this solution were transferred to a quartz cuvette which was stirred and thermostatted to 15 °C. After 17 hours the conversion was measured to be 5.6% by rp-HPLC (calibrated using 1,3,5-trimethoxybenzene as an internal standard added after cessation of irradiation and averaged across three wavelengths).

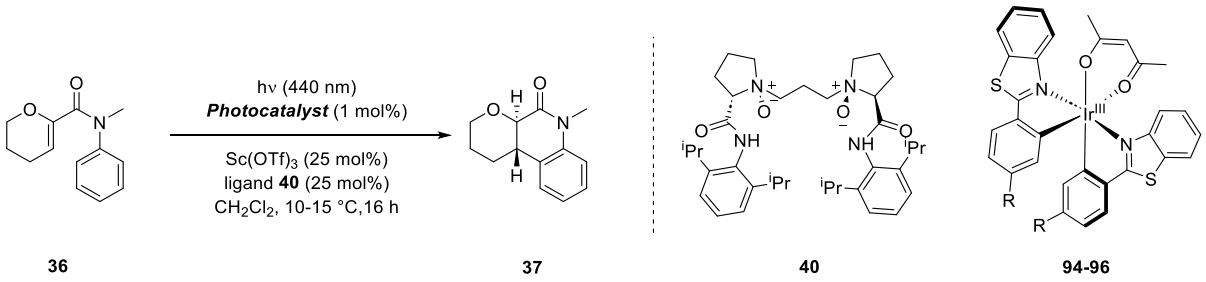
$$\Phi = \frac{no.moles\ \mathbf{2}}{f\ t\ (1 - 10^{-A})} = 0.003$$

Using **Equation S2** and the previously measured photon flux, the quantum yield was determined to be 0.003, which is consistent with a non-chain process.

## I.4.3 Weakly Reducing Photocatalyst Study

To probe whether the reaction was proceeding *via* a photoredox pathway or an energy transfer pathway, the reaction was carried out with a number of photocatalysts with appropriate triplet energies and redox properties.[18]

Table S6 Reaction outcomes with weakly reducing photocatalysts **94-96**




| Photocatalyst | $E_T$ 10% | $E_{ox}$ ($Ir^{*III}/Ir^{iV}$) (V) | Yield | er |
|---|---|---|---|---|
| **94** (R = F) | 56.3 | 1.12 | 33% | 76:24 |
| **95** (R = H) | 54.8 | 1.27 | 15% | 79:21 |
| **96** (R = $CF_3$) | 53.6 | 0.8 | 8% | 88:12 |

As can be seen from the above, increasing yield appears to correlate with increasing triplet energy, while increasing enantioselectivity appears to correlate with decreasing triplet energy. These observations are in line with expectations for a triplet energy transfer pathway wherein bound substrate (with a marginally lower triplet energy) selectively undergoes triplet energy transfer.

There is no correlation between excited state oxidation potential and yield or enantioselectivity, as could be expected if a selective photoredox pathway were in operation.

## I.4.4 Electrochemical Measurements

### Determination of Substrate (36) Redox Potentials and the Effect of $Sc(OTf)_3$

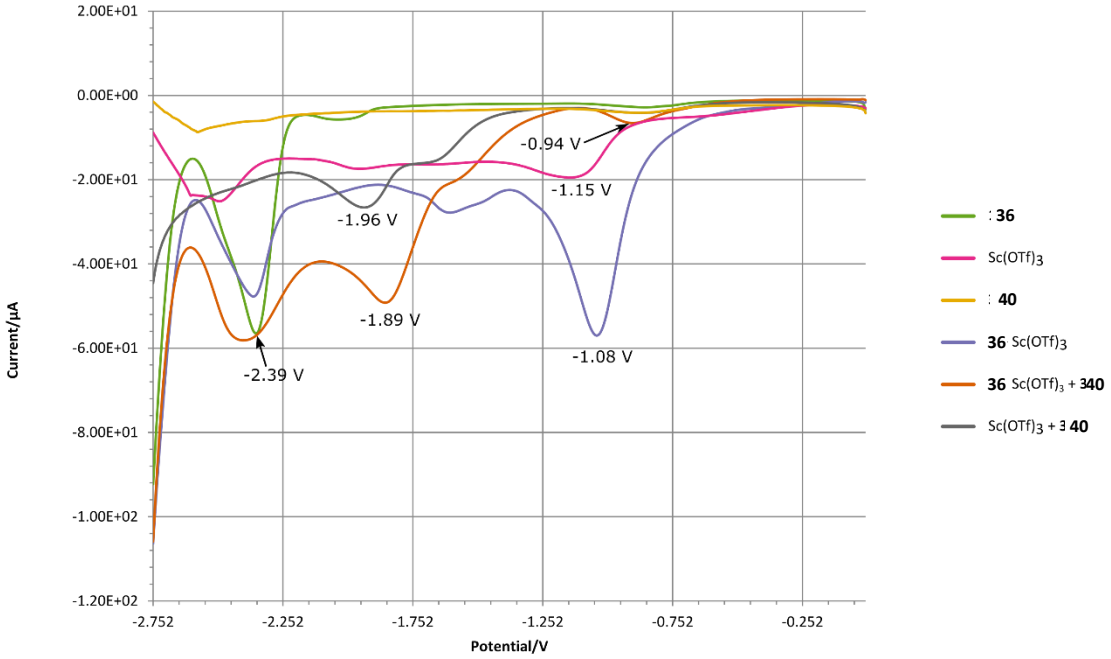



Figure S23 Square-wave voltammograms of reaction substrate (**36**) (green), the effect of $Sc(OTf)_3$ (lilac), $Sc(OTf)_3$ and **40** (orange), and of $Sc(OTf)_3$ alone (pink), **40** alone (yellow), and $Sc(OTf)_3$ and **40** (gray) quoted vs SCE.

Samples were measured at 0.01 M concentration in MeCN with tetra-N-butylammonium hexafluorophosphate, $Bu_4NPF_6$ ($TBAPF_6$) as supporting electrolyte.

### I.4.5 Stern-Volmer Quenching

A stock solution of **50** in argon sparged dichloromethane (25 mL, 0.5 µM) was prepared. Stock solutions of substrate **36** (40 mM in **1**, 0.5 µm in **50**) and scandium + **3** complex (4 mM in complex, 0.5 µm in **50**) were then prepared using this solution. A fourth solution of scandium + **3** complex with **50** was prepared by combining equal volumes of the prepared solutions. A cloudy solution was obtained and so this solution was syringe filtered to yield a solution suitable for fluorometric studies.

For each study an initial emission spectrum of the catalyst solution was recorded. One of the other three solutions was then added in measured volumes and the emission spectrum was rerecorded. If the dopant quenches the excited state photocatalyst, we expect the emission intensity to decrease as the concentration of dopant increases.

The resulting data were plotted according to the Stern-Volmer relationship:

$$\frac{I_0}{I} = k_q[Q] + 1$$

Where $I_0$ is the emission intensity of the photocatalyst in the absence of quencher, and I is the emission of the photocatalyst at a known quencher concentration, a graph plotting (I0/I) against quencher concentration ([Q]) should give a straight line with y intercept of 1 and a gradient quantifying the rate of quenching (kq).

**Addition of scandium + 3 complex**

In the addition of scandium complex to the photocatalyst no decrease in emission was recorded even at high concentrations of proposed quencher.

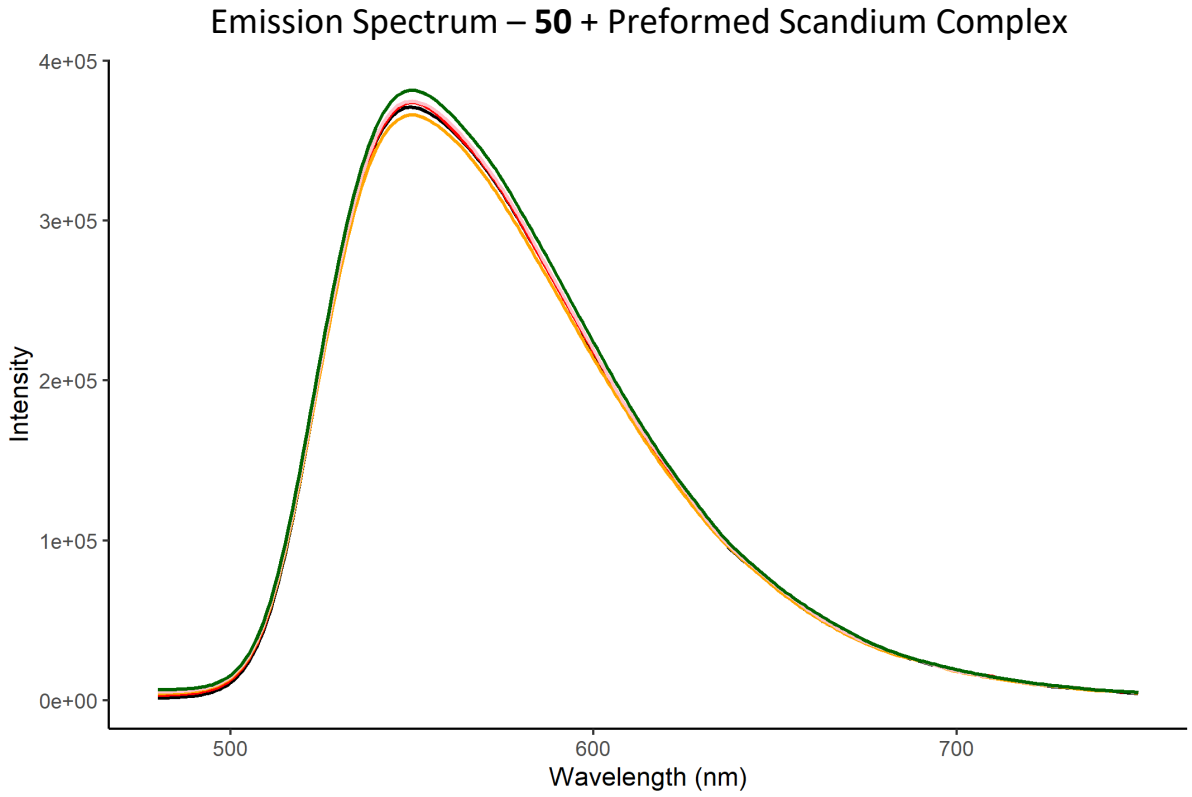



Figure S24 Stern-Volmer Quenching of PC (4) with preformed scandium complex. Concentrations of complex are: 0 mM (black), 0.67 mM (red), 1.14 mM (orange), 1.5 mM (pink), 1.78 mM (blue), 2 mM (green). **50** is 0.5 µM in all cases

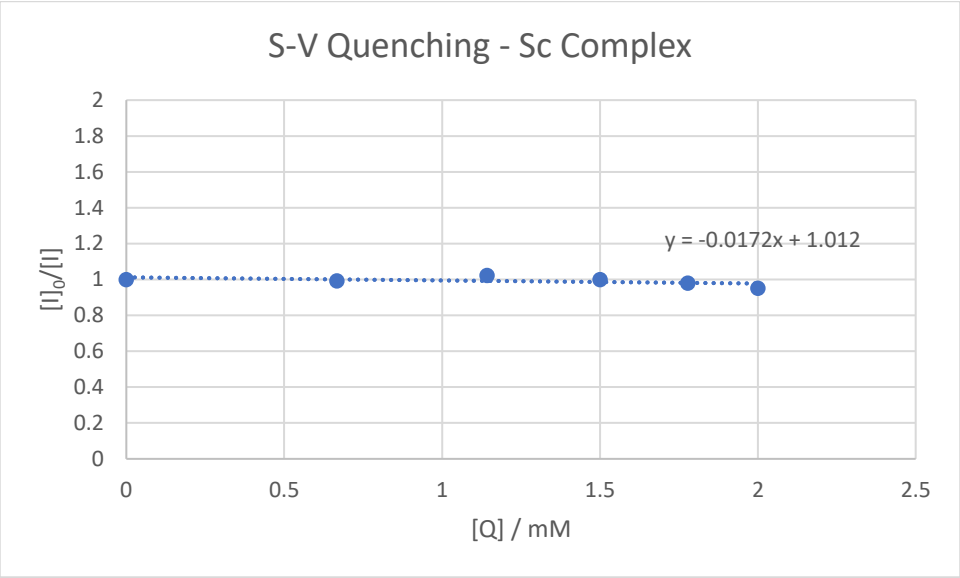



Figure S25 Stern-Volmer plot for **50** + preformed scandium complex

### Addition of substrate (36) complex

In the addition of substrate to the photocatalyst it was noted that additional emission was observed from the substrate itself. In the region where the substrate is not emissive ($\lambda > 650$ nm) no change in emission was observed even at thigh concentrations

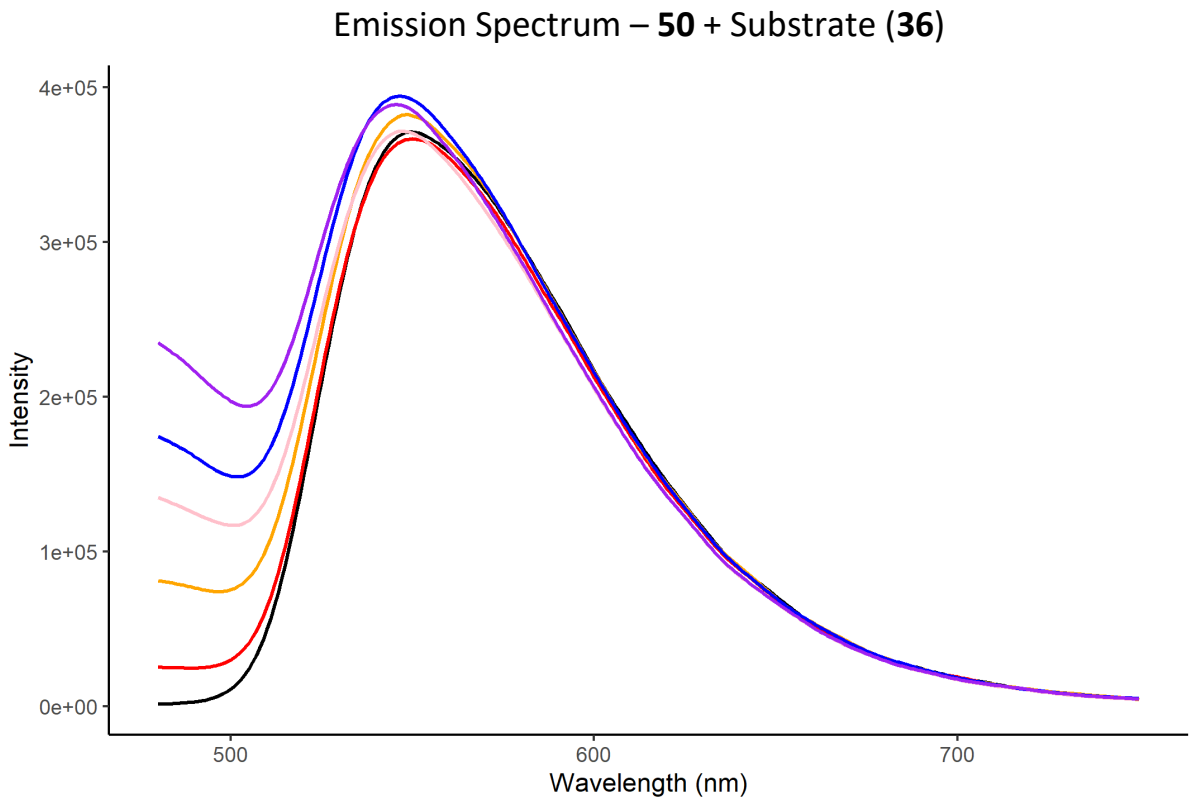



Figure S26 Stern-Volmer Quenching of PC (**50**) with substrate (**36**). Concentrations of **36** are: 0 mM (black), 1.9 mM (red), 6.7 mM (orange), 11.4 mM (pink), 15 mM (blue), 20 mM (purple). **50** is 0.5 µM in all cases.

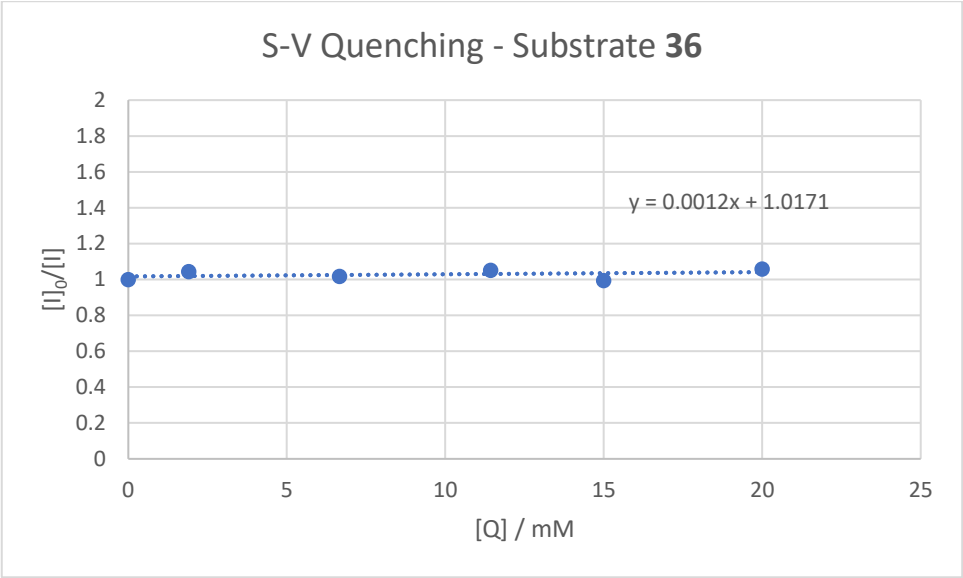



Figure S27 Stern-Volmer plot for **50** + substrate (**36**)

### **Addition of scandium +** 40 **complex + substrate (**36**)**

Due to solubility issues, the concentration of scandium complex was limited (maximum 2 mM). The concentration of substrate (**36**) was tenfold. Emission arising from the substrate itself was again observed, but no quenching outside of the substrate's emission range (λ>650 nm) was observed.

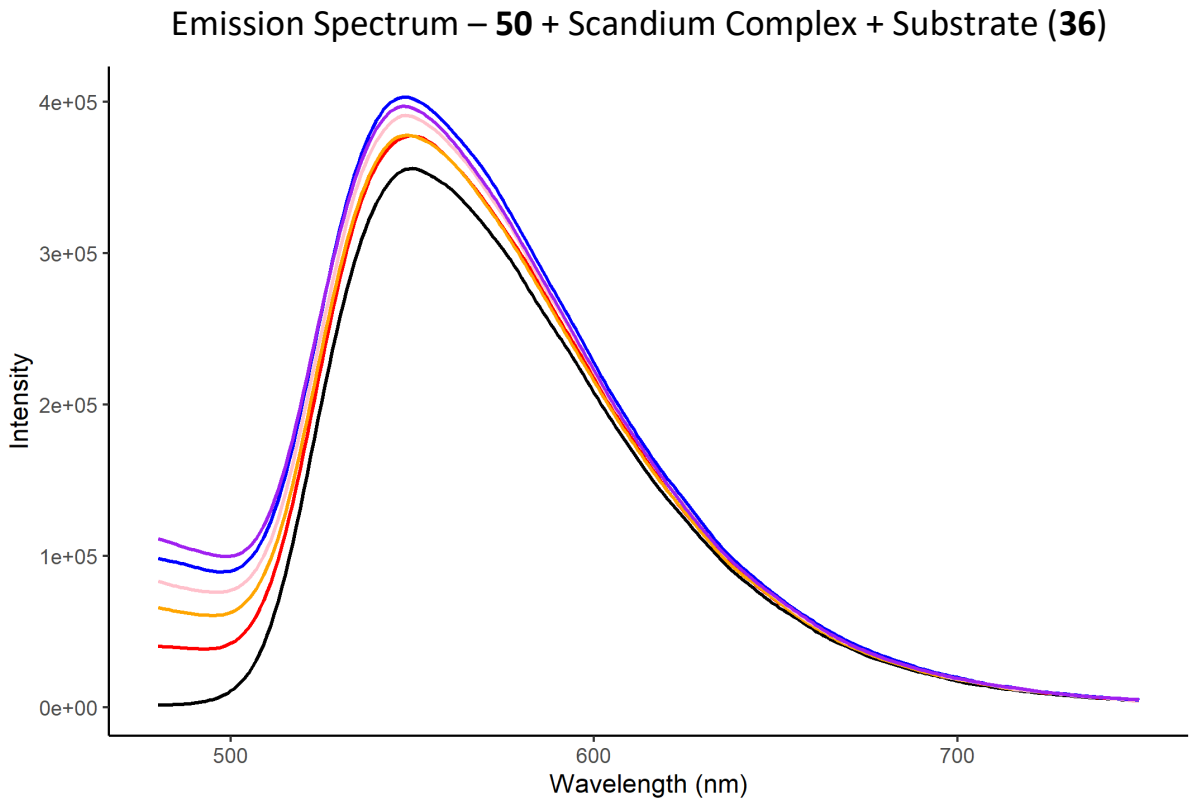



Figure S28 Stern-Volmer Quenching of PC (**50**) with scandium + **40** complex and substrate (**36**). Concentrations of **36** are: 0 (black), 0.17 (red), 0.29 (orange), 0.38 (pink), 0.44 (blue), 0.5 (purple). **50** is 0.5 µM in all cases.

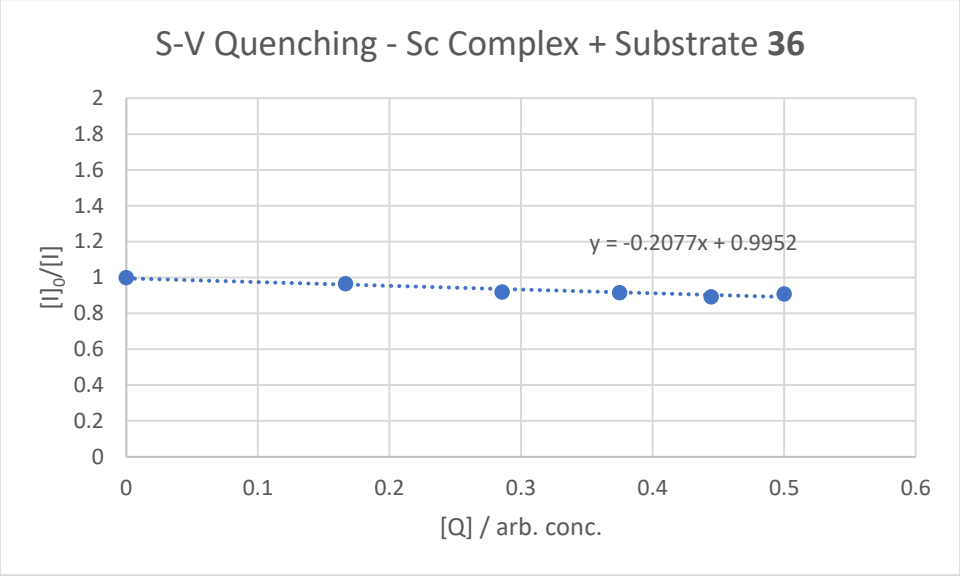



Figure S 29 Stern-Volmer plot for **50** + preformed scandium complex + substrate (**36**)

### I.4.6 UV-Vis Absorbance Spectra

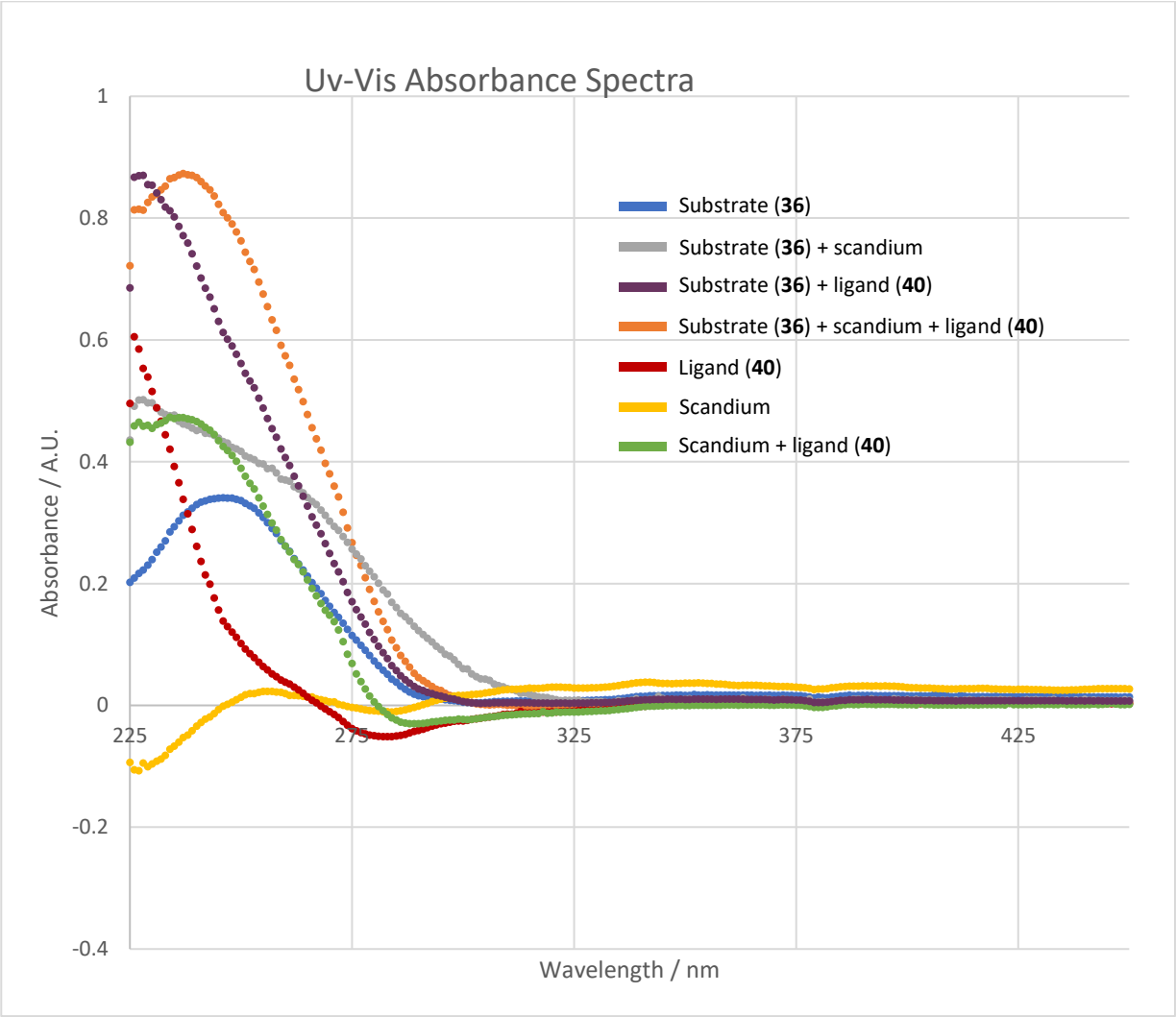
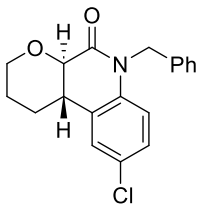



Figure S30 UV-Vis absorbance spectra of reaction components. substrate (**36**), blue, substrate (**36**) + scandium, grey, substrate (**36**) + ligand (**40**), purple, substrate (**36**) + scandium + ligand (**40**), orange, ligand (**40**), red, scandium, yellow, scandium + ligand (**40**), green.

## I.5 X-ray Crystallography

Single crystal X-ray diffraction was carried out by Owen A. Smith using a (Rigaku) Oxford Diffraction/Agilent Supernovae A diffractometer (Cu-$K_\alpha$ radiation, $\lambda$ = 1.54180 Å) equipped with a graphite monochromator within the Department of Chemistry, University of Oxford. Samples were mounted in perfluoropoly-ethyl ether oil and cooled to 150 K during the data collection by a $N_2$ Crysostream open-flow cooling device.[194] The raw frame data was integrated and reduced using CrysalisPro. CRYSTALS[15,16] was used to obtain an *ab initio* solution using SuperFlip[17] embedded within CRYSTALS and for structure refinement.

**(4a*R*,10b*S*)-6-Benzyl-9-chloro-2,3,6,10b-tetrahydro-1*H*-pyrano[2,3-c]quinolin-5(4a*H*)-one (86)**




**86**

Crystals of x-ray quality were grown by vapour diffusion of pentane into a solution of **86** (94.5:5.5 e.r.) in $CH_2Cl_2$. A void in the crystal structure containing heavily disordered solvent was treated with PLATON SQUEEZE.[18] The flack x parameter was refined to 0.004(9). Bayesian analysis of the Bijvoet pairs gave the Hooft y parameter as 0.000(2) allowing the absolute structure determination of **86**.

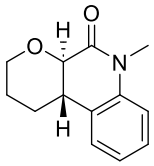
| | | |
|---|---|---|
| Identification Code | 031OS21 (CCDC 2192820) | |
| Empirical Formula | C19 H18 Cl N O2 | |
| $M_r$ | 327.81 | |
| Temperature | 150 K | |
| Wavelength | λ = 1.54180 Å (Cu $K_\alpha$) | |
| Crystal System | hexagonal | |
| Space Group | P 65 | |
| Unit Cell Dimensions | a = 19.8511(2) Å | α = 90° |
| | b = 19.8511(2) Å | β = 90° |
| | c = 7.64350(10) Å | γ = 120° |
| Volume | 2608.51(6) ($Å^3$) | |
| Z | 6 | |
| Density (Calculated) | 1.252 Mg $m^{-3}$ | |
| Absorption Coefficient | 2.011 $mm^{-1}$ | |
| Crystal Size | 0.05 x 0.06 x 0.45 $mm^3$ | |
| Theta range for data collection | 4.455 to 72.827° | |
| Index Ranges | -24<=h<=23 , -24<=k<=24 , -9<=l<=9 | |
| Reflections Collected | 51007 | |
| Independent Reflections | 3468 [R(int) = 0.054] | |
| Completeness to theta = 72.827° | 99.9% | |
| Absorption Correction | multi-scan | |
| Refinement method | Full-matrix least-squares on $F^2$ | |
| Goodness-of-fit on $F^2$ | 1.0068 | |
| Final R indices [I>2sigma(I)] | R1 = 0.0450, wR2 = 0.1160 | |
| R indices (all data) | R1 = 0.0457, wR2 = 0.1171 | |
| Flack x parameter | 0.004(9) | |
| Parsons' q parameter | 0.004(9) | |
| Hooft y parameter | 0.000(2) | |

# I.6 HPLC Traces for Chiral Compounds

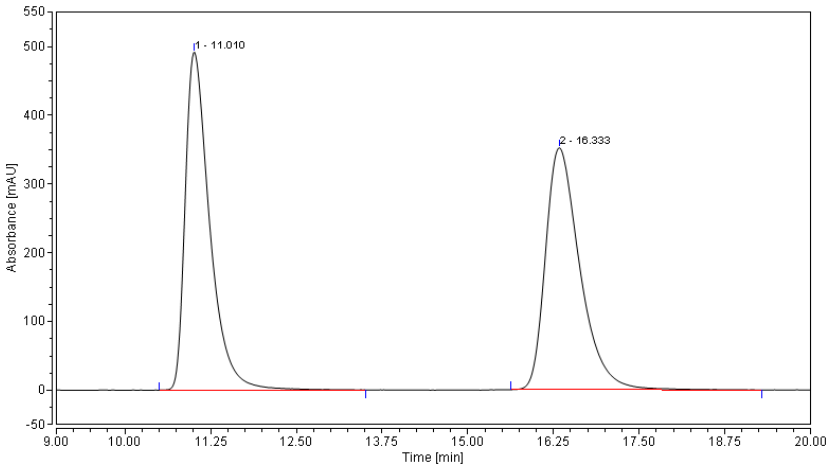
**(4a*R*,10b*S*)-6-Methyl-2,3,6,10b-tetrahydro-1*H*-pyrano[2,3-*c*]quinolin-5(4a*H*)-one (37)**

**Chiral HPLC:** (Chiralpak OD-H, 30% $^{i}$PrOH, 70% hexane, 1.0 mL min$^{-1}$, λ = 210 nm) $\tau_R$ (major) = 11.1 min, $\tau_R$ (minor) = 16.5 min.

**Racemic**

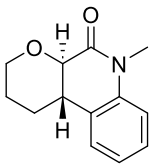


*(rac)*-**37**

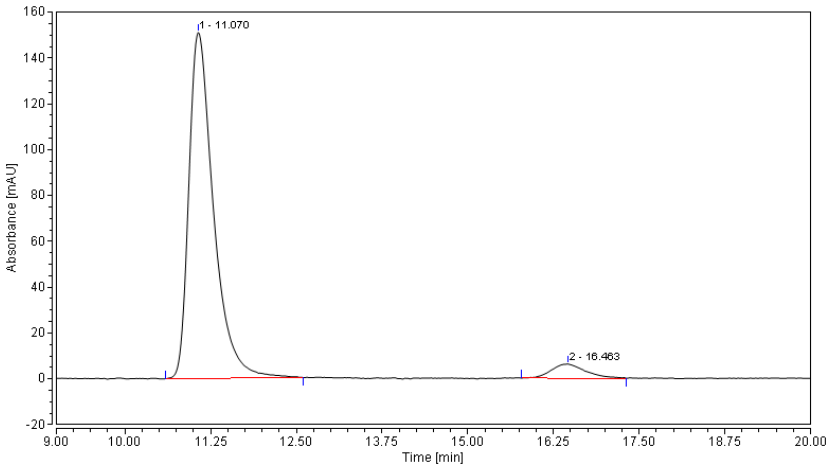



| No. | Retention Time (min) | Area (mAU*min) | Height (mAU) | Relative Area (%) |
|---|---|---|---|---|
| 1 | 11.010 | 203.568 | 491.786 | 49.86 |
| 2 | 16.333 | 204.734 | 351.968 | 50.14 |
| Total: | | 408.302 | 843.754 | 100.00 |

**Enantioselective**



**37**

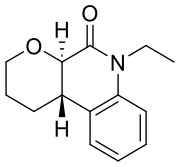



| No. | Retention Time (min) | Area (mAU*min) | Height (mAU) | Relative Area (%) |
|---|---|---|---|---|
| 1 | 11.070 | 62.899 | 151.094 | 94.55 |
| 2 | 16.463 | 3.627 | 6.211 | 5.45 |
| Total: | | 66.526 | 157.305 | 100.00 |

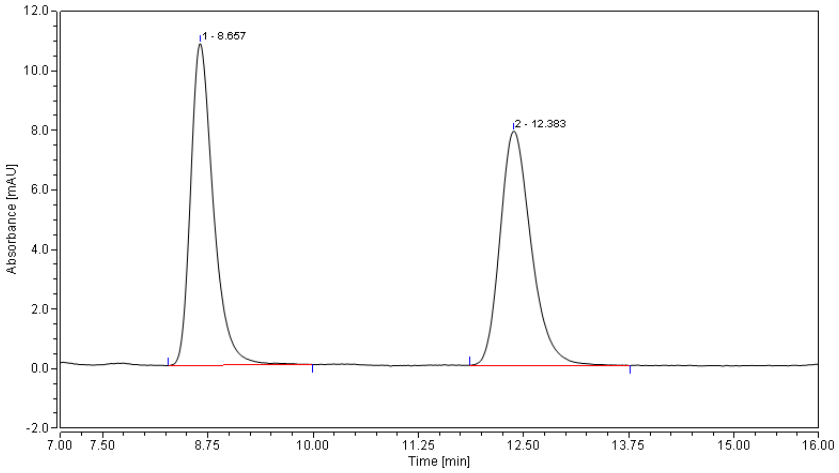
**(4a*R*,10b*S*)-6-Ethyl-2,3,6,10b-tetrahydro-1*H*-pyrano[2,3-c]quinolin-5(4a*H*)-one (60)**

**Chiral HPLC:** (Chiralpak OD-H, 30% $^{i}$PrOH, 70% hexane, 1.0 mL min$^{-1}$, λ = 260 nm) $\tau_R$ (major) = 8.6 min, $\tau_R$ (minor) = 12.4 min.

**Racemic**

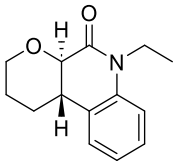


(*rac*)-**60**

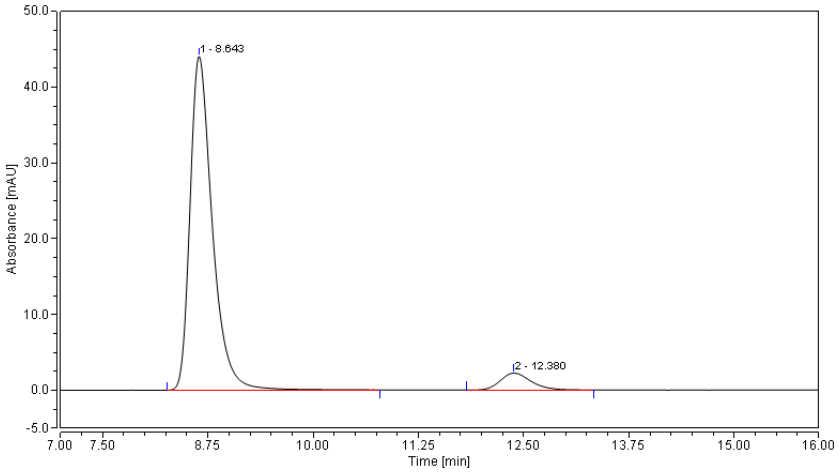



| No. | Retention Time (min) | Area (mAU*min) | Height (mAU) | Relative Area (%) |
|---|---|---|---|---|
| 1 | 8.657 | 3.388 | 10.813 | 50.07 |
| 2 | 12.383 | 3.378 | 7.866 | 49.93 |
| **Total:** | | 6.766 | 18.679 | 100.00 |

**Enantioselective**



**60**

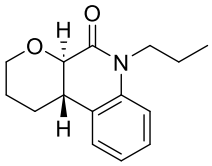



| No. | Retention Time (min) | Area (mAU*min) | Height (mAU) | Relative Area (%) |
|---|---|---|---|---|
| 1 | 8.643 | 13.508 | 44.052 | 93.40 |
| 2 | 12.380 | 0.954 | 2.235 | 6.60 |
| **Total:** | | 14.462 | 46.286 | 100.00 |

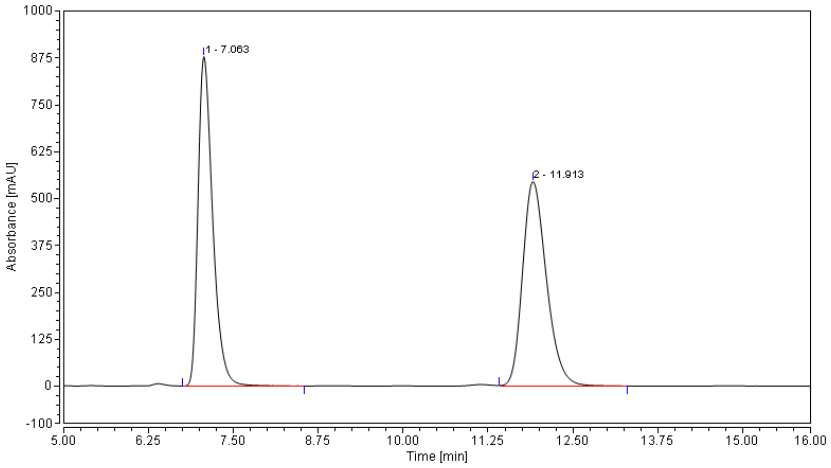
**(4a*R*,10b*S*)-6-Propyl-2,3,6,10b-tetrahydro-1*H*-pyrano[2,3-*c*]quinolin-5(4a*H*)-one (61)**

**Chiral HPLC:** (Chiralpak OD-H, 30% $^{i}$PrOH, 70% hexane, 1.0 mL min$^{-1}$, λ = 210 nm) $\tau_R$ (major) = 7.1 min, $\tau_R$ (minor) = 12.0 min.

**Racemic**

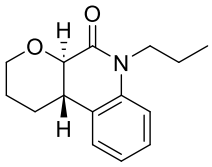


*(rac)*-**61**

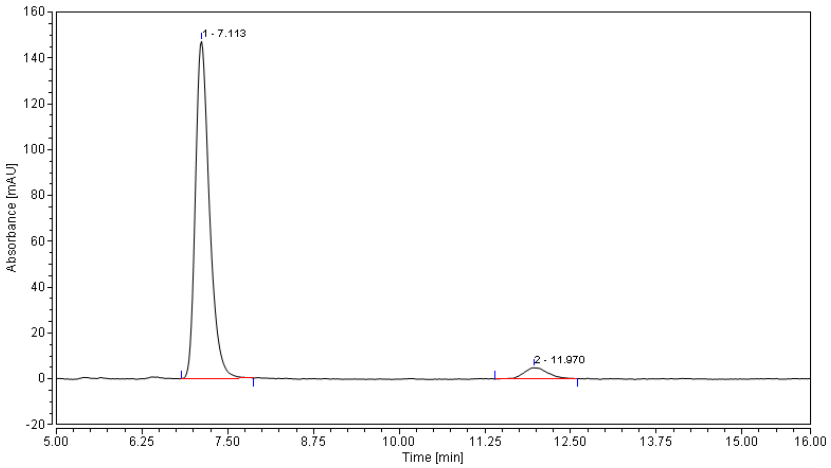



| No. | Retention Time (min) | Area (mAU*min) | Height (mAU) | Relative Area (%) |
|---|---|---|---|---|
| 1 | 7.063 | 220.115 | 878.849 | 49.74 |
| 2 | 11.913 | 222.381 | 545.415 | 50.26 |
| Total: | | 442.495 | 1424.264 | 100.00 |

**Enantioselective**



**61**

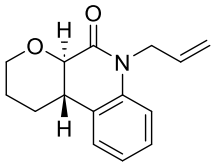



| No. | Retention Time (min) | Area (mAU*min) | Height (mAU) | Relative Area (%) |
|---|---|---|---|---|
| 1 | 7.113 | 34.889 | 147.221 | 94.52 |
| 2 | 11.970 | 2.025 | 4.924 | 5.48 |
| Total: | | 36.913 | 152.146 | 100.00 |

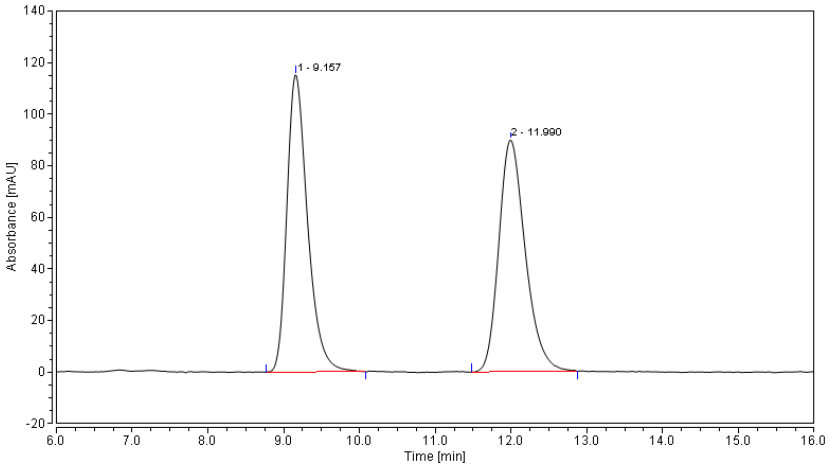
**(4a*R*,10b*S*)-6-Allyl-2,3,6,10b-tetrahydro-1*H*-pyrano[2,3-*c*]quinolin-5(4a*H*)-one (62)**

**Chiral HPLC:** (Chiralpak OD-H, 30% $^{i}$PrOH, 70% hexane, 1.0 mL min$^{-1}$, λ = 210 nm) $\tau_R$ (major) = 9.2 min, $\tau_R$ (minor) = 12.0 min.

**Racemic**

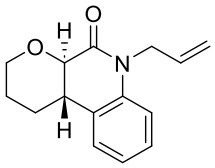


*(rac)*-**62**

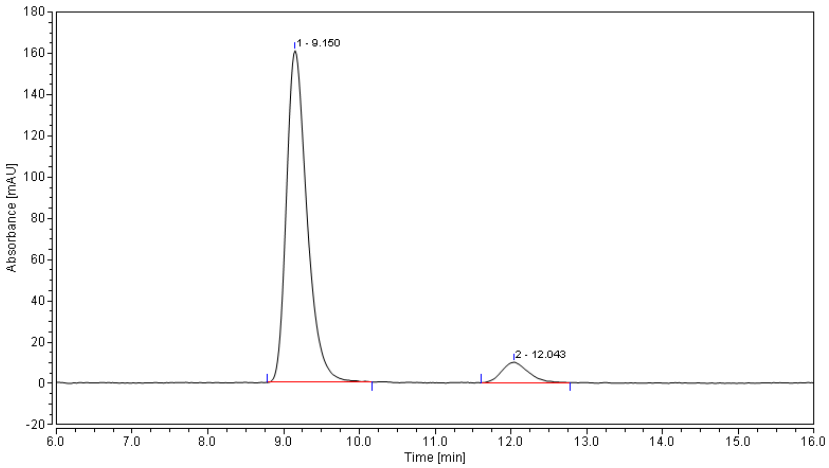



| No. | Retention Time (min) | Area (mAU*min) | Height (mAU) | Relative Area (%) |
|---|---|---|---|---|
| 1 | 9.157 | 36.484 | 115.459 | 50.03 |
| 2 | 11.990 | 36.445 | 89.948 | 49.97 |
| Total: | | 72.929 | 205.406 | 100.00 |

**Enantioselective**



**62**

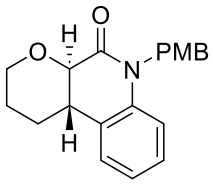



| No. | Retention Time (min) | Area (mAU*min) | Height (mAU) | Relative Area (%) |
|---|---|---|---|---|
| 1 | 9.150 | 50.640 | 160.888 | 92.53 |
| 2 | 12.043 | 4.086 | 9.948 | 7.47 |
| Total: | | 54.726 | 170.836 | 100.00 |

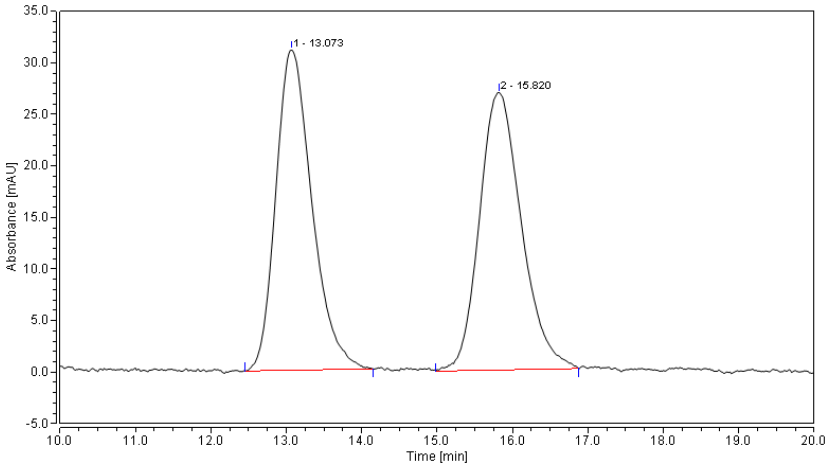
**(4a*R*,10b*S*)-6-(4-Methoxybenzyl)-2,3,6,10b-tetrahydro-1*H*-pyrano[2,3-*c*]quinolin-5(4a*H*)-one (63)**

**Chiral HPLC:** (Chiralpak OD-H, 30% $^{i}$PrOH, 70% hexane, 1.0 mL min$^{-1}$, $\lambda$ = 210 nm) $\tau_R$ (major) = 13.0 min, $\tau_R$ (minor) = 15.8 min.

**Racemic**

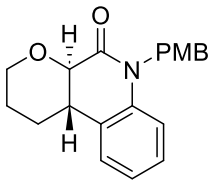



*(rac)*-**63**

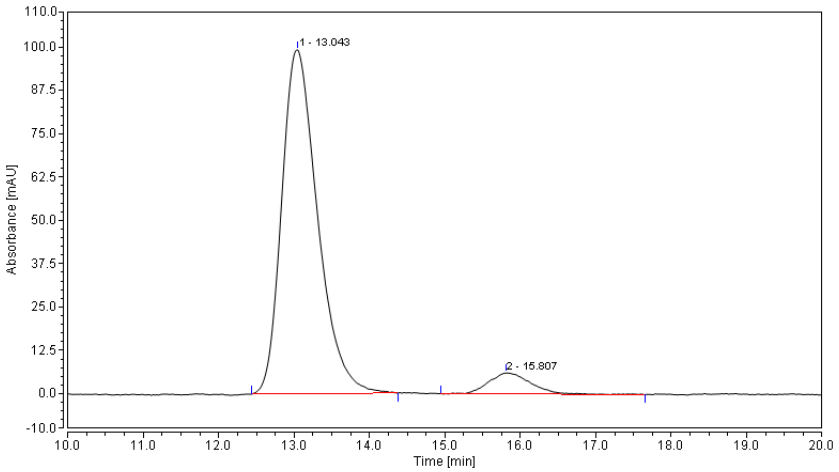



| No. | Retention Time (min) | Area (mAU*min) | Height (mAU) | Relative Area (%) |
|---|---|---|---|---|
| 1 | 13.073 | 17.247 | 31.079 | 49.84 |
| 2 | 15.820 | 17.357 | 26.922 | 50.16 |
| Total: | | 34.604 | 58.001 | 100.00 |

**Enantioselective**




**63**

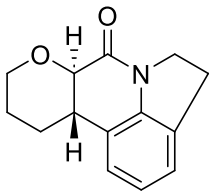



| No. | Retention Time (min) | Area (mAU*min) | Height (mAU) | Relative Area (%) |
|---|---|---|---|---|
| 1 | 13.043 | 54.693 | 99.249 | 93.22 |
| 2 | 15.807 | 3.979 | 6.043 | 6.78 |
| Total: | | 58.672 | 105.291 | 100.00 |

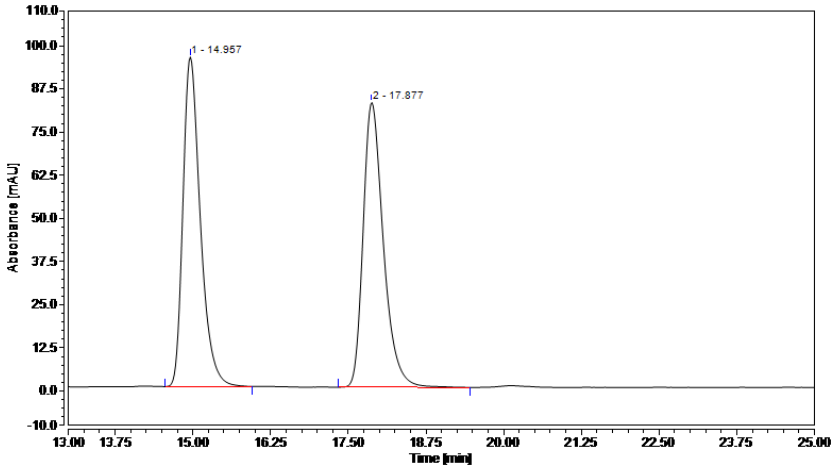
**(4a*R*,10b*S*)-6-Ethyl-2,3,6,10b-tetrahydro-1*H*-pyrano[2,3-c]quinolin-5(4a*H*)-one (64)**

**Chiral HPLC:** (Chiralpak IB N-3, 30% $^{i}$PrOH, 70% hexane, 1.0 mL min$^{-1}$, $\lambda$ = 210 nm) $\tau_R$ (major) = 15.0 min, $\tau_R$ (minor) = 17.9 min.

**Racemic**

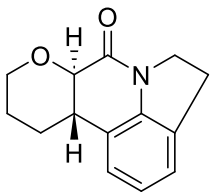


(*rac*)-**64**

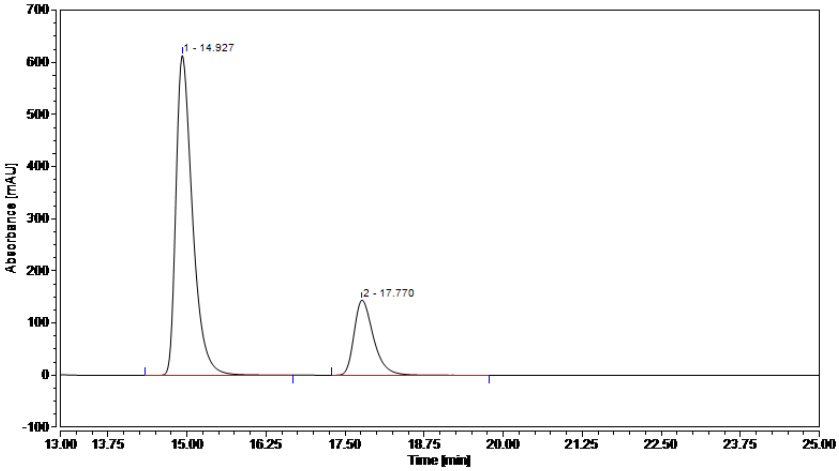



| No. | Retention Time (min) | Area (mAU*min) | Height (mAU) | Relative Area (%) |
|---|---|---|---|---|
| 1 | 14.957 | 31.084 | 95.569 | 50.00 |
| 2 | 17.877 | 31.089 | 82.522 | 50.00 |
| **Total:** | | 62.172 | 178.091 | 100.00 |

**Enantioselective**



**64**

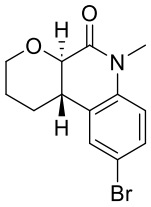



| No. | Retention Time (min) | Area (mAU*min) | Height (mAU) | Relative Area (%) |
|---|---|---|---|---|
| 1 | 14.927 | 186.154 | 613.760 | 78.34 |
| 2 | 17.770 | 51.461 | 144.311 | 21.66 |
| **Total:** | | 237.615 | 758.071 | 100.00 |

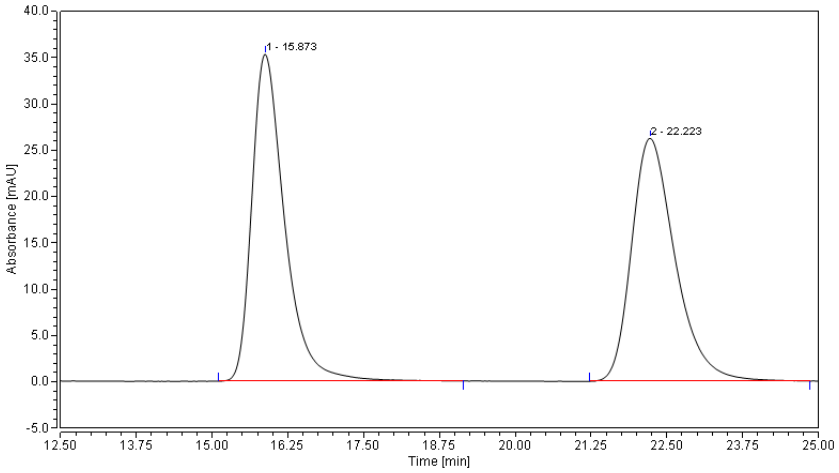
**(4a*R*,10b*S*)-9-Bromo-6-methyl-2,3,6,10b-tetrahydro-1*H*-pyrano[2,3-*c*]quinolin-5(4a*H*)-one (66)**

**Chiral HPLC:** (Chiralpak OD-H, 30% $^{i}$PrOH, 70% hexane, 1.0 mL min$^{-1}$, λ = 254 nm) $\tau_R$ (major) = 15.9 min, $\tau_R$ (minor) = 22.1 min.

**Racemic**

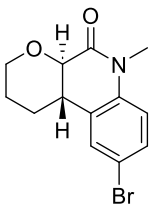


(*rac*)-**66**

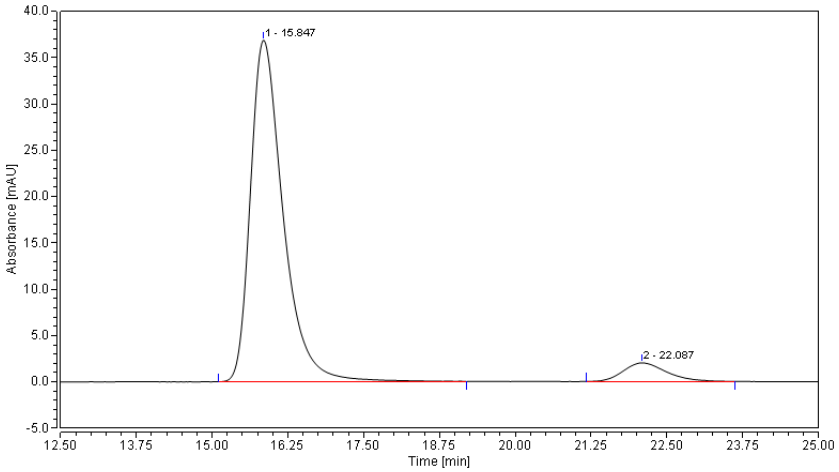



| No. | Retention Time (min) | Area (mAU*min) | Height (mAU) | Relative Area (%) |
|---|---|---|---|---|
| 1 | 15.873 | 22.118 | 35.283 | 50.05 |
| 2 | 22.223 | 21.788 | 26.215 | 49.30 |
| **Total:** | | 44.190 | 62.071 | 100.00 |

**Enantioselective**



**66**

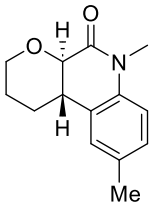



| No. | Retention Time (min) | Area (mAU*min) | Height (mAU) | Relative Area (%) |
|---|---|---|---|---|
| 1 | 15.847 | 23.017 | 36.865 | 93.22 |
| 2 | 22.087 | 1.674 | 2.019 | 6.78 |
| **Total:** | | 24.691 | 38.884 | 100.00 |

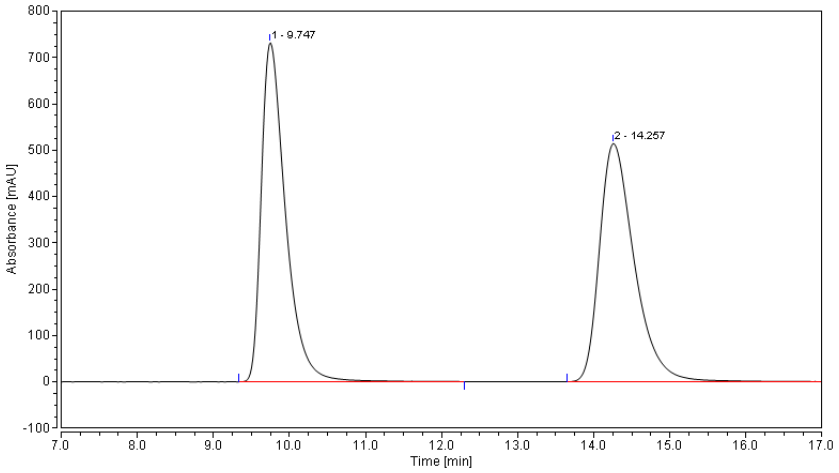
**(4a*R*,10b*S*)-6,9-Dimethyl-2,3,6,10b-tetrahydro-1*H*-pyrano[2,3-c]quinolin-5(4a*H*)-one (67)**

**Chiral HPLC:** (Chiralpak OD-H, 30% $^{i}$PrOH, 70% hexane, 1.0 mL min$^{-1}$, λ = 260 nm) $\tau_R$ (major) = 9.8 min, $\tau_R$ (minor) = 14.4 min.

**Racemic**

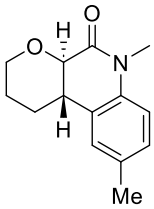



*(rac)*-**67**

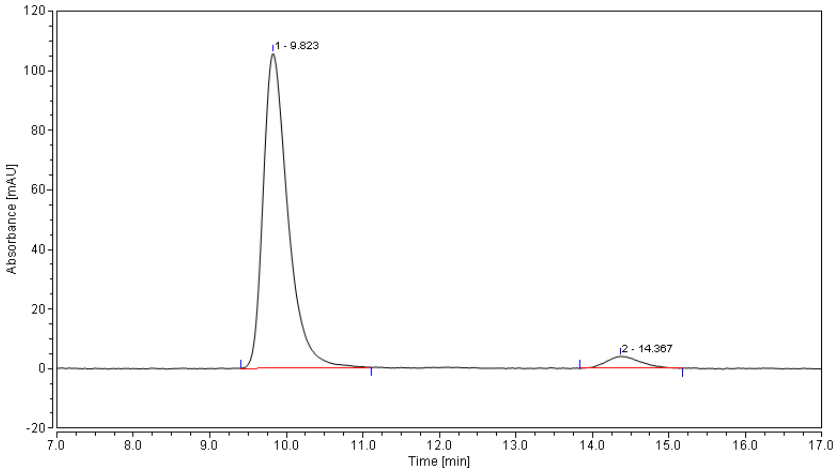



| No. | Retention Time (min) | Area (mAU*min) | Height (mAU) | Relative Area (%) |
|---|---|---|---|---|
| 1 | 9.747 | 271.226 | 732.107 | 49.89 |
| 2 | 14.257 | 272.409 | 514.365 | 50.11 |
| **Total:** | | 543.634 | 1246.472 | 100.00 |

**Enantioselective**




**67**

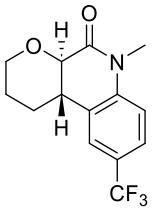



| No. | Retention Time (min) | Area (mAU*min) | Height (mAU) | Relative Area (%) |
|---|---|---|---|---|
| 1 | 9.823 | 39.541 | 105.756 | 94.85 |
| 2 | 14.367 | 2.147 | 4.016 | 5.15 |
| **Total:** | | 41.688 | 109.772 | 100.00 |

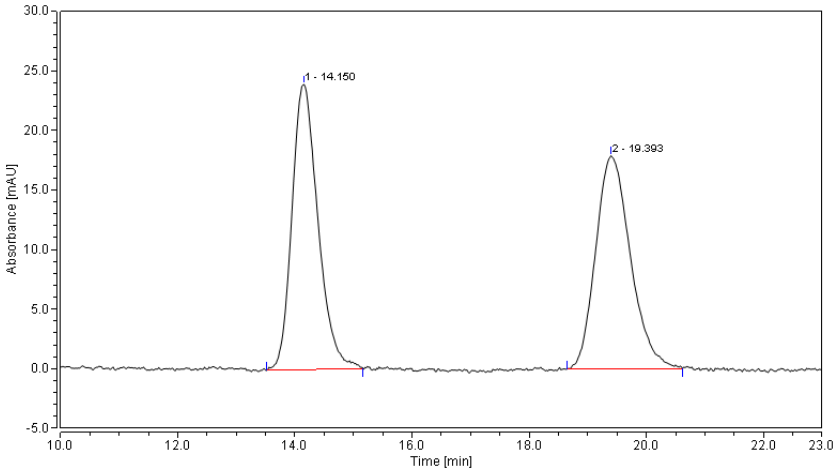
**(4a*R*,10b*S*)-6-Methyl-9-(trifluoromethyl)-2,3,6,10b-tetrahydro-1*H*-pyrano[2,3-*c*]quinolin-5(4a*H*)-one (68)**

**Chiral HPLC:** (Chiralpak OD-H, 30% $^{i}$PrOH, 70% hexane, 1.0 mL min$^{-1}$, λ = 210 nm) $\tau_R$ (major) = 14.2 min, $\tau_R$ (minor) = 19.4 min.

**Racemic**

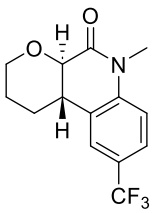


(*rac*)-**68**

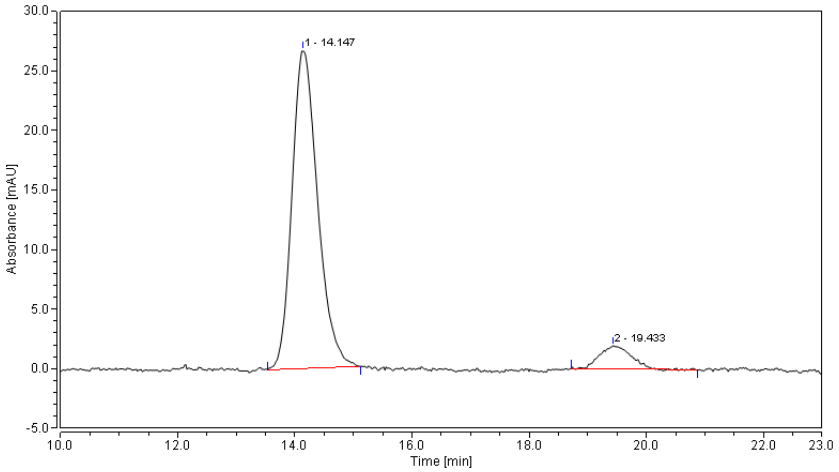



| No. | Retention Time (min) | Area (mAU*min) | Height (mAU) | Relative Area (%) |
|---|---|---|---|---|
| 1 | 14.150 | 12.348 | 24.000 | 50.10 |
| 2 | 19.393 | 12.301 | 17.913 | 49.90 |
| **Total:** | | 24.649 | 41.913 | 100.00 |

**Enantioselective**



**68**

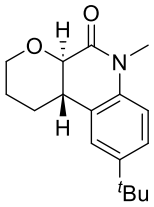



| No. | Retention Time (min) | Area (mAU*min) | Height (mAU) | Relative Area (%) |
|---|---|---|---|---|
| 1 | 14.147 | 13.590 | 26.717 | 91.82 |
| 2 | 19.433 | 1.211 | 1.988 | 8.18 |
| **Total:** | | 14.801 | 28.705 | 100.00 |

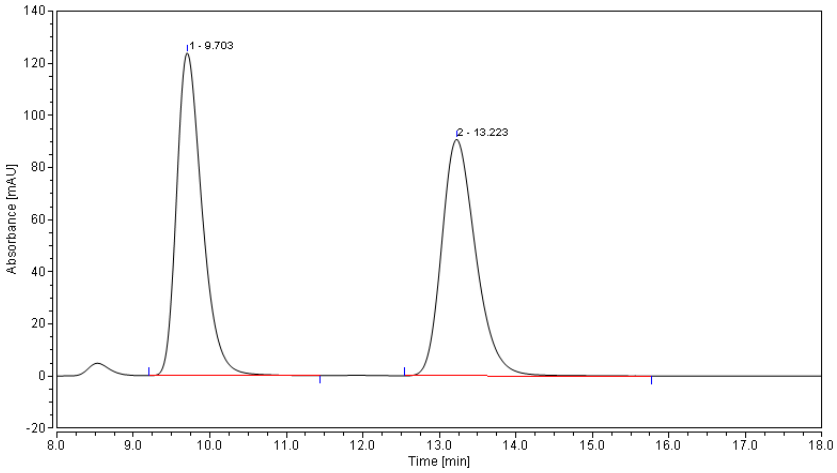
**(4a*R*,10b*S*)-9-(*Tert*-butyl)-6-methyl-2,3,6,10b-tetrahydro-1*H*-pyrano[2,3-c]quinolin-5(4a*H*)-one (69)**

**Chiral HPLC:** (Chiralpak OD-H, 30% $^{i}$PrOH, 70% hexane, 1.0 mL min$^{-1}$, λ = 270 nm) $\tau_R$ (major) = 9.8 min, $\tau_R$ (minor) = 13.2 min.

**Racemic**

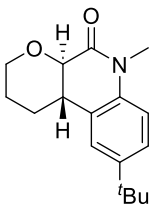



(*rac*)-**69**

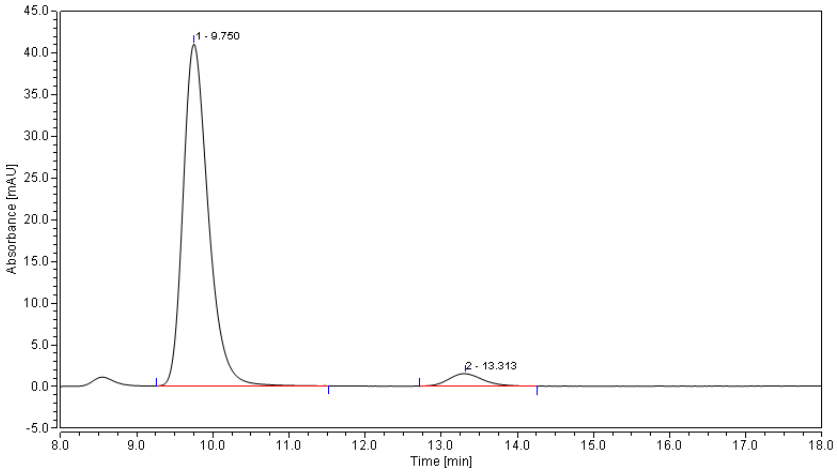



| No. | Retention Time (min) | Area (mAU*min) | Height (mAU) | Relative Area (%) |
|---|---|---|---|---|
| 1 | 9.703 | 47.894 | 123.868 | 50.61 |
| 2 | 13.223 | 46.748 | 90.741 | 49.39 |
| **Total:** | | 94.642 | 214.609 | 100.00 |

**Enantioselective**




**69**



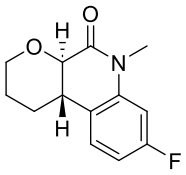

| No. | Retention Time (min) | Area (mAU*min) | Height (mAU) | Relative Area (%) |
|---|---|---|---|---|
| 1 | 9.750 | 15.681 | 41.024 | 95.28 |
| 2 | 13.313 | 0.776 | 1.497 | 4.72 |
| **Total:** | | 16.457 | 42.521 | 100.00 |

**(4a*R*,10b*S*)-8-Fluoro-6-methyl-2,3,6,10b-tetrahydro-1*H*-pyrano[2,3-*c*]quinolin-5(4a*H*)-one (72), and (4a*R*,10b*S*)-10-Fluoro-6-methyl-2,3,6,10b-tetrahydro-1*H*-pyrano[2,3-*c*]quinolin-5(4a*H*)-one (72b)**

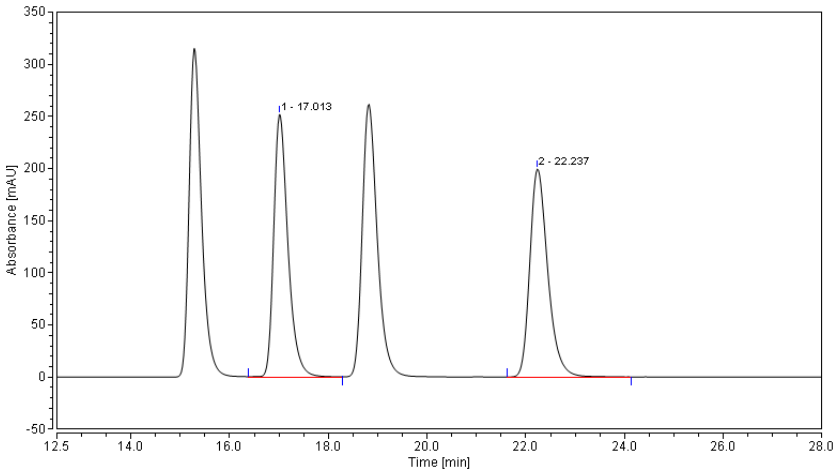
**(4a*R*,10b*S*)-8-Fluoro-6-methyl-2,3,6,10b-tetrahydro-1*H*-pyrano[2,3-*c*]quinolin-5(4a*H*)-one (72)**

**Chiral HPLC:** (Chiralpak IB N-3, 25% $^{i}$PrOH, 75% hexane, 1.0 mL min$^{-1}$, $\lambda$ = 210 nm) $\tau_R$ (major) = 17.0 min, $\tau_R$ (minor) = 22.3 min.

**Racemic**

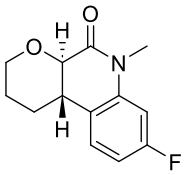


*(rac)*-**72**

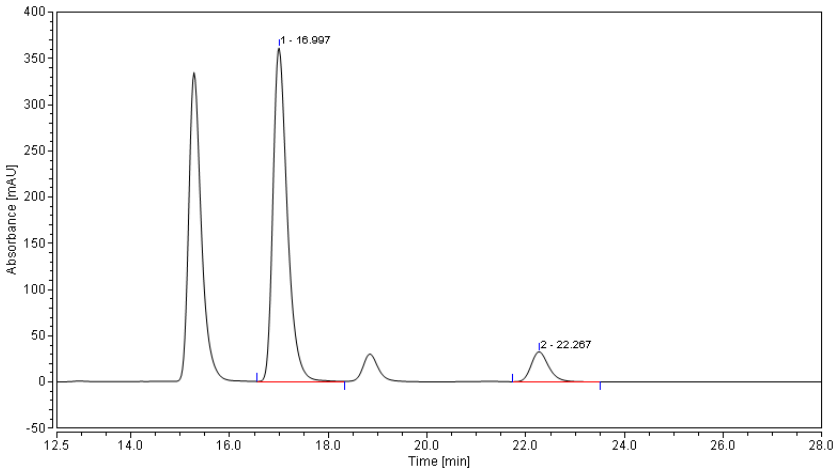



| No. | Retention Time (min) | Area (mAU*min) | Height (mAU) | Relative Area (%) |
|---|---|---|---|---|
| 1 | 17.013 | 84.238 | 251.994 | 50.02 |
| 2 | 22.237 | 84.182 | 199.732 | 49.98 |
| **Total:** | | 168.42 | 451.726 | 100.00 |

**Enantioselective**



**72**

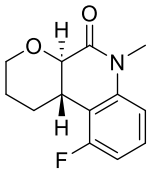



| No. | Retention Time (min) | Area (mAU*min) | Height (mAU) | Relative Area (%) |
|---|---|---|---|---|
| 1 | 16.997 | 121.490 | 360.833 | 90.03 |
| 2 | 22.267 | 13.452 | 32.464 | 9.97 |
| **Total:** | | 134.942 | 393.297 | 100.00 |

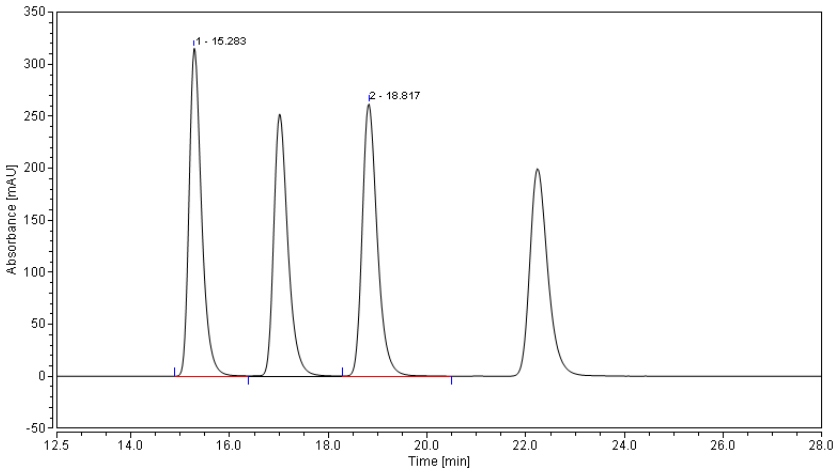
**(4a*R*,10b*S*)-10-Fluoro-6-methyl-2,3,6,10b-tetrahydro-1*H*-pyrano[2,3-*c*]quinolin-5(4a*H*)-one (72b)**

**Chiral HPLC:** (Chiralpak IB N-3, 25% $^{i}$PrOH, 75% hexane, 1.0 mL min$^{-1}$, $\lambda$ = 210 nm) $\tau_R$ (major) = 15.3 min, $\tau_R$ (minor) = 18.8 min.

**Racemic**

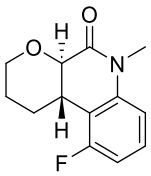


*(rac)*-**72b**

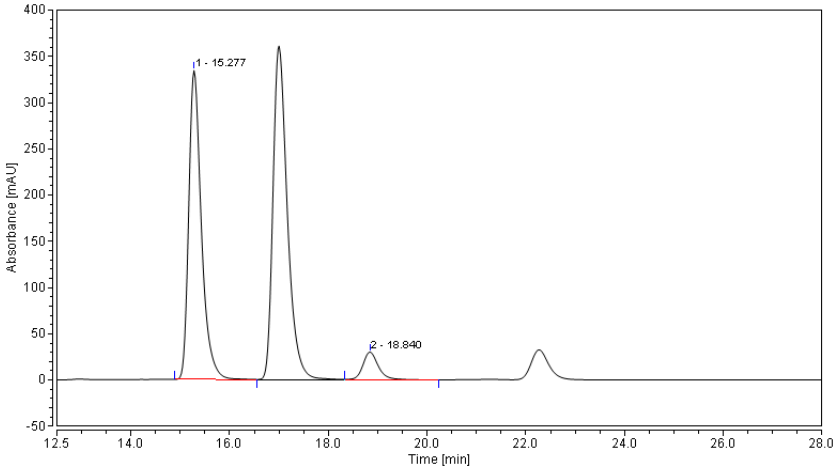



| No. | Retention Time (min) | Area (mAU*min) | Height (mAU) | Relative Area (%) |
|---|---|---|---|---|
| 1 | 15.283 | 92.385 | 315.391 | 49.96 |
| 2 | 18.817 | 92.534 | 262.069 | 50.04 |
| **Total:** | | 184.919 | 577.460 | 100.00 |

**Enantioselective**



**72b**



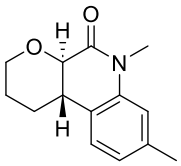

| No. | Retention Time (min) | Area (mAU*min) | Height (mAU) | Relative Area (%) |
|---|---|---|---|---|
| 1 | 15.277 | 99.067 | 334.192 | 90.09 |
| 2 | 18.840 | 10.901 | 29.982 | 9.91 |
| **Total:** | | 109.968 | 364.174 | 100.00 |

**(4a*R*,10b*S*)-6,8-Dimethyl-2,3,6,10b-tetrahydro-1*H*-pyrano[2,3-*c*]quinolin-5(4a*H*)-one (73), and (4a*R*,10b*S*)-6,10-dimethyl-2,3,6,10b-tetrahydro-1*H*-pyrano[2,3-*c*]quinolin-5(4a*H*) (91)**

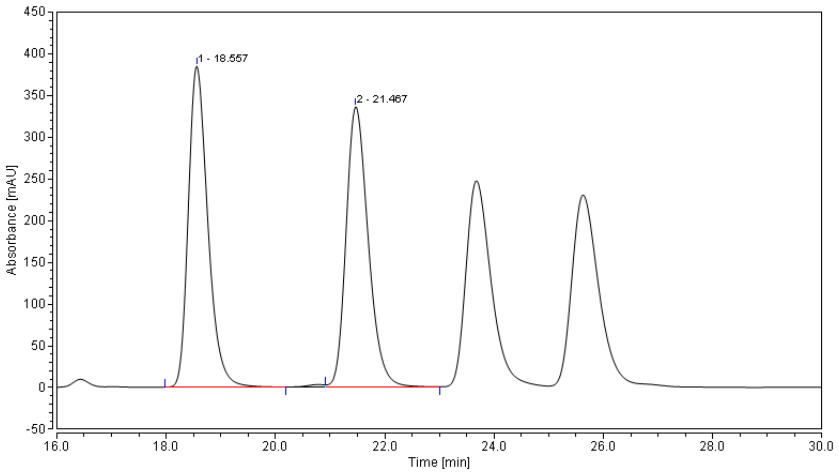
**(4a*R*,10b*S*)-6,8-Dimethyl-2,3,6,10b-tetrahydro-1*H*-pyrano[2,3-*c*]quinolin-5(4a*H*)-one (73)**

**Chiral HPLC:** (Chiralpak IG-3, 20% $^{i}$PrOH, 80% hexane, 1.0 mL min$^{-1}$, λ = 210 nm) $\tau_R$ (major) = 18.6 min, $\tau_R$ (minor) = 21.4 min.

**Racemic**

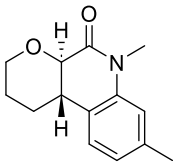


(*rac*)-**73**

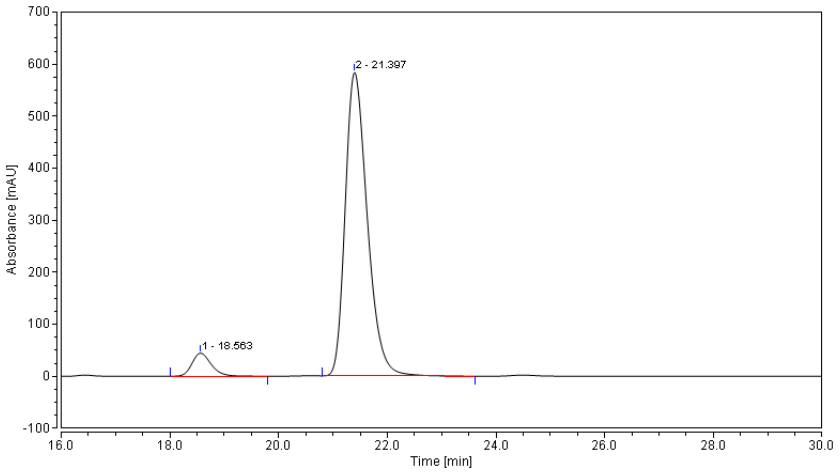



| No. | Retention Time (min) | Area (mAU*min) | Height (mAU) | Relative Area (%) |
|---|---|---|---|---|
| 1 | 18.557 | 159.021 | 385.017 | 50.15 |
| 2 | 21.467 | 158.075 | 336.339 | 49.85 |
| **Total:** | | 317.096 | 721.357 | 100.00 |

**Enantioselective**



**73**

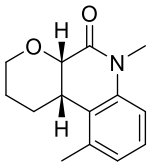



| No. | Retention Time (min) | Area (mAU*min) | Height (mAU) | Relative Area (%) |
|---|---|---|---|---|
| 1 | 18.563 | 18.138 | 44.307 | 6.20 |
| 2 | 21.397 | 274.554 | 583.765 | 93.80 |
| **Total:** | | 292.692 | 628.072 | 100.00 |

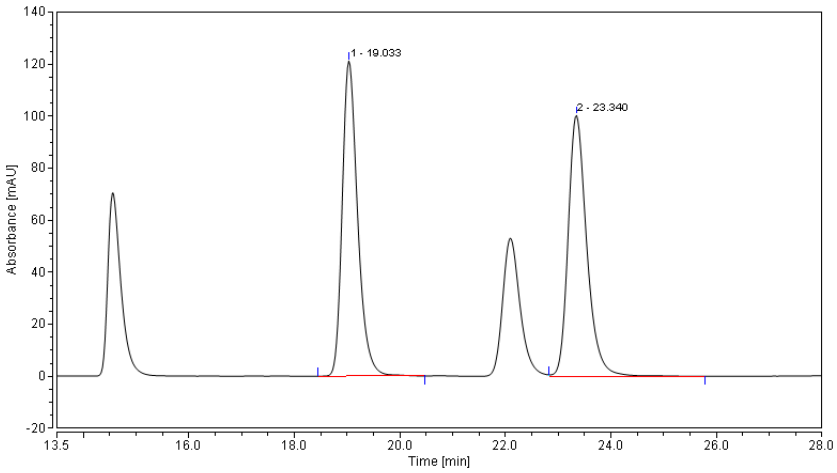
**(4a*R*,10b*S*)-6,8-Dimethyl-2,3,6,10b-tetrahydro-1*H*-pyrano[2,3-*c*]quinolin-5(4a*H*)-one (91)**

**Chiral HPLC:** (Chiralpak IB N-3, 15% $^{i}$PrOH, 85% hexane, 1.0 mL min$^{-1}$, $\lambda$ = 222 nm) $\tau_R$ (major) = 19.0 min, $\tau_R$ (minor) = 23.3 min..

**Racemic**

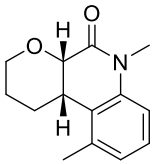


(*rac*)-**91**

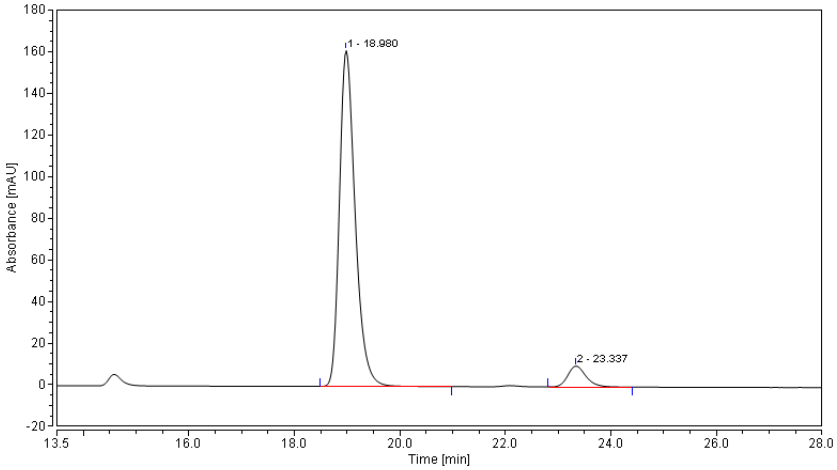



| No. | Retention Time (min) | Area (mAU*min) | Height (mAU) | Relative Area (%) |
|---|---|---|---|---|
| 1 | 19.033 | 41.036 | 121.263 | 49.97 |
| 2 | 23.340 | 41.084 | 100.422 | 50.03 |
| **Total:** | | 82.120 | 221.685 | 100.00 |

**Enantioselective**



**91**



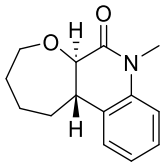

| No. | Retention Time (min) | Area (mAU*min) | Height (mAU) | Relative Area (%) |
|---|---|---|---|---|
| 1 | 18.980 | 55.884 | 161.512 | 93.21 |
| 2 | 23.337 | 4.068 | 10.082 | 6.79 |
| **Total:** | | 59.952 | 171.594 | 100.00 |

**(5a*R*,11b*S*)-7-Methyl-1,2,3,4,7,11b-hexahydrooxepino[2,3-*c*]quinolin-6(5a*H*)-one (85)**

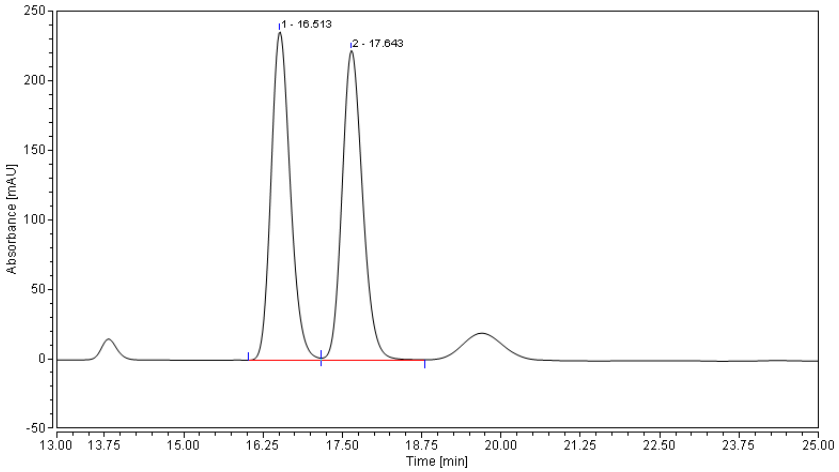
## Using 50

**Chiral HPLC:** (Chiralpak IG-3, 25% $^{i}$PrOH, 75% hexane, 1.0 mL min$^{-1}$, λ = 210 nm) $\tau_R$ (major) = 16.5 min, $\tau_R$ (minor) = 17.7 min.

**Racemic**

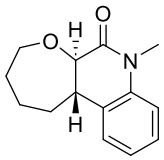


(*rac*)-**85**

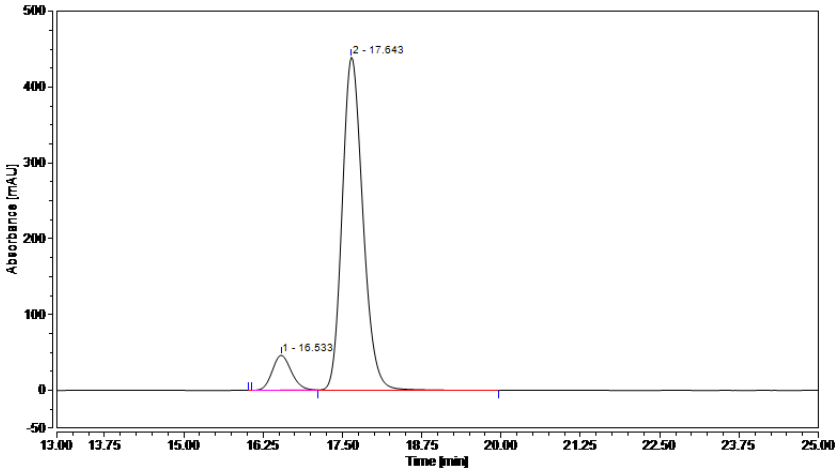



| No. | Retention Time (min) | Area (mAU*min) | Height (mAU) | Relative Area (%) |
|---|---|---|---|---|
| 1 | 16.513 | 83.015 | 236.480 | 49.88 |
| 2 | 17.643 | 83.399 | 222.767 | 50.12 |
| **Total:** | | 166.414 | 459.247 | 100.00 |

**Enantioselective**



**85**

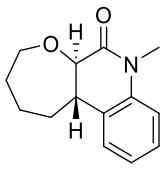



| No. | Retention Time (min) | Area (mAU*min) | Height (mAU) | Relative Area (%) |
|---|---|---|---|---|
| 1 | 16.533 | 15.893 | 45.898 | 8.71 |
| 2 | 17.643 | 166.666 | 439.575 | 91.29 |
| **Total:** | | 182.559 | 485.473 | 100.00 |

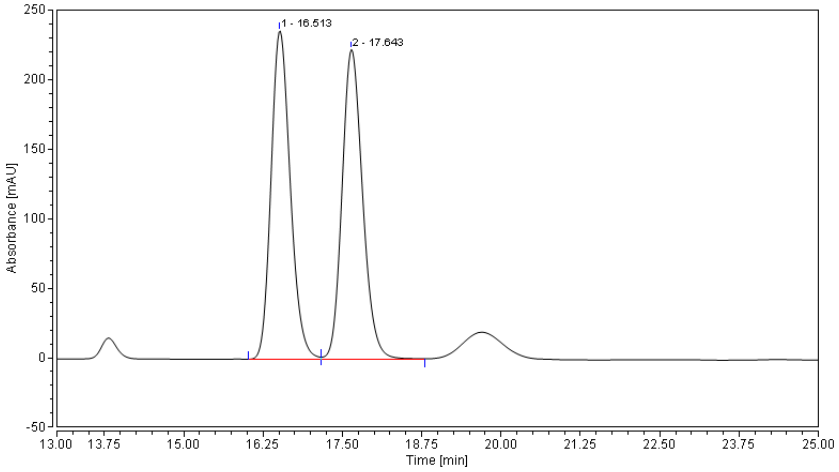
## Using $Ir(Fppy)_3$

**Chiral HPLC:** (Chiralpak IG-3, 25% $^{i}$PrOH, 75% hexane, 1.0 mL min$^{-1}$, $\lambda$ = 210 nm) $\tau_R$ (major) = 16.5 min, $\tau_R$ (minor) = 17.7 min.

**Racemic**

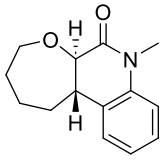


(*rac*)-**85**

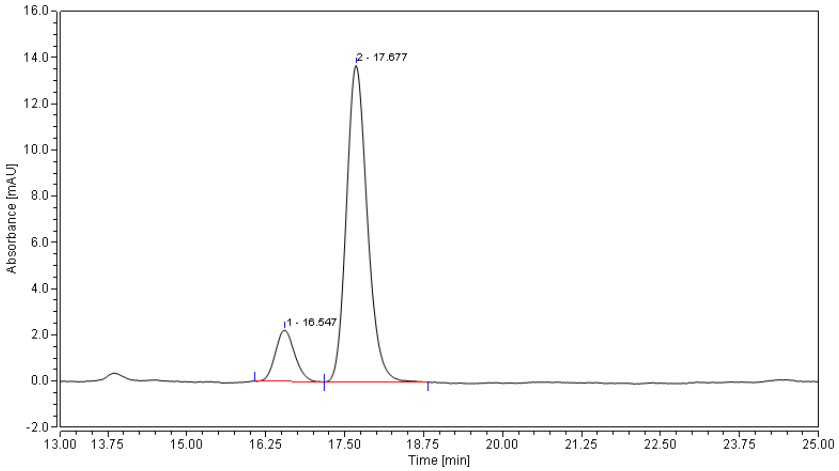



| No. | Retention Time (min) | Area (mAU*min) | Height (mAU) | Relative Area (%) |
|---|---|---|---|---|
| 1 | 16.513 | 83.015 | 236.480 | 49.88 |
| 2 | 17.643 | 83.399 | 222.767 | 50.12 |
| **Total:** | | 166.414 | 459.247 | 100.00 |

**Enantioselective**



**85**

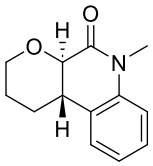



| No. | Retention Time (min) | Area (mAU*min) | Height (mAU) | Relative Area (%) |
|---|---|---|---|---|
| 1 | 16.547 | 0.789 | 2.214 | 13.01 |
| 2 | 17.677 | 5.271 | 13.718 | 86.99 |
| **Total:** | | 6.060 | 15.932 | 100.0 |

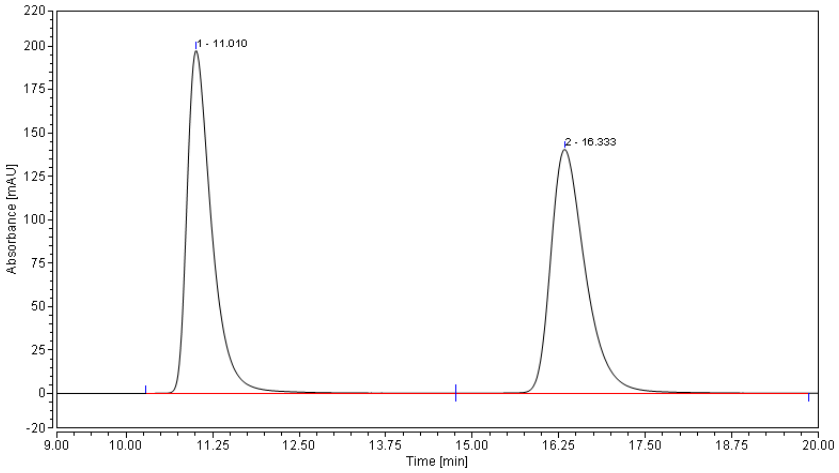
**(4a*R*,10b*S*)-6-Methyl-2,3,6,10b-tetrahydro-1*H*-pyrano[2,3-*c*]quinolin-5(4a*H*)-one-4a,7,8,9,10-$d_5$ (88)**

**Chiral HPLC:** (Chiralpak IB N-3, 30% $^{i}$PrOH, 70% hexane, 1.0 mL min$^{-1}$, $\lambda$ = 210 nm) $\tau_R$ (major) = 11.1 min, $\tau_R$ (minor) = 16.6 min.

**Racemic**

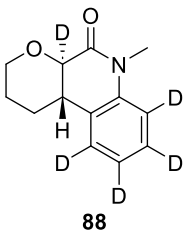


*(rac)*-**37**

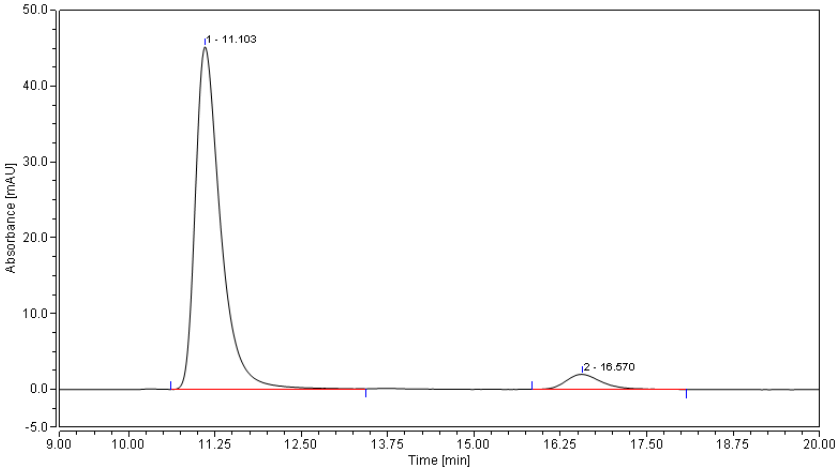



| No. | Retention Time (min) | Area (mAU*min) | Height (mAU) | Relative Area (%) |
|---|---|---|---|---|
| 1 | 11.010 | 81.682 | 197.420 | 50.00 |
| 2 | 16.333 | 81.678 | 140.439 | 50.00 |
| **Total:** | | 163.360 | 337.859 | 100.00 |

**Enantioselective**



**88**

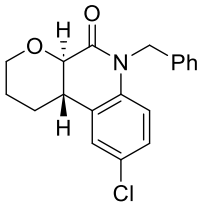



| No. | Retention Time (min) | Area (mAU*min) | Height (mAU) | Relative Area (%) |
|---|---|---|---|---|
| 1 | 11.103 | 19.074 | 45.196 | 94.06 |
| 2 | 16.570 | 1.204 | 1.987 | 5.94 |
| **Total:** | | 20.278 | 47.182 | 100.00 |

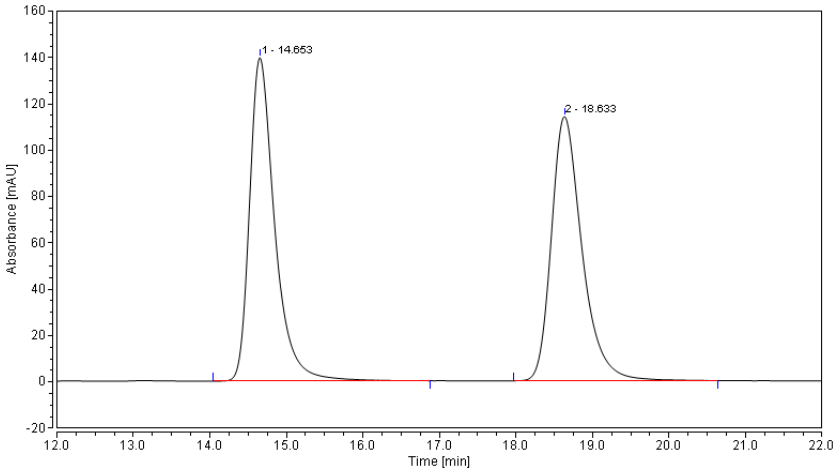
**(4a*R*,10b*S*)-6-Benzyl-9-chloro-2,3,6,10b-tetrahydro-1*H*-pyrano[2,3-c]quinolin-5(4a*H*)-one (86)**

**Chiral HPLC:** (Chiralpak IF-3, 50% $^{i}$PrOH, 50% hexane, 1.0 mL min$^{-1}$, $\lambda$ = 210 nm) $\tau_R$ (major) = 14.7 min, $\tau_R$ (minor) = 18.5 min.

**Racemic**

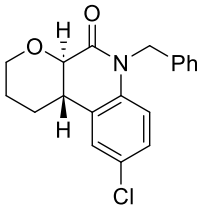



(*rac*)-**86**

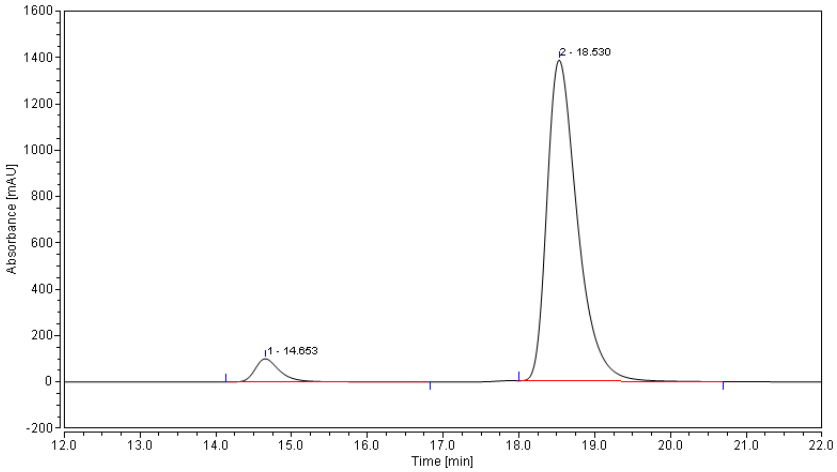



| No. | Retention Time (min) | Area (mAU*min) | Height (mAU) | Relative Area (%) |
|---|---|---|---|---|
| 1 | 14.653 | 53.151 | 139.649 | 50.11 |
| 2 | 18.633 | 52.919 | 114.096 | 49.89 |
| **Total:** | | 106.071 | 253.746 | 100.00 |

**Enantioselective**




**86**




| No. | Retention Time (min) | Area (mAU*min) | Height (mAU) | Relative Area (%) |
|---|---|---|---|---|
| 1 | 14.653 | 37.916 | 99.892 | 5.58 |
| 2 | 18.530 | 641.915 | 1385.648 | 94.42 |
| **Total:** | | 679.831 | 1485.540 | 100.00 |

# Part II:

# Enantiomerisation Processes of Indolyl-Naphthyl Atropisomers

# II.1 General Procedures for Kinetic Data Collection

**Procedure for 4**

A 1.75 ml vial containing an 8 mm × 3 mm stirrer bar, capped with a polypropylene cap with a 26s gauge hole and thread sealed with teflon tape was clamped in an 80 °C oil-bath stirring at 900 rpm and allowed to equilibrate for ca. 1 h. After this time a 1.75 ml vial containing the appropriate mass of **126** (Table 1.1) was removed from the freezer and allowed to warm to room temperature for 8.5 min before 250 µl Acros toluene, 99.85 %, Extra Dry, AcroSeal® was added *via* inerted syringe. 10 s later the vial was homogenised using a vortex mixer at 2800 rpm for 40 s. The solution was then drawn into an inerted sharped 1 ml syringe and the sharp of the syringe placed through the hole in the cap of the vial in the oil-bath. 10 min after removal from the freezer, the plunger was depressed and a second timer started to denote the start of the run. Aliquots of volume 0.5 µl – 1.0 µl were withdrawn at timepoints shown in Table 1.2 and diluted with 200 µl of cold 2 % *iso*-propanol in hexane into 250 µl autosampler vials cooled to 0 °C. An additional zero time-point was taken by rinsing the transfer syringe with 1 % *iso*-propanol in hexane.

Table S7 Masses of **126** required for each end concentration on dissolution in 250 µl of toluene

| Concentration (mol/kg) | 0.2 | 0.1 | 0.05 | 0.025 |
|---|---|---|---|---|
| Mass **126** (mg) | 13.1 | 6.5 | 3.3 | 1.6 |

Table S8 Time points for erosion studies of **126**

| **Pt (#)** | **1** | **2** | **3** | **4** | **5** | **6** | **7** | **8** | **9** | **10** |
|---|---|---|---|---|---|---|---|---|---|---|
| **Time (s)** | 0 | 60 | 120 | 180 | 240 | 300 | 360 | 420 | 480 | 540 |
| **Pt (#)** | **11** | **12** | **13** | **14** | **15** | **16** | **17** | **18** | **19** | **20** |
| **Time (s)** | 600 | 660 | 720 | 780 | 840 | 900 | 960 | 1020 | 1080 | 1140 |
| **Pt (#)** | **21** | **22** | **23** | **24** | **25** | **26** | **27** | **28** | **29** | **30** |
| **Time (s)** | 1200 | 1350 | 1500 | 1650 | 1800 | 1950 | 2100 | 2250 | 2400 | 2550 |
| **Pt (#)** | **31** | **32** | **33** | **34** | **35** | **36** | **37** | **38** | **39** | **40** |
| **Time (s)** | 2700 | 2850 | 3000 | 3150 | 3300 | 3450 | 3600 | 3900 | 4200 | 4500 |
| **Pt (#)** | **41** | **42** | **43** | **44** | **45** | **46** | | | | |
| **Time (s)** | 4800 | 5100 | 5400 | 6000 | 6600 | 7200 | | | | |

**Procedure for 129 and 131**

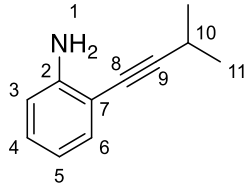
A 1.75 ml vial containing an 8 mm × 3 mm stirrer bar, capped with a polypropylene cap with a 26s gauge hole and thread sealed with teflon tape was clamped in a 155 °C oil-bath stirring at 900 rpm and allowed to equilibrate for ca. 1 h. After this time a 1.75 ml vial containing 1.7 mg of **129** or **131** was removed from the freezer and allowed to warm to room temperature for 8.5 min before 250 µl Tokyo Chemical Industries, > 98 %, 1,2,4-trimethylbenzene was added via inerted syringe. 10 s later the vial was homogenised using a vortex mixer at 2800 rpm for 40 s. The solution was then drawn into an inerted sharped 1 ml syringe and the sharp of the syringe placed through the hole in the cap of the vial in the oil-bath. 10 min after removal from the freezer, the plunger was depressed and a second timer started to denote the start of the run. Aliquots of volume 0.5 µl– 1.0 µl were withdrawn according to Table 1.3 and diluted with 200 µl of cold 1 % *iso*-propanol in hexane into 250 µl autosampler vials cooled to 0 °C. An additional zero timepoint was taken by rinsing the transfer syringe with 1 % *iso*-propanol in hexane.

Table S9 Time points for erosion studies of **129** and **131**

| **Pt** | **1** | **2** | **3** | **4** | **5** | **6** | **7** | **8** | **9** | **10** |
|---|---|---|---|---|---|---|---|---|---|---|
| **Time (s)** | 0 | 120 | 240 | 480 | 600 | 720 | 840 | 960 | 1080 | 1200 |
| **Pt (#)** | **11** | **12** | **13** | **14** | **15** | **16** | **17** | **18** | **19** | **20** |
| **Time (s)** | 1800 | 1800 | 2400 | 3000 | 3300 | 3600 | 4500 | 5400 | 6300 | 7200 |
| **Pt (#)** | **21** | **22** | **23** | **24** | **25** | **26** | | | | |
| **Time (s)** | 1500 | 9000 | 10800 | 14400 | 21600 | 36000 | | | | |

# II.2 Experimental Data for Compounds

**2-(3-Methylbut-1-yn-1-yl)aniline, 127**




This compound was prepared according to a literature procedure[20]

To a round-bottom flask containing a stirrer bar was added 2-iodoaniline (4.38 g, 20 mmol, 1.0 eq.), CuI (76 mg, 0.4 mmol, 0.02 eq.), and $PdCl_2(PPh_3)_2$ (140mg, 0.2 mmol, 0.01 eq.). The flask was then evacuated and backfilled with argon three times before 3-methyl-1-butyne (2.46 ml, 24 mmol, 1.2 eq.), and freshly sparged di*iso*propylamine (22.4 ml, 80 mmol, 16.0 eq.) and dimethyl-formamide (20 ml, 1.0 M) were added. The reaction was stirred at room temperature overnight before being quenched with sat. aq. $NH_4Cl$. The reaction mixture was then extracted with diethyl ether (3 × 40 ml), before the combined organic layers were dried over $MgSO_4$, filtered, and concentrated to dryness. The crude product was purified by flash column chromatography (ethyl acetate:pentane; 1:19) to yield **127** as a yellow oil (3.16 g, 99% yield).

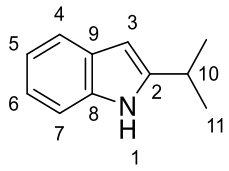
**FTIR** (film) *v* /cm$^{-1}$ 3474, 3379, 2969, 2931, 2870, 1612, 1493, 1455, 1383, 1363, 1320, 1264, 1244, 1216, 1157, 1098, 1031, 942, 852, 745 (str), 667;

**$^1$H NMR** (400 MHz, $CDCl_3$) $\delta$ = 7.32 – 7.24 (m, 1H, H-6), 7.11 (ddd, *J* = 8.1, 7.3, 1.6 Hz, 1H, H-4), 6.75 – 6.65 (m, 2H, H-3,5), 4.08 (s, 2H, H-1), 2.87 (hept, *J* = 6.9 Hz, 1H, H-10), 1.33 (d, *J* = 6.9 Hz, 6H, H-11);

**$^{13}$C NMR** (101 MHz, $CDCl_3$) $\delta$ = 147.5 (quat., C-2), 132.0 (CH, C-6), 128.8 (CH, C-4), 117.9 (CH, C-5), 114.2 (CH, C-3), 108.9 (quat., C-7), 101.3 (quat., C-9), 76.2 (quat., C-8), 23.3 (CH3, C-11), 22.9 (CH2, C-11'), 21.1 (CH, C-10);

**LRMS** (ESI$^+$) mass calculated for $C_{11}H_{14}N$ ([M+H]$^+$) = 160.1, mass found = 160.0;

**2-*Iso*propyl-1H-indole, 128**




This compound was prepared according to a literature procedure[21]

To a solution of **127** (3.16 g, 27.5 mmol, 1.0 eq.) in dry acetonitrile (100 ml, 0.2 M) was added $PdCl_2$ (463 mg, 0.9 mmol, 0.05 eq.). The reaction mixture was brought to reflux for 1 h before being cooled to room temperature and poured onto $H_2O$ (100 ml). The mixture was then extracted with ethyl acetate (3 × 50 ml), before the organic layers were combined, dried over $MgSO_4$, filtered, and concentrated to dryness. The crude product was purified by flash column chromatography (dichloromethane: pentane; 3:17) to yield **128** as a white solid (2.51 g, 79% yield).

*or*

To a solution of *o*-toluidine (5.3 ml, 50 mmol, 1.0 eq.) and triethyl amine (7.0 ml, 50 mmol, 1.0 eq.) in dichloromethane (35 mL, 1.5 M) at 0 °C was added isobutyryl chloride (5.8 mL, 55 mmol, 1.1 eq.) dropwise. After complete addition the solution was refluxed for 3 h. After complete consumption of starting materials, the reaction mixture was cooled and hydrochloric acid (1.0 M, 15 mL) was added slowly. The biphasic mixture was then extracted with dichloromethane (3 x 15 mL), the organic layers were combined and washed with water (15 mL), dried over $MgSO_4$, filtered and evaporated to dryness. To the resulting solid was added dry tetrahydrofuran (100 mL, 0.5 M) and the solution was cooled to 0 °C and the vessel was flushed with argon. *n*-Butyllithium (50 mL, 2.5 M in hexanes, 2.5 eq.) was then added dropwise and the resulting solution was allowed to stir at room temperature overnight. Upon completion, the reaction was quenched with sat. aq. $NH_4Cl$ (15 mL) and extracted with ethyl acetate (3 x 30 mL). The organic layers were dried over $MgSO_4$, filtered, and evaporated to dryness. Purification was by silica plug, eluting with toluene to afford **128** as a white solid (3.68 g, 46% yield).

**m.p.** 62-66 °C

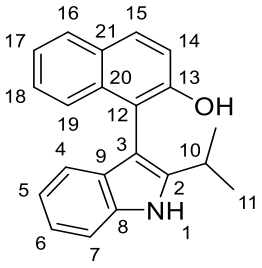
**FTIR** (film) $\nu$ /cm$^{-1}$ 3386 (str), 3050, 2966, 2871, 1547, 1461, 1411, 1382, 1341, 1302, 1130, 781, 749 (str), 688, 630, 610;

**$^1$H-NMR** (400 MHz, $CDCl_3$) $\delta$ = 7.91 (s, 1H, H-1), 7.56 (ddd, *J* = 7.6, 1.0, 1.0 Hz, 1H, H-4), 7.33 (d, *J* = 8.1 Hz, 1H, H-7), 7.18 – 7.07 (m, 2H, H-5,6), 6.25 (s, 1H, H-3), 3.08 (hept, *J* = 6.9 Hz, 1H, H-10), 1.38 (d, *J* = 6.9 Hz, 6H, H-11);

**$^{13}$C NMR** (101 MHz, $CDCl_3$) $\delta$ = 146.0 (quat., C-2), 135.9 (quat., C-9), 128.7 (quat., C-8), 121.2 (CH, C-6), 120.0 (CH, C-4), 119.8 (CH, C-5), 110.5 (CH, C-7), 97.4 (CH, C-3), 27.8 (CH, C-10), 22.5 (2CH3, C-11);

**LRMS** (ESI$^+$) mass calculated for $C_{11}H_{14}N$ ([M+H]$^+$) = 160.1, mass found = 160.0;

**1-(2-*Iso*propyl-1H-indol-3-yl)naphthalen-2-ol, 126**




To a solution of **128** (1.0 g, 6.3 mmol, 1.1 eq.) and 2-naphthol (820 mg, 5.7 mmol, 1.0 eq.) in 1:1 hexafluoroispropanol:dichloromethane (14 ml, 0.4 M) was added iron$^{III}$ chloride (90 mg, 0.56 mmol, 0.1 eq.) and di-*tert*-butyl peroxide (1.25 ml, 6.8 mmol, 1.2 eq.). The mixture was allowed to stir for 16 h before being concentrated to dryness, loaded onto silica, and purified by flash column chromatography (dichloromethane:pentane; 1:1) to give **126** as a white solid (1.25 g, 73 % yield).

**m.p.** 104-108 °C

**FTIR** (film) $\nu$ /cm$^{-1}$ 3477, 3410, 3336, 3055, 2958, 2867, 1619, 1595, 1458, 1195, 1167, 1137, 815, 750 (str);

**$^1$H NMR** (400 MHz, $CDCl_3$) $\delta$ = 8.37 (s, 1H, H-1), 7.96 – 7.86 (m, 2H, H-15,16), 7.51 – 7.42 (m, 2H, H-7,19), 7.45 – 7.31 (m, 3H, H-14,17,18), 7.29 (ddd, *J* = 8.2, 7.0, 1.3 Hz, 1H, H-6), 7.20 (ddd, *J* = 7.9, 0.9, 0.9 Hz, 1H, H-4), 7.12 (ddd, *J* = 7.9, 7.0, 1.1 Hz, 1H, H-5), 5.51 (s, 1H, H-22), 2.99 (qq, *J* = 7.0, 7.0 Hz, 1H, H-10), 1.26 (d, *J* = 7.0 Hz, 3H, H-11), 1.22 (d, *J* = 7.0 Hz, 3H, H-11');

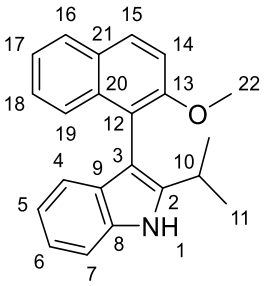
**$^{13}$C NMR** (101 MHz, $CDCl_3$) $\delta$ = 152.3 (quat., C-13), 144.9 (quat., C-2), 136.0 (quat., C-8), 134.7 (quat., C-2-), 139.6 (CH, C-15), 129.2 (quat., C-21), 128.9 (quat., C-9), 128.2 (CH, C-16), 126.4 (CH, C-18), 125.2 (CH, C-19), 123.2 (CH, C-17), 122.2 (CH, C-6), 120.4 (CH, C-5), 119.5 (CH, C-4), 117.0 (CH, C-14), 113.2 (quat., C-12), 110.9 (CH, C-7), 102.6 (quat., C-3), 26.5 (CH, C-10), 22.6 ($CH_3$, C-11), 22.5 ($CH_3$, C11');

**LRMS** ($ESI^+$) mass calculated for $C_{21}H_{20}NO$ ($[M+H]^+$) = 302.2, mass found = 302.2; HRMS ($ESI^+$) mass calculated for $C_{21}H_{20}NO$ ($[M+H]^+$) = 302.1539, mass found = 302.1541, Δ 0.5 ppm;

Enantiopure (> 99.5 % e.e.) **126** for use in erosion studies was obtained *via* semi-preparative HPLC (250mm × 10mm Ø YMC Chiral-SA column, 5.0 mL min$^{-1}$, *iso*-propanol:hexane; 16:84)

**$[\alpha]_D^{25}$** = +100 (*c* 0.10, $CHCl_3$)

**2-isopropyl-3-(2-methoxynaphthalen-1-yl)-1H-indole, 129**




To a solution of **126** (480 mg, 1.6 mmol, 1.0 eq.) in acetone (8 ml, 0.4 M) was added potassium carbonate (1.1 g, 8.0 mmol, 5.0 eq.), followed by dimethylsulfate (455 µl, 4.8 mmol, 3.0 eq.). The reaction was allowed to stir at room temperature for 1 h before being quenched with 5 % aq. $NH_4OH$ (25 ml), extracted with diethyl ether (3 × 25 ml), dried over $MgSO_4$, filtered, and concentrated *in vacuo*. The crude produce was purified by flash column chromatography (ethyl acetate: pentane; 1:9) to yield **129** as a white solid (454 mg, 90% yield).

**m.p.** 125-127 °C

**FTIR** (film) *v* /cm$^{-1}$ 3415, 2957, 1621, 1593, 1506, 1488, 1462, 1429, 1386, 1249, 1231, 1185, 1172, 1142, 1114, 1097, 851, 799, 777, 764, 748, 720, 705, 674

**$^1$H NMR** (400 MHz, $CDCl_3$) $\delta$ = 8.13 (s, 1H, H-1), 7.91 (d, *J* = 9.0 Hz, 1H, H-15), 7.85 (ddd, *J* = 8.2, 0.9, 0.9 Hz, 1H, H-16), 7.52 (dddd, *J* = 8.4, 1.6, 0.8, 0.8 Hz, 1H, H-19), 7.45 – 7.38 (m, 2H, H-14,7), 7.30 (m, H-17,18), 7.15 (ddd, *J* = 8.1, 6.7, 1.5 Hz, 1H, H-6), 7.09 – 6.93 (m, 2H, H-4,5), 3.80 (s, 3H, H-22), 2.94 (qq, *J* = 7.0, 7.0 Hz, 1H, H-10), 1.28 (d, *J* = 7.0 Hz, 3H, H-11), 1.18 (d, *J* = 7.0 Hz, 3H, H-11');

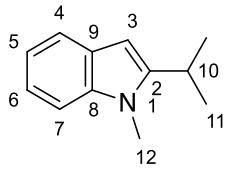
**$^{13}$C NMR** (101 MHz, $CDCl_3$) $\delta$ = 155.5 (quat., C-13), 142.9 (quat., C-2), 135.4 (quat., C-8), 134.9 (quat., C-21), 129.5 (quat., C-9), 129.2 (quat., C-20), 128.9 (CH, C-10), 127.8 (CH, C-16), 126.1 (CH, C-19), 126.0 (CH, C-18), 123.4 (CH, C-17), 121.1 (CH, C-6), 119.5 (2CH, C-4,5), 118.1 (quat., C-12), 114.1 (CH, C-14), 110.5 (CH, C-7), 106.0 (quat., C-3), 56.6 ($CH_3$, C-22), 26.5 (CH, C-10), 22.5 ($CH_3$, C-11), 22.2 ($CH_3$, C-11');

**HRMS** ($ESI^+$) mass calculated for $C_{22}H_{22}NO$ ($[M+H]^+$) = 316.1696, mass found = 316.1696, Δ 0.2 ppm;

Enantiopure (> 99.5 % e.e.) **129** for use in erosion studies was obtained *via* semi-preparative HPLC (250mm × 10mm ØYMC Chiral-SA column, 5.0 mL min$^{-1}$, isopropanol:hexane; 1:99)

**$[\alpha]_D^{25}$** = -94 (*c* 0.10, $CHCl_3$)

**2-*Iso*propyl-1-methyl-1H-indole, 130**




This compound was prepared according to a literature procedure[22]

To a solution of **5** (500mg, 3.14mmol, 1.0 eq.) in acetone (8 ml, 0.4 M) was added potassium *tert*-butoxide (527 mg, 4.71 mmol, 1.5 eq.), followed by dimethylsulfate (600 µl, 6.28 mmol, 2.0 eq.). The reaction was allowed to stir at room temperature for 1 h before being quenched with 5 % aq. $NH_4OH$ (25 ml), extracted with diethyl ether (3 × 25 ml), dried over $MgSO_4$, filtered, and concentrated *in vacuo*. The crude produce was purified by flash column chromatography (dichloromethane:pentane; 1:19) to yield **8** as a yellow oil (386 mg, 71% yield).

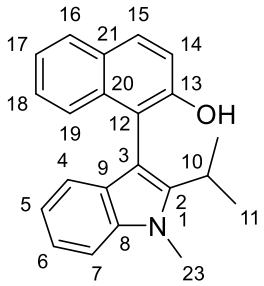
**FTIR** (film) *v* /cm$^{-1}$ 3053, 2965, 2931, 2874, 1611, 1541, 1467, 1296, 1296, 1232, 1171, 774, 747, 730, 675, 624;

**$^1$H NMR** (400 MHz, $CDCl_3$) $\delta$ = 7.56 (dddd, *J* = 7.8, 1.5, 0.7, 0.7 Hz, 1H, H-4), 7.28 (ddd, *J* = 8.3, 0.9, 0.9 Hz, 1H, H-7), 7.17 (dddd, *J* = 8.1, 7.3, 1.3, 0.7 Hz, 1H, H-5), 7.08 (ddd, *J* = 7.0, 7.0, 0.9 Hz, 1H, H-6), 6.20 (s, 1H, H-3), 3.71 (s, 3H, H-12), 3.10 (hept, *J* = 6.8 Hz, 1H, H-10), 1.39 – 1.32 (m, 6H, H-11);

**$^{13}$C NMR** (101 MHz, $CDCl_3$) $\delta$ = 147.6 (quat., C-2), 137.4 (quat., C-9), 127.8 (quat., C-8), 120.6 (CH, C5), 119.9 (CH, C-4), 119.2 (CH, C-6), 108.7 (CH, C-7), 96.2 (CH, C-3), 29.4 (CH3, C-12), 25.9 (CH, C-10), 22.6 (2CH3, C-11);

LRMS (ESI$^+$) mass calculated for $C_{12}H_{16}N$ ([M+H]$^+$) = 174.1, mass found = 174.2;

**1-(2-*Iso*propyl-1-methyl-1H-indol-3-yl)naphthalen-2-ol, 131**




To a solution of **130** (380 mg, 2.2 mmol, 1.1 eq.) and 2-naphthol (288 mg, 2.0 mmol, 1.0 eq.) in 1:1 hexafluoroispropanol:dichloromethane (5.0 ml, 0.4 M) was added iron$^{III}$ chloride (32 mg, 0.2 mmol, 0.1 eq.) and di-*tert*-butyl peroxide (441 µl, 2.4 mmol, 1.2 eq.). The mixture was allowed to stir for 16 h before being concentrated to dryness, loaded onto silica, and purified by flash column chromatography (dichloromethane:pentane; 4:6) to give **131** as a light yellow solid (274 mg, 43% yield).

**m.p.** 112-114 °C

**FTIR** (film) v /cm$^{-1}$ 3373 (w), 3056 (w), 2962 (w), 2161 (w), 2035 (w), 1620 (w), 1596, 1541, 1514, 1466, 1320, 1266, 1207, 1188, 1143, 1013, 962, 782, 743 (str), 706;

**$^1$H NMR** (400 MHz, $CDCl_3$) $\delta$ = 7.89 – 7.80 (m, 2H, H-15,16), 7.42 (ddd, *J* = 8.3, 0.9, 0.9 Hz, 1H, H-7), 7.38 – 7.21 (m, 5H, H-6,14,17,18,19), 7.07 – 6.98 (m, 2H, H-4,5), 5.35 (d, *J* = 0.5 Hz, 1H, *O*-H), 3.92 (s, 3H, H-23), 3.17 (qq, *J* = 7.1, 7.1 Hz, 1H, H-10), 1.22 (d, *J* = 7.2 Hz, 3H, H-11), 1.17 (d, *J* = 7.2 Hz, 3H, H-11');

**$^{13}$C NMR** (101 MHz, $CDCl_3$) $\delta$ = 152.3 (quat., C-13), 145.2 (quat., C-2), 137.7 (quat., C-8), 135.0 (quat., C20), 129.4 (CH, C-15), 129.0 (quat., C-21), 128.4 (quat., C-9), 128.0 (CH, C-16), 126.1 (CH, C-19), 125.5 (CH, C-18), 123.0 (CH, C-17), 121.8 (CH, C-6), 120.0 (CH, C-4), 119.3 (CH, C-5), 116.8 (CH, C-14), 114.2 (quat., C-12), 108.9 (CH, C-7), 102.2 (quat., C-3), 30.7 (CH3, C-23), 26.7 (CH, C-10), 21.3 ($CH_3$, C-11), 21.1 (CH3, C-11');

**LRMS** ($ESI^+$) mass calculated for $C_{22}H_{22}NO$ ($[M+H]^+$) = 316.2, mass found = 316.2; HRMS ($ESI^+$) mass calculated for $C_{22}H_{22}NO$ ($[M+H]^+$) = 316.1696, mass found = 316.1696, Δ 0.0 ppm;

Enantiopure (> 99.5 % e.e.) **131** for use in erosion studies was obtained *via* semi-preparative HPLC (250mm × 10mm ØYMC Chiral-SA column, 5.0 mL $min^{-1}$, dichloromethane:hexane; 1:99)

**$[\alpha]_D^{25}$** = +100 (*c* 0.10, $CHCl_3$)

# II.3 Rate Laws and Kinetic Formulae

## II.3.1 Rate Laws

**First-Order Reversible Enantiomerisation**

For the reaction:

$$R \underset{k_{ent}}{\overset{k_{ent}}{\rightleftharpoons}} S$$

Let *k* be the rate of enantiomerisation and [*R*] and [*S*] be the mole fractions of enantiomers R and S. The rate equation for this reaction is:

$$\frac{d[R]}{dt} = -k_{ent}[R] + k_{ent}[S]$$

But if [*R*] and [*S*] are mole fractions, [*R*] + [*S*] = 1. Therefore:

$$\frac{d[R]}{dt} = -k_{ent}[R] + k_{ent}(1 - [R])$$

$$\frac{d[R]}{dt} = -k_{ent}[R] - k_{ent}[R] + k_{ent}$$

$$\frac{d[R]}{dt} = k_{ent}(1 - 2[R])$$

Rearranging for integration gives:

$$\int_{[R]_0}^{[R]} \left(\frac{1}{1-2[R]}\right) d[R] = \int_{t_0}^{t} k_{ent}\, dt \,^{\ddagger}$$

$$-\frac{1}{2}\ln(1-2[R]) + \frac{1}{2}\ln(1-2[R]_0) = k_{ent}t - k_{ent}\, t_0$$

If $t_0 = 0$

$$-\frac{1}{2}\ln(1-2[R]) + \frac{1}{2}\ln(1-2[R]_0) = k_{ent}t$$

$$\ln\left(\frac{1-2[R]_0}{1-2[R]}\right) = 2k_{ent}\, t$$

‡ Integration is by substitution where $u = 1 - 2[R] \Rightarrow \frac{du}{d[R]} = -2$

$$\therefore d[R] = -\frac{1}{2}du \text{ and } \int_{1-2[R]_0}^{1-2[R]} -\frac{1}{2u}\, du = \int_{t_0}^{t} k_{ent}\, dt$$

Because [*R*] is defined as the mole fraction of the R enantiomer of the compound, 1-2[*R*] corresponds to the e.e. of the bulk solution:

$$\ln\left(\frac{e.e._0}{e.e._t}\right) = 2k_{ent}\,t$$

A plot of $\ln\left(\frac{e.e._0}{e.e._t}\right)$ *vs* t will therefore give a line with slope $2k_{ent}$, where $k_{ent}$ is the rate of enantiomerisation. $2k_{ent}$ itself is the rate of racemisation, $k_{rac}$, a bulk property.

### II.3.2 Formulae

**Barrier to Rotation**

To determine the barrier to rotation from a measured rate of enantiomerisation, a form of the Eyring equation is used:

$$\Delta G^{\ddagger} = \ln\left(\frac{k_B T}{h k_{ent}}\right) RT$$

where $\Delta G^{\ddagger}$ is the free energy barrier to rotation, $k_B$ is the boltzmann constant, $T$ is temperature, $h$ is the planck constant, $k_{ent}$ is the rate of enantiomerisation, and $R$ is the universal gas constant.

**The Eyring Equation**

Calculation of half-lives to racemisation at room temperature necessitates the determination of the rate of racemisation, $k_{rac}$ at room temperature. The Eyring equation can also be used to determine this value using $k_{rac}$ measured at a different temperature. The general equation takes the form:

$$k = \frac{\kappa\, k_B T}{h} e^{-\frac{\Delta G^{\ddagger}}{R\,T}}$$

where $k$ is the rate constant, κ is the transmission coefficient, $k_B$ is the boltzmann constant, $T$ is temperature, $h$ is the planck constant, $\Delta G^{\ddagger}$ is the free energy barrier to rotation, and $R$ is the universal gas constant.

Assuming no change in $\Delta G^{\ddagger}$ with changing temperature:

$$\frac{k_{T_1}}{k_{T_2}} = \frac{T_1}{T_2} e^{\frac{\Delta G^{\ddagger}}{R}\left(\frac{1}{T_2} - \frac{1}{T_1}\right)}$$

where $k_{T1}$ is the rate at temperature $T_1$ and $k_{T2}$ is the rate at temperature $T_2$.

## II.4 HPLC Data

**Analytical HPLC**

HPLC analysis of aliquots of **126** and **129** was carried out using a CHIRALPAK® IC column at a flow rate of 1.0 ml/ min with 1.5 % *iso*-propanol in hexane as the mobile phase. HPLC analysis of aliquots was carried out using a CHIRALPAK® IC column at a flow rate of 1.0 ml/ min with 1 % *iso*-propanol in hexane as the mobile phase. Injection volumes and absorbance collection wavelengths were chosen to maximise signal to noise ration and minimise the presence of any impurities in the recorded chromatogram. All data was recorded as relative peak areas of the enantiomers of relevant compound and converted to e.e.s according to the formula:

$$e.e. = \frac{A_{maj} - A_{min}}{A_{maj} + A_{min}} \times 100$$

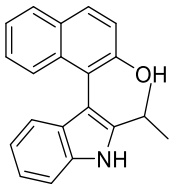
**Semi-Preparative HPLC**

Semi-preparative HPLC was carried using a YMC® Chiral-SA column thermostatted to 5 °C at a flow rate of 5.0 ml/ min with 16 % *iso*-propanol in hexane as the mobile phase for **126**, 1% *iso*-propanol in hexane as the mobile phase for **129**, and 1 % dichloromethane in hexane as the mobile phase for **131**. Fractions were collected in 250 ml schott bottles maintained at −18 °C in an ice/brine bath. Upon completion of the semi-preparative run care was taken to keep the resulting solution below 0 °C before evaporation of solvent at 0 °C. The resulting solid was stored at −18 °C.

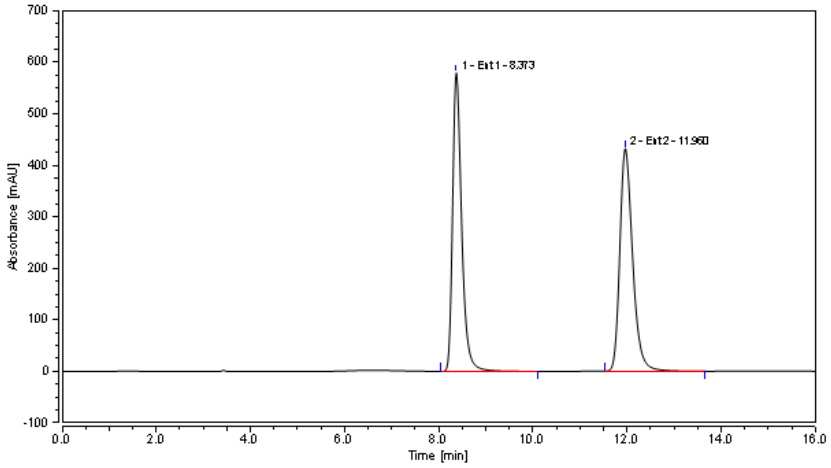
**4a*R*,10b*S*)-6-Methyl-2,3,6,10b-tetrahydro-1*H*-pyrano[2,3-*c*]quinolin-5(4a*H*)-one (126)**

**Chiral HPLC:** (Chiralpak IC, 1.5% $^{i}$PrOH, 98.5% hexane, 1.0 mL min$^{-1}$, $\lambda$ = 222 nm) $\tau_R$ (major) = 8.4 min, $\tau_R$ (minor) = 11.9 min.

**Racemic**

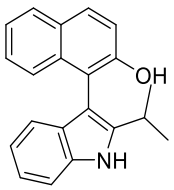



*(rac)*-**126**

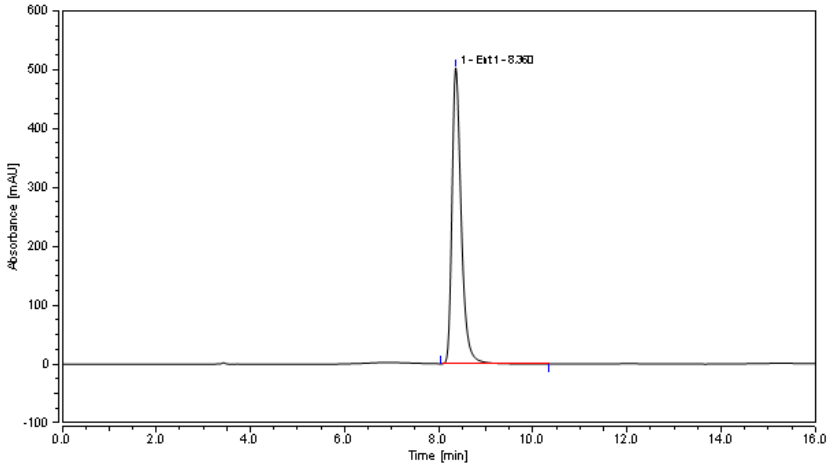



| No. | Retention Time (min) | Area (mAU*min) | Height (mAU) | Relative Area (%) |
|---|---|---|---|---|
| 1 | 8.373 | 129.317 | 579.432 | 48.74 |
| 2 | 11.960 | 135.984 | 431.875 | 51.26 |
| Total: | | 265.300 | 1011.307 | 100.00 |

**Resolved**




**126**

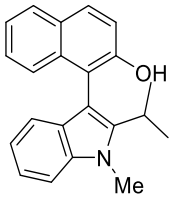



| No. | Retention Time (min) | Area (mAU*min) | Height (mAU) | Relative Area (%) |
|---|---|---|---|---|
| 1 | 8.350 | 230.239 | 1021.848 | 99.76 |
| 2 | 12.037 | 0.545 | 1.623 | 0.24 |
| Total: | | 230.785 | 1023.471 | 100.00 |

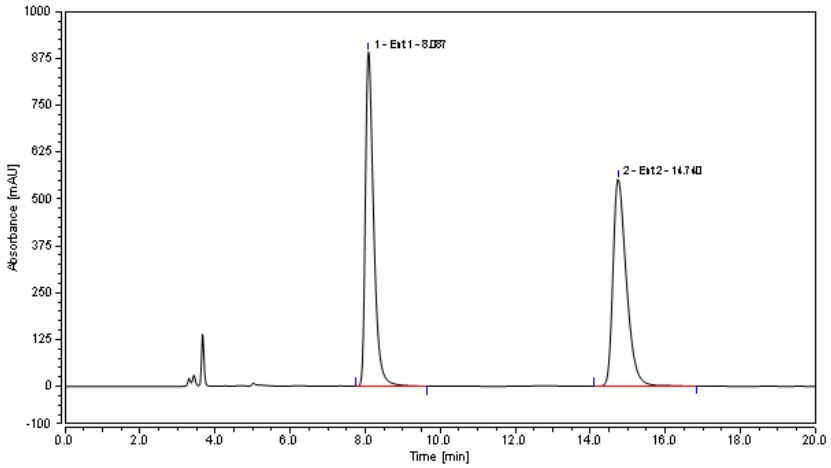
**4a*R*,10b*S*)-6-Methyl-2,3,6,10b-tetrahydro-1*H*-pyrano[2,3-*c*]quinolin-5(4a*H*)-one (131)**

**Chiral HPLC:** (Chiralpak IC, 1% $^{i}$PrOH, 99% hexane, 1.0 mL min$^{-1}$, $\lambda$ = 210 nm) $\tau_R$ (major) = 8.1 min, $\tau_R$ (minor) = 14.9 min.

**Racemic**

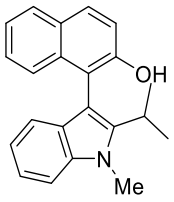



*(rac)*-**131**

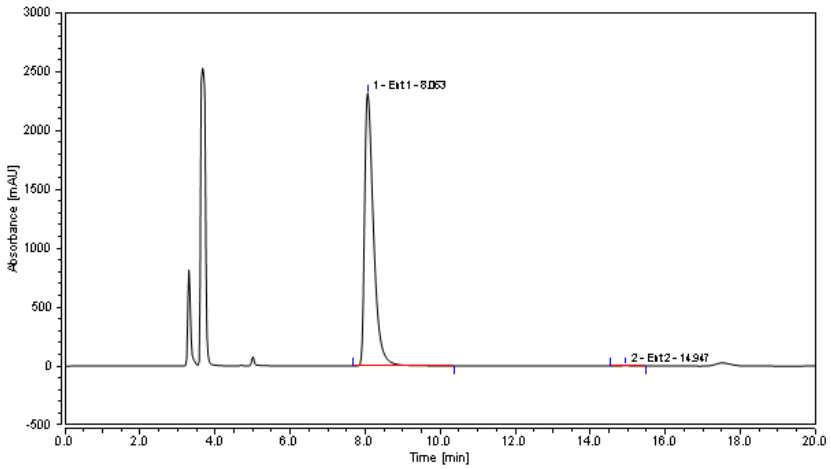



| No. | Retention Time (min) | Area (mAU*min) | Height (mAU) | Relative Area (%) |
|---|---|---|---|---|
| 1 | 8.087 | 227.848 | 892.403 | 49.89 |
| 2 | 14.740 | 228.877 | 553.647 | 50.11 |
| Total: | | 456.726 | 1446.051 | 100.00 |

**Resolved**




**131**

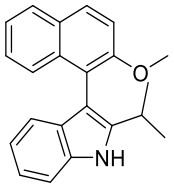



| No. | Retention Time (min) | Area (mAU*min) | Height (mAU) | Relative Area (%) |
|---|---|---|---|---|
| 1 | 8.063 | 639.112 | 2317.812 | 99.82 |
| 2 | 14.947 | 1.123 | 2.910 | 0.18 |
| Total: | | 640.236 | 2320.722 | 100.00 |

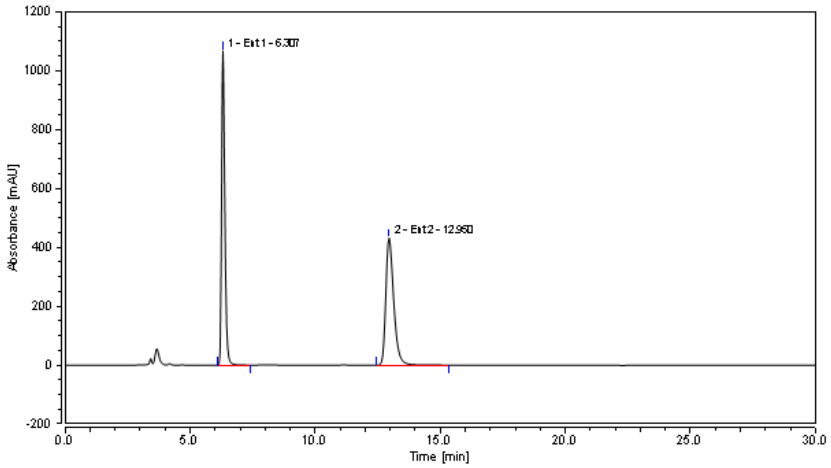
**4a*R*,10b*S*)-6-Methyl-2,3,6,10b-tetrahydro-1*H*-pyrano[2,3-*c*]quinolin-5(4a*H*)-one (126)**

**Chiral HPLC:** (Chiralpak IC, 1.5% $^{i}$PrOH, 98.5% hexane, 1.0 mL min$^{-1}$, $\lambda$ = 210 nm) $\tau_R$ (major) = 13.2 min, $\tau_R$ (minor) = 6.3 min.

**Racemic**

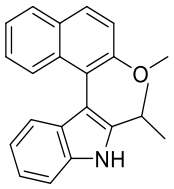


*(rac)*-**126**

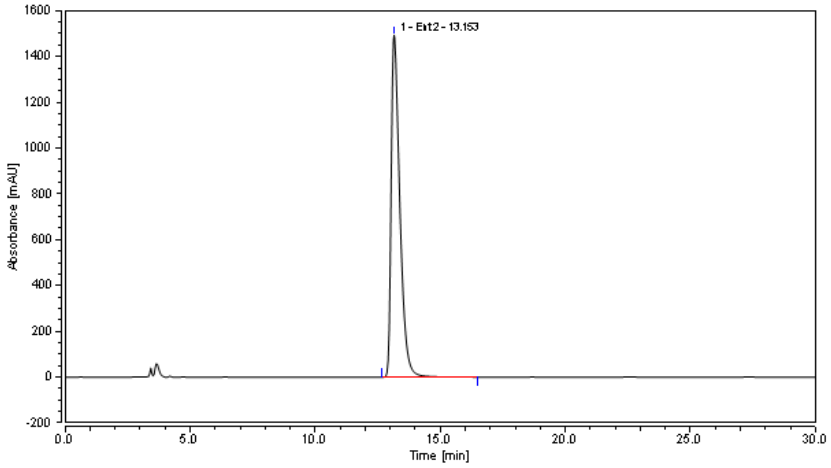



| No. | Retention Time (min) | Area (mAU*min) | Height (mAU) | Relative Area (%) |
|---|---|---|---|---|
| 1 | 6.307 | 158.536 | 1067.688 | 49.99 |
| 2 | 12.950 | 158.619 | 432.820 | 50.01 |
| Total: | | 317.155 | 1500.508 | 100.00 |

**Resolved**



**126**

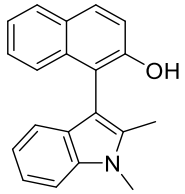



| No. | Retention Time (min) | Area (mAU*min) | Height (mAU) | Relative Area (%) |
|---|---|---|---|---|
| 1 | n.a. | n.a. | n.a. | n.a. |
| 2 | 13.153 | 599.041 | 1493.815 | 100.00 |
| Total: | | 599.041 | 1493.815 | 100.00 |

# II.5 Collated Erosion Data

## II.5.1 Data for 111 at 22 °C

Table S10 Erosion data for **111.** The erosion study was carried as described and analysed by normal phase chiral HPLC




**111**

| t (min) | Ent 1 rel area (%) | Ent 2 rel area (%) | e.e. (%) | $\ln\left(\frac{e.e._0}{e.e._t}\right)$ |
|---|---|---|---|---|
| 1099 | 99.5 | 0.5 | 99 | 0.0101 |
| 4225 | 98.0 | 2.0 | 96 | 0.0408 |
| 9990 | 96.5 | 3.5 | 93 | 0.0726 |
| 15151 | 95.5 | 4.5 | 91 | 0.0943 |
| 20317 | 94.5 | 5.5 | 89 | 0.1165 |
| 23417 | 93.5 | 6.5 | 87 | 0.1393 |
| 30442 | 92.0 | 8.0 | 84 | 0.1744 |
| 34855 | 91.0 | 9.0 | 82 | 0.1985 |
| 40791 | 89.5 | 10.5 | 79 | 0.2357 |
| 45187 | 88.0 | 12.0 | 76 | 0.2744 |
| 50503 | 86.0 | 14.0 | 72 | 0.3285 |

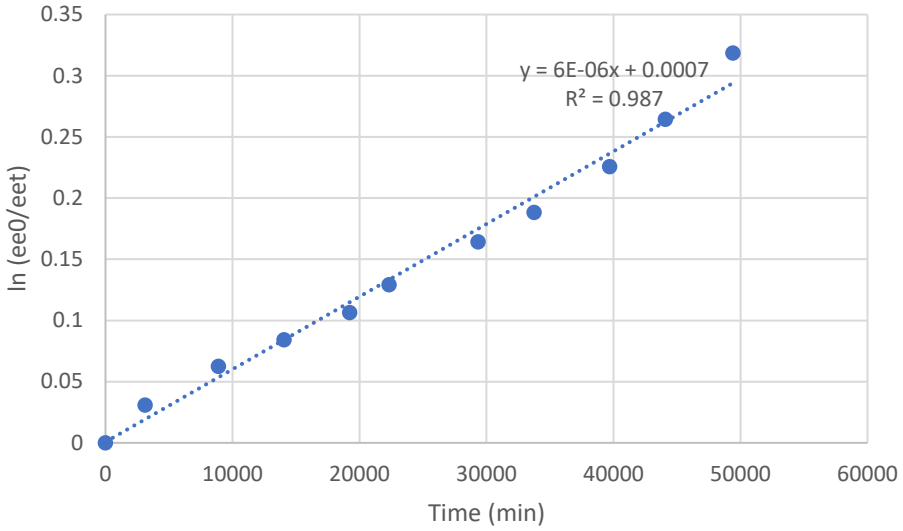



Figure S31 First order plot for **111**

$m = k_{rac} = 6 \times 10^{-6}\ min^{-1} = 9.9 \times 10^{-8}\ s^{-1}$

$k_{ent} = 4.95 \times 10^{-8}\ s^{-1}$

$\Delta G^{\ddagger}$ (22 °C) = 27.1 kcal $mol^{-1}$

$T_{½}$ (22 °C) = 81 days; $T_{½}$ (25 °C) = 50 days;

## II.5.2 Data for 126 recorded at 80 °C in toluene

### 0.2 Molal

| | Run 1 | | | Run 2 | | | Run 3 | | |
|---|---|---|---|---|---|---|---|---|---|
| t (s) | Ent 1 rel area (%) | Ent 2 rel area (%) | e.e. (%) | Ent 1 rel area (%) | Ent 2 rel area (%) | e.e. (%) | Ent 1 rel area (%) | Ent 2 rel area (%) | e.e. (%) |
| 0 | 99.750 | 0.250 | 99.50 | 99.755 | 0.245 | 99.51 | 100.000 | 0.000 | 100.00 |
| 60 | 99.740 | 0.260 | 99.48 | 100.000 | 0.000 | 100.00 | 99.810 | 0.190 | 99.62 |
| 120 | 99.480 | 0.520 | 98.96 | 99.540 | 0.460 | 99.08 | 99.545 | 0.455 | 99.09 |
| 180 | 99.165 | 0.835 | 98.33 | 99.155 | 0.845 | 98.31 | 99.210 | 0.790 | 98.42 |
| 240 | 98.620 | 1.380 | 97.24 | 98.530 | 1.470 | 97.06 | 98.670 | 1.330 | 97.34 |
| 300 | 97.870 | 2.130 | 95.74 | 97.935 | 2.065 | 95.87 | 97.990 | 2.010 | 95.98 |
| 360 | 96.840 | 3.160 | 93.68 | 97.005 | 2.995 | 94.01 | 96.985 | 3.015 | 93.97 |
| 420 | 95.640 | 4.360 | 91.28 | 95.855 | 4.145 | 91.71 | 95.885 | 4.115 | 91.77 |
| 480 | 94.000 | 6.000 | 88.00 | 94.230 | 5.770 | 88.46 | 94.440 | 5.560 | 88.88 |
| 540 | | | | 92.175 | 7.825 | 84.35 | 92.305 | 7.695 | 84.61 |
| 600 | 89.045 | 10.955 | 78.09 | 89.785 | 10.215 | 79.57 | 89.845 | 10.155 | 79.69 |
| 660 | 85.570 | 14.430 | 71.14 | 86.400 | 13.600 | 72.80 | 86.970 | 13.030 | 73.94 |
| 720 | 81.420 | 18.580 | 62.84 | 82.650 | 17.350 | 65.30 | 83.105 | 16.895 | 66.21 |
| 780 | 76.775 | 23.225 | 53.55 | 78.270 | 21.730 | 56.54 | 78.595 | 21.405 | 57.19 |
| 840 | 71.630 | 28.370 | 43.26 | 73.425 | 26.575 | 46.85 | 74.155 | 25.845 | 48.31 |
| 900 | 67.140 | 32.860 | 34.28 | 69.015 | 30.985 | 38.03 | 69.255 | 30.745 | 38.51 |
| 960 | 62.960 | 37.040 | 25.92 | 64.625 | 35.375 | 29.25 | 65.370 | 34.630 | 30.74 |
| 1020 | 60.040 | 39.960 | 20.08 | 60.990 | 39.010 | 21.98 | 61.815 | 38.185 | 23.63 |
| 1080 | 57.475 | 42.525 | 14.95 | 58.025 | 41.975 | 16.05 | 59.020 | 40.980 | 18.04 |
| 1140 | 55.440 | 44.560 | 10.88 | 55.910 | 44.090 | 11.82 | 57.120 | 42.880 | 14.24 |
| 1200 | 54.250 | 45.750 | 8.50 | 54.460 | 45.540 | 8.92 | 55.315 | 44.685 | 10.63 |
| 1350 | 52.085 | 47.915 | 4.17 | 52.115 | 47.885 | 4.23 | 52.700 | 47.300 | 5.40 |
| 1500 | 51.105 | 48.895 | 2.21 | 51.030 | 48.970 | 2.06 | 51.530 | 48.470 | 3.06 |
| 1650 | 50.570 | 49.430 | 1.14 | 50.545 | 49.455 | 1.09 | 50.885 | 49.115 | 1.77 |
| 1800 | 50.310 | 49.690 | 0.62 | 50.280 | 49.720 | 0.56 | 50.555 | 49.445 | 1.11 |
| 1950 | 50.165 | 49.835 | 0.33 | 50.105 | 49.895 | 0.21 | 50.355 | 49.645 | 0.71 |
| 2100 | 50.070 | 49.930 | 0.14 | 50.045 | 49.955 | 0.09 | 50.245 | 49.755 | 0.49 |
| 2250 | 50.100 | 49.900 | 0.20 | 49.930 | 50.070 | -0.14 | 50.125 | 49.875 | 0.25 |
| 2400 | 50.125 | 49.875 | 0.25 | 49.860 | 50.140 | -0.28 | 50.075 | 49.925 | 0.15 |
| 2550 | 50.095 | 49.905 | 0.19 | 49.915 | 50.085 | -0.17 | 49.910 | 50.090 | -0.18 |
| 2700 | 50.065 | 49.935 | 0.13 | 49.860 | 50.140 | -0.28 | 49.920 | 50.080 | -0.16 |
| 2850 | 49.990 | 50.010 | -0.02 | 49.855 | 50.145 | -0.29 | 49.915 | 50.085 | -0.17 |
| 3000 | 50.040 | 49.960 | 0.08 | 49.870 | 50.130 | -0.26 | 49.880 | 50.120 | -0.24 |
| 3150 | 49.925 | 50.075 | -0.15 | 49.850 | 50.150 | -0.30 | 49.820 | 50.180 | -0.36 |
| 3300 | 49.965 | 50.035 | -0.07 | 49.755 | 50.245 | -0.49 | 49.870 | 50.130 | -0.26 |
| 3450 | 50.760 | 49.240 | 1.52 | 49.620 | 50.380 | -0.76 | 49.860 | 50.140 | -0.28 |
| 3600 | 49.825 | 50.175 | -0.35 | 49.985 | 50.015 | -0.03 | 49.810 | 50.190 | -0.38 |
| 3900 | 50.080 | 49.920 | 0.16 | 49.890 | 50.110 | -0.22 | 49.845 | 50.155 | -0.31 |
| 4200 | 49.935 | 50.065 | -0.13 | | | | 49.900 | 50.100 | -0.20 |
| 4500 | 49.825 | 50.175 | -0.35 | 49.990 | 50.010 | -0.02 | 49.850 | 50.150 | -0.30 |
| 4800 | 49.920 | 50.080 | -0.16 | 49.890 | 50.110 | -0.22 | 49.860 | 50.140 | -0.28 |
| 5100 | 49.765 | 50.235 | -0.47 | 49.950 | 50.050 | -0.10 | 49.840 | 50.160 | -0.32 |
| 5400 | 49.700 | 50.300 | -0.60 | 49.955 | 50.045 | -0.09 | 49.680 | 50.320 | -0.64 |
| 6000 | 49.790 | 50.210 | -0.42 | 49.900 | 50.100 | -0.20 | 49.740 | 50.260 | -0.52 |
| 6600 | 49.800 | 50.200 | -0.40 | 49.810 | 50.190 | -0.38 | 49.825 | 50.175 | -0.35 |
| 7200 | 49.765 | 50.235 | -0.47 | 49.775 | 50.225 | -0.45 | 49.865 | 50.135 | -0.27 |

### 0.1 Molal

| | Run 1 | | | Run 2 | | | Run 3 | | |
|---|---|---|---|---|---|---|---|---|---|
| t (s) | Ent 1 rel area (%) | Ent 2 rel area (%) | e.e. (%) | Ent 1 rel area (%) | Ent 2 rel area (%) | e.e. (%) | Ent 1 rel area (%) | Ent 2 rel area (%) | e.e. (%) |
| 0 | 99.86 | 0.14 | 99.72 | 99.915 | 0.085 | 99.83 | 99.78 | 0.22 | 99.56 |
| 60 | 99.77 | 0.23 | 99.54 | 99.695 | 0.305 | 99.39 | 99.675 | 0.325 | 99.35 |
| 120 | 99.52 | 0.48 | 99.04 | 99.48 | 0.52 | 98.96 | 99.52 | 0.48 | 99.04 |
| 180 | 99.05 | 0.95 | 98.1 | 99.06 | 0.94 | 98.12 | 99.195 | 0.805 | 98.39 |
| 240 | 98.45 | 1.55 | 96.9 | 98.415 | 1.585 | 96.83 | 98.71 | 1.29 | 97.42 |
| 300 | 97.495 | 2.505 | 94.99 | 97.505 | 2.495 | 95.01 | 98.05 | 1.95 | 96.10 |
| 360 | 96.205 | 3.795 | 92.41 | 96.07 | 3.93 | 92.14 | 97.11 | 2.89 | 94.22 |
| 420 | 94.555 | 5.445 | 89.11 | 94.555 | 5.445 | 89.11 | 95.805 | 4.195 | 91.61 |
| 480 | 92.405 | 7.595 | 84.81 | 92.66 | 7.34 | 85.32 | 94.11 | 5.89 | 88.22 |
| 540 | 89.6 | 10.4 | 79.2 | 90.07 | 9.93 | 80.14 | 91.775 | 8.225 | 83.55 |
| 600 | 86.775 | 13.225 | 73.55 | 87.215 | 12.785 | 74.43 | 89.285 | 10.715 | 78.57 |
| 660 | 83.395 | 16.605 | 66.79 | 84.03 | 15.97 | 68.06 | 85.975 | 14.025 | 71.95 |
| 720 | 79.85 | 20.15 | 59.7 | 80.55 | 19.45 | 61.1 | | | |
| 780 | 76.67 | 23.33 | 53.34 | 77.395 | 22.605 | 54.79 | 79.32 | 20.68 | 58.64 |
| 840 | 73.405 | 26.595 | 46.81 | 74.4 | 25.6 | 48.8 | 76.145 | 23.855 | 52.29 |
| 900 | 70.615 | 29.385 | 41.23 | 71.375 | 28.625 | 42.75 | 73.605 | 26.395 | 47.21 |
| 960 | 68.265 | 31.735 | 36.53 | 69.74 | 30.26 | 39.48 | 71.09 | 28.91 | 42.18 |
| 1020 | 66.09 | 33.91 | 32.18 | 67.105 | 32.895 | 34.21 | 69.25 | 30.75 | 38.50 |
| 1080 | 64.42 | 35.58 | 28.84 | 65.42 | 34.58 | 30.84 | 67.945 | 32.055 | 35.89 |
| 1140 | 63.01 | 36.99 | 26.02 | 64.175 | 35.825 | 28.35 | 66.58 | 33.42 | 33.16 |
| 1200 | 61.75 | 38.25 | 23.5 | 63.005 | 36.995 | 26.01 | 65.685 | 34.315 | 31.37 |
| 1350 | 59.565 | 40.435 | 19.13 | 61.07 | 38.93 | 22.14 | 63.58 | 36.42 | 27.16 |
| 1500 | 58.13 | 41.87 | 16.26 | 59.675 | 40.325 | 19.35 | 62.185 | 37.815 | 24.37 |
| 1650 | 57.075 | 42.925 | 14.15 | 58.68 | 41.32 | 17.36 | 61.075 | 38.925 | 22.15 |
| 1800 | 56.305 | 43.695 | 12.61 | 57.795 | 42.205 | 15.59 | 60.285 | 39.715 | 20.57 |
| 1950 | 55.685 | 44.315 | 11.37 | 57.21 | 42.79 | 14.42 | 59.66 | 40.34 | 19.32 |
| 2100 | 55.135 | 44.865 | 10.27 | 56.635 | 43.365 | 13.27 | 59.115 | 40.885 | 18.23 |
| 2250 | 54.685 | 45.315 | 9.37 | 56.145 | 43.855 | 12.29 | 58.84 | 41.16 | 17.68 |
| 2400 | 54.295 | 45.705 | 8.59 | 55.745 | 44.255 | 11.49 | 58.42 | 41.58 | 16.84 |
| 2550 | 53.955 | 46.045 | 7.91 | 55.435 | 44.565 | 10.87 | 57.98 | 42.02 | 15.96 |
| 2700 | 53.63 | 46.37 | 7.26 | 55.025 | 44.975 | 10.05 | 57.68 | 42.32 | 15.36 |
| 2850 | 53.365 | 46.635 | 6.73 | 54.755 | 45.245 | 9.51 | 57.48 | 42.52 | 14.96 |
| 3000 | 53.145 | 46.855 | 6.29 | 54.52 | 45.48 | 9.04 | 57.265 | 42.735 | 14.53 |
| 3150 | 52.94 | 47.06 | 5.88 | 54.235 | 45.765 | 8.47 | 56.955 | 43.045 | 13.91 |
| 3300 | 52.79 | 47.21 | 5.58 | 54.025 | 45.975 | 8.05 | 56.905 | 43.095 | 13.81 |
| 3450 | 52.625 | 47.375 | 5.25 | 53.83 | 46.17 | 7.66 | 56.665 | 43.335 | 13.33 |
| 3600 | 52.48 | 47.52 | 4.96 | 53.685 | 46.315 | 7.37 | 56.385 | 43.615 | 12.77 |
| 3900 | 52.18 | 47.82 | 4.36 | 53.33 | 46.67 | 6.66 | 56.085 | 43.915 | 12.17 |
| 4200 | 51.905 | 48.095 | 3.81 | 53.03 | 46.97 | 6.06 | 55.98 | 44.02 | 11.96 |
| 4500 | 51.73 | 48.27 | 3.46 | 52.765 | 47.235 | 5.53 | 55.68 | 44.32 | 11.36 |
| 4800 | 51.49 | 48.51 | 2.98 | 52.5 | 47.5 | 5 | 55.31 | 44.69 | 10.62 |
| 5100 | 51.325 | 48.675 | 2.65 | 52.285 | 47.715 | 4.57 | 55.205 | 44.795 | 10.41 |
| 5400 | 51.22 | 48.78 | 2.44 | 52.16 | 47.84 | 4.32 | 55.01 | 44.99 | 10.02 |
| 6000 | 51.01 | 48.99 | 2.02 | 51.835 | 48.165 | 3.67 | 54.67 | 45.33 | 9.34 |
| 6600 | 50.87 | 49.13 | 1.74 | 51.565 | 48.435 | 3.13 | 54.32 | 45.68 | 8.64 |
| 7200 | 50.72 | 49.28 | 1.44 | 51.3 | 48.7 | 2.6 | 54.065 | 45.935 | 8.13 |

**0.05 Molal**

| | Run 1 | | | Run 2 | | | Run 3 | | |
|---|---|---|---|---|---|---|---|---|---|
| t (s) | Ent 1 rel area (%) | Ent 2 rel area (%) | e.e. (%) | Ent 1 rel area (%) | Ent 2 rel area (%) | e.e. (%) | Ent 1 rel area (%) | Ent 2 rel area (%) | e.e. (%) |
| 0 | 99.615 | 0.385 | 99.23 | 99.925 | 0.075 | 99.85 | 99.925 | 0.075 | 99.85 |
| 60 | 99.165 | 0.835 | 98.33 | 99.880 | 0.120 | 99.76 | 99.585 | 0.415 | 99.17 |
| 120 | 99.650 | 0.350 | 99.30 | 99.780 | 0.220 | 99.56 | 99.680 | 0.320 | 99.36 |
| 180 | 99.350 | 0.650 | 98.70 | 99.710 | 0.290 | 99.42 | 99.455 | 0.545 | 98.91 |
| 240 | 99.105 | 0.895 | 98.21 | 99.615 | 0.385 | 99.23 | 99.150 | 0.850 | 98.30 |
| 300 | 98.650 | 1.350 | 97.30 | 99.540 | 0.460 | 99.08 | 98.740 | 1.260 | 97.48 |
| 360 | 98.060 | 1.940 | 96.12 | 99.440 | 0.560 | 98.88 | 98.175 | 1.825 | 96.35 |
| 420 | 97.215 | 2.785 | 94.43 | 99.340 | 0.660 | 98.68 | 97.535 | 2.465 | 95.07 |
| 480 | 96.300 | 3.700 | 92.60 | 99.235 | 0.765 | 98.47 | 96.735 | 3.265 | 93.47 |
| 540 | 95.380 | 4.620 | 90.76 | 99.085 | 0.915 | 98.17 | 95.785 | 4.215 | 91.57 |
| 600 | 94.210 | 5.790 | 88.42 | 98.925 | 1.075 | 97.85 | 94.710 | 5.290 | 89.42 |
| 660 | 92.735 | 7.265 | 85.47 | 98.725 | 1.275 | 97.45 | 93.435 | 6.565 | 86.87 |
| 720 | 91.260 | 8.740 | 82.52 | 98.460 | 1.540 | 96.92 | 91.920 | 8.080 | 83.84 |
| 780 | 89.815 | 10.185 | 79.63 | 98.170 | 1.830 | 96.34 | 90.245 | 9.755 | 80.49 |
| 840 | 88.245 | 11.755 | 76.49 | 97.815 | 2.185 | 95.63 | 88.695 | 11.305 | 77.39 |
| 900 | 86.625 | 13.375 | 73.25 | 97.420 | 2.580 | 94.84 | 86.965 | 13.035 | 73.93 |
| 960 | 85.105 | 14.895 | 70.21 | 96.955 | 3.045 | 93.91 | 84.955 | 15.045 | 69.91 |
| 1020 | 83.530 | 16.470 | 67.06 | 96.420 | 3.580 | 92.84 | 83.015 | 16.985 | 66.03 |
| 1080 | 82.150 | 17.850 | 64.30 | 95.715 | 4.285 | 91.43 | 81.105 | 18.895 | 62.21 |
| 1140 | 80.990 | 19.010 | 61.98 | 94.805 | 5.195 | 89.61 | 79.505 | 20.495 | 59.01 |
| 1200 | 79.705 | 20.295 | 59.41 | 93.885 | 6.115 | 87.77 | 78.050 | 21.950 | 56.10 |
| 1350 | 77.275 | 22.725 | 54.55 | 90.950 | 9.050 | 81.90 | 75.425 | 24.575 | 50.85 |
| 1500 | 75.475 | 24.525 | 50.95 | 87.880 | 12.120 | 75.76 | 73.435 | 26.565 | 46.87 |
| 1650 | 74.365 | 25.635 | 48.73 | 84.875 | 15.125 | 69.75 | 72.195 | 27.805 | 44.39 |
| 1800 | 73.145 | 26.855 | 46.29 | 82.270 | 17.730 | 64.54 | 71.230 | 28.770 | 42.46 |
| 1950 | 72.365 | 27.635 | 44.73 | 80.330 | 19.670 | 60.66 | 70.555 | 29.445 | 41.11 |
| 2100 | 71.690 | 28.310 | 43.38 | 78.860 | 21.140 | 57.72 | 69.950 | 30.050 | 39.90 |
| 2250 | 71.085 | 28.915 | 42.17 | 77.720 | 22.280 | 55.44 | 69.445 | 30.555 | 38.89 |
| 2400 | 70.520 | 29.480 | 41.04 | 76.875 | 23.125 | 53.75 | 68.830 | 31.170 | 37.66 |
| 2550 | 69.955 | 30.045 | 39.91 | 76.120 | 23.880 | 52.24 | 68.535 | 31.465 | 37.07 |
| 2700 | 69.585 | 30.415 | 39.17 | 75.510 | 24.490 | 51.02 | 68.160 | 31.840 | 36.32 |
| 2850 | 69.150 | 30.850 | 38.30 | 74.980 | 25.020 | 49.96 | 67.860 | 32.140 | 35.72 |
| 3000 | 68.585 | 31.415 | 37.17 | 74.395 | 25.605 | 48.79 | 67.575 | 32.425 | 35.15 |
| 3150 | 68.305 | 31.695 | 36.61 | 73.885 | 26.115 | 47.77 | 67.275 | 32.725 | 34.55 |
| 3300 | 67.855 | 32.145 | 35.71 | 73.485 | 26.515 | 46.97 | 67.040 | 32.960 | 34.08 |
| 3450 | 67.575 | 32.425 | 35.15 | 73.025 | 26.975 | 46.05 | 66.790 | 33.210 | 33.58 |
| 3600 | 67.275 | 32.725 | 34.55 | 72.620 | 27.380 | 45.24 | 66.530 | 33.470 | 33.06 |
| 3900 | 66.550 | 33.450 | 33.10 | 71.895 | 28.105 | 43.79 | 66.075 | 33.925 | 32.15 |
| 4200 | 66.055 | 33.945 | 32.11 | 71.145 | 28.855 | 42.29 | 65.695 | 34.305 | 31.39 |
| 4500 | 65.470 | 34.530 | 30.94 | 70.495 | 29.505 | 40.99 | 65.395 | 34.605 | 30.79 |
| 4800 | 64.975 | 35.025 | 29.95 | 69.880 | 30.120 | 39.76 | 65.060 | 34.940 | 30.12 |
| 5100 | 64.505 | 35.495 | 29.01 | 69.205 | 30.795 | 38.41 | 64.755 | 35.245 | 29.51 |
| 5400 | 64.050 | 35.950 | 28.10 | 68.625 | 31.375 | 37.25 | 64.475 | 35.525 | 28.95 |
| 6000 | 63.265 | 36.735 | 26.53 | 67.440 | 32.560 | 34.88 | 63.885 | 36.115 | 27.77 |
| 6600 | 62.585 | 37.415 | 25.17 | 66.395 | 33.605 | 32.79 | 63.485 | 36.515 | 26.97 |
| 7200 | 61.890 | 38.110 | 23.78 | 65.345 | 34.655 | 30.69 | 63.030 | 36.970 | 26.06 |

**0.025 Molal**

| | Run 1 | | | Run 2 | | |
|---|---|---|---|---|---|---|
| t (s) | Ent 1 rel area | Ent 2 rel area | e.e. (%) | Ent 1 rel area | Ent 2 rel area | e.e. (%) |
| 0 | | | | 99.920 | 0.080 | 99.84 |
| 60 | 100.000 | 0.000 | 100.00 | 99.825 | 0.175 | 99.65 |
| 120 | 99.720 | 0.280 | 99.44 | 99.740 | 0.260 | 99.48 |
| 180 | 99.600 | 0.400 | 99.20 | 99.660 | 0.340 | 99.32 |
| 240 | 99.475 | 0.525 | 98.95 | 99.555 | 0.445 | 99.11 |
| 300 | 99.325 | 0.675 | 98.65 | 99.475 | 0.525 | 98.95 |
| 360 | 99.195 | 0.805 | 98.39 | 99.350 | 0.650 | 98.70 |
| 420 | 98.990 | 1.010 | 97.98 | 99.235 | 0.765 | 98.47 |
| 480 | 98.780 | 1.220 | 97.56 | 99.085 | 0.915 | 98.17 |
| 540 | 98.550 | 1.450 | 97.10 | 98.920 | 1.080 | 97.84 |
| 600 | 98.385 | 1.615 | 96.77 | 98.730 | 1.270 | 97.46 |
| 660 | 98.070 | 1.930 | 96.14 | 98.435 | 1.565 | 96.87 |
| 720 | 97.850 | 2.150 | 95.70 | 98.150 | 1.850 | 96.30 |
| 780 | 97.510 | 2.490 | 95.02 | 97.805 | 2.195 | 95.61 |
| 840 | 97.185 | 2.815 | 94.37 | 97.330 | 2.670 | 94.66 |
| 900 | 96.800 | 3.200 | 93.60 | 96.800 | 3.200 | 93.60 |
| 960 | 96.395 | 3.605 | 92.79 | 96.165 | 3.835 | 92.33 |
| 1020 | 96.010 | 3.990 | 92.02 | 95.440 | 4.560 | 90.88 |
| 1080 | 95.605 | 4.395 | 91.21 | 94.515 | 5.485 | 89.03 |
| 1140 | 95.175 | 4.825 | 90.35 | 93.590 | 6.410 | 87.18 |
| 1200 | 94.695 | 5.305 | 89.39 | 92.510 | 7.490 | 85.02 |
| 1350 | 93.550 | 6.450 | 87.10 | 89.755 | 10.245 | 79.51 |
| 1500 | 92.505 | 7.495 | 85.01 | 86.645 | 13.355 | 73.29 |
| 1650 | 91.370 | 8.630 | 82.74 | 84.155 | 15.845 | 68.31 |
| 1800 | 90.410 | 9.590 | 80.82 | 82.010 | 17.990 | 64.02 |
| 1950 | 89.515 | 10.485 | 79.03 | 80.830 | 19.170 | 61.66 |
| 2100 | 88.580 | 11.420 | 77.16 | | | |
| 2250 | 88.045 | 11.955 | 76.09 | 78.100 | 21.900 | 56.20 |
| 2400 | 87.300 | 12.700 | 74.60 | 77.290 | 22.710 | 54.58 |
| 2550 | 86.785 | 13.215 | 73.57 | 76.510 | 23.490 | 53.02 |
| 2700 | 86.260 | 13.740 | 72.52 | 76.050 | 23.950 | 52.10 |
| 2850 | 85.910 | 14.090 | 71.82 | 75.305 | 24.695 | 50.61 |
| 3000 | 85.395 | 14.605 | 70.79 | 74.815 | 25.185 | 49.63 |
| 3150 | 85.105 | 14.895 | 70.21 | 74.450 | 25.550 | 48.90 |
| 3300 | 84.715 | 15.285 | 69.43 | 74.075 | 25.925 | 48.15 |
| 3450 | 84.455 | 15.545 | 68.91 | 73.710 | 26.290 | 47.42 |
| 3600 | 84.070 | 15.930 | 68.14 | 73.410 | 26.590 | 46.82 |
| 3900 | 83.515 | 16.485 | 67.03 | 72.845 | 27.155 | 45.69 |
| 4200 | 82.860 | 17.140 | 65.72 | 72.235 | 27.765 | 44.47 |
| 4500 | 82.395 | 17.605 | 64.79 | 71.825 | 28.175 | 43.65 |
| 4800 | 81.750 | 18.250 | 63.50 | 71.345 | 28.655 | 42.69 |
| 5100 | 81.295 | 18.705 | 62.59 | 71.030 | 28.970 | 42.06 |
| 5400 | 80.730 | 19.270 | 61.46 | 70.635 | 29.365 | 41.27 |
| 6000 | 79.870 | 20.130 | 59.74 | 69.975 | 30.025 | 39.95 |
| 6600 | 78.980 | 21.020 | 57.96 | 69.475 | 30.525 | 38.95 |

| | | | | | | |
|---|---|---|---|---|---|---|
| 7200 | 78.175 | 21.825 | 56.35 | 68.825 | 31.175 | 37.65 |

**0.025 Molal cont'd**

| | | Run 3 | | | Run 4 | |
|---|---|---|---|---|---|---|
| t (s) | Ent 1 rel area (%) | Ent 2 rel area (%) | e.e. (%) | Ent 1 rel area (%) | Ent 2 rel area (%) | e.e. (%) |
| 0 | 99.935 | 0.065 | 99.87 | 99.930 | 0.070 | 99.86 |
| 60 | 99.655 | 0.345 | 99.31 | 99.805 | 0.195 | 99.61 |
| 120 | 99.670 | 0.330 | 99.34 | 99.720 | 0.280 | 99.44 |
| 180 | 99.575 | 0.425 | 99.15 | 99.605 | 0.395 | 99.21 |
| 240 | 99.520 | 0.480 | 99.04 | 99.415 | 0.585 | 98.83 |
| 300 | 99.425 | 0.575 | 98.85 | 99.270 | 0.730 | 98.54 |
| 360 | 99.265 | 0.735 | 98.53 | 99.120 | 0.880 | 98.24 |
| 420 | 99.190 | 0.810 | 98.38 | 98.915 | 1.085 | 97.83 |
| 480 | 99.060 | 0.940 | 98.12 | 98.690 | 1.310 | 97.38 |
| 540 | 98.930 | 1.070 | 97.86 | 98.470 | 1.530 | 96.94 |
| 600 | 98.780 | 1.220 | 97.56 | 98.240 | 1.760 | 96.48 |
| 660 | | | | 97.935 | 2.065 | 95.87 |
| 720 | 98.455 | 1.545 | 96.91 | 97.620 | 2.380 | 95.24 |
| 780 | 98.360 | 1.640 | 96.72 | 97.310 | 2.690 | 94.62 |
| 840 | 98.190 | 1.810 | 96.38 | 96.915 | 3.085 | 93.83 |
| 900 | 98.050 | 1.950 | 96.10 | 96.490 | 3.510 | 92.98 |
| 960 | 97.860 | 2.140 | 95.72 | 96.065 | 3.935 | 92.13 |
| 1020 | 97.705 | 2.295 | 95.41 | 95.605 | 4.395 | 91.21 |
| 1080 | 97.575 | 2.425 | 95.15 | 95.115 | 4.885 | 90.23 |
| 1140 | 97.375 | 2.625 | 94.75 | 94.645 | 5.355 | 89.29 |
| 1200 | 97.215 | 2.785 | 94.43 | 94.120 | 5.880 | 88.24 |
| 1350 | 96.810 | 3.190 | 93.62 | 92.570 | 7.430 | 85.14 |
| 1500 | 96.350 | 3.650 | 92.70 | 91.065 | 8.935 | 82.13 |
| 1650 | 95.925 | 4.075 | 91.85 | 90.215 | 9.785 | 80.43 |
| 1800 | 95.445 | 4.555 | 90.89 | 88.700 | 11.300 | 77.40 |
| 1950 | 95.005 | 4.995 | 90.01 | 87.610 | 12.390 | 75.22 |
| 2100 | 94.565 | 5.435 | 89.13 | 86.605 | 13.395 | 73.21 |
| 2250 | 94.150 | 5.850 | 88.30 | 85.750 | 14.250 | 71.50 |
| 2400 | 93.715 | 6.285 | 87.43 | 84.970 | 15.030 | 69.94 |
| 2550 | 93.280 | 6.720 | 86.56 | 84.175 | 15.825 | 68.35 |
| 2700 | 92.875 | 7.125 | 85.75 | 84.035 | 15.965 | 68.07 |
| 2850 | 92.480 | 7.520 | 84.96 | 82.625 | 17.375 | 65.25 |
| 3000 | 92.135 | 7.865 | 84.27 | 81.905 | 18.095 | 63.81 |
| 3150 | 91.570 | 8.430 | 83.14 | 81.115 | 18.885 | 62.23 |
| 3300 | 91.430 | 8.570 | 82.86 | 80.370 | 19.630 | 60.74 |
| 3450 | 91.100 | 8.900 | 82.20 | 79.370 | 20.630 | 58.74 |
| 3600 | 90.825 | 9.175 | 81.65 | 78.705 | 21.295 | 57.41 |
| 3900 | 89.960 | 10.040 | 79.92 | 77.350 | 22.650 | 54.70 |
| 4200 | 89.660 | 10.340 | 79.32 | 75.950 | 24.050 | 51.90 |
| 4500 | 88.915 | 11.085 | 77.83 | 74.620 | 25.380 | 49.24 |
| 4800 | 88.355 | 11.645 | 76.71 | 73.540 | 26.460 | 47.08 |
| 5100 | 87.870 | 12.130 | 75.74 | 72.335 | 27.665 | 44.67 |
| 5400 | 87.360 | 12.640 | 74.72 | 71.280 | 28.720 | 42.56 |
| 6000 | 86.550 | 13.450 | 73.10 | 69.240 | 30.760 | 38.48 |
| 6600 | 85.665 | 14.335 | 71.33 | 67.300 | 32.700 | 34.60 |
| 7200 | 84.920 | 15.080 | 69.84 | 65.430 | 34.570 | 30.86 |

**Data Analysis and R Scripts**

**Linear Regression**

For analysis of erosion studies following first-order kinetics linear least squares regression was carried out to determine the line of best fit. This was completed using Microsoft excel.

**Non-Linear Regression**

Non-linear regression was carried out to fit data collected from erosion studies of **4**. Regression was carried out using nonlinear weighted least squares ("nls") methods which uses a relative-offset convergence criterion to compare the numerical imprecision at the current parameter estimates to the residual sum-of-squares. A five parameter logistic curve was chosen for fitting due to its similarity in shape to the data to be fitted and because we did not seek physically meaningful parameterisation at the projects current stage. The equation takes the form:

$$y = h + \frac{h + i}{\left(1 + \left(\frac{x}{j}\right)^{k}\right)^{l}}$$

where h, i, j, k, and l are parameters to be fitted by nls methods and x and y are, in this instance, time and e.e., respectively. The fitted parameters are summarised below:

Upon parameterisation, equations of best fit were inputted to Mathematica to determine the solution to the roots of the third derivative of the equation. These correspond to the points at which the rate of change of the rate of change are maximal, which are reproducible approximations of the points at which the enantiomerisation appears to change regimes.

Table S11 – Fitted parameters

| | **0.2 molal** | **0.1 molal** | **0.05 molal** | **0.025 molal** |
|---|---|---|---|---|
| h | -0.02141 | 3.21427 | 22.27789 | -14.17073 |
| i | 98.33881 | 91.85182 | 54.18045 | 127.39377 |
| j | 20.2488 | 10.1654 | 13.03006 | 15.8615 |
| k | 3.91197 | 4.33591 | 3.86647 | 3.59347 |
| l | 3.58554 | 0.4743 | 0.28391 | 0.07939 |

The ee and slope at these resulting times were then evaluated for each concentration and the values plotted (Figure S32).

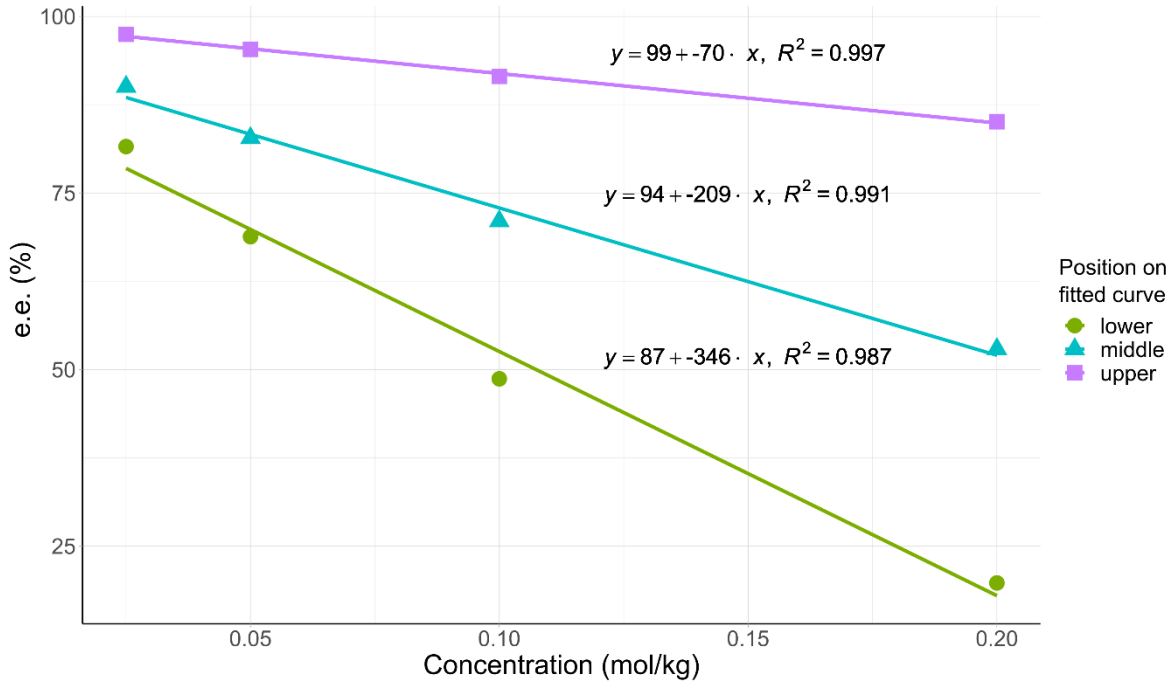



Figure S1 Fitted plots of points of inflection

**R Script for Non-Linear Regression**

The code used to carry out non-linear regression is given below for the data relating to **4**.

```
library(ggplot2)
library(grDevices)
library(cwhmisc)
library(graphics)
library(plyr)
library(dplyr)
library(tidyr)
library(Rcpp)
library(jtools)
library(Hmisc)
setwd("C:/Users/pearse.solon/Desktop/PRx Explt Data/Plots/Non-Lin_Fit")
a<-readxl::read_xlsx("Raw_All.xlsx")
b<-gather(a, conc, e.e., c1...2:c4...13, factor_key=TRUE)
levels(b$conc)[levels(b$conc)=="c1...2"] <- "0.2"
levels(b$conc)[levels(b$conc)=="c1...3"] <- "0.2"
levels(b$conc)[levels(b$conc)=="c1...4"] <- "0.2"
levels(b$conc)[levels(b$conc)=="c2...5"] <- "0.1"
levels(b$conc)[levels(b$conc)=="c2...6"] <- "0.1"
levels(b$conc)[levels(b$conc)=="c2...7"] <- "0.1"
levels(b$conc)[levels(b$conc)=="c3...7"] <- "0.05"
levels(b$conc)[levels(b$conc)=="c3...8"] <- "0.05"
levels(b$conc)[levels(b$conc)=="c3...9"] <- "0.05"
levels(b$conc)[levels(b$conc)=="c4...10"] <- "0.025"
```

```
levels(b$conc)[levels(b$conc)=="c4...11"]                    <-   "0.025"
levels(b$conc)[levels(b$conc)=="c4...12"]                    <-   "0.025"
levels(b$conc)[levels(b$conc)=="c4...13"]                    <-   "0.025"
e <- ddply(b, c("tm",      "conc"), summarise,
N          = sum(!is.na(e.e.)),
ee = mean(e.e., na.rm=TRUE),
sd         = sd(e.e., na.rm=TRUE),
se         = sd / sqrt(N))
c<-split(e,e$conc)
c1 <- c$‘0.2‘
c2 <- c$‘0.1‘
c3 <- c$‘0.05‘
c4 <- c$‘0.025‘
d1<-mutate(c1, CN=paste0(c1$conc," (N=3)"))
d2<-mutate(c2, CN=paste0(c2$conc," (N=2)"))
d3<-mutate(c3, CN=paste0(c3$conc," (N=3)"))
d4<-mutate(c4, CN=paste0(c4$conc," (N=4)"))
f<-rbind(d1,d2,d3,d4)
modelc1<- nls(ee~h+((h+i)/((1+((tm/j)^k))^l)), d1, start = list(h = 3, i = 90 ,
j = 10, k = 4, l = 0.5))
hm1<-coefficients(modelc1)[1]
im1<-coefficients(modelc1)[2]
jm1<-coefficients(modelc1)[3]
km1<-coefficients(modelc1)[4]
lm1<-coefficients(modelc1)[5]
modelc2<- nls(ee~h+((h+i)/((1+((tm/j)^k))^l)), d2, start = list(h = 3, i = 90 ,
j = 10, k = 4, l = 0.5))
hm2<-coefficients(modelc2)[1]
im2<-coefficients(modelc2)[2]
jm2<-coefficients(modelc2)[3]
km2<-coefficients(modelc2)[4]
lm2<-coefficients(modelc2)[5]
modelc3<- nls(ee~h+((h+i)/((1+((tm/j)^k))^l)), d3, start = list(h = 3, i = 90 ,
j = 10, k = 4, l = 0.5))
hm3<-coefficients(modelc3)[1]
im3<-coefficients(modelc3)[2]
jm3<-coefficients(modelc3)[3]
km3<-coefficients(modelc3)[4]
lm3<-coefficients(modelc3)[5]
modelc4<- nls(ee~h+((h+i)/((1+((tm/j)^k))^l)), d4, start = list(h = 3, i = 90 ,
j = 10, k = 4, l = 0.5))
hm4<-coefficients(modelc4)[1]
im4<-coefficients(modelc4)[2]
jm4<-coefficients(modelc4)[3]
km4<-coefficients(modelc4)[4]
lm4<-coefficients(modelc4)[5]
pc1<-ggplot(d1, aes(tm, ee)) +geom_point()+geom_smooth(method = "nls", formula =
y~h+((h+i)/((1+((x/j)^k))^l)), method.args=list(start = list(h = hm1, i = im1 ,
j = jm1, k=km1, l=lm1)), data = d1, se = FALSE)+theme_light() +
xlab("Time (min)") + ylab("e.e.")
pc2<-ggplot(d2, aes(tm, ee)) +geom_point()+geom_smooth(method = "nls", formula =
y~h+((h+i)/((1+((x/j)^k))^l)), method.args=list(start = list(h = hm2, i = im2 ,
j = jm2, k=km2, l=lm2)), data = d2, se = FALSE)+theme_light() +
```

```
xlab("Time (min)") + ylab("e.e.
pc3<-ggplot(d3, aes(tm, ee)) +geom_point()+geom_smooth(method = "nls", formula =
y~h+((h+i)/((1+((x/j)^k))^l)), method.args=list(start = list(h = hm3, i = im3 ,
j = jm3, k=km3, l=lm3)), data = d3, se = FALSE)+theme_light() +
xlab("Time (min)") + ylab("e.e.")
pc4<-ggplot(d4, aes(tm, ee)) +geom_point()+geom_smooth(method = "nls", formula =
y~h+((h+i)/((1+((x/j)^k))^l)), method.args=list(start = list(h = hm4, i = im4 ,
j = jm4, k=km4, l=lm4)), data = d4, se = FALSE)+theme_light()
+ xlab("Time (min)") + ylab("e.e.")
pc1e<-ggplot(d1, aes(tm, ee)) +geom_point()+geom_smooth(method = "nls", formula =
y~h+((h+i)/((1+((x/j)^k))^l)), method.args=list(start = list(h = hm1, i = im1 ,
j = jm1, k=km1, l=lm1)), data = d1, se = FALSE)+theme_light() +
geom_errorbar(aes(ymin=ee-se,
ymax=ee+se), width = 0.1) + xlab("Time (min)") + ylab("e.e.")
pc2e<-ggplot(d2, aes(tm, ee)) +geom_point()+geom_smooth(method = "nls", formula =
y~h+((h+i)/((1+((x/j)^k))^l)), method.args=list(start = list(h = hm2, i = im2 ,
j = jm2, k=km2, l=lm2)), data = d2, se = FALSE)+theme_light() +
geom_errorbar(aes(ymin=ee-se,
ymax=ee+se), width = 0.1) + xlab("Time (min)") + ylab("e.e.")
pc3e<-ggplot(d3, aes(tm, ee)) +geom_point()+geom_smooth(method = "nls", formula =
y~h+((h+i)/((1+((x/j)^k))^l)), method.args=list(start = list(h = hm3, i = im3 ,
j = jm3, k=km3, l=lm3)), data = d3, se = FALSE)+theme_light() +
geom_errorbar(aes(ymin=ee-se,
ymax=ee+se), width = 0.1) + xlab("Time (min)") + ylab("e.e.")
pc4e<-ggplot(d4, aes(tm, ee)) +geom_point()+geom_smooth(method = "nls", formula =
y~h+((h+i)/((1+((x/j)^k))^l)), method.args=list(start = list(h = hm4, i = im4 ,
j = jm4, k=km4, l=lm4)), data = d4, se = FALSE)+theme_light() +
geom_errorbar(aes(ymin=ee-se,
ymax=ee+se), width = 0.1) + xlab("Time (min)") + ylab("e.e.")
all <- ggplot(f, aes(x=tm, y=ee, colour=CN)) +
geom_errorbar(aes(ymin=ee-se, ymax=ee+se), width=.3) +
geom_point() + theme_light() + labs(x = "Time (min)", y = "e.e. (%)",
color = "Conc. \n (mol/kg)") + theme(legend.title.align = 0.5)
extrafont::loadfonts(device="win")
all2<-ggplot(f, aes(x=tm, y=ee, colour=CN, family="Arial")) +
geom_errorbar(aes(ymin=ee-se, ymax=ee+se), width=.3) +
geom_point() + theme_light() + labs(x = "Time (min)", y = "e.e. (%)",
color = "Conc. \n (mol/kg)", family="Arial") + theme(legend.title.align = 0.5)
everything<-all2+geom_smooth(method = "nls", formula =
y~h+((h+i)/((1+((x/j)^k))^l)), method.args=list(start = list(h = hm1, i = im1 ,
j = jm1, k=km1, l=lm1)), data = d1, se = FALSE)+
geom_smooth(method = "nls", formula = y~h+((h+i)/((1+((x/j)^k))^l)),
method.args=list(start = list(h = hm2, i = im2 , j = jm2, k=km2, l=lm2)),
data = d2, se = FALSE)+
geom_smooth(method = "nls", formula = y~h+((h+i)/((1+((x/j)^k))^l)),
method.args=list(start = list(h = hm3, i = im3 , j = jm3, k=km3, l=lm3)),
data = d3, se = FALSE)+
geom_smooth(method = "nls", formula = y~h+((h+i)/((1+((x/j)^k))^l)),
method.args=list(start = list(h = hm4, i = im4 , j = jm4, k=km4, l=lm4)),
data = d4, se = FALSE)+
theme(text=element_text(size=16))
all3 <-ggplot(f, aes(x=tm, y=ee, colour=CN, guide_legend(reverse=TRUE))) +
geom_errorbar(aes(ymin=ee-se, ymax=ee+se), width=.5) +
```

```
geom_point(aes(shape=CN), size=3) + theme_light() +
labs(x = "Time (min)", y = "e.e. (%)") + theme(legend.title.align = 0.5)
everythingbw<-all3+geom_smooth(method = "nls", formula =
y~h+((h+i)/((1+((x/j)^k))^l)), method.args=list(start = list(h = hm1, i = im1 ,
j = jm1, k=km1, l=lm1)), data = d1, se = FALSE)+
geom_smooth(method = "nls", formula = y~h+((h+i)/((1+((x/j)^k))^l)),
method.args=list(start = list(h = hm2, i = im2 , j = jm2, k=km2, l=lm2)),
data = d2, se = FALSE)+
geom_smooth(method = "nls", formula = y~h+((h+i)/((1+((x/j)^k))^l)),
method.args=list(start = list(h = hm3, i = im3 , j = jm3, k=km3, l=lm3)),
data = d3, se = FALSE)+
geom_smooth(method = "nls", formula = y~h+((h+i)/((1+((x/j)^k))^l)),
method.args=list(start = list(h = hm4, i = im4 , j = jm4, k=km4, l=lm4)),
data = d4, se = FALSE)+
theme(text=element_text(size=16))+scale_colour_grey()
everythingshape<-all3+geom_smooth(method = "nls", formula =
y~h+((h+i)/((1+((x/j)^k))^l)), method.args=list(start = list(h = hm1, i = im1 ,
j = jm1, k=km1, l=lm1)), data = d1, se = FALSE)+
geom_smooth(method = "nls", formula = y~h+((h+i)/((1+((x/j)^k))^l)),
method.args=list(start = list(h = hm2, i = im2 , j = jm2, k=km2, l=lm2)),
data = d2, se = FALSE)+
geom_smooth(method = "nls", formula = y~h+((h+i)/((1+((x/j)^k))^l)),
method.args=list(start = list(h = hm3, i = im3 , j = jm3, k=km3, l=lm3)),
data = d3, se = FALSE)+
geom_smooth(method = "nls", formula = y~h+((h+i)/((1+((x/j)^k))^l)),
method.args=list(start = list(h = hm4, i = im4 , j = jm4, k=km4, l=lm4)),
data = d4, se = FALSE)+
theme(text=element_text(size=16))
everythingshapes<-everythingshape+labs(color="Conc. \n (mol/kg)", shape="Conc. \n
(mol/kg)")+
theme(panel.border = element_blank(), axis.line =
element_line(colour = "black")) +
guides(colour = guide_legend(reverse=T), shape=guide_legend(reverse=T))+
scale_color_manual(values=c("#c77cff", "#00BFC4", "#7CAE00", "#F8766d"))+
scale_shape_manual(values=c(15, 17, 18, 19))
everythingshapes
cairo_ps(filename = "everythingshapes.eps",
width = 13, height = 7, pointsize = 12,
fallback_resolution = 300)
print(everythingshapes)
dev.off()
```

This gives the following plot and processed data:

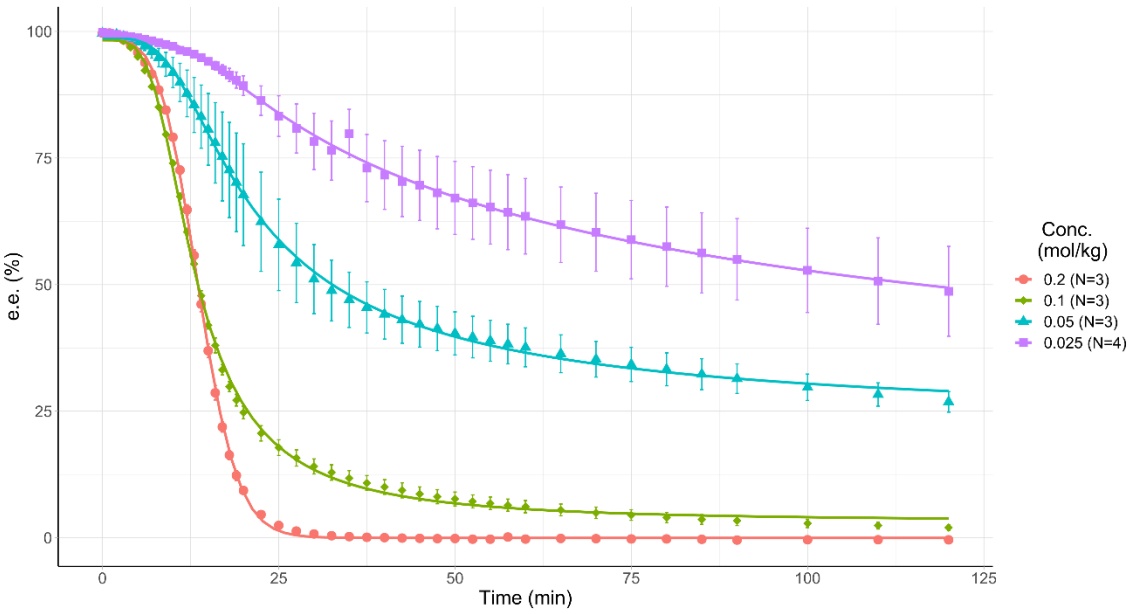



Figure S2 Processed data and fitted lines plot

| t (m) | Concentration (mol/kg) | N | mean e.e. (%) | sd | se |
|---|---|---|---|---|---|
| 0 | 0.2 | 3 | 99.67 | 0.2858 | 0.1650 |
| 1 | 0.2 | 3 | 99.70 | 0.2691 | 0.1553 |
| 2 | 0.2 | 3 | 99.04 | 0.0723 | 0.0418 |
| 3 | 0.2 | 3 | 98.35 | 0.0586 | 0.0338 |
| 4 | 0.2 | 3 | 97.21 | 0.1419 | 0.0819 |
| 5 | 0.2 | 3 | 95.86 | 0.1201 | 0.0694 |
| 6 | 0.2 | 3 | 93.89 | 0.1801 | 0.1040 |
| 7 | 0.2 | 3 | 91.59 | 0.2673 | 0.1543 |
| 8 | 0.2 | 3 | 88.45 | 0.4402 | 0.2541 |
| 9 | 0.2 | 2 | 84.48 | 0.1838 | 0.1300 |
| 10 | 0.2 | 3 | 79.12 | 0.8911 | 0.5145 |
| 11 | 0.2 | 3 | 72.63 | 1.4080 | 0.8129 |
| 12 | 0.2 | 3 | 64.78 | 1.7434 | 1.0066 |
| 13 | 0.2 | 3 | 55.76 | 1.9413 | 1.1208 |
| 14 | 0.2 | 3 | 46.14 | 2.5988 | 1.5004 |
| 15 | 0.2 | 3 | 36.94 | 2.3161 | 1.3372 |
| 16 | 0.2 | 3 | 28.64 | 2.4678 | 1.4248 |
| 17 | 0.2 | 3 | 21.90 | 1.7765 | 1.0256 |
| 18 | 0.2 | 3 | 16.35 | 1.5662 | 0.9043 |
| 19 | 0.2 | 3 | 12.31 | 1.7335 | 1.0008 |
| 20 | 0.2 | 3 | 9.35 | 1.1282 | 0.6514 |
| 22.5 | 0.2 | 3 | 4.60 | 0.6935 | 0.4004 |
| 25 | 0.2 | 3 | 2.44 | 0.5393 | 0.3114 |
| 27.5 | 0.2 | 3 | 1.33 | 0.3790 | 0.2188 |
| 30 | 0.2 | 3 | 0.76 | 0.3017 | 0.1742 |
| 32.5 | 0.2 | 3 | 0.42 | 0.2610 | 0.1507 |
| 35 | 0.2 | 3 | 0.24 | 0.2179 | 0.1258 |
| 37.5 | 0.2 | 3 | 0.10 | 0.2122 | 0.1225 |
| 40 | 0.2 | 3 | 0.04 | 0.2816 | 0.1626 |
| 42.5 | 0.2 | 3 | -0.05 | 0.2108 | 0.1217 |
| 45 | 0.2 | 3 | -0.10 | 0.2108 | 0.1217 |
| 47.5 | 0.2 | 3 | -0.16 | 0.1353 | 0.0781 |
| 50 | 0.2 | 3 | -0.14 | 0.1908 | 0.1102 |
| 52.5 | 0.2 | 3 | -0.27 | 0.1082 | 0.0624 |
| 55 | 0.2 | 3 | -0.27 | 0.2103 | 0.1214 |
| 57.5 | 0.2 | 3 | 0.16 | 1.2020 | 0.6940 |
| 60 | 0.2 | 3 | -0.25 | 0.1940 | 0.1120 |
| 65 | 0.2 | 3 | -0.12 | 0.2495 | 0.1440 |
| 70 | 0.2 | 2 | -0.17 | 0.0495 | 0.0350 |
| 75 | 0.2 | 3 | -0.22 | 0.1779 | 0.1027 |
| 80 | 0.2 | 3 | -0.22 | 0.0600 | 0.0346 |
| 85 | 0.2 | 3 | -0.30 | 0.1861 | 0.1074 |
| 90 | 0.2 | 3 | -0.44 | 0.3066 | 0.1770 |
| 100 | 0.2 | 3 | -0.38 | 0.1637 | 0.0945 |
| 110 | 0.2 | 3 | -0.38 | 0.0252 | 0.0145 |
| 120 | 0.2 | 3 | -0.40 | 0.1102 | 0.0636 |

| t (m) | Concentration (mol/kg) | N | mean e.e. (%) | sd | se |
|---|---|---|---|---|---|
| 0 | 0.1 | 3 | 99.70 | 0.1358 | 0.0784 |
| 1 | 0.1 | 3 | 99.43 | 0.1002 | 0.0578 |
| 2 | 0.1 | 3 | 99.01 | 0.0462 | 0.0267 |
| 3 | 0.1 | 3 | 98.20 | 0.1620 | 0.0935 |
| 4 | 0.1 | 3 | 97.05 | 0.3223 | 0.1861 |
| 5 | 0.1 | 3 | 95.37 | 0.6352 | 0.3667 |
| 6 | 0.1 | 3 | 92.92 | 1.1310 | 0.6530 |
| 7 | 0.1 | 3 | 89.94 | 1.4434 | 0.8333 |
| 8 | 0.1 | 3 | 86.12 | 1.8393 | 1.0619 |
| 9 | 0.1 | 3 | 80.96 | 2.2889 | 1.3215 |
| 10 | 0.1 | 3 | 75.52 | 2.6806 | 1.5477 |
| 11 | 0.1 | 3 | 68.93 | 2.6886 | 1.5522 |
| 12 | 0.1 | 2 | 60.40 | 0.9899 | 0.7000 |
| 13 | 0.1 | 3 | 55.59 | 2.7391 | 1.5814 |
| 14 | 0.1 | 3 | 49.30 | 2.7740 | 1.6016 |
| 15 | 0.1 | 3 | 43.73 | 3.1081 | 1.7945 |
| 16 | 0.1 | 3 | 39.40 | 2.8259 | 1.6315 |
| 17 | 0.1 | 3 | 34.96 | 3.2266 | 1.8629 |
| 18 | 0.1 | 3 | 31.86 | 3.6333 | 2.0977 |
| 19 | 0.1 | 3 | 29.18 | 3.6411 | 2.1022 |
| 20 | 0.1 | 3 | 26.96 | 4.0201 | 2.3210 |
| 22.5 | 0.1 | 3 | 22.81 | 4.0567 | 2.3421 |
| 25 | 0.1 | 3 | 19.99 | 4.0931 | 2.3631 |
| 27.5 | 0.1 | 3 | 17.89 | 4.0259 | 2.3244 |
| 30 | 0.1 | 3 | 16.26 | 4.0217 | 2.3219 |
| 32.5 | 0.1 | 3 | 15.04 | 4.0107 | 2.3156 |
| 35 | 0.1 | 3 | 13.92 | 4.0200 | 2.3210 |
| 37.5 | 0.1 | 3 | 13.11 | 4.2157 | 2.4340 |
| 40 | 0.1 | 3 | 12.31 | 4.1852 | 2.4163 |
| 42.5 | 0.1 | 3 | 11.58 | 4.0717 | 2.3508 |
| 45 | 0.1 | 3 | 10.89 | 4.1148 | 2.3757 |
| 47.5 | 0.1 | 3 | 10.40 | 4.1866 | 2.4171 |
| 50 | 0.1 | 3 | 9.95 | 4.1952 | 2.4221 |
| 52.5 | 0.1 | 3 | 9.42 | 4.0984 | 2.3662 |
| 55 | 0.1 | 3 | 9.15 | 4.2232 | 2.4383 |
| 57.5 | 0.1 | 3 | 8.75 | 4.1482 | 2.3949 |
| 60 | 0.1 | 3 | 8.37 | 3.9993 | 2.3090 |
| 65 | 0.1 | 3 | 7.73 | 4.0134 | 2.3172 |
| 70 | 0.1 | 3 | 7.28 | 4.2090 | 2.4301 |
| 75 | 0.1 | 3 | 6.78 | 4.0964 | 2.3651 |
| 80 | 0.1 | 3 | 6.20 | 3.9588 | 2.2856 |
| 85 | 0.1 | 3 | 5.88 | 4.0416 | 2.3334 |
| 90 | 0.1 | 3 | 5.59 | 3.9472 | 2.2789 |
| 100 | 0.1 | 3 | 5.01 | 3.8396 | 2.2168 |
| 110 | 0.1 | 3 | 4.50 | 3.6493 | 2.1069 |
| 120 | 0.1 | 3 | 4.06 | 3.5750 | 2.0640 |

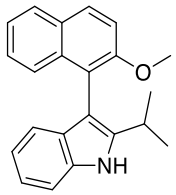
| t (m) | Concentration (mol/kg) | N | mean e.e. (%) | sd | se |
|---|---|---|---|---|---|
| 0 | 0.05 | 3 | 99.64 | 0.3580 | 0.2067 |
| 1 | 0.05 | 3 | 99.09 | 0.7186 | 0.4149 |
| 2 | 0.05 | 3 | 99.41 | 0.1361 | 0.0786 |
| 3 | 0.05 | 3 | 99.01 | 0.3703 | 0.2138 |
| 4 | 0.05 | 3 | 98.58 | 0.5647 | 0.3260 |
| 5 | 0.05 | 3 | 97.95 | 0.9799 | 0.5657 |
| 6 | 0.05 | 3 | 97.12 | 1.5314 | 0.8842 |
| 7 | 0.05 | 3 | 96.06 | 2.2914 | 1.3230 |
| 8 | 0.05 | 3 | 94.85 | 3.1679 | 1.8290 |
| 9 | 0.05 | 3 | 93.50 | 4.0646 | 2.3467 |
| 10 | 0.05 | 3 | 91.90 | 5.1799 | 2.9906 |
| 11 | 0.05 | 3 | 89.93 | 6.5500 | 3.7817 |
| 12 | 0.05 | 3 | 87.76 | 7.9602 | 4.5958 |
| 13 | 0.05 | 3 | 85.49 | 9.4091 | 5.4323 |
| 14 | 0.05 | 3 | 83.17 | 10.8001 | 6.2354 |
| 15 | 0.05 | 3 | 80.67 | 12.2734 | 7.0861 |
| 16 | 0.05 | 3 | 78.01 | 13.7706 | 7.9505 |
| 17 | 0.05 | 3 | 75.31 | 15.1902 | 8.7700 |
| 18 | 0.05 | 3 | 72.65 | 16.3004 | 9.4110 |
| 19 | 0.05 | 3 | 70.20 | 16.8750 | 9.7428 |
| 20 | 0.05 | 3 | 67.76 | 17.4080 | 10.0505 |
| 22.5 | 0.05 | 3 | 62.43 | 16.9598 | 9.7918 |
| 25 | 0.05 | 3 | 57.86 | 15.6355 | 9.0272 |
| 27.5 | 0.05 | 3 | 54.29 | 13.5635 | 7.8309 |
| 30 | 0.05 | 3 | 51.10 | 11.7987 | 6.8120 |
| 32.5 | 0.05 | 3 | 48.83 | 10.4009 | 6.0050 |
| 35 | 0.05 | 3 | 47.00 | 9.4454 | 5.4533 |
| 37.5 | 0.05 | 3 | 45.50 | 8.7631 | 5.0594 |
| 40 | 0.05 | 3 | 44.15 | 8.4839 | 4.8982 |
| 42.5 | 0.05 | 3 | 43.07 | 8.0646 | 4.6561 |
| 45 | 0.05 | 3 | 42.17 | 7.7957 | 4.5008 |
| 47.5 | 0.05 | 3 | 41.33 | 7.5872 | 4.3804 |
| 50 | 0.05 | 3 | 40.37 | 7.3615 | 4.2502 |
| 52.5 | 0.05 | 3 | 39.64 | 7.1129 | 4.1066 |
| 55 | 0.05 | 3 | 38.92 | 7.0190 | 4.0524 |
| 57.5 | 0.05 | 3 | 38.26 | 6.7919 | 3.9213 |
| 60 | 0.05 | 3 | 37.62 | 6.6439 | 3.8359 |
| 65 | 0.05 | 3 | 36.35 | 6.4636 | 3.7318 |
| 70 | 0.05 | 3 | 35.26 | 6.0959 | 3.5195 |
| 75 | 0.05 | 3 | 34.24 | 5.8462 | 3.3753 |
| 80 | 0.05 | 3 | 33.28 | 5.6154 | 3.2420 |
| 85 | 0.05 | 3 | 32.31 | 5.2887 | 3.0534 |
| 90 | 0.05 | 3 | 31.43 | 5.0553 | 2.9187 |
| 100 | 0.05 | 3 | 29.73 | 4.5058 | 2.6014 |
| 110 | 0.05 | 3 | 28.31 | 3.9828 | 2.2995 |
| 120 | 0.05 | 3 | 26.84 | 3.5210 | 2.0328 |

| t (m) | Concentration (mol/kg) | N | mean e.e. (%) | sd | se |
|---|---|---|---|---|---|
| 0 | 0.025 | 3 | 99.86 | 0.0153 | 0.0088 |
| 1 | 0.025 | 4 | 99.64 | 0.2825 | 0.1413 |
| 2 | 0.025 | 4 | 99.43 | 0.0597 | 0.0299 |
| 3 | 0.025 | 4 | 99.22 | 0.0716 | 0.0358 |
| 4 | 0.025 | 4 | 98.98 | 0.1209 | 0.0605 |
| 5 | 0.025 | 4 | 98.75 | 0.1863 | 0.0931 |
| 6 | 0.025 | 4 | 98.47 | 0.1964 | 0.0982 |
| 7 | 0.025 | 4 | 98.17 | 0.3086 | 0.1543 |
| 8 | 0.025 | 4 | 97.81 | 0.3971 | 0.1986 |
| 9 | 0.025 | 4 | 97.44 | 0.4837 | 0.2419 |
| 10 | 0.025 | 4 | 97.07 | 0.5261 | 0.2630 |
| 11 | 0.025 | 3 | 96.29 | 0.5173 | 0.2987 |
| 12 | 0.025 | 4 | 96.04 | 0.7257 | 0.3629 |
| 13 | 0.025 | 4 | 95.49 | 0.9138 | 0.4569 |
| 14 | 0.025 | 4 | 94.81 | 1.1017 | 0.5509 |
| 15 | 0.025 | 4 | 94.07 | 1.3845 | 0.6923 |
| 16 | 0.025 | 4 | 93.24 | 1.6746 | 0.8373 |
| 17 | 0.025 | 4 | 92.38 | 2.0760 | 1.0380 |
| 18 | 0.025 | 4 | 91.41 | 2.6511 | 1.3255 |
| 19 | 0.025 | 4 | 90.39 | 3.1898 | 1.5949 |
| 20 | 0.025 | 4 | 89.27 | 3.9057 | 1.9528 |
| 22.5 | 0.025 | 4 | 86.34 | 5.8214 | 2.9107 |
| 25 | 0.025 | 4 | 83.28 | 8.0177 | 4.0089 |
| 27.5 | 0.025 | 4 | 80.83 | 9.6953 | 4.8477 |
| 30 | 0.025 | 4 | 78.28 | 11.0993 | 5.5497 |
| 32.5 | 0.025 | 4 | 76.48 | 11.7016 | 5.8508 |
| 35 | 0.025 | 3 | 79.83 | 8.2899 | 4.7861 |
| 37.5 | 0.025 | 4 | 73.02 | 13.2681 | 6.6340 |
| 40 | 0.025 | 4 | 71.64 | 13.5649 | 6.7824 |
| 42.5 | 0.025 | 4 | 70.38 | 13.8739 | 6.9370 |
| 45 | 0.025 | 4 | 69.61 | 13.8797 | 6.9399 |
| 47.5 | 0.025 | 4 | 68.16 | 14.2841 | 7.1420 |
| 50 | 0.025 | 4 | 67.13 | 14.4274 | 7.2137 |
| 52.5 | 0.025 | 4 | 66.12 | 14.3535 | 7.1768 |
| 55 | 0.025 | 4 | 65.30 | 14.6097 | 7.3048 |
| 57.5 | 0.025 | 4 | 64.32 | 14.8044 | 7.4022 |
| 60 | 0.025 | 4 | 63.51 | 14.9026 | 7.4513 |
| 65 | 0.025 | 4 | 61.84 | 14.8955 | 7.4477 |
| 70 | 0.025 | 4 | 60.35 | 15.4086 | 7.7043 |
| 75 | 0.025 | 4 | 58.88 | 15.4802 | 7.7401 |
| 80 | 0.025 | 4 | 57.50 | 15.6305 | 7.8152 |
| 85 | 0.025 | 4 | 56.27 | 15.8693 | 7.9347 |
| 90 | 0.025 | 4 | 55.00 | 16.0611 | 8.0305 |
| 100 | 0.025 | 4 | 52.82 | 16.6377 | 8.3188 |
| 110 | 0.025 | 4 | 50.71 | 17.0839 | 8.5419 |
| 120 | 0.025 | 4 | 48.68 | 17.7556 | 8.8778 |

## II.5.3 Data for methylated analogues

### Data for 129 recorded at 155 °C in 1,2,4-trimethylbenzene

Table S12 Erosion data for **129** at 155 °C and 0.025 molal. The erosion study was carried as described and analysed by normal phase chiral HPLC




**129**

| t (s) | Ent 1 rel area (%) | Ent 2 rel area (%) | e.e. (%) | $\ln\left(\frac{e.e._0}{e.e._t}\right)$ |
|---|---|---|---|---|
| 0 | 99.95 | 0.05 | 99.9 | 0 |
| 120 | 99.075 | 0.925 | 98.15 | 0.017673 |
| 240 | 98.26 | 1.74 | 96.52 | 0.034419 |
| 360 | 97.395 | 2.605 | 94.79 | 0.052506 |
| 480 | 96.52 | 3.48 | 93.04 | 0.07114 |
| 600 | 95.685 | 4.315 | 91.37 | 0.089252 |
| 720 | 94.835 | 5.165 | 89.67 | 0.108033 |
| 840 | 94.025 | 5.975 | 88.05 | 0.126265 |
| 960 | 93.205 | 6.795 | 86.41 | 0.145066 |
| 1080 | 92.41 | 7.59 | 84.82 | 0.163638 |
| 1200 | 91.6 | 8.4 | 83.2 | 0.182922 |
| 1500 | 89.675 | 10.325 | 79.35 | 0.230301 |
| 1800 | 87.86 | 12.14 | 75.72 | 0.277127 |
| 2100 | 86.125 | 13.875 | 72.25 | 0.324037 |
| 2400 | 84.505 | 15.495 | 69.01 | 0.369918 |
| 2700 | 82.89 | 17.11 | 65.78 | 0.417854 |
| 3000 | 81.55 | 18.45 | 63.1 | 0.459449 |
| 3300 | 80.01 | 19.99 | 60.02 | 0.509492 |
| 3600 | 78.7 | 21.3 | 57.4 | 0.554125 |
| 4500 | 75.02 | 24.98 | 50.04 | 0.691347 |
| 5400 | 72.39 | 27.61 | 44.78 | 0.802408 |
| 6300 | 69.805 | 30.195 | 39.61 | 0.925088 |
| 7200 | 68.055 | 31.945 | 36.11 | 1.0176 |

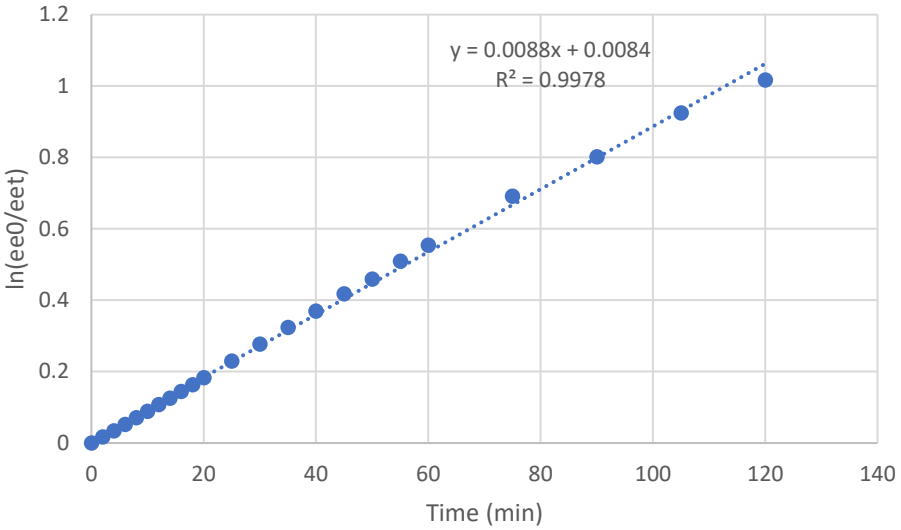



Figure S34 First order plot of erosion data for **129**

$m = k_{rac} = 1.46 \times 10^{-4}\ s^{-1}$

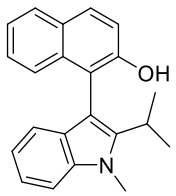
$k_{ent} = 7.3 \times 10^{-5}\ s^{-1}$

$\Delta G^{\ddagger}$ (155 °C) = 33.5 kcal $mol^{-1}$

$T_{½}$ (155 °C) = 79 min; $T_{½}$ (25 °C) = 6,000 years

**Data for 131 recorded at 155 °C in 1,2,4-trimethylbenzene**

Table S13 Erosion data for **131** at 155 °C and 0.025 molal. The erosion study was carried as described and analysed by normal phase chiral HPLC.




**131**

| t (s) | Ent 1 rel area (%) | Ent 2 rel area (%) | e.e. (%) | $\ln\left(\frac{e.e._0}{e.e._t}\right)$ |
|---|---|---|---|---|
| 0 | 100.000 | 0.000 | 100.00 | 0.0000 |
| 120 | 99.110 | 0.890 | 98.22 | 0.0180 |
| 240 | 98.555 | 1.445 | 97.11 | 0.0293 |
| 480 | 97.580 | 2.420 | 95.16 | 0.0496 |
| 600 | 97.290 | 2.710 | 94.58 | 0.0557 |
| 720 | 96.225 | 3.775 | 92.45 | 0.0785 |
| 840 | 97.230 | 2.770 | 94.46 | 0.0570 |
| 960 | 96.855 | 3.145 | 93.71 | 0.0650 |
| 1080 | 96.425 | 3.575 | 92.85 | 0.0742 |
| 1200 | 96.085 | 3.915 | 92.17 | 0.0815 |
| 1500 | 93.800 | 6.200 | 87.60 | 0.1324 |
| 1800 | 94.875 | 5.125 | 89.75 | 0.1081 |
| 1800 | 94.890 | 5.110 | 89.78 | 0.1078 |
| 2400 | 93.930 | 6.070 | 87.86 | 0.1294 |
| 3000 | 92.820 | 7.180 | 85.64 | 0.1550 |
| 3300 | 92.710 | 7.290 | 85.42 | 0.1576 |
| 3600 | 90.995 | 9.005 | 81.99 | 0.1986 |
| 4500 | 90.370 | 9.630 | 80.74 | 0.2139 |
| 5400 | 87.615 | 12.385 | 75.23 | 0.2846 |
| 6300 | 87.450 | 12.550 | 74.90 | 0.2890 |
| 7200 | 84.425 | 15.575 | 68.85 | 0.3732 |
| 9000 | 83.370 | 16.630 | 66.74 | 0.4044 |
| 10800 | 80.185 | 19.815 | 60.37 | 0.5047 |
| 14400 | 75.800 | 24.200 | 51.60 | 0.6616 |
| 21600 | 67.495 | 32.505 | 34.99 | 1.0501 |
| 36000 | 61.365 | 38.635 | 22.73 | 1.4815 |

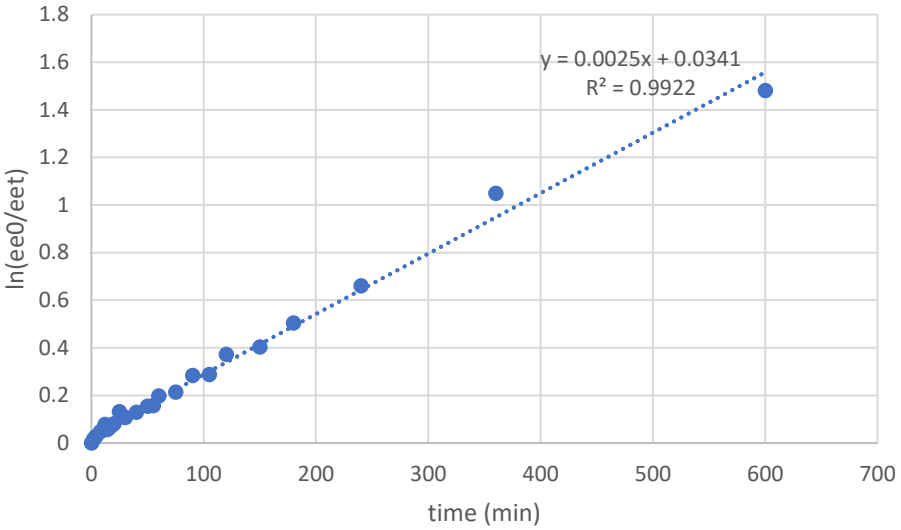



Figure S35 First order plot of erosion data for **131**

$m = k_{rac} = 4.2 \times 10^{-5}\ s^{-1}$

$k_{ent} = 2.1 \times 10^{-5}\ s^{-1}$

$\Delta G^{\ddagger}$ (155 °C) = 34.5 kcal $mol^{-1}$

$T_{½}$ (155 °C) = 273 min; $T_{½}$ (25 °C) = 36,000 years

## II.5.4 NMR Studies

**Dilution Study**

Dilution studies were carried out in toluene-$d_8$. Concentrations are volumetrically equivalent to the stated molalities (calculated for toluene-$h_8$).

| Conc (molal) | *N*-H Shift (ppm) | *O*-HShift (ppm) |
|---|---|---|
| 0.2 | 7.3311 | 5.2955 |
| 0.16 | 7.2865 | 5.2506 |
| 0.128 | 7.2778 | 5.2413 |
| 0.1024 | 7.2726 | 5.2371 |
| 0.08192 | 7.2614 | 5.2228 |
| 0.065536 | 7.2559 | 5.2175 |
| 0.052429 | 7.2488 | 5.2107 |
| 0.041943 | 7.2458 | 5.2072 |
| 0.033554 | 7.2437 | 5.2050 |
| 0.026844 | 7.2421 | 5.2029 |
| 0.021475 | 7.2404 | 5.2010 |
| 0.01718 | 7.2380 | 5.1983 |
| 0.013744 | 7.2376 | 5.1981 |

*N*-H Stacked

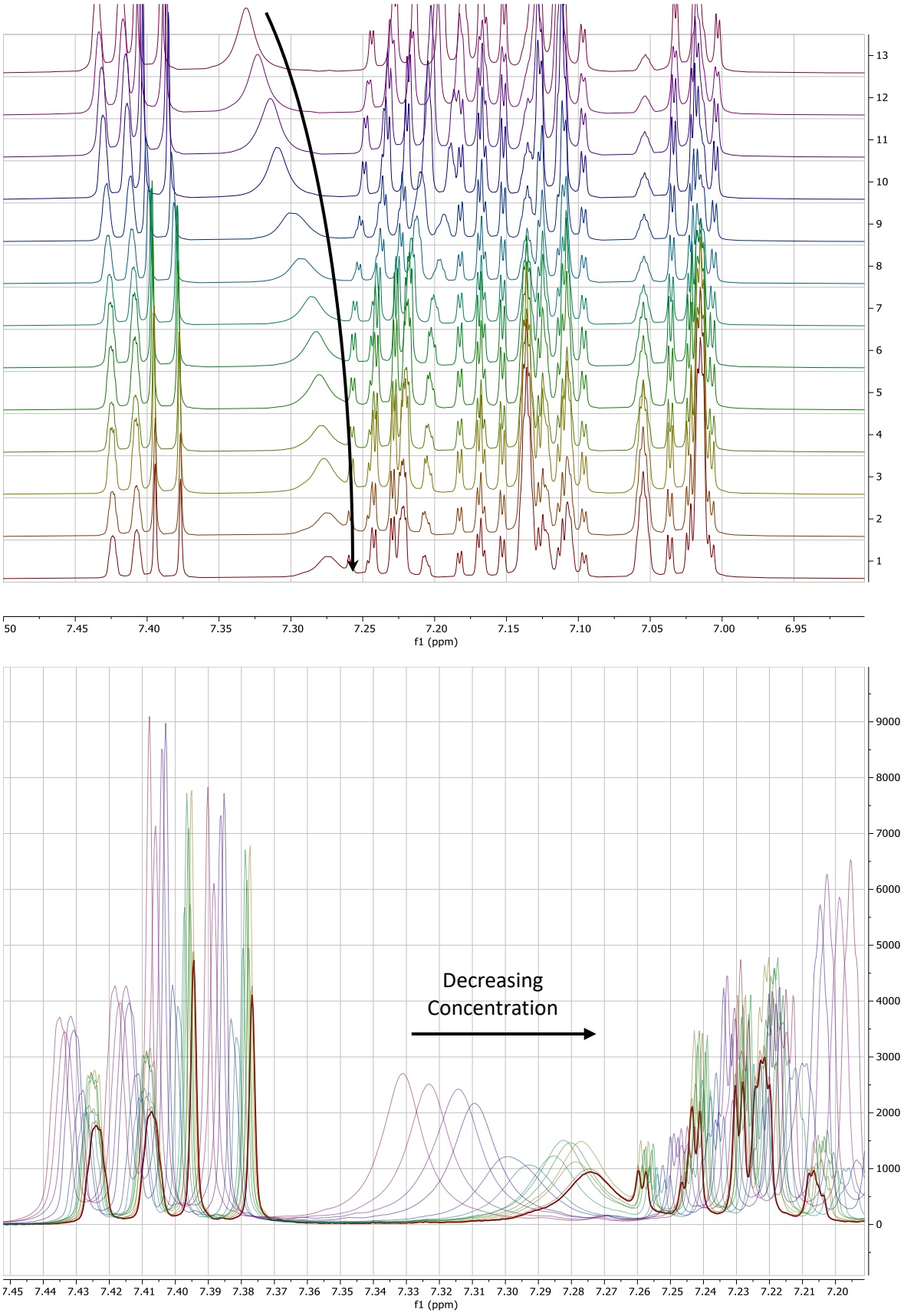



Figure S36 *N*-H shift decreases with concentration. Top: stacked; bottom: superimposed

*O*-H Stacked

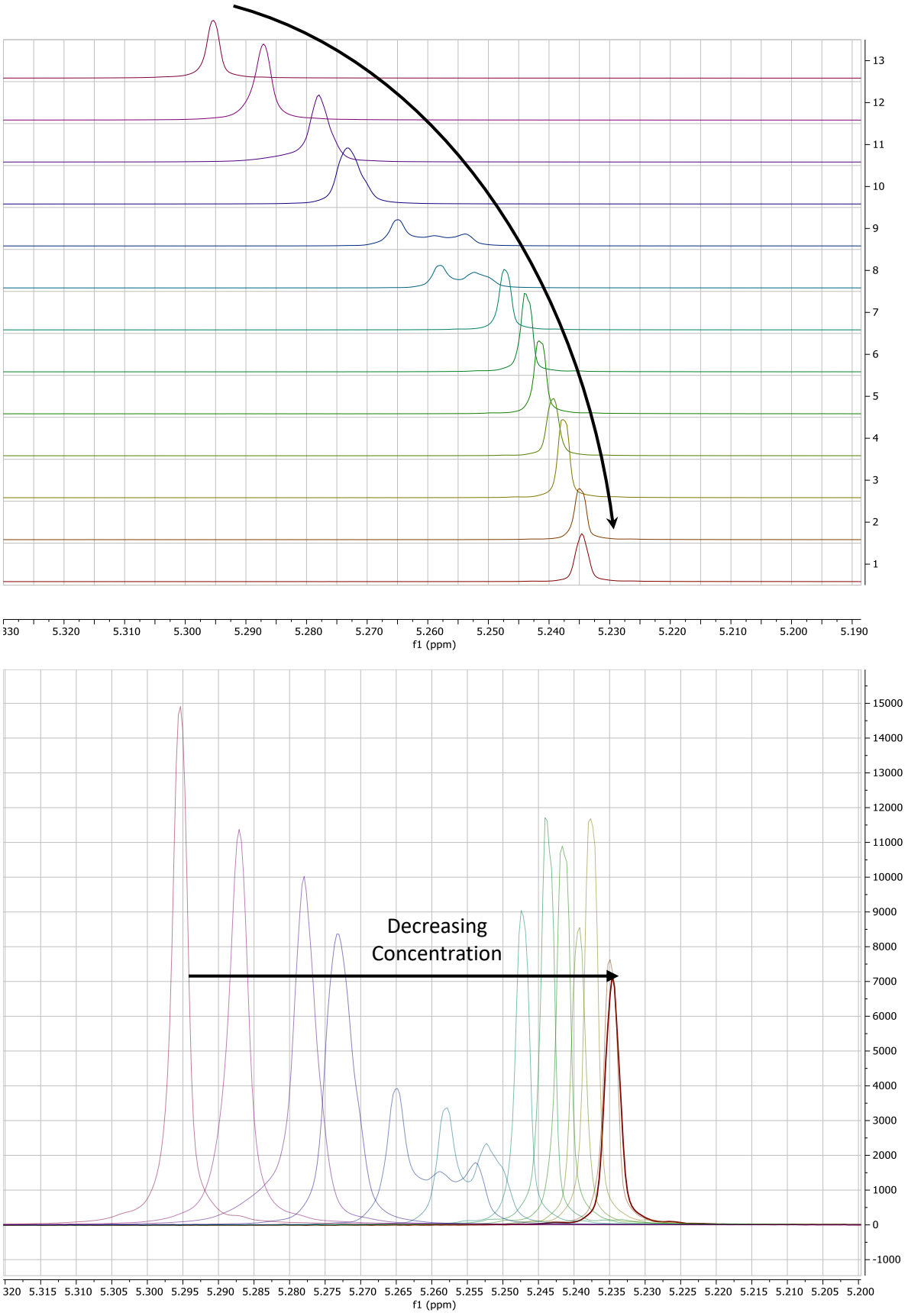



Figure S37 *O*-H shift decreases with concentration. Top: stacked; bottom: superimposed

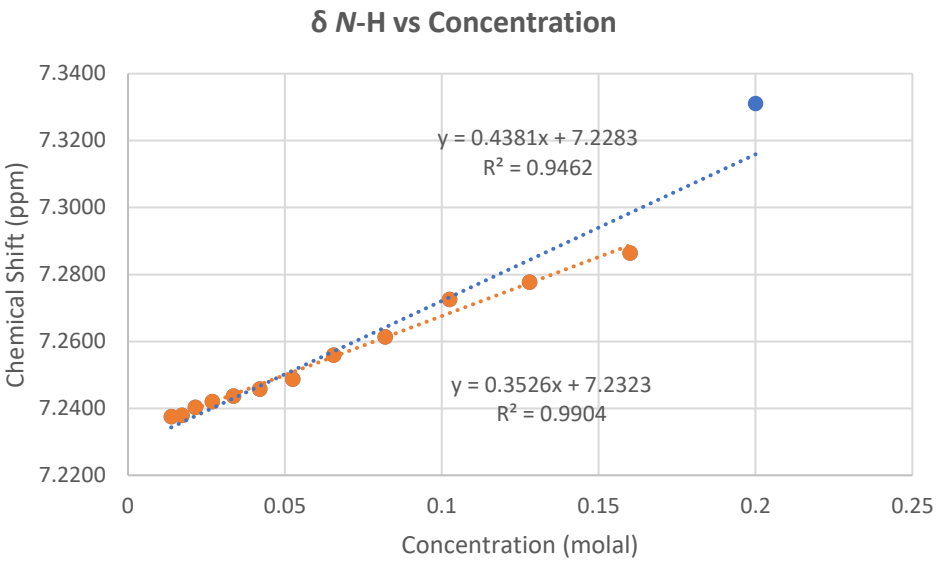



Figure S38 Plot of *N*-H shift vs. concentration

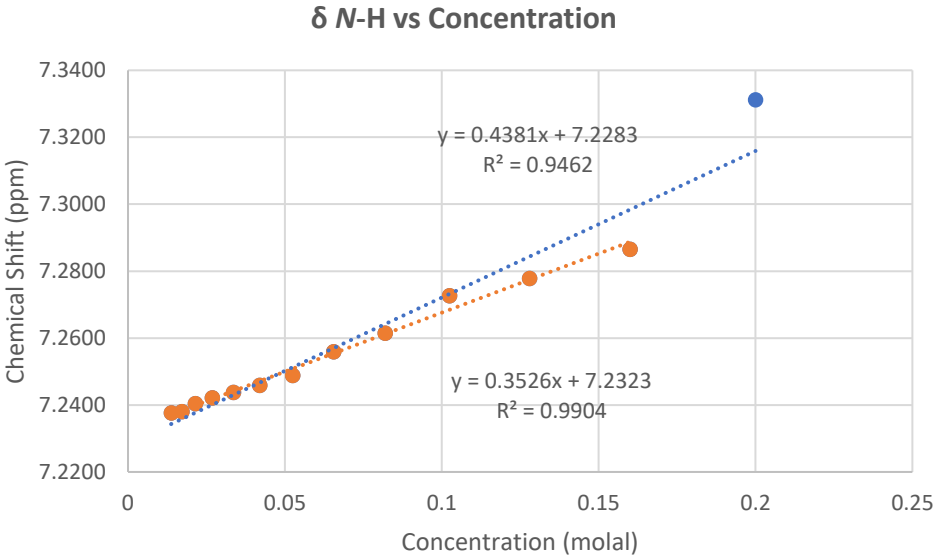



Figure S39 Plot of *O*-H shift vs. concentration

**DOSY**

DOSY spectra were collected for samples at 25 °C and at concentrations of 0.05 molal. Relaxation delays were set to 5 x the slowest relaxing nucleus of interest. Pulse lengths and delays were optimised to ensure that spectra at 95% gpz6 strength were 5 – 10% the intensity of spectra recorded at 5% gpz6 strength. Data were processed by applying line broadening of 1.0 Hz and zero filled to half the number of points recorded in the direct dimension (64k -> 32k)

2-D DOSY

## (ent)-126

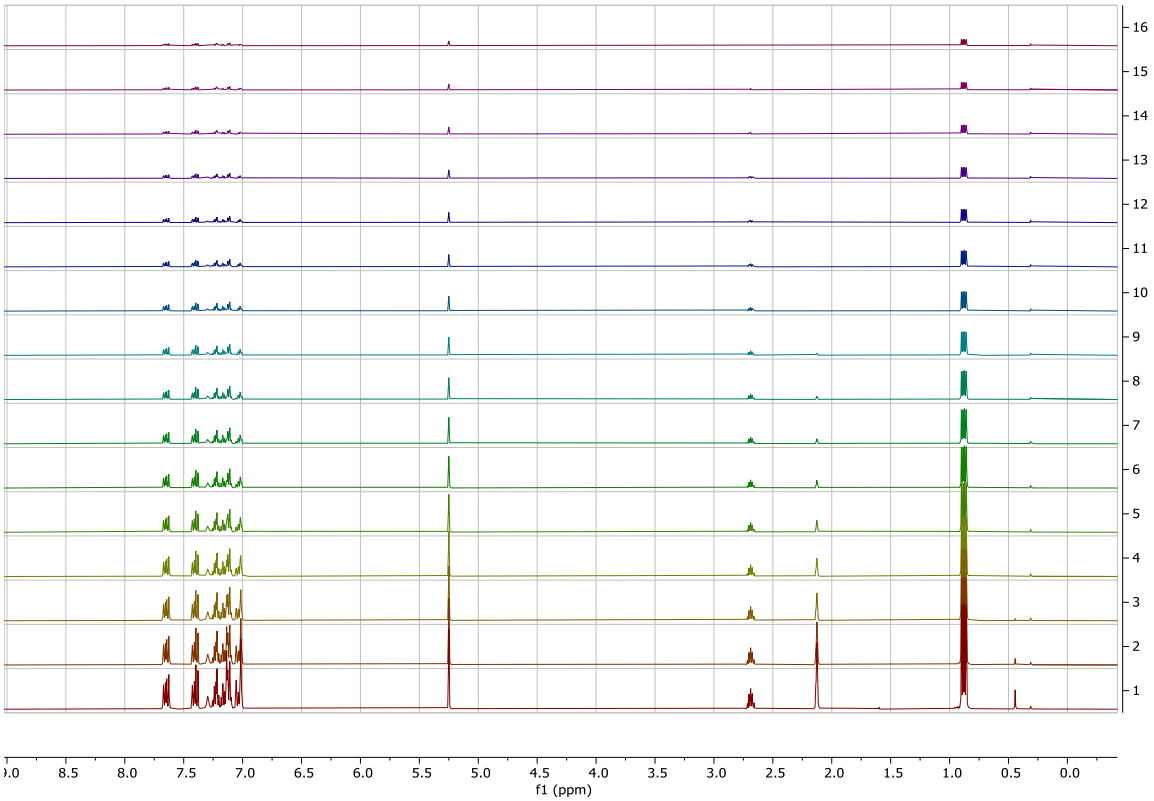



Figure S40 Stacked plot for (ent)-**126**

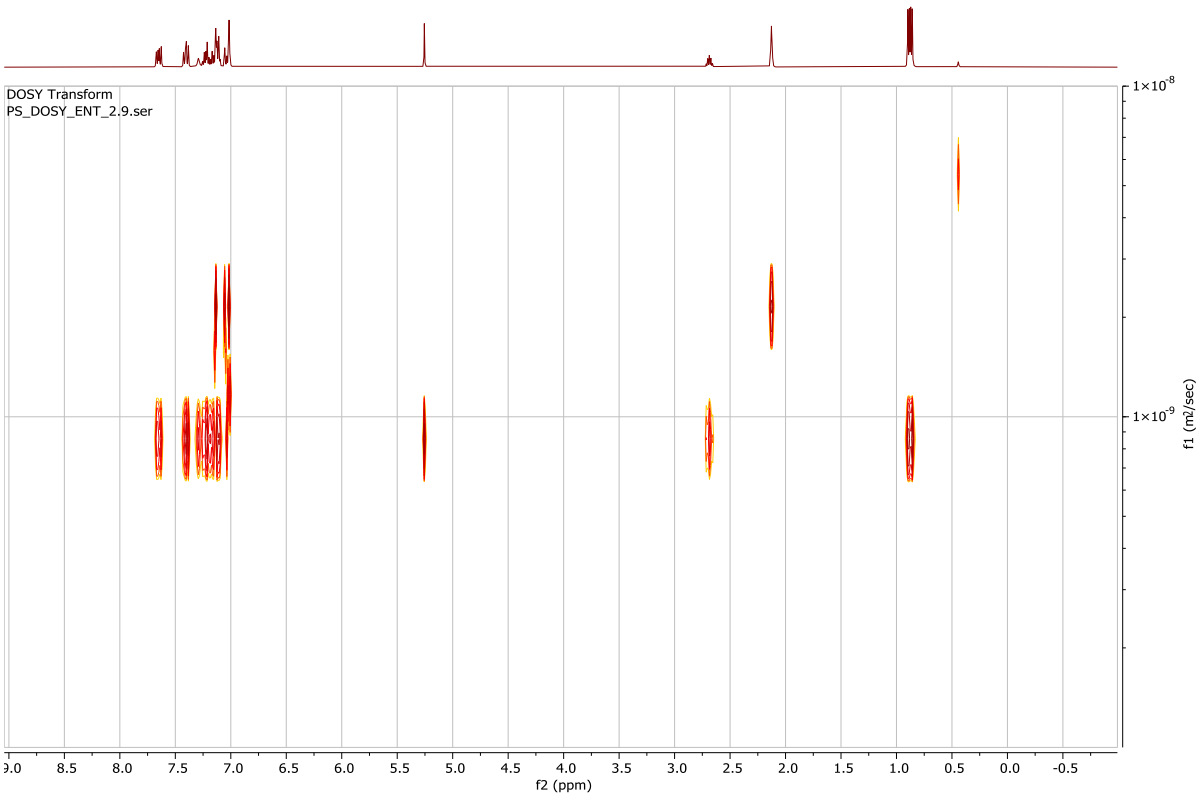
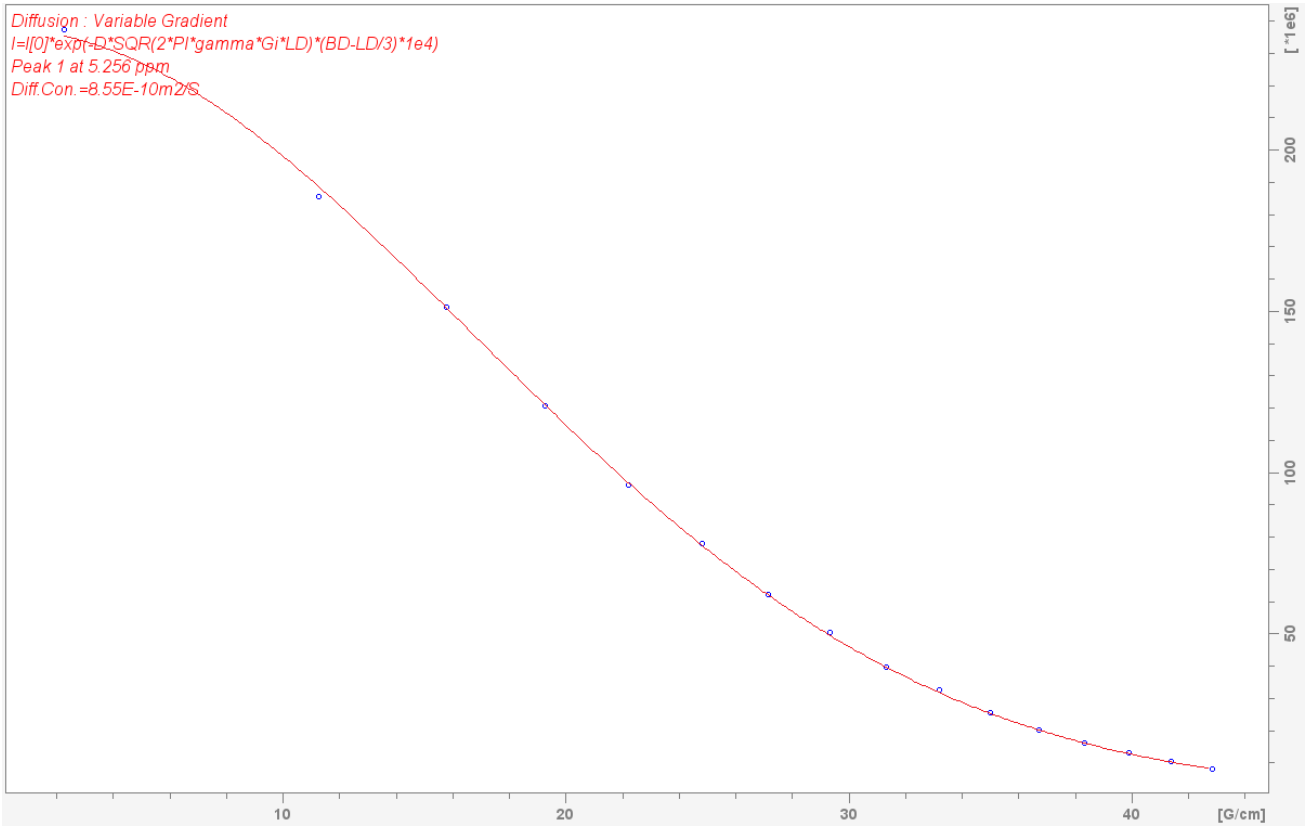



Figure S41 2-D plot for (ent)-**126**

Peak Fitting:

Points were fitted to: I=I[0]*exp(-D*SQR(2*PI*gamma*Gi*LD)*(BD-LD/3)*1e4)




16 points for Peak 1,

Peak Point = 5.256 ppm

Converged after 35 iterations!

Results Comp. 1

I[0] = 7.269e-01

Diff Con. = 8.550e-10 m2/s

Gamma = 4.258e+03 Hz/G

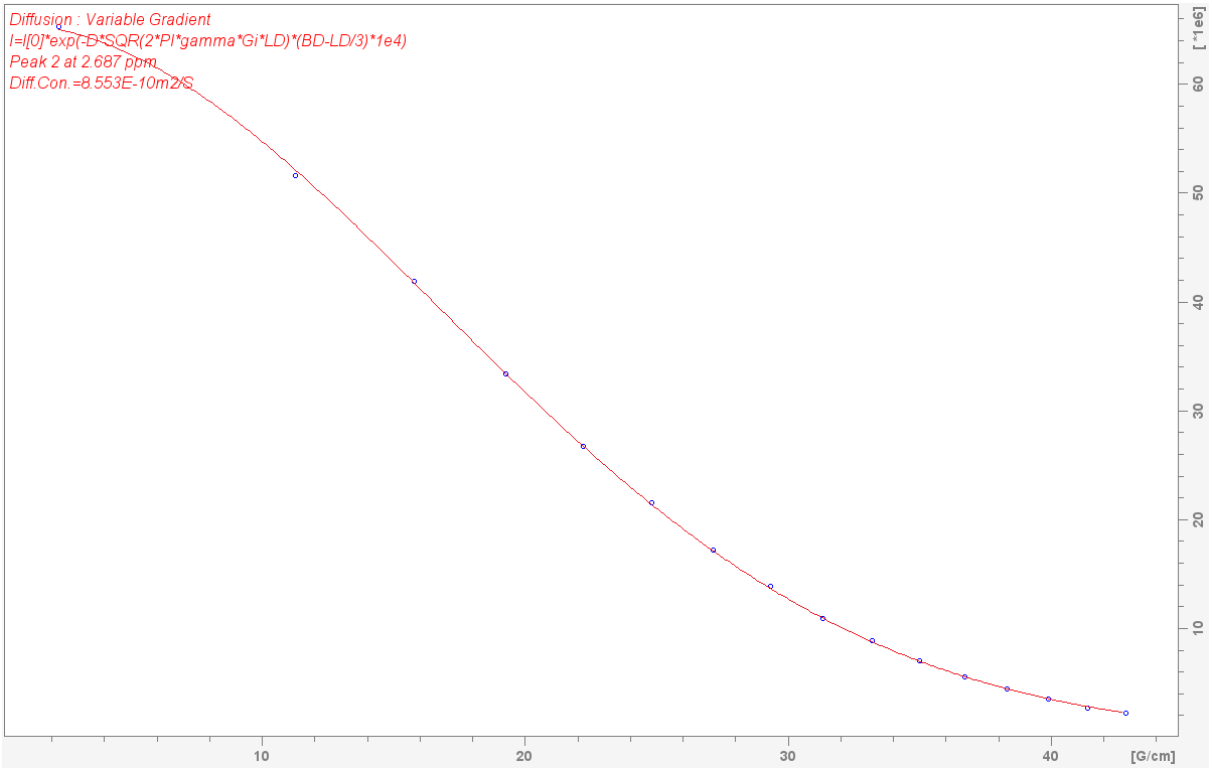
Little Delta = 2.000m

Big Delta = 74.900m

RSS = 1.348e-04

SD = 2.903e-03

| Point | Gradient | Expt | Calc | Difference |
|---|---|---|---|---|
| 1 | 2.25E+00 | 7.27E-01 | 7.20E-01 | -6.21E-03 |
| 2 | 1.13E+01 | 5.68E-01 | 5.77E-01 | 8.96E-03 |
| 3 | 1.58E+01 | 4.63E-01 | 4.62E-01 | -9.37E-04 |
| 4 | 1.93E+01 | 3.70E-01 | 3.70E-01 | 5.74E-04 |
| 5 | 2.22E+01 | 2.95E-01 | 2.97E-01 | 1.62E-03 |
| 6 | 2.48E+01 | 2.39E-01 | 2.38E-01 | -1.29E-03 |
| 7 | 2.72E+01 | 1.91E-01 | 1.91E-01 | -1.34E-04 |
| 8 | 2.93E+01 | 1.55E-01 | 1.53E-01 | -2.22E-03 |
| 9 | 3.13E+01 | 1.23E-01 | 1.22E-01 | -2.10E-04 |
| 10 | 3.32E+01 | 1.00E-01 | 9.80E-02 | -2.21E-03 |
| 11 | 3.50E+01 | 7.91E-02 | 7.85E-02 | -5.78E-04 |
| 12 | 3.67E+01 | 6.27E-02 | 6.29E-02 | 2.09E-04 |
| 13 | 3.83E+01 | 5.07E-02 | 5.04E-02 | -2.84E-04 |
| 14 | 3.99E+01 | 4.07E-02 | 4.04E-02 | -2.98E-04 |
| 15 | 4.14E+01 | 3.25E-02 | 3.24E-02 | -1.19E-04 |
| 16 | 4.28E+01 | 2.58E-02 | 2.59E-02 | 1.55E-04 |




16 points for Peak 2,

Peak Point = 2.687 ppm

Converged after 46 iterations!

Results Comp. 1

I[0] = 2.009e-01

Diff Con. = 8.553e-10 m2/s

Gamma = 4.258e+03 Hz/G

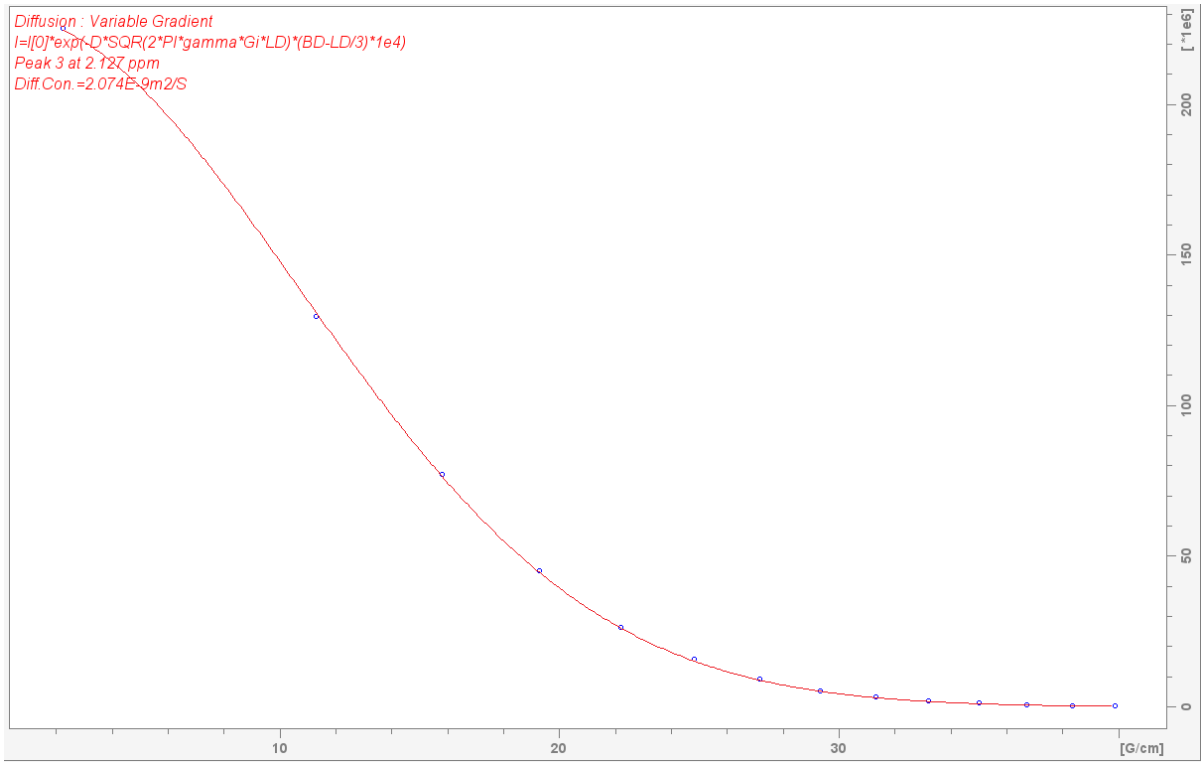
Little Delta = 2.000m

Big Delta = 74.900m

RSS = 3.295e-06

SD = 4.538e-04

| Point | Gradient | Expt | Calc | Difference |
|---|---|---|---|---|
| 1 | 2.25E+00 | 2.00E-01 | 1.99E-01 | -7.45E-04 |
| 2 | 1.13E+01 | 1.58E-01 | 1.60E-01 | 1.36E-03 |
| 3 | 1.58E+01 | 1.28E-01 | 1.28E-01 | -4.43E-04 |
| 4 | 1.93E+01 | 1.02E-01 | 1.02E-01 | 1.57E-04 |
| 5 | 2.22E+01 | 8.18E-02 | 8.20E-02 | 1.55E-04 |
| 6 | 2.48E+01 | 6.60E-02 | 6.57E-02 | -3.14E-04 |
| 7 | 2.72E+01 | 5.28E-02 | 5.26E-02 | -1.32E-04 |
| 8 | 2.93E+01 | 4.25E-02 | 4.22E-02 | -3.73E-04 |
| 9 | 3.13E+01 | 3.37E-02 | 3.38E-02 | 8.49E-05 |
| 10 | 3.32E+01 | 2.75E-02 | 2.71E-02 | -3.92E-04 |
| 11 | 3.50E+01 | 2.16E-02 | 2.17E-02 | 3.98E-05 |
| 12 | 3.67E+01 | 1.72E-02 | 1.74E-02 | 1.93E-04 |
| 13 | 3.83E+01 | 1.39E-02 | 1.39E-02 | 2.36E-05 |
| 14 | 3.99E+01 | 1.11E-02 | 1.12E-02 | 5.83E-05 |
| 15 | 4.14E+01 | 8.52E-03 | 8.93E-03 | 4.10E-04 |
| 16 | 4.28E+01 | 7.02E-03 | 7.16E-03 | 1.39E-04 |




14 points for Peak 3,

Peak Point = 2.127 ppm

Converged after 42 iterations!

Results Comp. 1

I[0] = 7.019e-01

Diff Con. = 2.074e-09 m2/s

Gamma = 4.258e+03 Hz/G

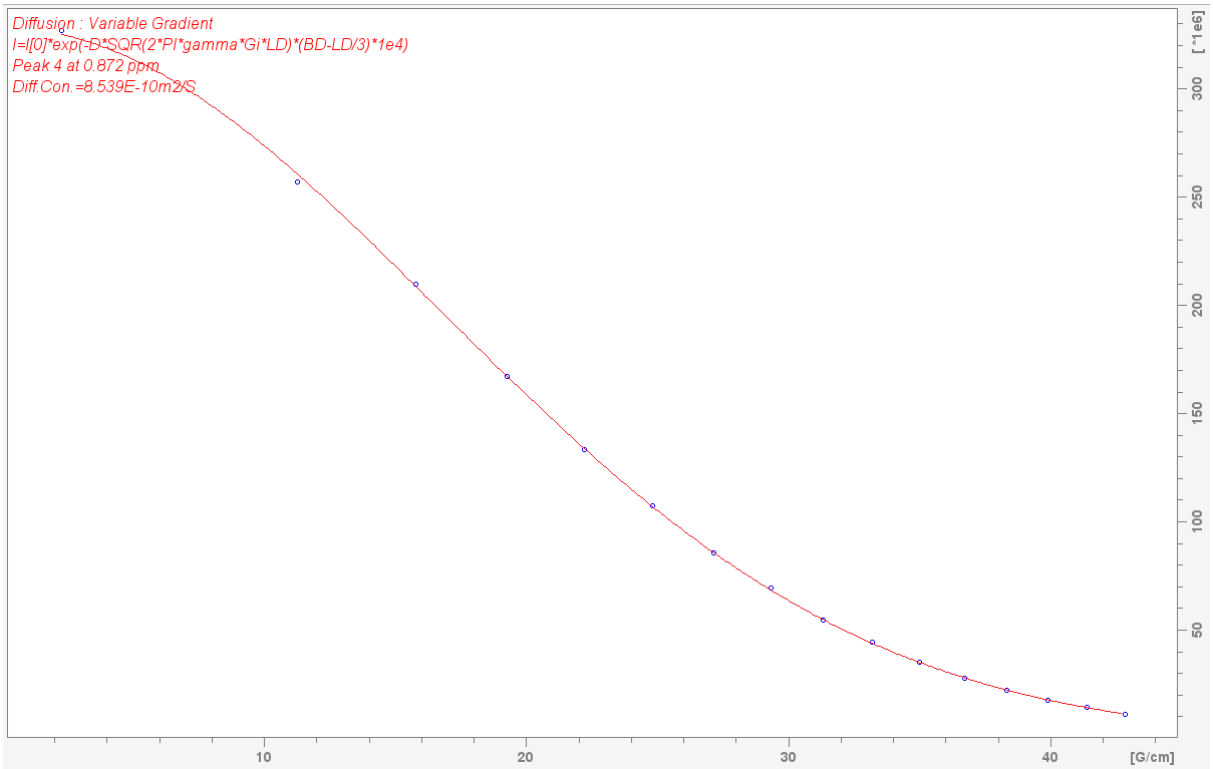
Little Delta = 2.000m

Big Delta = 74.900m

RSS = 3.375e-05

SD = 1.553e-03

| Point | Gradient | Expt | Calc | Difference |
|---|---|---|---|---|
| 1 | 2.25E+00 | 6.88E-01 | 6.86E-01 | -1.82E-03 |
| 2 | 1.13E+01 | 3.96E-01 | 4.01E-01 | 4.81E-03 |
| 3 | 1.58E+01 | 2.36E-01 | 2.34E-01 | -1.64E-03 |
| 4 | 1.93E+01 | 1.38E-01 | 1.37E-01 | -1.04E-03 |
| 5 | 2.22E+01 | 8.05E-02 | 7.99E-02 | -5.90E-04 |
| 6 | 2.48E+01 | 4.80E-02 | 4.67E-02 | -1.26E-03 |
| 7 | 2.72E+01 | 2.82E-02 | 2.73E-02 | -9.30E-04 |
| 8 | 2.93E+01 | 1.64E-02 | 1.59E-02 | -4.47E-04 |
| 9 | 3.13E+01 | 9.62E-03 | 9.31E-03 | -3.11E-04 |
| 10 | 3.32E+01 | 5.84E-03 | 5.44E-03 | -4.04E-04 |
| 11 | 3.50E+01 | 3.59E-03 | 3.18E-03 | -4.17E-04 |
| 12 | 3.67E+01 | 1.83E-03 | 1.86E-03 | 2.55E-05 |
| 13 | 3.83E+01 | 1.28E-03 | 1.08E-03 | -1.94E-04 |
| 14 | 3.99E+01 | 7.21E-04 | 6.33E-04 | -8.79E-05 |




16 points for Peak 4,

Peak Point = 0.872 ppm

Converged after 30 iterations!

Results Comp. 1

I[0] = 1.004e+00

Diff Con. = 8.539e-10 m2/s

Gamma = 4.258e+03 Hz/G

Little Delta = 2.000m

Big Delta = 74.900m

RSS = 1.718e-04

SD = 3.277e-03

| Point | Gradient | Expt | Calc | Difference |
|---|---|---|---|---|
| 1 | 2.25E+00 | 1.00E+00 | 9.94E-01 | -5.70E-03 |
| 2 | 1.13E+01 | 7.87E-01 | 7.97E-01 | 1.04E-02 |
| 3 | 1.58E+01 | 6.42E-01 | 6.39E-01 | -3.26E-03 |
| 4 | 1.93E+01 | 5.12E-01 | 5.12E-01 | -4.36E-04 |
| 5 | 2.22E+01 | 4.09E-01 | 4.10E-01 | 1.60E-03 |
| 6 | 2.48E+01 | 3.30E-01 | 3.29E-01 | -1.15E-03 |
| 7 | 2.72E+01 | 2.63E-01 | 2.64E-01 | 4.27E-04 |
| 8 | 2.93E+01 | 2.14E-01 | 2.11E-01 | -2.78E-03 |
| 9 | 3.13E+01 | 1.69E-01 | 1.69E-01 | 1.46E-04 |
| 10 | 3.32E+01 | 1.38E-01 | 1.36E-01 | -2.34E-03 |
| 11 | 3.50E+01 | 1.09E-01 | 1.09E-01 | -1.91E-04 |
| 12 | 3.67E+01 | 8.63E-02 | 8.71E-02 | 8.58E-04 |
| 13 | 3.83E+01 | 6.94E-02 | 6.98E-02 | 4.05E-04 |
| 14 | 3.99E+01 | 5.55E-02 | 5.60E-02 | 4.31E-04 |
| 15 | 4.14E+01 | 4.46E-02 | 4.48E-02 | 2.38E-04 |
| 16 | 4.28E+01 | 3.48E-02 | 3.59E-02 | 1.14E-03 |

## rac-126

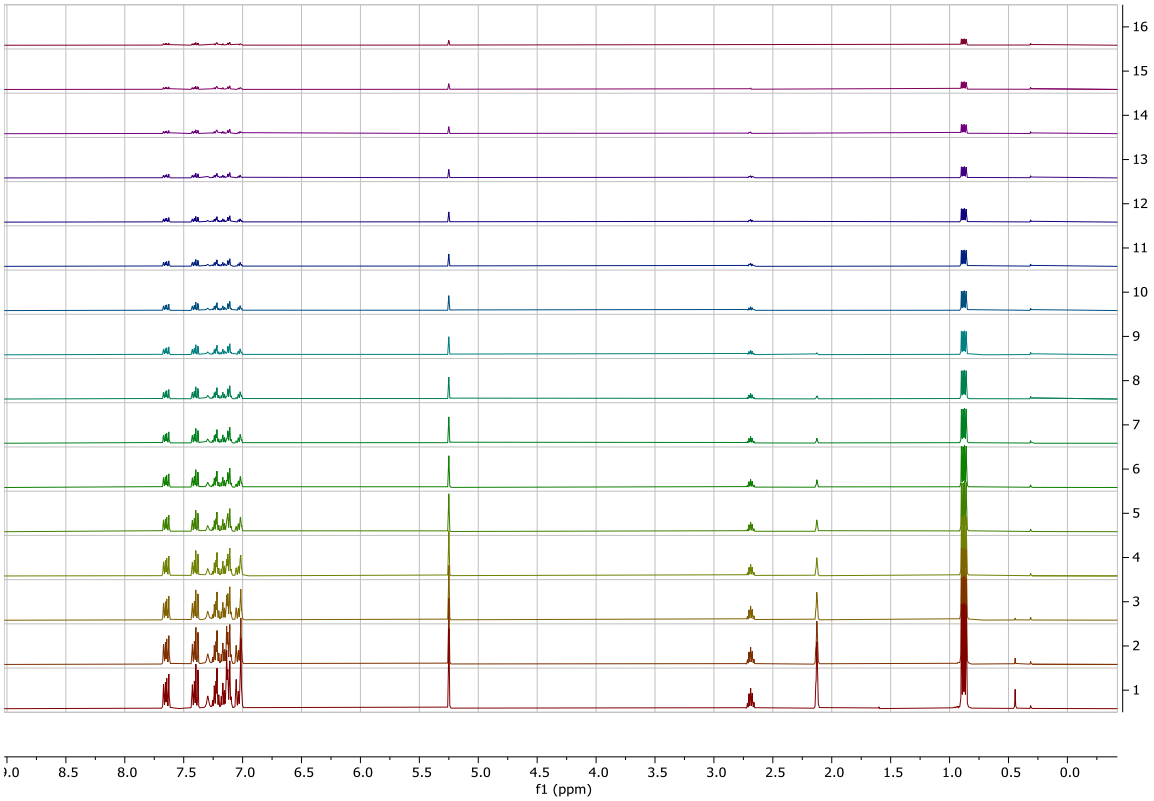



Figure S42 Stacked plot for (rac)-**126**

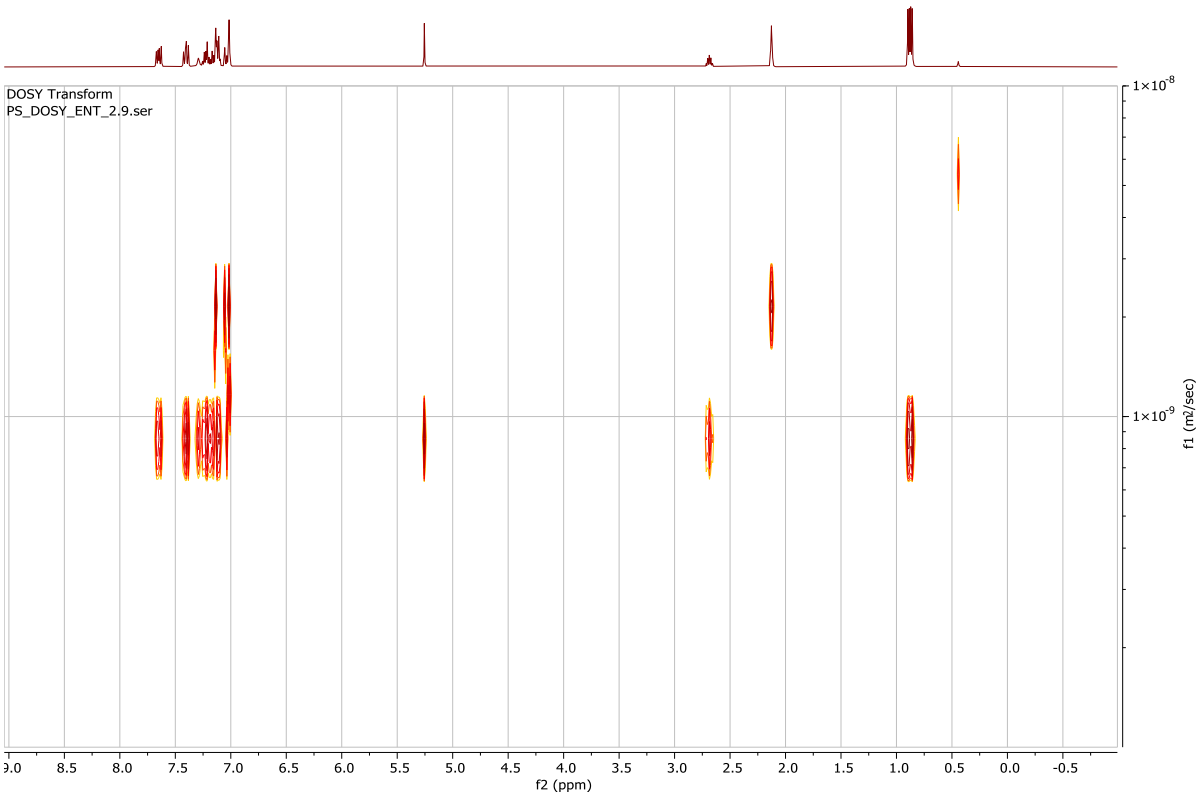
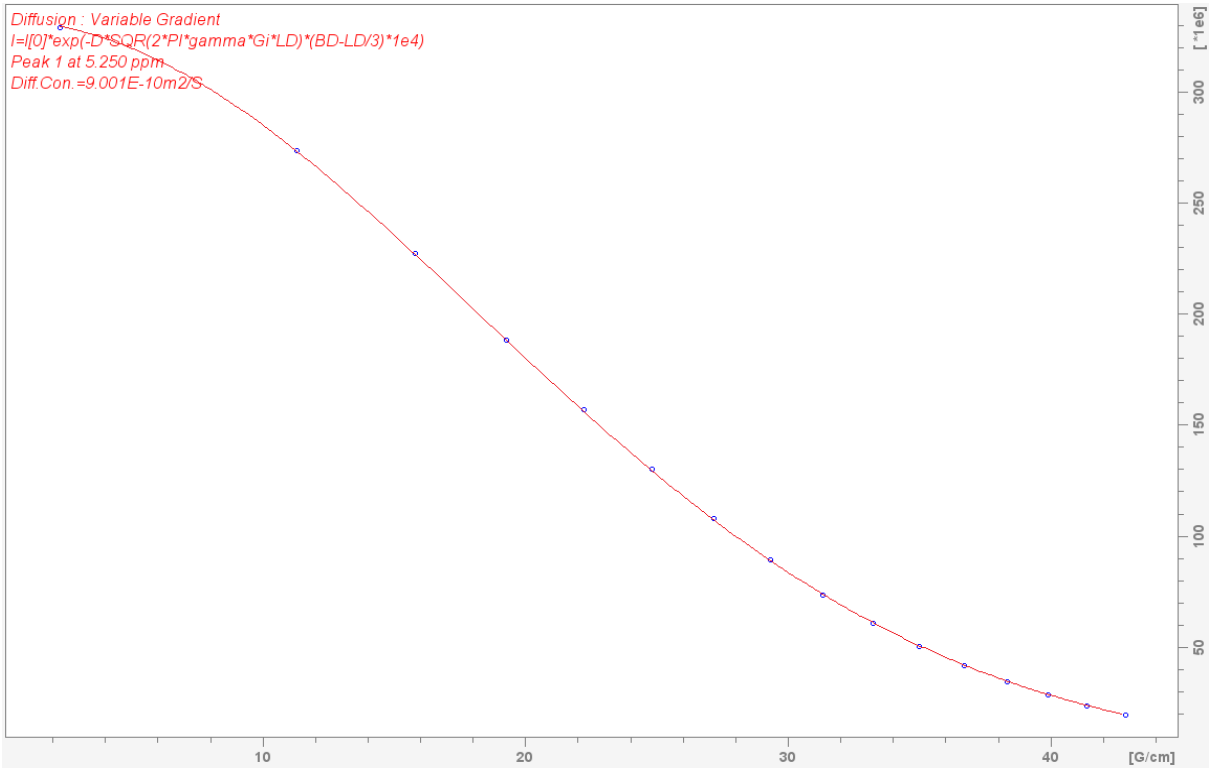



Figure S 43 2-D plot for (rac)-**126**

Peak Fitting:

Points were fitted to: I=I[0]*exp(-D*SQR(2*PI*gamma*Gi*LD)*(BD-LD/3)*1e4)




16 points for Peak 1,

Peak Point = 5.250 ppm

Converged after 37 iterations!

Results Comp. 1

I[0] = 7.636e-01

Diff Con. = 9.001e-10 m2/s

Gamma = 4.258e+03 Hz/G

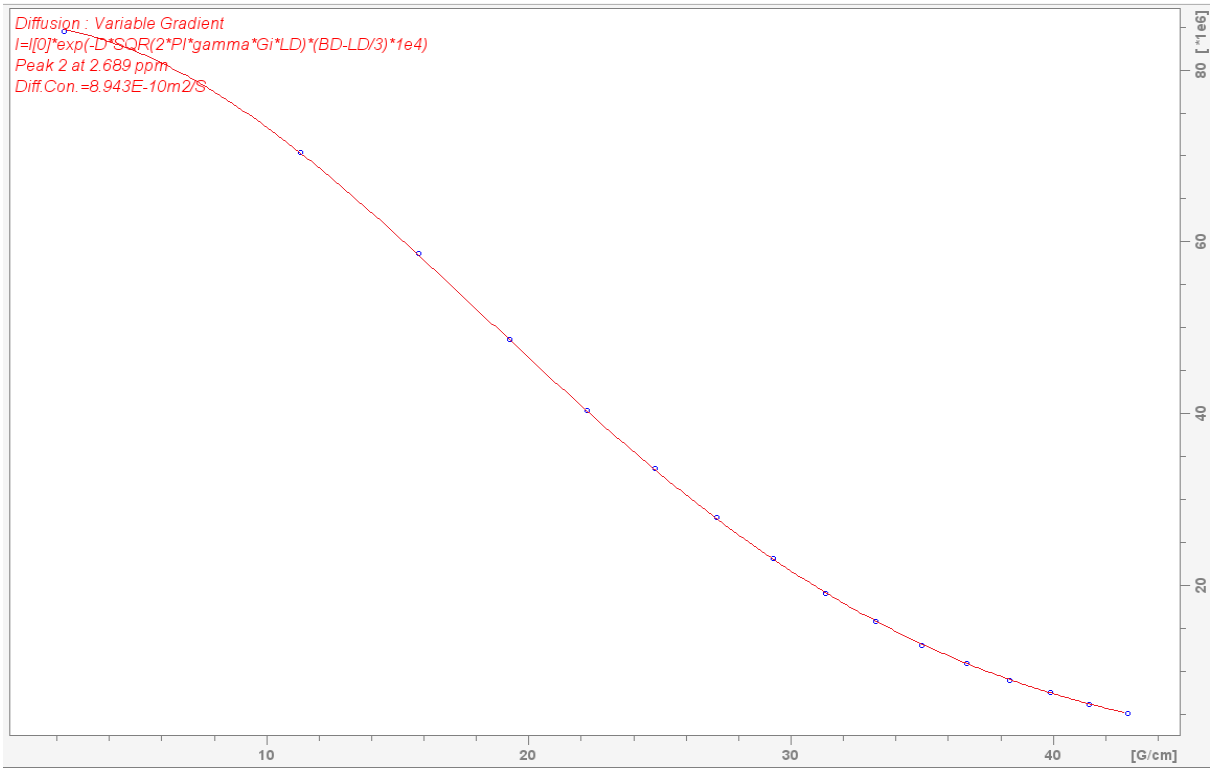
Little Delta = 2.000m

Big Delta = 59.900m

RSS = 1.279e-05

SD = 8.940e-04

| Point | Gradient | Expt | Calc | Difference |
|---|---|---|---|---|
| 1 | 2.25E+00 | 7.57E-01 | 7.58E-01 | 1.20E-03 |
| 2 | 1.13E+01 | 6.29E-01 | 6.29E-01 | 1.32E-04 |
| 3 | 1.58E+01 | 5.23E-01 | 5.22E-01 | -5.37E-04 |
| 4 | 1.93E+01 | 4.34E-01 | 4.33E-01 | -3.80E-04 |
| 5 | 2.22E+01 | 3.61E-01 | 3.60E-01 | -1.23E-03 |
| 6 | 2.48E+01 | 3.00E-01 | 2.99E-01 | -1.37E-03 |
| 7 | 2.72E+01 | 2.49E-01 | 2.48E-01 | -1.36E-03 |
| 8 | 2.93E+01 | 2.06E-01 | 2.06E-01 | 3.19E-05 |
| 9 | 3.13E+01 | 1.70E-01 | 1.71E-01 | 6.01E-04 |
| 10 | 3.32E+01 | 1.41E-01 | 1.42E-01 | 8.45E-04 |
| 11 | 3.50E+01 | 1.17E-01 | 1.18E-01 | 1.01E-03 |
| 12 | 3.67E+01 | 9.65E-02 | 9.77E-02 | 1.24E-03 |
| 13 | 3.83E+01 | 8.05E-02 | 8.11E-02 | 6.41E-04 |
| 14 | 3.99E+01 | 6.64E-02 | 6.73E-02 | 9.27E-04 |
| 15 | 4.14E+01 | 5.51E-02 | 5.59E-02 | 7.80E-04 |
| 16 | 4.28E+01 | 4.60E-02 | 4.64E-02 | 4.02E-04 |




16 points for Peak 2,

Peak Point = 2.689 ppm

Converged after 52 iterations!

Results Comp. 1

I[0] = 1.963e-01

Diff Con. = 8.943e-10 m2/s

Gamma = 4.258e+03 Hz/G

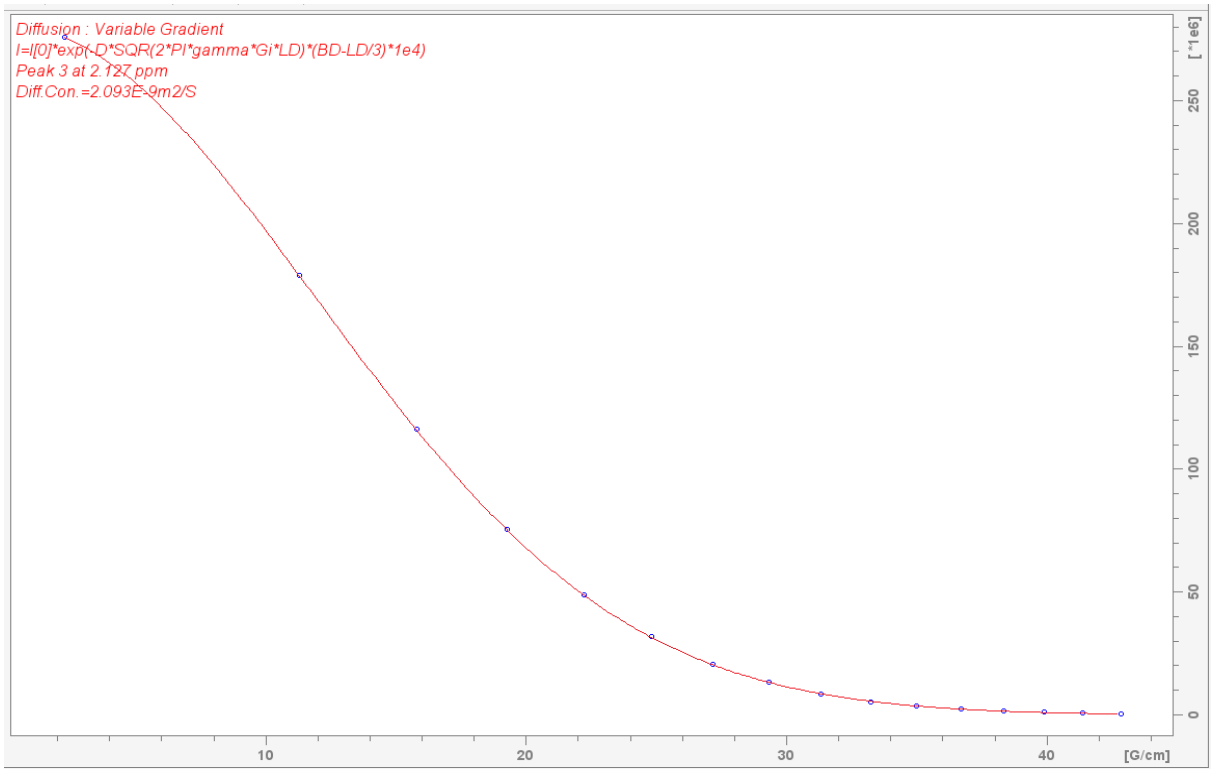
Little Delta = 2.000m

Big Delta = 59.900m

RSS = 1.129e-06

SD = 2.656e-04

| Point | Gradient | Expt | Calc | Difference |
|---|---|---|---|---|
| 1 | 2.25E+00 | 1.94E-01 | 1.95E-01 | 5.13E-04 |
| 2 | 1.13E+01 | 1.62E-01 | 1.62E-01 | -9.11E-05 |
| 3 | 1.58E+01 | 1.35E-01 | 1.35E-01 | -4.16E-04 |
| 4 | 1.93E+01 | 1.12E-01 | 1.12E-01 | -1.91E-04 |
| 5 | 2.22E+01 | 9.31E-02 | 9.30E-02 | -1.10E-04 |
| 6 | 2.48E+01 | 7.76E-02 | 7.73E-02 | -3.58E-04 |
| 7 | 2.72E+01 | 6.44E-02 | 6.42E-02 | -1.39E-04 |
| 8 | 2.93E+01 | 5.35E-02 | 5.34E-02 | -1.13E-04 |
| 9 | 3.13E+01 | 4.42E-02 | 4.44E-02 | 1.55E-04 |
| 10 | 3.32E+01 | 3.66E-02 | 3.69E-02 | 2.82E-04 |
| 11 | 3.50E+01 | 3.03E-02 | 3.06E-02 | 3.13E-04 |
| 12 | 3.67E+01 | 2.53E-02 | 2.55E-02 | 2.10E-04 |
| 13 | 3.83E+01 | 2.08E-02 | 2.12E-02 | 4.01E-04 |
| 14 | 3.99E+01 | 1.76E-02 | 1.76E-02 | -3.83E-05 |
| 15 | 4.14E+01 | 1.44E-02 | 1.46E-02 | 2.41E-04 |
| 16 | 4.28E+01 | 1.21E-02 | 1.22E-02 | 9.92E-05 |




16 points for Peak 3,

Peak Point = 2.127 ppm

Converged after 47 iterations!

Results Comp. 1

I[0] = 6.450e-01

Diff Con. = 2.093e-09 m2/s

Gamma = 4.258e+03 Hz/G

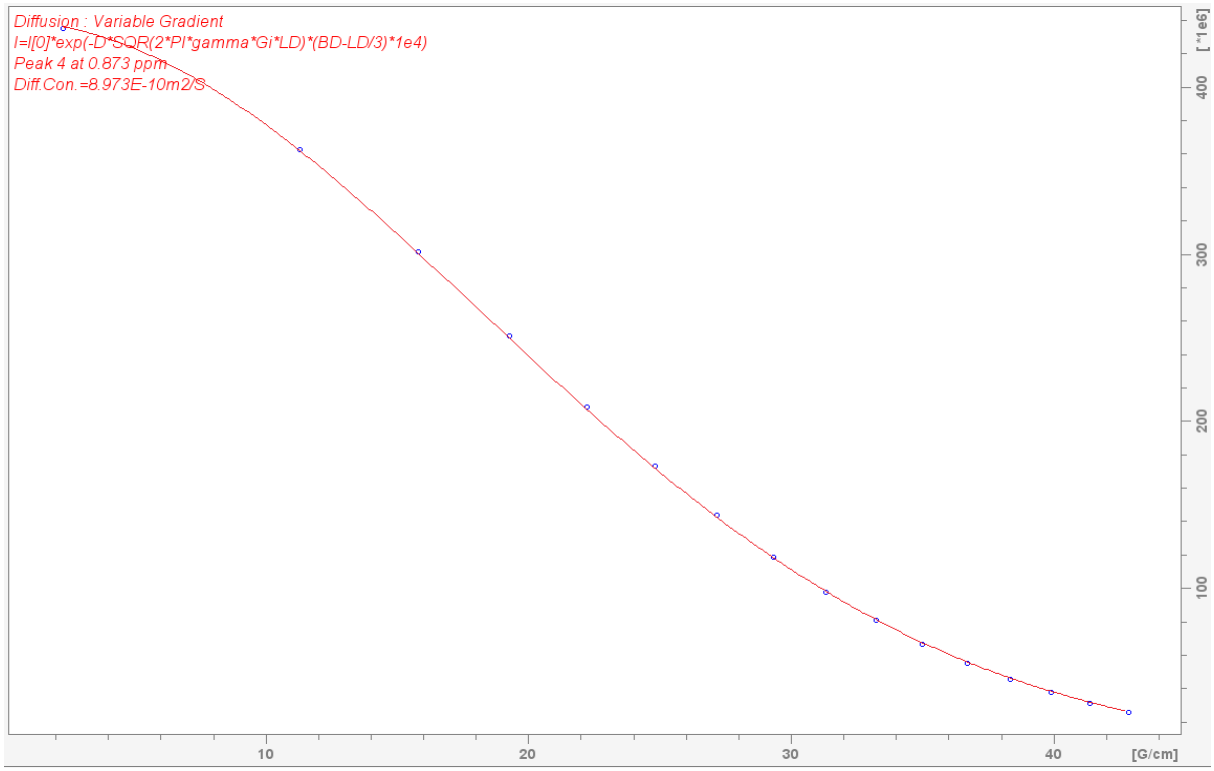
Little Delta = 2.000m

Big Delta = 59.900m

RSS = 6.751e-07

SD = 2.054e-04

| Point | Gradient | Expt | Calc | Difference |
|---|---|---|---|---|
| 1 | 2.25E+00 | 6.33E-01 | 6.34E-01 | 9.34E-05 |
| 2 | 1.13E+01 | 4.11E-01 | 4.11E-01 | -4.46E-05 |
| 3 | 1.58E+01 | 2.67E-01 | 2.67E-01 | -4.10E-05 |
| 4 | 1.93E+01 | 1.73E-01 | 1.73E-01 | -3.17E-04 |
| 5 | 2.22E+01 | 1.12E-01 | 1.12E-01 | -2.41E-05 |
| 6 | 2.48E+01 | 7.29E-02 | 7.28E-02 | -1.10E-04 |
| 7 | 2.72E+01 | 4.70E-02 | 4.72E-02 | 1.59E-04 |
| 8 | 2.93E+01 | 3.03E-02 | 3.06E-02 | 3.66E-04 |
| 9 | 3.13E+01 | 1.95E-02 | 1.99E-02 | 4.00E-04 |
| 10 | 3.32E+01 | 1.25E-02 | 1.29E-02 | 4.13E-04 |
| 11 | 3.50E+01 | 8.17E-03 | 8.36E-03 | 1.86E-04 |
| 12 | 3.67E+01 | 5.32E-03 | 5.42E-03 | 1.00E-04 |
| 13 | 3.83E+01 | 3.54E-03 | 3.52E-03 | -2.01E-05 |
| 14 | 3.99E+01 | 2.36E-03 | 2.28E-03 | -7.99E-05 |
| 15 | 4.14E+01 | 1.57E-03 | 1.48E-03 | -8.92E-05 |
| 16 | 4.28E+01 | 9.58E-04 | 9.60E-04 | 1.54E-06 |




16 points for Peak 4,

Peak Point = 0.873 ppm

Converged after 29 iterations!

Results Comp. 1

I[0] = 1.011e+00

Diff Con. = 8.973e-10 m2/s

Gamma = 4.258e+03 Hz/G

Little Delta = 2.000m

Big Delta = 59.900m

RSS = 5.660e-05

SD = 1.881e-03

| Point | Gradient | Expt | Calc | Difference |
|---|---|---|---|---|
| 1 | 2.25E+00 | 1.00E+00 | 1.00E+00 | 3.66E-03 |
| 2 | 1.13E+01 | 8.35E-01 | 8.34E-01 | -1.01E-03 |
| 3 | 1.58E+01 | 6.93E-01 | 6.92E-01 | -9.96E-04 |
| 4 | 1.93E+01 | 5.77E-01 | 5.75E-01 | -2.30E-03 |
| 5 | 2.22E+01 | 4.80E-01 | 4.78E-01 | -2.62E-03 |
| 6 | 2.48E+01 | 3.99E-01 | 3.97E-01 | -1.95E-03 |
| 7 | 2.72E+01 | 3.31E-01 | 3.30E-01 | -1.72E-03 |
| 8 | 2.93E+01 | 2.74E-01 | 2.74E-01 | 2.55E-04 |
| 9 | 3.13E+01 | 2.26E-01 | 2.27E-01 | 1.16E-03 |
| 10 | 3.32E+01 | 1.87E-01 | 1.89E-01 | 1.95E-03 |
| 11 | 3.50E+01 | 1.55E-01 | 1.57E-01 | 2.04E-03 |
| 12 | 3.67E+01 | 1.28E-01 | 1.30E-01 | 1.96E-03 |
| 13 | 3.83E+01 | 1.06E-01 | 1.08E-01 | 1.88E-03 |
| 14 | 3.99E+01 | 8.83E-02 | 8.99E-02 | 1.64E-03 |
| 15 | 4.14E+01 | 7.32E-02 | 7.47E-02 | 1.48E-03 |
| 16 | 4.28E+01 | 6.12E-02 | 6.20E-02 | 8.20E-04 |

**rac-131**

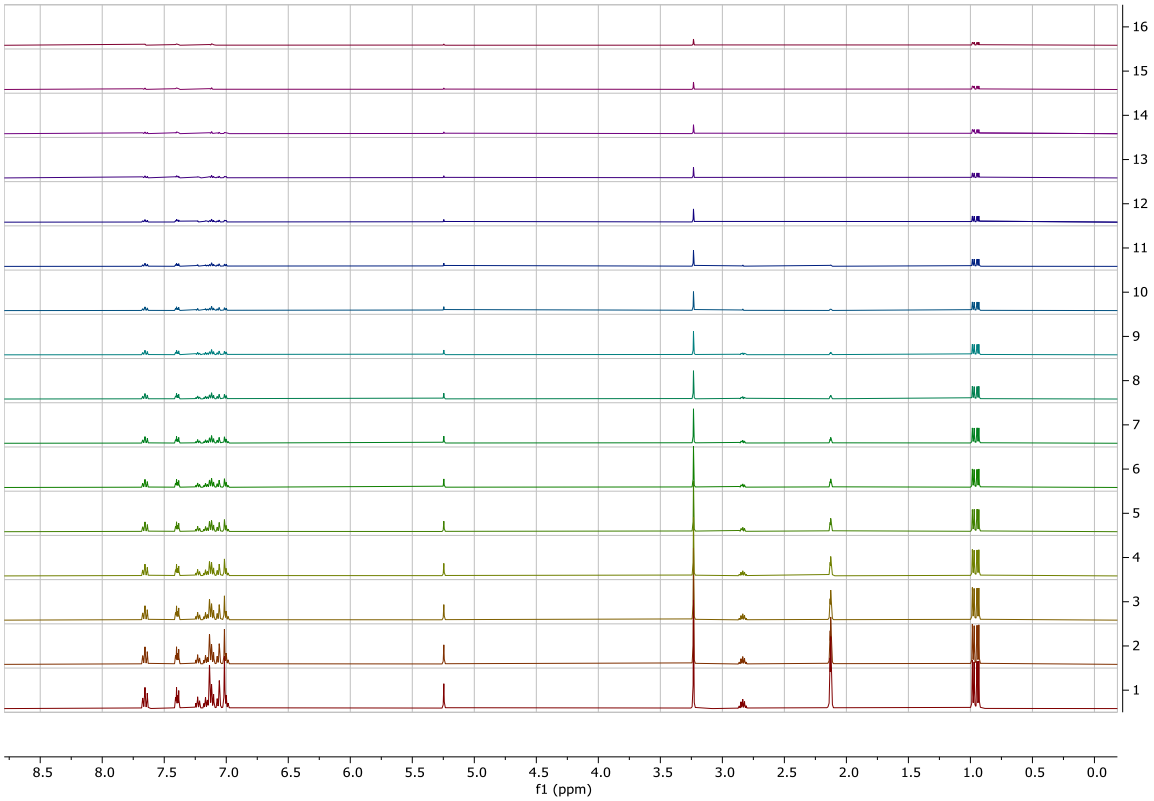



Figure S44 Stacked plot for (rac)-**131**

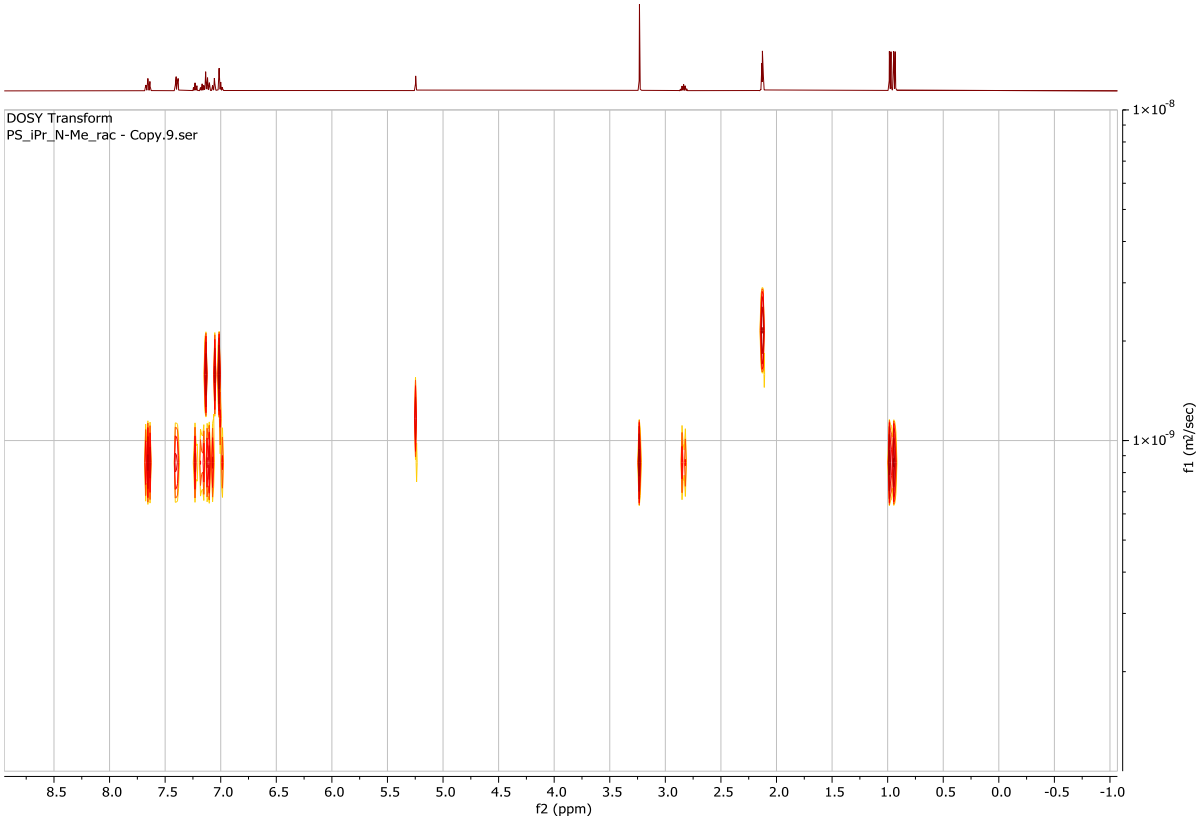
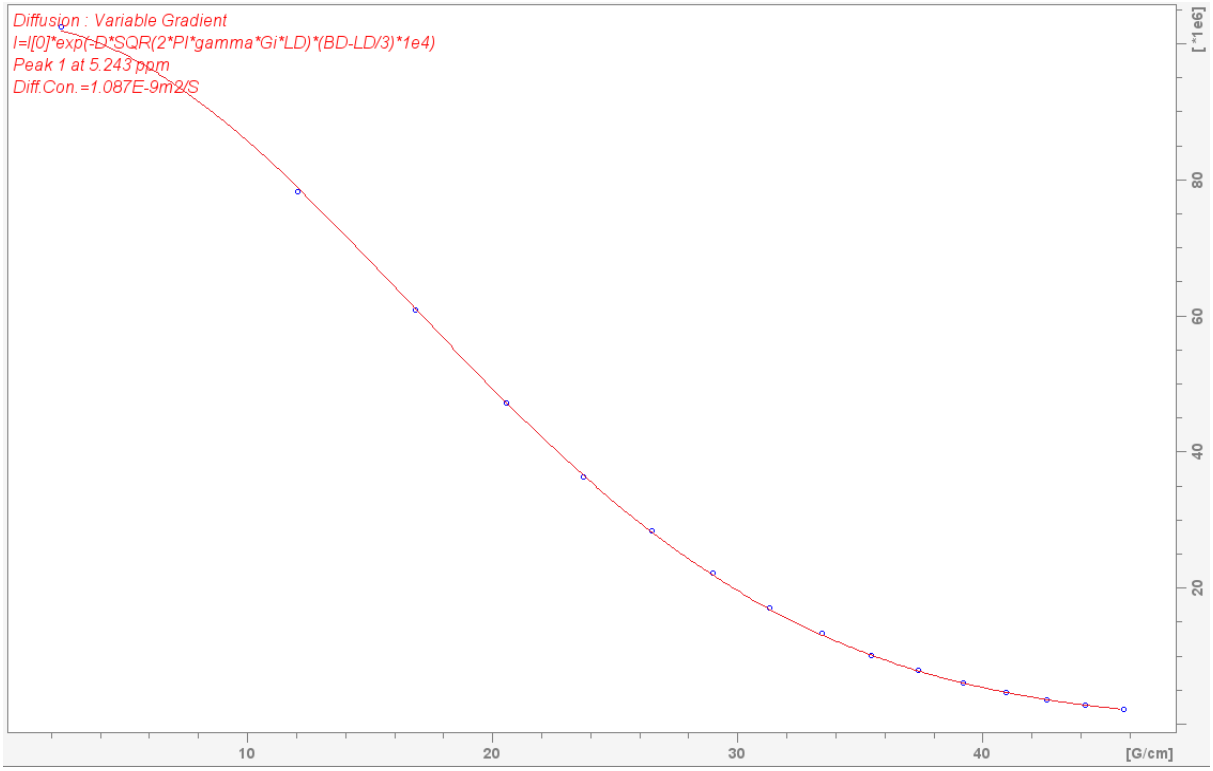



Figure S45 2-D plot for (rac)-**131**

Peak Fitting:
Points were fitted to: I=I[0]*exp(-D*SQR(2*PI*gamma*Gi*LD)*(BD-LD/3)*1e4)

*N-Me,* ***131***




16 points for Peak 1,

Peak Point = 5.243 ppm

Converged after 50 iterations!

Results Comp. 1

I[0] = 2.627e-01

Diff Con. = 1.087e-09 m2/s

Gamma = 4.258e+03 Hz/G

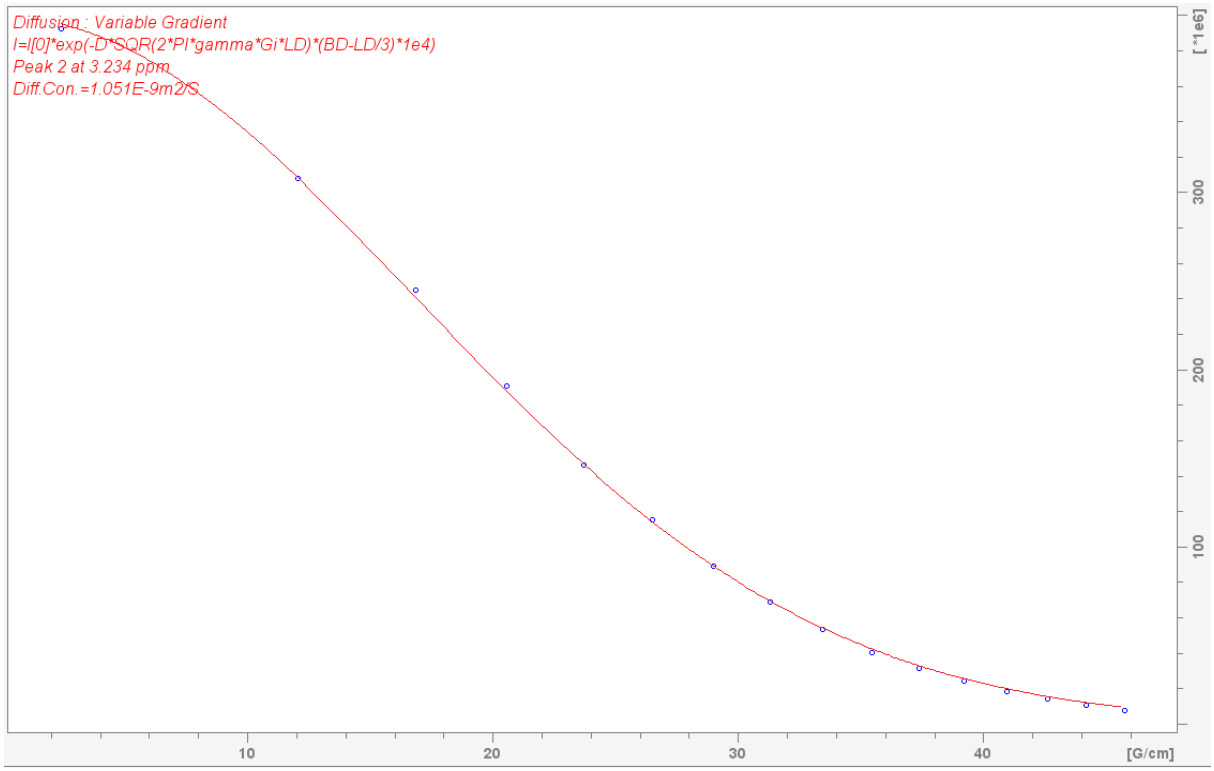
Little Delta = 2.000m

Big Delta = 59.900m

RSS = 6.641e-06

SD = 6.443e-04

| Point | Gradient | Expt | Calc | Difference |
|---|---|---|---|---|
| 1 | 2.41E+00 | 2.61E-01 | 2.60E-01 | -1.39E-03 |
| 2 | 1.20E+01 | 1.99E-01 | 2.01E-01 | 1.79E-03 |
| 3 | 1.69E+01 | 1.55E-01 | 1.56E-01 | 4.10E-04 |
| 4 | 2.06E+01 | 1.21E-01 | 1.20E-01 | -8.13E-05 |
| 5 | 2.37E+01 | 9.27E-02 | 9.32E-02 | 5.10E-04 |
| 6 | 2.65E+01 | 7.26E-02 | 7.21E-02 | -4.33E-04 |
| 7 | 2.90E+01 | 5.64E-02 | 5.58E-02 | -6.06E-04 |
| 8 | 3.13E+01 | 4.35E-02 | 4.32E-02 | -2.66E-04 |
| 9 | 3.35E+01 | 3.40E-02 | 3.34E-02 | -5.38E-04 |
| 10 | 3.55E+01 | 2.59E-02 | 2.59E-02 | -2.15E-05 |
| 11 | 3.74E+01 | 2.04E-02 | 2.00E-02 | -3.48E-04 |
| 12 | 3.92E+01 | 1.56E-02 | 1.55E-02 | -8.37E-05 |
| 13 | 4.09E+01 | 1.19E-02 | 1.20E-02 | 4.54E-05 |
| 14 | 4.26E+01 | 9.26E-03 | 9.28E-03 | 1.71E-05 |
| 15 | 4.42E+01 | 7.03E-03 | 7.18E-03 | 1.46E-04 |
| 16 | 4.57E+01 | 5.46E-03 | 5.55E-03 | 9.65E-05 |




16 points for Peak 2,

Peak Point = 3.234 ppm

Converged after 27 iterations!

Results Comp. 1

I[0] = 1.018e+00

Diff Con. = 1.051e-09 m2/s

Gamma = 4.258e+03 Hz/G

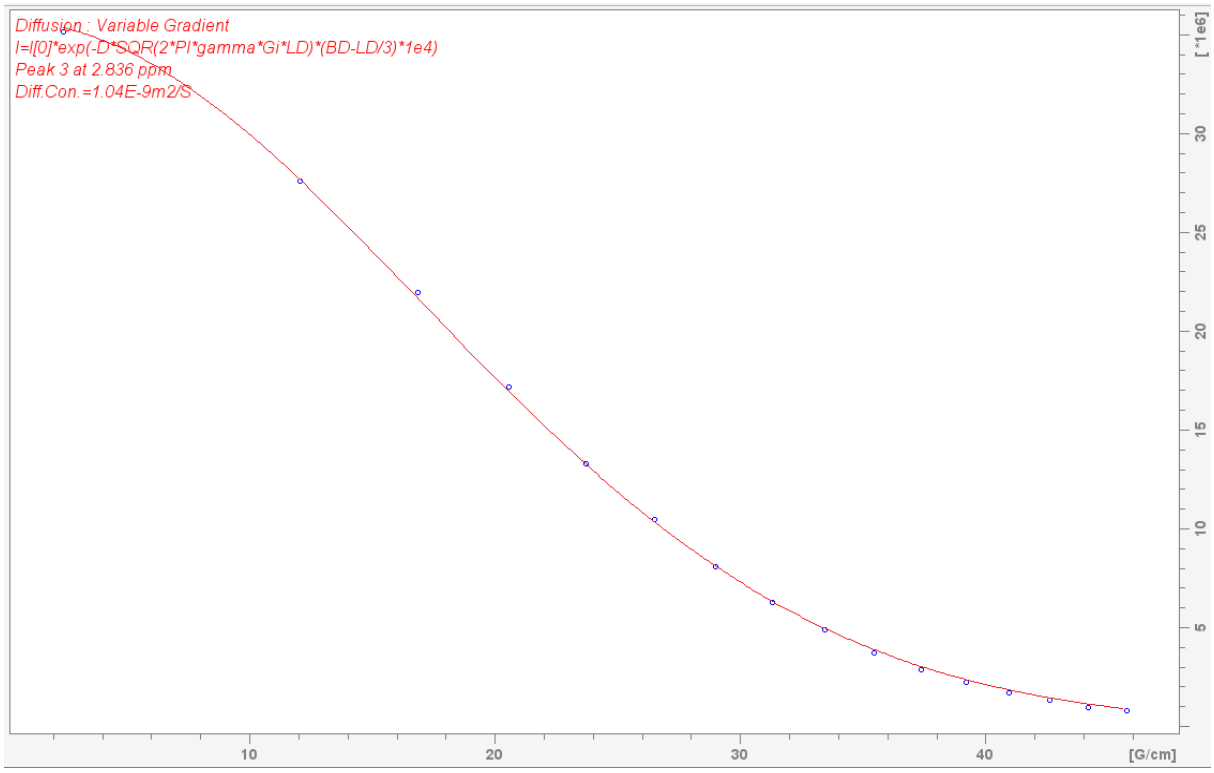
Little Delta = 2.000m

Big Delta = 59.900m

RSS = 4.010e-04

SD = 5.006e-03

| Point | Gradient | Expt | Calc | Difference |
|---|---|---|---|---|
| 1 | 2.41E+00 | 1.00E+00 | 1.01E+00 | 7.21E-03 |
| 2 | 1.20E+01 | 7.85E-01 | 7.86E-01 | 1.26E-03 |
| 3 | 1.69E+01 | 6.24E-01 | 6.14E-01 | -1.05E-02 |
| 4 | 2.06E+01 | 4.87E-01 | 4.79E-01 | -8.25E-03 |
| 5 | 2.37E+01 | 3.73E-01 | 3.74E-01 | 7.01E-04 |
| 6 | 2.65E+01 | 2.94E-01 | 2.92E-01 | -2.49E-03 |
| 7 | 2.90E+01 | 2.28E-01 | 2.28E-01 | -4.98E-04 |
| 8 | 3.13E+01 | 1.75E-01 | 1.78E-01 | 2.33E-03 |
| 9 | 3.35E+01 | 1.36E-01 | 1.39E-01 | 2.80E-03 |
| 10 | 3.55E+01 | 1.02E-01 | 1.08E-01 | 5.88E-03 |
| 11 | 3.74E+01 | 8.03E-02 | 8.45E-02 | 4.19E-03 |
| 12 | 3.92E+01 | 6.14E-02 | 6.59E-02 | 4.52E-03 |
| 13 | 4.09E+01 | 4.71E-02 | 5.15E-02 | 4.33E-03 |
| 14 | 4.26E+01 | 3.59E-02 | 4.02E-02 | 4.22E-03 |
| 15 | 4.42E+01 | 2.68E-02 | 3.14E-02 | 4.58E-03 |
| 16 | 4.57E+01 | 2.02E-02 | 2.45E-02 | 4.24E-03 |




16 points for Peak 3,

Peak Point = 2.836 ppm

Converged after 52 iterations!

Results Comp. 1

I[0] = 9.109e-02

Diff Con. = 1.040e-09 m2/s

Gamma = 4.258e+03 Hz/G

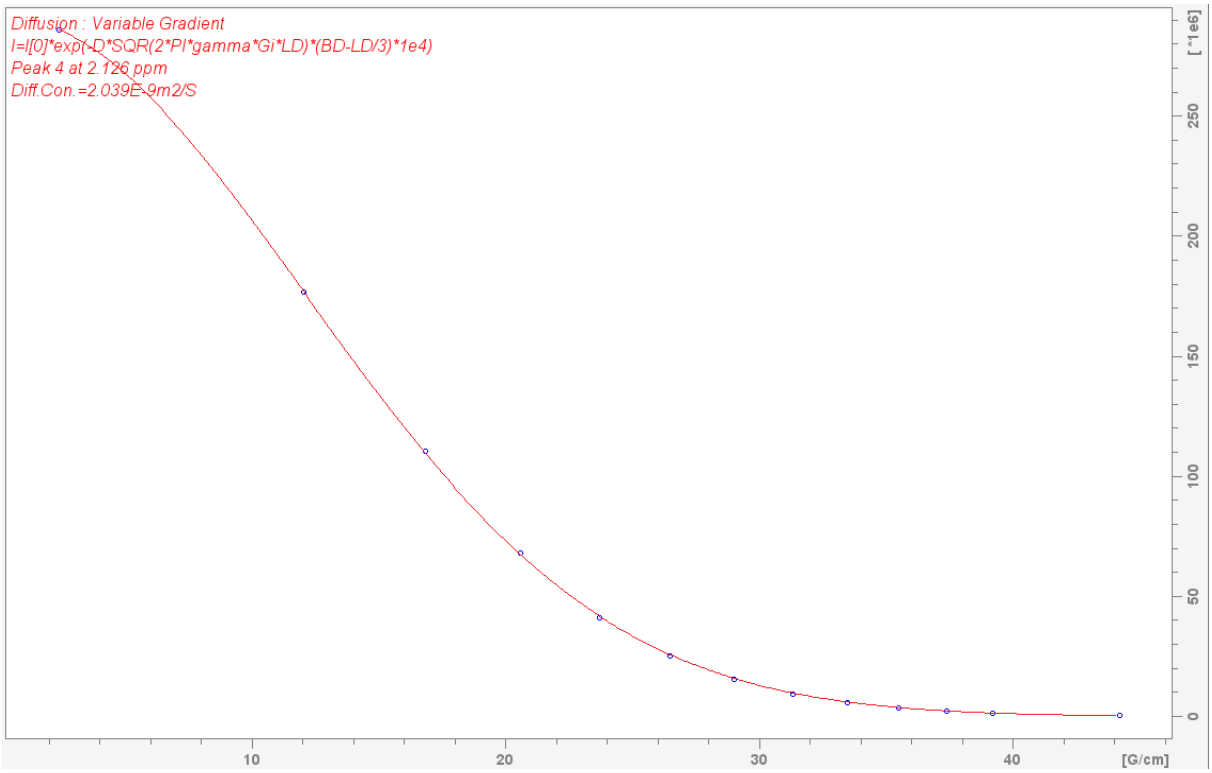
Little Delta = 2.000m

Big Delta = 59.900m

RSS = 2.734e-06

SD = 4.134e-04

| Point | Gradient | Expt | Calc | Difference |
|---|---|---|---|---|
| 1 | 2.41E+00 | 8.96E-02 | 9.02E-02 | 5.69E-04 |
| 2 | 1.20E+01 | 7.04E-02 | 7.06E-02 | 1.65E-04 |
| 3 | 1.69E+01 | 5.60E-02 | 5.52E-02 | -8.25E-04 |
| 4 | 2.06E+01 | 4.38E-02 | 4.32E-02 | -6.57E-04 |
| 5 | 2.37E+01 | 3.39E-02 | 3.38E-02 | -1.04E-04 |
| 6 | 2.65E+01 | 2.67E-02 | 2.64E-02 | -3.00E-04 |
| 7 | 2.90E+01 | 2.07E-02 | 2.07E-02 | 3.68E-05 |
| 8 | 3.13E+01 | 1.60E-02 | 1.62E-02 | 2.37E-04 |
| 9 | 3.35E+01 | 1.24E-02 | 1.27E-02 | 2.58E-04 |
| 10 | 3.55E+01 | 9.51E-03 | 9.91E-03 | 4.01E-04 |
| 11 | 3.74E+01 | 7.35E-03 | 7.75E-03 | 4.06E-04 |
| 12 | 3.92E+01 | 5.72E-03 | 6.07E-03 | 3.43E-04 |
| 13 | 4.09E+01 | 4.29E-03 | 4.75E-03 | 4.60E-04 |
| 14 | 4.26E+01 | 3.33E-03 | 3.71E-03 | 3.82E-04 |
| 15 | 4.42E+01 | 2.51E-03 | 2.91E-03 | 4.01E-04 |
| 16 | 4.57E+01 | 1.98E-03 | 2.27E-03 | 2.94E-04 |




13 points for Peak 4,

Peak Point = 2.126 ppm

Converged after 43 iterations!

Results Comp. 1

I[0] = 7.442e-01

Diff Con. = 2.039e-09 m2/s

Gamma = 4.258e+03 Hz/G

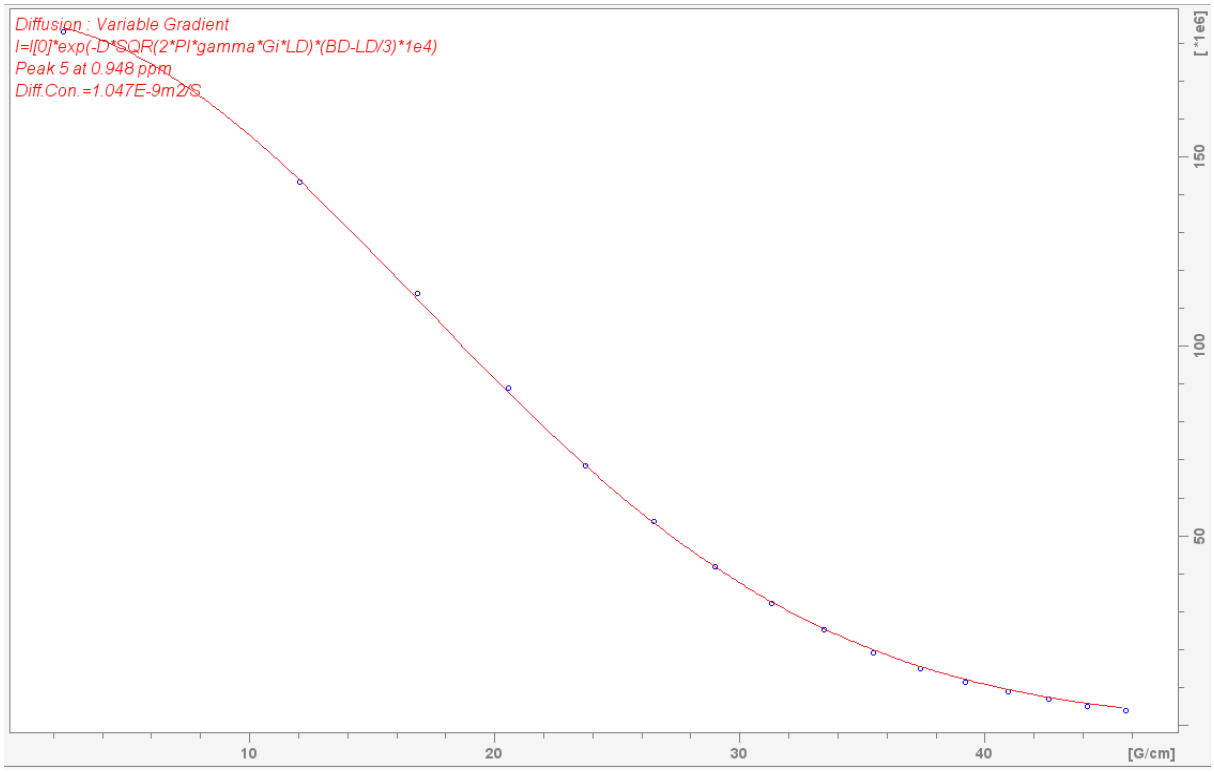
Little Delta = 2.000m

Big Delta = 59.900m

RSS = 2.379e-05

SD = 1.353e-03

| Point | Gradient | Expt | Calc | Difference |
|---|---|---|---|---|
| 1 | 2.41E+00 | 8.96E-02 | 9.02E-02 | 5.69E-04 |
| 2 | 1.20E+01 | 7.04E-02 | 7.06E-02 | 1.65E-04 |
| 3 | 1.69E+01 | 5.60E-02 | 5.52E-02 | -8.25E-04 |
| 4 | 2.06E+01 | 4.38E-02 | 4.32E-02 | -6.57E-04 |
| 5 | 2.37E+01 | 3.39E-02 | 3.38E-02 | -1.04E-04 |
| 6 | 2.65E+01 | 2.67E-02 | 2.64E-02 | -3.00E-04 |
| 7 | 2.90E+01 | 2.07E-02 | 2.07E-02 | 3.68E-05 |
| 8 | 3.13E+01 | 1.60E-02 | 1.62E-02 | 2.37E-04 |
| 9 | 3.35E+01 | 1.24E-02 | 1.27E-02 | 2.58E-04 |
| 10 | 3.55E+01 | 9.51E-03 | 9.91E-03 | 4.01E-04 |
| 11 | 3.74E+01 | 7.35E-03 | 7.75E-03 | 4.06E-04 |
| 12 | 3.92E+01 | 5.72E-03 | 6.07E-03 | 3.43E-04 |
| 13 | 4.09E+01 | 4.29E-03 | 4.75E-03 | 4.60E-04 |
| 14 | 4.26E+01 | 3.33E-03 | 3.71E-03 | 3.82E-04 |
| 15 | 4.42E+01 | 2.51E-03 | 2.91E-03 | 4.01E-04 |
| 16 | 4.57E+01 | 1.98E-03 | 2.27E-03 | 2.94E-04 |




16 points for Peak 5,

Peak Point = 0.948 ppm

Converged after 44 iterations!

Results Comp. 1

I[0] = 4.740e-01

Diff Con. = 1.047e-09 m2/s

Gamma = 4.258e+03 Hz/G

Little Delta = 2.000m

Big Delta = 59.900m

RSS = 6.030e-05

SD = 1.941e-03

| Point | Gradient | Expt | Calc | Difference |
|---|---|---|---|---|
| 1 | 2.41E+00 | 4.67E-01 | 4.69E-01 | 2.46E-03 |
| 2 | 1.20E+01 | 3.65E-01 | 3.67E-01 | 1.12E-03 |
| 3 | 1.69E+01 | 2.91E-01 | 2.86E-01 | -4.29E-03 |
| 4 | 2.06E+01 | 2.27E-01 | 2.24E-01 | -3.28E-03 |
| 5 | 2.37E+01 | 1.75E-01 | 1.75E-01 | 2.76E-04 |
| 6 | 2.65E+01 | 1.37E-01 | 1.37E-01 | -7.73E-04 |
| 7 | 2.90E+01 | 1.07E-01 | 1.07E-01 | -4.00E-04 |
| 8 | 3.13E+01 | 8.20E-02 | 8.33E-02 | 1.30E-03 |
| 9 | 3.35E+01 | 6.44E-02 | 6.51E-02 | 6.85E-04 |
| 10 | 3.55E+01 | 4.90E-02 | 5.08E-02 | 1.89E-03 |
| 11 | 3.74E+01 | 3.79E-02 | 3.97E-02 | 1.85E-03 |
| 12 | 3.92E+01 | 2.93E-02 | 3.10E-02 | 1.73E-03 |
| 13 | 4.09E+01 | 2.25E-02 | 2.42E-02 | 1.73E-03 |
| 14 | 4.26E+01 | 1.73E-02 | 1.89E-02 | 1.62E-03 |
| 15 | 4.42E+01 | 1.31E-02 | 1.48E-02 | 1.73E-03 |
| 16 | 4.57E+01 | 1.01E-02 | 1.16E-02 | 1.51E-03 |

**Summary and Mass Calculation**

Summary:

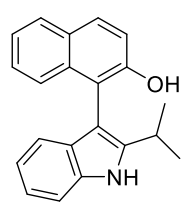
| Peak | Ent **126** | Rac **126** | Rac **131** |
|---|---|---|---|
| Peak 1 ($m^2 s^{-1}$) | 8.550E-10 | 9.001E-10 | 1.087E-09 |
| Peak 2 ($m^2 s^{-1}$) | 8.553E-10 | 8.943E-10 | 1.051E-09 |
| Peak 3($m^2 s^{-1}$) | 8.539E-10 | 8.973E-10 | 1.040E-09 |
| Peak 4 ($m^2 s^{-1}$) | | - | 1.047E-09 |
| Average ($m^2 s^{-1}$) | 8.547E-10 | 8.972E-10 | 1.056E-09 |
| Tol ref ($m^2 s^{-1}$) | 2.074E-09 | 2.093E-09 | 2.039E-09 |
| Approximate mass (Da)[4] | 412 | 386 | 283 |

[4] Masses were calculated using the method of Stalke et al.[1]

## II.5.6 Alternative erosion conditions

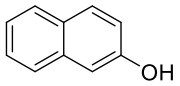
### Additive Spiking

Table S14 Spiked erosion dat for **126** + 2-naphthol *or* indole. Solids were prepared to give a final concentration of 0.025 molal in **126** and 0.175 molal in spiking compound on dissolution in 150 µL toluene.

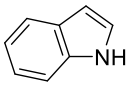



**126**

+




*-or-*




| | Indole | | | 2-Naphthol | | |
|---|---|---|---|---|---|---|
| t (s) | Ent 1 rel area (%) | Ent 2 rel area (%) | e.e. (%) | Ent 1 rel area (%) | Ent 2 rel area (%) | e.e. (%) |
| 0 | 100 | 0 | 100 | 100 | 0 | 100 |
| 60 | - | - | - | 100 | 0 | 100 |
| 120 | 100 | 0 | 100 | 100 | 0 | 100 |
| 180 | 100 | 0 | 100 | 100 | 0 | 100 |
| 240 | 100 | 0 | 100 | 100 | 0 | 100 |
| 300 | 100 | 0 | 100 | 100 | 0 | 100 |
| 360 | 100 | 0 | 100 | 100 | 0 | 100 |
| 420 | 100 | 0 | 100 | 100 | 0 | 100 |
| 480 | 100 | 0 | 100 | 100 | 0 | 100 |
| 540 | 100 | 0 | 100 | 100 | 0 | 100 |
| 600 | 100 | 0 | 100 | 100 | 0 | 100 |
| 660 | 100 | 0 | 100 | 100 | 0 | 100 |
| 720 | 100 | 0 | 100 | 100 | 0 | 100 |
| 780 | 100 | 0 | 100 | 100 | 0 | 100 |
| 840 | 100 | 0 | 100 | 100 | 0 | 100 |
| 900 | 100 | 0 | 100 | 100 | 0 | 100 |
| 960 | 100 | 0 | 100 | 100 | 0 | 100 |
| 1020 | 100 | 0 | 100 | 100 | 0 | 100 |
| 1080 | 100 | 0 | 100 | 100 | 0 | 100 |
| 1140 | 100 | 0 | 100 | 100 | 0 | 100 |
| 1200 | 100 | 0 | 100 | 100 | 0 | 100 |
| 1350 | 100 | 0 | 100 | 100 | 0 | 100 |
| 1500 | 100 | 0 | 100 | 100 | 0 | 100 |
| 1650 | 100 | 0 | 100 | 100 | 0 | 100 |
| 1800 | 100 | 0 | 100 | 100 | 0 | 100 |
| 1950 | 100 | 0 | 100 | 100 | 0 | 100 |
| 2100 | 100 | 0 | 100 | 100 | 0 | 100 |
| 2250 | 100 | 0 | 100 | 100 | 0 | 100 |
| 2400 | 100 | 0 | 100 | 100 | 0 | 100 |

| | | | | | | |
|---|---|---|---|---|---|---|
| 2550 | 100 | 0 | 100 | 100 | 0 | 100 |
| 2700 | 100 | 0 | 100 | 100 | 0 | 100 |
| 2850 | 100 | 0 | 100 | 100 | 0 | 100 |
| 3000 | 100 | 0 | 100 | 100 | 0 | 100 |
| 3150 | 100 | 0 | 100 | 100 | 0 | 100 |
| 3300 | 100 | 0 | 100 | 100 | 0 | 100 |
| 3450 | 100 | 0 | 100 | 100 | 0 | 100 |
| 3600 | 100 | 0 | 100 | 100 | 0 | 100 |
| 3900 | 100 | 0 | 100 | 100 | 0 | 100 |
| 4200 | 100 | 0 | 100 | 100 | 0 | 100 |
| 4500 | 100 | 0 | 100 | 100 | 0 | 100 |
| 4800 | 100 | 0 | 100 | 100 | 0 | 100 |
| 5100 | 100 | 0 | 100 | 100 | 0 | 100 |
| 5400 | 100 | 0 | 100 | 100 | 0 | 100 |
| 6000 | 100 | 0 | 100 | 100 | 0 | 100 |
| 6600 | 99.605 | 0.395 | 99.21 | 100 | 0 | 100 |
| 7200 | 99.015 | 0.985 | 98.03 | 100 | 0 | 100 |

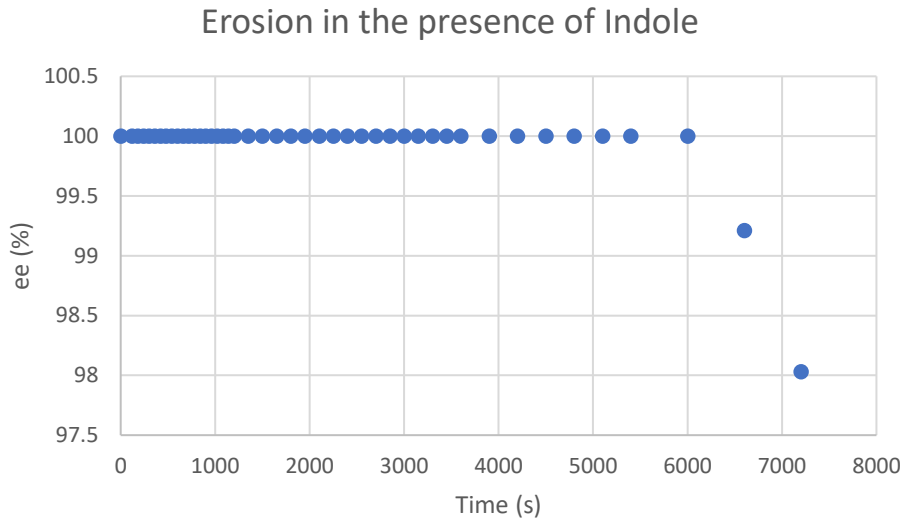



Figure S46 Plotted erosion data in the presence of indole

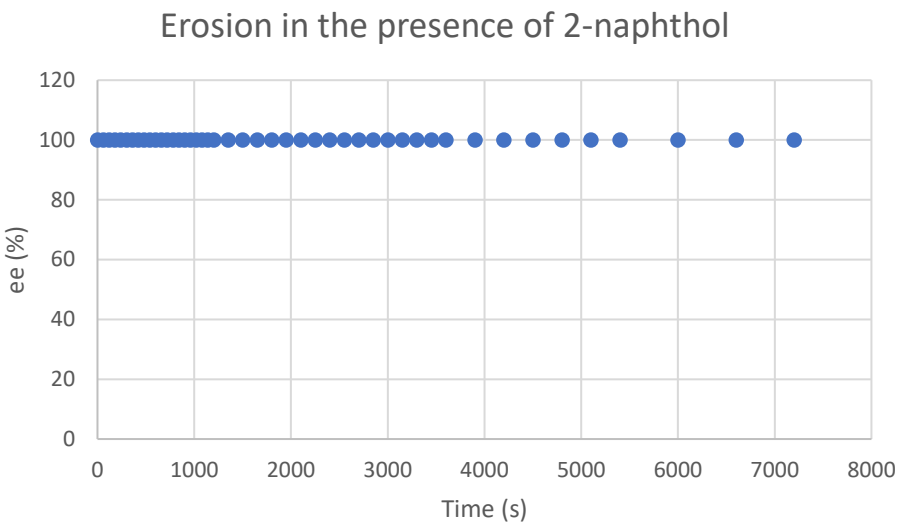
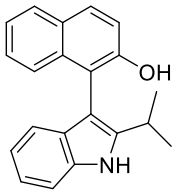



Figure S47 Plotted erosion data in the presence of 2-naphthol

**Hydrogen Bonding Solvents**

## Butanol – 0.2 molal 80 °C

Table S15 Erosion data for **126** in butanol. The erosion study was carried as described and analysed by normal phase chiral HPLC.




**126**

| t (s) | Ent 1 rel area (%) | Ent 2 rel area (%) | e.e. (%) | t (s) | Ent 1 rel area (%) | Ent 2 rel area (%) | e.e. (%) |
|---|---|---|---|---|---|---|---|
| 0 | 99.565 | 0.435 | 99.13 | 1800 | 75.385 | 24.615 | 50.77 |
| 60 | 99.105 | 0.895 | 98.21 | 1950 | 74.94 | 25.06 | 49.88 |
| 120 | 97.785 | 2.215 | 95.57 | 2100 | 74.375 | 25.625 | 48.75 |
| 180 | 96.01 | 3.99 | 92.02 | 2250 | 74.055 | 25.945 | 48.11 |
| 240 | 94.385 | 5.615 | 88.77 | 2400 | 73.735 | 26.265 | 47.47 |
| 300 | 92.865 | 7.135 | 85.73 | 2550 | 73.35 | 26.65 | 46.7 |
| 360 | 91.385 | 8.615 | 82.77 | 2700 | 73.06 | 26.94 | 46.12 |
| 420 | 90.06 | 9.94 | 80.12 | 2850 | 72.77 | 27.23 | 45.54 |
| 480 | 88.705 | 11.295 | 77.41 | 3000 | 72.46 | 27.54 | 44.92 |
| 540 | 87.475 | 12.525 | 74.95 | 3150 | 72.265 | 27.735 | 44.53 |
| 600 | 86.425 | 13.575 | 72.85 | 3300 | 71.905 | 28.095 | 43.81 |
| 660 | 85.41 | 14.59 | 70.82 | 3450 | 71.825 | 28.175 | 43.65 |
| 720 | 84.375 | 15.625 | 68.75 | 3600 | 71.59 | 28.41 | 43.18 |
| 780 | 83.44 | 16.56 | 66.88 | 3900 | 71.19 | 28.81 | 42.38 |
| 840 | 82.585 | 17.415 | 65.17 | 4200 | 70.795 | 29.205 | 41.59 |
| 900 | 81.725 | 18.275 | 63.45 | 4500 | 70.405 | 29.595 | 40.81 |
| 960 | 80.91 | 19.09 | 61.82 | 4800 | 70.045 | 29.955 | 40.09 |
| 1020 | 80.29 | 19.71 | 60.58 | 5100 | 69.74 | 30.26 | 39.48 |
| 1080 | 79.58 | 20.42 | 59.16 | 5400 | 69.435 | 30.565 | 38.87 |
| 1140 | 79.02 | 20.98 | 58.04 | 6000 | 68.805 | 31.195 | 37.61 |
| 1200 | 78.42 | 21.58 | 56.84 | 6600 | 68.255 | 31.745 | 36.51 |
| 1350 | 77.48 | 22.52 | 54.96 | 7200 | 67.78 | 32.22 | 35.56 |
| 1500 | 76.61 | 23.39 | 53.22 | | | | |
| 1650 | 75.995 | 24.005 | 51.99 | | | | |

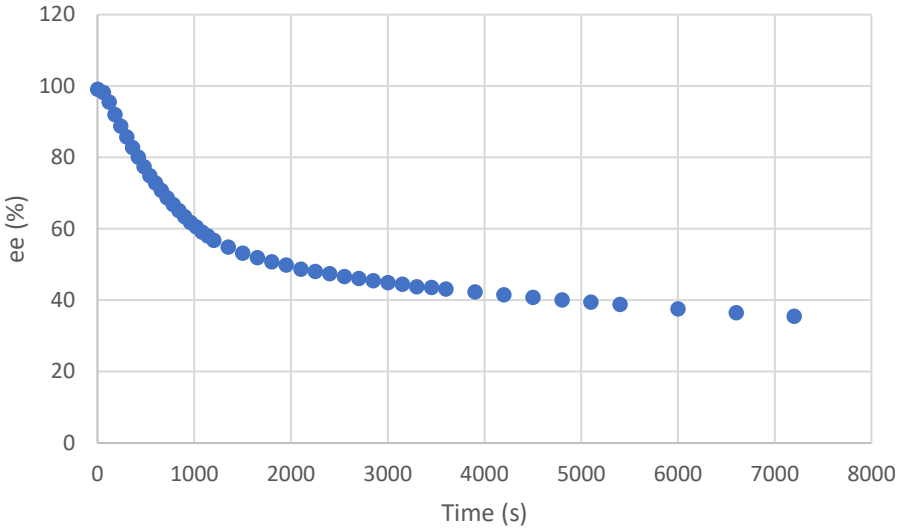
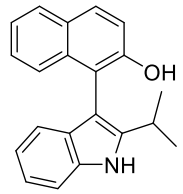



Figure S48 Plotted erosion data for **126** in butanol

## DMSO – 0.2 molal 155 °C

Table S16 Erosion data for **126** in DMSO at 120 °C. The erosion study was carried as described and analysed by reverse phase chiral HPLC (36.5% IPA in $H_2O$, 1 ml/min, 4.6 mm x 25 cm IC, $\tau_R$ 16.5, 18.3 min).




**126**

| | **0.2 molal** | | | | **0.1 molal** | | | |
|---|---|---|---|---|---|---|---|---|
| t (s) | Ent 1 rel area (%) | Ent 2 rel area (%) | e.e. (%) | $\ln\left(\frac{e.e_0}{e.e_t}\right)$ | Ent 1 rel area (%) | Ent 2 rel area (%) | e.e. (%) | $\ln\left(\frac{e.e_0}{e.e_t}\right)$ |
| 0 | 100 | 0 | 100 | 0.0000 | 100 | 0 | 100 | 0.0000 |
| 240 | 99.715 | 0.285 | 99.43 | 0.0057 | 99.5 | 0.5 | 99 | 0.0101 |
| 480 | 99.16 | 0.84 | 98.32 | 0.0169 | 99.28 | 0.72 | 98.56 | 0.0145 |
| 720 | 98.805 | 1.195 | 97.61 | 0.0242 | 98.985 | 1.015 | 97.97 | 0.0205 |
| 960 | 98.395 | 1.605 | 96.79 | 0.0326 | 98.63 | 1.37 | 97.26 | 0.0278 |
| 1200 | 97.945 | 2.055 | 95.89 | 0.0420 | 98.255 | 1.745 | 96.51 | 0.0355 |
| 1680 | 96.615 | 3.385 | 93.23 | 0.0701 | 97.585 | 2.415 | 95.17 | 0.0495 |
| 2160 | 92.185 | 7.815 | 84.37 | 0.1700 | 96.75 | 3.25 | 93.5 | 0.0672 |
| 2640 | 78.3 | 21.7 | 56.6 | 0.5692 | 95.9 | 4.1 | 91.8 | 0.0856 |
| 3120 | 68.22 | 31.78 | 36.44 | 1.0095 | 95.115 | 4.885 | 90.23 | 0.1028 |
| 3600 | 60.43 | 39.57 | 20.86 | 1.5673 | 94.265 | 5.735 | 88.53 | 0.1218 |
| 4200 | 55.89 | 44.11 | 11.78 | 2.1388 | 93.215 | 6.785 | 86.43 | 0.1458 |
| 4800 | 53.995 | 46.005 | 7.99 | 2.5270 | 92.095 | 7.905 | 84.19 | 0.1721 |
| 5400 | 52.855 | 47.145 | 5.71 | 2.8630 | 91.03 | 8.97 | 82.06 | 0.1977 |
| 6000 | 51.855 | 48.145 | 3.71 | 3.2941 | 89.94 | 10.06 | 79.88 | 0.2246 |
| 6600 | 51.32 | 48.68 | 2.64 | 3.6344 | 89.28 | 10.72 | 78.56 | 0.2413 |
| 7200 | 51.01 | 48.99 | 2.02 | 3.9021 | 88.2 | 11.8 | 76.4 | 0.2692 |

| | 0.05 molal | | | | 0.025 molal | | | |
|---|---|---|---|---|---|---|---|---|
| t (s) | Ent 1 rel area (%) | Ent 2 rel area (%) | e.e. (%) | $\ln\left(\frac{e.e_{\cdot 0}}{e.e_{\cdot t}}\right)$ | Ent 1 rel area | Ent 2 rel area (%) | e.e. (%) | $\ln\left(\frac{e.e_{\cdot 0}}{e.e_{\cdot t}}\right)$ |
| 0 | 100 | 0 | 100 | 0.0000 | 100 | 0 | 100 | 0.0000 |
| 240 | 99.095 | 0.905 | 98.19 | 0.0183 | 98.85 | 1.15 | 97.7 | 0.0233 |
| 480 | 98.605 | 1.395 | 97.21 | 0.0283 | 98.455 | 1.545 | 96.91 | 0.0314 |
| 720 | 97.71 | 2.29 | 95.42 | 0.0469 | 97.485 | 2.515 | 94.97 | 0.0516 |
| 960 | 97.28 | 2.72 | 94.56 | 0.0559 | 96.93 | 3.07 | 93.86 | 0.0634 |
| 1200 | 96.65 | 3.35 | 93.3 | 0.0694 | 96.265 | 3.735 | 92.53 | 0.0776 |
| 1680 | 95.615 | 4.385 | 91.23 | 0.0918 | 95.23 | 4.77 | 90.46 | 0.1003 |
| 2160 | 94.36 | 5.64 | 88.72 | 0.1197 | 94.24 | 5.76 | 88.48 | 0.1224 |
| 2640 | 93.395 | 6.605 | 86.79 | 0.1417 | 93.185 | 6.815 | 86.37 | 0.1465 |
| 3120 | 92.4 | 7.6 | 84.8 | 0.1649 | 92.125 | 7.875 | 84.25 | 0.1714 |
| 3600 | 91.345 | 8.655 | 82.69 | 0.1901 | 91.065 | 8.935 | 82.13 | 0.1969 |
| 4200 | 90.13 | 9.87 | 80.26 | 0.2199 | 90.27 | 9.73 | 80.54 | 0.2164 |
| 4800 | 89.69 | 10.31 | 79.38 | 0.2309 | 89.16 | 10.84 | 78.32 | 0.2444 |
| 5400 | 88.445 | 11.555 | 76.89 | 0.2628 | 87.885 | 12.115 | 75.77 | 0.2775 |
| 6000 | 87.465 | 12.535 | 74.93 | 0.2886 | 86.59 | 13.41 | 73.18 | 0.3122 |
| 6600 | 86.305 | 13.695 | 72.61 | 0.3201 | 85.58 | 14.42 | 71.16 | 0.3402 |
| 7200 | 85.22 | 14.78 | 70.44 | 0.3504 | 84 | 16 | 68 | 0.3857 |

Untransformed plots

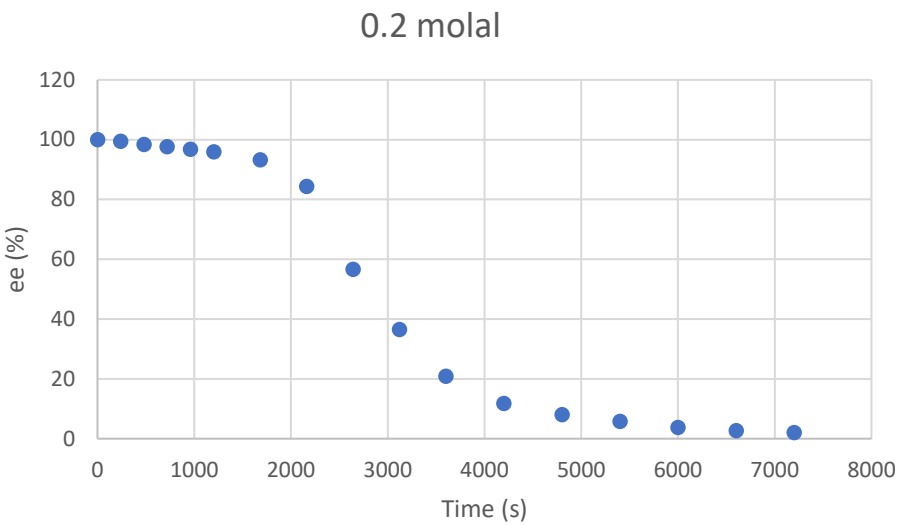



Figure S49 Plotted erosion data for **126** in DMSO at 0.2 molal

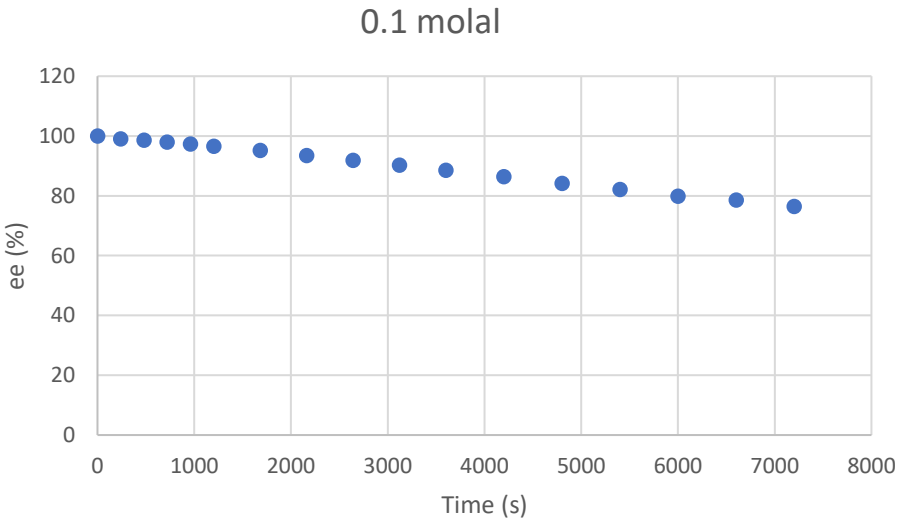



Figure S50 Plotted erosion data for **126** in DMSO at 0.1 molal

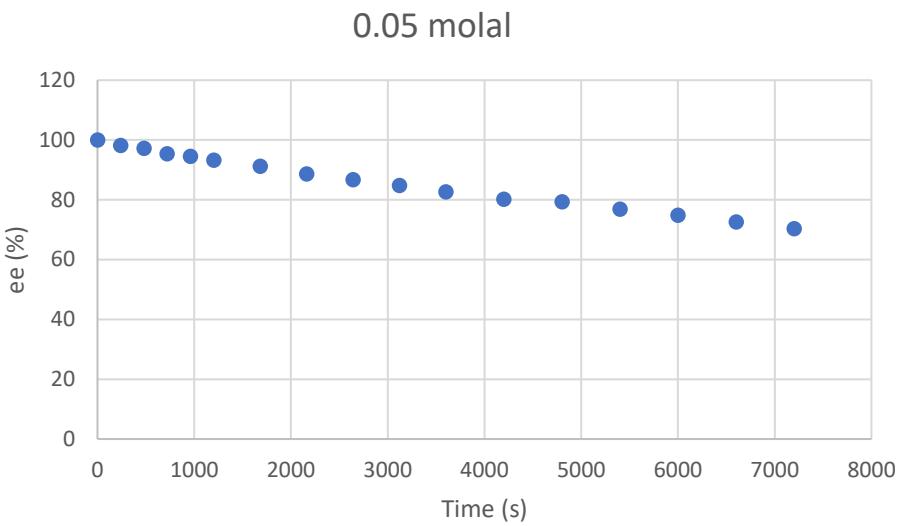



Figure S51 Plotted erosion data for **126** in DMSO at 0.05 molal

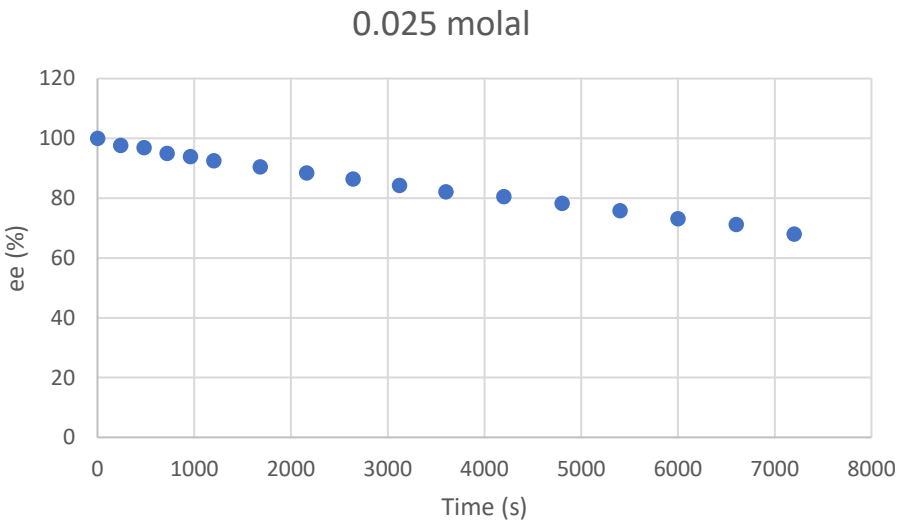



Figure S52 Plotted erosion data for **126** in DMSO at 0.025 molal

Ln plots

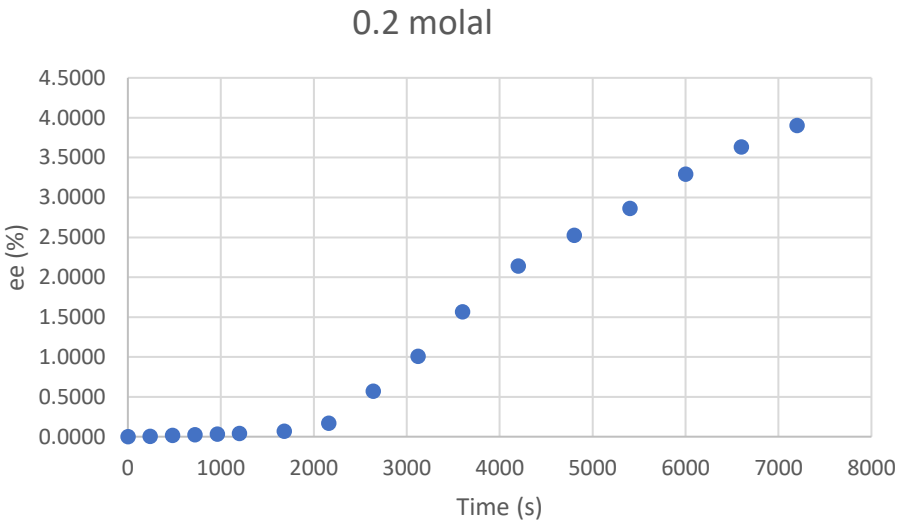



Figure S53 First order plot for **126** in DMSO at 0.2 molal

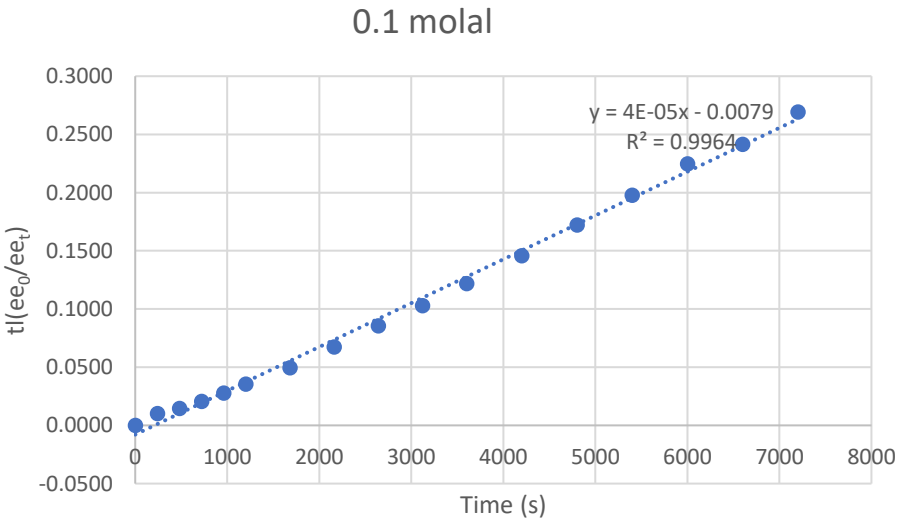



Figure S54 First order plot for **126** in DMSO at 0.1 molal

$m = k_{rac} = 3.8 \times 10^{-5}\ s^{-1}$

$k_{ent} = 1.9 \times 10^{-5}\ s^{-1}$

$\Delta G^{\ddagger}$ (155 °C) = 34.6 kcal $mol^{-1}$

$T_{½}$ (155 °C) = 5 hours; $T_{½}$ (25 °C) = 42,800 years

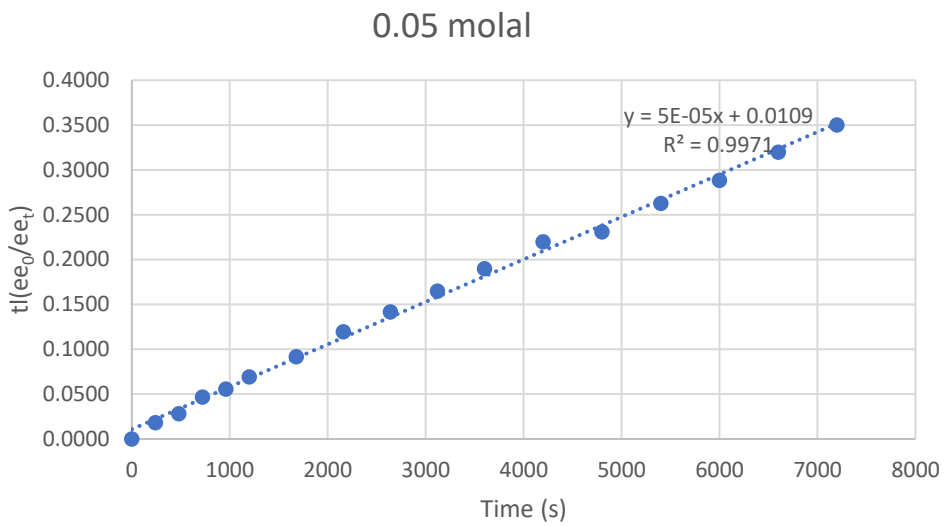



Figure S55 First order plot for **126** in DMSO at 0.05 molal

$m = k_{rac} = 4.7 \times 10^{-5}\ s^{-1}$

$k_{ent} = 2.4 \times 10^{-5}\ s^{-1}$

$\Delta G^{\ddagger}$ (155 °C) = 34.4 kcal $mol^{-1}$

$T_{½}$ (155 °C) = 4 hours; $T_{½}$ (25 °C) = 30,800 years

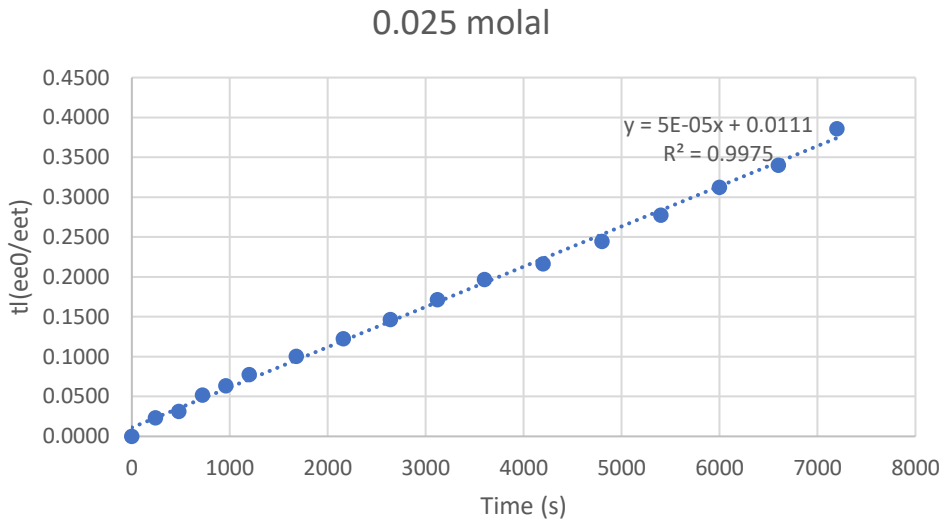



Figure S56 First order plot for **126** in DMSO at 0.025 molal

$m = k_{rac} = 5.0 \times 10^{-5}\ s^{-1}$

$k_{ent} = 2.5 \times 10^{-5}\ s^{-1}$

$\Delta G^{\ddagger}$ (155 °C) = 34.4 kcal $mol^{-1}$

$T_{½}$ (155 °C) = 3.8 hours; $T_{½}$ (25 °C) = 28,100 years

**Spiking Data**

## Ent Spike

Table S17 Erosion data for **126** with opposite enantiomer added. The erosion study was carried out in toluene at 80 °C. Solid enantiopure *R*-**126** was added to solid enantiopure *S*-**126** to create a scalemic mixture with 70% ee. The erosion study was then run as described and monitored by chiral normal phase HPLC




| t (s) | Ent 1 rel area (%) | Ent 2 rel area (%) | e.e. (%) | t (s) | Ent 1 rel area (%) | Ent 2 rel area (%) | e.e. (%) |
|---|---|---|---|---|---|---|---|
| 0 | 79.625 | 20.375 | 59.25 | 1500 | 61.84 | 38.16 | 23.68 |
| 60 | 85.635 | 14.365 | 71.27 | 1650 | 61.38 | 38.62 | 22.76 |
| 120 | 85.17 | 14.83 | 70.34 | 1800 | 60.97 | 39.03 | 21.94 |
| 180 | 84.38 | 15.62 | 68.76 | 1950 | 60.625 | 39.375 | 21.25 |
| 240 | 83.135 | 16.865 | 66.27 | 2100 | 60.27 | 39.73 | 20.54 |
| 300 | 81.43 | 18.57 | 62.86 | 2400 | 59.72 | 40.28 | 19.44 |
| 360 | 79.565 | 20.435 | 59.13 | 2550 | 59.52 | 40.48 | 19.04 |
| 420 | 77.535 | 22.465 | 55.07 | 2700 | 59.27 | 40.73 | 18.54 |
| 480 | 75.535 | 24.465 | 51.07 | 2850 | 59.07 | 40.93 | 18.14 |
| 540 | 73.53 | 26.47 | 47.06 | 3000 | 58.89 | 41.11 | 17.78 |
| 600 | 71.83 | 28.17 | 43.66 | 3150 | 58.715 | 41.285 | 17.43 |
| 660 | 70.43 | 29.57 | 40.86 | 3300 | 58.545 | 41.455 | 17.09 |
| 720 | 69.055 | 30.945 | 38.11 | 3450 | 58.5 | 41.5 | 17 |
| 780 | 67.855 | 32.145 | 35.71 | 3600 | 58.3 | 41.7 | 16.6 |
| 840 | 66.97 | 33.03 | 33.94 | 3900 | 57.9 | 42.1 | 15.8 |
| 900 | 66.155 | 33.845 | 32.31 | 4200 | 57.63 | 42.37 | 15.26 |
| 960 | 65.415 | 34.585 | 30.83 | 4500 | 57.345 | 42.655 | 14.69 |
| 1020 | 64.73 | 35.27 | 29.46 | 4800 | 57.115 | 42.885 | 14.23 |
| 1080 | 64.155 | 35.845 | 28.31 | 5100 | 57.025 | 42.975 | 14.05 |
| 1140 | 63.73 | 36.27 | 27.46 | 5400 | 56.805 | 43.195 | 13.61 |
| 1200 | 63.33 | 36.67 | 26.66 | 6000 | 56.25 | 43.75 | 12.5 |
| 1350 | 62.52 | 37.48 | 25.04 | 6600 | 56.03 | 43.97 | 12.06 |
| | | | | 7200 | 55.475 | 44.525 | 10.95 |

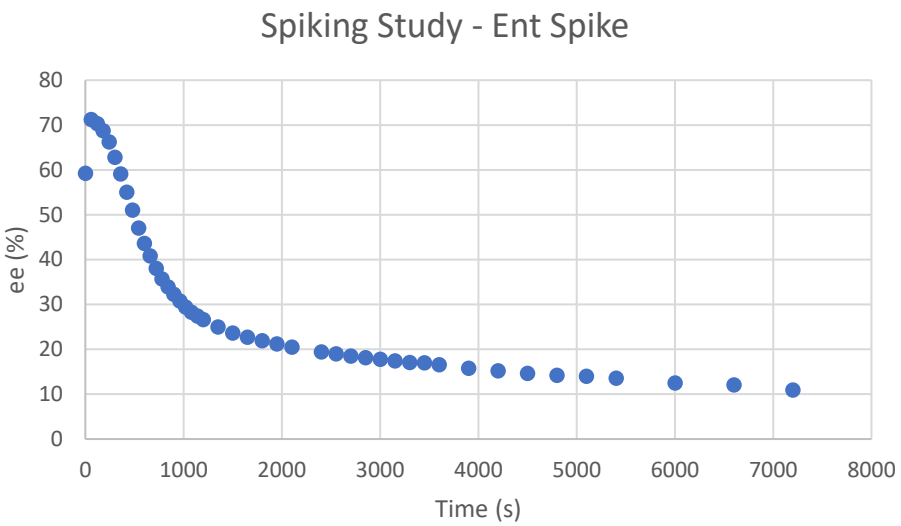



Figure S57 Plot of erosion data for **126** with opposite enantiomer added

## Racemic Spike

Table S18 Erosion data for **126** with racemate added. The erosion study was carried out in toluene at 80 °C. Solid racemic **126** was added to solid enantiopure **126** to create a scalemic mixture with 70% ee. The erosion study was then run as described and monitored by chiral normal phase HPLC




| t (s) | Ent 1 rel area (%) | Ent 2 rel area (%) | e.e. (%) | t (s) | Ent 1 rel area (%) | Ent 2 rel area (%) | e.e. (%) |
|---|---|---|---|---|---|---|---|
| 0 | 85.38 | 14.62 | 70.76 | 1500 | 79.48 | 20.52 | 58.96 |
| 120 | 85.3 | 14.7 | 70.6 | 1650 | 78.275 | 21.725 | 56.55 |
| 240 | 86.345 | 13.655 | 72.69 | 1800 | 75.875 | 24.125 | 51.75 |
| 300 | 85.565 | 14.435 | 71.13 | 1950 | 73.105 | 26.895 | 46.21 |
| 360 | 85.2 | 14.8 | 70.4 | 2100 | 69.74 | 30.26 | 39.48 |
| 420 | 84.83 | 15.17 | 69.66 | 2250 | 66.12 | 33.88 | 32.24 |
| 360 | 85.12 | 14.88 | 70.24 | 2400 | 62.635 | 37.365 | 25.27 |
| 420 | 84.735 | 15.265 | 69.47 | 2550 | 59.605 | 40.395 | 19.21 |
| 480 | 84.595 | 15.405 | 69.19 | 2700 | 57.11 | 42.89 | 14.22 |
| 540 | 84.735 | 15.265 | 69.47 | 2850 | 55.425 | 44.575 | 10.85 |
| 600 | 84.74 | 15.26 | 69.48 | 3000 | 53.52 | 46.48 | 7.04 |
| 660 | 84.55 | 15.45 | 69.1 | 3150 | 52.77 | 47.23 | 5.54 |
| 720 | 84.725 | 15.275 | 69.45 | 3300 | 51.985 | 48.015 | 3.97 |
| 780 | 84.545 | 15.455 | 69.09 | 3450 | 51.715 | 48.285 | 3.43 |
| 840 | 84.405 | 15.595 | 68.81 | 3600 | 51.13 | 48.87 | 2.26 |
| 900 | 84.225 | 15.775 | 68.45 | 3900 | 50.46 | 49.54 | 0.92 |
| 960 | 83.95 | 16.05 | 67.9 | 4200 | 50.205 | 49.795 | 0.41 |
| 1020 | 83.86 | 16.14 | 67.72 | 4500 | 50.2 | 49.8 | 0.4 |
| 1080 | 83.57 | 16.43 | 67.14 | 4800 | 50 | 50 | 0 |
| 1140 | 83.135 | 16.865 | 66.27 | 5100 | 49.995 | 50.005 | -0.01 |
| 1200 | 82.305 | 17.695 | 64.61 | 5400 | 50.02 | 49.98 | 0.04 |
| 1350 | 80.905 | 19.095 | 61.81 | 6000 | 50.635 | 49.365 | 1.27 |
| | | | | 6600 | 50.41 | 49.59 | 0.82 |

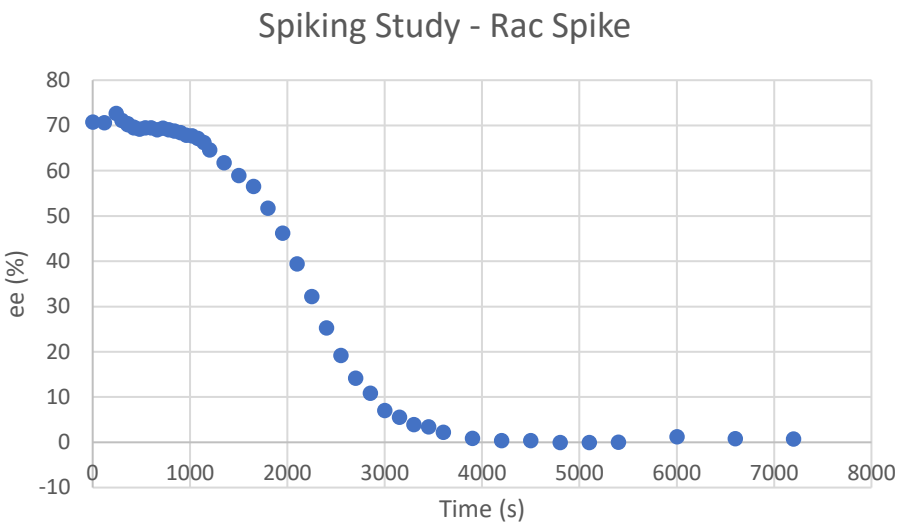



Figure S58 Plot of erosion data for **126** with racemate added.

# II.6 X-Ray Crystallography

**Computing details**

Data collection: SuperNova, (Oxford Diffraction, 2010); cell refinement: *CrysAlis PRO* (Rigaku Oxford Diffraction, 2017); data reduction: *CrysAlis PRO* (Rigaku Oxford Diffraction, 2017); program(s) used to solve structure: Superflip (Palatinus & Chapuis, 2007); program(s) used to refine structure: *CRYSTALS* (Betteridge *et al.*, 2003); molecular graphics: *CAMERON* (Watkin *et al.*, 1996); software used to prepare material for publication: *CRYSTALS* (Betteridge *et al.*, 2003).

**References**

Betteridge, P. W., Carruthers, J. R., Cooper, R. I., Prout, K. & Watkin, D. J. (2003). *J. Appl. Cryst.* **36**, 1487.

Oxford Diffraction, (2010). Supernova User Manual.

Palatinus, L. & Chapuis, G. (2007). *J. Appl. Cryst.* **40**, 786–790.

Parsons,S., Flack, H.D. and Wagner, T. Acta Cryst. (2013). B69, 249?259

Rigaku Oxford Diffraction (2017). *CrysAlis PRO*.

Watkin, D. J., Prout, C. K. & Pearce, L. J. (1996). *CAMERON*, Chemical Crystallography Laboratory, Oxford, UK.

**(global)**

*Crystal data*

| | |
|---|---|
| $C_{21}H_{19}NO$ | $D_x$ = 1.220 Mg m$^{-3}$ |
| $M_r$ = 301.39 | Melting point: not measured K |
| Orthorhombic, $P2_12_12_1$ | Cu *K*a radiation, l = 1.54180 Å |
| Hall symbol: P 2ac 2ab | Cell parameters from 14185 reflections |
| *a* = 9.9920 (1) Å | q = 3.8–75.5° |
| *b* = 12.7687 (2) Å | m = 0.58 mm$^{-1}$ |
| *c* = 25.7221 (4) Å | *T* = 150 K |
| *V* = 3281.75 (8) Å$^3$ | Block, colourless |
| *Z* = 8 | 0.36 × 0.18 × 0.11 mm |
| *F*(000) = 1279.991 | |

*Data collection*

| | |
|---|---|
| Oxford Diffraction SuperNova diffractometer | 6283 reflections with $I > 2.0s(I)$ |
| Focussing mirrors monochromator | $R_{int} = 0.055$ |
| w scans | $q_{max} = 76.3°$, $q_{min} = 3.4°$ |
| Absorption correction: multi-scan *CrysAlis PRO* (Rigaku Oxford Diffraction, 2017) | $h = -12 \rightarrow 9$ |
| $T_{min} = 0.66$, $T_{max} = 0.94$ | $k = -15 \rightarrow 15$ |
| 28871 measured reflections | $l = -32 \rightarrow 30$ |
| 6811 independent reflections | |

*Refinement*

| | |
|---|---|
| Refinement on $F^2$ | Hydrogen site location: difference Fourier map |
| Least-squares matrix: full | H atoms treated by a mixture of independent and constrained refinement |
| $R[F^2 > 2s(F^2)] = 0.042$ | Method = Modified Sheldrick $w = 1/[s^2(F^2) + (0.09P)^2 + 0.25P]$, where $P = (\max(F_o^2,0) + 2F_c^2)/3$ |
| $wR(F^2) = 0.120$ | $(D/s)_{max} = 0.040$ |
| $S = 0.94$ | $D\rho_{max} = 0.30$ e Å$^{-3}$ |
| 6810 reflections | $D\rho_{min} = -0.21$ e Å$^{-3}$ |
| 432 parameters | Absolute structure: Parsons, Flack & Wagner (2013), 2834 Friedel Pairs |
| 12 restraints | Absolute structure parameter: 0.16 (13) |
| Primary atom site location: other | |

*Fractional atomic coordinates and isotropic or equivalent isotropic displacement parameters (Å$^2$) for (global)*

| | *x* | *y* | *z* | $U_{iso}$*/$U_{eq}$ |
|---|---|---|---|---|
| O1 | 0.59130 (16) | 0.45458 (12) | 0.67660 (5) | 0.0470 |
| C2 | 0.70314 (19) | 0.50359 (14) | 0.65862 (7) | 0.0365 |
| C3 | 0.74068 (17) | 0.50248 (13) | 0.60696 (6) | 0.0317 |
| C4 | 0.85647 (17) | 0.55962 (14) | 0.59163 (7) | 0.0353 |
| C5 | 0.93333 (19) | 0.61385 (15) | 0.62955 (9) | 0.0429 |

| | | | | |
|---|---|---|---|---|
| C6 | 1.0487 (2) | 0.66984 (17) | 0.61308 (12) | 0.0583 |
| C7 | 1.0846 (2) | 0.67548 (19) | 0.56202 (13) | 0.0641 |
| C8 | 1.0079 (2) | 0.62301 (17) | 0.52483 (11) | 0.0578 |
| C9 | 0.8978 (2) | 0.56535 (16) | 0.53872 (8) | 0.0453 |
| C10 | 0.8913 (2) | 0.61100 (17) | 0.68186 (9) | 0.0527 |
| C11 | 0.7791 (2) | 0.55861 (17) | 0.69640 (7) | 0.0489 |
| C12 | 0.66322 (16) | 0.43861 (14) | 0.56916 (6) | 0.0322 |
| C13 | 0.56960 (18) | 0.47274 (14) | 0.53360 (6) | 0.0336 |
| N14 | 0.52630 (16) | 0.38756 (12) | 0.50505 (6) | 0.0370 |
| C15 | 0.58896 (17) | 0.29802 (14) | 0.52209 (6) | 0.0348 |
| C16 | 0.67675 (16) | 0.32717 (14) | 0.56256 (6) | 0.0326 |
| C17 | 0.75253 (18) | 0.25114 (14) | 0.58759 (6) | 0.0355 |
| C18 | 0.73722 (19) | 0.14724 (15) | 0.57272 (7) | 0.0403 |
| C19 | 0.6491 (2) | 0.11986 (15) | 0.53260 (7) | 0.0430 |
| C20 | 0.57420 (19) | 0.19378 (16) | 0.50654 (7) | 0.0403 |
| C21 | 0.51674 (19) | 0.58191 (14) | 0.52511 (7) | 0.0379 |
| C22 | 0.4384 (2) | 0.61935 (17) | 0.57237 (8) | 0.0491 |
| C23 | 0.4300 (3) | 0.59147 (17) | 0.47652 (9) | 0.0557 |
| O24 | 0.39791 (14) | 0.62717 (10) | 0.71057 (5) | 0.0413 |
| C25 | 0.28415 (17) | 0.62926 (14) | 0.74070 (6) | 0.0338 |
| C26 | 0.22795 (16) | 0.53931 (13) | 0.76010 (6) | 0.0302 |
| C27 | 0.10897 (16) | 0.54770 (13) | 0.79079 (6) | 0.0310 |
| C28 | 0.04094 (17) | 0.45816 (15) | 0.80965 (7) | 0.0362 |
| C29 | -0.07156 (19) | 0.46831 (16) | 0.83997 (8) | 0.0441 |
| C30 | -0.1214 (2) | 0.56840 (18) | 0.85273 (9) | 0.0487 |
| C31 | -0.06052 (18) | 0.65625 (15) | 0.83411 (8) | 0.0420 |
| C32 | 0.05575 (17) | 0.64857 (14) | 0.80253 (7) | 0.0342 |
| C33 | 0.1191 (2) | 0.73848 (14) | 0.78139 (7) | 0.0374 |
| C34 | 0.22948 (19) | 0.72957 (14) | 0.75100 (7) | 0.0381 |
| C35 | 0.29271 (16) | 0.43719 (13) | 0.75031 (6) | 0.0300 |
| C36 | 0.36266 (17) | 0.37904 (13) | 0.78610 (6) | 0.0313 |
| N37 | 0.41441 (15) | 0.29170 (11) | 0.76220 (6) | 0.0344 |

| | | | | |
|---|---|---|---|---|
| C38 | 0.38080 (18) | 0.29319 (14) | 0.71044 (7) | 0.0344 |
| C39 | 0.30315 (17) | 0.38300 (13) | 0.70136 (6) | 0.0322 |
| C40 | 0.25926 (19) | 0.40585 (15) | 0.65073 (7) | 0.0396 |
| C41 | 0.2985 (2) | 0.33809 (18) | 0.61093 (7) | 0.0502 |
| C42 | 0.3766 (2) | 0.25013 (17) | 0.62086 (8) | 0.0504 |
| C43 | 0.4189 (2) | 0.22554 (15) | 0.67037 (8) | 0.0435 |
| C44 | 0.38912 (18) | 0.40136 (14) | 0.84265 (6) | 0.0359 |
| C45 | 0.5392 (2) | 0.40526 (18) | 0.85391 (8) | 0.0466 |
| C46 | 0.3180 (2) | 0.32244 (19) | 0.87759 (7) | 0.0469 |
| H61 | 1.1002 | 0.7045 | 0.6369 | 0.0706* |
| H71 | 1.1606 | 0.7160 | 0.5524 | 0.0759* |
| H81 | 1.0340 | 0.6270 | 0.4892 | 0.0710* |
| H91 | 0.8472 | 0.5277 | 0.5136 | 0.0531* |
| H101 | 0.9427 | 0.6471 | 0.7059 | 0.0641* |
| H111 | 0.7493 | 0.5614 | 0.7309 | 0.0569* |
| H171 | 0.8141 | 0.2697 | 0.6148 | 0.0429* |
| H181 | 0.7895 | 0.0962 | 0.5893 | 0.0463* |
| H191 | 0.6430 | 0.0485 | 0.5237 | 0.0490* |
| H201 | 0.5118 | 0.1739 | 0.4795 | 0.0493* |
| H211 | 0.5937 | 0.6297 | 0.5215 | 0.0438* |
| H221 | 0.4097 | 0.6907 | 0.5685 | 0.0725* |
| H222 | 0.3590 | 0.5756 | 0.5753 | 0.0725* |
| H223 | 0.4931 | 0.6132 | 0.6038 | 0.0738* |
| H231 | 0.4112 | 0.6655 | 0.4702 | 0.0831* |
| H232 | 0.4830 | 0.5662 | 0.4475 | 0.0833* |
| H233 | 0.3468 | 0.5497 | 0.4794 | 0.0838* |
| H281 | 0.0746 | 0.3911 | 0.8024 | 0.0409* |
| H291 | -0.1177 | 0.4067 | 0.8514 | 0.0535* |
| H301 | -0.1987 | 0.5747 | 0.8736 | 0.0581* |
| H311 | -0.0927 | 0.7234 | 0.8418 | 0.0508* |
| H331 | 0.0815 | 0.8061 | 0.7882 | 0.0438* |
| H341 | 0.2715 | 0.7893 | 0.7380 | 0.0449* |

| | | | | |
|---|---|---|---|---|
| H401 | 0.2040 | 0.4652 | 0.6438 | 0.0463* |
| H411 | 0.2692 | 0.3511 | 0.5750 | 0.0616* |
| H421 | 0.4027 | 0.2061 | 0.5931 | 0.0615* |
| H431 | 0.4742 | 0.1651 | 0.6773 | 0.0512* |
| H441 | 0.3522 | 0.4707 | 0.8494 | 0.0410* |
| H451 | 0.5594 | 0.4284 | 0.8896 | 0.0694* |
| H452 | 0.5799 | 0.3350 | 0.8492 | 0.0689* |
| H453 | 0.5851 | 0.4530 | 0.8294 | 0.0686* |
| H461 | 0.3356 | 0.3373 | 0.9138 | 0.0698* |
| H462 | 0.2208 | 0.3227 | 0.8722 | 0.0684* |
| H463 | 0.3480 | 0.2515 | 0.8711 | 0.0689* |
| H2 | 0.4589 (19) | 0.3888 (13) | 0.4830 (8) | 0.0449 (19)* |
| H3 | 0.465 (2) | 0.2441 (14) | 0.7757 (6) | 0.0410 (19)* |
| H4 | 0.553 (3) | 0.419 (2) | 0.6549 (10) | 0.071 (2)* |
| H241 | 0.423 (3) | 0.5653 (15) | 0.7073 (11) | 0.0607 (19)* |

*Atomic displacement parameters (Å²) for (global)*

| | $U^{11}$ | $U^{22}$ | $U^{33}$ | $U^{12}$ | $U^{13}$ | $U^{23}$ |
|---|---|---|---|---|---|---|
| O1 | 0.0575 (8) | 0.0523 (8) | 0.0311 (6) | -0.0145 (7) | 0.0066 (6) | -0.0030 (6) |
| C2 | 0.0418 (9) | 0.0377 (8) | 0.0299 (8) | -0.0033 (7) | -0.0039 (7) | 0.0007 (6) |
| C3 | 0.0319 (8) | 0.0337 (8) | 0.0295 (7) | 0.0013 (6) | -0.0033 (6) | -0.0010 (6) |
| C4 | 0.0318 (8) | 0.0310 (8) | 0.0432 (9) | 0.0046 (6) | -0.0012 (7) | 0.0013 (7) |
| C5 | 0.0350 (9) | 0.0346 (8) | 0.0590 (11) | 0.0004 (7) | -0.0156 (8) | 0.0053 (8) |
| C6 | 0.0375 (10) | 0.0418 (10) | 0.0956 (19) | -0.0042 (8) | -0.0223 (11) | 0.0129 (11) |
| C7 | 0.0320 (9) | 0.0497 (12) | 0.111 (2) | -0.0002 (9) | 0.0116 (12) | 0.0225 (13) |
| C8 | 0.0487 (11) | 0.0458 (11) | 0.0789 (16) | 0.0046 (9) | 0.0276 (11) | 0.0077 (11) |
| C9 | 0.0436 (10) | 0.0405 (9) | 0.0519 (11) | 0.0038 (8) | 0.0124 (8) | -0.0003 (8) |
| C10 | 0.0604 (12) | 0.0455 (10) | 0.0521 (11) | -0.0107 (9) | -0.0283 (10) | 0.0015 (9) |
| C11 | 0.0709 (13) | 0.0489 (10) | 0.0269 (8) | -0.0068 (10) | -0.0138 (9) | 0.0004 (7) |
| C12 | 0.0338 (8) | 0.0378 (8) | 0.0251 (7) | -0.0025 (6) | 0.0008 (6) | -0.0011 (6) |
| C13 | 0.0369 (8) | 0.0374 (8) | 0.0265 (7) | -0.0039 (7) | -0.0005 (6) | -0.0023 (6) |
| N14 | 0.0418 (8) | 0.0400 (8) | 0.0291 (7) | -0.0024 (6) | -0.0050 (6) | -0.0041 (6) |
| C15 | 0.0374 (8) | 0.0414 (9) | 0.0256 (7) | -0.0026 (7) | 0.0039 (6) | -0.0043 (6) |
| C16 | 0.0334 (8) | 0.0389 (8) | 0.0255 (7) | -0.0043 (6) | 0.0058 (6) | -0.0026 (6) |
| C17 | 0.0366 (8) | 0.0424 (9) | 0.0275 (7) | 0.0000 (7) | 0.0040 (6) | -0.0011 (6) |
| C18 | 0.0447 (9) | 0.0390 (9) | 0.0372 (8) | 0.0033 (7) | 0.0087 (7) | 0.0015 (7) |
| C19 | 0.0500 (10) | 0.0371 (9) | 0.0417 (10) | -0.0035 (8) | 0.0119 (8) | -0.0104 (7) |
| C20 | 0.0428 (9) | 0.0452 (9) | 0.0331 (8) | -0.0053 (8) | 0.0057 (7) | -0.0103 (7) |
| C21 | 0.0403 (9) | 0.0368 (9) | 0.0366 (9) | -0.0062 (7) | -0.0065 (7) | 0.0009 (7) |
| C22 | 0.0525 (11) | 0.0463 (10) | 0.0485 (11) | 0.0104 (9) | 0.0004 (9) | 0.0018 (8) |
| C23 | 0.0762 (15) | 0.0439 (10) | 0.0471 (11) | -0.0021 (10) | -0.0232 (11) | 0.0053 (9) |
| O24 | 0.0464 (7) | 0.0359 (6) | 0.0416 (7) | -0.0076 (6) | 0.0123 (6) | -0.0016 (5) |
| C25 | 0.0353 (8) | 0.0366 (8) | 0.0294 (7) | -0.0036 (7) | -0.0024 (6) | -0.0021 (6) |
| C26 | 0.0323 (8) | 0.0320 (7) | 0.0262 (7) | 0.0002 (6) | -0.0039 (6) | -0.0011 (6) |
| C27 | 0.0314 (8) | 0.0356 (8) | 0.0262 (7) | 0.0020 (6) | -0.0041 (6) | -0.0002 (6) |
| C28 | 0.0309 (8) | 0.0370 (8) | 0.0407 (9) | 0.0036 (7) | -0.0001 (7) | 0.0030 (7) |
| C29 | 0.0348 (9) | 0.0460 (10) | 0.0515 (11) | 0.0022 (8) | 0.0053 (8) | 0.0090 (8) |
| C30 | 0.0353 (9) | 0.0573 (12) | 0.0536 (11) | 0.0121 (9) | 0.0102 (8) | 0.0071 (9) |

| | | | | | | |
|---|---|---|---|---|---|---|
| C31 | 0.0386 (9) | 0.0428 (9) | 0.0447 (10) | 0.0137 (8) | -0.0007 (7) | -0.0011 (8) |
| C32 | 0.0351 (8) | 0.0361 (8) | 0.0313 (8) | 0.0076 (7) | -0.0064 (6) | -0.0004 (6) |
| C33 | 0.0455 (10) | 0.0326 (8) | 0.0342 (8) | 0.0065 (7) | -0.0072 (7) | -0.0026 (6) |
| C34 | 0.0464 (10) | 0.0320 (8) | 0.0359 (8) | -0.0055 (7) | -0.0038 (7) | 0.0019 (6) |
| C35 | 0.0305 (7) | 0.0321 (8) | 0.0273 (7) | -0.0030 (6) | 0.0034 (6) | -0.0023 (6) |
| C36 | 0.0316 (7) | 0.0318 (7) | 0.0304 (8) | 0.0006 (6) | 0.0038 (6) | -0.0010 (6) |
| N37 | 0.0374 (7) | 0.0318 (7) | 0.0341 (7) | 0.0042 (6) | 0.0034 (6) | -0.0016 (5) |
| C38 | 0.0362 (8) | 0.0358 (8) | 0.0311 (8) | -0.0074 (7) | 0.0098 (6) | -0.0050 (6) |
| C39 | 0.0340 (8) | 0.0350 (8) | 0.0277 (7) | -0.0083 (6) | 0.0053 (6) | -0.0032 (6) |
| C40 | 0.0447 (9) | 0.0456 (10) | 0.0285 (8) | -0.0142 (8) | 0.0023 (7) | -0.0005 (7) |
| C41 | 0.0634 (12) | 0.0612 (12) | 0.0260 (8) | -0.0277 (10) | 0.0075 (8) | -0.0057 (8) |
| C42 | 0.0596 (12) | 0.0534 (11) | 0.0382 (10) | -0.0241 (10) | 0.0211 (9) | -0.0167 (9) |
| C43 | 0.0440 (9) | 0.0399 (9) | 0.0467 (10) | -0.0100 (8) | 0.0173 (8) | -0.0133 (8) |
| C44 | 0.0398 (9) | 0.0399 (9) | 0.0281 (8) | 0.0044 (7) | -0.0015 (6) | -0.0023 (6) |
| C45 | 0.0445 (10) | 0.0562 (11) | 0.0391 (9) | -0.0074 (9) | -0.0050 (8) | 0.0010 (8) |
| C46 | 0.0454 (10) | 0.0661 (13) | 0.0293 (8) | -0.0062 (9) | 0.0007 (7) | 0.0031 (8) |

*Geometric parameters (Å, º) for (global)*

| | | | |
|---|---|---|---|
| O1—C2 | 1.362 (2) | O24—C25 | 1.376 (2) |
| O1—H4 | 0.817 (17) | O24—H241 | 0.833 (17) |
| C2—C3 | 1.381 (2) | C25—C26 | 1.372 (2) |
| C2—C11 | 1.419 (2) | C25—C34 | 1.417 (3) |
| C3—C4 | 1.423 (2) | C26—C27 | 1.431 (2) |
| C3—C12 | 1.486 (2) | C26—C35 | 1.477 (2) |
| C4—C5 | 1.422 (3) | C27—C28 | 1.416 (2) |
| C4—C9 | 1.424 (3) | C27—C32 | 1.426 (2) |
| C5—C6 | 1.421 (3) | C28—C29 | 1.374 (3) |
| C5—C10 | 1.410 (3) | C28—H281 | 0.939 |
| C6—C7 | 1.363 (4) | C29—C30 | 1.410 (3) |
| C6—H61 | 0.915 | C29—H291 | 0.958 |
| C7—C8 | 1.396 (4) | C30—C31 | 1.363 (3) |
| C7—H71 | 0.953 | C30—H301 | 0.945 |

| | | | |
|---|---|---|---|
| C8—C9 | 1.371 (3) | C31—C32 | 1.421 (3) |
| C8—H81 | 0.955 | C31—H311 | 0.937 |
| C9—H91 | 0.951 | C32—C33 | 1.419 (3) |
| C10—C11 | 1.358 (3) | C33—C34 | 1.357 (3) |
| C10—H101 | 0.926 | C33—H331 | 0.958 |
| C11—H111 | 0.936 | C34—H341 | 0.933 |
| C12—C13 | 1.379 (2) | C35—C36 | 1.374 (2) |
| C12—C16 | 1.439 (2) | C35—C39 | 1.440 (2) |
| C13—N14 | 1.382 (2) | C36—N37 | 1.374 (2) |
| C13—C21 | 1.507 (2) | C36—C44 | 1.506 (2) |
| N14—C15 | 1.375 (2) | N37—C38 | 1.373 (2) |
| N14—H2 | 0.880 (16) | N37—H3 | 0.864 (16) |
| C15—C16 | 1.411 (2) | C38—C39 | 1.404 (3) |
| C15—C20 | 1.398 (3) | C38—C43 | 1.397 (2) |
| C16—C17 | 1.389 (3) | C39—C40 | 1.405 (2) |
| C17—C18 | 1.389 (3) | C40—C41 | 1.397 (3) |
| C17—H171 | 0.961 | C40—H401 | 0.954 |
| C18—C19 | 1.401 (3) | C41—C42 | 1.391 (4) |
| C18—H181 | 0.938 | C41—H411 | 0.984 |
| C19—C20 | 1.378 (3) | C42—C43 | 1.378 (3) |
| C19—H191 | 0.942 | C42—H421 | 0.946 |
| C20—H201 | 0.968 | C43—H431 | 0.966 |
| C21—C22 | 1.523 (3) | C44—C45 | 1.528 (3) |
| C21—C23 | 1.526 (3) | C44—C46 | 1.526 (3) |
| C21—H211 | 0.986 | C44—H441 | 0.974 |
| C22—H221 | 0.960 | C45—H451 | 0.985 |
| C22—H222 | 0.973 | C45—H452 | 0.992 |
| C22—H223 | 0.980 | C45—H453 | 0.989 |
| C23—H231 | 0.977 | C46—H461 | 0.968 |
| C23—H232 | 0.971 | C46—H462 | 0.981 |
| C23—H233 | 0.990 | C46—H463 | 0.968 |
| | | | |

| | | | |
|---|---|---|---|
| C2—O1—H4 | 114 (2) | C25—O24—H241 | 109 (2) |
| O1—C2—C3 | 123.04 (16) | O24—C25—C26 | 121.77 (16) |
| O1—C2—C11 | 115.71 (16) | O24—C25—C34 | 116.18 (15) |
| C3—C2—C11 | 121.24 (17) | C26—C25—C34 | 122.04 (16) |
| C2—C3—C4 | 118.83 (15) | C25—C26—C27 | 118.54 (15) |
| C2—C3—C12 | 119.58 (15) | C25—C26—C35 | 119.83 (15) |
| C4—C3—C12 | 121.54 (15) | C27—C26—C35 | 121.61 (14) |
| C3—C4—C5 | 119.91 (17) | C26—C27—C28 | 121.82 (15) |
| C3—C4—C9 | 121.80 (17) | C26—C27—C32 | 119.63 (15) |
| C5—C4—C9 | 118.29 (17) | C28—C27—C32 | 118.54 (15) |
| C4—C5—C6 | 118.6 (2) | C27—C28—C29 | 120.73 (17) |
| C4—C5—C10 | 118.78 (17) | C27—C28—H281 | 119.8 |
| C6—C5—C10 | 122.6 (2) | C29—C28—H281 | 119.4 |
| C5—C6—C7 | 121.8 (2) | C28—C29—C30 | 120.42 (19) |
| C5—C6—H61 | 120.0 | C28—C29—H291 | 119.3 |
| C7—C6—H61 | 118.1 | C30—C29—H291 | 120.2 |
| C6—C7—C8 | 119.4 (2) | C29—C30—C31 | 120.42 (17) |
| C6—C7—H71 | 119.3 | C29—C30—H301 | 119.9 |
| C8—C7—H71 | 121.3 | C31—C30—H301 | 119.7 |
| C7—C8—C9 | 121.3 (2) | C30—C31—C32 | 120.60 (17) |
| C7—C8—H81 | 118.9 | C30—C31—H311 | 121.7 |
| C9—C8—H81 | 119.8 | C32—C31—H311 | 117.7 |
| C4—C9—C8 | 120.6 (2) | C27—C32—C31 | 119.23 (16) |
| C4—C9—H91 | 118.0 | C27—C32—C33 | 118.91 (15) |
| C8—C9—H91 | 121.4 | C31—C32—C33 | 121.84 (16) |
| C5—C10—C11 | 121.41 (18) | C32—C33—C34 | 121.01 (16) |
| C5—C10—H101 | 117.3 | C32—C33—H331 | 119.0 |
| C11—C10—H101 | 121.2 | C34—C33—H331 | 120.0 |
| C2—C11—C10 | 119.79 (19) | C25—C34—C33 | 119.79 (16) |
| C2—C11—H111 | 119.8 | C25—C34—H341 | 119.9 |
| C10—C11—H111 | 120.3 | C33—C34—H341 | 120.2 |
| C3—C12—C13 | 127.86 (16) | C26—C35—C36 | 125.85 (14) |

| | | | |
|---|---|---|---|
| C3—C12—C16 | 124.80 (15) | C26—C35—C39 | 127.21 (15) |
| C13—C12—C16 | 107.32 (15) | C36—C35—C39 | 106.82 (15) |
| C12—C13—N14 | 108.44 (15) | C35—C36—N37 | 109.28 (15) |
| C12—C13—C21 | 128.77 (15) | C35—C36—C44 | 129.38 (15) |
| N14—C13—C21 | 122.79 (15) | N37—C36—C44 | 121.30 (15) |
| C13—N14—C15 | 110.03 (14) | C36—N37—C38 | 109.29 (14) |
| C13—N14—H2 | 124.5 (11) | C36—N37—H3 | 127.8 (10) |
| C15—N14—H2 | 124.7 (11) | C38—N37—H3 | 122.8 (10) |
| N14—C15—C16 | 107.39 (15) | N37—C38—C39 | 107.92 (14) |
| N14—C15—C20 | 130.73 (17) | N37—C38—C43 | 129.79 (18) |
| C16—C15—C20 | 121.85 (17) | C39—C38—C43 | 122.17 (18) |
| C12—C16—C15 | 106.82 (15) | C35—C39—C38 | 106.67 (15) |
| C12—C16—C17 | 133.41 (16) | C35—C39—C40 | 133.47 (17) |
| C15—C16—C17 | 119.76 (16) | C38—C39—C40 | 119.76 (16) |
| C16—C17—C18 | 118.66 (17) | C39—C40—C41 | 117.59 (19) |
| C16—C17—H171 | 120.9 | C39—C40—H401 | 121.2 |
| C18—C17—H171 | 120.4 | C41—C40—H401 | 121.2 |
| C17—C18—C19 | 120.69 (18) | C40—C41—C42 | 121.55 (19) |
| C17—C18—H181 | 118.5 | C40—C41—H411 | 120.0 |
| C19—C18—H181 | 120.8 | C42—C41—H411 | 118.4 |
| C18—C19—C20 | 121.91 (17) | C41—C42—C43 | 121.70 (18) |
| C18—C19—H191 | 117.4 | C41—C42—H421 | 119.7 |
| C20—C19—H191 | 120.7 | C43—C42—H421 | 118.6 |
| C15—C20—C19 | 117.11 (17) | C38—C43—C42 | 117.2 (2) |
| C15—C20—H201 | 121.6 | C38—C43—H431 | 120.9 |
| C19—C20—H201 | 121.3 | C42—C43—H431 | 121.9 |
| C13—C21—C22 | 110.80 (15) | C36—C44—C45 | 111.20 (15) |
| C13—C21—C23 | 113.07 (15) | C36—C44—C46 | 111.25 (15) |
| C22—C21—C23 | 109.67 (18) | C45—C44—C46 | 111.51 (16) |
| C13—C21—H211 | 108.2 | C36—C44—H441 | 106.1 |
| C22—C21—H211 | 106.4 | C45—C44—H441 | 107.9 |
| C23—C21—H211 | 108.4 | C46—C44—H441 | 108.6 |

| | | | |
|---|---|---|---|
| C21—C22—H221 | 111.6 | C44—C45—H451 | 112.8 |
| C21—C22—H222 | 107.5 | C44—C45—H452 | 110.4 |
| H221—C22—H222 | 108.0 | H451—C45—H452 | 107.5 |
| C21—C22—H223 | 110.3 | C44—C45—H453 | 110.7 |
| H221—C22—H223 | 109.2 | H451—C45—H453 | 108.3 |
| H222—C22—H223 | 110.2 | H452—C45—H453 | 106.8 |
| C21—C23—H231 | 108.8 | C44—C46—H461 | 110.7 |
| C21—C23—H232 | 107.0 | C44—C46—H462 | 112.1 |
| H231—C23—H232 | 107.4 | H461—C46—H462 | 108.3 |
| C21—C23—H233 | 111.9 | C44—C46—H463 | 111.8 |
| H231—C23—H233 | 111.8 | H461—C46—H463 | 107.1 |
| H232—C23—H233 | 109.6 | H462—C46—H463 | 106.6 |

*Hydrogen-bond geometry (Å, º) for (global)*

| *D*—H···*A* | *D*—H | H···*A* | *D*···*A* | *D*—H···*A* |
|---|---|---|---|---|
| N37—H3···O24$^{i}$ | 0.86 | 2.06 | 2.902 (3) | 166 (2) |
| O24—H241···O1 | 0.83 | 2.33 | 3.058 (3) | 146 (3) |

Symmetry code: (i) -*x*+1, *y*-1/2, -*z*+3/2.

Document origin: *publCIF* [Westrip, S. P. (2010). *J. Apply. Cryst.*, **43**, 920-925].

# II.7 MATLAB SimBiology

## II.7.1 Simulations

**Trimer Model**

$$\mathrm{R} + \mathrm{R} \underset{k_r}{\overset{k_f}{\rightleftharpoons}} \mathrm{RR} \qquad \text{(AC 1.0)}$$

$$\mathrm{S} + \mathrm{S} \underset{k_r}{\overset{k_f}{\rightleftharpoons}} \mathrm{SS} \qquad \text{(AC 1.1)}$$

$$\mathrm{R} + \mathrm{S} \underset{k_{r_1}}{\overset{k_{f_1}}{\rightleftharpoons}} \mathrm{RS} \qquad \text{(AC 1.2)}$$

$$\mathrm{RR} \underset{k_{r_2}}{\overset{k_{f_2}}{\rightleftharpoons}} \mathrm{RS} \underset{k_{f_2}}{\overset{k_{r_2}}{\rightleftharpoons}} \mathrm{SS} \qquad \text{(AC 1.3)}$$

$$\mathrm{RS} + \mathrm{R} \underset{k_{f_7}}{\overset{k_{r_7}}{\rightleftharpoons}} \mathrm{RS} + \mathrm{S} \qquad \text{(AC 1.4)}$$

$$\mathrm{RS} + \mathrm{R} \underset{k_{r_5}}{\overset{k_{f_5}}{\rightleftharpoons}} \mathrm{SS} + \mathrm{R} \qquad \text{(AC 1.5)}$$

$$\mathrm{RR} + \mathrm{S} \underset{k_{f_5}}{\overset{k_{r_5}}{\rightleftharpoons}} \mathrm{RS} + \mathrm{S} \qquad \text{(AC 1.6)}$$

$$\mathrm{RR} + \mathrm{S} \underset{k_{r_6}}{\overset{k_{f_6}}{\rightleftharpoons}} \mathrm{SS} + \mathrm{R} \qquad \text{(AC 1.7)}$$

**Quantities**

| | Quantity Name | Type | Scope | Value | Initial Value |
|---|---|---|---|---|---|
| 1 | unnamed | compartment | Trimeric_TS | 1 | 1 |
| 2 | R | species | unnamed | 0.55 | 0.55 |
| 3 | RR | species | unnamed | 0.225 | 0.225 |
| 4 | S | species | unnamed | 0 | 0 |
| 5 | SS | species | unnamed | 0 | 0 |
| 6 | RS | species | unnamed | 0 | 0 |
| 7 | kf | parameter | Trimeric_TS | 1 | 1 |
| 8 | kr | parameter | Trimeric_TS | 1 | 1 |
| 9 | kf_1 | parameter | Trimeric_TS | 1 | 1 |
| 10 | kr_1 | parameter | Trimeric_TS | 1 | 1 |
| 11 | kf_2 | parameter | Trimeric_TS | 1 | 1 |
| 12 | kr_2 | parameter | Trimeric_TS | 1 | 1 |
| 13 | kf_5 | parameter | Trimeric_TS | 1 | 1 |

| | Quantity Name | Type | Scope | Value | Initial Value |
|---|---|---|---|---|---|
| 14 | kr_5 | parameter | Trimeric_TS | 1 | 1 |
| 15 | kf_6 | parameter | Trimeric_TS | 1 | 1 |
| 16 | kr_6 | parameter | Trimeric_TS | 1 | 1 |

**Reactions**

| | Reactions |
|---|---|
| 1 | R + R <-> RR |
| | *kf*R*R - kr*RR* |
| 2 | S + S <-> SS |
| | *kf*S*S - kr*SS* |
| 3 | R + S <-> RS |
| | *kf_1*R*S - kr_1*RS* |
| 4 | RR <-> RS |
| | *kf_2*RR - kr_2*RS* |
| 5 | SS <-> RS |
| | *kf_2*SS - kr_2*RS* |
| 6 | RS + S <-> RR + S |
| | *kf_5*RS*S - kr_5*RR*S* |
| 7 | RS + S <-> R + RS |
| | *kf_6*RS*S - kr_6*R*RS* |
| 8 | R + SS <-> RR + S |
| | *kr_6*R*SS - kf_6*RR*S* |
| 9 | R + SS <-> R + RS |
| | *kr_5*R*SS - kf_5*R*RS* |

**Observables**

| | Observables |
|---|---|
| 1 | cR = 100*(2*RR + R + RS) |
| 2 | ee = 100*((R + 2*RR + RS)-(S + 2*SS + RS)) |

**Model Equations**

**ODEs**

| | ODEs |
|---|---|
| 1 | d(R)/dt = 1/unnamed*(-2*(kf*R*R-kr*RR) - (kf_1*R*S-kr_1*RS) + (kf_6*RS*S-kr_6*R*RS) - (kr_6*R*SS-kf_6*RR*S)) |
| 2 | d(RR)/dt = 1/unnamed*((kf*R*R-kr*RR) - (kf_2*RR-kr_2*RS) + (kf_5*RS*S-kr_5*RR*S) + (kr_6*R*SS-kf_6*RR*S)) |
| 3 | d(S)/dt = 1/unnamed*(-2*(kf*S*S-kr*SS) - (kf_1*R*S-kr_1*RS) - (kf_6*RS*S-kr_6*R*RS) + (kr_6*R*SS-kf_6*RR*S)) |

| | ODEs |
|---|---|
| 4 | d(SS)/dt = 1/unnamed*((kf*S*S-kr*SS) - (kf_2*SS-kr_2*RS) - (kr_6*R*SS-kf_6*RR*S) - (kr_5*R*SS-kf_5*R*RS)) |
| 5 | d(RS)/dt = 1/unnamed*((kf_1*R*S-kr_1*RS) + (kf_2*RR-kr_2*RS) + (kf_2*SS-kr_2*RS) - (kf_5*RS*S-kr_5*RR*S) + (kr_5*R*SS-kf_5*R*RS)) |

**Program Setup**

**Data Step**

**Data Map**

| Classification | Value |
|---|---|
| group | |
| independent | Column1 |
| response | Column2 ~ ee |

**Variant and Dose Setup Step**

**Variant and Dose Setup**

| Group |
|---|
| |
| 1 |

**Fit Step**

**Estimated Parameters**

| Name | Transformation | Initial Untransformed Value | Untransformed Bounds |
|---|---|---|---|
| kf | log | 1 | [1e-10 10000000000] |
| kr | log | 1 | [1e-10 10000000000] |
| kf_1 | log | 1 | [1e-10 10000000000] |
| kr_1 | log | 1 | [1e-10 10000000000] |
| kf_2 | log | 1 | [1e-10 10000000000] |
| kr_2 | log | 1 | [1e-10 10000000000] |
| kf_5 | log | 1 | [1e-10 10000000000] |
| kr_5 | log | 1 | [1e-10 10000000000] |
| kf_6 | log | 1 | [1e-10 10000000000] |
| kr_6 | log | 1 | [1e-10 10000000000] |

**Error Model**

Use the same error model for each response: constant

**Algorithm Settings**

| Property | Value |
|---|---|
| EstimationFcn | scattersearch |
| MaxIterations | auto |
| FunctionTolerance | 1e-08 |
| MaxStallIterations | 50 |
| MaxTime | Inf |
| NumInitialPoints | auto |
| NumTrialPoints | auto |
| XTolerance | 1e-06 |
| LocalSolver | lsqnonlin |

**Local Solver Settings**

| Property | Value |
|---|---|
| StepTolerance | 1e-08 |
| FunctionTolerance | 1e-08 |
| OptimalityTolerance | 1e-06 |
| MaxIterations | 400 |

**Post Processing: Calculate Observables Step**

**Observables to Calculate**

| | Expression |
|---|---|
| 1 | ee = 100*((R + 2*RR + RS)-(S + 2*SS + RS)) |

**Program Results**

**Fit Step**

**Unpooled Parameter Estimates**

| | kf | | kr | | kf_1 | | kr_1 | |
|---|---|---|---|---|---|---|---|---|
| Group | Estimate | Standard Error | Estimate | Standard Error | Estimate | Standard Error | Estimate | Standard Error |
| One group | 2.4764e-05 | 6.8586e-07 | 3.9875e-05 | 8.8729e-07 | 890.5782 | 10.9993 | 0.0093239 | 0.00012925 |

| kf_2 | | kr_2 | | kf_5 | |
|---|---|---|---|---|---|
| Estimate | Standard Error | Estimate | Standard Error | Estimate | Standard Error |
| 0.00012123 | 1.4649e-06 | 0.00022977 | 2.9795e-06 | 0.78022 | 0.00047562 |

| kr_5 | | kf_6 | | kr_6 | |
|---|---|---|---|---|---|
| Estimate | Standard Error | Estimate | Standard Error | Estimate | Standard Error |
| 571.8213 | 6.3878 | 0.00097608 | 1.6406e-05 | 0.0046795 | 1.8639e-05 |

**Statistics**

| Group | AIC | BIC | LogLikelihood | DFE | MSE | SSE |
|---|---|---|---|---|---|---|
| One group | -5.4198 | 12.8667 | 12.7099 | 36 | 0.043052 | 1.5499 |

**Unpooled Beta**

| | kf | | kr | |
|---|---|---|---|---|
| **Group** | **Estimate** | **StandardError** | **Estimate** | **StandardError** |
| One group | -10.6061 | 0.027696 | -10.1298 | 0.022252 |

| kf_1 | | kr_1 | |
|---|---|---|---|
| **Estimate** | **Standard Error** | **Estimate** | **StandardError** |
| 6.7919 | 0.012351 | -4.6752 | 0.013862 |

| kf_2 | | kr_2 | | kf_5 | |
|---|---|---|---|---|---|
| **Estimate** | **StandardError** | **Estimate** | **StandardError** | **Estimate** | **StandardError** |
| -9.0178 | 0.012083 | -8.3784 | 0.012968 | -0.24818 | 0.0006096 |

| kr_5 | | kf_6 | | kr_6 | |
|---|---|---|---|---|---|
| **Estimate** | **StandardError** | **Estimate** | **StandardError** | **Estimate** | **StandardError** |
| 6.3488 | 0.011171 | -6.932 | 0.016808 | -5.3646 | 0.0039831 |

**Residuals**

| Column1 | Column2 | Column1 | Column2 |
|---|---|---|---|
| 0 | 0.33 | 2400 | -0.21012 |
| 60 | -0.086641 | 2550 | -0.17805 |
| 120 | 0.038529 | 2700 | -0.17326 |
| 180 | 0.00035702 | 2850 | -0.15071 |
| 240 | 0.14551 | 3000 | -0.19639 |
| 300 | 0.14339 | 3150 | -0.086154 |
| 360 | 0.29475 | 3300 | -0.098142 |
| 420 | 0.15517 | 3450 | -0.54337 |
| 480 | 0.075543 | 3600 | -0.13939 |
| 540 | -0.13793 | 3900 | -0.28228 |
| 600 | -0.084757 | 4200 | -0.24819 |
| 660 | -0.14871 | 4500 | -0.19452 |
| 720 | -0.097597 | 4800 | -0.20086 |
| 780 | 0.094272 | 5100 | -0.12605 |
| 840 | 0.28828 | 5400 | 0.019512 |
| 900 | 0.13731 | 6000 | -0.045007 |
| 960 | -0.062752 | 6600 | -0.048769 |
| 1020 | -0.32627 | 7200 | -0.028952 |
| 1080 | -0.14449 | | |
| 1140 | -0.039987 | | |
| 1200 | 0.09872 | | |
| 1350 | 0.2593 | | |
| 1500 | 0.02306 | | |
| 1650 | -0.11409 | | |
| 1800 | -0.18528 | | |
| 1950 | -0.17936 | | |
| 2100 | -0.19947 | | |
| 2250 | -0.18798 | | |

**Covariance Matrix**

| Group | Parameters | log(kf) | log(kr) | log(kf_1) | log(kr_1) |
|---|---|---|---|---|---|
| One group | log(kf) | 4.704e-13 | 3.6607e-13 | -6.3956e-06 | -5.2824e-11 |
| One group | log(kr) | 3.6607e-13 | 7.8729e-13 | -8.2188e-06 | -6.8359e-11 |
| One group | log(kf_1) | -6.3956e-06 | -8.2188e-06 | 120.9848 | 0.00059037 |
| One group | log(kr_1) | -5.2824e-11 | -6.8359e-11 | 0.00059037 | 1.6705e-08 |

| Group | Parameters | log(kf) | log(kr) | log(kf_1) | log(kr_1) |
|---|---|---|---|---|---|
| One group | log(kf_2) | -1.5627e-14 | -1.8577e-13 | 9.9736e-07 | -4.1582e-11 |
| One group | log(kr_2) | -1.3329e-12 | -3.8622e-13 | 7.1099e-06 | 2.5234e-10 |
| One group | log(kf_5) | 2.6511e-10 | 2.5289e-10 | -0.0031795 | -5.1098e-08 |
| One group | log(kr_5) | -2.1926e-07 | 2.4953e-07 | 19.5315 | -0.00038756 |
| One group | log(kf_6) | -3.3611e-12 | -5.276e-13 | 2.3241e-05 | 4.1475e-10 |
| One group | log(kr_6) | -9.2526e-12 | -9.2236e-12 | 0.00015512 | 6.148e-10 |

| log(kf_2) | log(kr_2) | log(kf_5) | log(kr_5) | log(kf_6) | log(kr_6) |
|---|---|---|---|---|---|
| -1.5627e-14 | -1.3329e-12 | 2.6511e-10 | -2.1926e-07 | -3.3611e-12 | -9.2526e-12 |
| -1.8577e-13 | -3.8622e-13 | 2.5289e-10 | 2.4953e-07 | -5.276e-13 | -9.2236e-12 |
| 9.9736e-07 | 7.1099e-06 | -0.0031795 | 19.5315 | 2.3241e-05 | 0.00015512 |
| -4.1582e-11 | 2.5234e-10 | -5.1098e-08 | -0.00038756 | 4.1475e-10 | 6.148e-10 |
| 2.1459e-12 | 1.001e-12 | -1.6441e-11 | -3.9637e-06 | 1.8116e-12 | 6.0089e-12 |
| 1.001e-12 | 8.8777e-12 | -1.0724e-09 | -1.1215e-05 | 1.795e-11 | 1.7664e-11 |
| -1.6441e-11 | -1.0724e-09 | 2.2622e-07 | 0.00086406 | -2.4942e-09 | -3.3986e-09 |
| -3.9637e-06 | -1.1215e-05 | 0.00086406 | 40.8045 | -1.4879e-05 | -2.1966e-06 |
| 1.8116e-12 | 1.795e-11 | -2.4942e-09 | -1.4879e-05 | 2.6914e-10 | 5.8093e-11 |
| 6.0089e-12 | 1.7664e-11 | -3.3986e-09 | -2.1966e-06 | 5.8093e-11 | 3.4741e-10 |

**Error Model**

| Group | Response | ErrorModel | a |
|---|---|---|---|
| One group | Column2 | constant | 0.18356 |

**Program Plots**

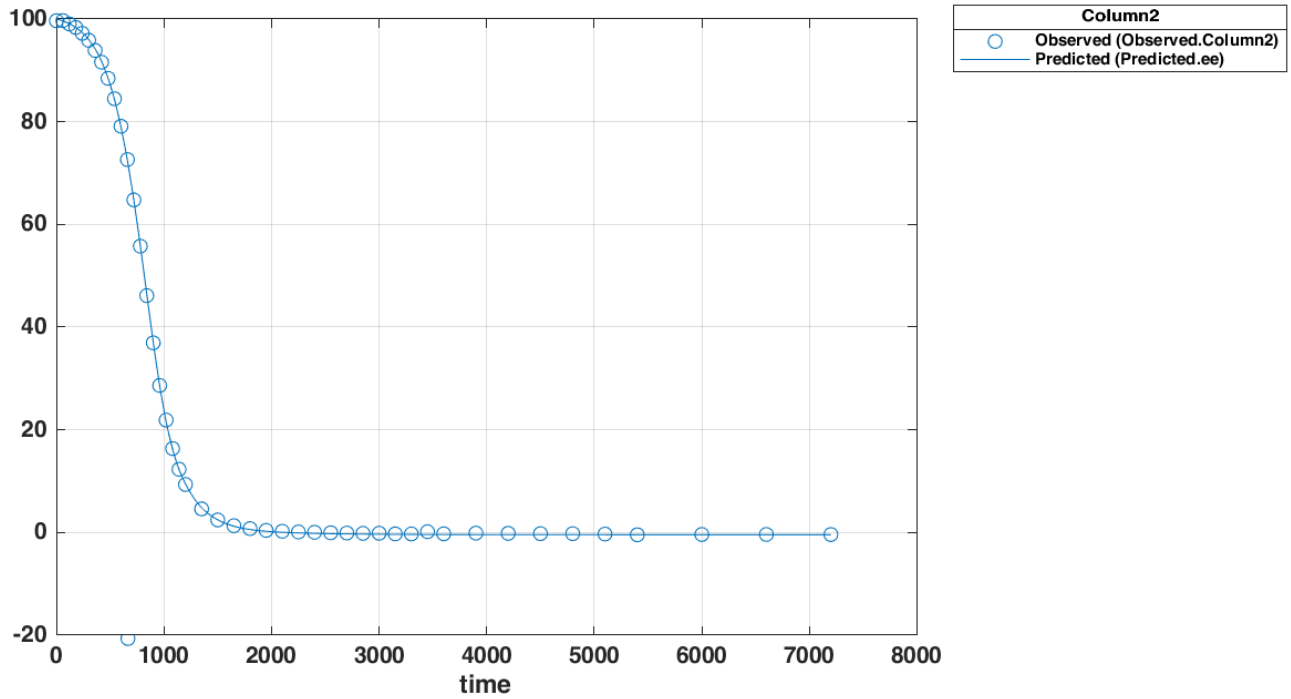



Figure 1 : Fit Plot

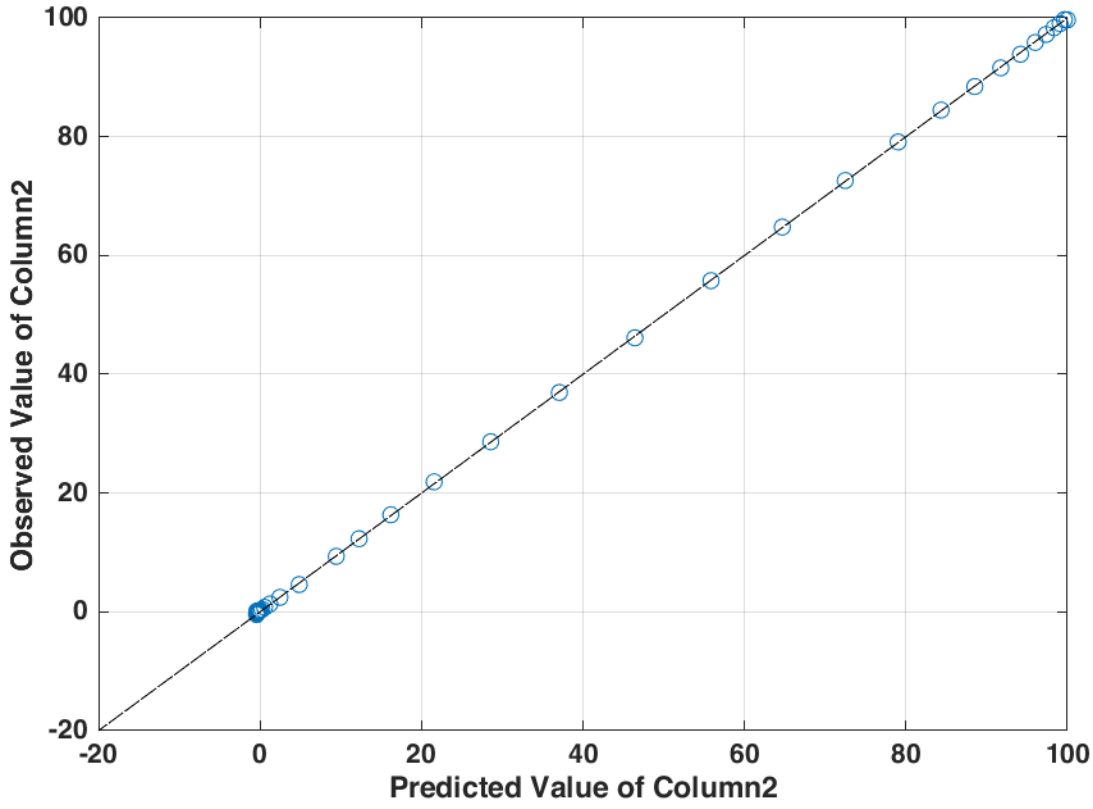



Figure 2 : Actual_vs_predicted Plot

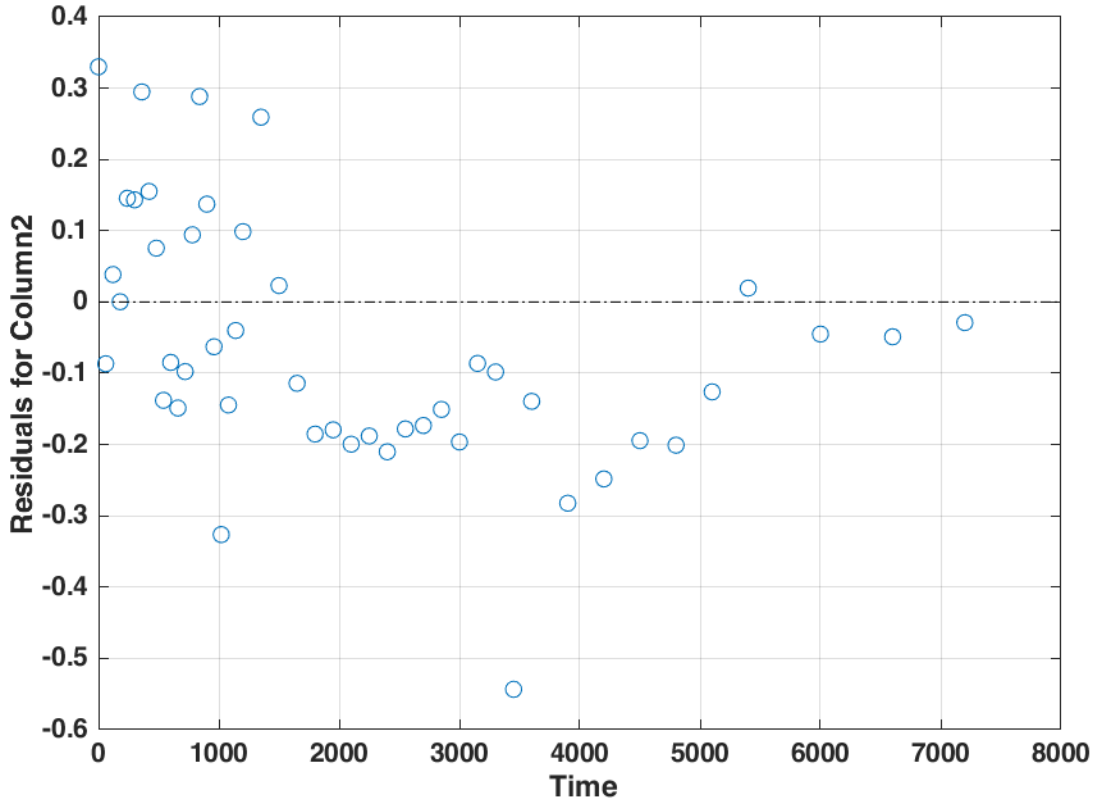



Figure 3 :

Residuals Plot

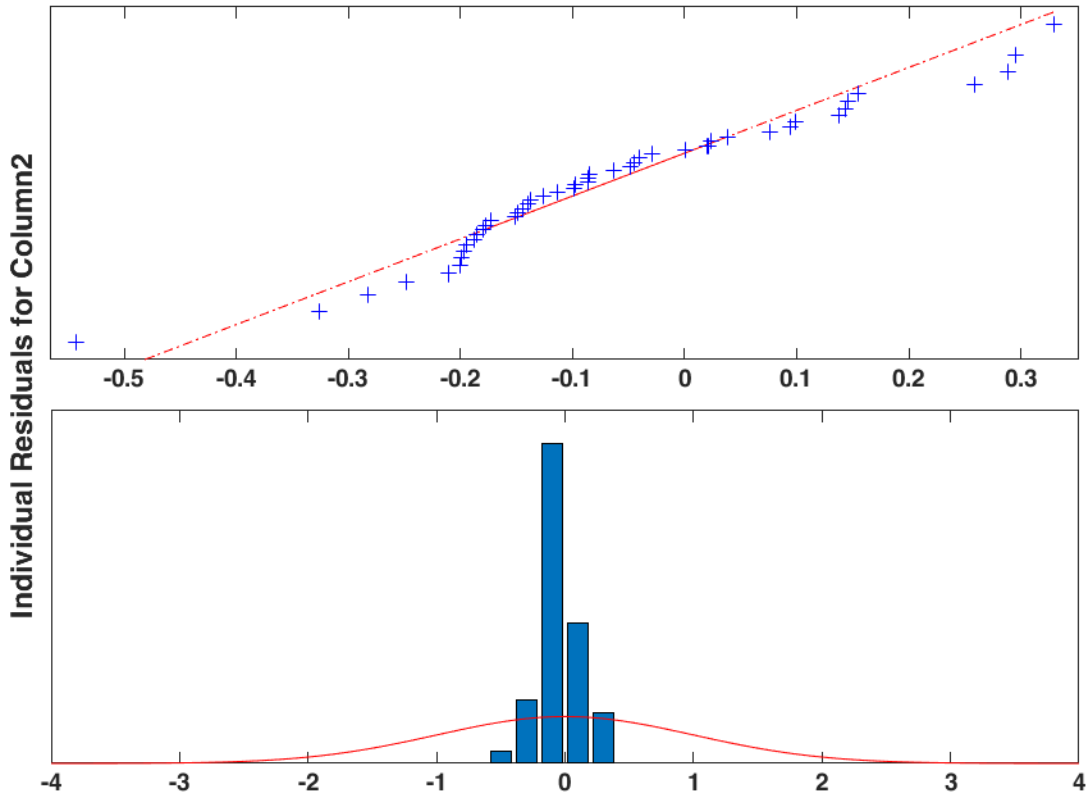



Figure 4 :

Residual_distribution Plot

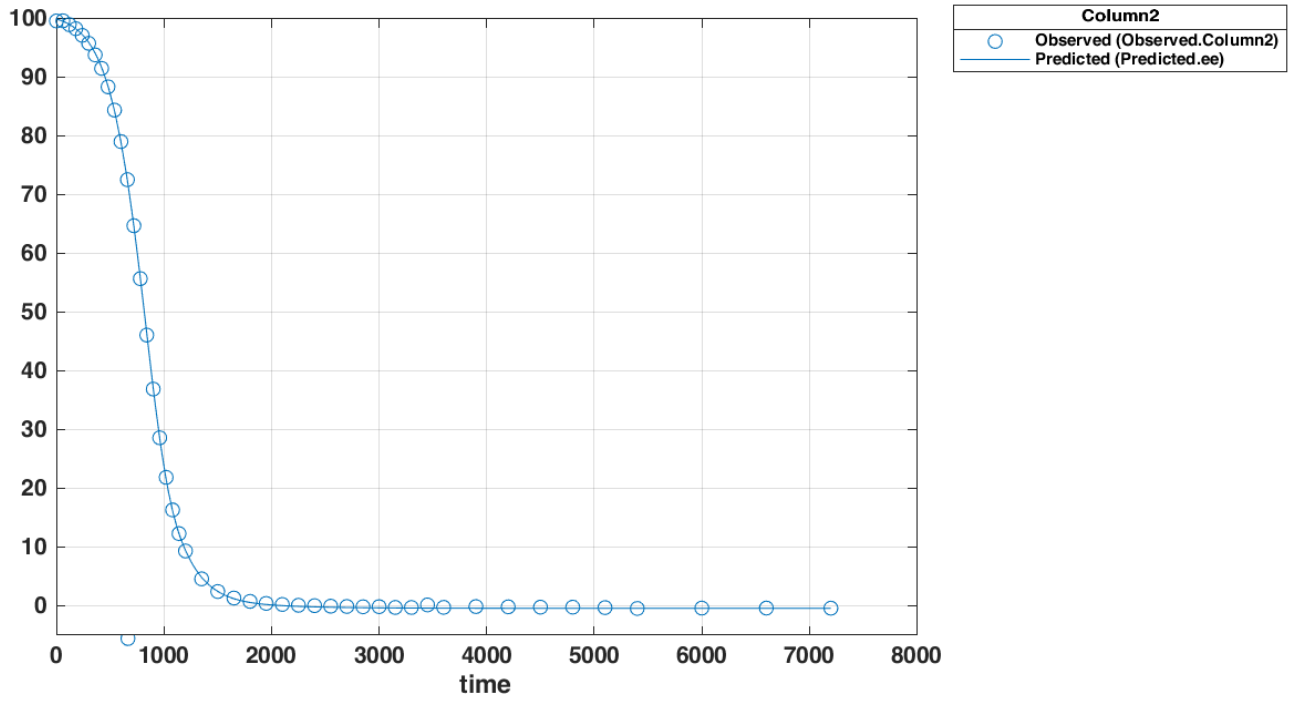



Figure 5 : Fit Plot

**Fit Code**

```
function args = runprogram(model, cs, data, variantsStruct, dosesStruct)

% Initialize arguments.
args.input.model    = model;
args.input.cs       = cs;
args.input.data     = data;
args.input.variants = variantsStruct;
args.input.doses    = dosesStruct;

% Run fit.
args = runFit(args);


end

% --------------------------------------------------------------------
function args = runFit(args)

% Extract the input arguments.
input    = args.input;
data     = input.data;
model    = input.model;
cs       = input.cs;
variants = input.variants.modelStep;
doses    = input.doses.modelStep;

% Set the active configuration set.
originalConfigset = getconfigset(model, 'active');
setactiveconfigset(model, cs);
```

```
% Restore the original configset after the task has completed running.
cleanupConfigset = onCleanup(@() restoreActiveConfigset(model, originalConfigset));

% Turn off observables.
observables       = model.Observables;
activateState     = get(observables, {'Active'});
cleanupObservables = onCleanup(@() restoreObservables(observables, activateState));
set(observables, 'Active', false);

% Turn on observables.
obsNames    = {'cR', 'ee'};
observables = sbioselect(model.Observables, 'Name', obsNames);
set(observables, 'Active', true);

% Define a description of the data.
groupedDataObj                          = groupedData(data);
groupedDataObj.Properties.GroupVariableName      = 'Column3';
groupedDataObj.Properties.IndependentVariableName = 'Column1';

% Define objects being estimated and their initial estimates.
estimatedInfoObj = estimatedInfo({'log(kf)', 'log(kr)', 'log(kf_1)', 'log(kr_1)', 'log(kf_2)', 'log(kr_2)', 'log(kf_5)',
'log(kr_5)', 'log(kf_6)', 'log(kr_6)'});
estimatedInfoObj(1).InitialValue = 2.4764e-05;
estimatedInfoObj(1).Bounds       = [1e-10 100000];
estimatedInfoObj(2).InitialValue = 3.9875e-05;
estimatedInfoObj(2).Bounds       = [1e-10 100000];
estimatedInfoObj(3).InitialValue = 890.5782;
estimatedInfoObj(3).Bounds       = [1e-10 100000];
estimatedInfoObj(4).InitialValue = 0.0093239;
estimatedInfoObj(4).Bounds       = [1e-10 100000];
estimatedInfoObj(5).InitialValue = 0.00012123;
estimatedInfoObj(5).Bounds       = [1e-10 100000];
estimatedInfoObj(6).InitialValue = 0.00022977;
estimatedInfoObj(6).Bounds       = [1e-10 100000];
estimatedInfoObj(7).InitialValue = 0.78022;
estimatedInfoObj(7).Bounds       = [1e-10 100000];
estimatedInfoObj(8).InitialValue = 571.8213;
estimatedInfoObj(8).Bounds       = [1e-10 100000];
estimatedInfoObj(9).InitialValue = 0.00097608;
estimatedInfoObj(9).Bounds       = [1e-10 100000];
estimatedInfoObj(10).InitialValue = 0.0046795;
estimatedInfoObj(10).Bounds      = [1e-10 100000];

% Get the variants needed from the model.
v1  = sbioselect(getvariant(model), 'Name', 'ee_rub_values');

% Create the group specific variant array.
variants1 = {v1; v1; v1; v1};

% Build table of variants.
variantList = [variants4, variants3, variants2, variants1];

% Convert cell matrix to a cell with one column.
variantsForFit = cell(size(variantList, 1), 1);
for i = 1:numel(variantsForFit)
   next            = variantList(i, :);
   variantsForFit{i} = [next{:}];
end
```

```
% Build array of doses.
dosesForFit = [];

% Define response information.
responseMap = {'cR = Column2'};

% Define Algorithm options.
options                 = struct;
options.MaxIterations     = 'auto';
options.FunctionTolerance  = 1e-08;
options.MaxStallIterations = 50;
options.MaxTime           = Inf;
options.NumInitialPoints   = 'auto';
options.NumTrialPoints     = 'auto';
options.XTolerance        = 1e-06;
options.LocalSolver       = 'lsqnonlin';

% Build local solver options
localSolverOptions                    = optimoptions('lsqnonlin');
localSolverOptions.StepTolerance         = 1e-08;
localSolverOptions.FunctionTolerance     = 1e-08;
localSolverOptions.OptimalityTolerance    = 1e-06;
localSolverOptions.MaxIterations         = 400;
localSolverOptions.MaxFunctionEvaluations = 4000;

% Set local solver options to scattersearch
options.LocalOptions = localSolverOptions;

% Define fit problem.
f            = fitproblem('FitFunction', 'sbiofit');
f.Data        = groupedDataObj;
f.Model       = model;
f.Estimated    = estimatedInfoObj;
f.ResponseMap  = responseMap;
f.ErrorModel   = 'constant';
f.Variants     = variantsForFit;
f.Doses       = dosesForFit;
f.FunctionName = 'scattersearch';
f.Options      = options;
f.ProgressPlot = true;
f.UseParallel  = false;
f.Pooled       = true;

% Estimate parameter values.
[results, simdataI] = f.fit;

% Configure the names of the resulting simulation data.
for i = 1:length(simdataI)
   simdataI(i).Name = 'SimData Individual';
end

% Assign output arguments.
args.output.results  = results;
args.output.simdataI = simdataI;

end

% ---------------------------------------------------------------------------
function restoreActiveConfigset(model, cs)
```

```
% Restore active configset.
setactiveconfigset(model, cs);

end

% ---------------------------------------------------------------------
function restoreObservables(observables, active)

for i = 1:length(observables)
   set(observables(i), 'Active', active{i});
end

end
```

**Tetramer Model**

$$\mathrm{R} + \mathrm{R} \underset{kr}{\overset{kf}{\rightleftharpoons}} \mathrm{RR} \qquad (\mathrm{AC2.1})$$

$$\mathrm{S} + \mathrm{S} \underset{kr}{\overset{kf}{\rightleftharpoons}} \mathrm{SS} \qquad (\mathrm{AC2.2})$$

$$\mathrm{R} + \mathrm{S} \underset{kr_1}{\overset{kf_1}{\rightleftharpoons}} \mathrm{RS} \qquad (\mathrm{AC2.3})$$

$$\mathrm{RR} \underset{kr_2}{\overset{kf_2}{\rightleftharpoons}} \mathrm{RS} \underset{kf_2}{\overset{kr_2}{\rightleftharpoons}} \mathrm{SS} \qquad (\mathrm{AC2.4})$$

$$\mathrm{RR} + \mathrm{RS} \underset{kr_3}{\overset{kf_3}{\rightleftharpoons}} 2\,\mathrm{RS} \underset{kf_3}{\overset{kr_3}{\rightleftharpoons}} \mathrm{SS} + \mathrm{RS} \qquad (\mathrm{AC2.5})$$

**Model: Dimer_dimer_AC**

**Quantities**

| | Quantity Name | Type | Scope | Value | Initial Value |
|---|---|---|---|---|---|
| 1 | unnamed | compartment | Dimer_dimer_AC | 1 | 1 |
| 2 | R | species | unnamed | 0.55 | 0.55 |
| 3 | RR | species | unnamed | 0.225 | 0.225 |
| 4 | S | species | unnamed | 0 | 0 |
| 5 | SS | species | unnamed | 0 | 0 |
| 6 | RS | species | unnamed | 0 | 0 |
| 7 | kf | parameter | Dimer_dimer_AC | 1 | 1 |
| 8 | kr | parameter | Dimer_dimer_AC | 1 | 1 |
| 9 | kf_1 | parameter | Dimer_dimer_AC | 1 | 1 |
| 10 | kr_1 | parameter | Dimer_dimer_AC | 1 | 1 |
| 11 | kf_2 | parameter | Dimer_dimer_AC | 1 | 1 |
| 12 | kr_2 | parameter | Dimer_dimer_AC | 1 | 1 |
| 13 | kf_3 | parameter | Dimer_dimer_AC | 1 | 1 |

| | Quantity Name | Type | Scope | Value | Initial Value |
|---|---|---|---|---|---|
| 14 | kr_3 | parameter | Dimer_dimer_AC | 1 | 1 |

**Reactions**

| | Reactions |
|---|---|
| 1 | R + R <-> RR |
| | *kf*R*R - kr*RR* |
| 2 | S + S <-> SS |
| | *kf*S*S - kr*SS* |
| 3 | R + S <-> RS |
| | *kf_1*R*S - kr_1*RS* |
| 4 | RR <-> RS |
| | *kf_2*RR - kr_2*RS* |
| 5 | SS <-> RS |
| | *kf_2*SS - kr_2*RS* |
| 6 | RS + RR <-> 2 RS |
| | *kf_3*RS*RR - kr_3*RS^2* |
| 7 | RS + SS <-> 2 RS |
| | *kf_3*RS*SS - kr_3*RS^2* |

**Observables**

| | Observables |
|---|---|
| 1 | ee = 100*((R + 2*RR + RS) - (S + 2*SS + RS)) |

**Model Equations**

**ODEs**

| | ODEs |
|---|---|
| 1 | d(R)/dt = 1/unnamed*(-2*(kf*R*R-kr*RR) - (kf_1*R*S-kr_1*RS)) |
| 2 | d(RR)/dt = 1/unnamed*((kf*R*R-kr*RR) - (kf_2*RR-kr_2*RS) - (kf_3*RS*RR-kr_3*RS^2)) |
| 3 | d(S)/dt = 1/unnamed*(-2*(kf*S*S-kr*SS) - (kf_1*R*S-kr_1*RS)) |
| 4 | d(SS)/dt = 1/unnamed*((kf*S*S-kr*SS) - (kf_2*SS-kr_2*RS) - (kf_3*RS*SS-kr_3*RS^2)) |
| 5 | d(RS)/dt = 1/unnamed*((kf_1*R*S-kr_1*RS) + (kf_2*RR-kr_2*RS) + (kf_2*SS-kr_2*RS) + (kf_3*RS*RR-kr_3*RS^2) + (kf_3*RS*SS-kr_3*RS^2)) |

**Program Setup**

1. **Data Step**

**Data Map**

| Classification | Value |
|---|---|
| group | |
| independent | Column1 |
| response | Column2 ~ ee |

2. **Variant and Dose Setup Step**

**Variant and Dose Setup**

| Group |
|---|
| |
| 1 |

3. **Fit Step**

**Estimated Parameters**

| Name | Transformation | Initial Untransformed Value | Untransformed Bounds |
|---|---|---|---|
| kf | log | 1 | [1e-10 10000000000] |
| kr | log | 1 | [1e-10 10000000000] |
| kf_1 | log | 1 | [1e-10 10000000000] |
| kr_1 | log | 1 | [1e-10 10000000000] |
| kf_2 | log | 1 | [1e-10 10000000000] |
| kr_2 | log | 1 | [1e-10 10000000000] |
| kf_3 | log | 1 | [1e-10 10000000000] |
| kr_3 | log | 1 | [1e-10 10000000000] |

**Error Model**

Use the same error model for each response: constant

**Algorithm Settings**

| Property | Value |
|---|---|
| EstimationFcn | scattersearch |
| MaxIterations | auto |
| FunctionTolerance | 1e-08 |
| MaxStallIterations | 50 |
| MaxTime | Inf |
| NumInitialPoints | auto |
| NumTrialPoints | auto |
| XTolerance | 1e-06 |
| LocalSolver | lsqnonlin |

**Local Solver Settings**

| Property | Value |
|---|---|
| StepTolerance | 1e-08 |
| FunctionTolerance | 1e-08 |
| OptimalityTolerance | 1e-06 |
| MaxIterations | 400 |

**4. Post Processing: Calculate Observables Step**

**Observables to Calculate**

| | Expression |
|---|---|
| 1 | ee = 100*((R + 2*RR + RS) - (S + 2*SS + RS)) |

**Program Results**

**5. Fit Step**

**Unpooled Parameter Estimates**

| kf | | kr | | kf_1 | | kr_1 | |
|---|---|---|---|---|---|---|---|
| **Estimate** | **Standard Error** | **Estimate** | **Standard Error** | **Estimate** | **Standard Error** | **Estimate** | **Standard Error** |
| 0.0020945 | 1.6119e-06 | 1.2323e-05 | 2.1762e-05 | 0.45762 | 0.0017372 | 367.477 | 0.14024 |

| kf_2 | | kr_2 | | kf_3 | | kr_3 | |
|---|---|---|---|---|---|---|---|
| **Estimate** | **Standard Error** | **Estimate** | **Standard Error** | **Estimate** | **Standard Error** | **Estimate** | **Standard Error** |
| 8.1885e-05 | 1.3427e-06 | 4.5744e-07 | 4.4179e-09 | 40.0136 | 0.25583 | 6.2354e-10 | 7.9847e-07 |

**Statistics**

| Group | AIC | BIC | LogLikelihood | DFE | MSE | SSE |
|---|---|---|---|---|---|---|
| One group | 4.5696 | 19.1987 | 5.7152 | 38 | 0.055282 | 2.1007 |

**Unpooled Beta**

| kf | | kr | | kf_1 | | kr_1 | |
|---|---|---|---|---|---|---|---|
| **Estimate** | **Standard Error** | **Estimate** | **Standard Error** | **Estimate** | **Standard Error** | **Estimate** | **Standard Error** |
| -6.1684 | 0.00076956 | -11.304 | 1.7659 | -0.78172 | 0.0037961 | 5.9067 | 0.00038164 |

| kf_2 | | kr_2 | | kf_3 | | kr_3 | |
|---|---|---|---|---|---|---|---|
| **Estimate** | **Standard Error** | **Estimate** | **Standard Error** | **Estimate** | **Standard Error** | **Estimate** | **Standard Error** |
| -9.4102 | 0.016397 | -14.5976 | 0.009658 | 3.6892 | 0.0063936 | -21.1956 | 1280.535 |

**Residuals**

| Column1 | Column2 | Column1 | Column2 | Column1 | Column2 |
|---|---|---|---|---|---|
| 0 | 0.33 | 960 | 0.06084 | 3000 | 0.14598 |
| 60 | 0.0041347 | 1020 | -0.16875 | 3150 | 0.26864 |
| 120 | 0.19349 | 1080 | -0.0556 | 3300 | 0.27129 |
| 180 | 0.1861 | 1140 | -0.096233 | 3450 | -0.16246 |
| 240 | 0.32629 | 1200 | -0.13006 | 3600 | 0.2525 |

| Column1 | Column2 | Column1 | Column2 | Column1 | Column2 |
|---|---|---|---|---|---|
| 300 | 0.28591 | 1350 | 0.15348 | 3900 | 0.12422 |
| 360 | 0.37546 | 1500 | 0.1536 | 4200 | 0.16574 |
| 420 | 0.16534 | 1650 | 0.14122 | 4500 | 0.22299 |
| 480 | 0.025311 | 1800 | 0.095978 | 4800 | 0.219 |
| 540 | -0.22137 | 1950 | 0.084978 | 5100 | 0.29582 |
| 600 | -0.16944 | 2100 | 0.052191 | 5400 | 0.44248 |
| 660 | -0.21657 | 2250 | 0.06914 | 6000 | 0.37991 |
| 720 | -0.15607 | 2400 | 0.062576 | 6600 | 0.37671 |
| 780 | 0.026707 | 2550 | 0.11406 | 7200 | 0.39671 |
| 840 | 0.22236 | 2700 | 0.13761 | 3000 | 0.14598 |
| 900 | 0.13977 | 2850 | 0.17561 | | |

**Covariance Matrix**

| Group | Parameters | log(kf) | log(kr) | log(kf_1) | log(kr_1) | log(kf_2) | log(kr_2) | log(kf_3) | log(kr_3) |
|---|---|---|---|---|---|---|---|---|---|
| One group | log(kf) | 2.5981e-12 | 5.6392e-12 | -1.6086e-10 | -1.0728e-08 | -1.9627e-13 | -2.2306e-15 | 2.0922e-08 | -2.7955e-13 |
| One group | log(kr) | 5.6392e-12 | 4.7359e-10 | -3.1035e-08 | 2.0182e-06 | -1.4201e-11 | 1.0499e-14 | 2.6131e-06 | -6.0286e-12 |
| One group | log(kf_1) | -1.6086e-10 | -3.1035e-08 | 3.0178e-06 | -9.713e-05 | 1.9914e-09 | -1.0288e-12 | -0.00037744 | 2.9998e-10 |
| One group | log(kr_1) | -1.0728e-08 | 2.0182e-06 | -9.713e-05 | 0.019668 | -1.8271e-08 | 1.1892e-10 | 0.0029316 | -5.1929e-08 |
| One group | log(kf_2) | -1.9627e-13 | -1.4201e-11 | 1.9914e-09 | -1.8271e-08 | 1.8027e-12 | -3.6246e-16 | -3.4301e-07 | 5.8541e-14 |
| One group | log(kr_2) | -2.2306e-15 | 1.0499e-14 | -1.0288e-12 | 1.1892e-10 | -3.6246e-16 | 1.9518e-17 | 8.2827e-11 | -7.7049e-16 |
| One group | log(kf_3) | 2.0922e-08 | 2.6131e-06 | -0.00037744 | 0.0029316 | -3.4301e-07 | 8.2827e-11 | 0.065449 | -1.0234e-08 |
| One group | log(kr_3) | -2.7955e-13 | -6.0286e-12 | 2.9998e-10 | -5.1929e-08 | 5.8541e-14 | -7.7049e-16 | -1.0234e-08 | 6.3755e-13 |

**Error Model**

| Group | Response | ErrorModel | a |
|---|---|---|---|
| One group | Column2 | constant | 0.2137 |

**Program Plots**

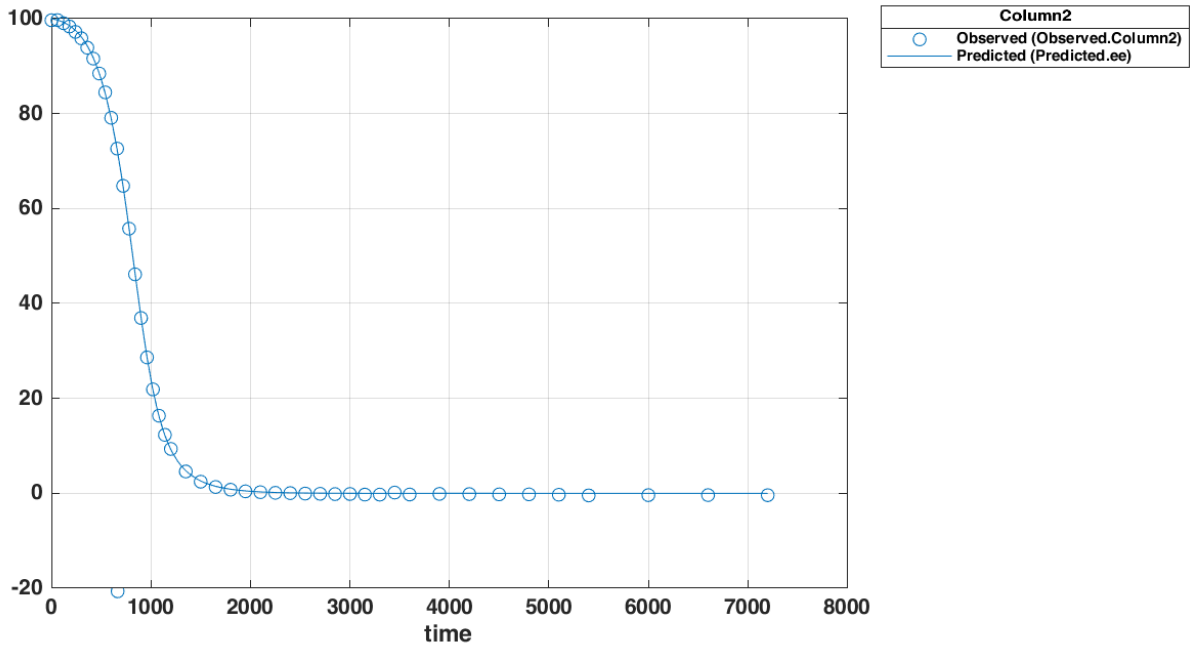



Figure 1 : Fit Plot

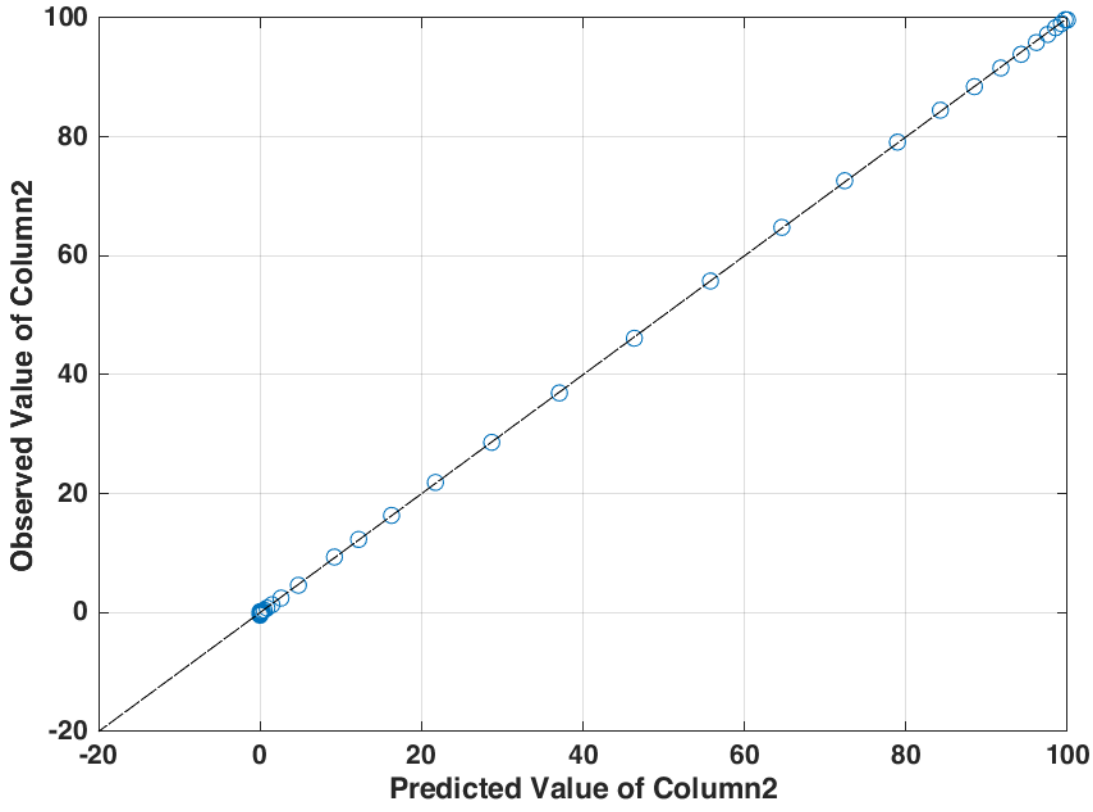



Figure 2 : Actual_vs_predicted Plot

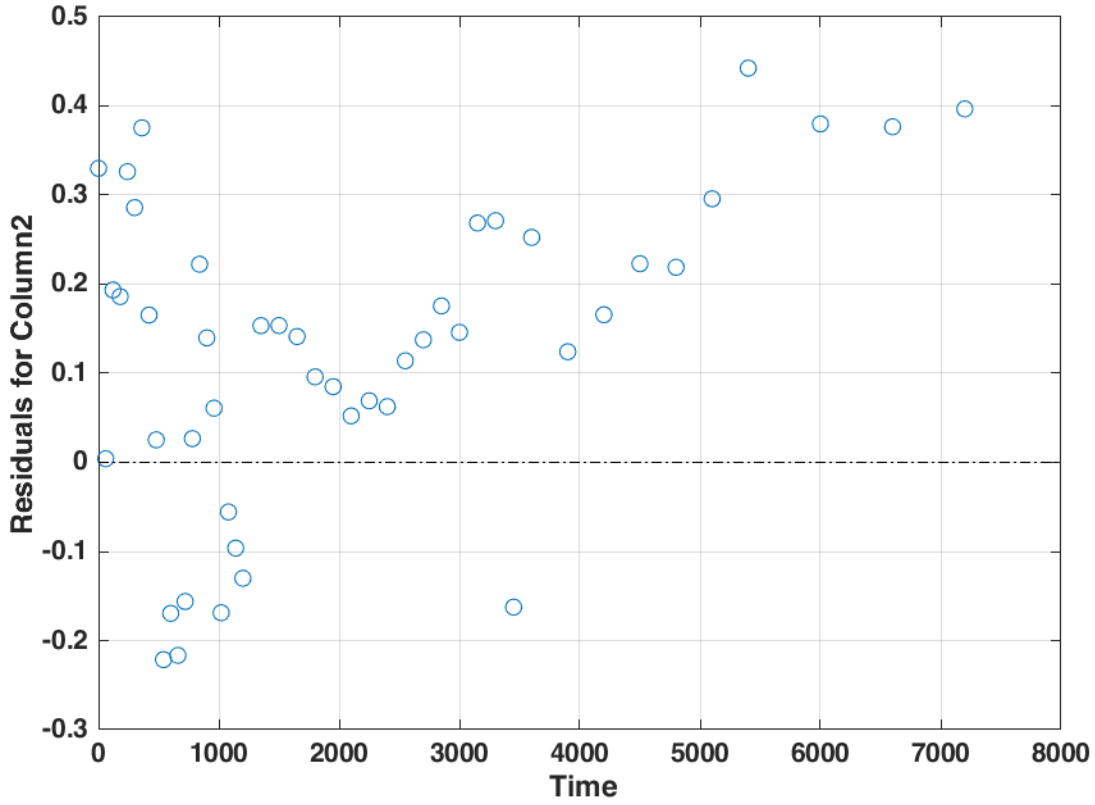



Figure3 : Residuals Plot

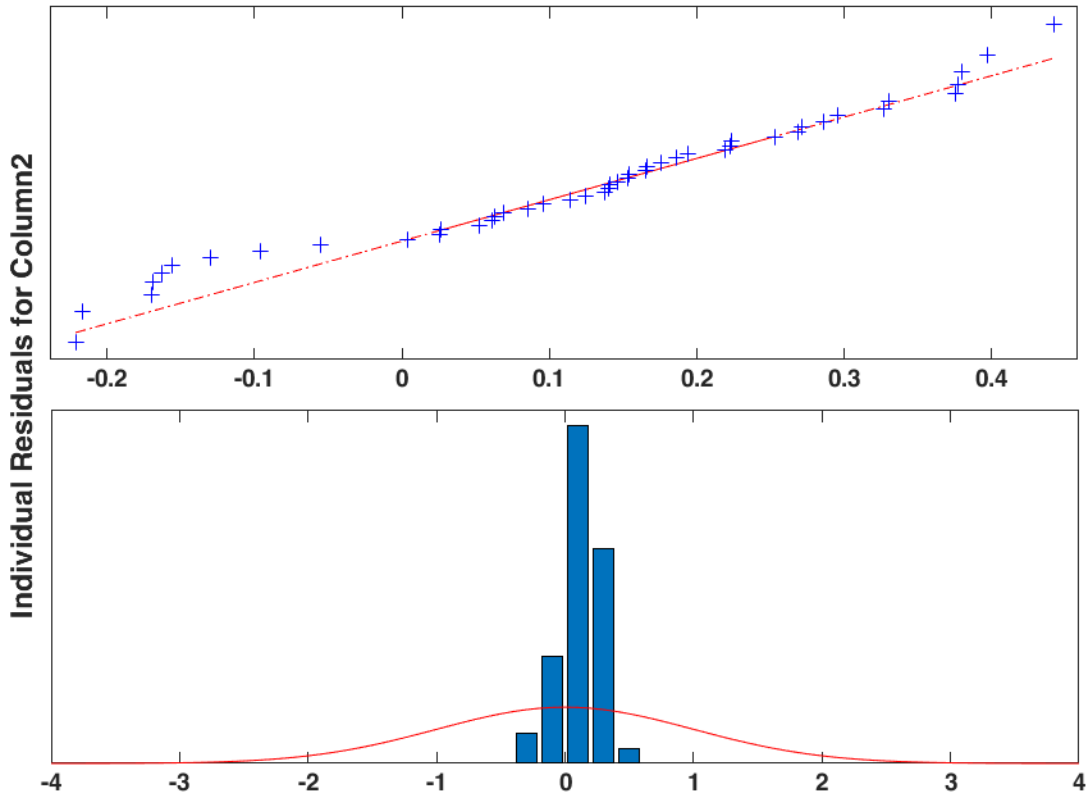



Figure4 : Residual_distribution Plot

**Fit Code**

```
function args = runprogram(model, cs, data, variantsStruct, dosesStruct)

% Initialize arguments.
args.input.model    = model;
args.input.cs       = cs;
args.input.data     = data;
args.input.variants = variantsStruct;
args.input.doses    = dosesStruct;

% Run fit.
args = runFit(args);


end

% ---------------------------------------------------------------------------
function args = runFit(args)

% Extract the input arguments.
input    = args.input;
data     = input.data;
model    = input.model;
cs       = input.cs;
variants = input.variants.modelStep;
doses    = input.doses.modelStep;

% Set the active configuration set.
originalConfigset = getconfigset(model, 'active');
setactiveconfigset(model, cs);

% Restore the original configset after the task has completed running.
cleanupConfigset = onCleanup(@() restoreActiveConfigset(model, originalConfigset));

% Turn off observables.
observables       = model.Observables;
activateState     = get(observables, {'Active'});
cleanupObservables = onCleanup(@() restoreObservables(observables, activateState));
set(observables, 'Active', false);

% Turn on observables.
obsNames    = {'ee'};
observables = sbioselect(model.Observables, 'Name', obsNames);
set(observables, 'Active', true);

% Define a description of the data.
groupedDataObj                          = groupedData(data);
groupedDataObj.Properties.GroupVariableName      = '';
groupedDataObj.Properties.IndependentVariableName = 'Column1';

% Define objects being estimated and their initial estimates.
estimatedInfoObj = estimatedInfo({'log(kf)', 'log(kr)', 'log(kf_1)', 'log(kr_1)', 'log(kf_2)', 'log(kr_2)', 'log(kf_3)',
'log(kr_3)'});
estimatedInfoObj(1).InitialValue = 1;
estimatedInfoObj(1).Bounds       = [1e-10 10000000000];
estimatedInfoObj(2).InitialValue = 1;
estimatedInfoObj(2).Bounds       = [1e-10 10000000000];
estimatedInfoObj(3).InitialValue = 1;
estimatedInfoObj(3).Bounds       = [1e-10 10000000000];
```

```
estimatedInfoObj(4).InitialValue = 1;
estimatedInfoObj(4).Bounds      = [1e-10 10000000000];
estimatedInfoObj(5).InitialValue = 1;
estimatedInfoObj(5).Bounds      = [1e-10 10000000000];
estimatedInfoObj(6).InitialValue = 1;
estimatedInfoObj(6).Bounds      = [1e-10 10000000000];
estimatedInfoObj(7).InitialValue = 1;
estimatedInfoObj(7).Bounds      = [1e-10 10000000000];
estimatedInfoObj(8).InitialValue = 1;
estimatedInfoObj(8).Bounds      = [1e-10 10000000000];

% Build array of doses.
dosesForFit = [];

% Define response information.
responseMap = {'ee = Column2'};

% Define Algorithm options.
options                 = struct;
options.MaxIterations     = 'auto';
options.FunctionTolerance  = 1e-08;
options.MaxStallIterations = 50;
options.MaxTime           = Inf;
options.NumInitialPoints   = 'auto';
options.NumTrialPoints     = 'auto';
options.XTolerance        = 1e-06;
options.LocalSolver       = 'lsqnonlin';

% Build local solver options
localSolverOptions                  = optimoptions('lsqnonlin');
localSolverOptions.StepTolerance      = 1e-08;
localSolverOptions.FunctionTolerance   = 1e-08;
localSolverOptions.OptimalityTolerance = 1e-06;
localSolverOptions.MaxIterations      = 400;

% Set local solver options to scattersearch
options.LocalOptions = localSolverOptions;

% Define fit problem.
f            = fitproblem('FitFunction', 'sbiofit');
f.Data        = groupedDataObj;
f.Model       = model;
f.Estimated    = estimatedInfoObj;
f.ResponseMap  = responseMap;
f.ErrorModel   = 'constant';
f.Doses       = dosesForFit;
f.FunctionName = 'scattersearch';
f.Options      = options;
f.ProgressPlot = true;
f.UseParallel  = false;
f.Pooled       = 'auto';

% Estimate parameter values.
[results, simdataI] = f.fit;

% Configure the names of the resulting simulation data.
for i = 1:length(simdataI)
   simdataI(i).Name = 'SimData Individual';
end
```

```
% Assign output arguments.
args.output.results  = results;
args.output.simdataI = simdataI;

end

% ------------------------------------------------------------------------
function restoreActiveConfigset(model, cs)

% Restore active configset.
setactiveconfigset(model, cs);

end

% ------------------------------------------------------------------------
function restoreObservables(observables, active)

for i = 1:length(observables)
   set(observables(i), 'Active', active{i});
end

end
```

### II.7.2 Concentration Based Fits

**Trimer**

**Quantities**

| | Quantity Name | Type | Scope | Value | Initial Value |
|---|---|---|---|---|---|
| 1 | unnamed | compartment | Trimeric_TS | 1 | 1 |
| 2 | R | species | unnamed | 0 | 0 |
| 3 | RR | species | unnamed | 0 | 0 |
| 4 | S | species | unnamed | 0 | 0 |
| 5 | SS | species | unnamed | 0 | 0 |
| 6 | RS | species | unnamed | 0 | 0 |
| 7 | kf | parameter | Trimeric_TS | 1 | 1 |
| 8 | kr | parameter | Trimeric_TS | 1 | 1 |
| 9 | kf_1 | parameter | Trimeric_TS | 1 | 1 |
| 10 | kr_1 | parameter | Trimeric_TS | 1 | 1 |
| 11 | kf_2 | parameter | Trimeric_TS | 1 | 1 |
| 12 | kr_2 | parameter | Trimeric_TS | 1 | 1 |
| 13 | kf_5 | parameter | Trimeric_TS | 1 | 1 |
| 14 | kr_5 | parameter | Trimeric_TS | 1 | 1 |
| 15 | kf_6 | parameter | Trimeric_TS | 1 | 1 |
| 16 | kr_6 | parameter | Trimeric_TS | 1 | 1 |

**Reactions**

| | Reactions |
|---|---|
| 1 | R + R <-> RR |
| | *kf*R*R - kr*RR* |
| 2 | S + S <-> SS |
| | *kf*S*S - kr*SS* |
| 3 | R + S <-> RS |
| | *kf_1*R*S - kr_1*RS* |
| 4 | RR <-> RS |
| | *kf_2*RR - kr_2*RS* |
| 5 | SS <-> RS |
| | *kf_2*SS - kr_2*RS* |
| 6 | RS + S <-> RR + S |
| | *kf_5*RS*S - kr_5*RR*S* |
| 7 | RS + S <-> R + RS |
| | *kf_6*RS*S - kr_6*R*RS* |
| 8 | R + SS <-> RR + S |

| | Reactions |
|---|---|
| | *kr_6*R*SS - kf_6*RR*S* |
| 9 | R + SS <-> R + RS |
| | *kr_5*R*SS - kf_5*R*RS* |

**Observables**

| | Observables |
|---|---|
| 1 | cR = 100*(2*RR + R + RS) |

**Model Equations**
**ODEs**

| | ODEs |
|---|---|
| 1 | d(R)/dt = 1/unnamed*(-2*(kf*R*R-kr*RR) - (kf_1*R*S-kr_1*RS) + (kf_6*RS*S-kr_6*R*RS) - (kr_6*R*SS-kf_6*RR*S)) |
| 2 | d(RR)/dt = 1/unnamed*((kf*R*R-kr*RR) - (kf_2*RR-kr_2*RS) + (kf_5*RS*S-kr_5*RR*S) + (kr_6*R*SS-kf_6*RR*S)) |
| 3 | d(S)/dt = 1/unnamed*(-2*(kf*S*S-kr*SS) - (kf_1*R*S-kr_1*RS) - (kf_6*RS*S-kr_6*R*RS) + (kr_6*R*SS-kf_6*RR*S)) |
| 4 | d(SS)/dt = 1/unnamed*((kf*S*S-kr*SS) - (kf_2*SS-kr_2*RS) - (kr_6*R*SS-kf_6*RR*S) - (kr_5*R*SS-kf_5*R*RS)) |
| 5 | d(RS)/dt = 1/unnamed*((kf_1*R*S-kr_1*RS) + (kf_2*RR-kr_2*RS) + (kf_2*SS-kr_2*RS) - (kf_5*RS*S-kr_5*RR*S) + (kr_5*R*SS-kf_5*R*RS)) |

**Program Setup**
**Data Step**
**Data Map**

| Classification | Value |
|---|---|
| group | Column3 |
| independent | Column1 |
| response | Column2 ~ cR |
| variant from data | Column4 ~ unnamed.RR |
| | UnitConversion: auto |
| variant from data | Column5 ~ unnamed.R |
| | UnitConversion: auto |

**Variant and Dose Setup Step**
**Variant and Dose Setup**

| Group | Variants1 | Variants2 | Variants3 | Doses1 |
|---|---|---|---|---|
| | Group Specific | Data | Data | Group Specific |
| 1 | | Column4 | Column5 | |
| 2 | | Column4 | Column5 | |
| 5 | | Column4 | Column5 | |
| 25 | | Column4 | Column5 | |

**Fit Step**
**Estimated Parameters (Pooled Fit)**

| Name | Transformation | Initial Untransformed Value | Untransformed Bounds |
|---|---|---|---|
| kf | log | 1 | [1e-10 10000000000] |
| kr | log | 1 | [1e-10 10000000000] |
| kf_1 | log | 1 | [1e-10 10000000000] |
| kr_1 | log | 1 | [1e-10 10000000000] |
| kf_2 | log | 1 | [1e-10 10000000000] |
| kr_2 | log | 1 | [1e-10 10000000000] |
| kf_5 | log | 1 | [1e-10 10000000000] |
| kr_5 | log | 1 | [1e-10 10000000000] |
| kf_6 | log | 1 | [1e-10 10000000000] |
| kr_6 | log | 1 | [1e-10 10000000000] |

**Error Model**
Use the same error model for each response: constant
**Algorithm Settings**

| Property | Value |
|---|---|
| EstimationFcn | scattersearch |
| MaxIterations | auto |
| FunctionTolerance | 1e-08 |
| MaxStallIterations | 50 |
| MaxTime | Inf |
| NumInitialPoints | auto |
| NumTrialPoints | auto |
| XTolerance | 1e-06 |
| LocalSolver | lsqnonlin |

**Local Solver Settings**

| Property | Value |
|---|---|
| StepTolerance | 1e-08 |
| FunctionTolerance | 1e-08 |
| OptimalityTolerance | 1e-06 |
| MaxIterations | 400 |

**Post Processing: Calculate Observables Step**
**Observables to Calculate**

| | Expression |
|---|---|
| 1 | cR = 100*(2*RR + R + RS) |

**Program Results**
**Fit Step**

**Pooled Parameter Estimates**

| Name | Estimate | StandardError |
|---|---|---|
| kf | 1.6917e-05 | 0.00093303 |
| kr | 0.0050453 | 2.9715e-06 |
| kf_1 | 1.6206 | 0.30741 |
| kr_1 | 0.055505 | 1.061e-05 |
| kf_2 | 0.00020816 | 4.8577e-07 |
| kr_2 | 5.5001e-08 | 2.6621e-10 |
| kf_5 | 1.0852 | 1.0361e-05 |
| kr_5 | 0.083525 | 4.0423e-05 |
| kf_6 | 9.0752 | 1.6958 |
| kr_6 | 0.024262 | 0.013803 |

**Statistics**

| Name | Value |
|---|---|
| AIC | -21.3317 |
| BIC | 10.7632 |
| LogLikelihood | 20.6658 |
| DFE | 173 |
| MSE | 0.049413 |
| SSE | 8.5485 |

**Pooled Beta**

| Name | Estimate | StandardError |
|---|---|---|
| log(kf) | -10.9872 | 55.1536 |
| log(kr) | -5.2893 | 0.00058897 |
| log(kf_1) | 0.48281 | 0.18969 |
| log(kr_1) | -2.8913 | 0.00019116 |
| log(kf_2) | -8.4772 | 0.0023336 |
| log(kr_2) | -16.7159 | 0.00484 |
| log(kf_5) | 0.081775 | 9.5478e-06 |
| log(kr_5) | -2.4826 | 0.00048396 |
| log(kf_6) | 2.2055 | 0.18686 |
| log(kr_6) | -3.7188 | 0.56892 |

**Residuals**

| Column3 | Column1 | Column2 | Column3 | Column1 | Column2 |
|---|---|---|---|---|---|
| 1 | 0 | 0.014833 | 1 | 3150 | 0.23777 |
| 1 | 60 | -0.01858 | 1 | 3300 | 0.25096 |
| 1 | 120 | -0.049543 | 1 | 3450 | 0.27137 |
| 1 | 180 | -0.064278 | 1 | 3600 | 0.28996 |
| 1 | 240 | -0.068748 | 1 | 3900 | 0.32153 |
| 1 | 300 | -0.056965 | 1 | 4200 | 0.34615 |
| 1 | 360 | -0.02111 | 1 | 4500 | 0.37096 |
| 1 | 420 | 0.024058 | 1 | 4800 | 0.40136 |
| 1 | 480 | 0.090607 | 1 | 5100 | 0.41714 |
| 1 | 540 | 0.19933 | 1 | 5400 | 0.43116 |
| 1 | 600 | 0.29599 | 1 | 6000 | 0.46026 |
| 1 | 660 | 0.42138 | 1 | 6600 | 0.48568 |
| 1 | 720 | 0.61665 | 1 | 7200 | 0.50819 |
| 1 | 780 | 0.60094 | 2 | 0 | 0.033 |
| 1 | 840 | 0.63982 | 2 | 60 | -0.071388 |
| 1 | 900 | 0.63123 | 2 | 120 | -0.11604 |
| 1 | 960 | 0.55889 | 2 | 180 | -0.17039 |
| 1 | 1020 | 0.49982 | 2 | 240 | -0.20207 |
| 1 | 1080 | 0.39218 | 2 | 300 | -0.24547 |
| 1 | 1140 | 0.28834 | 2 | 360 | -0.26982 |
| 1 | 1200 | 0.19292 | 2 | 420 | -0.3178 |
| 1 | 1350 | 0.022538 | 2 | 480 | -0.35017 |
| 1 | 1500 | -0.054741 | 2 | 540 | -0.37989 |
| 1 | 1650 | -0.065975 | 2 | 600 | -0.35908 |
| 1 | 1800 | -0.04415 | 2 | 660 | -0.31848 |
| 1 | 1950 | -0.012986 | 2 | 720 | -0.23032 |
| 1 | 2100 | 0.027747 | 2 | 780 | -0.096009 |
| 1 | 2250 | 0.061066 | 2 | 840 | 0.054303 |
| 1 | 2400 | 0.098149 | 2 | 900 | 0.15783 |
| 1 | 2550 | 0.133 | 2 | 960 | 0.2089 |
| 1 | 2700 | 0.16667 | 2 | 1020 | 0.1784 |
| 1 | 2850 | 0.19009 | 2 | 1080 | 0.12986 |
| 1 | 3000 | 0.21166 | 2 | 1140 | 0.041436 |
| 2 | 1200 | -0.043865 | 5 | 420 | -0.089521 |
| 2 | 1350 | -0.14191 | 5 | 480 | -0.099276 |
| 2 | 1500 | -0.17507 | 5 | 540 | -0.11143 |

| Column3 | Column1 | Column2 | Column3 | Column1 | Column2 |
|---|---|---|---|---|---|
| 2 | 1650 | -0.1659 | 5 | 600 | -0.12351 |
| 2 | 1800 | -0.15007 | 5 | 660 | -0.13314 |
| 2 | 1950 | -0.13178 | 5 | 720 | -0.14435 |
| 2 | 2100 | -0.12127 | 5 | 780 | -0.15944 |
| 2 | 2250 | -0.11252 | 5 | 840 | -0.17923 |
| 2 | 2400 | -0.10942 | 5 | 900 | -0.1992 |
| 2 | 2550 | -0.10203 | 5 | 960 | -0.21824 |
| 2 | 2700 | -0.098 | 5 | 1020 | -0.23793 |
| 2 | 2850 | -0.090875 | 5 | 1080 | -0.25829 |
| 2 | 3000 | -0.090901 | 5 | 1140 | -0.28201 |
| 2 | 3150 | -0.076133 | 5 | 1200 | -0.3022 |
| 2 | 3300 | -0.074934 | 5 | 1350 | -0.34737 |
| 2 | 3450 | -0.11736 | 5 | 1500 | -0.36882 |
| 2 | 3600 | -0.075723 | 5 | 1650 | -0.37394 |
| 2 | 3900 | -0.088803 | 5 | 1800 | -0.35618 |
| 2 | 4200 | -0.08513 | 5 | 1950 | -0.3393 |
| 2 | 4500 | -0.07988 | 5 | 2100 | -0.318 |
| 2 | 4800 | -0.08061 | 5 | 2250 | -0.29605 |
| 2 | 5100 | -0.072933 | 5 | 2400 | -0.27175 |
| 2 | 5400 | -0.058398 | 5 | 2550 | -0.24979 |
| 2 | 6000 | -0.064672 | 5 | 2700 | -0.23056 |
| 2 | 6600 | -0.064826 | 5 | 2850 | -0.21219 |
| 2 | 7200 | -0.062366 | 5 | 3000 | -0.1891 |
| 5 | 0 | 0.0089167 | 5 | 3150 | -0.17094 |
| 5 | 60 | 0.0014951 | 5 | 3300 | -0.15299 |
| 5 | 120 | -0.0301 | 5 | 3450 | -0.13686 |
| 5 | 180 | -0.044136 | 5 | 3600 | -0.12126 |
| 5 | 240 | -0.058726 | 5 | 3900 | -0.089376 |
| 5 | 300 | -0.070762 | 5 | 4200 | -0.062117 |
| 5 | 360 | -0.080819 | 5 | 4500 | -0.037657 |
| 5 | 4800 | -0.013387 | 25 | 2400 | -0.21301 |
| 5 | 5100 | 0.010413 | 25 | 2550 | -0.20738 |
| 5 | 5400 | 0.032788 | 25 | 2700 | -0.20559 |
| 5 | 6000 | 0.076094 | 25 | 2850 | -0.19314 |
| 5 | 6600 | 0.11165 | 25 | 3000 | -0.18421 |
| 5 | 7200 | 0.14795 | 25 | 3150 | -0.17489 |

| Column3 | Column1 | Column2 | Column3 | Column1 | Column2 |
|---|---|---|---|---|---|
| 25 | 0 | 0.0017917 | 25 | 3300 | -0.16704 |
| 25 | 60 | -0.0048897 | 25 | 3450 | -0.15532 |
| 25 | 120 | -0.01249 | 25 | 3600 | -0.14558 |
| 25 | 180 | -0.019815 | 25 | 3900 | -0.12556 |
| 25 | 240 | -0.02651 | 25 | 4200 | -0.10888 |
| 25 | 300 | -0.033327 | 25 | 4500 | -0.090755 |
| 25 | 360 | -0.039873 | 25 | 4800 | -0.073411 |
| 25 | 420 | -0.046702 | 25 | 5100 | -0.059455 |
| 25 | 480 | -0.053454 | 25 | 5400 | -0.043313 |
| 25 | 540 | -0.060833 | 25 | 6000 | -0.015681 |
| 25 | 600 | -0.069224 | 25 | 6600 | 0.010585 |
| 25 | 660 | -0.07358 | 25 | 7200 | 0.036203 |
| 25 | 720 | -0.085517 | | | |
| 25 | 780 | -0.094961 | | | |
| 25 | 840 | -0.10379 | | | |
| 25 | 900 | -0.11296 | | | |
| 25 | 960 | -0.122 | | | |
| 25 | 1020 | -0.13143 | | | |
| 25 | 1080 | -0.14013 | | | |
| 25 | 1140 | -0.14885 | | | |
| 25 | 1200 | -0.15647 | | | |
| 25 | 1350 | -0.17377 | | | |
| 25 | 1500 | -0.18648 | | | |
| 25 | 1650 | -0.2013 | | | |
| 25 | 1800 | -0.20788 | | | |
| 25 | 1950 | -0.21666 | | | |
| 25 | 2250 | -0.21668 | | | |

**Covariance Matrix**

| Name | log(kf) | log(kr) | log(kf_1) | log(kr_1) | log(kf_2) |
|---|---|---|---|---|---|
| log(kf) | 8.7055e-07 | 7.6131e-10 | -0.00012909 | 1.0582e-09 | -2.7989e-11 |
| log(kr) | 7.6131e-10 | 8.8301e-12 | -5.7086e-08 | 5.5905e-13 | -3.341e-13 |
| log(kf_1) | -0.00012909 | -5.7086e-08 | 0.094503 | 4.5705e-07 | -1.4478e-09 |
| log(kr_1) | 1.0582e-09 | 5.5905e-13 | 4.5705e-07 | 1.1258e-10 | -3.3402e-13 |
| log(kf_2) | -2.7989e-11 | -3.341e-13 | -1.4478e-09 | -3.3402e-13 | 2.3597e-13 |
| log(kr_2) | 6.1163e-15 | 1.1934e-16 | -4.4502e-12 | -2.8742e-16 | -1.1896e-16 |
| log(kf_5) | -9.361e-10 | -1.5194e-11 | -5.7765e-08 | 8.64e-12 | 1.0484e-12 |

| Name | log(kf) | log(kr) | log(kf_1) | log(kr_1) | log(kf_2) |
|---|---|---|---|---|---|
| log(kr_5) | -3.3457e-09 | 2.4032e-11 | -3.9139e-08 | 3.6546e-12 | -9.4006e-13 |
| log(kf_6) | -0.00019632 | 3.8398e-07 | 0.48855 | 2.7452e-06 | -1.8024e-08 |
| log(kr_6) | -1.1742e-05 | -1.4612e-08 | 0.00054392 | -3.0326e-08 | 2.3007e-10 |

| log(kr_2) | log(kf_5) | log(kr_5) | log(kf_6) | log(kr_6) |
|---|---|---|---|---|
| 6.1163e-15 | -9.361e-10 | -3.3457e-09 | -0.00019632 | -1.1742e-05 |
| 1.1934e-16 | -1.5194e-11 | 2.4032e-11 | 3.8398e-07 | -1.4612e-08 |
| -4.4502e-12 | -5.7765e-08 | -3.9139e-08 | 0.48855 | 0.00054392 |
| -2.8742e-16 | 8.64e-12 | 3.6546e-12 | 2.7452e-06 | -3.0326e-08 |
| -1.1896e-16 | 1.0484e-12 | -9.4006e-13 | -1.8024e-08 | 2.3007e-10 |
| 7.0866e-20 | -1.1947e-15 | 4.5521e-17 | -2.502e-11 | 9.3571e-14 |
| -1.1947e-15 | 1.0736e-10 | -7.5831e-11 | -1.2048e-06 | 1.6047e-08 |
| 4.5521e-17 | -7.5831e-11 | 1.634e-09 | -4.0371e-06 | 6.6625e-08 |
| -2.502e-11 | -1.2048e-06 | -4.0371e-06 | 2.8759 | -0.0049427 |
| 9.3571e-14 | 1.6047e-08 | 6.6625e-08 | -0.0049427 | 0.00019054 |

**Error Model**

| Response | ErrorModel | a |
|---|---|---|
| Column2 | constant | 0.21613 |

**Program Plots**

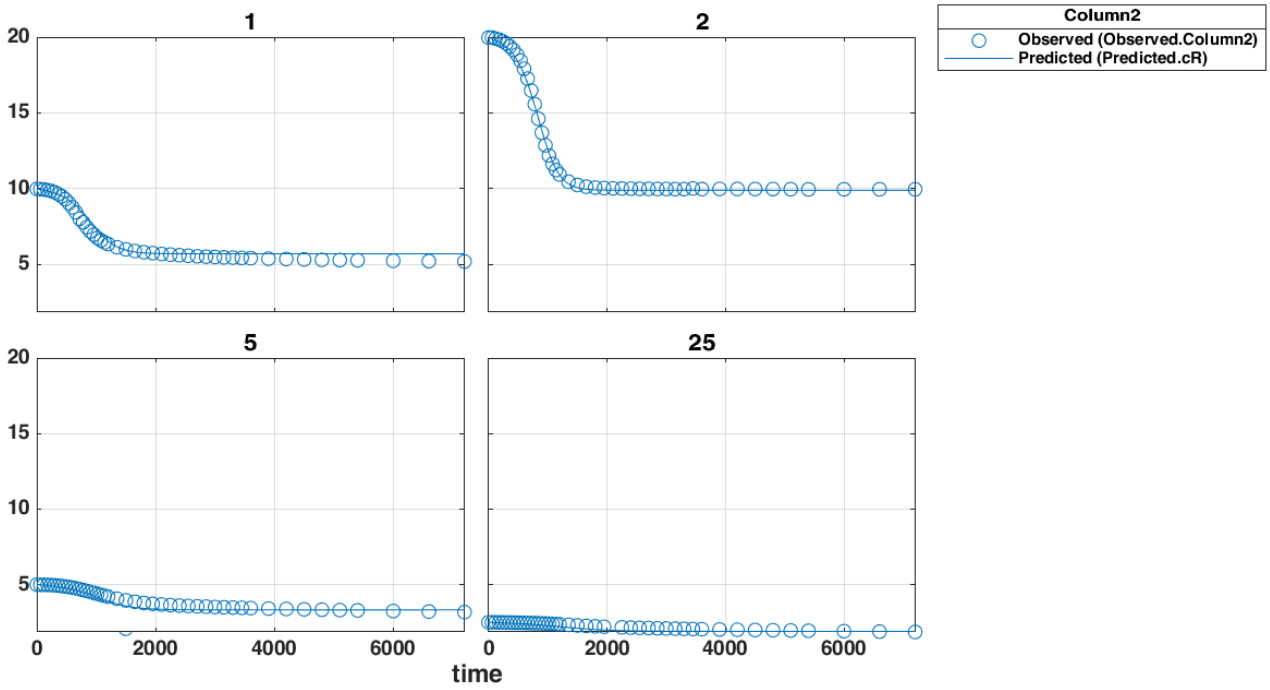



Figure 1 : Fit Plot

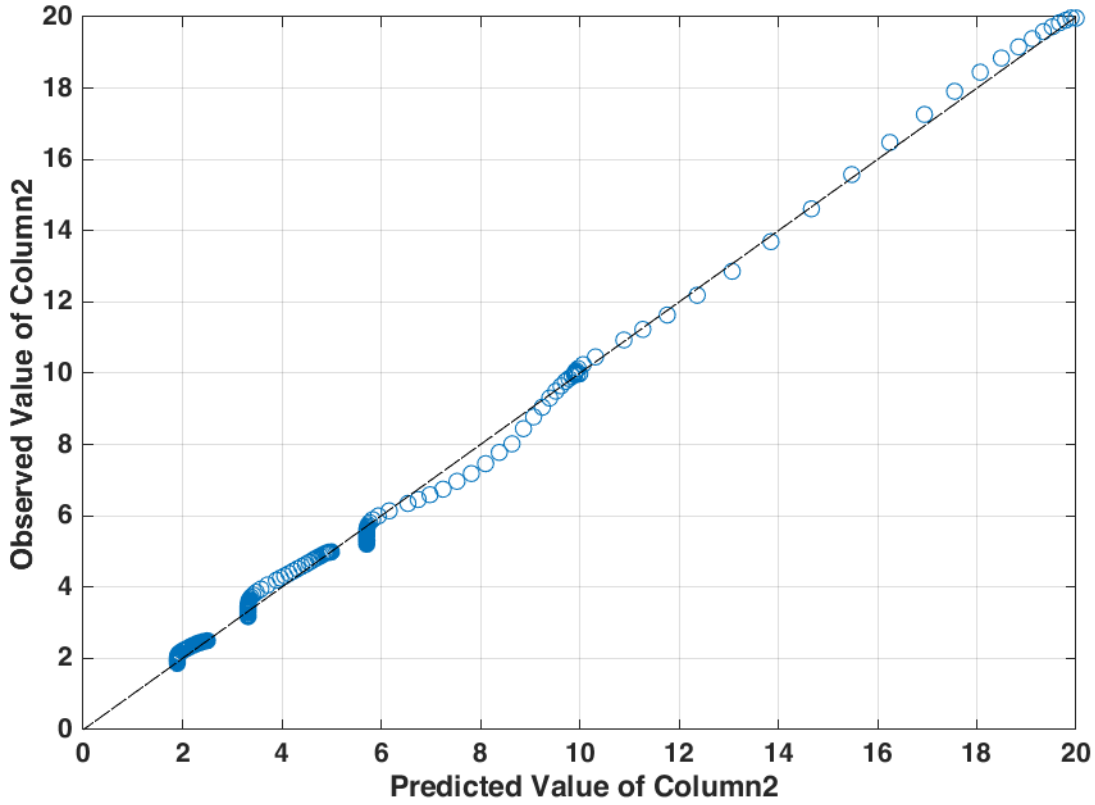



Figure 2 :

Actual_vs_predicted Plot

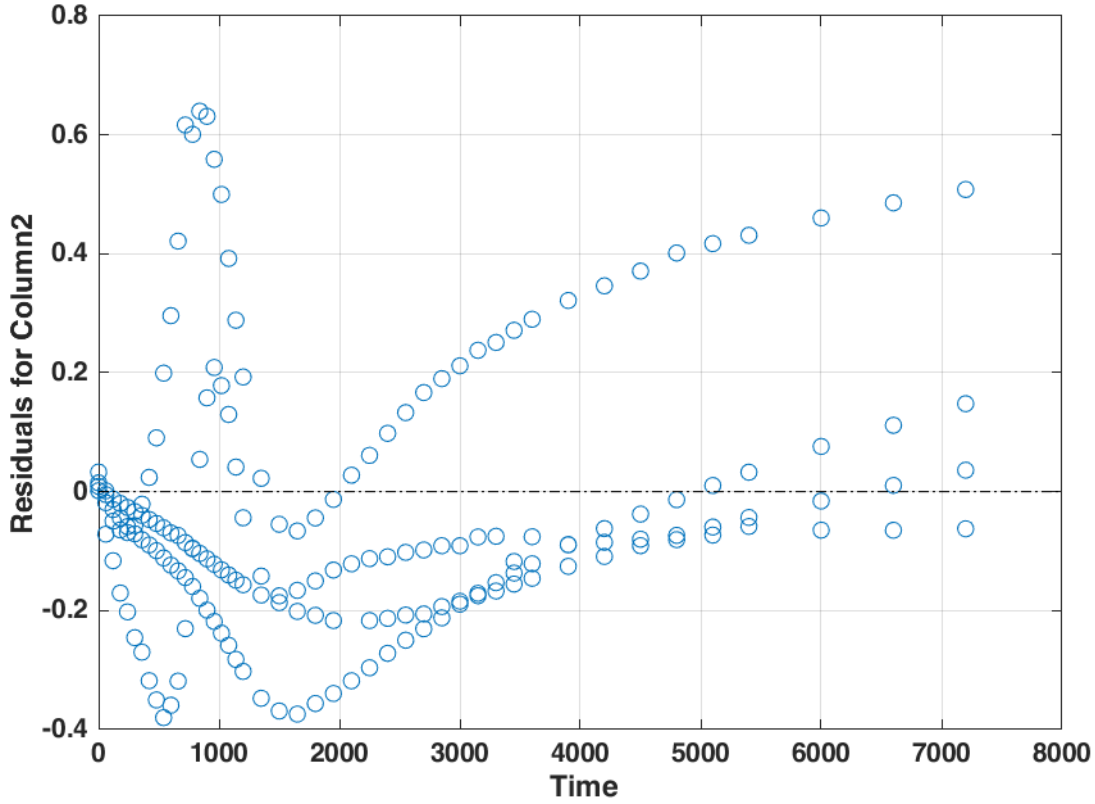



Figure 3 :

Residuals Plot

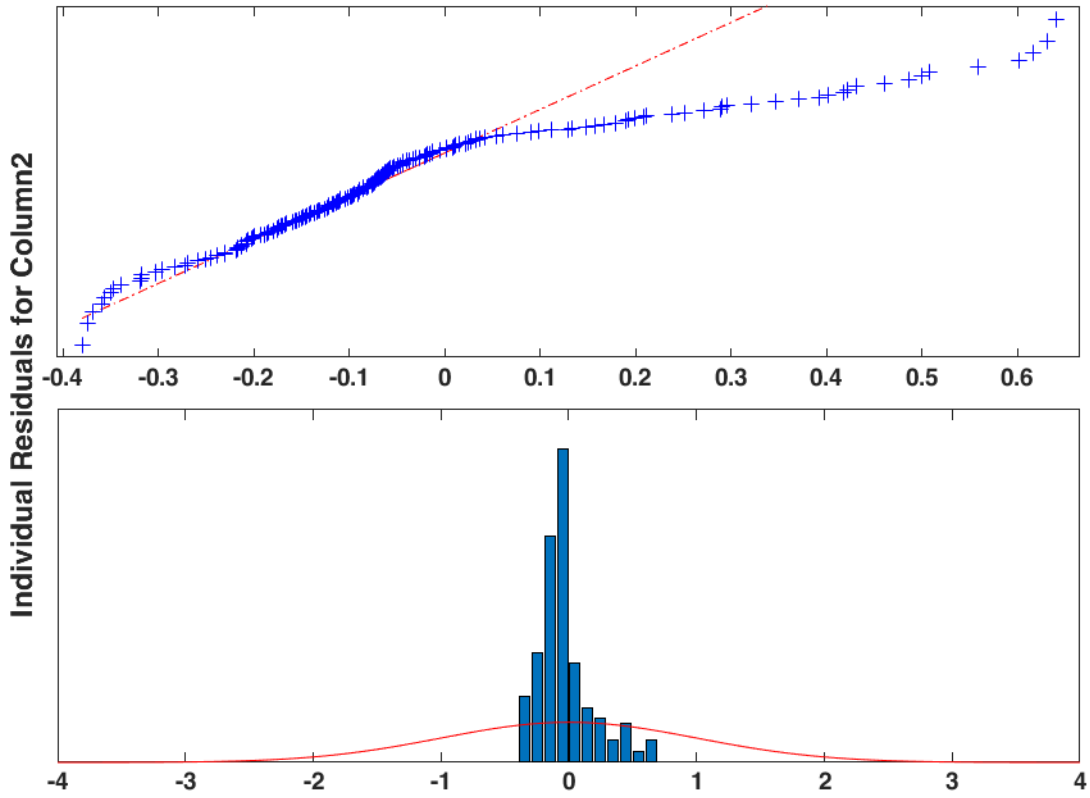



Figure 4 : Residual_distribution Plot

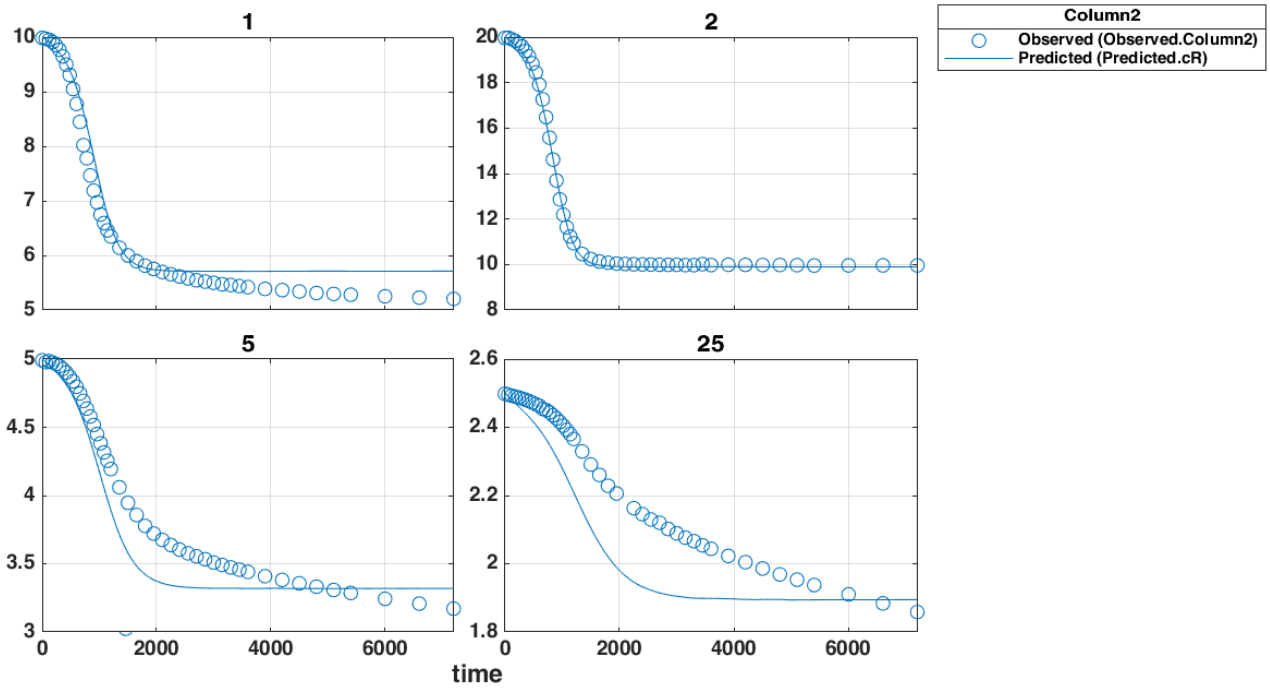



Figure 5 : Fit Plot

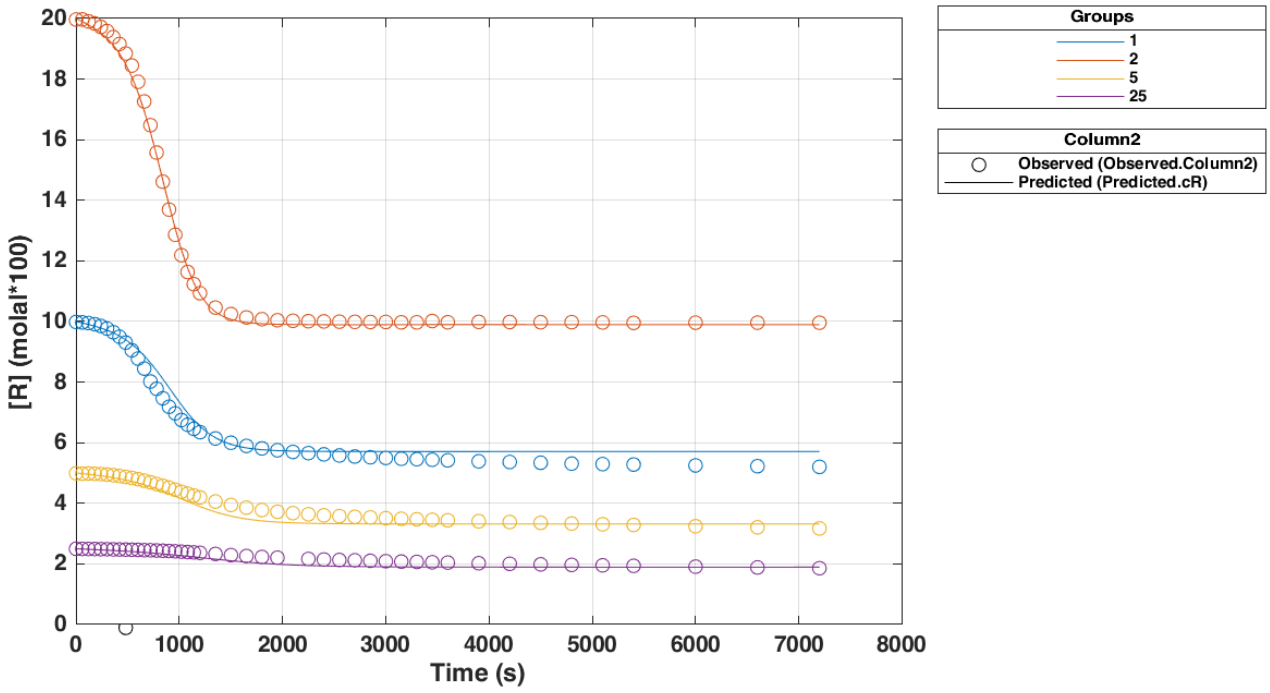



Figure 6 : Fit Plot

**Tetramer**

**Quantities**

| | Quantity Name | Type | Scope | Value | Initial Value |
|---|---|---|---|---|---|
| 1 | unnamed | compartment | Dimer_dimer_AC | 1 | 1 |
| 2 | R | species | unnamed | 0.55 | 0.55 |
| 3 | RR | species | unnamed | 0.225 | 0.225 |
| 4 | S | species | unnamed | 0 | 0 |
| 5 | SS | species | unnamed | 0 | 0 |
| 6 | RS | species | unnamed | 0 | 0 |
| 7 | kf | parameter | Dimer_dimer_AC | 1 | 96.3644 |
| 8 | kr | parameter | Dimer_dimer_AC | 1 | 0.00025638 |
| 9 | kf_1 | parameter | Dimer_dimer_AC | 1 | 8871.4218 |
| 10 | kr_1 | parameter | Dimer_dimer_AC | 1 | 0.055095 |
| 11 | kf_2 | parameter | Dimer_dimer_AC | 1 | 0.00013505 |
| 12 | kr_2 | parameter | Dimer_dimer_AC | 1 | 8.9024e-07 |
| 13 | kf_3 | parameter | Dimer_dimer_AC | 1 | 0.048474 |
| 14 | kr_3 | parameter | Dimer_dimer_AC | 0 | 0 |

**Reactions**

| | Reactions |
|---|---|
| 1 | R + R <-> RR |
| | *kf*R*R - kr*RR* |

| | Reactions |
|---|---|
| 2 | S + S <-> SS |
| | *kf*S*S - kr*SS* |
| 3 | R + S <-> RS |
| | *kf_1*R*S - kr_1*RS* |
| 4 | RR <-> RS |
| | *kf_2*RR - kr_2*RS* |
| 5 | SS <-> RS |
| | *kf_2*SS - kr_2*RS* |
| 6 | RS + RR <-> 2 RS |
| | *kf_3*RS*RR - kr_3*RS^2* |
| 7 | RS + SS <-> 2 RS |
| | *kf_3*RS*SS - kr_3*RS^2* |

**Observables**

| | Observables |
|---|---|
| 1 | ee = 100*((R + 2*RR ) - (S + 2*SS)) |
| 2 | cR = 100*(R + 2*RR + RS) |

**Model Equations**

**ODEs**

| | ODEs |
|---|---|
| 1 | d(R)/dt = 1/unnamed*(-2*(kf*R*R-kr*RR) - (kf_1*R*S-kr_1*RS)) |
| 2 | d(RR)/dt = 1/unnamed*((kf*R*R-kr*RR) - (kf_2*RR-kr_2*RS) - (kf_3*RS*RR-kr_3*RS^2)) |
| 3 | d(S)/dt = 1/unnamed*(-2*(kf*S*S-kr*SS) - (kf_1*R*S-kr_1*RS)) |
| 4 | d(SS)/dt = 1/unnamed*((kf*S*S-kr*SS) - (kf_2*SS-kr_2*RS) - (kf_3*RS*SS-kr_3*RS^2)) |
| 5 | d(RS)/dt = 1/unnamed*((kf_1*R*S-kr_1*RS) + (kf_2*RR-kr_2*RS) + (kf_2*SS-kr_2*RS) + (kf_3*RS*RR-kr_3*RS^2) + (kf_3*RS*SS-kr_3*RS^2)) |

**Program Setup**
**Model Setup**
**Variants**

| | Type | Name | variant1 |
|---|---|---|---|
| 1 | parameter | kf | 96.3644 |
| 2 | parameter | kr | 0.00025638 |
| 3 | parameter | kf_1 | 8871.4218 |
| 4 | parameter | kr_1 | 0.055095 |
| 5 | parameter | kf_2 | 0.00013505 |
| 6 | parameter | kr_2 | 8.9024e-07 |
| 7 | parameter | kf_3 | 0.048474 |

**Data Step**
**Data Map**

| Classification | Value |
|---|---|
| group | Column3 |
| independent | Column1 |
| response | Column2 ~ cR |
| variant from data | Column4 ~ unnamed.RR |
| | UnitConversion: auto |
| variant from data | Column5 ~ unnamed.R |
| | UnitConversion: auto |

**Variant and Dose Setup Step**
**Variant and Dose Setup**

| Group | Variants1 | Variants2 | Variants3 | Variants4 | Doses1 |
|---|---|---|---|---|---|
| | Baseline | Group Specific | Data | Data | Group Specific |
| 2 | variant1_feb2 | | Column4 | Column5 | |
| 1 | variant1_feb2 | | Column4 | Column5 | |
| 5 | variant1_feb2 | | Column4 | Column5 | |
| 25 | variant1_feb2 | | Column4 | Column5 | |

**Fit Step**
**Estimated Parameters (Pooled Fit)**

| Name | Transformation | Initial Untransformed Value | Untransformed Bounds |
|---|---|---|---|
| kf | log | 96.3644 | [1e-05 10000] |
| kr | log | 0.00025638 | [1e-05 10000] |
| kf_1 | log | 8871.4218 | [1e-05 10000] |
| kr_1 | log | 0.055095 | [1e-05 10000] |
| kf_2 | log | 0.00013505 | [1e-08 10000] |
| kr_2 | log | 8.9024e-07 | [1e-08 10000] |
| kf_3 | log | 0.048474 | [1e-08 10000] |

**Error Model**
Use the same error model for each response: constant
**Algorithm Settings**

| Property | Value |
|---|---|
| EstimationFcn | scattersearch |
| MaxIterations | auto |
| FunctionTolerance | 1e-16 |
| MaxStallIterations | 50 |
| MaxTime | Inf |
| NumInitialPoints | auto |
| NumTrialPoints | auto |
| XTolerance | 1e-12 |
| LocalSolver | fminsearch |

**Local Solver Settings**

| Property | Value |
|---|---|
| TolX | 1e-16 |
| TolFun | 1e-16 |
| MaxIter | 800 |

**Post Processing: Calculate Observables Step**
**Observables to Calculate**

| | Expression |
|---|---|
| 1 | ee = 100*((R + 2*RR ) - (S + 2*SS)) |
| 2 | cR = 100*(R + 2*RR + RS) |

**Program Results**
**Fit Step**
**Pooled Parameter Estimates**

| Name | Estimate | StandardError |
|---|---|---|
| kf | 96.3644 | 61.9954 |

| Name | Estimate | StandardError |
|---|---|---|
| kr | 0.00025638 | 0.00058757 |
| kf_1 | 8871.4156 | 43.0527 |
| kr_1 | 0.055095 | 0.0027016 |
| kf_2 | 0.00013505 | 1.5775e-05 |
| kr_2 | 8.9024e-07 | 1.6377e-07 |
| kf_3 | 0.048474 | 0.0024457 |

**Statistics**

| Name | Value |
|---|---|
| AIC | 227.2628 |
| BIC | 249.7292 |
| LogLikelihood | -106.6314 |
| DFE | 176 |
| MSE | 0.19524 |
| SSE | 34.363 |

**Pooled Beta**

| Name | Estimate | StandardError |
|---|---|---|
| log(kf) | 4.5681 | 0.64334 |
| log(kr) | -8.2689 | 2.2918 |
| log(kf_1) | 9.0906 | 0.004853 |
| log(kr_1) | -2.8987 | 0.049036 |
| log(kf_2) | -8.9099 | 0.11681 |
| log(kr_2) | -13.9318 | 0.18396 |
| log(kf_3) | -3.0267 | 0.050453 |

**Residuals**

| Column3 | Column1 | Column2 | Column3 | Column1 | Column2 |
|---|---|---|---|---|---|
| 1 | 0 | 0.014833 | 1 | 3300 | -0.33098 |
| 1 | 60 | -0.014351 | 1 | 3450 | -0.33808 |
| 1 | 120 | -0.042929 | 1 | 3600 | -0.34015 |
| 1 | 180 | -0.058419 | 1 | 3900 | -0.33838 |
| 1 | 240 | -0.064151 | 1 | 4200 | -0.33415 |
| 1 | 300 | -0.051427 | 1 | 4500 | -0.32087 |
| 1 | 360 | -0.0093188 | 1 | 4800 | -0.29873 |
| 1 | 420 | 0.050531 | 1 | 5100 | -0.28702 |
| 1 | 480 | 0.14329 | 1 | 5400 | -0.27532 |
| 1 | 540 | 0.29279 | 1 | 6000 | -0.24877 |
| 1 | 600 | 0.44742 | 1 | 6600 | -0.22437 |

| Column3 | Column1 | Column2 | Column3 | Column1 | Column2 |
|---|---|---|---|---|---|
| 1 | 660 | 0.64961 | 1 | 7200 | -0.20243 |
| 1 | 720 | 0.94053 | 2 | 0 | 0.033 |
| 1 | 780 | 1.0373 | 2 | 60 | -0.062883 |
| 1 | 840 | 1.201 | 2 | 120 | -0.11944 |
| 1 | 900 | 1.3228 | 2 | 180 | -0.20964 |
| 1 | 960 | 1.3784 | 2 | 240 | -0.30073 |
| 1 | 1020 | 1.4354 | 2 | 300 | -0.42611 |
| 1 | 1080 | 1.4242 | 2 | 360 | -0.55302 |
| 1 | 1140 | 1.3915 | 2 | 420 | -0.71863 |
| 1 | 1200 | 1.3362 | 2 | 480 | -0.87414 |
| 1 | 1350 | 1.1402 | 2 | 540 | -1.018 |
| 1 | 1500 | 0.90705 | 2 | 600 | -1.0838 |
| 1 | 1650 | 0.67798 | 2 | 660 | -1.082 |
| 1 | 1800 | 0.46914 | 2 | 720 | -0.96962 |
| 1 | 1950 | 0.28395 | 2 | 780 | -0.7418 |
| 1 | 2100 | 0.13486 | 2 | 840 | -0.43473 |
| 1 | 2250 | 0.0070203 | 2 | 900 | -0.13086 |
| 1 | 2400 | -0.08907 | 2 | 960 | 0.13629 |
| 1 | 2550 | -0.16223 | 2 | 1020 | 0.3085 |
| 1 | 2700 | -0.21499 | 2 | 1080 | 0.42621 |
| 1 | 2850 | -0.26078 | 2 | 1140 | 0.45559 |
| 1 | 3000 | -0.29336 | 2 | 1200 | 0.43524 |
| 1 | 3150 | -0.30994 | 2 | 1350 | 0.33671 |
| 2 | 1650 | 0.12175 | 5 | 720 | -0.035936 |
| 2 | 1800 | 0.065837 | 5 | 780 | -0.016612 |
| 2 | 1950 | 0.036881 | 5 | 840 | 0.0026194 |
| 2 | 2100 | 0.019573 | 5 | 900 | 0.025266 |
| 2 | 2250 | 0.013443 | 5 | 960 | 0.051109 |
| 2 | 2400 | 0.0090031 | 5 | 1020 | 0.077006 |
| 2 | 2550 | 0.012532 | 5 | 1080 | 0.10121 |
| 2 | 2700 | 0.014372 | 5 | 1140 | 0.11934 |
| 2 | 2850 | 0.01804 | 5 | 1200 | 0.13687 |
| 2 | 3000 | 0.015263 | 5 | 1350 | 0.15958 |
| 2 | 3150 | 0.027517 | 5 | 1500 | 0.16261 |
| 2 | 3300 | 0.027755 | 5 | 1650 | 0.14137 |
| 2 | 3450 | -0.015816 | 5 | 1800 | 0.11297 |

| Column3 | Column1 | Column2 | Column3 | Column1 | Column2 |
|---|---|---|---|---|---|
| 2 | 3600 | 0.025412 | 5 | 1950 | 0.064734 |
| 2 | 3900 | 0.012474 | 5 | 2100 | 0.010092 |
| 2 | 4200 | 0.016529 | 5 | 2250 | -0.047885 |
| 2 | 4500 | 0.022416 | 5 | 2400 | -0.10419 |
| 2 | 4800 | 0.022056 | 5 | 2550 | -0.16166 |
| 2 | 5100 | 0.029693 | 5 | 2700 | -0.21772 |
| 2 | 5400 | 0.044366 | 5 | 2850 | -0.26966 |
| 2 | 6000 | 0.038027 | 5 | 3000 | -0.31317 |
| 2 | 6600 | 0.037675 | 5 | 3150 | -0.35721 |
| 2 | 7200 | 0.039666 | 5 | 3300 | -0.39618 |
| 5 | 0 | 0.0089167 | 5 | 3450 | -0.43222 |
| 5 | 60 | 0.0021867 | 5 | 3600 | -0.46392 |
| 5 | 120 | -0.027913 | 5 | 3900 | -0.51594 |
| 5 | 180 | -0.04146 | 5 | 4200 | -0.55844 |
| 5 | 240 | -0.055576 | 5 | 4500 | -0.59063 |
| 5 | 300 | -0.06621 | 5 | 4800 | -0.61386 |
| 5 | 360 | -0.073051 | 5 | 5100 | -0.62883 |
| 5 | 420 | -0.075859 | 5 | 5400 | -0.63918 |
| 5 | 480 | -0.076214 | 5 | 6000 | -0.6441 |
| 5 | 540 | -0.074685 | 5 | 6600 | -0.64094 |
| 5 | 600 | -0.068159 | 5 | 7200 | -0.62603 |
| 5 | 660 | -0.053928 | 25 | 0 | 0.0017917 |
| 25 | 60 | -0.0055923 | 25 | 2550 | -0.18454 |
| 25 | 120 | -0.013332 | 25 | 2700 | -0.20558 |
| 25 | 180 | -0.0215 | 25 | 2850 | -0.21707 |
| 25 | 240 | -0.029532 | 25 | 3000 | -0.2327 |
| 25 | 300 | -0.037861 | 25 | 3150 | -0.24769 |
| 25 | 360 | -0.045858 | 25 | 3300 | -0.26388 |
| 25 | 420 | -0.053892 | 25 | 3450 | -0.27713 |
| 25 | 480 | -0.061453 | 25 | 3600 | -0.29142 |
| 25 | 540 | -0.069066 | 25 | 3900 | -0.31645 |
| 25 | 600 | -0.076969 | 25 | 4200 | -0.33996 |
| 25 | 660 | -0.080005 | 25 | 4500 | -0.35992 |
| 25 | 720 | -0.089722 | 25 | 4800 | -0.37773 |
| 25 | 780 | -0.096014 | 25 | 5100 | -0.39423 |
| 25 | 840 | -0.10076 | 25 | 5400 | -0.40747 |

| Column3 | Column1 | Column2 | Column3 | Column1 | Column2 |
|---|---|---|---|---|---|
| 25 | 900 | -0.10495 | 25 | 6000 | -0.43052 |
| 25 | 960 | -0.10819 | 25 | 6600 | -0.44573 |
| 25 | 1020 | -0.11112 | 25 | 7200 | -0.45417 |
| 25 | 1080 | -0.11275 | 25 | 3900 | -0.31645 |
| 25 | 1140 | -0.11401 | 25 | 4200 | -0.33996 |
| 25 | 1200 | -0.11397 | 25 | 4500 | -0.35992 |
| 25 | 1350 | -0.11259 | 25 | 4800 | -0.37773 |
| 25 | 1500 | -0.10971 | 25 | 5100 | -0.39423 |
| 25 | 1650 | -0.11439 | 25 | 5400 | -0.40747 |
| 25 | 1800 | -0.11754 | 25 | 6000 | -0.43052 |
| 25 | 1950 | -0.12957 | 25 | 6600 | -0.44573 |
| 25 | 2250 | -0.15362 | 25 | 7200 | -0.45417 |
| 25 | 2400 | -0.16877 | | | |

**Covariance Matrix**

| Name | log(kf) | log(kr) | log(kf_1) |
|---|---|---|---|
| log(kf) | 3843.4301 | 0.032578 | 104.5391 |
| log(kr) | 0.032578 | 3.4524e-07 | 0.00169 |
| log(kf_1) | 104.5391 | 0.00169 | 1853.5372 |
| log(kr_1) | 0.02352 | 5.0223e-07 | -0.016227 |
| log(kf_2) | -0.00014555 | -2.5815e-09 | -0.00016263 |
| log(kr_2) | 8.9722e-07 | 2.1156e-11 | 1.1004e-06 |
| log(kf_3) | -0.025488 | -5.4777e-07 | 0.014836 |

| | log(kr_1) | log(kf_2) | log(kr_2) | log(kf_3) |
|---|---|---|---|---|
| log(kf) | 0.02352 | -0.00014555 | 8.9722e-07 | -0.025488 |
| log(kr) | 5.0223e-07 | -2.5815e-09 | 2.1156e-11 | -5.4777e-07 |
| log(kf_1) | -0.016227 | -0.00016263 | 1.1004e-06 | 0.014836 |
| log(kr_1) | 7.2987e-06 | 2.1107e-08 | -2.2839e-10 | -5.8278e-06 |
| log(kf_2) | 2.1107e-08 | 2.4886e-10 | -2.5578e-12 | -2.0083e-08 |
| log(kr_2) | -2.2839e-10 | -2.5578e-12 | 2.6821e-14 | 2.179e-10 |
| log(kf_3) | -5.8278e-06 | -2.0083e-08 | 2.179e-10 | 5.9813e-06 |

**Error Model**

| Response | ErrorModel | a |
|---|---|---|
| Column2 | constant | 0.43333 |

**Program Plots**

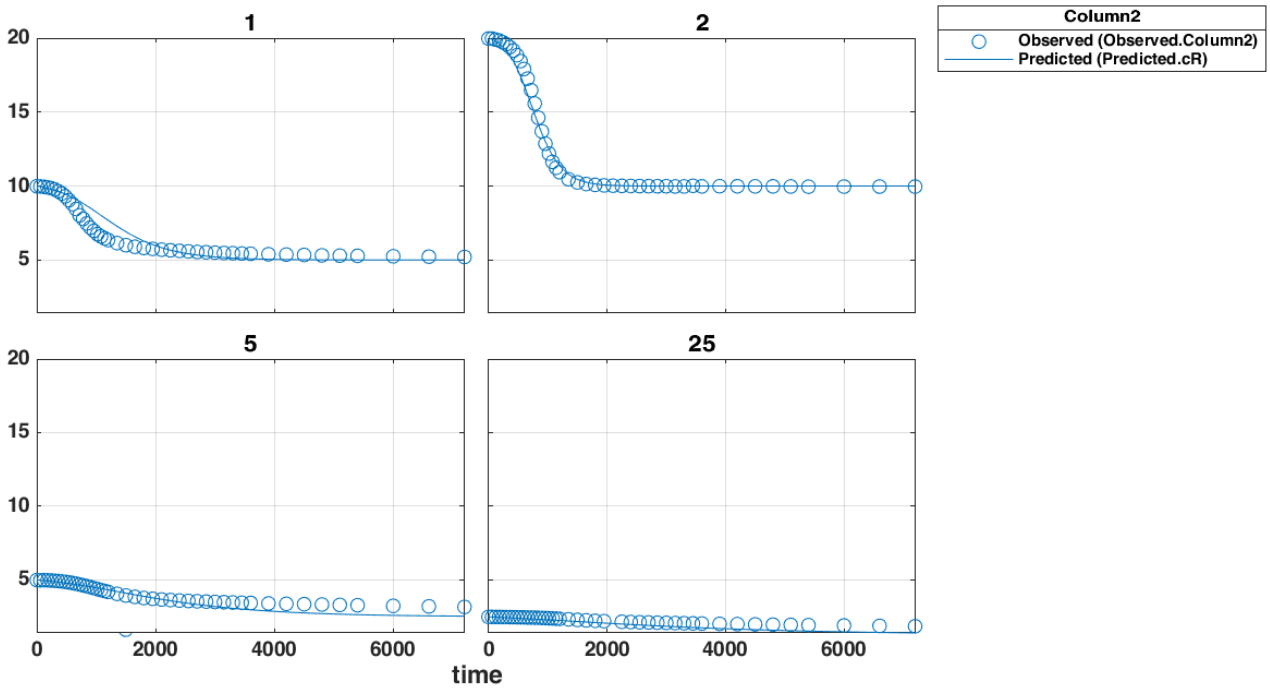



Figure 1 : Fit Plot

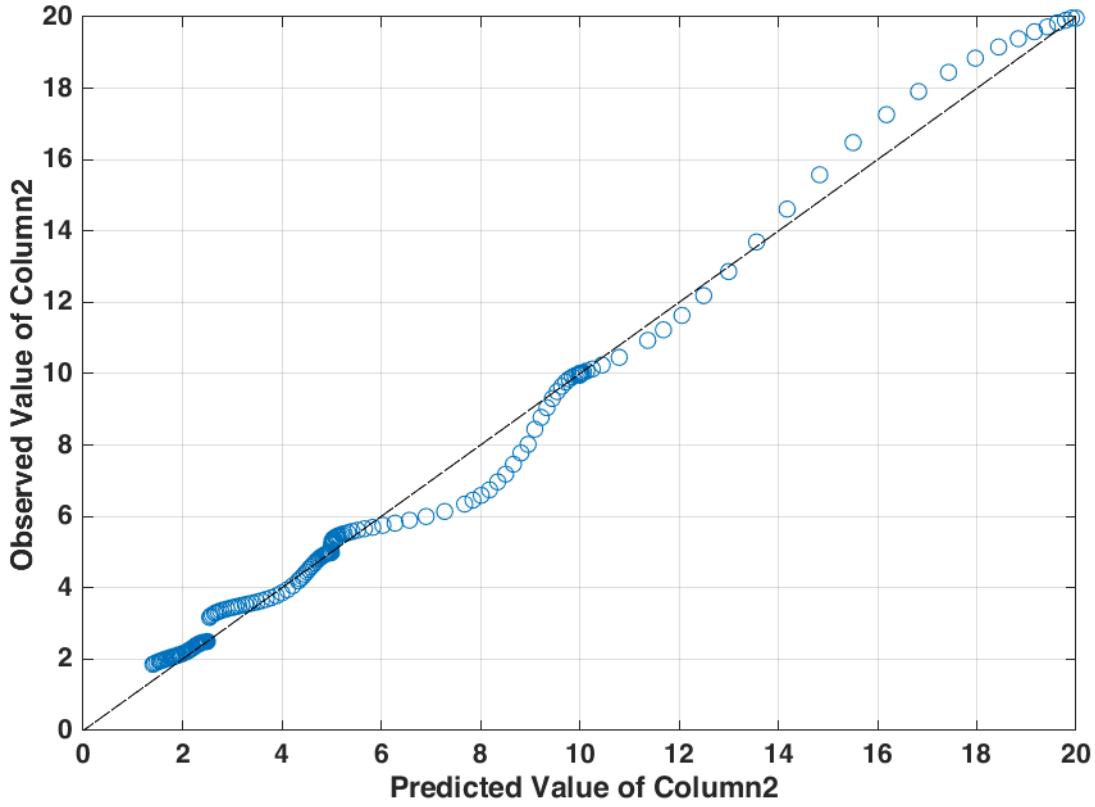



Figure 2 : Actual_vs_predicted Plot

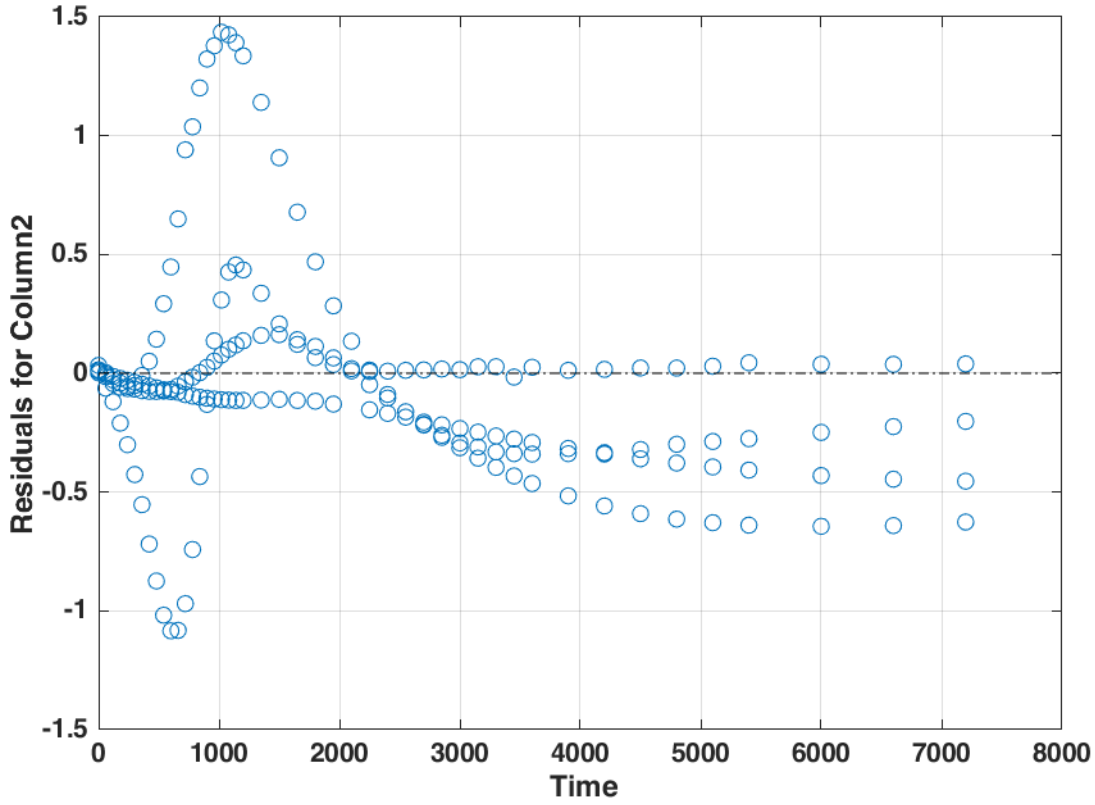



Figure 3 : Residuals Plot

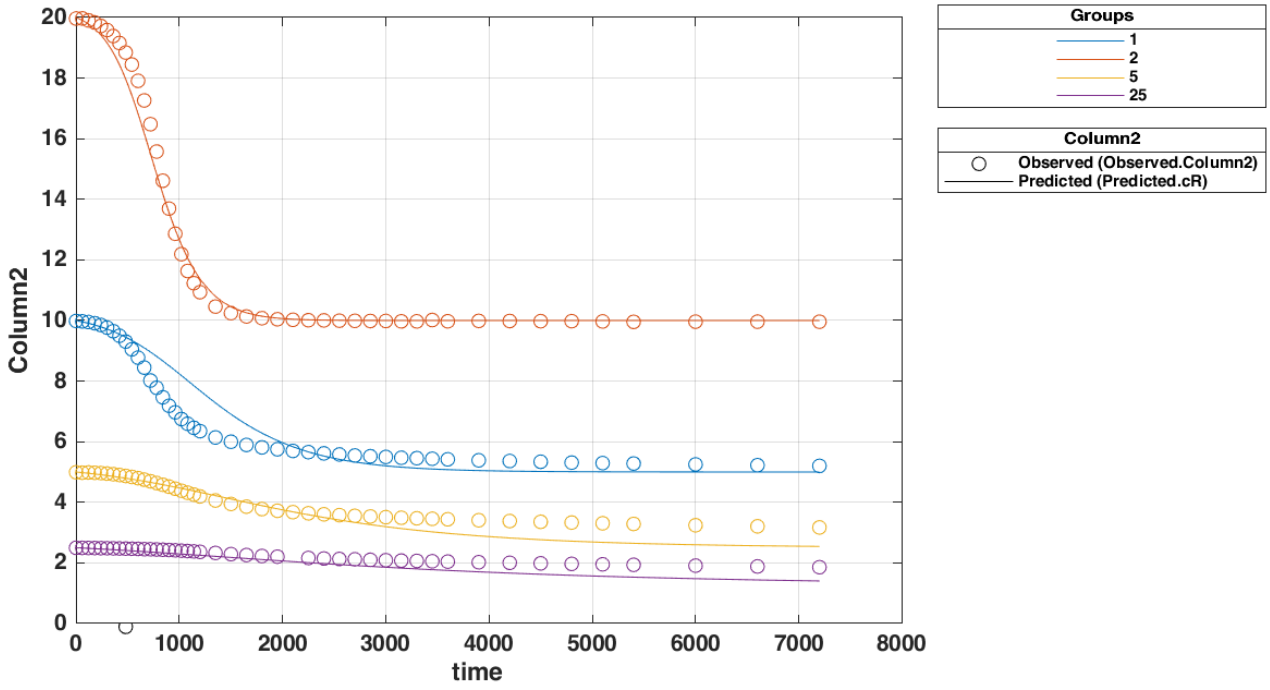



Figure 4 : Fit Plot

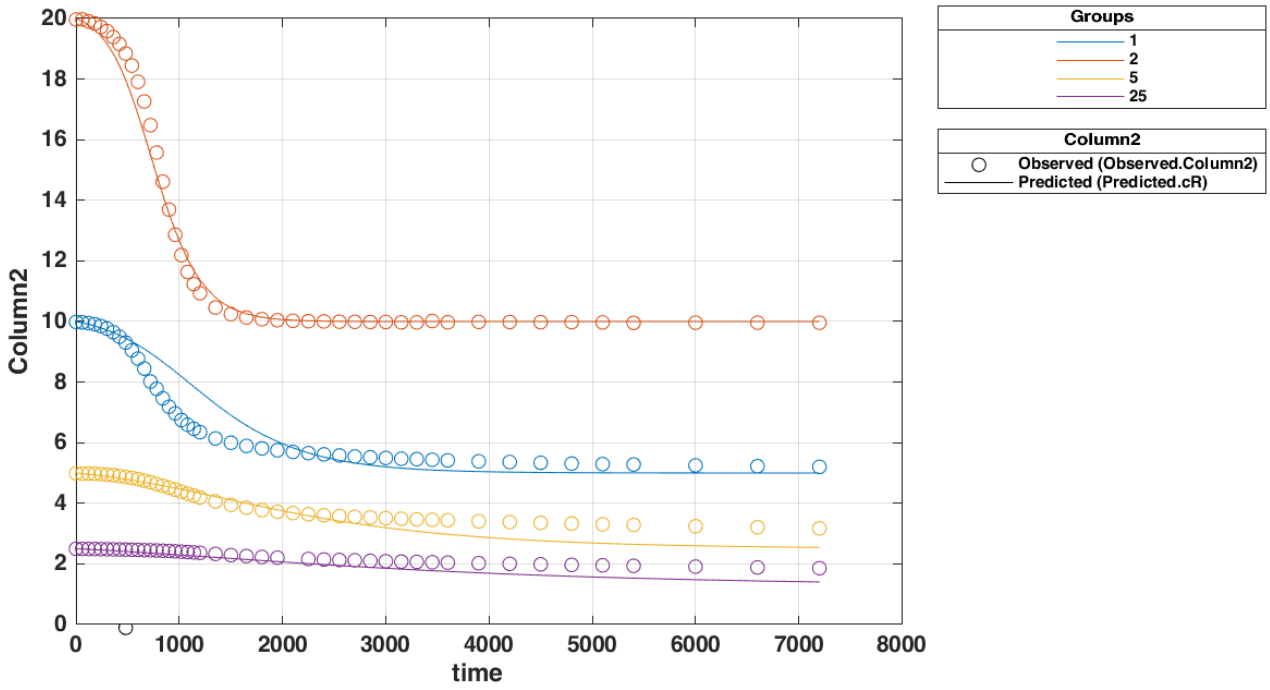



Figure 5 : Fit Plot

# References


1. Y. Guan, S. V. Shree Sowndarya, L. C. Gallegos, P. C. St John and R. S. Paton, *Chem. Sci.*, 2021, **12**, 12012-12026.
2. W. Li, X. Liu, X. Hao, Y. Cai, L. Lin and X. Feng, *Angew. Chem. Int. Ed. Engl.*, 2012, **51**, 8644-8647.
3. A. Singh, K. Teegardin, M. Kelly, K. S. Prasad, S. Krishnan and J. D. Weaver, *J. Organomet. Chem.*, 2015, **776**, 51-59.
4. B. Shen, W. Liu, W. Cao, X. Liu and X. Feng, *Org. Lett.*, 2019, **21**, 4713-4716.
5. B. A. Jones, P. Solon, M. V. Popescu, J. Y. Du, R. Paton and M. D. Smith, *J. Am. Chem. Soc.*, 2023, **145**, 171-178.
6. F. T. Oakes, F. A. Yang and J. F. Sebastian, *J. Org. Chem.*, 1982, **47**, 3094-3097.
7. J. J. Koenig, T. Arndt, N. Gildemeister, J. M. Neudorfl and M. Breugst, *J. Org. Chem.*, 2019, **84**, 7587-7605.
8. T. Ueda, H. Konishi and K. Manabe, *Org. Lett.*, 2012, **14**, 5370-5373.
9. S. Song, S. F. Zhu, L. Y. Pu and Q. L. Zhou, *Angew. Chem. Int. Ed. Engl.*, 2013, **52**, 6072-6075.
10. H. J. Kuhn, S. E. Braslavsky and R. Schmidt, *Pure and Applied Chemistry*, 1989, **61**, 187-210.
11. Y. J. Yuan, Z. T. Yu, H. L. Gao, Z. G. Zou, C. Zheng and W. Huang, *Chemistry*, 2013, **19**, 6340-6349.
12. J. R. Ochola and M. O. Wolf, *Org. Biomol. Chem.*, 2016, **14**, 9088-9092.
13. E. D. Nacsa and D. W. C. MacMillan, *J. Am. Chem. Soc.*, 2018, **140**, 3322-3330.
14. J. L. Brennan, T. E. Keyes and R. J. Forster, *Langmuir*, 2006, **22**, 10754-10761.
15. M. J. Oddy, D. A. Kusza and W. F. Petersen, *Org. Lett.*, 2021, **23**, 8963-8967.
16. M. Montalti, A. Credi, L. Prodi and M. T. Gandolfi, *Handbook of Photochemistry*, CRC Press, 2006.
17. Y. Xiong, DPhil, University of Oxford, 2018.
18. I. R. Laskar and T. M. Chen, *Chem. Mater.*, 2004, **16**, 111-117.
19. J. Cosier and A. M. Glazer, *J. Appl. Crystallogr.*, 1986, **19**, 105-107.
20. T. Saito, H. Nihei, T. Otani, T. Suyama, N. Furukawa and M. Saito, *Chem. Commun.*, 2008, 172-174.
21. K. Iritani, S. Matsubara and K. Utimoto, *Tetrahedron Lett.*, 1988, **29**, 1799-1802.
22. Z. Wen, J. Xu, Z. Wang, H. Qi, Q. Xu, Z. Bai, Q. Zhang, K. Bao, Y. Wu and W. Zhang, *Eur. J. Med. Chem.*, 2015, **90**, 184-194.